

UNIVERSITY OF LATVIA

FACULTY OF BIOLOGY



NINEĻA MIRIAMA VAINŠEĻBAUMA

**POLYPLOIDY-RELATED ATAVISTIC AND REPRODUCTIVE
EVOLUTIONARY ADAPTATIONS IN MALIGNANT TUMORS**

DOCTORAL THESIS

Submitted for the degree of PhD in the Natural Sciences

Subfield of Molecular Biology

Riga, 2023

The doctoral thesis was carried out at the Latvian Biomedical Research and Study Centre and University of Latvia, Faculty of Biology, Department of Molecular Biology from 2019 to 2023.

Form of the thesis: collection of articles/research papers in biology, subfield molecular biology.

Supervisor: Dr. hab. med. Jekaterina Ērenpreisa

Consultant: Prof. Alessandro Giuliani (Istituto Superiore di Sanità, Rome, Italy)

Reviewers:

1) Kenneth J. Pienta, MD, Prof. (Johns Hopkins University School of Medicine, Maryland, USA);

2) Aija Linē, Dr. biol. (LBMC);

3) Nikolajs Sjakste, Dr.hab. biol., Prof. (LU);

The thesis will be defended at the public session of the Doctoral Committee of _____, University of Latvia, at _____ on _____, 20____.

Chairman of the Doctoral Committee _____ (Kaspars Tārs)

Secretary of the Doctoral Committee _____ (Daina Eze)

© University of Latvia, 2023
© Nineļa Miriama Vainšeļbauma, 2023

ABSTRACT

Polyploidy (particularly polyploid giant cancer cells, or PGCCs) is a crucial factor in the complex evolutionary mechanism that drives cancer towards the attractor state of aggressiveness and therapy resistance. PGCCs are induced by treatment and repopulate tumors by depolyploidizing into mitotic progeny. This ploidy cycle involves a radical cell fate change encompassing reversible senescence that induces embryonic stemness, atavistic transition, and the expression of reproductive (meiotic, cancer-testis and germ cell) genes.

On the basis of this data, we have proposed a hypothesis that cancer treatment resistance development through cyclical polyploidy involves a process that atavistically recapitulates pre-programmed mechanisms of asexual reproduction from extant species. A bioinformatic approach focused mainly on analysis of large-scale *ex vivo* sample datasets was used for its investigation.

The relationship between ploidy and the sex chromosome complement was assessed through statistical analysis of male patient karyotypes from the Mitelman Database, revealing a link between X-disomy (XXY or XX,-Y) and near-triploidy, which suggests maternal genome duplication and may be indicative of a reproductive process akin to digynic parthenogenesis. X-disomic triploid karyotypes were also shown to coexist with diploid and tetraploid cell populations, suggesting their exchange through a triploid bridge. The comparison of diploid and polyploid normal tissues revealed a whole-transcriptome atavistic shift, ploidy-dependant activation of developmental bivalent genes, enrichment of cancer-associated functional modules, and circadian clock repression. Circadian deregulation was also associated with polyploidy in TCGA non-treated tumor sample data. In multiple TCGA tumor types, polyploidy was found to upregulate gametogenetic genes (GG) and drive enrichment of reproductive modules (oogenesis in particular) in their gene regulatory networks. Furthermore, GG were abundantly expressed and interconnected in the proteomes of malignant melanoma and breast carcinoma. Lastly, comparison of doxorubicin-treated MDA-MB-231 human breast cancer cell line transcriptomes with non-treated controls revealed the activation of functional modules related to embryogenesis (placentation and pregnancy) and senescence.

Overall, the results obtained over the course of this work indicate that polyploidy and the associated rewiring of the gene regulatory network may enable cancer cells to undergo an atavistic reproductive process (likely incorporating elements from different stages of evolution,

as well as different asexual modes of reproduction, however invariably involving the recombination genes of meiotic prophase) that should result in resistance to DNA damage and protection from loss of heterozygosity, allowing the malignancy to recur after treatment. The results support our hypothesis on the involvement of polyploidy-driven asexual reproduction cycles in somatic tumor evolution, without conflicting with other existing theories of cancer development. Potential practical applications of the results were also outlined.

KOPSAVILKUMS

Poliploīdija (it īpaši poliploīdās vēža ģigantsūnas šūnas jeb PGCC) ir svarīgs faktors sarežģītajā evolūcijas mehānismā, kas virza vēzi uz agresivitātes un rezistences pret terapiju atraktora stāvokli. PGCC veidojas pēc ārstēšanas un atjauno audzēja šūnu populāciju, depoliploidizējoties par mitotiskiem pēcnācējiem. Šis ploīdijas cikls ir saistīts ar radikālu šūnas likteņa maiņu, kas ietver atgriezenisko senescenci, kura inducē embrionālo cilmestību, atavistisko pāreju un reproduktīvo (meiotisko, vēža-gonādu un ģerminatīvo šūnu) gēnu ekspresiju.

Pamatojoties uz šiem datiem, esam izvirzījuši hipotēzi, ka vēža ārstēšanas rezistences attīstība caur ciklisko poliploīdiju ietver procesu, kas atavistiski atveido iepriekš ieprogrammētos eksistējošo sugu bezdzimumiskās reprodukcijas mehānismus. Šīs hipotēzes pārbaudei tika izmantota bioinformātiskā pieeja, kas galvenokārt vērsta uz lielapjoma *ex vivo* paraugu datu kopu analīzi.

Saistība starp ploīdiju un dzimumhromosomu stāvokli tika novērtēta, statistiski analizējot vīriešu dzimuma pacientu kariotipus no Mitelmana datubāzes; tika identificēta saikne starp X disomiju (XXY vai XX,-Y) un triploīdiju, kas liecina par maternālā genoma dubultošanos un potenciāli arī digīniskajai partenogēnēzei līdzīgu reproduktīvo procesu. Tika arī novērots, ka X-disomiskie triploīdie kariotipi pastāv līdzās diploīdo un tetraploīdo šūnu populācijām, kas liecina par to apmaiņu caur triploīdo tiltu. Salīdzinot diploīdos un poliploīdos normālos audus, tika atklāta visa transkriptoma atavistiskā nobīde, no ploīdijas atkarīgā bivalento attīstības gēnu aktivācija, ar vēzi saistītu funkcionālo moduļu bagātināšanās un cirkadiānā pulksteņa nomākšana. Cirkadiānā deregulācija bija saistīta ar poliploīdiju arī TCGA neārstēto audzēju paraugu datos. Vairākos TCGA audzēju tipos tika konstatēts, ka poliploīdija augšupregulē gametoģenētiskos gēnus (GG) un veicina reproduktīvo (tostarp ooģenēzes) moduļu bagātināšanos to gēnu regulācijas tīklos. Turklāt malignās melanomas un krūts karcinomas proteomos GG bija bagātīgi ekspresēti un savstarpēji saistīti tīklos. Visbeidzot, ar doksorubicīnu apstrādātas cilvēka krūts vēža MDA-MB-231 šūnu līnijas transkriptomu salīdzināšana ar neapstrādāto kontroli identificēja ar embriogēzi (grūtniecību un placentāciju) un senescenci asociēto funkcionālo moduļu aktivāciju.

Kopumā šī darba gaitā iegūtie rezultāti liecina, ka poliploīdija un ar to saistītā gēnu regulatorā tīkla pārkārtošanās var ļaut vēža šūnām veikt atavistisku reproduktīvo procesu (iespējams, ietverot elementus no dažādiem evolūcijas posmiem, kā arī dažādiem bezdzimumvairošanās veidiem, tomēr nemainīgi iesaistot mejozes profāzes rekombinācijas gēnus), kas varētu nodrošināt

rezistenci pret DNS bojājumiem un aizsardzību pret heterozigotiskuma zudumu, tādējādi dodot ļaundabīgajām audzējam iespēju atgriezties pēc ārstēšanas. Iegūtie rezultāti apstiprina mūsu hipotēzi par poliploidijas virzītu bezdzimumvairošanās ciklu iesaisti somatisko audzēju evolūcijā, nenonākot pretrunā ar citām esošajām vēža attīstības teorijām. Tika izklāstīts arī rezultātu potenciālais praktiskais pielietojums.

TABLE OF CONTENTS

TABLE OF CONTENTS	7
LIST OF ABBREVIATIONS	9
Introduction	10
1. Literature review	11
1.1. Polyploidy in cancer, and the fitness benefits it confers	11
1.2. Epigenetic reprogramming and embryonic-like features in polyploid cancer cells	17
1.3. Meiosis, asexual reproduction, and the cancer ploidy cycle	19
1.4. The “imposter among us”: atavistic co-option of traits in cancer evolution	21
1.5. The circadian clock and cancer	22
1.6. Cancer evolution in the light of complexity and Systems theory	23
2. Materials and Methods	26
2.1. The sources of data	26
2.1. Statistical analysis of 15 malignant and 5 benign tumor patient karyotype cohorts	28
2.2. Analysis of bivalent gene activity in polyploid normal tissues	28
2.3. Ploidy-related circadian deregulation assessment in TCGA tumors	29
2.4. Ploidy-related gametogenetic (GG) gene expression assessment in TCGA malignant tumor transcriptomes	30
2.5. GG gene expression and cooperation assessment on the protein level in high-throughput proteomics datasets of melanoma and breast carcinoma	31
2.6. Comparison of 100 nM doxorubicin-treated and untreated MDA-MB-231 transcriptomes	32
3. Results	34
3.1. Triploidy is associated with X chromosome disomy in male patient tumor karyotypes from the Mitelman Database	37
3.2. In normal tissues, polyploidy is associated with developmental bivalent gene activation, an atavistic reversal to an evolutionarily ancient phenotype, circadian deregulation, and carcinogenic pathways	74
3.3. Polyploidy is linked to circadian deregulation in malignant tumors from the TCGA database	96
3.4. Polyploidy upregulates gametogenetic genes and enriches meiotic modules in TCGA malignant tumors	121
3.5. Gametogenetic genes are expressed and networked in malignant melanoma and breast carcinoma proteomes	121
3.6. Reproductive functional modules related to embryogenesis are activated in MDA-MB-231 breast cancer cells after doxorubicin treatment and subsequent polyploidization via mitotic slippage	148
3.6.1. Mitotic slippage in MDA-MB-231 cells is associated with meiotic gene expression, alternative telomere lengthening, and the emergence of two distinct PGCC subtypes	148
3.6.2. The trophoblast-like capacity of supergiant PGCCs, and its cooperation with the reproductive PGCC function in the MDA-MB-231 model	177

4. Discussion	202
5. Conclusions	206
6. Theses for defense	207
7. Acknowledgements	208
References	209

LIST OF ABBREVIATIONS

BG	Bivalent genes
BP	Biological process
BRCA	Breast carcinoma
CC	Circadian clock
CCD	Clock correlation distance
CSCs	Cancer stem cells
DEGs	Differentially expressed genes
EMT	Epithelial-mesenchymal transition
ESCs	Embryonic stem cells
GEO	Gene Expression Omnibus
GG	Gametogenetic genes
GO	Gene Ontology
GRN	Gene regulatory network
iPSCs	Induced pluripotent stem cells
KEGG	Kyoto Encyclopedia of Genes and Genomes
LECA	Last eukaryote common ancestor
LOH	Loss of heterozygosity
MM	Malignant melanoma
MS	Mitotic slippage
PGCCs	Polyploid giant cancer cells
PGCs	Primordial germ cells
PPI	Protein-protein interactions
SASP	Senescence associated secretory phenotype
TCGA	The Cancer Genome Atlas
WGD	Whole-genome duplication

Introduction

Comprising a vast range of over 100 diseases and firmly settled among the top-ranking causes of death in the developed world, cancer is, without a doubt, one of humanity's most formidable foes. Despite decades of dedicated research and massive monetary investments, efforts to find a definitive cure of metastatic solid tumors have so far resulted in disappointment. At least one in 3 people is likely to get cancer at some point during their lifetime, with the risk increasing as we age (Sasieni et al., 2011). Now, what exactly makes cancer so lethal and hard to eradicate?

The reason why cancer is responsible for so many deaths lies in its ability to metastasize, spreading across the patient's organs and tissues and ultimately destroying their function. Advanced, metastatic disease, the manifestation of cancer responsible for the majority of its death toll (Treasure et al., 2021), is characterized by its capacity to continuously resist a variety of treatment modalities, evolving and adapting to challenges posed by chemo-, radio- or immunotherapy. Thus, metastatic cancer treatment is often a matter of when, rather than if, this resistance develops and the disease recurs (Korentzelos et al., 2020; Pienta et al., 2020).

Recent findings suggest that the root of cancer resistance and recurrence lies in a population of cells that survive therapy by polyploidizing and acquiring stemness properties and, upon cessation of treatment, de-polyploidize, releasing resistant progeny that re-enters the mitotic cell cycle and regrows the tumor. Such cells, called polyploid giant cancer cells or PGCCs, are characterized by extensive evolutionary modifications and epigenetic reprogramming, and likely represent important targets for future therapies (J. Chen et al., 2019; Lee et al., 2009; Moein et al., 2020).

In this study, we investigated the hypothesis that the cancer ploidy cycle involves a reproductive process that employs gametogenesis-related genes to resist treatment and maintain immortality.

The objective of this study was to use bioinformatics and systems biology methods to explore the potential link between polyploidy and evolutionary reproductive processes in cancer.

The tasks for reaching this objective were:

1. To investigate the relationship between the sex chromosome complement and the ploidy of cancer karyotype samples from the Mitelman Database of Chromosome Aberrations and Fusions in Cancer

2. To identify the impact of polyploidy on the transcriptome in normal and cancer material (both *ex vivo* samples and *in vitro* samples from genotoxically treated cell lines)
3. To further the investigation on the proteome level by assessing the expression and cooperation of gametogenesis-related proteins

1. Literature review

1.1. Polyploidy in cancer, and the fitness benefits it confers

Polyploidy, or an increase in the number of whole genome copies, is a well-known driving force of evolution. The emergence of new genes is documented to occur via gene duplication followed by mutation and neofunctionalization leading to new speciation (generative polyploidy) (Madlung, 2013; Wendel, 2000). Somatic polyploidy, in turn, bestows numerous evolutionary benefits via an increase in genome number. It is considered an important mechanism of adaptation to stress (Anatskaya & Vinogradov, 2022) and associated with improved endurance to functional and toxicity load (Anatskaya & Vinogradov, 2004; Pandit et al., 2013; Tan et al., 2016). Extra genomes can serve as a “shield” against deleterious mutations causing otherwise-lethal loss of heterozygosity, as well as confer “hybrid vigor”, or heterosis (Z. J. Chen, 2010; Comai, 2005).

As for generative polyploidy, another crucial evolutionary benefit it confers is the capability to shift the organism from sexual to asexual reproduction, which is beneficial in harsh conditions and the absence of mates (Archetti, 2022; Comai, 2005; Skejo et al., 2021). In particular, triploidy formed by the fusion of a reduced and unreduced gamete is considered the “bridge” between diploid sexual and polyploid asexual reproduction (Hojsgaard, 2018; Schinkel et al., 2017).

The mechanisms of polyploidization are quite diverse. They include endoreplication (i.e. endocycling and aborted mitosis) and cell fusion, both of which have been documented to play a role in cancer development (Lee et al., 2009).

Over 40-50% of cancers are documented to undergo a whole-genome duplication at some point in their development (Newcomb et al., 2021). WGD is potentiated by circumventing the regulatory checkpoints of the cell cycle (for example, loss-of-function mutations in TP53 prevent cell cycle arrest upon DNA damage detection) (Barnum & O’Connell, 2014; Mosieniak & Sikora, 2010). The timing of the WGD is variable, depending on cancer type (Boisselier et al., 2018; C.-H. Wu et al., 2021). Aneuploid and polyploid modal chromosome numbers are

associated with higher disease aggressiveness, therapy resistance and patient mortality (Sheltzer & Amon, 2011). While aneuploidy was initially thought to interfere with cell division, this paradox can be resolved through polyploidy-associated reprogramming and self-renewal (J. Erenpreisa et al., 2022).

Polyploid giant cancer cells (PGCCs) not only take the spotlight during cancer’s response to therapy, but are present, albeit in a smaller proportion, in many non-treated tumors as well (S. Zhang et al., 2014). Aside from the previously mentioned benefits of somatic cell polyploidy, the cyclical nature of polyploidization and depolyploidization in PGCCs warrants special attention. The crucial role of cyclical polyploidy in cancer evolution and adaptation to therapy has been studied in over 25 laboratories all over the world, with a detailed list thereof presented in Table 1.

Table 1. A summary of experimental evidence for anti-cancer treatment resistance acquired via reversible polyploidization of mammalian cancer cells (where the animal is not indicated, human material was investigated). PGCC – polyploid cancer giant cells. (republished from (Vainshelbaum et al., 2022)).

Cancer type	Anti-cancer treatments	Experiment type	Source
Burkitt’s lymphoma	Ionising radiation (single dose of 10 Gy)	<i>In vitro</i> , on two cell lines, separation of PGCC by FACS, clonogenicity of the labeled polyploid fraction; microscopy	(J. Erenpreisa, 2000; J. A. Erenpreisa et al., 2000; Illidge et al., 2000)
Transformed cell lines, cervical carcinoma, renal adenocarcinoma, neuroblastoma	Ionising radiation, etoposide	<i>In vitro</i> computerised video-time lapse microscopy recording polyploidisation followed by bursting or budding of	(Sundaram et al., 2004)

		small cells restarting mitosis	
Colon carcinoma (rat)	Cisplatin	<i>In vivo, ex vivo</i> DHD-K12-TRb (PROb) cells	(Puig et al., 2008)
Colorectal carcinoma	Nocodazole	<i>In vitro</i> (HCT116 cell line)	(Vitale et al., 2010)
Lymphoblastoma, Burkitt's lymphoma	Ionising radiation (single dose of 10 Gy)	<i>In vitro</i> (WI-L2-NS, TK6, Namalwa)	(Salmina et al., 2010)
Fibrosarcoma (mouse)	Doxorubicin	<i>In vitro</i> induced and isolated single giant cells' allografts causing metastatic cancer	(Weihua et al., 2011)
NK/Ly lymphoma (mouse)	Vinblastine	<i>In vivo</i>	(Horbay & Stoika, 2011)
Colorectal carcinoma	H ₂ O ₂	<i>In vitro</i> (HCT116 cell line and its derivatives)	(Park et al., 2011)
Breast carcinoma	Ionising radiation (single dose of 8 Gy)	Tumorigenic and non- tumorigenic breast cancer cell lines; tumor xenografts; <i>ex vivo</i> primary human breast cancer	(Lagadec et al., 2012)

Non-small cell lung cancer	camptothecin, doxorubicin, cisplatin	NCI-H1299 cell line <i>in vitro</i> and <i>ex vivo</i> (patient samples)	(Q. Wang et al., 2013)
Breast carcinoma	Genotoxic drugs and mTOR inhibitors	<i>In vitro</i> (T-47D and ZR-75-1 cell lines)	(Sharma et al., 2014)
Colorectal carcinoma	5-fluorouracil and oxaliplatin	<i>In vitro</i> (HCT-116 and Caco-2 cell lines); separation of PCGC by CoCl ₂	(Lopez-Sánchez et al., 2014)
Virally transformed rat fibroblasts	Ionising radiation	<i>In vitro</i> (E1A + E1B cells)	(Chitikova et al., 2014)
Ovarian adenocarcinoma, breast carcinoma	Cisplatin	<i>In vitro</i> (HEY, SKOv3 and MDA-MB-231 cell lines), separation of PCGC by CoCl ₂ ; tumor xenografts	(S. Zhang et al., 2014)
Multiple human tumor types	Etoposide, doxorubicin, ionising radiation	Cell lines, time-lapse video microscopy, tumor xenografts	(Díaz-Carballo et al., 2014, 2018)
Ovarian carcinoma	carboplatin	<i>In vitro</i> (SKVO3)	(Rohnalter et al., 2015)

Nevi-derived multinuclear melanoma cells	Doxycycline	<i>Ex vivo</i>	(Leikam et al., 2015)
Colorectal carcinoma	Doxorubicin	<i>In vitro</i> (HC116)	(Mosieniak et al., 2015)
Ovarian carcinoma	Paclitaxel	<i>In vitro</i> (HCT116 cell line)	(Niu et al., 2016)
Breast carcinoma	Doxorubicin + paclitaxel	Neoadjuvant therapy. Induction of depolyploidizing PCGCs positive for OCT4, SOX2, NANOG, and CD44, mainly occurring in resistant near-triploid cases.	(Gerashchenko et al., 2016)
Prostate carcinoma	Docetaxel	<i>In vitro</i> (PC3 cell line)	(Mittal et al., 2017)
Ovarian carcinoma	Paclitaxel	<i>In vitro</i> (Hey, SKOV3 and MDA-HGSC-1 cell lines)	(Niu et al., 2017)
Prostate carcinoma	Docetaxel	<i>In vitro</i> (PC3 cell line and resistant subline)	(Lin et al., 2019)
Glioblastoma	Ionising radiation	<i>In vitro</i> (T98G, A172, and resistant sublines)	(Kiseleva et al., 2019)

Breast carcinoma and mouse melanoma	5-fluorouracil	<i>In vitro</i> (MDA-MB-231 and B16-F10 cell lines); tumor xenografts	(Kudo-Saito et al., 2020)
Breast carcinoma (triple-negative)	Doxorubicin	<i>In vitro</i> . Resistant reversible polyploidisation. DNA cytometry 7 w., microscopy.	(Salmina et al., 2020)
Ovarian carcinoma	Cisplatin	<i>In vitro</i> (SCOV-3 and A2780 cell lines without/with acquired resistance)	(Adibi et al., 2021)

This so-called “ploidy cycle” involves the polyploidized survivors returning to diploidy through reduction mechanisms, with the resulting progeny displaying therapy resistance and serving to repopulate the tumor through regained mitotic division (Rajaraman et al., 2007; Sundaram et al., 2004). In their journey through the stages of the ploidy cycle, cancer cells undergo extensive epigenetic reprogramming (a cell fate change) that may allow them to renew the Hayflick limit (Fig.1), explaining the effective “reproductive immortality” of cancer (Erenpreiss, 1993; Sundaram et al., 2004).

Furthermore, PGCCs display unique morphological traits that may render them similar to protozoans or early embryos. The features of PGCCs and their evolutionary significance are discussed in detail in the following sections.

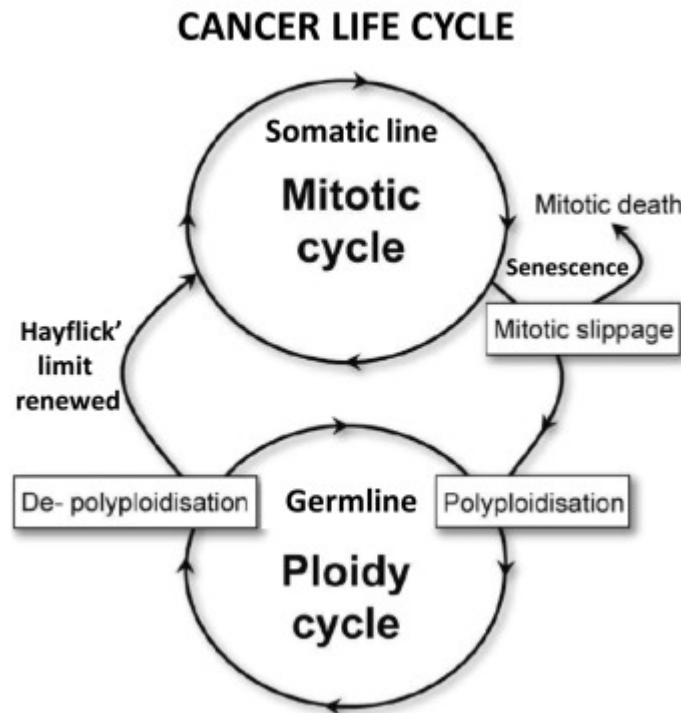


Figure 1. A graphical representation of the cancer life cycle model, showcasing cancer cells' ability to switch between mitotic para-diploidy and epigenetically reprogrammed polyploidy (republished from (J. Erenpreisa et al., 2022), modified from (J. Erenpreisa & Cragg, 2007)).

1.2. Epigenetic reprogramming and embryonic-like features in polyploid cancer cells

The existence of cancer stem cells (CSCs) - cancer cells with asymmetric division and differentiation potential that are responsible for creating the contents of the tumor- is considered to be one of the recent landmark discoveries in cancer biology research (Ayob & Ramasamy, 2018). Multiple studies on a variety of cancer types have hitherto observed PGCCs expressing stem cell markers, particularly embryonic ones (POU5F1, NANOG, SOX2) (Lagadec et al., 2012; Salmina et al., 2010). Another subset of cancer stemness markers are cancer-testis (CT) antigens - genes that are expressed in the testis, ovary, placenta and malignant tumor tissues, but not in normal somatic tissues (Gantchev et al., 2020; Gordeeva, 2018; Kalejs & Erenpreisa, 2005). Currently, there are over a thousand known CT genes (including both confirmed and predicted ones) (Almeida et al., 2009; C. Wang et al., 2016). In particular, genes such as PRAME and the MAGE family warrant attention, as they are heavily implicated in suppressing p53 and preventing cell differentiation (Epping et al., 2008; Wei et al., 2018; B. Yang et al., 2007; Zhao et al., 2022).

The process behind the origin of stemness properties in cancer cells, epigenetic reprogramming, is a complex interplay of different factors. One of its most crucial and, at a first glance, somewhat paradoxical components is cellular senescence - a stable arrest of the cell cycle that occurs in response to stress (oncogene activation, tumor suppressor deactivation, replicative stress, reactive oxygen species, epigenetic factors, and cancer treatment that inflicts DNA damage (Faggioli et al., 2022)).

Senescence, though tumor-suppressing in the short term, is associated with upregulation of both embryonic and adult stem cell markers, and activation of the Wnt pathway (Dou & Berger, 2018). The important proto-oncogene MYC, which is frequently amplified in aggressive cancers (Duffy et al., 2021), is in itself a factor of both senescence (Ko et al., 2018) and epigenetic reprogramming to stemness, used for iPSC generation alongside other Yamanaka factors (K. Takahashi & Yamanaka, 2006).

Another way senescent cells promote stemness is the auto- and paracrine stimulation via the senescence-associated secretory phenotype (SASP) (Faggioli et al., 2022). The senescent cell secretome contains interleukins, chemokines, growth factors, proteases, and extracellular matrix (ECM) components that altogether promote epigenetic reprogramming, inflammation and epithelial-mesenchymal transition (EMT), which is crucial for invasion and metastasis (Coppé et al., 2010).

Through DNA damage, senescence is linked to polyploidy, with PGCCs that form after treatment expressing such senescence markers as β -galactosidase and γ -H2AX - the marker of DNA double strand breaks (Niu et al., 2017; Salmina et al., 2020). This therapy-induced senescence in PGCCs has been found to be reversible via a subsequent “winning-out” of the stemness and self-renewal program that it itself stimulates (Huna et al., 2015; Salmina et al., 2017). Thus, PGCCs could be described as oscillating between senescence and stemness.

The similarities between PGCCs and certain phenotypes of embryogenesis do not end at the expression of embryonal stem cell marker genes. Malignant teratocarcinoma cells were found to be capable of differentiating into the three essential germ layers (Pierce, 1985; Pierce et al., 1982). Niu et al. observed the same phenomenon in PGCCs of ovarian cancer (Niu et al., 2017). Furthermore, expression of meiotic (MOS, REC8, SGO1 and 2, SPO11, DMC1, RAD51, synaptonemal complex proteins (SYCPs and SYCEs), STAG3, HORMADs) genes has also been stably detected in cancers (J. Erenpreisa et al., 2009; J. Erenpreisa & Cragg, 2010; Feichtinger & McFarlane, 2019; Gantchev et al., 2020; Ianzini et al., 2009; Rivera et al., 2015). Overall, these observations are in line with the embryonic theory of cancer, which has existed since the

19th century (Erenpreiss, 1993; J. Liu, 2020; Moein et al., 2020), and is currently enjoying a resurgence.

1.3. Meiosis, asexual reproduction, and the cancer ploidy cycle

Meiosis and sex appears to have evolved alongside eukaryotic cells themselves; the last common ancestor of current eukaryote taxa (LECA) was likely multinucleate, meiotic and sexually-reproducing (Skejo et al., 2021). The reason meiosis and sexual reproduction have become stably fixed in the biology of eukaryotes so early on in their evolutionary history lies in the benefits they confer. Meiotic interhomolog recombination represents a way to repair DNA damage (Bernstein et al., 2011; Bernstein & Bernstein, 2013); the same process induces heterozygosity and increases genetic variation of the offspring (reshuffling alleles). Meiosis is also a way to reduce ploidy (Roeder, 1997). The ability of an organism to shift between different ploidy levels is quite useful when it comes to persisting in variable environmental conditions (Lenormand et al., 2016). Overall, meiosis and sexual reproduction may be considered a form of stress response, with facultative sexual species (from *Paramecia* to plants and parthenogenetic vertebrates) favoring sexual reproduction over asexual reproduction in adverse conditions (Gerber & Kokko, 2018; Griffiths & Bonser, 2013; Ram & Hadany, 2016).

In the light of that knowledge, the increase and reduction of ploidy coupled with the expression of embryonic and meiotic genes (see Section 1.2) may seem, to some degree, indicative of reproductive process co-option for adaptive benefits. Since the environment inhabited by cancer cells can be quite hostile (hypoxia, the DNA-damaging chemotherapy and radiotherapy, replication stress), it makes sense that the benefits granted by meiosis would be of great use to their survival. Malignant tumors are also known to express germ cell-specific genes characteristic of both embryonic and adult germ cells (a gene set which partially overlaps with both cancer-testis genes and meiotic genes) (Bruggeman et al., 2020). This raises a possibility of not just reprogramming to stemness, but also a “soma-germ transition” process being involved in cancer evolution (Bruggeman et al., 2020). The cancer polyploidization-depolyploidization cycle hypothesis displayed in Fig. 1 has indeed been likened to a life cycle of an organism, with the mitotic descendants repopulating the tumor being compared to somatic cells and the epigenetically reprogrammed PGCCs - to a kind of “cancer germline”. The comparison with the life cycle hinges on the knowledge that advanced, resistant cancer is effectively immortal and the life cycle is the only hitherto known way in nature by which immortality is achieved (in this context, reproductive immortality - even if the parent organism dies, the passing-on of the germline ensures species survival)(Weismann, 1890). A soma-germ transition coupled to a

meiosis-like process which may even involve some mimic of syngamy (e.g. the segregation and conjugation of parental genomes, which has been observed in embryonal carcinoma (Salmina et al., 2019), and also seen earlier in senescent cell cultures and plants (Huskins, 1948; Walen, 2014)) seems like a logically feasible sequence.

Still, while the involvement of a reproductive process in cancer evolution and treatment resistance development is a tempting hypothesis, many questions still remain regarding its nature. Conventional meiosis involving a proper synaptonemal complex has never been observed via microscopic study (J. Erenpreisa et al., 2022). In fact, the ectopic expression of meiotic genes in somatic cancer cells is widely considered to interfere with normal mitosis leading to genome instability and mutability (Lindsey et al., 2013; Lingg et al., 2022). Still, cancer does not need to recapitulate the entire process of canonical gametic meiosis and sexual reproduction to reap evolutionary benefits from it. Furthermore, in somatic tumors, any hypothetical reproductive process would be an asexual one. In this context, it is important to mention the overlap between sexual and asexual reproductive machinery components. Some species of *Amoebozoa* express “meiotic toolkit” genes despite being obligate asexual, and also demonstrate cycling polyploidy. They likely use it for recombination between sister chromatids and gene conversion (Archetti, 2022; Maciver, 2016), as well as for “homologous chromosome counting” (Zickler & Kleckner, 2015) and elimination of excessive and/or damaged DNA (Goodkov et al., 2019), preventing loss of heterozygosity and lethal mutation accumulation, or Muller’s ratchet (Muller, 1964). Since meiosis, gametogenesis and sex appeared in the ancient predecessor of extant eukaryotes formed from an Archaea and bacteria fusion (LECA) (Skejo et al., 2021), the asexual reproduction of these eukaryotic organisms is secondary (Hofstatter et al., 2018). Furthermore, in the context of polyploidy (due to the higher abundance of allele copies) asexual reproduction was calculated to outweigh the benefits of sexual reproduction when it comes to minimizing loss of heterozygosity (LOH) (Archetti, 2022), which is rampant in cancers and would otherwise decrease fitness (X. Zhang & Sjöblom, 2021).

Still, it is by no means necessary for meiotic genes to perform only non-meiotic functions in an asexual life cycle, as such a life cycle does not need to rule out meiosis altogether (complete or, more likely, partial). For example, the automictic variant of parthenogenesis (which is of particular interest in the context of embryonic cancer theory and oocyte maturation gene (e.g. MOS) expression in cancer (J. Erenpreisa & Cragg, 2010), involves a meiotic step with two divisions, while in meiotic apomixis, the first meiotic division is obligate, and the second may be

suppressed (Archetti, 2004) or meiotic divisions in polyploids may proceed in an inverted order (Archetti 2021).

While there are some similarities between reproductive PGCCs and embryos (Niu et al., 2017), a curious direction of cancer cell fate change may be related to the other, no less crucial attribute of embryogenesis - placentation. Many CT genes, for example, are normally restricted to not just the testis and ovary, but the human placenta as well (Jungbluth et al., 2007). Furthermore, placenta-specific gene expression in cancer is a known marker of poor prognosis, and the process of invasion and metastasis shares some similarities with placenta evolution (Costanzo et al., 2018; Kshitiz et al., 2019). This knowledge warrants further investigation with regards to the cancer ploidy cycle.

Overall, taking into account the available literature, it appears that if a reproductive process is indeed involved in cancer evolution, it is an asexual one that incorporates characteristics/components of the meiotic cell cycle (that of its canonical form in humans, or, even more likely, some other evolutionary modification of it) and soma-germ transition (development of the cancer germline). Such a hypothesis is investigated and expanded upon by this study. The reason it seems feasible that reproductive mechanisms resembling that of other species may be involved in the evolution of malignant tumors lies in cancer's well-documented atavistic capabilities.

1.4. The “imposter among us”: atavistic co-option of traits in cancer evolution

The phenotypic differences between a normal cell and an advanced, epigenetically reprogrammed PGCC are vast. In fact, one of the distinctive features of advanced metastatic cancer is its apparent capability of transcending the species identity (Vincent, 2011), with some researchers even terming carcinogenesis a kind of speciation in itself (Pienta et al., 2020; Vincent, 2010). Particularly striking is the ability of cancer cells to borrow, or, more fittingly, co-opt traits from other lifeforms for the sake of survival and proliferation. This phenomenon, termed “atavistic transformation” or “phylostratigraphic shift”, involves the upregulation of ancient genes characteristic of unicellular (UC) and early multicellular organisms (MC), the downregulation of evolutionarily newer MC genes and the disruption of the balanced UC-MC interactions in the gene regulatory network (Trigos et al., 2018, 2019). The ploidy cycles of PGCCs (and alternative uses for meiotic genes) have a counterpart in amoebae (See Section 1.2), and the mechanism of depolyploidization likely represents a form of coenocytosis - cell division with postponed cellularisation within multinuclear cells created by a-cytokinetic karyotomy,

which is observed in protists, fungi and algae in nature, and associated with reproduction (Adl et al., 2012).

Furthermore, PGCCs and their descendant cells can have amoeboid-like morphology (motility, cytoskeleton, encystment) as well - the epithelial-mesenchymal-amoeboid transition is a crucial stage of invasion and metastasis (J. Erenpreisa et al., 2011, 2018; Graziani et al., 2022).

1.5. The circadian clock and cancer

One of the crucial regulators of both gene expression and organismal functions (such as, for example, sleep (Allada & Chung, 2010; Buhr & Takahashi, 2013)) is the circadian clock (CC). The CC is a molecular mechanism that couples said functions to the 24-hour day-night cycle, making them rhythmic through a web of autoregulatory transcriptional and translational feedback loops (this phenomenon is called the circadian rhythms). At least 20% of all mammalian genes (Storch et al., 2002) and 43% of protein-coding genes (R. Zhang et al., 2014) are controlled by the CC. When the “core” component of the CC oscillates, so do its numerous interactants. Said “core” CC component consists of 16 genes (CLOCK, ARNTL (BMAL1), ARNTL2, NPAS2, NR1D1, NR1D2, CRY1, CRY2, DBP, TEF, RORA, RO RB, RORC, PER1, PER2, and PER3) (Shilts et al., 2018; Y. Wu et al., 2019).

BMAL1/CLOCK dimers are transcriptional activators (both proteins are basic helix-loop-helix transcription factors), while PER/CRY dimers make up the repressive “arm” of the clock. The heterodimeric complex of BMAL1 and CLOCK binds the promoters and activates the expression of PER1, PER2, PER3, CRY1, and CRY2, which subsequently heterodimerize into PER/CRY complexes, translocate into the nucleus, and repress BMAL1/CLOCK (Langmesser et al., 2008). BMAL1 and CLOCK expression is renewed once E3 ubiquitin ligases deplete the PER/CRY dimers (J. S. Takahashi, 2017). The architecture of the CC also includes a feedback loop of nuclear receptors that rhythmically bind DNA - the activating RORs and repressive REV-ERBs (X. Yang, 2010). These receptors regulate, among other genes, the expression of BMAL1, and are themselves regulated by other clock genes, such as CLOCK, BMAL1, and DBP (Rijo-Ferreira & Takahashi, 2019).

Core clock genes are directly involved in regulating the checkpoints of the cell cycle (Farshadi et al., 2020). For example, BMAL1/CLOCK regulates transcription of the proto-oncogene c-Myc, which is involved in G0/G1 transition (Fu et al., 2002), while ATR/CHK2, which activates in response to DNA double-strand breaks introduced by ionizing radiation, is regulated by PER1. Furthermore, PER2 is involved in the stabilization of the master tumor suppressor p53 (Farshadi et al., 2020).

As such, considering that proper CC function is so crucial for maintaining proper cell division, it comes as no surprise that circadian deregulation is firmly associated with cancer development and progression (Savvidis & Koutsilieris, 2012; Sulli et al., 2019).

Crucially, CC function is also missing in embryonic stem cells (ESCs) and germ cells, and it develops as they differentiate (in mammals -during post-implantation embryo development). In fact, stemness and reprogramming factors interact and directly compete with both cell cycle inhibitors (senescence regulators) and some CC components. For example, c-Myc alone and in the form of MYC/MAX dimers inhibits CLOCK/BMAL1, while OCT4, NANOG and SOX2 respectively inhibit p21, p16 and p27 senescence regulators. This allows ESCs to bypass the G1/S checkpoint (Neganova & Lako, 2008). In the context of cancer, which is known to express these embryonal stemness markers (particularly in the PGCCs), this ability to bypass checkpoints would certainly be an evolutionary boon. Furthermore, circadian deregulation results in a lack of p53 stabilization, and there is evidence that is directly implicated in polyploidization - inactivating the circadian clock proteins PER1, PER2, and PER3 causes rampant ploidy increase in non-cancerous hepatocytes (Chao et al., 2017).

As such, CC function disruption can be potentially considered yet another piece of evidence for a similarity between polyploid cancer cells and early embryos, and thus, the vast adaptive potential of malignant tumors.

1.6. Cancer evolution in the light of complexity and Systems theory

Cancers (and biological entities in general, from cells to organs, organisms and populations) are complex, dynamic and adaptive systems (J. Erenpreisa & Giuliani, 2019). This type of system is characterized by high-dimensionality (a vast multitude of interacting components), stochasticity (random fluctuations around a state of dynamic equilibrium), heterogeneity (diversity of components) (Huang, 2021) and, crucially, a capacity to learn (Gyurkó et al., 2013). As such, to understand cancer and evolution on a holistic level, a systems biology approach grounded in dynamical systems theory is needed (Huang, 2021). This enables the assessment of not just the system's constituent parts, but also the emergent properties arising from their collective nonlinear interactions (Bizzarri et al., 2011; Huang et al., 2009).

For this purpose, it is most convenient to represent the biological system in question as a network. The biological interaction network can be constructed on different layers of organization - for example, the interactions of genes within a cell and cell types within a tissue/tumor (Bizzarri & Giuliani, 2022). This study in particular focuses on the gene regulatory network (GRN), where nodes represent the system's components (genes and the products of

their expression - RNA transcripts for the gene coexpression network, and proteoforms - for the protein-protein interaction (PPI) network), and the edges - their interactions. Biological networks are «critical networks» - not too densely connected (with many loosely interconnected nodes and a smaller number of crucial hub nodes), optimized in terms of balancing information transmission (Huang, 2021), as well as order and chaos, on the edge of which self-organization into new system states is known to occur (S. A. Kauffman & Johnsen, 1991; Prigogine & Stengers, 1984).

As such, from a systems biology viewpoint, cancer development is a rewiring of the GRN (critical transition) governing cell fate from a healthy to a diseased state. Now, what exactly defines a “diseased” interaction network?

Kaufmann (S. Kauffman, 1971) was the first to propose the idea of a “cancer attractor”. The idea of the attractor in the context of cell fate is best explained by invoking the concepts of Waddington’s epigenetic landscape and the state space. Waddington (Creighton & Waddington, 1958) envisioned cell differentiation as a marble (representing the cell’s current state) rolling down a hill, and eventually ending up in one of the branching furrows at its bottoms, which represent discrete differentiated states. This landscape can also be referred to as a “state-space” where coordinates represent different cell fates.

As defined by Huang (Huang, 2021), the system state S is represented by a vector of values of its constituent components, and a state-space is a dimensional reduction thereof. Upon perturbation, the values change, and so does the position of the cell upon the state-space. Since the interactions between the components of the system (e.g. genes inhibiting one another) create constraints, some areas of the state space are less accessible than others - hence, its topography of hills, valleys and furrows. This landscape can be quantified as a gradient of quasi-potential energy (U). Further drawing on the landscape metaphor, “elevation” on the landscape represents the difference of U between two positions in state space (ΔU). States occupying local minimums of U (the bottoms of valleys) are referred to as attractor states - they are stable and self-stabilizing upon perturbation (Lewin, 1999). Since a GRN is a critical network, the existence of multiple attractors is inherent to it via its capacity for self-organization. Overall, stochasticity inherent to the dynamic system, such as transcription fluctuation or transposon noise, makes cells within the same population slightly different, which influences cell fate transitions upon perturbation (decides the slope down which the proverbial “marble” of system state will roll, with the gradient of U amplifying the fluctuation) (Huang, 2021). An example of such a “decision” (the so-called critical transition, or bifurcation event), can be seen in cancer upon chemotherapy, nudging cells either towards death or survival through senescence-stemness

reprogramming and cyclical polyploidy (J. Erenpreisa et al., 2022; J. Erenpreisa & Giuliani, 2019). However, one high-impact perturbation of a high-dimensional system causes numerous bifurcation events, which is an important cause of heterogeneity within a tumor, cells reaching and stabilizing at a variety of attractor states. Events such as mutations or aneuploidies can fundamentally alter the GRN, rearranging the landscape itself and thus enabling access to previously unavailable states (Huang, 2021). According to the cancer attractor theory, cancer can be considered one of such states - evolutionarily preprogrammed during early evolution of life, yet normally unreachable or reachable only in other, more ancient lifeforms (Huang et al., 2005, 2009; S. Kauffman, 1971). As for the initial origins of this attractor, it is hypothesized that it may be one of defective regeneration - “tumors are wounds that never heal” (Dvorak, 1986). Attractors (as they are phenotypes) are subject to selective pressures, and evolutionarily unfavorable ones are made hard to access via the quasipotential landscape - this means they are sealed rather than destroyed (Huang, 2021). Given enough perturbations (and they are not in short supply - each cell in the body is subjected to tens of thousands of potential DNA lesions daily, and its repair mechanisms are accurate but imperfect (Tubbs & Nussenzweig, 2017) and bifurcation events in the complex system that is a cell, an attractor of resistant cancer is certain to be reached, cementing cancer as a grim fate inherent to multicellular organisms. The fact that bifurcation events are low-dimensional - influenced by a small number of key genes (the hubs of the GRN) - may provide a ray of hope (Huang, 2021). Still, advanced cancer treatment can't be a matter of simply targeting network hubs alone, considering that these hubs can be important for normal organismal function (Goh et al., 2007; Ibrahim et al., 2011).

In the context of cancer, another important functional characteristic of GRNs is their rigidity or plasticity. Rigid networks have a clearly defined modular and hierarchical structure, with few attractor states, and are effective for continuously encoding a specific function (“memory”). Plastic networks, on the other hand, are less centralized, with a high number of attractors that can switch easily (represented by a smoother epigenetic landscape). Such networks are optimal for learning and adapting to new stimuli (Csermely, 2021). While early-stage cancers are associated with network plasticity and late-stage cancers - with rigidity, the GRNs of cancer stem cells (among them, PGCCs and their progeny (J. Erenpreisa et al., 2022)) are known to switch between these two qualities. Seeing as rigid and plastic networks require different treatment approaches, this ambivalence of CSCs is particularly problematic and highlights the need of combined treatment approaches targeting not only cancer genes, but their first and second neighbors (Csermely, 2021).

2. Materials and Methods

2.1. The sources of data

Table 2. The summary of tumor and normal tissue datasets used in the current study.

Dataset	Publication	Sample type	N samples	Data source
Patient (male) tumor karyotypes from 15 solid malignant and 5 benign tumor types	I, II	<i>Ex vivo</i>	2928	Mitelman Database of Chromosome Aberrations and Gene Fusions in Cancer (Mitelman et al., 2000)
The human and mouse transcriptomes of normal diploid and endopolyploid tissues	IV	<i>Ex vivo</i>	11	The multi-species database of organ-specific transcriptomes from (Brawand et al., 2011)
Rsubread-recounted transcriptome data of patient tumor and matched normal samples (29 malignant tumor types)	V, VI	<i>Ex vivo</i>	10005 (9264 tumor and 741 normal)	The Cancer Genome Atlas (TCGA) (Cancer Genome Atlas Research Network et al., 2013) Gene Expression Omnibus dataset GSE62944 (Rahman et al.,

				2015)
ABSOLUTE purity and ploidy values of TCGA patient tumor samples (33 malignant tumor types)	V, VI	<i>Ex vivo</i>	10522	Supplementary materials of (Taylor et al., 2018)
Whole-proteome protein abundance matrix of malignant melanoma patient samples	VI	<i>Ex vivo</i>	505	Supplementary materials of the MM500 Melanoma Proteome Atlas study (Betancourt et al., 2021)
Whole-proteome protein abundance matrix of breast carcinoma patient samples	VI	<i>Ex vivo</i>	45	ProteomeXChange dataset PXD008841 (Johansson et al., 2019)
Transcriptome data of the doxorubicin-treated MDA-MB-231 breast cancer cell line	VII	<i>In vitro</i>	3 replicates of 5 time points (NT, D5, D8, D16, D22)	Latvian Biomedical Research and Study Center, Cancer Cell Biology and Melanoma Research Lab

This study relies on the bioinformatic analysis of tumor and normal sample data from open-access repositories (as well as our laboratory), which are listed in Table 2. The analysis assesses cancer evolution on the genomic (in the form of purity and ploidy values calculated from TCGA genome sequencing data, as well as cytogenetic data), transcriptomic, and proteomic levels.

Additionally, the study uses the following gene sets:

- Data on the evolutionary age (phylostratigraphy) of human protein-coding genes from (Trigos et al., 2017).
- The list of ESC bivalent genes from (Court & Arnaud, 2017).
- The CTDatabase's repertoire of high-evidence cancer-testis genes (Almeida et al., 2009).
- The meiotic gene set from the MeiosisOnline meiotic genes (Jiang et al., 2021), extended further based on currently available evidence.
- The cancer-germ cell gene set established by (Bruggeman et al., 2020).

2.1. Statistical analysis of 15 malignant and 5 benign tumor patient karyotype cohorts

Karyotype datasets from 15 solid malignant and 5 benign tumor types were obtained from the Mitelman Database of Chromosome Aberrations and Gene Fusions in Cancer (Mitelman et al., 2000). Male patient karyotypes were used exclusively due to the diversity of the sex chromosome complement (X and Y) that makes it easier to discern between paternal and maternal genome rearrangements.

Monoclonal karyotypes (2928 samples in total) were collected.

Pearson correlation analysis was performed on them using the numpy (Oliphant, 2006) and pandas (McKinney, 2010) Python packages to determine the relationship between ploidy and different sex chromosome karyotypes. The correlation was validated with principal component analysis (PCA). Matplotlib (Hunter, 2007) and seaborn (Waskom, 2021) Python packages were used for visualization.

Polyclonal samples containing X-disomic triploid karyotypes were filtered out separately to assess ploidy dynamics.

2.2. Analysis of bivalent gene activity in polyploid normal tissues

Differentially expressed genes acquired from both cross-species differential expression analysis and PCA were assessed for bivalency by comparison with the set of genes containing bivalent chromatin regions in human embryonic stem cells (Court & Arnaud, 2017). The

binomial test approach was used to calculate enrichment of the DEGs with bivalent genes. The upregulated and downregulated BGs were then subjected to phylostratigraphic assessment using the gene phylostratigraphy data from (Trigos et al., 2017), and the phylostratigraphic distributions of DEGs in general and bivalent DEGs in particular were plotted using matplotlib. The network association (in the form of a protein-protein interaction or PPI network) of the bivalent DEGs was assessed using the STRING database's (Szklarczyk et al., 2020) web interface, which also has the capability to perform GO (Harris et al., 2004) and KEGG (Kanehisa et al., 2016) enrichment analysis (modules with $p_{Adj} < 0.05$ classified as enriched). A separate STRING network and enrichment analysis was performed for the bivalent c-Myc interactants. The oncogenes and tumor suppressor genes found among the differentially expressed genes were also ordered by their phylostratigraphic status and plotted.

2.3. Ploidy-related circadian deregulation assessment in TCGA tumors

The CCD (Clock Correlation Distance) method (implemented via the `deltaccd` R package) developed by Shilts et al. was used to calculate the degree of circadian deregulation (the Δ CCD coefficient) (Shilts et al., 2018).

This method compares core CC gene coexpression (Spearman rank-based correlation) between samples used in the study and a pan-tissue reference matrix calculated from eight normal mouse time-series datasets. The Euclidean distance between core CC gene correlation vectors of the samples and the mouse reference is referred to as the Clock Correlation Distance (CCD). The difference between normal and reference CCD, and the tumor vs. reference CCD, known as the Δ CCD, serves as a coefficient of circadian dysregulation, with the “difference of differences” approach effectively negating the nuance of mouse–human comparison and accepting the common regulation of CC in mammals (Shilts et al., 2018).

TPM-normalised Rsubread-processed TCGA gene expression data was downloaded from the GSE62944 GEO dataset (Rahman et al., 2015) using GEOquery (Davis & Meltzer, 2007) in R. In order to ensure statistical power, only TCGA transcriptomics datasets counterpart by at least 35 available normal samples were selected, resulting in a final cohort of 11 cancer types and 6667 samples (613 normal and 6054 tumors).

Circadian deregulation in TCGA cancer samples was determined using the CCD method, and scaled Δ CCD values were obtained for each tumor type.

Tumor ploidy calculated from somatic DNA alteration data using the ABSOLUTE algorithm (Carter et al., 2012) was obtained from (Taylor et al., 2018). The relationship between the values

of scaled Δ CCD for each of the 11 tumor types and the respective proportion of WGD+ samples was investigated using Spearman correlation analysis.

2.4. Ploidy-related gametogenetic (GG) gene expression assessment in TCGA malignant tumor transcriptomes

A combined gametogenesis-related (GG) gene set, numbering a total of 1474 genes, was compiled from cancer–testis genes from the CTDatabase (Almeida et al., 2009), cancer–germ cell (primordial and adult male) genes from (Bruggeman et al., 2020) and the MeiosisOnline (Jiang et al., 2021) human meiosis-involved gene database that was updated with a manually-curated set of additional genes (SYCP1, SYCP2, SYCP3, SYCE1, SYCE2, HORMAD2, MAEL, MEIKIN, MEIOB, MEIOC, SYCE1L, TEX11, MAJIN, FAM9C, FAM9B, FAM9A, REC114, TEX19, BRME1, TEX14, MSH4, TEX15).

DEGs were selected from the TCGA WGD-associated gene expression dataset available in the supplementary materials of (Quinton et al., 2021) using a threshold of Benjamini-Hochberg $p_{Adj} < 0.05$ and $|\log_{2}FC| > 0.5$. Each of the 29 cancer types covered in the aforementioned study was assessed for enrichment with GG genes using a binomial test. The phylostratigraphic distribution of GG genes for the 17 eligible (>10 WGD-upregulated GG genes) tumor types was plotted after matching the genes with the phylostratigraphic data from (Trigos et al., 2017). The phylostratigraphic distribution of the whole GG gene set was also plotted and used for comparison with the former. The interconnection of ploidy-upregulated and ploidy-downregulated genes was assessed using network analysis. STRING PPI networks were constructed using the STRING web interface. Enriched ($p_{Adj} < 0.05$) GO and KEGG modules were subsequently identified using STRING's analysis function. Cancer types with ploidy-upregulated gene networks enriched for reproductive modules were subjected to coexpression network analysis to validate the interconnection of these DEGs in polyploid samples pertaining to the dataset in question rather than just a general database.

The co-expression network (unsigned, both positive and negative correlation coefficients above threshold recognized as an edge between genes) was obtained by computing pairwise Pearson correlations between DEGs.

A permutation approach similar to that described in (Censi et al., 2011) was used for determining the appropriate correlation coefficient threshold. A hard threshold of pairwise correlation coefficients was determined by comparing the number of edges (pairwise correlations equal to or exceeding the threshold in absolute value) between 50 randomly picked

sets of 300 genes and surrogate data - shufflings of these datasets across columns (50 shufflings for each set). This approach serves to determine a “mean correlation field” linking the genes (or, in the case of the proteomic data described in the next sections, the proteins), and the amount of noise/randomness present in the data. In this case, a list of 4 possible thresholds, ranging from 0.6 to 0.9, were tested in this manner, and a threshold of 0.6 was found to be sufficient to define an edge in the network, with the number of interactions in “real” data vastly and highly significantly (Wilcoxon test $p < 0.001$) exceeding that of surrogate data, indicating that the normalization procedure in the initial data was successful at reducing the noise.

The selected threshold was used to transform the correlation matrix into a binary adjacency matrix, which was imported into Cytoscape (Shannon et al., 2003) via the RCy3 R package (Gustavsen et al., 2019) and the aMatReader app (Settle et al., 2018). Cytoscape’s network analysis functionalities were used to acquire the network’s statistics and the prototyped Cytoscape network was fully visualized with the functionalities of the igraph and ggraph R packages. The giant components of the upregulated and downregulated gene networks were then extracted for further analysis. The resulting 12 coexpression networks (6 WGD-upregulated and 6 WGD-downregulated) were assessed for enriched GO and KEGG modules with the clusterprofileR package (Yu et al., 2012) and the enrichment analysis results were visualized as treemap plots using the rrvgo (Sayols, 2020) R package.

2.5. GG gene expression and cooperation assessment on the protein level in high-throughput proteomics datasets of melanoma and breast carcinoma

This analysis was performed to assess the relationships between GG gene expression in malignant tumor patient samples on the whole-proteome level. For that purpose, two high-throughput proteomics datasets of two malignancy types (malignant melanoma, or MM, and breast carcinoma, or BRCA) from public databases were used.

A matrix of high-throughput LC-MS/MS proteomics data (normalized relative protein abundance values) from 505 late-stage melanoma patient tumor samples and over 12 000 protein-coding genes was obtained from the supplementary materials of the MM500 Melanoma Proteome Atlas study (Betancourt et al., 2021). Hierarchical clustering (hclust in the R stats package) was performed to stratify the samples by abundance and value missingness. Cutting the tree at a height of 1400 (an ultrametrics based on Euclidean Distance) stratified the patient samples into 6 clusters (Figure 4). Patient Cluster 3 (n=142) was selected for further analysis due to technical considerations.

The low-expressed proteoforms were filtered out of the resulting 142-sample matrix, with a cutoff of at least 5 normalized relative expression units in at least 20% of the samples. For the rest, the missing values were replaced using minimum imputation (the log₂-scale value of the minimum possible measurement) with the assumption of low protein expression as the reason for their missingness.

A matrix of normalized relative protein abundances for 45 BRCA samples (grades 2-3) was obtained from the ProteomeXChange PXD008841 repository (Johansson et al., 2019). Unlike the MM dataset, the BRCA dataset had already been filtered to only include proteins expressed in every sample, for a total of 9995 proteins. As such, no further low-expression filtering was necessary.

In order to assess the possible presence of soma-germ transition and/or pseudo-meiotic features related to embryonalization in late-stage melanoma and grade 2-3 breast carcinoma, the GG gene set (n=1474) was used to filter out the proteins related to the aforementioned processes.

To investigate the relationship between the expressed proteins, the resulting GG protein abundance matrix was used to calculate pairwise correlations and construct a coexpression network with the same procedure as described in Section 2.4. In the proteome data, the threshold of 0.6 in absolute value was found to be sufficient. To determine the most interconnected network components or modules, the co-expression network was MCL-clustered with a granularity parameter of 2.5, implemented in Cytoscape's clusterMaker app (Morris et al., 2011). GO BP and KEGG enrichment analysis was performed as described in Section 2.4, but unlike the case of the TCGA transcriptomes, in which all genes in the database were used, for proteomics data, the whole proteome of the cancer dataset in question was input as the background gene set. The enrichment analysis was done separately on the whole giant component of the protein-protein coexpression network, and its most highly interconnected part (MCL cluster 1).

The NDEX database (Pratt et al., 2015) was used for depositing the networks.

2.6. Comparison of 100 nM doxorubicin-treated and untreated MDA-MB-231 transcriptomes

This part of the study compares transcriptomes of the breast adenocarcinoma MDA-MB-231 cell line (triple-negative, modal chromosome number 64) treated with 100 nM DOX (doxorubicin) for 24 h (four timepoints - the 5th, 8th, 16th and 22nd days post-DOX treatment) with non-treated samples. The libraries were sequenced with the DNBSEQ-G400 sequencing platform (MGI, China). Transcriptome FASTQ files were quality-checked with FastQC, trimmed

of adapters and low-quality reads with Cutadapt, pseudo-aligned to the GRCh38.p13 human transcriptome (downloaded from the GENCODE site) with Salmon (Patro et al., 2017), and then the tximport package (Soneson et al., 2015) in R was used to acquire gene-level count matrices for each sample.

Differential expression analysis comparing treated samples with the NT control at each timepoint was performed using edgeR (Robinson et al., 2010), obtaining differentially expressed genes (DEGs) with the glmQLFTest approach. The threshold for differential expression was selected to be $FDR < 0.05$ & $LogFC > 1$ (in absolute value). EdgeR's plotMDS visualization function was used to construct a MDS (multidimensional scaling) plot of the samples, while volcano plots of the DEGs were generated with EnhancedVolcano (Blighe et al., 2019). The resulting lists of upregulated and downregulated genes for each time point were subsequently subjected to GO enrichment analysis with the hypergeometric test method and Benjamini-Hochberg p-value correction ($p_{Adj} < 0.05$ threshold for enrichment) implemented in the clusterProfileR (T. Wu et al., 2021) package. The enrichment results were visualized in treemap plot form using the rrvgo R package.

The DEG lists (upregulated and downregulated genes separately) for each time point were assessed for statistically significant enrichment with bivalent genes using the binomial test method. The differentially expressed bivalent genes were assessed separately with GO enrichment analysis and the results were visualized as described in the previous section.

The whole-genome phylostratigraphy data separating the genes into evolutionary groups referred to as phylostrata was obtained from Trigos et al. 2017 (Trigos et al., 2017). There were 3590 bivalent genes with phylostratigraphic annotation. The phylostratigraphic distributions of differentially expressed genes at each of the time points were plotted with ggplot2 (Villanueva & Chen, 2019), with the whole-genome phylostratigraphic distribution serving as reference.

Due to the prevalence of 8th-phylostratum genes among upregulated genes, it was further decided to subject these 8th phylostratum DEGs to STRING PPI network analysis in order to determine the functional relationship between them. Protein-protein interaction data for these genes-of-interest was downloaded from the STRING database and visualized in network form using Cytoscape. After extracting the giant component of each network, the resulting networks were subjected to GO enrichment analysis with the ClueGO (Bindea et al., 2009) Cytoscape app. The resulting enriched GO modules were subsequently visualized in Enrichment Map format and deposited in the NDEX database.

3. Results

The results are presented here as 7 original publications.

The author's contribution to the publications:

Original article I

Vainshelbaum, N. M., Zayakin, P., Kleina, R., Giuliani, A., & Erenpreisa, J. (2019). Meta-Analysis of Cancer Triploidy: Rearrangements of Genome Complements in Male Human Tumors Are Characterized by XXY Karyotypes. *Genes*, 10(8), 613. <https://doi.org/10.3390/genes10080613>

Contribution: participated in the design of the study, performed bioinformatic meta-analysis of 2928 cancer karyotypes from the Mitelman Database of Chromosome Aberrations and Gene Fusions in Cancer, analyzed the literature on cancer triploidy, polyploidy's role in evolution, and digyny, visualized the results, majorly participated in the manuscript draft writing and editing until its final version.

Original article II

Salmina, K., Gerashchenko, B. I., Hausmann, M., **Vainshelbaum, N. M.**, Zayakin, P., Erenpreiss, J., Freivalds, T., Cragg, M. S., & Erenpreisa, J. (2019). When Three Isn't a Crowd: A Digyny Concept for Treatment-Resistant, Near-Triploid Human Cancers. *Genes*, 10(7), 551. <https://doi.org/10.3390/genes10070551>

Contribution: Analyzed literature on the topic of cancer triploidy. Continued the meta-analysis of Mitelman Database karyotypes, focusing on renal carcinoma. Contributed to writing part of the manuscript draft.

Original article III

Salmina, K., Bojko, A., Inashkina, I., Staniak, K., Dudkowska, M., Podlesniy, P., Rumnieks, F., **Vainshelbaum, N. M.**, Pjanova, D., Sikora, E., & Erenpreisa, J. (2020). "Mitotic Slippage" and Extranuclear DNA in Cancer Chemoresistance: A Focus on Telomeres. *International journal of molecular sciences*, 21(8), 2779. <https://doi.org/10.3390/ijms21082779>

Contribution: Prepared a literature review on gene conversion, alternative telomere lengthening and homologous recombination, performed statistical analysis and visualization of experimental data resulting from time-series in situ DNA cytometry of doxorubicin-treated MDA-MB-238 cells, as well as the data from RT-PCR and Selfie digital PCR of meiotic gene expression in that model.

Original article IV

Anatskaya, O. V., Vinogradov, A. E., **Vainshelbaum, N. M.**, Giuliani, A., & Erenpreisa, J. (2020). Phylostratic Shift of Whole-Genome Duplications in Normal Mammalian Tissues towards Unicellularity Is Driven by Developmental Bivalent Genes and Reveals a Link to Cancer. *International Journal of Molecular Sciences.*, 21(22), 8759. <https://doi.org/10.3390/ijms21228759>

Contribution: Performed gene phylostratigraphic analysis of ploidy-upregulated bivalent genes. Worked on data visualization and interpretation. Performed literature analysis on the topic of bivalent genes and their function in cancer.

Original article V

Vainshelbaum, N. M., Salmina, K., Gerashchenko, B. I., Lazovska, M., Zayakin, P., Cragg, M. S., Pjanova, D., & Erenpreisa, J. (2022). Role of the Circadian Clock "Death-Loop" in the DNA Damage Response Underpinning Cancer Treatment Resistance. *Cells*, 11(5), 880. <https://doi.org/10.3390/cells11050880>

Contribution: Assessed the association between circadian deregulation and polyploidy with the DeltaCCD bioinformatic method, using multiomic (transcriptomic data and ploidy values inferred from whole-genome copy number data with the ABSOLUTE algorithm) data of 6667 samples (11 tumor types) from the Cancer Genome Atlas (TCGA) database. Performed literature analysis on the topic of circadian deregulation in cancer. Majorly contributed to manuscript writing and editing.

Original article VI

Vainshelbaum, N. M., Giuliani, A., Salmina, K., Pjanova, D., & Erenpreisa, J. (2022).

The transcriptome and proteome networks of malignant tumours reveal atavistic attractors of polyploidy-related asexual reproduction. *International Journal of Molecular Sciences.*, 23(23), 14930. <https://doi.org/10.3390/ijms232314930>

Contribution: Majorly developed study aims and design, statistically (via binomial test) assessed gametogenetic (GG) gene expression in 29 TCGA tumor types, performed STRING and transcriptomic coexpression network analysis on 9 TCGA tumor types, performed proteomic coexpression analysis on proteomes of malignant melanoma and breast carcinoma, performed GO and KEGG enrichment analysis, visualized the results and performed their interpretation, performed literature analysis on the topic of meiotic, cancer-testis and germ cell gene expression in cancer, majorly contributed to writing and editing the manuscript.

Original article VII.

Salmina, K., **Vainshelbaum, N.M.**, Kreishmane, M., Inashkina, I., Cragg, M.S., Pjanova, D., Erenpreisa, J.

The Role of Mitotic Slippage in Creating a “Female Pregnancy-like System” in a Single Polyploid Giant Cancer Cell. *International Journal of Molecular Sciences*. 2023; 24(4):3237. <https://doi.org/10.3390/ijms24043237>.

Contribution: Performed differential gene expression analysis comparing DOX-treated MDA-MB-231 cell line samples with non-treated ones over 4 time points. Performed GO enrichment, phylostratigraphic and STRING network analysis on the aforementioned data. Assessed the enrichment of bivalent genes among differentially expressed genes. Contributed to result visualization, manuscript writing and editing.

3.1. Triploidy is associated with X chromosome disomy (duplication of the maternal genome) in male patient tumor karyotypes from the Mitelman Database

In this part of the project, karyotype statistical analysis was performed to investigate the link between ploidy (modal chromosome number) and the state of the sex chromosome complement (using male patients due to diversity of the X and Y chromosomes discerning maternal and paternal genomes). The analysis of 15 malignant tumor types revealed a strong positive Pearson correlation ($p < 0.01$) between the fraction of triploid karyotypes and the fraction of X-disomy in different triploidy ranges (58-80, 62-76 and 64-72 chromosomes). Principal component analysis subsequently confirmed the nature of this correlation to be non-random. The X-disomic triploid pattern was also found in smaller fractions among the 5 pre-cancerous conditions.

Furthermore, some polyclonal samples were found to contain triploid X-disomic subpopulations alongside diploid and tetraploid ones (as seen in Article II Table 1). This data supported the exchange between diploid and triploid subpopulations found in Article II on tissue cultures.

Overall, X-disomy in near-triploid cancers indicates a likely duplication of the maternal genome. This may be a sign of reproductive process function, judging from the phenomenon of digyny observed in plants and animals subject to hostile environmental conditions. Digyny is a fertilization of an unreduced diploid egg with a haploid sperm that results in the creation of a more stress-resistant triploid offspring imbued with the adaptive benefits of polyploidy (Austin, 1960). A schematic diagram of how a digyny-like process resulting in X-disomic triploid karyotypes may operate in PGCCs is shown in Article II Figure 5.

Article

Meta-Analysis of Cancer Triploidy: Rearrangements of Genome Complements in Male Human Tumors Are Characterized by XXY Karyotypes

Ninel M. Vainshelbaum ^{1,2}, Pawel Zayakin ¹ , Regina Kleina ³, Alessandro Giuliani ⁴ 
and Jekaterina Erenpreisa ^{1,*} 

¹ Cancer Research Division, Latvian Biomedical Research and Study Centre, LV-1067 Riga, Latvia

² Faculty of Biology, The University of Latvia, LV-1586 Riga, Latvia

³ Department of Pathology, Riga Stradins University, LV-1007 Riga, Latvia

⁴ Environment and Health Department, Istituto Superiore di Sanità, 00161 Rome, Italy

* Correspondence: katrina@biomed.lu.lv

Received: 5 April 2019; Accepted: 9 August 2019; Published: 13 August 2019



Abstract: Triploidy in cancer is associated with poor prognosis, but its origins remain unclear. Here, we attempted to differentiate between random chromosomal and whole-genome origins of cancer triploidy. *In silico* meta-analysis was performed on 15 male malignant and five benign tumor cohorts (2928 karyotypes) extracted from the Mitelman Database, comparing their ploidy and combinations of sex chromosomes. A distinct near-triploid fraction was observed in all malignant tumor types, and was especially high in seminoma. For all tumor types, X-chromosome doubling, predominantly observed as XXY, correlated strongly with the near-triploid state ($r \approx 0.9$, $p < 0.001$), negatively correlated with near-diploidy, and did not correlate with near-tetraploidy. A smaller near-triploid component with a doubled X-chromosome was also present in three of the five benign tumor types, especially notable in colon adenoma. Principal component analysis revealed a non-random correlation structure shaping the X-chromosome disomy distribution across all tumor types. We suggest that doubling of the maternal genome followed by pedogamic fusion with a paternal genome (a possible mimic of the fertilization aberration, 69, XXY digyny) associated with meiotic reprogramming may be responsible for the observed rearrangements of genome complements leading to cancer triploidy. The relatively frequent loss of the Y-chromosome results as a secondary factor from chromosome instability.

Keywords: cancer near-triploidy; male tumors; karyotype meta-analysis; XXY; whole-genome rearrangements; digyny

1. Introduction

Aneuploidy (an abnormal number of chromosomes) is a well-known hallmark of malignant tumors and is generally associated with their aggressive development [1,2]. With results of cancer genome sequencing projects revealing flaws in the mutation theory, its inability to explain chemoresistance, and for providing targeted therapies in general with limited clinical benefit, the aneuploidy theory of cancer proposed in the 19th century by David Hansemann and Theodor Boveri is enjoying a renaissance [3]. The aneuploidy theory posits that genome instability is causally responsible for the propagation of cancer. Currently, the evolution of cancer is viewed as a system behavior of a stress response with adaptive advantages of microevolution (including the Darwinian selection of the fittest mutant clones), which is followed by the further destabilization of the genome, leading to its crisis (chromothripsis), which results in a rapid and massive genome reorganization (punctuated evolution) unifying the diverse chromosomal and nuclear abnormalities [4,5]. The earlier stages of carcinogenesis

in this setting still remain obscure [6,7]. Recent advances in the molecular characterization of aneuploidy revealed that the search for the general mechanism of how aneuploidy contributes to cancer is becoming increasingly challenging: It appears that aneuploidy can be linked to diverse molecular pathways [8] and favors both tumor-suppressing and driving effects [9,10]. Another problem in the advance of chaotic adaptations in cancer evolution; this is the so-called “Muller’s ratchet” (Muller 1964), which was proved experimentally on bacteria [11]. In his works, H. Muller postulated that neutral and harmful mutations (also inevitably caused by structural chromosome imbalances) should sooner or later lead to the extinction of asexual species. However, such unicellular species have existed on Earth for aeons. The same relates to somatic tumors of mammals; as with protists, they are immortal and resistant to extinction, and we still do not have an answer for why this is the case. Interestingly, some agamic protists return in a cycle from heterogenic aneupolyploidy in the interphase and chromatin diminution in the endoprophase to strict euploidy in each metaphase and telophase [12,13], likely compensating for Muller’s ratchet by gene conversion in the polyploidy phase [14]. Moreover, chromothripsis, which affects the chromosome order, may cause the de-speciation of mammalian tumor cells. Indeed, the atavistic recapitulation in human tumor cells of the unicellular programs is becoming apparent [15–17]. Interestingly, this epigenetic shift is also associated with polyploidy [18–20], whereas polyploidy and aneuploidy in human cancer cells are linked, in turn, with chromothripsis [21], genome reprogramming, and the upregulation of a single cell organism gene module [3,18,20,22]. Thus, cancer aneuploidy involves both genetic and crucial epigenetic changes, requiring deliberate escape from the mitotic control.

It therefore appears that an exit from the “blind corner” of Muller’s ratchet may be provided by the option for the aneupolyploid genome to convert chaos into order using the ploidy cycle as it operates with the genome complements, in contrast to the mitotic cycles, whose task is to orderly segregate chromosomes. The reproductive ploidy (life) cycles are doubling and halving the whole genome complements in order with the help of meiosis, performing recombination and reduction [23,24]. The elements of this meiosis-like mechanism are likely implemented by the reprogrammed cancer cells in the asexual or parasexual “life-cycles”, which are reciprocally joined in tumors with mitotic cycles [25–28].

Among aneuploidies of solid tumors, a near-triploid karyotype is often a hallmark of chemotherapy resistance and thus of increased survival potential [29,30]. We paid attention to the fact that among the numerical sex chromosome aberrations in the tumors of male patients, the assertive acquisition of an extra X-chromosome and frequent loss of the Y-chromosome have been reported in several cases [31–37], particularly in association with triploidy in the male germ cell tumor seminoma [38].

Here, we decided to use the advantage of the presence of two different sex chromosomes, X and Y, in a normal diploid male karyotype, in an attempt to differentiate between two potential constituents of tumor near-triploidy: The chromosomal aberrations and the rearrangements of the whole-genome complements. For this purpose, we performed an *in silico* meta-analysis of the male tumor karyotypes deposited in the Mitelman Database of Chromosome Aberrations and Gene Fusions in Cancer [39].

2. Materials and Methods

The karyotypes from 15 male malignant solid tumor types (untreated and presented in the >50 number of cases), epithelial and mesenchymal, somatic and germinative, and karyotypes from five benign tumor types were obtained from the Mitelman Database of Chromosome Aberrations and Gene Fusions in Cancer [39] in the period of January–March, 2019. None of the male patient karyotypes were affected with congenital sex chromosome aberrations such as Klinefelter syndrome. The types of tumors and the number of patient karyotypes for each of them are presented in Table 1.

Table 1. The analyzed male tumor types, the number of karyotypes per cohort, the percentage share of near-triploidy (in the range of 62–76 chromosomes), and the percentage share of sex chromosome configurations containing a disomic X-chromosome. The karyotype XXY in most cases indicates near-triploidy with the three sex chromosome complement XXY. XX,-Y largely means a near-triploid karyotype from a male with the loss of the Y chromosome, where "-Y" indicates the third haploid chromosome set. Sex chromosomes XY,+X indicate a near-diploid male karyotype with the (not inherited) acquisition of the extra sex chromosome X. The diploid (or near-diploid) male karyotype X,-Y,+X means the (acquired) loss of sex chromosome Y and gain of sex chromosome X, while karyotype XXY,+Y is near-triploid by chromosome number, with a gain of chromosome Y.

N°	Malignant Tumor Type	Number of Karyotypes	% of Near-Triploidy (62–76)	XXY %	XX,-Y %	(XY,+X)+ (X,-Y,+X) %	XXY,+Y %
1	Seminoma	78	42.31	47.44	3.85	5.13	10.26
2	Osteosarcoma	61	27.87	24.59	3.28	0.00	6.56
3	Lung carcinoma	237	27.00	8.02	9.70	2.53	2.53
4	Gastric carcinoma	74	20.27	10.81	5.41	6.76	1.35
5	Head and neck squamous cell carcinoma	191	16.75	5.76	8.90	0.52	1.57
6	Colon adenocarcinoma	98	16.33	12.24	6.12	10.20	6.12
7	Transitional cell carcinoma	104	13.46	4.81	3.85	1.92	1.92
8	Chondrosarcoma	85	11.76	4.71	3.53	3.53	0.00
9	Malignant melanoma	134	10.45	5.22	3.73	2.24	2.24
10	Glioblastoma	215	10.23	7.44	1.40	0.00	1.40
11	Renal carcinoma	577	7.11	3.81	4.68	1.04	1.21
12	Mesothelioma	72	6.94	5.56	2.78	0.00	2.78
13	Rhabdomyosarcoma	92	6.52	3.26	1.09	3.26	0.00
14	Ewing sarcoma	228	3.51	3.95	0.00	3.51	0.88
15	Liposarcoma	147	3.40	1.36	1.36	0.00	0.00
Benign tumor type							
16	Colon adenoma	62	11.29	11.29	4.84	0.00	0.00
17	Astrocytoma	59	6.78	1.69	1.69	1.69	1.69
18	Lipoma	235	0.85	0.85	0.00	0.00	0.43
19	Renal adenoma and oncocytoma	48	0.00	0.00	2.08	0.00	0.00
20	Salivary gland adenoma	131	0.00	0.00	0.76	0.00	0.00

The tumor nomenclature used was based on the International Classification of Diseases for Oncology (ICD-O), the Systematized Nomenclature of Medicine (SNOMED), and the WHO Classification of Tumours of Soft Tissue and Bone—the same sources as the Mitelman database's nomenclature. Seminoma was the germ cell tumor. Among somatic tumors, the lung carcinoma cohort included a total of five lung tumor types (squamous cell carcinoma, adenosquamous carcinoma, adenocarcinoma, undifferentiated large cell carcinoma, and small cell carcinoma), united from the evidence that both bronchoepithelial and neuroendocrine lung stem cells likely have one common precursor [40]. The gastric carcinoma cohort comprised adenocarcinoma and undifferentiated carcinoma. These cases were not sorted by stages of the malignant process in the Mitelman database. Only monoclonal karyotypes comprising 2928 tumor cases in total were collected, filtering out the cases with polyclonal karyotypes, cases where several samples were obtained from one patient, and incomplete sex chromosome karyotypes. Using the data analysis tools of the numpy [41], pandas [42], and scipy [43] Python libraries, a statistical analysis of the available data was performed to determine the relationship between modal chromosome numbers and different sex chromosome karyotypes.

The 2013 edition of the International System for Human Cytogenetic Nomenclature (ISCN) defines near-triploidy as a modal chromosome number that falls in the 58–80 range [44]. In our study, the boundaries of triploidy were also narrowed to a medium-sized range spanning 62–76 chromosomes, and a narrower range spanning 66–72 chromosomes. The nomenclature of the sex chromosome karyotypes was used as presented in the Mitelman database using ISCN, where a sex chromosome complement is expressed as related to ploidy level.

Principal component analysis (PCA) was applied to the X-chromosome disomy (#X-disomy) distribution across different tumor types in order to check for the departure of the #X-disomy patterns

from randomness [45]. The departure from randomness of such a solution was estimated by means of the Bartlett-corrected chi-square as applied to maximum-likelihood factor extraction [46].

3. Results

3.1. Analysis of the Histograms of the Modal Chromosome Numbers in 15 Cohorts of Malignant Tumors

In all examined malignant solid tumor types, listed in Table 1, the aneuploid karyotypes were present. The summary histograms of the modal chromosome numbers of each cohort are presented in Figure 1.

It is seen that they include near-diploid karyotypes, near-triploid karyotypes, a degree of tetraploidy (high in rhabdomyosarcoma), and in some cases also hyper-tetraploid karyotypes. The near-triploid karyotypes were present in all malignant tumor types. Their percentage share for malignant tumor types 1–15 is presented in Table 1 in descending order. In particular, a high proportion of near-triploidy (42%) was observed for the germ tumor seminoma. In 14 examined somatic malignant tumor types, both epithelial and mesenchymal, the near-diploid karyotypes were predominating, while the proportion of near-triploid ones was less pronounced than in seminoma, albeit in a varying degree (Table 1, Figure 1). Osteosarcoma was a leader in triploidy (28%). Lung carcinoma also displayed a high proportion of near-triploid karyotypes (27%); other somatic tumors showed lower values.

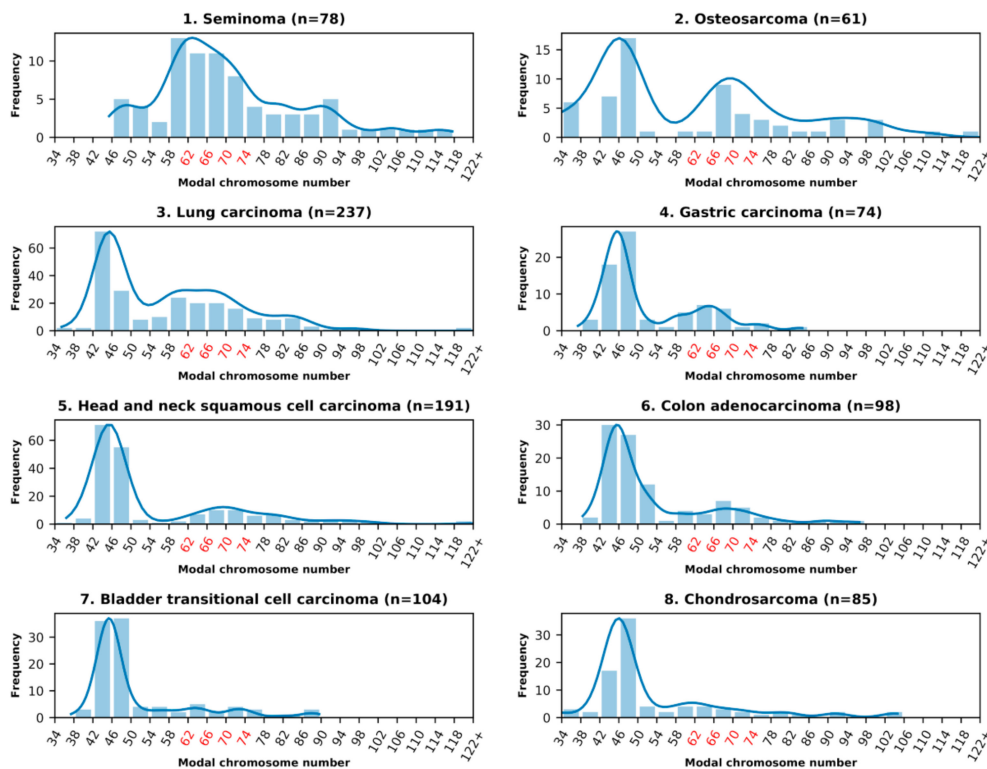


Figure 1. Cont.

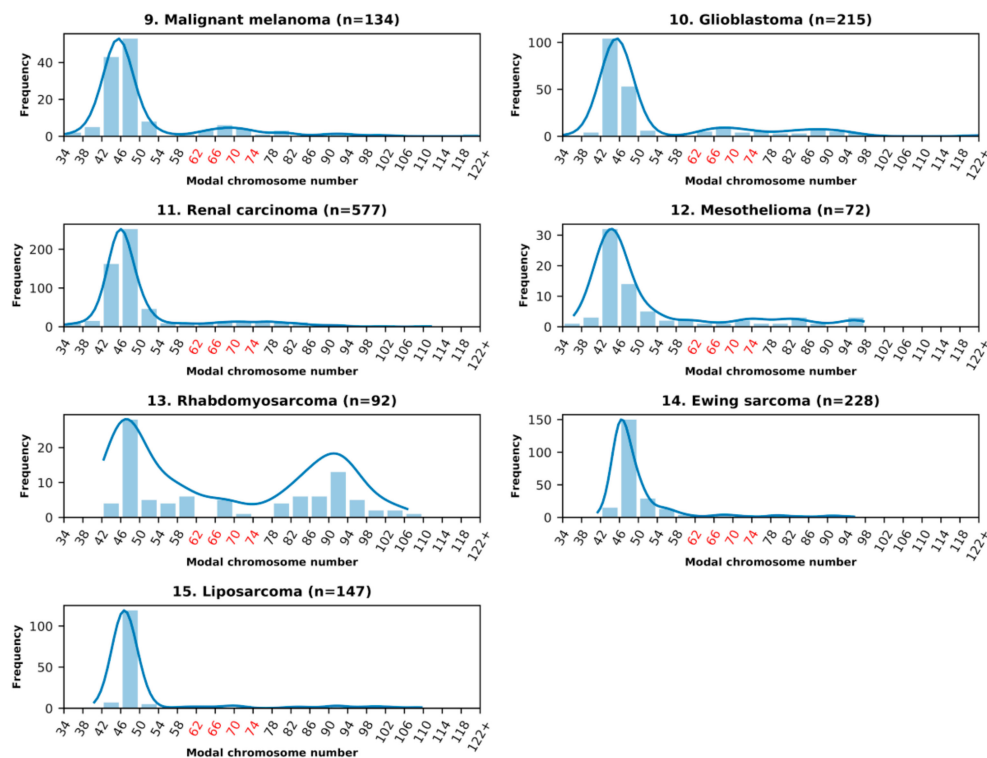


Figure 1. The modal chromosome number frequency histograms of 15 malignant tumor cohorts, numbered as listed in Table 1. The chromosome numbers within the (arbitrarily chosen) range of near-triploidy (62–76 chromosomes) are marked red.

3.2. Analysis of the Sex Chromosome Sets with #X-Disomy in Each Malignant Tumor Cohort in Relation to Ploidy for their Karyotypes

We also analyzed the sex chromosome sets with #X-disomy, which are presented alongside their percentage for each malignant tumor cohort in Table 1. It can be seen that the configuration XXY dominates in seminoma and is also predominant among #X-disomic karyotypes in 10 of 14 somatic malignant tumors. However, the proportion of the XX,-Y set is larger in them than in seminoma, while in head and neck (HN) squamous cell carcinoma, XX,-Y prevails over XXY. Other karyotypes with #X-disomy (XY,+X) + (X,-Y,+X) were a minority, with the exception of colon adenocarcinoma, where their proportion was comparatively high. Some of the (largely near-triploid) XXY karyotypes were also shown to possess an extra Y chromosome (especially evident in seminoma, osteosarcoma and colon adenocarcinoma); their percentage share is presented in Table 1.

Further, we compared the relationship of the karyotypes exhibiting #X-disomy with different ploidy ranges of the modal chromosome numbers for all malignant tumors and for only somatic tumor cohorts, excluding seminoma. The results of this comparative statistical analysis are shown in Figure 2.

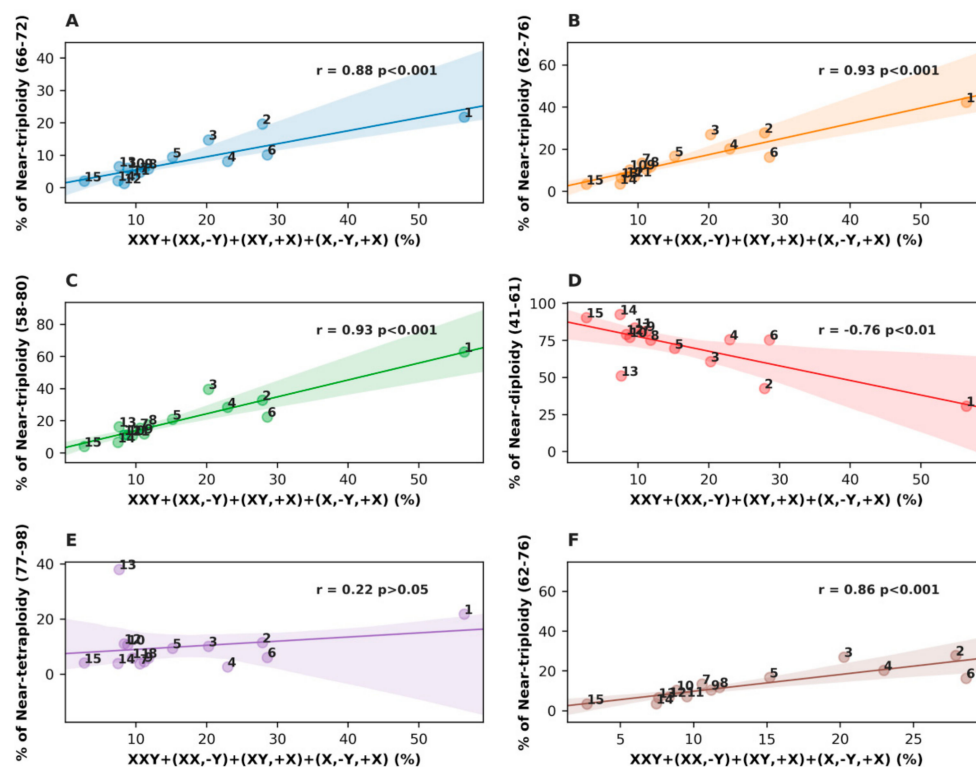


Figure 2. Results of the Pearson correlation analysis for all 15 patient karyotype cohorts of malignant tumors, evaluating the relationship between all karyotypes containing doubled X-chromosomes and ploidy in different chromosome ranges: (A) In relation to the narrow triploidy range (66–72 chromosomes); (B) in relation to the median triploidy range (62–76 chromosomes); (C) in relation to the wide (International System for Human Cytogenetic Nomenclature, ISCN) triploidy range (58–80 chromosomes); (D) in relation to the near-diploidy range (41–61 chromosomes); (E) in relation to near-tetraploidy range (77–98 chromosomes); and (F) only malignant somatic tumors are presented as related to the near-triploidy median range. The tumor cohort numbers are the same as in Table 1.

Strikingly, in spite of the many-fold differences in the proportions of the near-triploid karyotypes among 15 malignant tumor types, taken together, they provided a very high Pearson correlation between #X-disomic sex chromosome karyotypes and all tested ranges of near-triploidy, from the narrower range ($r = 0.88$; $p < 0.001$) to the median and widest range, equally ($r = 0.93$, $p < 0.001$) (Figure 2A–C). In the near-diploidy range (Figure 2D), the correlation was strongly negative ($r = -0.76$, $p < 0.01$), while in the near-tetraploidy range (Figure 2E), no correlation was observed. When excluding seminoma, the Pearson correlation of the somatic malignant tumor cohorts presented in Figure 2F in the median near-triploidy range was also convincingly strong ($r = 0.86$, $p < 0.001$).

Further, we examined the influence of different #X-disomic karyotypes on Pearson correlation in the median range of near-triploidy (62–78 chromosomes). The results are presented in Figure 3.

The results show a very high contribution of XXY karyotypes (Figure 3A) in the near-triploidy range ($r = 0.88$, $p < 0.001$), which remains the same, adding also near-diploid karyotypes with #X-disomy (Figure 3B). For somatic malignant tumors only, as presented in Figure 3C, this correlation with both karyotypes is smaller but still strong ($r = 0.75$, $p < 0.01$). The loss of #Y from #X-disomic near-triploid and near-diploid karyotypes presented for all malignant tumors in Figure 3D weakened the correlation with near-triploidy, but it still remained positive and statistically significant ($r = 0.54$, $p < 0.05$).

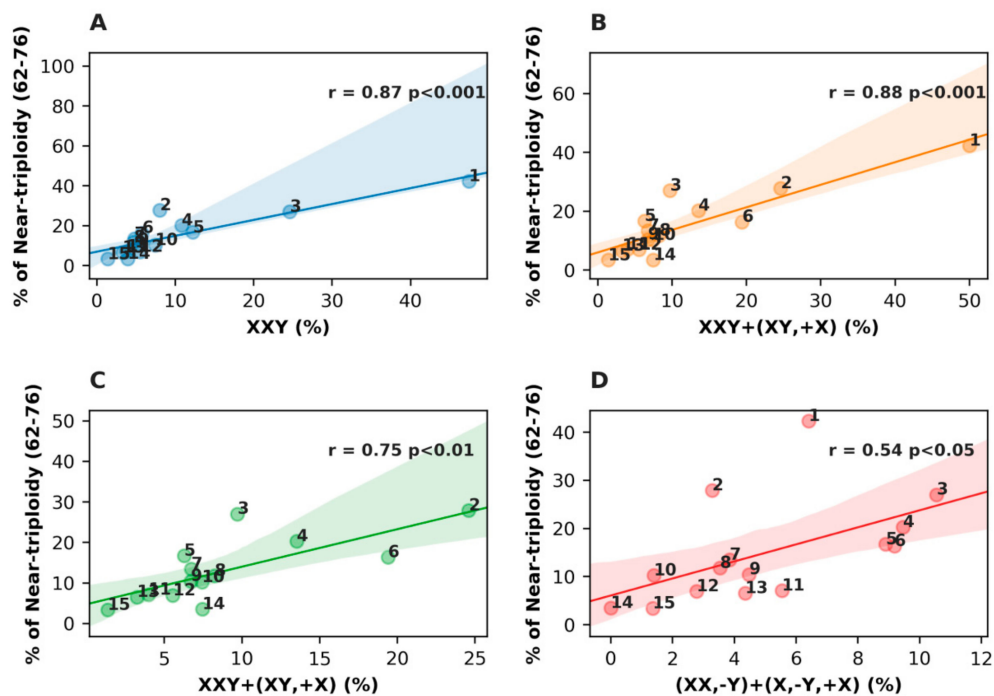


Figure 3. Results of the Pearson correlation analysis for malignant tumors evaluating the relationship between different karyotypes containing disomic X-chromosomes and ploidy in the median near-triploidy range. (A) For XXY and (B) XXY+(XY,+X) configurations; (C) X-disomic karyotypes with a Y chromosome; and (D) X-disomic karyotypes lacking a Y chromosome. The tumor cohort numbers are the same as in Table 1.

3.3. Analysis of All Sex Chromosome Configurations in Relation to Near-Triploidy in Malignant Tumors

The relationship between near-triploidy (62–76) and all sex chromosome sets is presented in a bar-plot form for all malignant tumors in Figure 4. Besides the already discussed issues of the prevailing association of #X-disomy with near-triploidy, Figure 4 also reveals that a small portion of XY karyotypes and X,-Y karyotypes are also near-triploid; in particular, this is pronounced in lung carcinoma. This is likely to be associated with the chromosome instability processes. Contrary to the karyotypes with a doubled X-chromosome, the compositions of sex chromosomes with doubled Y and one or an absent X (XYY or YY) were rare (and therefore not presented in this article), while 10 of 16 tumor types (seminoma, osteosarcoma, lung carcinoma, colon adenocarcinoma, gastric carcinoma, bladder transitional cell carcinoma, liposarcoma, chondrosarcoma, Ewing sarcoma, and glioblastoma) were lacking them. Only one near-triploid XYY karyotype was found in the entire analyzed dataset, in rhabdomyosarcoma.

As triploidy in association with #X-disomy was found in all malignant tumors, we were interested to find out whether these features could also be observed in premalignant somatic lesions. Thus, four available pairs of sufficiently large tumor cohorts were compared: Astrocytoma versus glioblastoma, colon adenoma versus adenocarcinoma, renal adenoma and oncocytoma versus renal carcinoma, and lipoma versus liposarcoma—and salivary gland adenoma was added as the fifth cohort. The results are presented in Table 1 (16–20) and Figure 5.

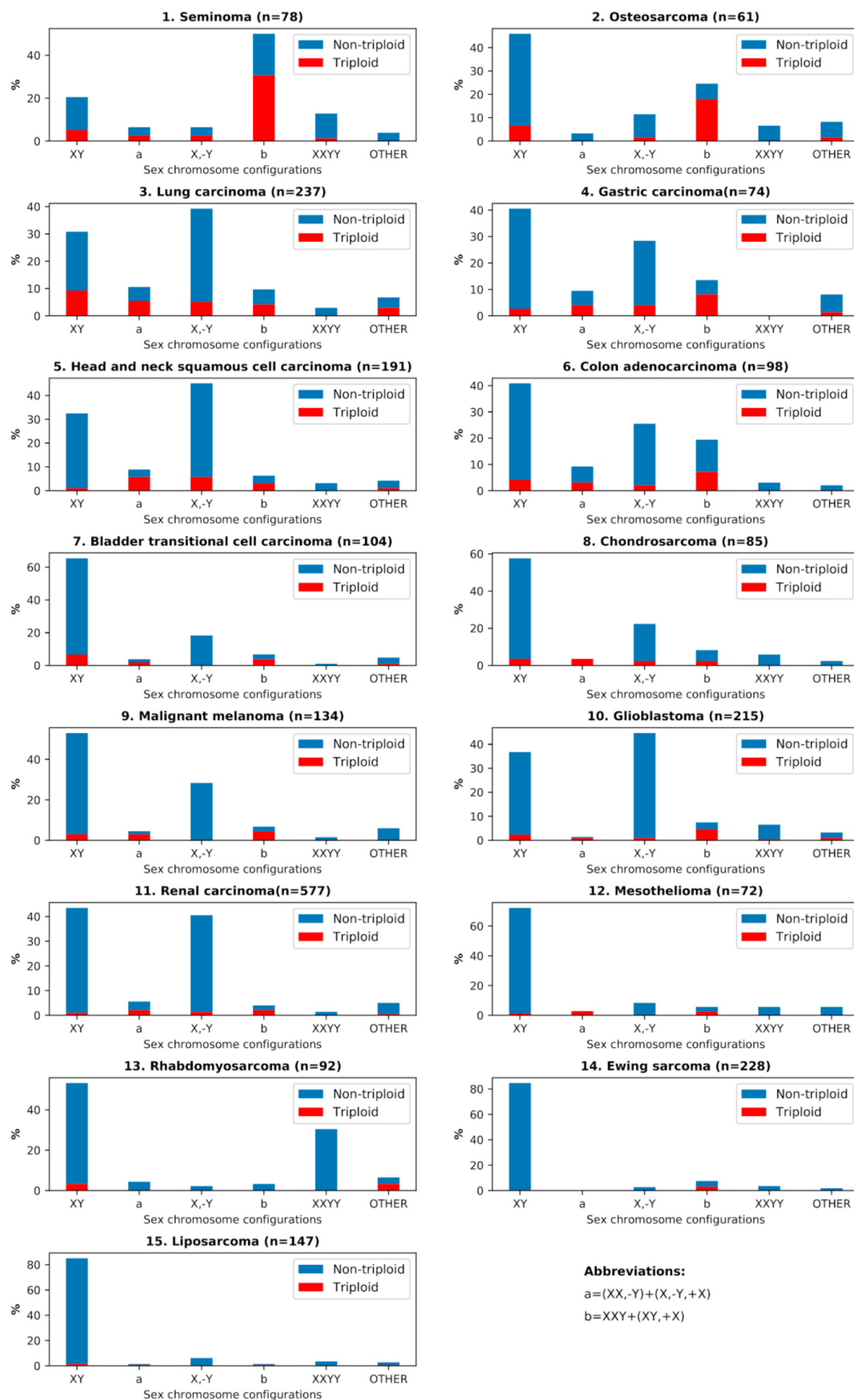


Figure 4. The percentages of different sex chromosome configurations and their respective percentages of near-triploidy (62–76 chromosomes) for all malignant tumor cohorts, numbered as listed in Table 1.

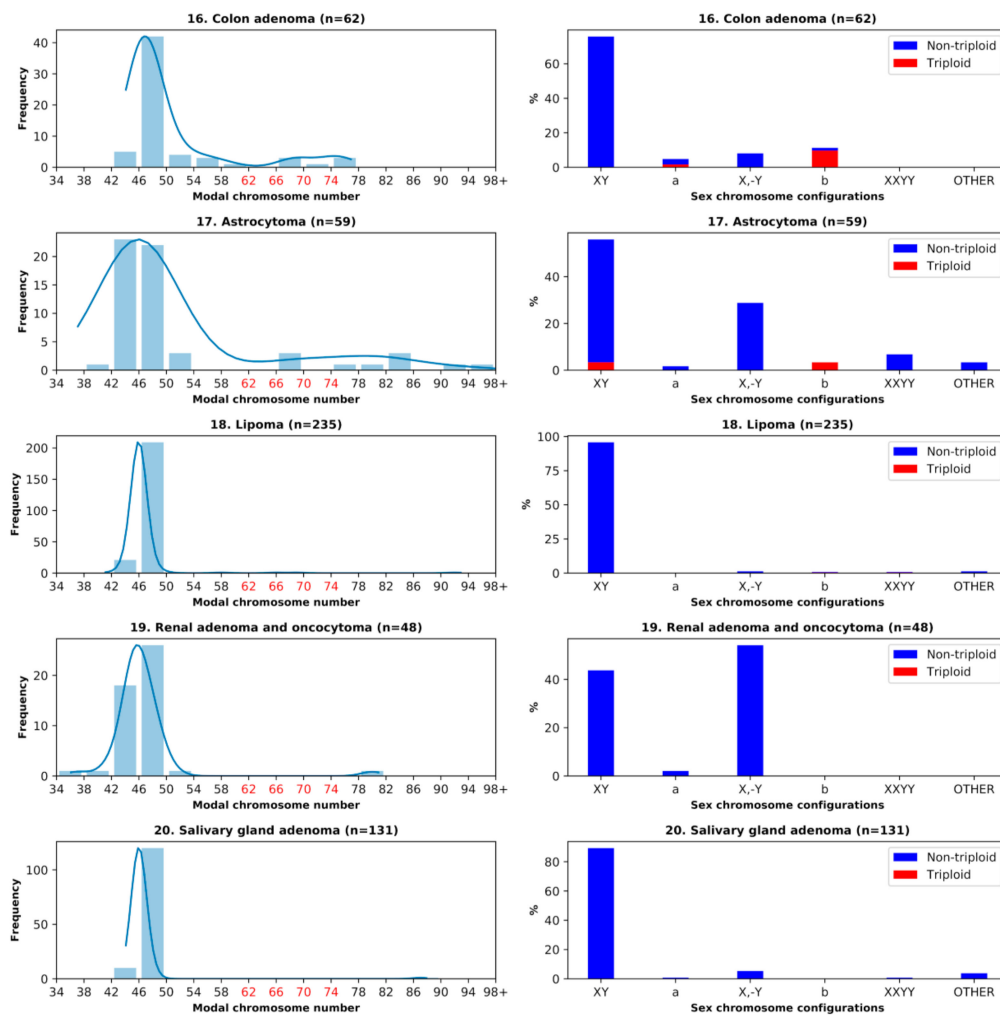


Figure 5. Benign tumor karyotypes. Left column: The histograms of the modal chromosome numbers, with near-triploidy marked red. Right column: The corresponding percentages of different sex chromosome configurations with #X-disomy and their respective percentages of near-triploidy (62–76 chromosomes) for five benign tumor cohorts. Designations (a,b) in the right column: (a) #X-disomic karyotypes lacking a Y chromosome (XX,-Y and X,-Y,+X); (b) #X-disomic karyotypes with a Y chromosome (XXY and XY,+X).

3.4. Benign Tumors: Study of the Doubled X-Chromosome Karyotypes and Near-Triploidy

In colon adenoma and adenocarcinoma, the proportion of #X-disomic karyotypes with near-triploidy was rather high; however, triploidy in adenoma was lower than in colon adenocarcinoma (11% vs. 16%, respectively). All triploid colon adenoma karyotypes except one were XXYY, while the remaining one was XX,-Y (Table 1, Figure 5). In astrocytoma, the total percentage of #X-disomy was more than two times lower compared to glioblastoma, and near-triploidy was also significantly lower (6.78% to glioblastoma's 10.23%), while liposarcoma surpassed lipoma 4-fold in triploidy, and more than 3-fold in #X-disomy proportions (although both were in the lower range of the two values). The renal adenoma and oncocytoma cohort was more than 4-fold poorer with #X-disomic karyotypes than its malignant counterpart (2.08% vs. 8.49%) and did not show near-triploidy. Salivary gland adenoma also did not display near-triploidy, and #X-disomy was almost absent as well (0.76%).

3.5. Principal Component Analysis (PCA)

PCA was applied for the exploration of the X-chromosome disomy (#X-disomy) pattern in order to demonstrate the non-randomness of different #X-disomy categories distribution in near-triploidy

across different tumor types. The initial four-dimension space having four different categories of #X-disomy as axes, namely #X-disomy (all types)_62–76 (chromosomes), #X-disomy (all types)_58–80, XXY+XX,-Y_62–76, and #X-disomy (all types)_66–72 and 15 malignant tumor types as statistical units, was submitted to PCA (Table 2).

Table 2. Principal component analysis (PCA) loading pattern.

Original Variables	Factor1	Factor2
#X disomy_62-76	0.96650	−0.23119
#X disomy_58-80	0.94894	−0.05406
XXY+XX,-Y_62-76	0.95938	−0.23271
#X disomy_66-72	0.69858	0.71287
% of Explained Variance	81.1	15.5

As evident from Table 2, the analysis ended up as a two-component solution, cumulatively explaining 96% of the total variance. The #X-disomy distribution highlighted a striking correlation structure, with a major “size” [45], first principal component (Factor1), and a minor “shape” component. The presence of very high and positive loadings (the Pearson correlation coefficient between the original variables and components) for Factor 1 corresponds to the fact that all the categories contribute “along the same direction” to the Factor 1 scores, and thus it is an integrated score of the “amount of #X-disomy”. The second “shape” component (Factor 2) explains 15% of the total variance, and this value mainly stems from the unique mesothelioma pattern (see Figure 6). It is worth noting that principal components are orthogonal to each other by construction, and therefore, “size” and “shape” are two independent latent concepts [47]. PCA thus showed an extremely ordered #X-disomy distribution in the near-triploid space of all tumor types. The presence of such a strong correlation structure is indicative of the non-random character of #X-disomy distribution in triploidy. As a matter of fact, a maximum likelihood approach to factor extraction [46] highlighted a very high statistical significance (Bartlett-corrected chi-square = 87.01, $p < 0.0001$) against the null hypothesis of no common factor.

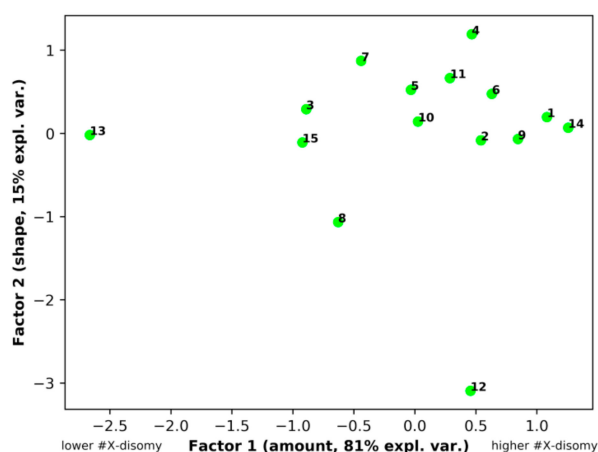


Figure 6. PCA results of the X-chromosome disomy distribution in the triploidy space for 15 malignant tumor types, designated as numbered in Table 1.

Commenting on the space distribution of #X-disomy for different tumor types, it should be noted that 12 of 14 somatic tumor types form a common “shape” cluster with the germ tumor seminoma underlying a common biological phenomenon. The peculiarity of mesothelioma (Nr 12) may be due to its (still unknown) highly plastic progenitors switching between different phenotypes depending on the local microenvironment [48]. Thus, the PCA results showed an extremely ordered X-chromosome

disomy distribution in the near-triploid space of all tumor types. The presence of such a strong correlation structure is indicative of the non-random character of #X-disomy distribution in triploidy. The emergence of a greatly major “size” component points toward a largely invariant pattern of disomy distribution among tumor types that mainly differ by the amount of #X-disomy, keeping the relative frequency of various tumor types largely constant.

4. Discussion

In this study, we hypothesized that tumor near-triploidy, which is associated with chemoresistance, may originate primarily from the rearrangement of whole-genome complements. Therefore, we attempted to differentiate it from aneuploidy resulting from chromosomal aberrations. As a method, we chose to analyze the sets of sex chromosomes in relation to modal chromosome numbers in male tumor karyotypes. Through all analyzed material representing 20 types of 2928 epithelial and mesenchymal, somatic and germ, malignant and benign male tumor karyotypes, we found that near-triploid karyotypes were characterized by X-chromosome disomy.

The simplest explanation for #X-disomic chromosomes would be their origin from the mis-segregation of sister chromatids in aberrant mitosis. The random mis-segregation of individual chromosomes is a well-known mitotic aberration in breakage–fusion–bridge cycles. Tumor aneuploidy concerning the re-arrangements of whole chromosomes and near-triploidy, in particular, has been hitherto explained mostly from the position of the random aberrations in mitotic cycles [2]. However, Pearson correlations carried out in our study established that a kind of aneuploidy represented by #X-disomy (with the dominating XXY karyotypes) showed a very high correlation ($r \sim 0.9$, $p < 0.001$) with triploidy, while PCA resulted in an extremely ordered X- chromosome disomy distribution in the near-triploid space of all tumor types, clearly indicating a departure from randomness.

In addition, #X-disomic tumors were clearly repulsing from the near-diploid chromosome range with a strong negative correlation, and thus collectively depart from the null hypothesis of the random origin of X chromosome mis-segregation.

It is also worth noting, in addition, that the dominating set of #X-disomy in male cells was XXY, while the XYY sets, which at random would exhibit a 50% possibility, were practically non-existent in the dataset (with only one among 2928 analyzed male tumor karyotypes being near-triploid XYY). This indicates that #X-disomy and near-triploidy of male tumor karyotypes are two facets of the same phenomenon, rather than stemming from random aberrant chromosome mis-segregation in a mitotic cycle.

We also found that somatic tumor types and seminoma are not only highly correlated together with #X-disomy related to near-triploidy by the Pearson coefficient and p -value, but also constituted a common “shape” cluster in PCA space. So, the identified novel phenomenon of the persuasive link between #X-disomy and near-triploidy dominated by the “feminized” XXY karyotype may not be of mitotic origin. Rather, it may possess meiotic features programmatically directed towards the oogenic pathway.

Although the above analysis points towards the concerted mis-segregation of the chromosome complement of the maternal genome, which would be expected in a process similar to oocyte development, the direct data confirming this process have not yet been elaborated. However, the study of Ozery-Flato et al. [49] on the same Mitelman database including 15,000 karyotypes of 62 tumor cohorts, among them 18 solid (some the same as we have explored), analyzing all aberrations identifiable by cytogenetic techniques, revealed the strongest association among mainly whole chromosome gains and losses, with the gains prevailing. This regularity was also confirmed by comparative genome hybridization analysis. The data of these researchers are supportive for our interpretation of XXY male tumor triploid karyotypes as resulting from the whole genome complements rearrangements of meiotic (for somatic tumors, pseudo-meiotic) origin.

How may this process proceed? XXYY sets could possibly serve as a starting point. A configuration of XXYY sex chromosomes was found to be present in each malignant tumor cohort of our tumor sets

(except for gastric carcinoma) and was particularly high in seminoma (10.3%). Although designated as triploid XXY,+Y (see the last column in Table 1), it can derive either from spermatocytes I or from the G2/mitotic slippage fraction of XXYY of any tumor. #X-disomic karyotypes did not display a statistically significant correlation with tetraploidy (Figure 2F). In other words, the absence of this correlation does not prove—but also does not deny—that the formation of XXY triploid karyotypes for male tumors can start from the G2/mitotic slippage (XXYY) phase as a meiosis-like process. In addition, our study of breast cancers showed that triploid stemlines contain, in addition, four times more $\geq 4C$ cells than the populations with a near diploid stem line [29].

Molecularly, and particularly in the case of reprogramming, this mito-meiotic trigger is feasible because the G2 mitotic recombination checkpoint is identical to the recombination checkpoint of the meiotic prophase and evolutionary derived from it [28,50]. The reprogramming shift may be favored by cell senescence and associated DNA damage [51], chromosome instability (CIN) itself [3], and also by the hyper-activation of the RAS-RAF/MOS-MEK-MAPK pathway, where the up-regulated RAS can induce either senescence or also be substitutive for MOS in oocyte maturation and active in fertilization [51,52]. In accordance with this, human somatic tumors ectopically express meiotic genes and proteins, and also enhance their synthesis after genotoxic challenge [53–59], while primordial male germ cells and their immediate progeny are able to undergo oogenesis in adverse conditions [60].

If so, a process similar to sexual digyny (the aberrant fusion of an unreduced maternal diploid gamete possessing the non-disjunct sister chromatids with a paternal haploid gamete), occurring here in a parasexual, pedogamic manner, could explain the persuasive formation of XXY triploid karyotypes in a proportion of male tumors. It is schematically presented on Figure 7 as starting with a glide into a meiotic prophase-like state from the mitotic G2 recombination checkpoint. The trigger between this survival pathway and death in mitotic catastrophe may depend on the actual concentration of the MOS-dependent undegraded cyclin B1 [28,51,61], while chromothripsis with its micronucleation may be part of this decision threshold [62,63].

The digyny-like process can use meiotic recombination for the effective repair of DNA damage and gene conversion, while the third genome can compensate for recessive lethal mutations (and also moderate the genome imbalance created by the inevitably joined CIN). Thus, this variant of the whole genome aberrations in triploid tumors can favor both their perpetuation and chemoresistance. More information on the evolutionary significance of digyny for adaptation to catastrophic environments and the alternation of the digyny cycle with a mitotic cycle in triploid tumors can be found in [64].

Our findings lead us to question if these revelations have any potentially predictive clinical significance. To this end, it is interesting to compare somatic tumors and seminoma, on one side, and colon adenoma and carcinoma, on the other side. Table 1 shows that seminoma has the highest proportion of XXY karyotypes (47%) and also a fraction of XX,-Y - likely due to the secondary loss of the Y-chromosome (together 56%); however, it possesses a relatively small fraction (5%) of less stable #X-disomic karyotypes (XY,+X)+(X,-Y,+X). On the contrary, somatic tumors display a higher proportion of more defective karyotypes—which, however, still maintain #X-disomy—and they still negatively correlate with near-diploidy. This points towards a primary origin of XXY triploidy and a secondary origin of unstable #X-disomic karyotypes derived from it, and also highlights the fact that somatic tumors have higher secondary CIN (involving the loss of single chromosomes, #Y and autosomes) than seminoma. In accordance with our suggestion that seminoma is less subjected to secondary CIN alterations, it was found that, except for a few driver mutations, seminoma has far less secondary passenger mutations in comparison with somatic cancers [65]. In the case of colon cancer, where the tumor suppressor adenomatous polyposis coli (*APC*) function loss occurs in early adenoma, the acquisition of a driver mutation *KRAS* in late adenoma, while the exaggerated chromosome and microsatellite instability further develops with cancer progression and loss of *TP53* function [66], the secondary stochastic CIN process degrading the triploidy partly overlaps and likely masks the germinative initiation by triploidy. Therefore, the colon adenoma is enriched with XXY triploidy, while adenocarcinoma accumulates, in addition, the near-diploid #X-disomic karyotypes. Interestingly,

and in accordance with this interpretation, Giaretti and colleagues [67] found that the incidence of mutations of the *KRAS2* and *TP53* genes was lowest among the DNA near-triploid and highest among the near-diploid cases of sporadic colorectal adenocarcinoma. Deeper investigation into the predictive potential of our findings is needed.

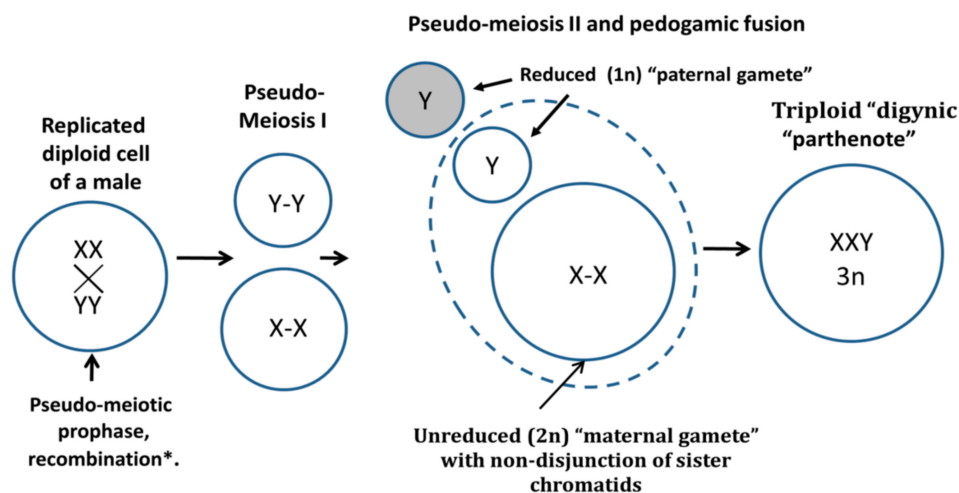


Figure 7. Schematic of the digyny-like formation of XXY triploid karyotypes in somatic male tumors. The reprogrammed male tumor cell triggers the aberrant molecular pathway of the pseudo-meiotic prophase from the G2-phase, undergoes recombination between cohered sisters and possibly also homologues, undergoes pseudo-meiosis I segregating maternal and paternal progenies with cohered sister chromatids, and triggers the reduction to haploidy of the “paternal gamete” in the pseudo-meiosis II and its pedogamic fusion with the unreduced diploid “maternal gamete”, resulting in triploid “digynic parthenote”.

5. Conclusions

The analysis of the karyotypes of 15 male malignant tumor types, germ and somatic, from the Mitelman database revealed a very high correlation between X-chromosome disomy (predominantly represented by XXY karyotypes) with triploidy, a negative correlation with near-diploidy, and no correlation with near-tetraploid modal chromosome numbers. In addition, principal component analysis revealed the strongly non-random nature of the #X-disomy and triploidy association and clustering of the germ tumor seminoma with somatic tumors in the PCA space. Collectively, this suggests that the disomy of the X-chromosome and triploidy in the typically XXY karyotypes in male tumors represent two facets of the same biological phenomenon: The rearrangement of the whole genome complements. A hypothesis of a digyny-like process (the aberrant fusion of two maternal genomes with one paternal genome) exploiting the elements of meiosis in reprogrammed tumor cells has been proposed. The analysis of partly defective XXY triploid karyotypes still maintaining #X-disomy allows us to suggest that chromosome instability may be largely secondary to the whole genome complement rearrangements. The potential for clinical predictions based on the comparison of colon adenoma and carcinoma and of seminoma with somatic malignant tumors is preliminarily discussed.

Author Contributions: Conceptualization, J.E.; methodology, R.K., N.M.V., P.Z. and A.G.; validation, N.M.V., A.G. and P.Z.; formal analysis, P.Z.; investigation, N.M.V. and A.G.; data curation, P.Z. and R.K., writing—original draft preparation, N.M.V.; writing—review and editing, J.E.; supervision, J.E.

Funding: This work has been supported by a grant of the European Regional Development Fund (ERDF) project No. 1.1.1.1/18/A/099 and Alfred Raisner memorial scholarship to N.M.V.

Acknowledgments: The cytogenetic advice of Aigars Dzalbs is highly appreciated.

Conflicts of Interest: The authors declare no conflict of interest.

References

- Holland, A.J.; Cleveland, D.W. Losing balance: The origin and impact of aneuploidy in cancer. *EMBO Rep.* **2012**, *13*, 501–514. [[CrossRef](#)] [[PubMed](#)]
- Pfau, S.J.; Amon, A. Chromosomal instability and aneuploidy in cancer: From yeast to man. *EMBO Rep.* **2012**, *13*, 515–527. [[CrossRef](#)] [[PubMed](#)]
- Pihan, G.A. Centrosome dysfunction contributes to chromosome instability, chromoanagenesis, and genome reprogramming in cancer. *Front. Oncol.* **2013**, *3*, 277. [[CrossRef](#)] [[PubMed](#)]
- Heng, H.H.; Bremer, S.W.; Stevens, J.B.; Horne, S.D.; Liu, G.; Abdallah, B.Y.; Ye, K.J.; Ye, C.J. Chromosomal instability (CIN): What it is and why it is crucial to cancer evolution. *Cancer Metastasis Rev.* **2013**, *32*, 325–340. [[CrossRef](#)] [[PubMed](#)]
- Liu, G.; Stevens, J.B.; Horne, S.D.; Abdallah, B.Y.; Ye, K.J.; Bremer, S.W.; Ye, C.J.; Chen, D.J.; Heng, H.H. Genome chaos: Survival strategy during crisis. *Cell Cycle* **2014**, *13*, 528–537. [[CrossRef](#)] [[PubMed](#)]
- Cross, W.C.; Graham, T.A.; Wright, N.A. New paradigms in clonal evolution: Punctuated equilibrium in cancer. *J. Pathol.* **2016**, *240*, 126–136. [[CrossRef](#)] [[PubMed](#)]
- Ly, P.; Cleveland, D.W. Rebuilding Chromosomes After Catastrophe: Emerging Mechanisms of Chromothripsis. *Trends Cell Biol.* **2017**, *27*, 917–930. [[CrossRef](#)]
- Ye, C.J.; Regan, S.; Liu, G.; Alemara, S.; Heng, H.H. Understanding aneuploidy in cancer through the lens of system inheritance, fuzzy inheritance and emergence of new genome systems. *Mol. Cytogenet.* **2018**, *11*, 31. [[CrossRef](#)]
- Weaver, B.A.A.; Silk, A.D.; Montagna, C.; Verdier-Pinard, P.; Cleveland, D.W. Aneuploidy acts both oncogenically and as a tumor suppressor. *Cancer Cell* **2007**, *11*, 25–36. [[CrossRef](#)]
- Sheltzer, J.M.; Ko, J.H.; Replogle, J.M.; Habibe Burgos, N.C.; Chung, E.S.; Meehl, C.M.; Sayles, N.M.; Passerini, V.; Storchova, Z.; Amon, A. Single-chromosome Gains Commonly Function as Tumor Suppressors. *Cancer Cell* **2017**, *31*, 240–255. [[CrossRef](#)]
- Andersson, D.I.; Hughes, D. Muller's ratchet decreases fitness of a DNA-based microbe. *Proc. Natl. Acad. Sci. USA* **1996**, *93*, 906–907. [[CrossRef](#)] [[PubMed](#)]
- Demin, S.Y.; Berdieva, M.A.; Goodkov, A.V. Cyclic Polyploidy in Obligate Agamic Amoebae. *Cell Tissue Biol.* **2019**, *13*, 242–246. [[CrossRef](#)]
- Raikov, I.B. *The Protozoan Nucleus; Cell Biology Monographs*; Springer: Wien, Austria, 1982; Volume 9, ISBN 9783709141380.
- Maciver, S.K. Asexual Amoebae Escape Muller's Ratchet through Polyploidy. *Trends Parasitol.* **2016**, *32*, 855–862. [[CrossRef](#)] [[PubMed](#)]
- Vincent, M.D. Cancer: Beyond speciation. *Adv. Cancer Res.* **2011**, *112*, 283–350.
- Trigos, A.S.; Pearson, R.B.; Papenfuss, A.T.; Goode, D.L. Altered interactions between unicellular and multicellular genes drive hallmarks of transformation in a diverse range of solid tumors. *Proc. Natl. Acad. Sci. USA* **2017**, *114*, 6406–6411. [[CrossRef](#)]
- Vinogradov, A.E.; Anatskaya, O.V. Evolutionary framework of the human interactome: Unicellular and multicellular giant clusters. *Biosystems* **2019**, *181*, 82–87. [[CrossRef](#)]
- Vazquez-Martin, A.; Anatskaya, O.V.; Giuliani, A.; Erenpreisa, J.; Huang, S.; Salmina, K.; Inashkina, I.; Huna, A.; Nikolsky, N.N.; Vinogradov, A.E. Somatic polyploidy is associated with the upregulation of c-MYC interacting genes and EMT-like signature. *Oncotarget* **2016**, *7*, 75235–75260. [[CrossRef](#)]
- Erenpreisa, J.; Giuliani, A.; Vinogradov, A.E.; Anatskaya, O.V.; Vazquez-Martin, A.; Salmina, K.; Cragg, M.S. Stress-induced polyploidy shifts somatic cells towards a pro-tumorigenic unicellular gene transcription network. *Cancer Hypotheses* **2018**, *1*, 1–20.
- Anatskaya, O.V.; Erenpreisa, J.; Giuliani, A.; Salmina, K.; Vinogradov, A.E. Polyploidy reprograms regulatory pathways towards unicellular mode: The role in stress response, drug resistance, growth and cancer. *Proc. Biopolym. Cell* **2019**, *35*, 2019.
- Notta, F.; Chan-Seng-Yue, M.; Lemire, M.; Li, Y.; Wilson, G.W.; Connor, A.A.; Denroche, R.E.; Liang, S.-B.; Brown, A.M.K.; Kim, J.C.; et al. A renewed model of pancreatic cancer evolution based on genomic rearrangement patterns. *Nature* **2016**, *538*, 378–382. [[CrossRef](#)]




22. Salmina, K.; Jankevics, E.; Huna, A.; Perminov, D.; Radovica, I.; Klymenko, T.; Ivanov, A.; Jascenko, E.; Scherthan, H.; Cragg, M.; et al. Up-regulation of the embryonic self-renewal network through reversible polyploidy in irradiated p53-mutant tumour cells. *Exp. Cell Res.* **2010**, *316*, 2099–2112. [CrossRef]
23. Kondrashov, A.S. Evolutionary Genetics of Life Cycles. *Annu. Rev. Ecol. Syst.* **1997**, *28*, 391–435. [CrossRef]
24. Kondrashov, A.S. The asexual ploidy cycle and the origin of sex. *Nature* **1994**, *370*, 213–216. [CrossRef]
25. Rajaraman, R.; Rajaraman, M.M.; Rajaraman, S.R.; Guernsey, D.L. Neosis—A paradigm of self-renewal in cancer. *Cell Biol. Int.* **2005**, *29*, 1084–1097. [CrossRef]
26. Erenpreisa, J.; Cragg, M.S. Cancer: A matter of life cycle? *Cell Biol. Int.* **2007**, *31*, 1507–1510. [CrossRef]
27. Erenpreisa, J.; Cragg, M.S. MOS, aneuploidy and the ploidy cycle of cancer cells. *Oncogene* **2010**, *29*, 5447–5451. [CrossRef]
28. Erenpreisa, J.; Kalejs, M.; Cragg, M.S. Mitotic catastrophe and endomitosis in tumour cells: An evolutionary key to a molecular solution. *Cell Biol. Int.* **2005**, *29*, 1012–1018. [CrossRef]
29. Gerashchenko, B.I.; Salmina, K.; Eglitis, J.; Huna, A.; Grjunberga, V.; Erenpreisa, J. Disentangling the aneuploidy and senescence paradoxes: A study of triploid breast cancers non-responsive to neoadjuvant therapy. *Histochem. Cell Biol.* **2016**, *145*, 497–508. [CrossRef]
30. Schulze, S.; Petersen, I. Gender and ploidy in cancer survival. *Cell. Oncol.* **2011**, *34*, 199–208. [CrossRef]
31. Di Oto, E.; Monti, V.; Cucchi, M.C.; Masetti, R.; Varga, Z.; Foschini, M.P. X chromosome gain in male breast cancer. *Hum. Pathol.* **2015**, *46*, 1908–1912. [CrossRef]
32. Yamamoto, K.; Nagata, K.; Kida, A.; Hamaguchi, H. Acquired gain of an X chromosome as the sole abnormality in the blast crisis of chronic neutrophilic leukemia. *Cancer Genet. Cytogenet.* **2002**, *134*, 84–87. [CrossRef]
33. Okada, Y.; Nishikawa, R.; Matsutani, M.; Louis, D.N. Hypomethylated X chromosome gain and rare isochromosome 12p in diverse intracranial germ cell tumors. *J. Neuropathol. Exp. Neurol.* **2002**, *61*, 531–538. [CrossRef]
34. Hunter, S.; Gramlich, T.; Abbott, K.; Varma, V. Y chromosome loss in esophageal carcinoma: An in situ hybridization study. *Genes Chromosomes Cancer* **1993**, *8*, 172–177. [CrossRef]
35. Park, S.-J.; Jeong, S.-Y.; Kim, H.J. Y chromosome loss and other genomic alterations in hepatocellular carcinoma cell lines analyzed by CGH and CGH array. *Cancer Genet. Cytogenet.* **2006**, *166*, 56–64. [CrossRef]
36. Bianchi, N.O. Y chromosome structural and functional changes in human malignant diseases. *Mutat. Res.* **2009**, *682*, 21–27. [CrossRef]
37. Duijf, P.H.G.; Schultz, N.; Benezra, R. Cancer cells preferentially lose small chromosomes. *Int. J. Cancer* **2013**, *132*, 2316–2326. [CrossRef]
38. Castedo, S.M.; de Jong, B.; Oosterhuis, J.W.; Seruca, R.; te Meerman, G.J.; Dam, A.; Schraffordt Koops, H. Cytogenetic analysis of ten human seminomas. *Cancer Res.* **1989**, *49*, 439–443.
39. Mitelman, F.; Johansson, B.; Mertens, F. Mitelman Database of Chromosome Aberrations and Gene Fusions in Cancer. Available online: <http://cgap.nci.nih.gov/Chromosomes/Mitelman> (accessed on 18 January 2019).
40. Onaitis, M.; Hanna, J. Cell of origin of lung cancer. *J. Carcinog.* **2013**, *12*, 6. [CrossRef]
41. Oliphant, T.E. *A guide to NumPy*; Trelgol Publishing: Spanish Fork, UT, USA, 2006.
42. McKinney, W. Data Structures for Statistical Computing in Python. In Proceedings of the 9th Python in Science Conference, Austin, TX, USA, 28 June–3 July 2010; van der Walt, S., Millman, J., Eds.; pp. 51–56.
43. Jones, E.; Oliphant, T.; Peterson, P. SciPy: Open Source Scientific Tools for Python. Available online: <http://www.scipy.org/> (accessed on 18 January 2019).
44. Shaffer, L.G.; McGowan-Jordan, J.; Schmid, M. International Standing Committee on Human Cytogenetic Nomenclature. In *ISCN 2013: An International System for Human Cytogenetic Nomenclature*; Shaffer, L.G., McGowan-Jordan, J., Schmid, M., Eds.; Karger Medical and Scientific Publishers: Basel, Switzerland, 2013; ISBN 9783318022537.
45. Jolicoeur, P.; Mosimann, J.E. Size and shape variation in the painted turtle. A principal component analysis. *Growth* **1960**, *24*, 339–354.
46. Bickel, P.J.; Doksum, K.A. *Mathematical Statistics: Basic Ideas and Selected Topics*; Holden-Day: San Francisco, CA, USA, 1977.
47. Giuliani, A. The application of principal component analysis to drug discovery and biomedical data. *Drug Discov. Today* **2017**, *22*, 1069–1076. [CrossRef]
48. Herrick, S.E.; Mutsaers, S.E. Mesothelial progenitor cells and their potential in tissue engineering. *Int. J. Biochem. Cell Biol.* **2004**, *36*, 621–642. [CrossRef]

49. Ozery-Flato, M.; Linhart, C.; Trakhtenbrot, L.; Izraeli, S.; Shamir, R. Large-scale analysis of chromosomal aberrations in cancer karyotypes reveals two distinct paths to aneuploidy. *Genome Biol.* **2011**, *12*, R61. [[CrossRef](#)]
50. Nasmyth, K. Disseminating the genome: Joining, resolving, and separating sister chromatids during mitosis and meiosis. *Annu. Rev. Genet.* **2001**, *35*, 673–745. [[CrossRef](#)]
51. Erenpreisa, J.; Cragg, M.S. Three steps to the immortality of cancer cells: Senescence, polyploidy and self-renewal. *Cancer Cell Int.* **2013**, *13*, 92. [[CrossRef](#)]
52. Erenpreiss, J. *Current Concepts of Malignant Growth. Part A: From A Normal Cell to Cancer*; Zvaigzne: Riga, Latvia, 1993.
53. Kalejs, M.; Ivanov, A.; Plakhins, G.; Cragg, M.S.; Emzinsh, D.; Illidge, T.M.; Erenpreisa, J. Upregulation of meiosis-specific genes in lymphoma cell lines following genotoxic insult and induction of mitotic catastrophe. *BMC Cancer* **2006**, *6*, 6. [[CrossRef](#)]
54. Ianzini, F.; Kosmacek, E.A.; Nelson, E.S.; Napoli, E.; Erenpreisa, J.; Kalejs, M.; Mackey, M.A. Activation of meiosis-specific genes is associated with depolyploidization of human tumor cells following radiation-induced mitotic catastrophe. *Cancer Res.* **2009**, *69*, 2296–2304. [[CrossRef](#)]
55. Vitale, I.; Senovilla, L.; Jemaà, M.; Michaud, M.; Galluzzi, L.; Kepp, O.; Nanty, L.; Criollo, A.; Rello-Varona, S.; Manic, G.; et al. Multipolar mitosis of tetraploid cells: Inhibition by p53 and dependency on Mos. *EMBO J.* **2010**, *29*, 1272–1284. [[CrossRef](#)]
56. Gorgoulis, V.G.; Zacharatos, P.; Mariatos, G.; Liloglou, T.; Kokotas, S.; Kastriakis, N.; Kotsinas, A.; Athanasiou, A.; Foukas, P.; Zoumpourlis, V.; et al. Deregulated expression of c-mos in non-small cell lung carcinomas: Relationship with p53 status, genomic instability, and tumor kinetics. *Cancer Res.* **2001**, *61*, 538–549.
57. Erenpreisa, J.; Cragg, M.S.; Salmina, K.; Hausmann, M.; Scherthan, H. The role of meiotic cohesin REC8 in chromosome segregation in γ irradiation-induced endopolyploid tumour cells. *Exp. Cell Res.* **2009**, *315*, 2593–2603. [[CrossRef](#)]
58. Chung, J.-Y.; Kitano, H.; Takikita, M.; Cho, H.; Noh, K.H.; Kim, T.W.; Ylala, K.; Hanaoka, J.; Fukuoka, J.; Hewitt, S.M. Synaptonemal complex protein 3 as a novel prognostic marker in early stage non-small cell lung cancer. *Hum. Pathol.* **2013**, *44*, 472–479. [[CrossRef](#)]
59. Lindsey, S.F.; Byrnes, D.M.; Eller, M.S.; Rosa, A.M.; Dabas, N.; Escandon, J.; Grichnik, J.M. Potential role of meiosis proteins in melanoma chromosomal instability. *J. Skin Cancer* **2013**, *2013*, 190109. [[CrossRef](#)]
60. Wang, L.; Cao, J.; Ji, P.; Zhang, D.; Ma, L.; Dym, M.; Yu, Z.; Feng, L. Oocyte-like cells induced from mouse spermatogonial stem cells. *Cell Biosci.* **2012**, *2*, 27. [[CrossRef](#)]
61. Erenpreisa, J.; Cragg, M.S. Mitotic death: A mechanism of survival? A review. *Cancer Cell Int.* **2001**, *1*, 1. [[CrossRef](#)]
62. Zhang, C.-Z.; Spektor, A.; Cornils, H.; Francis, J.M.; Jackson, E.K.; Liu, S.; Meyerson, M.; Pellman, D. Chromothripsis from DNA damage in micronuclei. *Nature* **2015**, *522*, 179–184. [[CrossRef](#)]
63. Mc Gee, M.M. Targeting the Mitotic Catastrophe Signaling Pathway in Cancer. *Mediat. Inflamm.* **2015**, *2015*, 146282. [[CrossRef](#)]
64. Salmina, K.; Gerashchenko, B.I.; Hausmann, M.; Vainshelbaum, N.M.; Zayakin, P.; Erenpreiss, J.; Freivalds, T.; Cragg, M.S.; Erenpreisa, J. When Three Isn't a Crowd: A Digyny Concept for Treatment-Resistant, Near-Triploid Human Cancers. *Genes* **2019**, *10*, 551. [[CrossRef](#)]
65. Cutcutache, I.; Suzuki, Y.; Tan, I.B.; Ramgopal, S.; Zhang, S.; Ramnarayanan, K.; Gan, A.; Lee, H.H.; Tay, S.T.; Ooi, A.; et al. Exome-wide Sequencing Shows Low Mutation Rates and Identifies Novel Mutated Genes in Seminomas. *Eur. Urol.* **2015**, *68*, 77–83. [[CrossRef](#)]
66. Armaghany, T.; Wilson, J.D.; Chu, Q.; Mills, G. Genetic alterations in colorectal cancer. *Gastrointest. Cancer Res.* **2012**, *5*, 19–27.
67. Giaretti, W.; Venesio, T.; Sciutto, A.; Prevosto, C.; Geido, E.; Risio, M. Near-diploid and near-triploid human sporadic colorectal adenocarcinomas differ for KRAS2 and TP53 mutational status. *Genes Chromosomes Cancer* **2003**, *37*, 207–213. [[CrossRef](#)]



Concept Paper

When Three Isn't a Crowd: A Digyny Concept for Treatment-Resistant, Near-Triploid Human Cancers

Kristine Salmina ¹, Bogdan I. Gerashchenko ², Michael Hausmann ³ ,
Ninel M. Vainshelbaum ^{1,4}, Pawel Zayakin ¹ , Juris Erenpreiss ^{5,6}, Talivaldis Freivalds ⁴,
Mark S. Cragg ⁷ and Jekaterina Erenpreisa ^{1,*} 

¹ Latvian Biomedical Research and Study Centre, LV-1067 Riga, Latvia

² R.E. Kavetsky Institute of Experimental Pathology, Oncology and Radiobiology, National Academy of Sciences of Ukraine, 03022 Kyiv, Ukraine

³ Kirchhoff Institute for Physics, Heidelberg University, D-69120 Heidelberg, Germany

⁴ Institute of Cardiology and Regenerative Medicine, University of Latvia, LV-1004 Riga, Latvia

⁵ Riga Stradins University, LV-1007 Riga, Latvia

⁶ Clinic IVF-Riga, LV-1010 Riga, Latvia

⁷ Centre for Cancer Immunology, University of Southampton, Southampton SO16 6YD, UK

* Correspondence: katrina@biomed.lu.lv

Received: 30 April 2019; Accepted: 19 June 2019; Published: 19 July 2019



Abstract: Near-triploid human tumors are frequently resistant to radio/chemotherapy through mechanisms that are unclear. We recently reported a tight association of male tumor triploidy with XXY karyotypes based on a meta-analysis of 15 tumor cohorts extracted from the Mitelman database. Here we provide a conceptual framework of the digyny-like origin of this karyotype based on the germline features of malignant tumors and adaptive capacity of digyny, which supports survival in adverse conditions. Studying how the recombinatorial reproduction via diploidy can be executed in primary cancer samples and HeLa cells after DNA damage, we report the first evidence that diploid and triploid cell sub-populations constitutively coexist and inter-change genomes via endoreduplicated polyploid cells generated through genotoxic challenge. We show that irradiated triploid HeLa cells can enter tripolar mitosis producing three diploid sub-subnuclei by segregation and pairwise fusions of whole genomes. Considering the upregulation of meiotic genes in tumors, we propose that the reconstructed diploid sub-cells can initiate pseudo-meiosis producing two “gametes” (diploid “maternal” and haploid “paternal”) followed by digynic-like reconstitution of a triploid stemline that returns to mitotic cycling. This process ensures tumor survival and growth by (1) DNA repair and genetic variation, (2) protection against recessive lethal mutations using the third genome.

Keywords: near-triploid cancer; radioresistance; chemoresistance; reprogramming; digyny; polynuclear cancer cells; tripolar mitosis; pedogamy; tumor blastomeres

“All basic traits inherent in cancer cells are displayed in gametes and vice versa”

Janis-Olgerts Erenpreiss [1]

1. Introduction

Organismal triploidy in humans is known to be lethal and causes early spontaneous abortions [2]. In contrast, aneuploidy is a well-tolerated characteristic hallmark of most human tumors [3–5]. Moreover, many established tumor cell lines used as models for cancer research or pharmacological studies exhibit near-triploidy [6] and many chemotherapy-resistant cancers display it in vivo [7–9]. In the accompanying article [10] we recently presented data for the origin of tumor triploidy based on the in silico meta-analysis of 2928 karyotypes from 15 malignant solid tumor types of male patients

from the Mitelman database [11]. We provided evidence that triploidy very likely initially occurs through whole genome rearrangements when one paternal genome is added to two copies of the maternal genome (XXY karyotype correlating with near-triploidy, $r = 0.88$, $p < 0.001$). Such a karyotype can be formed by a digyny-like process (Figure 1). For female tumors, this karyotype should be triploid XXX (~69XXX). To obtain this outcome, a separation of parental genomes and sister chromatid non-disjunction in maternal genomes using an aberrant meiotic pathway can be presumed to occur at some stage of tumor development that involves the gametogenic reprogramming of somatic tumor cells.

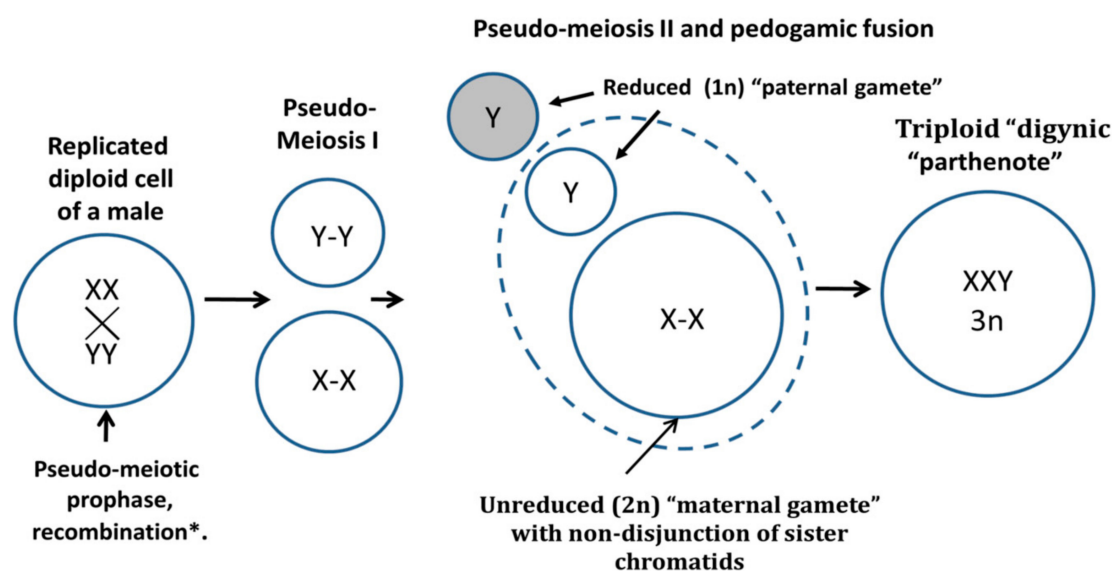


Figure 1. A conceptual schematic of the digyny-like formation of XXY triploid karyotypes in somatic male tumors revealed in the Mitelman karyotypes database data [10,11]. The reprogrammed male tumour cell triggers from G2-phase the aberrant molecular pathway of meiosis (here termed pseudo-meiosis), undergoes recombination between cohesed sisters and homologues *, pseudo-meiosis I segregating maternal, and paternal progenies with cohesed sister chromatids, reduction to haploidy of the “paternal gamete” in the pseudo-meiosis II and its pedogamic fusion with the unreduced diploid “maternal gamete” resulting in triploid “digynic parthenote”. * For recombination details, which are aberrant, see [12].

Below we briefly review the literature data which may give a hint for tackling the problem of cancer triploidy from this point. For a better understanding of the conceptual terms, we provide the reader with a Glossary.

1.1. Glossary

Near-triploidy—DNA content of the stem line, determined in relation to G1 diploidy DNA content, which is close to 1.5. [9,13]. For human karyotypes, near-triploidy is defined from the modal chromosome number, close to $3n = 69$ chromosomes [10]. The confidence interval is chosen depending on the research object, method precision, and tasks.

Digyny—refers to the process of an unreduced maternal gamete becoming fertilized by a haploid sperm (reduced paternal gamete). The result of digyny is a triploid zygote.

Unreduced maternal gamete—the oocyte which does not undergo the second meiotic division and remains diploid.

Digyny-like—the process similar to digyny supposedly occurring in tumor cells of somatic origin reprogrammed to the epigenetic state of the germline (“maternal and paternal gametes”).

Parthenote—an organism produced from an unfertilized ovum, which in human is incapable of developing beyond the early embryonic stages.

Germline—germ cells each descended or developed from earlier cells in the series, regarded as continuing through successive generations of an organism (life-cycles).

Endoreduplication (also referred to as endocycling) is the replication of the nuclear genome in the absence of mitosis, which leads to elevated nuclear gene content and polyploidy.

Pseudo-meiosis (somatic meiosis) is an asexual ploidy cycle.

Ploidy cycle—includes the doubling(s) of ploidy (asexual by endoreduplication or sexual by fertilization) and its halving in reduction division(s). “The ploidy cycle provides the potential for orderly reduction which needs (1) cohesion of sister chromatids; (2) omission of DNA replication; and (3) pairing and recombination of homologous chromosomes, which is usually present but may be optional for somatic reduction” [14].

Meiomitosis—currently a poorly defined term used in particular for mitotic tumor cells, which undergo endoreduplication and in which the meiotic machinery is partially expressed. In these cells, chiasma occurs and sister chromatids are fully or partially linked together with cohesion. These cells reduce ploidy and again return to mitosis [15,16].

Parasexual process—any form of reproduction in which the recombination of genes occurs by a process other than the gamete fusion [17].

Pedogamy—reproduction by the fusion of gametes derived from the same parent cell [18].

Triploid bridge—an epistatic synonym of digyny. Unreduced egg cell formation in diploids represents the first step (a bridge) toward asexual reproduction [19]. It appears that a triploid bridge between sexual diploidy and asexual polyploidy can evolutionarily operate in both directions [20].

Neosis—the term introduced by R. Rajaraman [21,22] for a parasexual process in tumor cells resuming immortality and proliferation potential by particular de-polyploidization cycles of polyploidized senescing mother cells.

Diplochromosome—a chromosome containing four chromatids produced by two rounds of replication without chromatid separation (due to their unresolved cohesion).

1.2. Digyny in Developmental Biology and Human Diploid-Triploid Mosaicism

In developmental biology, the XXY triploid karyotype is referred to as “digyny”, which is the most common form of whole genome aneuploidy in plants and animals [20,23,24], however, it is rarely encountered in human pathology [25]. Digyny most often arises from aberrant fertilization of an unreduced diploid egg cell by a monoploid sperm leading to a sterile triploid organism [26]. Two rounds of endoreduplication before meiosis instead of one also often favor failed reduction of the gamete in the unisexual reproduction [27]. In rare pathology of diploid-triploid human mosaics, a delayed digyny was also described—by incorporation of a pronucleus from a second polar body into one embryonic blastomere developed from an unreduced gamete [28].

In nature, a “triploid bridge” to asexual reproduction appears as an adaptation to adverse environmental conditions or can be artificially induced by them. In such cases, sexual organisms produce an increased number of unreduced oocytes so that after fertilization triploid sterile individuals appear [29]. Development “with a purpose” of the three-genome organisms seems strange because meiosis ensuring a reproductive process by recombination and ordered reduction “takes only two to tango” [30], while the third is odd. However, triploid individuals have two advantages—(1) the third genome is compatible with mitosis and diminishes the frequency of recessive lethal mutations and so favors clonal survival in a poor environment, (2) a sterile triploid conserves the energy otherwise needed for sex [20,24]. Therefore, the short-term advantage of digyny is even exploited in fish aquaculture when the female fish are treated with hydrostatic pressure, cold- or heat-shock to prevent their oocyte maturation in order to produce artificial triploid food-fish after fertilization [31].

From this data, the constitutive karyotype of near-triploid human male tumors ~69XXY found by us in silico in male malignant tumors and known chemoresistance of cancer triploidy motivated us to hypothesize that a process similar to digyny can occur in somatic tumor cells. Digyny is associated with gametogenesis. How can it be related to cancer?

1.3. Cancer Reprogramming To the Embryonality

Cancer (stem) cells can be reprogrammed to the epigenetic state of the cleavage embryo or even the germ cell [32]. This trait heralded by expression of totipotency cycle gene *POU5F1* [33], is started with the emergence of illicit tetraploidy triggered from G2-phase/mitotic slippage, particularly enhanced by genotoxic stress [34–36]. The reprogramming to the embryonal stemness of tumor cells was found in aggressive tumors in vivo [37] and recently documented by single-cell transcriptome sequencing in chemoresistant basal breast cancer and melanoma [38,39]. These facts correspond to the embryological theory of cancer and its gametogenic variant, known since the 19th century [1,40–44] and coming into power again in the 21st century [35,36,45–47]. Cancer cells were hypothesized to undergo a life-cycle-like process of reversible polyploidy for self-renewing “neosis” [21,22], producing a “germ” [35,48] comparable with sporogenesis [49,50]. In the following, this process will be termed pseudo-meiosis as displaying common features with meiosis. Pseudo-meiosis of somatic tumor cells is likely part of this asexual life-cycle as the relevant processes including cohesion of sister chromatids, recombination, and reduction divisions omitting the S-phase, with an expression of relevant meiotic genes, were reported for multiple treatment-resistant tumor cell lines [12,51–54], also in vivo [55,56]. Still, the details of the whole process (currently also termed meiomitosis) remain obscure [15,16].

1.4. Segregation of Haploid Genomes Is Coupled to Endoreduplication by Spindle Dysfunction

To get from diploidy to the digyny-like triploidy, segregation of haploid genomes should occur. Normally, it takes place in sexual meiosis but has been also described in the asexual life cycles, with meiotic elements. Segregation of haploid genomes by cycling polyploidy in the life cycle of radiolarian *Aulacantha* was first described by C. Grell [57]. This multi-step process was shown by him and further by others to operate with bi-chromatid chromosomes linked end-to-end in haploid genome entities, undergoing polyploidization (through a dysfunctional spindle), somatic pairing, followed by multipolar and bipolar mitoses, and final release of haploid spores [57,58]. Separation of autonomous duplicated parental haploid sets in diploid tissues induced by colchicine (which causes spindle dysfunction) or spontaneously by stress is known for plants, fungi, animals, [59], senescing cells, and was related by Walen [60,61] to human cancer. We recently provided evidence from human diploid embryonal carcinoma that segregation of parental genomes composed of bi-chromatid chromosomes with closed telomere ends, linked end-to-end, in a peculiar pro-metaphase possessing a dysfunctional mitotic spindle and forming a tetraploid cell, is followed by parental genome fusion and conjugation of homologues, recombination, and reduction divisions that restore diploidy [12]. From this data, it follows that separation of haploid genomes is likely evolutionary pre-programmed from the asexual life-cycles of haploid protists. It is coupled to endoreduplication, the cohesion of sister chromatids, and needs a dysfunctional spindle, which otherwise would separate them.

1.5. The Spindle Checkpoint Is Weak in the Preimplantation Embryo and Polyploidizing Tumor Cells

It is now established that a spindle arrest checkpoint is not fully functioning during the first four embryonal cleavage stages. The early blastomeres are genetically unstable [62–64] and frequently mixoploidy in vitro [65]. Moreover, in *Drosophila* the whole embryo remains multinucleated until de-polyploidization by cellularization, which occurs only at the blastocyst stage [66].

Importantly, during the first four cleavage divisions, along with the weakness of the spindle checkpoint, the parental genomes in normal mouse and human embryo also keep in mitotic plates as separate groups [67], that is while the blastomeres remain totipotent. Interestingly, the polyploidization of human tumor cells induced by the genotoxic challenge also usually proceeds until “a totipotency checkpoint”, the ploidy number (four endocycles) equivalent of the 32-cell morula, from which de-polyploidization including cellularization producing resistant mitotic progeny starts from day ~6–7 [68–71]. The multinucleated giant single cells matured to this point are capable of initiating tumor growth upon transplantation in animals [50,72,73].

1.6. Digynic Zygotes in Human In Vitro Fertilization (IVF) Clinic

Interesting information for our analysis of cancer triploidy is coming from the IVF clinic. Triploid zygotes are often observed there (with a frequency of 12%) and the most frequent cause is digyny—fertilization of unreduced oocytes by a haploid sperm [74]. Digynic triploid zygotes most often divide by tripolar mitosis [75].

In summary, the literature analysis suggests that endoreduplication coupled with reprogramming to embryonic germline totipotency and separation of parental haploid genomes through the dysfunctional spindle, and likely the tripolar mitosis, with poorly explored relationship to pseudo-meiosis, may be involved in the origin of digyny-like whole genome triploidy in radio-chemoresistant human tumors.

2. Materials and Methods

2.1. Patient Samples, Cell Lines, and Treatment

Breast cancer patient tissue specimens were collected after the patient's informed consent was obtained in accordance with the regulations of the Committee of Medical Ethics of Latvia [9]. HeLa cervix carcinoma cells and Namalwa Burkitt's lymphoma cells were obtained from ATCC. The HeLa cell culture was grown as a monolayer in flasks or on glass coverslips in F-10 medium (Hyclone Pittsburgh, PA, USA) containing 10% fetal bovine serum (FBS) (Hyclone, Pittsburgh, PA, USA) and antibiotics (Penicillin-streptomycin, Sigma P4333, Ronkonkoma, NY, USA) at 37 °C in a 5% CO₂ humidified incubator (Sanyo, Watford, UK). ATCC cells were grown as suspension cultures in RPMI-1640 medium supplied with 10% FBS (Sigma).

For the experimental studies shown here, cells were maintained in the log phase of growth, and treated with a single, acute 10 Gy dose of gamma radiation using a Gulmay D3 225 X-ray source (Krefeld, Germany) at a dose rate of 0.77 Gy/min. After irradiation, cell cultures were maintained by replenishing culture medium every 2–3 days and sampled over a two-week period post-irradiation. For Aurora B-kinase detection in some specified experiments, the proteasome inhibitor 10 μM lactacystin was added to the culture medium for 2 h before cell harvest.

2.2. Fluorescent In Situ Hybridization (FISH)

The fluorescent in situ hybridization (FISH) protocol has been described in detail previously [76]. In brief, HeLa cells were harvested, treated with 75 mM KCl at room temperature for 10 min and fixed with five changes of methanol/glacial acetic acid (3:1). The cell suspension was dropped onto slides and allowed to dry. Fluorescence labelled pericentric satellite DNA probes (Q-BIOgene–Molecular Cytogenetics/Diagnostics, Illkirch Graffenstaden, France) specific for chromosomes #6, #10, and #X were used and hybridized according to the manufacturer's protocol. The cell nuclei were counterstained with DAPI (4',6-diamidino-2-phenylindole) (ThermoFisher, Waltham, MS, USA) and embedded in the antifade mounting medium. The cover glass on the slides was sealed with rubber cement. These chromosomes were chosen as containing three normal copies and not participating in clonal markers [77]. The number of fluorescent chromosome labels per individual nuclei was counted in 500–800 cells 24 and 48 h after irradiation and compared to the non-irradiated control.

2.3. DNA Image Cytometry

Cells were grown on coverslips, prepared as cytopins or as smears and imprints on poly-L-lysine-coated microscopy slides (from breast cancer material), air-dried and fixed in ethanol:Acetone (1:1) for >30 min at 4 °C and then air-dried again. Slides were then hydrolyzed with 5N HCl for 20 min at room temperature. They were further washed in distilled water (5 × 1 min) and stained for 10 min with 0.05% toluidine blue (TB) in 50% citrate-phosphate McIlvain buffer at pH 4. After staining, samples were shortly rinsed in distilled water followed by blotting to dry and dehydration in butanol for 2 × 3 min at 37 °C. Samples were then incubated twice in xylene for 3 min at room temperature

before being embedded in DPX. Digital images were collected at 100×10 magnification using L03-10 microscope (Ergolux, Leitz, Germany) equipped with DXC 390P color video camera (Sony, Tokyo, Japan) calibrated in the green channel. DNA content was measured as the integral optical density (IOD), using Image-Pro Plus 4.1 software (Media Cybernetics, Rockville, MD, USA). The stoichiometry of DNA staining was verified using the values obtained for metaphases compared to anaphases and telophases (ratio 2:0); arbitrary diploid (2C) DNA values were averaged from measuring 50 anaphases in non-treated tumor cells. The reference 2C DNA value and variation coefficient for DNA staining method were assessed in normal human leukocytes ($\approx 2\%$). The device error was estimated at 0.5%. The integral error of the DNA staining for DNA index (DI) determination in breast cancer was assumed 10%; for HeLa mitotic cells the variation of the DNA C-value reached 20%.

2.4. Immunofluorescence

Immunofluorescence staining was performed as described [78]. The Aurora B kinase antibody (ab2254) was purchased from Abcam (Cambridge, UK), α -Tubulin (T5168) from Sigma, and Lamin B1 (sc-6216) from Santa Cruz (Dallas, TX, USA). For microscopic observations, a fluorescence light microscope Ergolux L03-10 (Leitz) equipped with a color video camera (Sony DXC 390P, Tokyo, Japan) was used (Objective $\times 100$, magnification $\times 1000$). To capture fluorescent images, in addition to separate optical filters, a three-band BRG (blue, red, green) optical filter (Leica, Wetzlar, Germany) was used.

2.5. In Silico Study of the Mitelman Database

The in-silico study of the Mitelman database was performed as described in the accompanying article [10,11]. *Nota bene*: For the sex chromosomes, chromothripsis was specifically filtered out by our bioinformatic pipeline, to allow us to document whole genome rearrangements [10].

3. Results

After assuming that a digyny-like process can convert diploid tumor cells into triploidy “digynic parthenotes”, we suggest as a working hypothesis, that on its side, the near-triploid tumor cell line uses the endoreduplication platform to create the diploid stemline, capable of undergoing the recombinatorial pseudo-meiosis and reciprocal exchange with “digyny”.

We report below some data relevant to this hypothesis from our studies of male tumors from the Mitelman database and from chemoresistance study of breast cancer tumors in patients. Next, we searched for the evidence and mechanisms of the reversible conversion of triploidy into diploidy in the well-known tumor model cervical carcinoma HeLa. We provoked resistant near-triploid cervical carcinoma HeLa cells (with a modal chromosome number 69 [79]) by one hit of ionizing irradiation (10 Gy) to follow the cell division events over the two-week course.

3.1. A Triploid Cell-Line May Coexist with Cycling Diploidy in Patient Tumors

3.1.1. Male Tumors (Renal Carcinoma)

Analysis of histograms of modal chromosome numbers in large 15 cohorts of monoclonal tumor types from the Mitelman database presented in [10] revealed near-diploid, near-triploid, and also near-tetraploid karyotypes in each tumor type. One can suggest that “monoclonal” near-triploid tumors could contain or give rise to a small amount of diploid and tetraploid sub-clones (which may be hidden in a dormant state). Some examples of the reported polyclonal karyotypes from male renal carcinoma with near-triploid XXY, diploid, and tetraploid clones from the Mitelman karyotype database (exemplified in Table 1) are compatible with this assumption.

Table 1. Some examples of the polyclonal karyotypes (numbered in columns) from male renal carcinoma with near-triploid XXY, near-diploid, and near-tetraploid clones, extracted from the Mitelman karyotype database. (Chr—modal chromosome number, Sex—sex chromosome complement).

Case	Chr1	Sex1	Chr2	Sex2	Chr3	Sex3	Chr4	Sex4
1	70	XXY	46	XY	42	XXY	45	XXY
2	75	XXY	68	XXY	87	XXXXYY	48	XY
3	46	XX, -Y	45	XX, -Y	62	XX, -Y		
4	74	XXY	46	X, -Y	46	XY		

3.1.2. Female Tumors (Breast Cancer)

The coexistence of the cycling triploid with the cycling diploid stemline was clearly seen in our study of breast cancer in patients [9]. In cases of chemoresistance, a cycling and endocycling triploidy (3C, 6C, 12C, 24C) was found in each DNA cytometry histogram, both in the diagnostic biopsy and material from the same patient post-neoadjuvant therapy (Figure S1). In one case (case 30), the triploid clone evolved from a very small cycling sub-clone in initial tumor biopsy to become the dominant stemline after non-successful chemotherapy (Figure S1). The study also revealed that in breast cancer tumors with a near-triploid stemline the hyper-tetraploid cell fraction (DNA C value > 4.5) was 4-times larger ($p = 0.003$) than in near-diploid tumors [9], indirectly pointing towards the role of endocycles in the origin of triploidy. Similarly, Kim et al. [39], in a single cell study, noticed the emergence of the triploid clone in the case of resistant to therapy basal breast cancer.

3.2. Diploid, Tetraploid, and Haploid Cell Nuclei Are Induced after Irradiation of Near-Triploid Cervical Carcinoma HeLa Cells

The model of a single 10 Gy irradiation hit of HeLa cells has been previously established in the prolonged life-imaging digital studies in the lab of Ianzini and MacKay [80], while HeLa cell response in this model during two weeks post-damage using life-imaging, DNA cytometry, and immunofluorescence was further reported in the joint studies with Ianzini/MacKay, our and Hausmann labs in Heidelberg [78,81]. In particular, it was shown that HeLa cells polyploidize in response to this irradiation hit, while cell clonal regrowth starting from day 7–9 is provided by de-polyploidization of a small proportion of still-persisting giant cells. In the current research, following treatment of HeLa cells with a single dose of 10 Gy irradiation, cells were sampled and FISH was applied for centromeres of three chromosomes #6, #10, #X (presented as triples without markers in a HeLa carcinoma genome). The relative proportions were determined in 500–800 cell nuclei for each chromosome label per nucleus. The representative FISH patterns of triploid, diploid and tetraploid nuclei are shown on Figure 2.

As seen in Figure 3A, the non-treated population consisted on average of 94% cell nuclei, trisomic by all three centromeric-labels (NB: hexa-somy indicating to triploidy cycling was also observed), however a very small proportion of diploid (disomic) and tetraploid (tetrasomic) cell nuclei and a negligible amount of haploidy (monosomy) were also present. At 48 h after 10 Gy irradiation the proportion of triploid cells decreased to 88% on average, while the proportion of diploid and tetraploid cells correspondingly increased. In addition, a tiny subpopulation of haploid nuclei also appeared (Figure 3A). When analyzed by χ -squared test (Table 2), the change of each label from non-treated culture to 48 h post-irradiation showed its statistical significance, while all three labels changed in accord. This leads us to suggest that triploid cells began the rearrangement of the whole genomes to produce diploid and tetraploid fractions.

We were therefore interested to see if and how this tendency developed and examined the DNA ploidy by in situ cytometry on further days after irradiation.

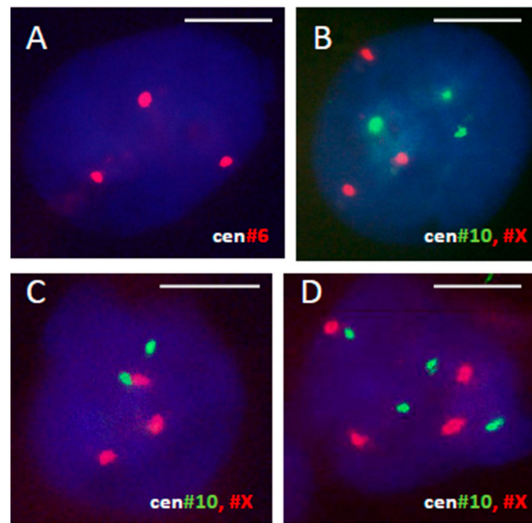


Figure 2. Representative fluorescent in situ hybridization (FISH) patterns revealing (A,B) triploid, (C) diploid, and (D) tetraploid cell nuclei 48 h after 10 Gy hit in HeLa cells using centromeric labels for three chromosomes, #6, 10, X.

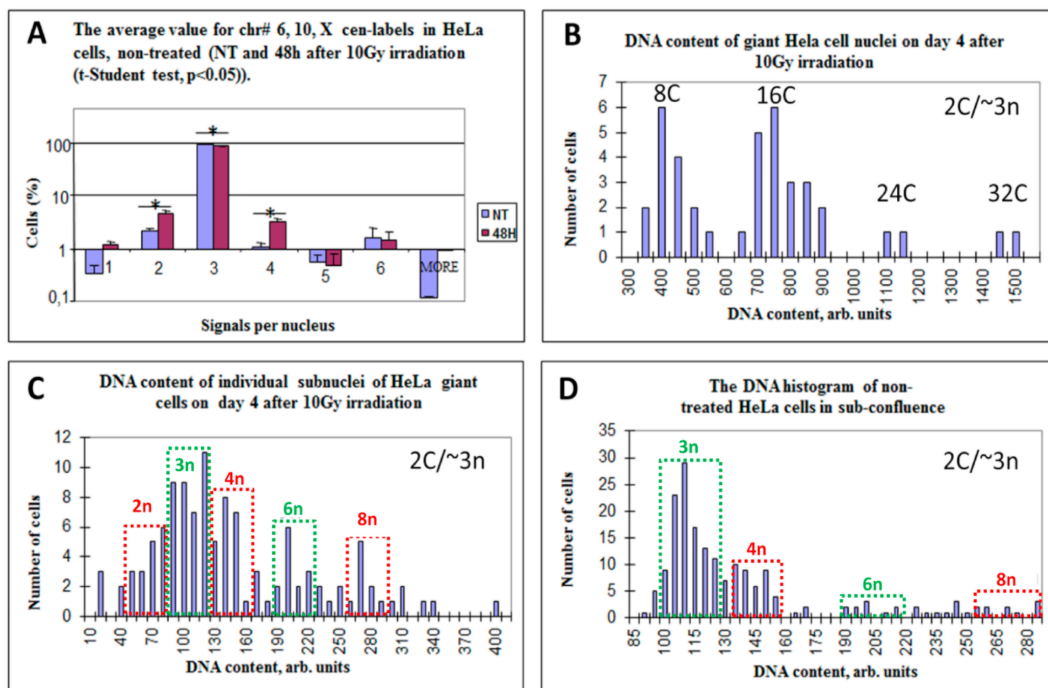


Figure 3. Endoreduplication and emergence of diploidy in the near-triploid HeLa cell line after 10 Gy-irradiation. (A) The decrease of the proportion of triploid nuclei and a corresponding increase of the proportion of diploid and tetraploid cell nuclei are presented as an average value for chr #6, #10, #X cen-labels in non-treated controls and 48 h after irradiation (*t*-student-test, $p < 0.05$). Percentage of cells is presented in logarithmic scale. (B) DNA content (presented as integrated optical density in arbitrary units) in giant cell nuclei on day four post-irradiation. The ploidy of 2C, roughly corresponding to $\sim 3n$, was determined from anaphase halves of bipolar mitoses of the control ($n = 50$). (C) Heterogeneity of the giant cell sub-nuclei on day four post-irradiation (obtained from 116 giant cells as determined by DNA cytometry, and expressed and converted for convenience into \sim ploidy numbers showing triploid (3n) and hexaploid (6n) nuclei along with about 50% of diploid nuclei and their multiples (2n, 4n, 8n); (D) Non-treated HeLa cells harvested in sub-confluence, composed of the dominant 3n stemline, while the diploid stemline endocycling to 8n is also seen (mostly accumulated in the 4n-fraction). On (C,D), the diploid endocycling stemline fractions are enframed in red, while triploid, in green dashed boxes.

Table 2. Statistically significant and concordant increase of the proportion of diploid and tetraploid cell nuclei tested by FISH centromeres labels of three chromosomes at 48 h post 10 Gy irradiation of HeLa cells.

Share of Cell Nuclei with a Certain Number of Centromere Signals		Chromosome X		Chromosome 6		Chromosome 10	
		Number of Nuclei	%	Number of Nuclei	%	Number of Nuclei	%
Diploid and tetraploid nuclei	NT	19	3.1	17	3.1	23	3.4
Triploid and other cell nuclei	NT	586	96.9	523	96.9	649	96.6
Diploid and tetraploid nuclei	48h	53	10.2	34	6.2	54	7.0
Triploid and other cell nuclei	48h	466	89.8	518	93.8	714	93.0
χ -squared test, <i>p</i> -value		2.4·10 ⁻²⁰		3.6·10 ⁻⁵		3.7·10 ⁻¹²	

3.3. Multinucleated Giant Cells Contain DNA with Odd and Even Ploidy Numbers

As reported previously [78], on the first day most irradiated HeLa cells were delayed in the G2-arrest, from day two, 82% of live-imaged HeLa cells ($n = 645$) underwent the chromosome-bridged post-telophase bi-nucleation, becoming tetraploid and many started the asynchronous bipolar divisions of two sub-nuclei (exemplified in Figure 4A). These divisions were also a-cytokinetic, and thus, by day three, 70% cells became octoploid (composed typically of two 4C sub-nuclei), in the following days the ploidy and multi-nucleation increased. By day 4–5, the multinucleated polyploid giant cancer cells (PGCC) composed of ~50% of the population and contained largely 8C, 16C, 24C, and 32C DNA in total (Figure 3B). DNA cytometry of individual sub-nuclei of the 4-day PGCCs reveals in them odd and even *n*-value numbers. C-value was determined from anaphase halves of the DNA content in bipolar mitoses of untreated cultures. Therefore, it should be kept in mind that for near-triploid HeLa, a 2C value roughly corresponds to ~3*n*. Subsequently, the derived ploidy numbers of the sub-nuclei were 2*n*, 3*n*, 4*n*, 6*n*, and 8*n* (Figure 3C). The sub-nuclei of PGCC were mostly bridged, indicating their origin from a common mother. Live-imaging showed that only 3% of cells in 72 h underwent fusion of non-sister cells [78]. Interestingly, the DNA histogram of the non-treated population taken at sub-confluence on day six (Figure 3D), also showed the same odd and even fractions (except 2*n*), however, the ploidy doubling fractions 6*n* and 8*n* were minor. The sub-nuclei in PGCCs with odd and even genome numbers were often arranged in giant cells radially and also frequently contained a near-haploid subnucleus (rarely two-three of them), and a few micronuclei (Figure 4B,C).

In summary, a genotoxic challenge apparently caused the entrance of HeLa cells into endomitotic a-cytokinetic cycles, starting from bi-nucleated on day two and reaching by day three majorly 8C/12*n* and by day 4, 16C/24*n* ploidy. This response was heralded by the emergence of the increasing number of diploid, tetraploid, and octoploid subnuclei coexisting with triploidy (and also haploidy) in the same PGCCs. How could they achieve that? The answer was likely found in tripolar mitosis.

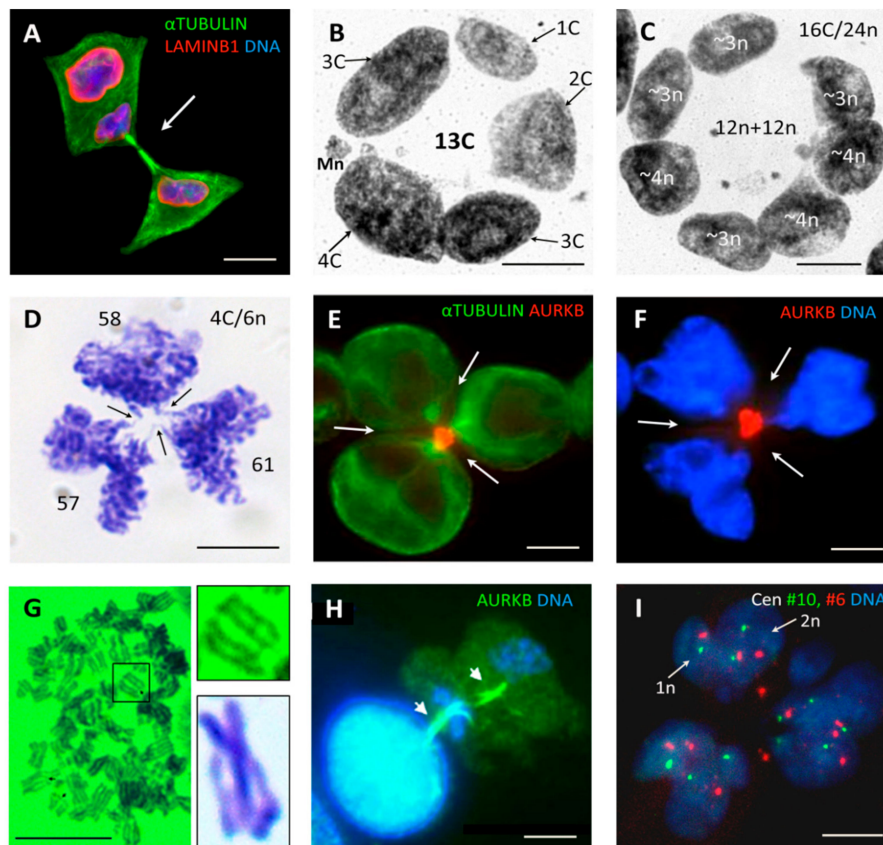


Figure 4. Divisions and multi-nucleation of the genotoxically damaged tumor cells. (A) HeLa cell, on day two post-irradiation (10 Gy): One subnucleus in a bi-nucleated cell is being divided (arrow). (B) A processed for image analysis (DNA bridges were deleted) multinucleated giant HeLa cell nucleus on day six post-irradiation containing sub-nuclei with even and odd proportions of DNA content, along which a near-haploid ($\sim 1C$) sub-nucleus and a micronucleus (Mn) were seen; (C) A processed for image analysis (DNA bridges were deleted) multinucleated giant HeLa cell on day nine post-irradiation containing four $\sim 3n$ and three $\sim 4n$ sub-nuclei with a similar sum DNA content; (D) The anaphase of the multipolar mitosis of an irradiated HeLa cell with chromosome bridges between the karyokinesis products of three bilobed groups, a finding indicative of the pair-wise fusion of segregated neighboring genomes (stained with toluidine blue for DNA). The arrows show indentations in the bridges between these pairwise fused products of three karyotomies due to incomplete or ongoing cleavage by radial cytotomy; (E,F) Radial cleavage furrows bringing three Aurora KB-positive mid-bodies to the fused one of their spindle poles together, potentially segregating the progeny with pedogamically fused bilobed nuclei; (G) The diplochromosomic metaphase of a HeLa cell on day five post-irradiation (10 Gy) (stained with Toluidine blue for DNA), resembling the diakinetik stage of meiosis with often intertwined or DNA-bridged (arrows) two pairs of cohesed sisters. On insert enlarged: (a) The enframed bridged diplochromosome and an example of the chiasma found between diplochromosomes of the irradiated Namalwa cell line; (H) Two subsequent divisions of the tetraploid sub-nucleus of a giant Namalwa cell to a haploid pair of nuclei on day five post-irradiation (10 Gy) are seen, displaying two persisting mid-bodies (shown by the arrows). Persistence of two subsequent mid-bodies and \sim haploidy in DNA content of the final anaphase figures suggest that the second division closely followed the first division, omitting the S-phase. This sample was collected after 2-h treatment with the proteasome inhibitor—lactacystin; The brightness in the DAPI channel was enhanced to highlight small nuclei of the second anaphase; (I) The FISH sample for centromeres #6 and #10 of HeLa cells on day four post-irradiation (10 Gy) shows (arrows) haploid (monosomic) and diploid (disomic) lobes of a sub-nucleus resulting after multipolar karyokinesis. Bars = 10 μ m. Figure 4A–C,H are reproduced from [78], with permission of the publishers.

3.4. Tripolar Mitosis of Endoreduplicated Cells May Convert Triploidy into Diploidy

Along with rare bipolar divisions, tripolar mitotic figures were seen in irradiated HeLa cells more often than in control, at the end of the second day and onwards, until recovery of the triploid clonogenic cell line. In some tripolar ana-telophase-like figures 48 h after irradiation, the chromosome bridges were observed between three bilobed chromosome groups, indicating the pairwise fusion of karyokinesis products (chromosome groups of a similar size) at each of three neighbor poles (Figure 4D). The arrowed indentations of the chromosome bridges between these pairwise fused products are due to incomplete, failed or ongoing cleavage by the radial cytokinesis. Cytometry revealed that three bilobed groups contained equal (with 4% variation) DNA content corresponding $\sim 2n$, testifying to the division of the replicated near-triploid cell into three diploid groups, where each likewise was formed by the fusion of two haploid genomes ($6n:3 = 2n$). The radial cleavage furrows potentially segregating the progeny with fused bilobed sub-nuclei and bringing three mid-bodies together are seen in (Figure 4E,F). Most tumor segregations appeared less precise, however, the reported observation shows namely that the tripolar mitosis of a replicated triploid $6n$ cell can convert triploidy into diploidy demonstrating a pair-wise fusion of haploid genomes (see schematic on Figure 5, central upper figure). If endoreduplication forms a larger $8C/12n$ cell, it can potentially produce by tripolar mitosis three $4n$ cells ($12n:3 = 4n$) or by tetrapolar mitosis four $3n$ cells ($12n:4 = 3n$). This may have occurred with the nucleus of a PGCC on Figure 4C containing four $3n$ and three $4n$ sub-nuclei, each group making the same $12n$ ($\sim 8C$) DNA amount as measured by DNA cytometry. Those apparently represent the products of tripolar and tetrapolar divisions of two $8C$ subnuclei in the same giant cell. The prerequisites for such whole genome rearrangements would be the grouping and segregation of the haploid chromosome entities and non-separation of sister chromatids. Therefore, it is worth to mention as shown previously, that the chromosomal ends in acytokinetic multipolar mitoses of HeLa cells were usually seen closed [12,81].

So, we found here that near-triploid HeLa cells begin to increasingly produce the diploid and tetraploid subfractions after irradiation, likely by a-cytokinetic tripolar mitosis of near-triploid cells endoreduplicated to $6n$ and $12n$ and that their proportion increased from $\sim 6\%$ on day two to $\sim 40\text{--}50\%$ on days 3–6. Thus, a tetraploid fraction composed of doubled parental genomes ($\sim 4nXXYY$) could be reconstituted from a triploid one. It could further enter pseudo-meiosis and potentially produce a recombined unreduced diploid maternal pseudo-gamete and recombined reduced paternal haploid pseudo-gamete (this process is schematically represented for a male tumor on Figure 1). This process can take place either in the individualized cells—the diplochromosomic metaphases segregating bi-chromatids (presented on Figure 4G) may have a relationship to this process. However, it is not excluded that the whole pseudo-meiosis (recombination and reduction), as well as the digyny-like pedogamic process (fusion between an unreduced diploid “maternal gamete” and a haploid reduced “paternal gamete”), can take place at the site—on the platform of a polyploid giant cancer cell. A two-step asymmetric reduction division from a PGCC in irradiated lymphoma cells (reproduced here on Figure 4H) and occasional finding of two-parted HeLa giant cells sub-nuclei composed from a monosomic and disomic parts seen by centromere #6 and #10 FISH (Figure 4I) provide a hint for such an option. A non-sister fusion between diploid and haploid cells is not excluded as well, taking into consideration the very rare, but still found in vivo (Figure S2) divisions of free haploid tumor cells.

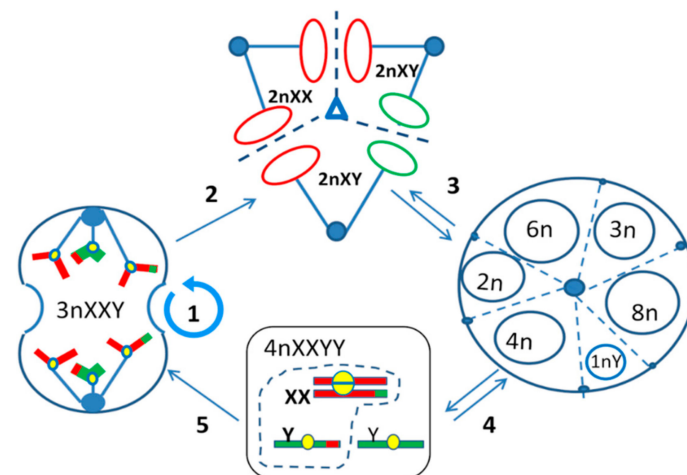


Figure 5. The Digyny Concept of meio-mitosis applied to near-triploid male tumor cells. (1) A digynic triploidy tumor cell line ($3nXXY$) undergoes mitotic cycles replicating and segregating sister chromatids for growth of the tumor mass. To perform recombinative renewal, it first closes telomere ends, and after replication segregates the genomes of the $3nXXY(x2)$ cell in (2) tripolar mitosis as 2:2:2 by pairwise fusing the haploid whole genome products of karyokinesis (red circles for arbitrary maternal, green, for paternal genomes) at each pole. (3) A diploid progeny ($2nXY$) endoreduplicates to $4n$ $XXYY$, and to $8n$; a triploid subnucleus can also endoreplicate to $6n$; $1n$ Y can be also (rarer) produced in tripolar mitosis (3:2:1); (4) $4n$ as a subnucleus of the polyploid giant cancer cell (PGCC) or as a free cell enters the recombinative pseudo-meiosis followed by one-step reduction division (for “maternal” sub-nucleus) and two-step reduction (for “paternal” sub-nucleus). A digyny-like fusion in $3n$ XXY subcell is processed (a dashed box). Alternatively (less likely), one non-recombined $1nY$ subnucleus from tripolar mitosis of a triploid cell (3:2:1) can fuse with two recombined, unreduced maternal genomes of a pseudo-meiotic diploid sub-cell. (5) A renewed digynic triploid cell restarts mitotic cycling, the process constitutive for tumor near-triploidy and favoring cell survival by compensating lethal recessive mutations. The near-diploid tumors can also enter this hybrid cycle induced through endoreduplication and multipolar mitosis, and thus be converted into triploid digynic stem-line if influenced by senescence, oncogenes, and genotoxic therapy.

3.5. Summary of Results

The presented results provide the first evidence that in somatic human tumors the diploid and triploid compartments may constitutively co-exist and exchange the whole genomes in the same tumor. The study of irradiated near-triploid HeLa cells revealed that diploid subcells are produced after genotoxic insult in induced endopolyploid tumor cells through euploid whole genome segregations and fusions in tripolar mitosis.

4. Discussion

From the study of 15 male malignant tumor types with near-triploid XXY karyotypes assembled from the Mitelman karyotype database presented in the accompanying paper [10] and DNA cytometry of resistant triploid breast cancer, we suggested the association of the near-triploid XXY karyotypes (XXX for females) with a digyny-like pedogamic process—somewhat like an aberrant unisexual “fertilization”. From the literature analysis and experimental evidence presented here the whole process can be deduced as follows (Figure 5). The mitotically cycling near-triploid “digynic” tumor cell (Figure 5(1)), when challenged by stress, undergoes tripolar mitosis for the reconstruction of diploidy by segregating and fusing haploid genomes (Figure 5(2)). For that, these cells possibly use the platform of transient multinucleated giant cells enclosing resulting diploid and triploid sub-nuclei and their replicas (Figure 5(3)). In turn, the replicated diploid subnuclei/cells ($4n$) are capable of undergoing the recombinative pseudo-meiosis and creating pseudo-gametes. The parental

pseudo-gametes (unreduced maternal and reduced paternal) pedogamically fuse, to reconstitute the triploidy digynic-like tumor stem line $3n\ XXY$ (Figure 5(4)). The latter, representing a triploid “parthenote”, stops further differentiation and returns in the genetically renewed, recombined form into a mitotic cycle (Figure 5(5)). On recovery, this mitotic clonogenic cycling becomes dominant again, increasing the tumor mass. It follows, that diploid and triploid sub-lines exchange whole haploid genomes. Somewhat in accord, Kroeger et al. [82] recently published the necessity for a hybrid epithelial-and mesenchymal state (Snail–Wnt-driven) for the growth of basal breast cancer suggesting the epithelial and mesenchymal cells cooperate as two sub-populations of tumors. Could they correspond to the diploid and triploid sub-lines? This is a question for future projects. Our hypothesis was stimulated by the previously published study of the chemoresistant triploid breast cancer [9] and the polyclonal karyotypes in male renal carcinoma, which were assessed here. Moreover, single-cell transcriptome sequencing tumor analysis also points to the polyclonal adaptive nature of cancer chemoresistance [83]. The current study on irradiated near-triploid HeLa cells brought us to PGCC—an analogue by its expression profile of the blastula embryo [35,36,47] and to tripolar mitoses in them.

Further, we should compare our results with a series of studies performed in the late 1960s to the mid-1970s [84–87], which essentially coincide with our observations. The authors used the multiple primary cultures of normal diploid mouse fibroblasts and Rhesus monkey kidney epithelial cells, applying DNA densitometry and cytogenetic analysis. They found that, contrary to bipolar mitosis occurring in diploid cells, the endoreduplicated tetraploid cells emerging in senescing cultures in a small proportion (~3% cells) from day 15–20 majorly undergo tripolar mitoses. Those were analyzed without applying spreading and spindle poisons. The euploid segregation of the genomes in haploid, diploid, and triploid ana-telophase groups by tripolar mitosis was reported in this article series published by two groups on two mammalian species. The genetic material of the initially diploid culture is most often segregating in tripolar mitosis as the multiples of haploid genomes in a $3n:3n:2n$ ratio—so, through endoreduplication the diploidy gives birth to triploidy. In turn, the resulting triploid cells most often segregate the genomes (after re-replication) by tripolar mitosis in a $2n:2n:2n$ ratio, thus triploidy could recurrently give birth to diploidy. This is namely the same as what we have found as a “nervus probandi” on Figure 4D for near-triploid endoreduplicated HeLa cells. Segregations of triploids to haploidy were also found by these authors ($3n:2n:1n$), but far less frequently. Although, as they also found the cytokinesis was defective or delayed, all subcells segregated after tripolar mitosis still could further divide by bipolar mitosis, except haploid YO, which existed only within a multinucleated mother. Importantly, Palitti and Rizzoni [85] scored the frequency of different variants of euploid segregations in tripolar mitoses of tetraploid and triploid cells from 77 primary diploid mouse cultures and tested as the null hypothesis if those segregate the genomes (i) in random and (ii) sending sister chromatids to different poles. This model was disproved by real scores—segregations were not random (some variants were several-fold preferred over the theoretically possible ones) and the chromatids could be not (or preferentially were not) separated, indicating a weak spindle.

Rizzoni et al [87] concluded that in mammalian somatic euploid cells there seems to exist a supra-chromosomal organization of the genome in haploid sets, which displays itself in the euploid segregations through multipolar mitosis. As to the analysis of segregation of the sex chromosomes, [86], the digynic formula $3nXXY$ was preferentially found, while $3n\ XYY$ (diandry) also occurred but two times less frequently. Moreover, the authors were highly surprised to reveal XX-diploid cells in male mouse fibroblast cultures after multi-polar mitoses of polyploid cells.

Finally, Pera and Scholtz [88] described the sharp conversion of the normal male mouse diploid fibroblast cell line into triploidy after ~12 months of cultivation (likely occurring due to oncogenic transformation). Two triploid cell lines comprising 85% of the population could be distinguished and isolated, one with the karyotype $3n\ XXY$, the other with $3n\ XYY$. In ~1% of the culture, diploid cells with two X or two Y chromosomes were found. Haploid, tetraploid, hexaploidy, and octoploid mitoses were also observed at a low percentage. The involvement of the meiotic component in tripolar

segregations of diploid mammalian cells, which may be responsible for XXY karyotype and diploid XX male cells, was suggested.

We also decided to additionally extract from the Mitelman database the malignant tumor karyotypes with double X and double Y tetraploid and diploid karyotypes presented in Table 3 for comparison with the above literature data. YO haploid karyotypes were never encountered, and also YY were practically absent (or could exist as an exception only with fragmented X-chromosome), while XX diploid karyotypes were present in seven of 15 tumor cohorts and XXYY were present everywhere (except gastric cancer).

Summarizing this part of the discussion, we conclude that the German and Italian groups of the 1970s revealed on normal mammalian cells the same regularity, which we were able to “fish out” using the X chromosome disomy “hook” from the 2928 male tumor karyotypes on the digyny-like origin of triploidy from Mitelman database. Without this approach, the somatic digyny in tumors is obscured by the overlaying chromosome instability and not easily seen.

Namely, these data presume the segregation of parental genomes as suprachromosomal entities, reconstruction of diploidy from triploidy and vice versa through multipolar divisions of endoreduplicated cells, as well as a preferential doubling of maternal genomes in male tumors, shown and discussed in [10].

The details of a pseudo-meiotic process remained less clear. The existence of a pseudo-meiotic process in irradiated HeLa cells was studied by Ianzini et al. [53] in collaboration with our laboratory, mostly by qPCR, where up-regulation of MOS, cyclin B1, meiotic cohesin REC8 (increased 3-fold on day three and 10-fold on day five, with repeating peaks on day 10 and 25), meiotic recombinase DMC1, and SYCP3 were found. The overexpressed meiotic protein SCP3 was even suggested as a prognostic marker for cervical carcinomas [89]. However, pseudo-meiosis in tumors seems to be occurring even without conventional synaptonemal complexes [12]. More studies on this issue are needed in the future.

Table 3. The proportions of tetraploid and diploid karyotypes possessing two X chromosomes, and the almost-absent karyotypes with two Y-chromosomes for 15 male malignant tumor cohorts from the Mitelman database.

Malignant Tumor Type	Number of Karyotypes	XXYY (%)	X ₁ -Y ₁ +X (%)	YY ₁ -X (or with Fragmented X) (%)
Seminoma	78	12.82	2.56	0.00
Osteosarcoma	61	6.56	0	0.00
Lung carcinoma	237	2.95	0.84	0.00
Gastric carcinoma	74	0.00	4.05	0.00
Head and neck squamous cell carcinoma	191	3.14	0	0.00
Colon adenocarcinoma	98	3.06	3.06	0.00
Transitional cell carcinoma	104	0.96	0	0.00
Chondrosarcoma	85	5.88	0	0.00
Malignant melanoma	134	1.49	0.75	0.00
Glioblastoma	215	6.51	0	0.00
Renal carcinoma	577	1.39	0.87	0.17
Mesothelioma	72	5.56	0	0.00
Rhabdomyosarcoma *	92	30.43	3.26	1.09
Ewing sarcoma	228	3.51	0	0.00
Liposarcoma	147	3.40	0	0.00

* Rhabdomyosarcoma is an outlier as originating from multi-nuclear cells.

Interestingly, concerning meiotic kinase MOS and quite in accord with our current data, Vitale et al [90] found in colon cancer p53-null cells treated with nocodazole that multipolar mitosis in induced transient tetraploidy cells was dependent on upregulation of this kinase, which inhibited the coalescence of supernumerary centrosomes and finally favored selection of less aneuploid progeny.

Multipolar mitosis in tumors has been extensively studied and explained by the dysfunctional spindle assembly checkpoint leading to nearly random segregation of sister chromatids between poles [91,92], then the role of cytokinesis failure in the asymmetric segregation of chromosomes into two daughter cells was highlighted [93]. However, it seems that the rules applicable to the regulation of mitosis as such may be non-applicable for tripolar mitosis in the germ-like PGCCs. Further detailed studies are needed but currently it appears that in the latter not the chromatids but the genomes are segregated, reassorted and fused in a pedogamic manner at the background of the weak spindle checkpoint. The same can be said about a-cytokinesis. In fact, radial cytokinesis releasing progeny from PGCC is postponed [12] and, by analogy with such in *Drosophila* egg chambers [94], is inherently unequal.

5. Conclusions

Considering the nature of the complex process involving the PGCC, it seems to be evolutionary pre-programmed and aimed for the atavistic response mode for cell survival in adverse conditions, operating with the whole genomes in a parasexual life cycle of tumor cells. The molecular background of the endoreduplicated pseudo-blastula in the conditions of oncogenic and/or genotoxic stress likely favors the adaptive triploid digyny-like process assisted through tripolar mitosis. The exchange between reproductive (with meiotic elements) diploid and clonogenic triploid subfractions supports the tumor immortality by recombinative genetic variation, on one side, and protects from recessive lethal mutations with the selection of the fittest clones, on the other side. These whole-genome rearrangements do not exclude chromosome instability because stochastic noise and occasional chromothripsis are also inevitably needed for the optimization of the inheritance system [95].

The digyny concept also does not contradict but essentially complement the paradigm of the somatic mutation/clonal selection origin of cancer.

Supplementary Materials: The following are available online at <http://www.mdpi.com/2073-4425/10/7/551/s1>, Figure S1: DNA content histograms of two locally advanced triple-negative breast cancer cases (Stage III) before and after neoadjuvant chemotherapy (denoted as NAC) using standard doses of paclitaxel and doxorubicin, Figure S2: Microphotograph of TB-DNA-stained diagnostic biopsy cell nuclei of the triple negative case 17.

Author Contributions: Conceptualization, J.E. (Jekaterina Erenpreisa); methodology, J.E. (Jekaterina Erenpreisa) and K.S.; validation, P.Z. and T.F.; formal analysis M.H. and P.Z.; investigation, K.S., B.I.G., M.H. and J.E. (Jekaterina Erenpreisa); data curation, J.E. (Juris Erenpreiss); writing-original draft preparation, K.S.; writing-review and editing, J.E. (Jekaterina Erenpreisa), P.Z., M.H. and J.E. (Juris Erenpreiss), visualization, J.E. (Jekaterina Erenpreisa) and T.F., supervision, J.E. (Jekaterina Erenpreisa).

Funding: Baltisch-Deutsches HochschulKontor (2015) project, European Regional Development Fund (ERDF) project No. 1.1.1.1/18/A/099, Alfred Raister memorial scholarship of the Latvian University to Ninel M. Vainshelbaum. Michael Hausmann was supported by the Heidelberg University Mobility Grant for International Research Cooperation within the excellence initiative II of the Deutsche Forschungsgemeinschaft (DFG) for laboratory exchange and discussions.

Acknowledgments: Elizabeth A. Kosmacek is acknowledged for performing some cytometry experiments on HeLa cell line under a collaboration between the Erenpreisa's (BMC, Latvia) and the Ianzini/Mackey's (Iowa University, USA) laboratories.

Conflicts of Interest: The authors declare no conflict of interest. The funders had no role in the design of the study; in the collection, analyses, or interpretation of data; in the writing of the manuscript, or in the decision to publish the results.

References

1. Erenpreiss, J. *Current Concepts of Malignant Growth. Part A: From a Normal Cell to Cancer*; Zvaigzne: Riga, Latvia, 1993.

2. Inhorn, S.L.; Therman, E.; Patau, K. Cytogenetic studies in spontaneous human abortion. *Am. J. Clin. Pathol.* **1964**, *42*, 528.
3. Hanahan, D.; Weinberg, R.A. Hallmarks of cancer: The next generation. *Cell* **2011**, *144*, 646–674. [[CrossRef](#)] [[PubMed](#)]
4. Sheltzer, J.M.; Amon, A. The aneuploidy paradox: Costs and benefits of an incorrect karyotype. *Trends Genet.* **2011**, *27*, 446–453. [[CrossRef](#)] [[PubMed](#)]
5. Holland, A.J.; Cleveland, D.W. Losing balance: The origin and impact of aneuploidy in cancer. *EMBO Rep.* **2012**, *13*, 501–514. [[CrossRef](#)] [[PubMed](#)]
6. Jo, Y.; Choi, N.; Kim, K.; Koo, H.-J.; Choi, J.; Kim, H.N. Chemoresistance of cancer cells: Requirements of tumor microenvironment-mimicking models in anti-cancer drug development. *Theranostics* **2018**, *8*, 5259–5275. [[CrossRef](#)] [[PubMed](#)]
7. Teixeira, M.T.; Pandis, N.; Heim, S. Tumours of the Breast. In *Cancer Cytogenetics*, 3rd ed.; Heim, S., Mitelman, F., Eds.; Wiley: Hoboken, NJ, USA, 1995; pp. 493–516.
8. Swanton, C.; Nicke, B.; Schuett, M.; Eklund, A.C.; Ng, C.; Li, Q.; Hardcastle, T.; Lee, A.; Roy, R.; East, P.; et al. Chromosomal instability determines taxane response. *Proc. Natl. Acad. Sci. USA* **2009**, *106*, 8671–8676. [[CrossRef](#)] [[PubMed](#)]
9. Gerashchenko, B.I.; Salmina, K.; Eglitis, J.; Huna, A.; Grjunberga, V.; Erenpreisa, J. Disentangling the aneuploidy and senescence paradoxes: A study of triploid breast cancers non-responsive to neoadjuvant therapy. *Histochem. Cell Biol.* **2016**, *145*, 497–508. [[CrossRef](#)]
10. Vainshelbaum, N.M.; Zayakin, P.; Kleina, R.; Erenpreisa, J. Meta-analysis of cancer triploidy: Whole-genome rearrangements in male human tumours are characterised by XXY karyotypes. *Genes* **2019**, accepted for publication.
11. Mitelman, F.; Johansson, B.; Mertens, F. Mitelman Database of Chromosome Aberrations and Gene Fusions in Cancer. Available online: <http://cgap.nci.nih.gov/Chromosomes/Mitelman> (accessed on 1 January 2019).
12. Salmina, K.; Huna, A.; Kalejs, M.; Pjanova, D.; Scherthan, H.; Cragg, M.S.; Erenpreisa, J. The cancer aneuploidy paradox: In the light of evolution. *Genes* **2019**, *10*, 83. [[CrossRef](#)]
13. Giaretti, W.; Venesio, T.; Sciutto, A.; Prevosto, C.; Geido, E.; Risio, M. Near-diploid and near-triploid human sporadic colorectal adenocarcinomas differ for KRAS2 and TP53 mutational status. *Genes Chromosomes Cancer* **2003**, *37*, 207–213. [[CrossRef](#)]
14. Kondrashov, A.S. The asexual ploidy cycle and the origin of sex. *Nature* **1994**, *370*, 213–216. [[CrossRef](#)] [[PubMed](#)]
15. Yant, L.; Bomblies, K. Genome management and mismanagement—Cell-level opportunities and challenges of whole-genome duplication. *Genes Dev.* **2015**, *29*, 2405–2419. [[CrossRef](#)] [[PubMed](#)]
16. Tsang, M.; Gantchev, J.; Netchiporouk, E.; Moreau, L.; Ghazawi, F.M.; Glassman, S.; Sasseville, D.; Litvinov, I.V. A study of meiomitosis and novel pathways of genomic instability in cutaneous T-cell lymphomas (CTCL). *Oncotarget* **2018**, *9*, 37647. [[CrossRef](#)] [[PubMed](#)]
17. Collins, U.K. *Collins English Dictionary*; Collins: Glasgow, Scotland, 2014; ISBN 9780007522743.
18. Stevenson, A. *Oxford Dictionary of English*; Oxford University Press: New York, NY, USA, 2010; ISBN 9780199571123.
19. Schinkel, C.C.F.; Kirchheimer, B.; Dullinger, S.; Geelen, D.; De Storme, N.; Hörandl, E. Pathways to polyploidy: Indications of a female triploid bridge in the alpine species *Ranunculus kuepferi* (Ranunculaceae). *Plant Syst. Evol.* **2017**, *303*, 1093–1108. [[CrossRef](#)] [[PubMed](#)]
20. Comai, L. The advantages and disadvantages of being polyploid. *Nat. Rev. Genet.* **2005**, *6*, 836–846. [[CrossRef](#)]
21. Sundaram, M.; Guernsey, D.L.; Rajaraman, M.M.; Rajaraman, R. Neosis: A novel type of cell division in cancer. *Cancer Biol. Ther.* **2004**, *3*, 207–218. [[CrossRef](#)] [[PubMed](#)]
22. Rajaraman, R.; Rajaraman, M.M.; Rajaraman, S.R.; Guernsey, D.L. Neosis—A paradigm of self-renewal in cancer. *Cell Biol. Int.* **2005**, *29*, 1084–1097. [[CrossRef](#)]
23. Harlan, J.R.; deWet, J.M.J.; On, Ö. Winge and a Prayer: The origins of polyploidy. *Bot. Rev.* **1975**, *41*, 361–390. [[CrossRef](#)]
24. Otto, S.P. The evolutionary consequences of polyploidy. *Cell* **2007**, *131*, 452–462. [[CrossRef](#)]
25. Pawlowitzki, I.H.; Cenani, A. Sporadic triploid cells in human blood and fibroblast cultures. *Humangenetik* **1967**, *5*, 65–69. [[CrossRef](#)]

26. Austin, C.R. Anomalies of fertilization leading to triploidy. *J. Cell. Comp. Physiol.* **1960**, *56* (Suppl. 1), 1–15. [[CrossRef](#)]
27. Neaves, W.B.; Baumann, P. Unisexual reproduction among vertebrates. *Trends Genet.* **2011**, *27*, 81–88. [[CrossRef](#)]
28. Daniel, A.; Wu, Z.; Darmanian, A.; Collins, F.; Jackson, J. Three different origins for apparent triploid/diploid mosaics. *Prenat. Diagn.* **2003**, *23*, 529–534. [[CrossRef](#)]
29. Mason, A.S.; Pires, J.C. Unreduced gametes: Meiotic mishap or evolutionary mechanism? *Trends Genet.* **2015**, *31*, 5–10. [[CrossRef](#)]
30. Roeder, G.S. Meiotic chromosomes: It takes two to tango. *Genes Dev.* **1997**, *11*, 2600–2621. [[CrossRef](#)]
31. Zhou, L.; Gui, J. Natural and artificial polyploids in aquaculture. *Aquac. Fish.* **2017**, *2*, 103–111. [[CrossRef](#)]
32. Sell, S.; Nicolini, A.; Ferrari, P.; Biava, P.M. Cancer: A problem of developmental biology; scientific evidence for reprogramming and differentiation therapy. *Curr. Drug Targets* **2016**, *17*, 1103–1110. [[CrossRef](#)]
33. Yeom, Y.I.; Fuhrmann, G.; Ovitt, C.E.; Brehm, A.; Ohbo, K.; Gross, M.; Hübner, K.; Schöler, H.R. Germline regulatory element of Oct-4 specific for the totipotent cycle of embryonal cells. *Development* **1996**, *122*, 881–894.
34. Salmina, K.; Jankevics, E.; Huna, A.; Perminov, D.; Radovica, I.; Klymenko, T.; Ivanov, A.; Jascenko, E.; Scherthan, H.; Cragg, M.; et al. Up-regulation of the embryonic self-renewal network through reversible polyploidy in irradiated p53-mutant tumour cells. *Exp. Cell Res.* **2010**, *316*, 2099–2112. [[CrossRef](#)]
35. Erenpreisa, J.; Salmina, K.; Huna, A.; Jackson, T.R.; Vazquez-Martin, A.; Cragg, M.S. The “virgin birth”, polyploidy, and the origin of cancer. *Oncoscience* **2015**, *2*, 3–14. [[CrossRef](#)]
36. Niu, N.; Mercado-Uribe, I.; Liu, J. Dedifferentiation into blastomere-like cancer stem cells via formation of polyploid giant cancer cells. *Oncogene* **2017**, *36*, 4887–4900. [[CrossRef](#)]
37. Ben-Porath, I.; Thomson, M.W.; Carey, V.J.; Ge, R.; Bell, G.W.; Regev, A.; Weinberg, R.A. An embryonic stem cell-like gene expression signature in poorly differentiated aggressive human tumors. *Nat. Genet.* **2008**, *40*, 499–507. [[CrossRef](#)]
38. Shaffer, S.M.; Dunagin, M.C.; Torborg, S.R.; Torre, E.A.; Emert, B.; Krepler, C.; Beqiri, M.; Sproesser, K.; Brafford, P.A.; Xiao, M.; et al. Rare cell variability and drug-induced reprogramming as a mode of cancer drug resistance. *Nature* **2017**, *546*, 431–435. [[CrossRef](#)]
39. Kim, C.; Gao, R.; Sei, E.; Brandt, R.; Hartman, J.; Hatschek, T.; Crosetto, N.; Foukakis, T.; Navin, N.E. Chemoresistance evolution in triple-negative breast cancer delineated by single-cell sequencing. *Cell* **2018**, *173*, 879–893. [[CrossRef](#)]
40. Cohnheim, J. *Vorlesungen über Allgemeine Pathologie. Ein Handbuch für Ärzte und Studierende*; Hirschwald: Berlin, Germany, 1880.
41. Barry Pierce, G.; Johnson, L.D. Differentiation and cancer. *In Vitro* **1971**, *7*, 140–145. [[CrossRef](#)]
42. Pierce, G.B. The cancer cell and its control by the embryo. Rous-Whipple Award lecture. *Am. J. Pathol.* **1983**, *113*, 117–124.
43. Virchow, R.; Chance, F.; Goodsir, J.; Osborn, S.; King’s College London; Pathological Institute of Berlin; St. Thomas’s Hospital. *Cellular Pathology as Based upon Physiological and Pathological Histology*; Twenty Lectures Delivered in the Pathological Institute of Berlin during the Months of February, March, and April; John Churchill: London, UK, 1860.
44. Ērenpreisa, J.; Dālmāne, A.; Ērenpreiss, J. Jānis Oļģerts Ērenpreiss and his theory of carcinogenesis. *Acta Med. Hist. Rigensia Riga* **2000**, *25*, 281–285. [[CrossRef](#)]
45. Vinnitsky, V. The development of a malignant tumor is due to a desperate asexual self-cloning process in which cancer stem cells develop the ability to mimic the genetic program of germline cells. *Intrinsically Disord. Proteins* **2014**, *2*, e29997. [[CrossRef](#)]
46. Cofre, J.; Abdelhay, E. Cancer is to embryology as mutation is to genetics: Hypothesis of the cancer as embryological phenomenon. *Sci. World J.* **2017**, *2017*, 3578090. [[CrossRef](#)]
47. Chen, J.; Niu, N.; Zhang, J.; Qi, L.; Shen, W.; Donkena, K.V.; Feng, Z.; Liu, J. Polyploid giant cancer cells (PGCCs): The evil roots of cancer. *Curr. Cancer Drug Targets* **2019**, *19*, 360–367. [[CrossRef](#)]
48. Erenpreisa, J.; Cragg, M.S. Cancer: A matter of life cycle? *Cell Biol. Int.* **2007**, *31*, 1507–1510. [[CrossRef](#)]
49. Buikis, I.; Harju, L.; Freivalds, T. Origin of microcells in the human sarcoma cell line HT-1080. *Anal. Cell. Pathol.* **1999**, *18*, 73–85. [[CrossRef](#)]

50. Zhang, S.; Mercado-Uribe, I.; Xing, Z.; Sun, B.; Kuang, J.; Liu, J. Generation of cancer stem-like cells through the formation of polyploid giant cancer cells. *Oncogene* **2014**, *33*, 116–128. [[CrossRef](#)]
51. Kalejs, M.; Ivanov, A.; Plakhins, G.; Cragg, M.S.; Emzinsh, D.; Illidge, T.M.; Erenpreisa, J. Upregulation of meiosis-specific genes in lymphoma cell lines following genotoxic insult and induction of mitotic catastrophe. *BMC Cancer* **2006**, *6*, 6. [[CrossRef](#)]
52. Erenpreisa, J.; Cragg, M.S.; Salmina, K.; Hausmann, M.; Scherthan, H. The role of meiotic cohesin REC8 in chromosome segregation in γ irradiation-induced endopolyploid tumour cells. *Exp. Cell Res.* **2009**, *315*, 2593–2603. [[CrossRef](#)]
53. Ianzini, F.; Kosmacek, E.A.; Nelson, E.S.; Napoli, E.; Erenpreisa, J.; Kalejs, M.; Mackey, M.A. Activation of meiosis-specific genes is associated with depolyploidization of human tumor cells following radiation-induced mitotic catastrophe. *Cancer Res.* **2009**, *69*, 2296–2304. [[CrossRef](#)]
54. Erenpreisa, J.; Kalejs, M.; Cragg, M.S. Mitotic catastrophe and endomitosis in tumour cells: An evolutionary key to a molecular solution. *Cell Biol. Int.* **2005**, *29*, 1012–1018. [[CrossRef](#)]
55. Gorgoulis, V.G.; Zacharatos, P.; Mariatos, G.; Liloglou, T.; Kokotas, S.; Kastrinakis, N.; Kotsinas, A.; Athanasiou, A.; Foukas, P.; Zoumpourlis, V.; et al. Deregulated expression of *c-mos* in non-small cell lung carcinomas: Relationship with *p53* status, genomic instability, and tumor kinetics. *Cancer Res.* **2001**, *61*, 538–549.
56. Klymiuk, I.; Kenner, L.; Adler, T.; Busch, D.H.; Boersma, A.; Irmeler, M.; Fridrich, B.; Gailus-Durner, V.; Fuchs, H.; Leitner, N.; et al. In vivo functional requirement of the mouse *Ifitm1* gene for germ cell development, interferon mediated immune response and somitogenesis. *PLoS ONE* **2012**, *7*, e44609. [[CrossRef](#)]
57. Grell, K.G. Die Chromosomen von *Aulacantha scolymantha* Haeckel. *Arch. Protistenkd* **1953**, *99*, 1–54.
58. Raïkov, I.B. *The Protozoan Nucleus, Morphology and Evolution*; Springer: Wien, Austria, 1982.
59. Huskins, C.L. Chromosome multiplication and reduction in somatic tissues; their possible relation to differentiation, reversion and sex. *Nature* **1948**, *161*, 80–83. [[CrossRef](#)]
60. Walen, K. Normal human cells acquiring proliferative advantage to hyperplasia-like growth-morphology: Aberrant progeny cells associated with endopolyploid and haploid divisions. *Cancer Clin. Oncol.* **2013**, *2*. [[CrossRef](#)]
61. Walen, K.H. Neoplastic-like cell changes of normal fibroblast cells associated with evolutionary conserved maternal and paternal genomic autonomous behavior (Gonomy). *J. Cancer Ther.* **2014**, *5*, 860–877. [[CrossRef](#)]
62. Delhanty, J.D.; Handyside, A.H. The origin of genetic defects in the human and their detection in the preimplantation embryo. *Hum. Reprod. Update* **1995**, *1*, 201–215. [[CrossRef](#)]
63. Zernicka-Goetz, M.; Huang, S. Stochasticity versus determinism in development: A false dichotomy? *Nat. Rev. Genet.* **2010**, *11*, 743–744. [[CrossRef](#)]
64. Vanneste, E.; Voet, T.; Le Caignec, C.; Ampe, M.; Konings, P.; Melotte, C.; Debrock, S.; Amyere, M.; Vikkula, M.; Schuit, F.; et al. Chromosome instability is common in human cleavage-stage embryos. *Nat. Med.* **2009**, *15*, 577–583. [[CrossRef](#)]
65. Hansis, C. Analysis of Oct-4 expression and ploidy in individual human blastomeres. *Mol. Hum. Reprod.* **2001**, *7*, 155–161. [[CrossRef](#)]
66. Wolpert, L.; Beddington, R.; Jessell, T.; Lawrence, P.; Meyerowitz, E.; Smith, J. *Principles of Development*, 2nd ed.; Oxford University Press: Oxford, UK, 2002; Volume 77, p. 327.
67. Mayer, W.; Smith, A.; Fundele, R.; Haaf, T. Spatial separation of parental genomes in preimplantation mouse embryos. *J. Cell Biol.* **2000**, *148*, 629–634. [[CrossRef](#)]
68. Illidge, T.; Cragg, M.; Fringe, B.; Olive, P.; Erenpreisa, J. Polyploid giant cells provide a survival mechanism for p53 mutant cells after DNA damage. *Cell Biol. Int.* **2000**, *24*, 621–633. [[CrossRef](#)]
69. Erenpreisa, J.A.; Cragg, M.S.; Fringes, B.; Sharakhov, I.; Illidge, T.M. Release of mitotic descendants by giant cells from irradiated Burkitt's lymphoma cell line. *Cell Biol. Int.* **2000**, *24*, 635–648. [[CrossRef](#)]
70. Erenpreisa, J.; Kalejs, M.; Ianzini, F.; Kosmacek, E.A.; Mackey, M.A.; Emzinsh, D.; Cragg, M.S.; Ivanov, A.; Illidge, T.M. Segregation of genomes in polyploid tumour cells following mitotic catastrophe. *Cell Biol. Int.* **2005**, *29*, 1005–1011. [[CrossRef](#)]
71. Erenpreisa, J.; Cragg, M.S.; Anisimov, A.P.; Illidge, T.M. Tumor cell embryonicity and the ploidy number 32n: Is it a developmental checkpoint? *Cell Cycle* **2011**, *10*, 1873–1874. [[CrossRef](#)]

72. Weihua, Z.; Lin, Q.; Ramoth, A.J.; Fan, D.; Fidler, I.J. Formation of solid tumors by a single multinucleated cancer cell. *Cancer* **2011**, *117*, 4092–4099. [[CrossRef](#)]
73. Mirzayans, R.; Andrais, B.; Murray, D. Roles of polyploid/multinucleated giant cancer cells in metastasis and disease relapse following anticancer treatment. *Cancers* **2018**, *10*, 118. [[CrossRef](#)]
74. Rosenbusch, B.E. Mechanisms giving rise to triploid zygotes during assisted reproduction. *Fertil. Steril.* **2008**, *90*, 49–55. [[CrossRef](#)]
75. Kalatova, B.; Jesenska, R.; Hlinka, D.; Dudas, M. Tripolar mitosis in human cells and embryos: Occurrence, pathophysiology and medical implications. *Acta Histochem.* **2015**, *117*, 111–125. [[CrossRef](#)]
76. Schwarz-Finsterle, J.; Scherthan, H.; Huna, A.; González, P.; Mueller, P.; Schmitt, E.; Erenpreisa, J.; Hausmann, M. Volume increase and spatial shifts of chromosome territories in nuclei of radiation-induced polyploidizing tumour cells. *Mutat. Res.* **2013**, *756*, 56–65. [[CrossRef](#)]
77. Macville, M.; Schröck, E.; Padilla-Nash, H.; Keck, C.; Ghadimi, B.M.; Zimonjic, D.; Popescu, N.; Ried, T. Comprehensive and definitive molecular cytogenetic characterization of HeLa cells by spectral karyotyping. *Cancer Res.* **1999**, *59*, 141–150.
78. Erenpreisa, J.; Ivanov, A.; Wheatley, S.P.; Kosmacek, E.A.; Ianzini, F.; Anisimov, A.P.; Mackey, M.; Davis, P.J.; Plakhins, G.; Illidge, T.M. Endopolyploidy in irradiated p53-deficient tumour cell lines: Persistence of cell division activity in giant cells expressing Aurora-B kinase. *Cell Biol. Int.* **2008**, *32*, 1044–1056. [[CrossRef](#)]
79. Ghosh, S.; Ghosh, I. Variation of stemline karyotype in a HeLa cell line. *Z. Krebsforsch. Klin. Onkol.* **1975**, *84*, 129–133. [[CrossRef](#)]
80. Ianzini, F.; Mackey, M.A. Development of the large scale digital cell analysis system. *Radiat. Prot. Dosim.* **2002**, *99*, 289–293. [[CrossRef](#)]
81. Erenpreisa, J.; Salmina, K.; Huna, A.; Kosmacek, E.A.; Cragg, M.S.; Ianzini, F.; Anisimov, A.P. Polyploid tumour cells elicit paradiplod progeny through depolyploidizing divisions and regulated autophagic degradation. *Cell Biol. Int.* **2011**, *35*, 687–695. [[CrossRef](#)]
82. Kröger, C.; Afeyan, A.; Mraz, J.; Eaton, E.N.; Reinhardt, F.; Khodor, Y.L.; Thiru, P.; Bierie, B.; Ye, X.; Burge, C.B.; et al. Acquisition of a hybrid E/M state is essential for tumorigenicity of basal breast cancer cells. *Proc. Natl. Acad. Sci. USA* **2019**, *116*, 7353–7362. [[CrossRef](#)]
83. Navin, N.E. The first five years of single-cell cancer genomics and beyond. *Genome Res.* **2015**, *25*, 1499–1507. [[CrossRef](#)]
84. Pera, F.; Schwarzacher, H.G. Die Verteilung der Chromosomen auf die Tochterzellkerne multipolarer Mitosen in euploiden Gewebekulturen von *Microtus agrestis*. *Chromosoma* **1969**, *26*, 337–354. [[CrossRef](#)]
85. Palitti, F.; Rizzoni, M. Pattern of DNA segregation in multipolar anelophases of different ploidy in euploid and aneuploid mammalian cells cultivated in vitro. *Genetica* **1972**, *43*, 130–147.
86. Pera, F.; Rainer, B. Studies of multipolar mitoses in euploid tissue cultures. I. Somatic reduction to exactly haploid and triploid chromosome sets. *Chromosoma (Berl.)* **1973**, *42*, 71–86. [[CrossRef](#)]
87. Rizzoni, M.; Palitti, F.; Perticone, P. Euploid segregation through multipolar mitosis in mammalian cell cultures. Identification of triploid, haploid, and segregating diploid cells in a diploid-euploid primary culture of rhesus kidney cells. *Chromosoma* **1974**, *45*, 151–162. [[CrossRef](#)]
88. Pera, F.; Scholz, P. Polyploidization in vitro: Formation of a predominantly triploid cell population in an originally diploid tissue culture of *Microtus agrestis*. *Hum. Genet.* **1974**, *21*, 17–26. [[CrossRef](#)]
89. Cho, H.; Noh, K.H.; Chung, J.-Y.; Takikita, M.; Chung, E.J.; Kim, B.W.; Hewitt, S.M.; Kim, T.W.; Kim, J.-H. Synaptonemal complex protein 3 is a prognostic marker in cervical cancer. *PLoS ONE* **2014**, *9*, e98712. [[CrossRef](#)]
90. Vitale, I.; Senovilla, L.; Jemaà, M.; Michaud, M.; Galluzzi, L.; Kepp, O.; Nanty, L.; Criollo, A.; Rello-Varona, S.; Manic, G.; et al. Multipolar mitosis of tetraploid cells: Inhibition by p53 and dependency on Mos. *EMBO J.* **2010**, *29*, 1272–1284. [[CrossRef](#)]
91. Stewenius, Y.; Gorunova, L.; Jonson, T.; Larsson, N.; Høglund, M.; Mandahl, N.; Mertens, F.; Mitelman, F.; Gisselsson, D. Structural and numerical chromosome changes in colon cancer develop through telomere-mediated anaphase bridges, not through mitotic multipolarity. *Proc. Natl. Acad. Sci. USA* **2005**, *102*, 5541–5546. [[CrossRef](#)]
92. Gisselsson, D.; Håkanson, U.; Stoller, P.; Marti, D.; Jin, Y.; Rosengren, A.H.; Stewenius, Y.; Kahl, F.; Panagopoulos, I. When the genome plays dice: Circumvention of the spindle assembly checkpoint and near-random chromosome segregation in multipolar cancer cell mitoses. *PLoS ONE* **2008**, *3*, e1871. [[CrossRef](#)]

93. Gisselsson, D.; Jin, Y.; Lindgren, D.; Persson, J.; Gisselsson, L.; Hanks, S.; Sehic, D.; Mengelbier, L.H.; Øra, I.; Rahman, N.; et al. Generation of trisomies in cancer cells by multipolar mitosis and incomplete cytokinesis. *Proc. Natl. Acad. Sci. USA* **2010**, *107*, 20489–20493. [[CrossRef](#)]
94. Lin, H.; Yue, L.; Spradling, A.C. The *Drosophila* fusome, a germline-specific organelle, contains membrane skeletal proteins and functions in cyst formation. *Development* **1994**, *120*, 947–956.
95. Ye, C.J.; Regan, S.; Liu, G.; Alemara, S.; Heng, H.H. Understanding aneuploidy in cancer through the lens of system inheritance, fuzzy inheritance and emergence of new genome systems. *Mol. Cytogenet.* **2018**, *11*, 31. [[CrossRef](#)]



© 2019 by the authors. Licensee MDPI, Basel, Switzerland. This article is an open access article distributed under the terms and conditions of the Creative Commons Attribution (CC BY) license (<http://creativecommons.org/licenses/by/4.0/>).

3.2. In normal tissues, polyploidy is associated with developmental bivalent gene activation, an atavistic reversal to an evolutionarily ancient phenotype, circadian deregulation, and carcinogenic pathways

The main focus of this manuscript was to bioinformatically assess the impact of polyploidy on the normal transcriptome, and then explore the findings in the context of two phenomena inherent to cancer development and evolution: atavistic shifts (Trigos et al., 2017; Vinogradov, 2010) and the activation of bivalent genes - a largely embryogenesis-related subgroup of genes with both activating and repressive histone modifications that enable rapid activity modulation and epigenetic plasticity (Bernhart et al., 2016; Zaidi et al., 2017).

The differentially expressed genes identified in normal endopolyploid human and mouse organs via a combination of cross-species differential gene expression analysis and PCA revealed that even in normal tissues, polyploidy enables atavistic transformation to a more ancient phenotype, associated with activation of bivalent genes that largely originated in ancient phylostratigraphic categories (phylostrata) and enable rapid cell fate switching. Furthermore, polyploidy was shown to upregulate oncogenes, downregulate tumor suppressor genes, activate the bivalent interactome of the key oncogene and cell fate regulator c-Myc, and suppress circadian clock function. Overall, these findings suggest that polyploidy alone may be sufficient to create an environment that would benefit cancer development.



Article

Phylostratic Shift of Whole-Genome Duplications in Normal Mammalian Tissues towards Unicellularity Is Driven by Developmental Bivalent Genes and Reveals a Link to Cancer

Olga V. Anatskaya ^{1,*}, Alexander E. Vinogradov ^{1,*}, Ninel M. Vainshelbaum ^{2,3},
Alessandro Giuliani ⁴ and Jekaterina Erenpreisa ^{2,*}

¹ Department of Bioinformatics and Functional Genomics, Institute of Cytology, Russian Academy of sciences, 194064 St. Petersburg, Russia

² Department of Oncology, Latvian Biomedical Research and Study Centre, Cancer Research Division, LV-1067 Riga, Latvia; ninela.vainshelbaum@biomed.lu.lv

³ Faculty of Biology, University of Latvia, LV-1586 Riga, Latvia

⁴ Istituto Superiore di Sanità, 00161 Rome, Italy; alessandro.giuliani@iss.it

* Correspondence: olga.anatskaya@gmail.com (O.V.A.); aevin@incras.ru (A.E.V.); katrina@biomed.lu.lv (J.E.)

† These authors equally contributed to this work.

Received: 24 September 2020; Accepted: 17 November 2020; Published: 19 November 2020



Abstract: Tumours were recently revealed to undergo a phylostratic and phenotypic shift to unicellularity. As well, aggressive tumours are characterized by an increased proportion of polyploid cells. In order to investigate a possible shared causation of these two features, we performed a comparative phylostratigraphic analysis of ploidy-related genes, obtained from transcriptomic data for polyploid and diploid human and mouse tissues using pairwise cross-species transcriptome comparison and principal component analysis. Our results indicate that polyploidy shifts the evolutionary age balance of the expressed genes from the late metazoan phylostrata towards the upregulation of unicellular and early metazoan phylostrata. The up-regulation of unicellular metabolic and drug-resistance pathways and the downregulation of pathways related to circadian clock were identified. This evolutionary shift was associated with the enrichment of ploidy with bivalent genes ($p < 10^{-16}$). The protein interactome of activated bivalent genes revealed the increase of the connectivity of unicellulars and (early) multicellulars, while circadian regulators were depressed. The mutual polyploidy-*c-MYC*-bivalent genes-associated protein network was organized by gene-hubs engaged in both embryonic development and metastatic cancer including driver (proto)-oncogenes of viral origin. Our data suggest that, in cancer, the atavistic shift goes hand-in-hand with polyploidy and is driven by epigenetic mechanisms impinging on development-related bivalent genes.

Keywords: polyploidy; unicellularity; early multicellularity; embryonality; cancer; bivalent genes; viral-origin oncogenes

1. Introduction

Whole-genome duplications (WGD) and recurrent polyploidization, providing a source for gene divergence and adaptability to environmental changes, are central in the evolution of biodiversity [1–3]. Polyploid cells are also present in the tissues of vertebrates: in humans and other mammals, cells with multiplied genomes appear during normal organogenesis of definitive and provisional organs (placenta, heart, brain, liver, skin, blood) [4–10]. Polyploidy also arises in response to stress, wounding, and in cancer [11–18].

The relationship between polyploidy and stemness, both found as typical features of aggressive tumours [19–22], may be associated with the re-activation of evolutionarily ancient programs. The observations show that malignant cells often acquire the phenotypes and reproductive behaviour of unicellular organisms through transient polyploidy “life-cycle”, which is reciprocally linked with a cell cycle [23–27]. This behaviour is characteristic for cancer cells resistant to therapeutic treatments [28].

The atavistic theory of oncogenesis suggests that cancer is a reversal from a multicellular to a unicellular state [7,29–33]. The two giant clusters were revealed in the human coexpression gene network (also based on bulk tissue analysis): a widely expressed cluster enriched in genes of unicellular origin enriching the cancer tissues and the other giant cluster of multicellular genes [34,35]. Phylostratigraphic tracking of the genes involved in cancer [36] suggests their link to the emergence of multicellularity in metazoan, many cancer genes have a viral origin and even the typical somatic mutations of the cancer genes can be traced as ancestral [37].

In turn, the studies of Trigos and colleagues [38,39] also showed that the genes of unicellular origin are overexpressed in human cancers as compared to their normal counterpart tissues, whereas the genes appearing at multicellular stages of evolution were downregulated. Moreover, in tumours, the interaction between the unicellularity and multicellularity gene networks is weakened [38,40].

The upregulation of the unicellular giant cluster in cancer cells was shown in the single-cells transcriptomes of various cancer types and in invasive as compared with non-invasive cancer [35,41]. These two clusters can be defined as “echoing” a proper dynamical attractor given, strictly speaking, they are not mutually exclusive (both in cancer and normal cell genes from both clusters are activated). The prevalence of ancient unicellular state of cancer cells with respect to normal tissue corresponds to a partial “going back” to the more ancient unicellular pattern preceding the rise of multicellularity. This implies we do not expect that cancer cells become ‘identical to unicellular organism’ but that lose some phenotypic characters essential for the existence of an organized tissue like contact inhibition, the crucial role played by shape changes in cancer development is consistent with this view [42,43].

The epigenetic mechanisms favouring transition to unicellularity and cancerogenesis and, thus, the proposed evolution reversal of human cancer cells remain unclear. Since oncogenesis is frequently associated with polyploidy [2,26,44–47], we suggested the involvement of polyploidy in this process and addressed here the phylostratigraphy and protein networks of the genes differentially expressed in polyploid versus diploid tissues.

We choose this approach, because mammalian homologous tissues differ by cell ploidy levels [1,2,5,8,12]. Some species have predominantly polyploid heart and diploid liver (pig and primates), whereas others possess mainly polyploid liver and predominantly diploid heart (rodents) [1,5,8]. Here, we rely on this fact to generate a balanced factorial design with a criss-cross distribution of ploidy/tissue across human and mouse that allows to separate ploidy effect from both tissue and species influences (see Methods).

To promote understanding of the epigenetic nature of ploidy-associated gene regulation, we also investigated how polyploidy influences the expression of bivalent genes. Bivalent genes are characterized by epigenetic ambiguity, bearing in their promoters or enhancers two opposite epigenetic modifications of the histone H3, the repressing H3K27me3 and the activating H3K4me3, poised for transcription but capable for its rapid activation. These poised genes were established in embryonic stem cells [48,49] and are the main players in the early and post-implantation development and cell fate change. Changes of bivalent chromatin coincide with the increased expression of developmental genes in cancer and are also likely involved there in the epigenetic changes [50–55]. On a more general ground the notion of cancer as ‘development gone awry’ supports the focus on such genes [56].

The obtained results indicate that polyploidy activates unicellular metabolic pathways and ancient programs of development related to carcinogenesis. This evolutionary retour is accompanied by the activation of bivalent genes and deregulation of circadian rhythms. Altogether, these results provide evidence that polyploidy is an important driver of epigenetic changes linked to cancer that may reorganize gene regulatory networks.

2. Results

2.1. Polyploidy Causes Transition of Gene Phylostratic Balance towards Evolutionary Old Unicellular Phylostrata

To find out whether polyploidy affects the expression of genes of various evolutionary ages, we first applied pairwise cross-species transcriptome comparison to polyploid vs. diploid organs in human and mouse (human heart vs. mouse heart and mouse liver vs. human liver). Then we evaluated the effects of polyploidy at various thresholds of the expression difference. This evaluation gave 584 upregulated and 711 downregulated genes at two-fold difference and 1028 upregulated and 887 downregulated genes at a 1.3-fold difference (Tables S1 and S2).

Phylostratic distribution of ploidy-associated genes was analysed by grouping genes according to their age of evolutionary origin taken from [38]. Our data indicated that polyploidy is associated with the upregulation of ancient genes originating in unicellular ancestors (1-3 phylostrata) and the downregulation of genes starting with phylostratum 6 (Bilateria) and onwards, while the early multicellularity strata 4–5 (Metazoa and Eumetazoa) did not reveal a clear difference (Figure 1A,B).

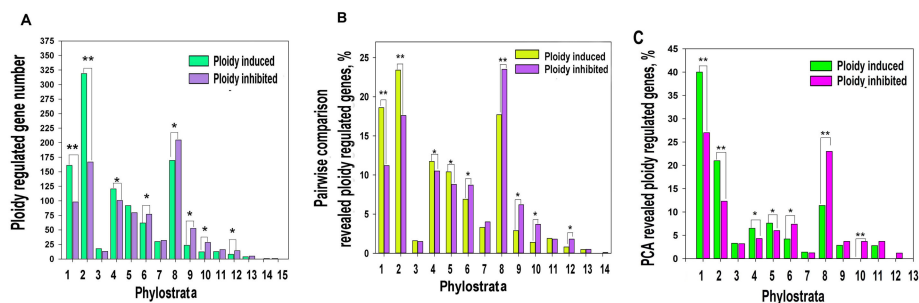


Figure 1. Ploidy associated gene distribution across evolutionary phylostrata. Phylostratigraphy of ploidy associated genes revealed by pairwise cross-species (criss-cross) comparison (A,B) and by PCA (C). This figure illustrates that polyploidy shifts the gene age balance of expressed genes from metazoan phylostrata (6–16, Bilateria and later) towards unicellular phylostrata (1–3) via transitional early metazoan phylostrata (4–5) * $p < 0.05$ for the difference, ** $p < 0.01$ for the difference. Gene expression difference above two-fold. The phylostrata are as follows: 1—cellular organisms, 2—Eukaryota, 3—Opisthokonta, 4—Metazoa, 5—Eumetazoa, 6—Bilateria, 7—Chordata, 8—Euteleostomi, 9—Amniota, 10—Mammalia, 11—Theria, 12—Eutheria, 13—Euarchontoglires, 14—Catarrhini, 15—Homininae.

To verify this result with a well-known traditional approach, we applied principal component analysis (PCA). PCA identified 103 upregulated and 96 downregulated genes having above two standard deviations. Of these genes, 78 and 87 genes demonstrated a more than two-fold expression difference (Tables S1 and S2). With excluding the tissue-specific component, the phylostratic distribution of PCA-revealed genes also indicated the activation by polyploidy of evolutionarily conserved programs (genes from phylostrata 1–3) and the suppression of young programs maintaining multicellularity (phylostrata 6–13, Figure 1C). The phylostrata 4–5 were up-regulated.

2.2. Polyploidy Activates Recapitulation of Evolutionary Developmental Programs Associated with Carcinogenesis

To investigate the functional consequences of ploidy-associated phylostrata rearrangement at the gene module level, we performed gene module enrichment analysis for genes with more than two-fold expression difference between polyploid vs. diploid organs. The results are presented in Table S3. For unicellular phylostrata (1–3) the main effects of polyploidy were the induction of modules related to drug ABC pump and drug metabolism (hsa02010;GO:0017144), protein and ribosome synthesis (hsa01230;hsa03010), oxidation-reduction (GO:0055114) and energy metabolism

(both aerobic respiration and carbohydrate metabolism (GO:0019752; GO:0008152; GO:0044262; hsa00051). This picture is seen from the higher significance of enrichment and the larger gene number for upregulated genes than for downregulated ones. For the up-regulated by polyploidy early metazoan phylostrata (4–5) our data reveal the upregulation of modules related to embryonic development (GO:0009790), stem cell commitment (GO:0045165), pluripotency (hsa04550) and Kegg pathways of carcinogenesis (hsa05200; hsa05205). The phylostrata 6–8 were down-regulated by polyploidy. They are involved in the development of the multicellular organism complexity. The downregulated genes of the 6–8 strata were mostly enriched in biological processes related to immunity (GO:0002682), inflammation (GO:0050727) and communication (GO:0010646) that are the specific biological features of multi-cellularity. Consistently, multicellular phylostrata (10–15, i.e., Mammalia and later) were not enriched for gene modules depending on polyploidy.

The results of functional enrichment of PCA-ploidy-revealed genes for old phylostrata were consistent with the results of pair-wise cross-species comparison (Table S4). Thus, the carcinogenesis pathways favoured by polyploidy appear in the early metazoan (strata 4–5) in one pack with embryogenesis and cell fate change (stemness commitment), associated with asexual reproduction.

Similar changes in the general phylostratigraphic landscape shifted towards unicellularity found here for polyploidy were previously shown for tumorigenesis as such [38]. The authors also paid attention to the enrichment of the intermediate between unicellularity and multicellularity phylostrata with cancer driver genes [40]. In comparison with our data, this similarity suggests that polyploidy may favour the epigenetic evolutionary shift of normal cells to cancer. The interactome of *c-MYC* proto-oncogene provides a useful link to verify this suggestion because *c-MYC* is an important regulator of both ploidy and cancer.

2.3. *c-MYC* Induction Drives Polyploidy-Associated Transcriptomic Changes towards Unicellularity

c-MYC is a regulator of the normal cell cycle. However, when over-expressed it disjoins replication from cell division and favours polyploidy [57,58]. Moreover, while the overexpressed non-mutant (often amplified) *c-MYC* is a powerful reprogramming factor and oncogene, its downregulation in transgenic mice causes tumour regression [59–62].

The pleiotropic *c-MYC* is capable to drive the opposite processes, proliferation versus apoptosis and is acting as a master activator of the bivalent genes involved in the epigenetic regulation of development [60,63–65].

Here we evaluated the phylostratic distribution of ploidy-dependent *c-MYC* -interacting genes at two-fold expression difference (Tables S5 and S6) and explored its link through polyploidy with bivalent genes (Figure 2). The data on ploidy -Myc-ploidy-related gene phylostratigraphic changes repeat the ploidy-dependent relationships (compare with Figure 1)

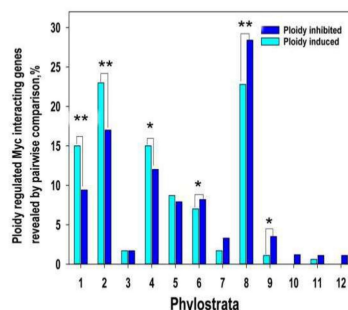


Figure 2. Ploidy associated *c-MYC* interacting gene distribution across evolutionary phylostrata. This figure illustrates that *c-MYC* -interacting genes repeat pattern of all ploidy related gene age distribution. Gene age is shifted from young multicellular phylostrata (6–16) towards unicellular phylostrata (1–3 phylostrata) via transitional metazoan phylostrata (4–5). * $p < 0.05$ for the difference, ** $p < 0.01$. Gene expression difference is above two-fold.

It is clear that the non-mutant *c-MYC* should elaborate these effects in the epigenetic modus. Therefore, we paid attention to the fact that *c-MYC* controls gene transcription by activating bivalent genes.

2.4. The Phylostratigraphic Polyploidy-Associated Effect of *c-MYC* Is Associated with the Regulation of Bivalent Genes

The genome-wide studies indicate that the overexpressed *c-MYC* demethylates the H3K27me3 repressive domain of bivalent genes and thereby switches these genes to the active state [63,64], it also activates Polymerase II paused in bivalent genes [53]. To find out whether overexpressed Myc also increases expression of ploidy-related bivalent genes, we first identified these genes among ploidy-regulated *c-MYC* interacting genes with expression difference above two-fold. Genes of interest were identified using the list of bivalent genes in human embryonic stem cells [54]. Our data identified 60 bivalent genes of 161 ploidy-upregulated Myc interactants and 27 bivalent genes among 101 ploidy-downregulated *c-MYC* interactants (Figure 3A,B, Tables S7 and S8).

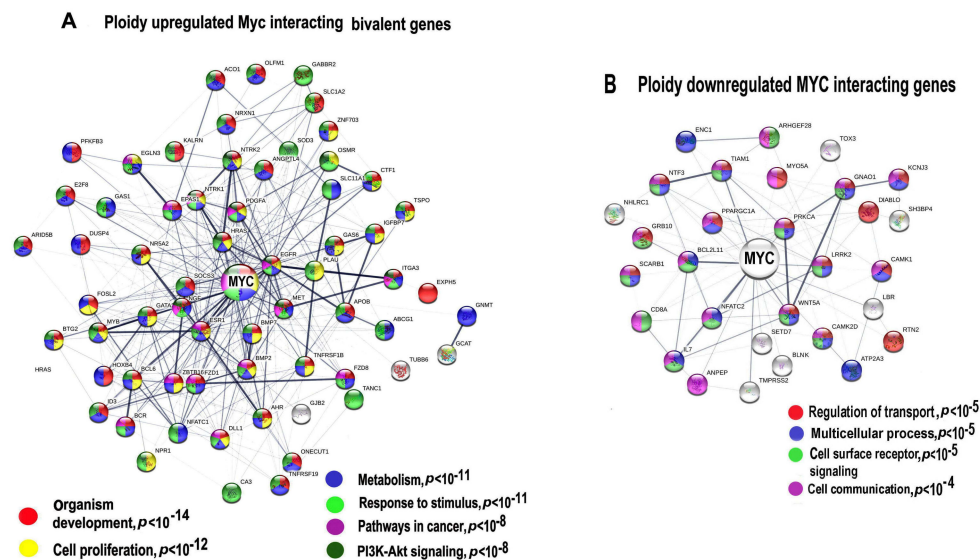


Figure 3. Protein interaction networks (PPIs) for ploidy associated *c-MYC*-interacting bivalent genes. PPI for upregulated (A) and downregulated (B) genes. Gene expression difference is above two-fold. The networks are constructed with server String. Gene pathway enrichment was found using the same server.

Protein interaction network presented in Figure 3A indicates the Myc interacting and ploidy upregulated bivalent genes. Gene module functional enrichment analysis indicated that these genes are enriched in pathways of development, proliferation, stress response, and pathways in cancer with high significance. Figure 3B that presents *c-MYC* interacting ploidy downregulated genes shows that the cell surface-mediated functions (transport, reception, communication) are downregulated.

It is important to note that the network for the upregulated bivalent genes shows higher connectivity (13.5 connection per a node) compared to the downregulated genes (only 5.13 connections per a node), which implies that *c-MYC* and polyploidy-induced activity of bivalent genes considerably increases epigenetic plasticity of protein interaction network. It should be noted that the overexpressed functional pack again included a tandem of development and carcinogenesis modules, which we have found in the ploidy-related gene phylostratigraphic analysis. Therefore, we decided to extend the investigation of bivalent genes in relation to ploidy and gene phylostrata through the entire transcriptome.

2.5. Ploidy-Associated Genes Are Enriched in Bivalent Genes of the Entire Genome, Prevailing among Unicellular and Eumetazoan Phylostrata.

We compared the genes with above two-fold expression difference dependent on polyploidy (vs. diploidy) with bivalent genes in human embryonic stem cells [54]. Among the 584 up and 711 downregulated by ploidy genes (Tables S1 and S2) we found 267 (45.7%) and 222 (31.6%) of up-and down-regulated bivalent genes, respectively (Tables S9 and S10). The results of the binomial test indicate that bivalent genes enrich ploidy-upregulated genes compared to the entire transcriptome (3024 vs. 14093) with high significance ($p < 10^{-16}$ binomial test). For the downregulated genes the significance was $p < 10^{-8}$ (for 21.3 vs. 31.2%), respectively. These results indicate that polyploidy mostly induced bivalent genes.

The percentage of phylostratigraphic distribution of ploidy associated bivalent and common genes is shown in Figure 4. The bivalent genes, comprising ~21% of the human genome, originated in evolution in all phylostrata but in the larger proportion with development of multicellularity, from phylostratum 4 (Metazoa) to 8 (Euteleostomi). The distribution of the expression of the ploidy upregulated bivalent genes by phylostrata is different from that for all bivalent genes. It is clearly seen that these genes repeat the general effect of all ploidy-regulated genes and *c-MYC*-ploidy regulated genes. Among the ploidy upregulated bivalent genes prevail the proportions of phylostrata 1 (Prokaryota) to 5 (Eumetazoa). Proportions of phylostrata 6 and 7 (Bilateria and Chordata) are ambivalent. Proportions of phylostrata 8 (Euteleostomi) to 10 (Mammalia) show clear decrease (Figure 4). The ploidy downregulated bivalent genes generally repeat the pattern for all bivalent genes.

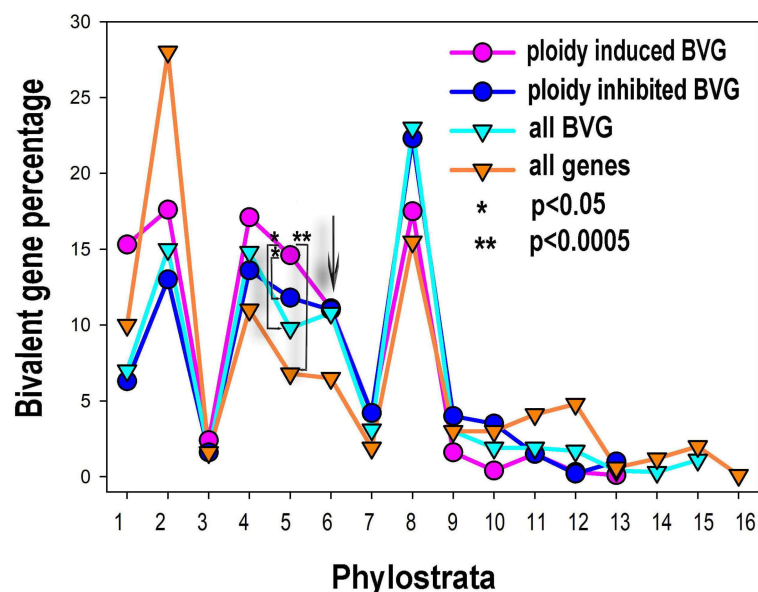


Figure 4. The percentual proportions of gene origins and distribution of bivalent genes (BVG) in the phylostratic tree of life (strata 1–16) and the effect of polyploidy on it. The upregulation of bi-valent genes by polyploidy includes strata 1, 2 (unicellularians), stratum 4 (metazoa) and, prominently, stratum 5 (eumetazoa—the appearance of embryo, germ layer, and gastrulation). The arrowed cross-point starting down-regulation of bivalent genes by polyploidy in late metazoa falls upon stratum 6 (bilateria).

2.6. Protein Interaction Networks for Ploidy-Associated Bivalent Genes Are Involved in the Upregulation of the Developmental and Carcinogenesis Genes and the Downregulation of the Networks Related to Differentiation Biological Quality and Circadian Clock

We constructed protein interaction networks (PPIs) for ploidy up- and downregulated bivalent genes marked with H3K27me3 and H3K4me3 in human ESC using the String server. We also included *c-MYC* that is not a bivalent gene, but it is of particular interest because this important oncogene is an inducer of bivalent genes [64]. The networks were constructed for genes with above two-fold expression

difference. Then we extracted the whole connected component from the up- and downregulated networks and clustered them using the same server. For the upregulated genes the network contains 165 bivalent of 267 ploidy upregulated bivalent genes (62%). For the ploidy downregulated bivalent genes it contains 63 genes of 222 (24%). As in the case of *c-MYC*, the striking difference in gene numbers of the connected components of up- and downregulated networks (163 vs. 63) by bivalent genes in the whole transcriptome, despite approximately the same numbers of up- and downregulated genes, shows that the upregulated by ploidy bivalent genes create essentially more functional connections and master regulators compared to the downregulated genes. Below we provide a functional description of the up and downregulated PPIs (Figure 5A,B). It is clearly seen that the upregulated network contains more hub regulators than the downregulated network (29 vs. 13).

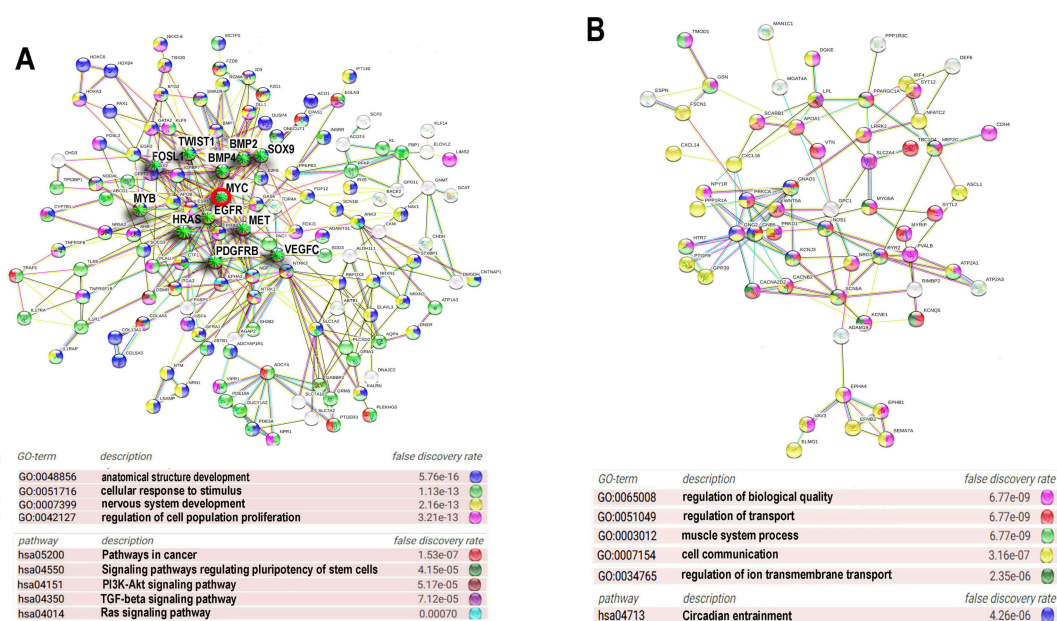


Figure 5. Protein interaction networks for ploidy associated bivalent genes. The most connected components of protein interaction networks of upregulated (A) and downregulated (B) bivalent genes constructed using STRING server. Gene expression difference is above two-fold. Gene module analysis and node degree evaluation was done using the same server. The titles of GO biological processes are given with false discovery rate. The important drivers of carcinogenesis are marked with green asterisks. Myc oncogene is marked with a red circle.

The PPI for the ploidy upregulated bivalent genes (Figure 5A) is enriched in the GO biological processes related to the development of anatomical structures (GO:0048856) and the nervous system (GO:007399), proliferation (GO:0042127), response to stress and stimulus (GO:0051716), and in KEGG pathways involved in the regulation of pluripotency (hsa04550), pathway of carcinogenesis (hsa05200) and several pro-carcinogenic and development related pathways, including *PI3K-AKT* (hsa04151) *TGFβ* (hsa04350) and *RAS* (hsa04014) signalling pathways (Figure 5A). It is important to note that this PIN unifies proteins involved both in development and metastatic cancer that comprise dense functional nucleus of the induced network and are the hub proteins with high degree of connectivity originating from 1–6 phylostrata genes (Table 1). The PPI for the downregulated genes is enriched for GO biological processes participating in transport (GO:0051049, GO:0034765), cell communication (GO:0007154), regulation of biological quality (GO:0065008), muscle system processes (GO:0003012) and circadian entrainment (hsa04713). Thus, the functional picture provided by PPI for the upregulated genes indicates that ploidy-related bivalent genes are associated with the induction of embryonic developmental programs including drivers of carcinogenesis (Figure 5A, Table 1). PPI for the downregulated genes illustrates the depression of circadian clocks.

Table 1. Characteristics of the central hubs of Myc-related network of proteins encoded by bivalent genes upregulated by polyploidy (presented in Figure 5A).

Gene/ Protein	Folds Up-Regulation	Number of Connections	Phylo Stratum	Function Involvement in Cancer	References
<i>BMP4</i>	3.24	26	4	Development, cell motility, oncogene	[66]
<i>BMP2</i>	3.84	14	5	Development, cell motility, oncogene	[67]
<i>c-MYC</i>	3.2	29	3	Stemness, proliferation, apoptosis, polyploidy induction, driver oncogene	[68]
<i>MET</i>	3.7	15	6	Embryonic development, proliferation; when mutationally activated is involved in multiple cancers	[69]
<i>MYB</i>	3.8	8	2	Development of colon epithelial progenitors, high in gastric, colon, and breast cancer	[70]
<i>HRAS</i>	3.6	19	1	Proliferation, senescence, germ development, driver oncogene	[71,72]
<i>EGFR</i>	4.94	34	6	Epithelium development, driver oncogene	[73]
<i>PDGFRB</i>	2.23	15	6	Development, cancer-related angiogenesis	[74]
<i>VEGFC</i> (C)	2.88	12	5	Blood vessels development, cancer-related angiogenesis	[74]
<i>SOX9</i>	3.86	15	4	Germ (male) and skeleton development	[75]
<i>TWIST1</i>	2.53	11	2	Mesoderm development, motility, metastatic cancer	[76]
<i>FOSL1</i>	2.19	11	5	Early stress response, reinforces Myc, oncogenesis	[77]

2.7. The Relation of Cancer Driver Genes to Polyploidy, Bivalency and Their Phylostratigraphic Origin

To obtain more evidence concerning features of carcinogenesis, we evaluated the expression of tumour suppressors and oncogenes in relation to polyploidy based on the list from [78]. The obtained data presented in Figure 6, together with phylostratic origin of genes, indicates that polyploidy is associated with preferential downregulation of tumour suppressors and strong upregulation of many oncogenes. It is important to note that the upregulated oncogenes were more strongly enriched with bivalent genes than the downregulated oncogenes and tumour suppressors ($p < 0.02$ for all comparisons, binomial test). The notably down-regulated by polyploidy tumour suppressors belong to DNA damage response: *ATR*, (2nd phylostratum), *ATR* (2nd), *CHEK2* (2nd), *CHEK1* (3rd), *TP53* (5th)—however, its protein inhibitor *MDM2* (seen in the column for oncogenes) is also inhibited; apoptosis executor Fas, prominent tumour suppressor *PTEN* (2nd) and the E-cadherin-associated gene *CDH1* (8th phylostratum). Thus, cell communication is suppressed by polyploidy, while cells become more tolerant to DNA damage and inhibit apoptosis.

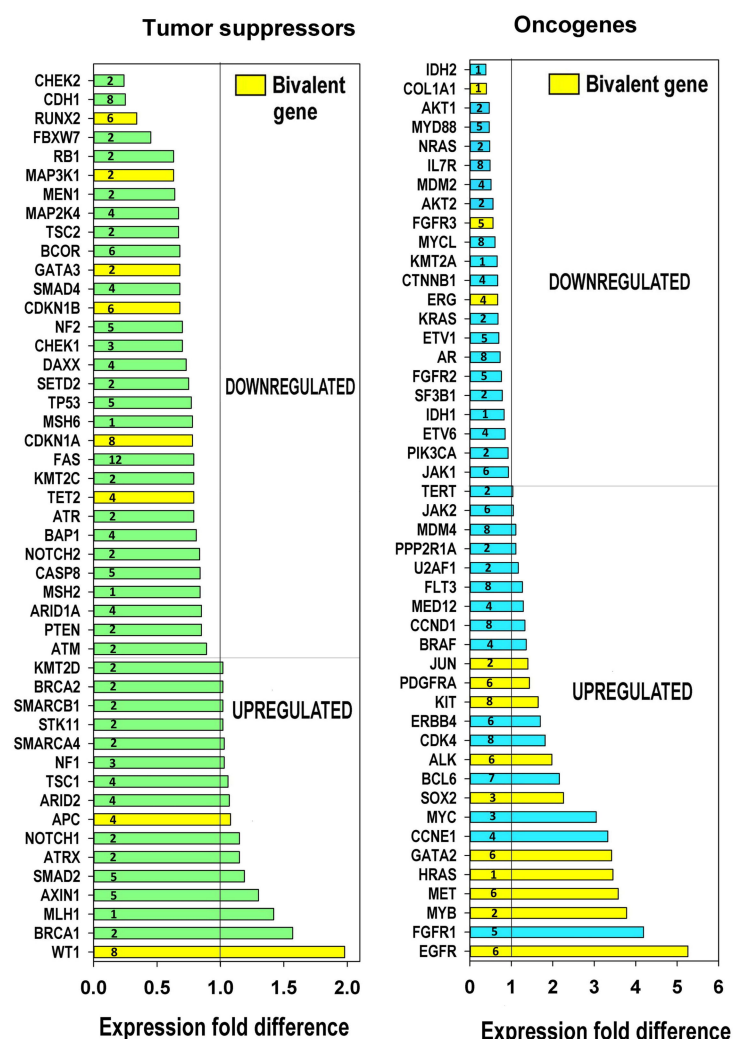


Figure 6. Ploidy associated tumor suppressors and oncogenes. This figure illustrates the downregulation of tumour suppressors, the upregulation of oncogenes and the enrichment of the induced oncogenes with bivalent genes $p < 0.05$, binomial test. The phylostrata numbers of gene evolutionary origins are indicated.

Among the prominent oncogenes upregulated by polyploidy, we find a master transcription factor (TF) of early stress response Jun (2nd phylostratum), *KIT*-tyrosine-protein-kinase (6th); among 3–5-fold upregulated oncogenes, we see *GATA 2* TF (6th) responsible for embryonic development, *c-MYC* TF (3rd, viral origin); *MYB* TF (2nd, viral origin); *MET* Tyrosin-protein-kinase (6th)—often a target for avian leukemia retrovirus [79] *HA-RAS* G-protein (1st phylostratum, viral origin)—the most common oncogene in at least 30% of all tumours and, finally, its upstream regulator *EGFR* (6th); both are bivalent (Table S9).

Clearly, in this analysis, we have used the transcriptome data from polyploid tissues, where the activated protooncogenes were not mutated. In addition to their relation to bivalency and embryonic development, we see that the main tumour suppressor *TP53* and strong oncogene *EGFR* belong to the intermediate phylostrata 5–6, while many important driver oncogenes of this list activated by polyploidy are from the earliest evolutionary phylostrata. Furthermore, the most often involved in carcinogenesis prominent complementary pair of oncogenes *c-MYC* and *HRAS* (phylostrata 1–3) are of the most ancient origin.

3. Discussion

Despite extensive development of therapies, metastatic cancer disease remains incurable, resulting in high morbidity and mortality [80]. The association of aggressive incurable cancer with polyploid giant cells has been shown [28]. The extraordinary resistance to extinction therapies suggests that cancers recapitulate the phylogenetic endurance acquired in the long evolution of the lifeforms on Earth [81]. The cancer genome sequencing projects compromised, to some extent, a somatic mutation theory [82,83]. In recent times, the epigenetic aspects of the whole genome regulation in cancer stepped forward and are now intensively explored. One of these aspects is associated with typical for cancers whole genome duplications, or polyploidy (and aneuploidy inevitably linked to it), as a feature characteristically accompanying tumour growth and aggravating with tumour aggression [18]. The genetic sequences of polyploidy and aneuploidy in the microevolution of cancer were in the focus of studies for rather a long time [84,85]. However, the epigenetic aspects of aneuploidy became also attractive [86,87]. Considering a possible atavistic effect of cancer polyploidy, the phylostratigraphic analysis considering the evolutionary origin of genes and the change of their expression balance may be helpful.

Therefore, an interesting epigenetic approach may represent the study of the phylostratigraphic effect of polyploidy of not mutant normal mammalian tissues. In this paper we have investigated these issues by bioinformatical means using transcriptome data of polyploid versus diploid cells of normal human heart and mouse liver.

We have revealed that polyploidy changes the phylostratigraphic balance of the mammalian cellular network in favour of the enhanced expression of the evolutionary most ancient gene phylostrata—prokaryotic, early eukaryotic and early metazoan (1–5 phylostrata) up to bilateria, after which the trend is changed to the opposite. Although found here in normal polyploid tissues, this shift is surprisingly similar to the changes revealed for tumours when compared with normal counterparts [34–36,38]. With this revelation we arrive to the immediate conclusion: this epigenetic shift in tumours to the unicellular and early multicellular forms of life is associated or at least highly favoured by polyploidization.

The question arises—how it is regulated (or rather disregulated)? One of the mechanisms found in our study—it is by use of so-called bivalent genes, the epigenetically modified by histone H3 repressive and activating modifications of the same gene promoter or enhancer, namely by their prevailing activation. The particularity of bivalent genes comprising ~21% of human genes and employed for cell fate change in development is that they are poised (paused) but can be rapidly activated. That means that they favour cell fate change by the rules of non-equilibrium thermodynamics, in particular by critical state transition [88].

It is known now that the chromatin conformation at the supranucleosome and higher levels of the genome architecture is much a subject of the biophysical processes which assemble the active and inactive chromatin in two separate self-organizing high-order domains [89–93]. Self-organization is an important driving force of evolution [94]. On one hand, polyploidy is well known as driving gene diversification and speciation in evolution [1], which is a slow process. On the other hand, its epigenetic effect causing rapid reorganization of the transcriptional regulatory network after genome duplication was shown [95,96].

It can be reasoned that multiplication in polyploid cells of the identical chromosome alleles with the identical epigenetic status of bivalent genes should not just linearly increase their epigenetic effect proportionally to gene dosage but potentiate it by the thermodynamics of structural self-organization (phase transition). The role of the closely-juxtaposed DNA fibres' electrostatic forces yielding fine-tuned structure-specific recognition and pairing [97,98] should also contribute in the chromatin self-organization by polyploidy. A similar thought on the potentiating structural effect of additional DNA by the chromatin modifiers and transcription factors has been proposed earlier [99,100].

The Kegg “pathways in carcinogenesis”, along with the genes known as being mutants in cancers [101], also include many developmental genes. Here we revealed that this developmental

component is largely introduced through the polyploidy-dependent enrichment of the expression networks with the activated bivalent genes upregulated by *c-MYC* master hub (stratum 3). While in general gene evolution the proportion of bivalent genes increases from phylostrata 3 to 8, the polyploidy is mostly affected by enrichment with expression of bivalency in the phylostrata of Prokaryote and Eumetazoa (1–5). Very likely, that it is achieved by Myc up-regulating both polyploidy and bivalency. Thus, the carcinogenic *H-RAS-c-MYC* feed-back loop (strata 1–3) linked to developmental genes of early metazoans (strata 4–5) enriched with developmental pathways becomes involved, while stratum 6 (Bilateria) becomes a cross-point of the ambivalence (with repulsion from vertebrates).

c-MYC-mtH-RAS complementary pair has been distinguished in the early cancer chemical carcinogenesis research in a two-hit theory of cancer with Myc determining immortality and cancer initiation and *H-RAS* mutant in the codon 12 or 61 accomplishing cancer promotion [71,102]. Afterwards, ample studies have extended this theory by demonstrating that a potent oncogenicity of Myc can be further enhanced by collaborations with not only *RAS* mutant but also many extracellular growth stimuli that activate *RAS*, such as epidermal growth factor and its receptor (*EGFR*) or transforming growth factors [103,104]. The found phylostratic effect of ploidy-associated *c-MYC* collaborating with bivalent genes, e.g., both *H-RAS* (stratum 1) and *EGFR* (stratum 6) may explain its critical role in cancer initiation when overexpressed, and cancer regression when locked [59,60,62]. This phylostratic effect induced by the oncogenic potency of *c-MYC* linked to induced polyploidy, metabolic stemness, and bivalency likely creates the evolutionary “cancer attractor” postulated by Kauffman [94] as situated close to the summit of metaphoric Waddington Hill of the development potential [105,106]. Moreover, the upregulated *c-MYC* cooperates with mutant ras through programming inflammation and suppressing the tumour immunity [61], and *c-MYC* acts by cell selection promoting proliferation versus apoptosis depending on the supply of growth factors [60]. Likely, this trigger can occur through asymmetric cell division of epigenetically diverged bi-nuclear cells [107,108]. In fact, the main actors of this complex “story” including the complementary *c-MYC* and *RAS* pair can be found in Table 1 describing tumour and stromal components (like angiogenesis) of the polyploidy-dependent “cancer attractor”.

Interestingly, cnidaria (Hydra), an organism where the basic processes of the multicellularity were established represents phylogenetically the oldest organisms, where the tumours were revealed [109].

The early eukaryotic gene cluster in human genome is more stable than the cluster of complex metazoans (starting from vertebrates and peaking in acquired number of new genes at stratum 8) [38,40,41]. The unicellular gene network is responsible for basic cellular functions and also for resistance to extinction elaborated through series of earth catastrophes in billion years—we highlighted here that the genes responsible for DNA damage response, drug resistance, early stress response, and the proto-oncogenes of the viral origin, are from the 1–3 phylostrata. These likely act through feedback loops as the driving belts epigenetically attracting the cells from the basin of early metazoans into a unicellularity network.

On the other hand, the basic evolutionary processes of the early embryonal development of mammals are conserved from their origin in Eumetazoa, stratum 5 [110]. Therefore, aggressive cancer associated with polyploidy and multinuclearity often bears the features of the early embryo [111,112], including such inalienable components of morphogenesis as cell motility and angiogenesis. Moreover, through polyploidy, the *TP53* cancer mutants can acquire the phenotypical features of more ancient unicellular eukaryotes (“amoeboidisation”) [24,27,33,108,113,114], in line with the atavistic theory of cancer [29,30,33,115,116], confirmed by gene phylostratigraphic analysis [38] and here.

The early metazoans are tolerant to polyploidy because use it reversibly in their life-cycles [117]; it is sufficient to mention *Amoeba vulgaris* and *Entamoeba histolytica* [33,118,119] and amoebal slime molds [120]. When associated with polyploidy, as we found, the bivalent genes increase the connectivity and basin of attraction and become embedded in the network with the oncogene hubs of the viral origin, such as *c-MYC*, *H-RAS*, *MYB*—originated and having strong established interactions in the older strata (1–2–3). Moreover, polyploidy permits DNA replication but stops cell division and induces suppression

of the bivalent genes regulating circadian rhythms, which entrain many cellular processes, including cell cycles [121]. The cell-autonomous circadian timers established already in cyanobacteria are composed of a transcription–translation-based auto-regulatory feedback loops [122]. Apparently, this detrainment is an important factor causing along with epigenetic bivalency a metastable dynamic state, which can also favour a reshape and glide from the multi-cellular to unicellular gene expression network.

However, de-polyploidisation, in turn, can probably cause the back-shift of the transcription network: the two cycles, polyploidy (life-cycle-like) and diploidy (cell cycle) are reciprocally linked in tumours [23,87]; the recovery diploid fraction reciprocally downregulates the expression of amoebal genes in polyploidized human breast cancer treated with anticancer drugs; in addition, the amoebal giant cells can play a “nursing” function for the reproductive cell line [27]. Without any doubt, the constitutively activating mutations of oncogenes increase, push and likely stabilize the epigenetic shift to unicellularity. Such prominent tumour suppressors as *TP53* and *HYPPO/YAP* pathway, which also serve as guardians of the barrier to polyploidy [123], normally prevent the carcinogenic epigenetic shift to unicellularity caused by overcoming this barrier.

4. Methods

4.1. Data Sources and Comparative Criss-Cross Analysis

In this study we applied the method of reciprocal pair-wise cross-species transcriptome comparison that we used previously [12,57,124]. We choose this approach, because mammalian homologous tissues differ by cell ploidy levels [1,2,5,8,12]. Certain species have predominantly polyploid heart and diploid liver (pig and primates), whereas others possess mainly polyploid liver and predominantly diploid heart (rodents) [1,5,8]. Humans have highly polyploid hearts where cardiomyocytes contain nuclei with 4–16 genomes, whereas mouse hearts, on the contrary, consist of cardiomyocytes with mostly diploid nuclei [12]. At the same time, human hepatocytes are mostly diploid, whereas mouse hepatocytes contain nuclei with 4–8 genomes [5,12]. This inverse pattern of polyploidization enables identifying pure ploidy specific effects since it removes species-specific and tissue-specific noise [12]. In this study we applied pairwise cross species transcriptome comparison and principal component analysis (PCA) to comparisons of polyploid vs. diploid tissues: human heart vs. mouse heart and mouse liver vs. human liver. In the present work there are three main advancements over previous studies. Firstly, here we made the functional analysis of all ploidy-associated genes based on the whole-transcriptome data. Previously, the analysis was limited to the *c-MYC* interactome only [58,124]. Secondly, we studied the gene evolutionary origin (phylostratic distribution of all polyploidy-associated genes), which is important for cancer research in the context of the main contradiction arising between the unicellular and multicellular level features in tissue organization [34,38,41]. Thirdly, we addressed possible epigenetic mechanisms underlying ploidy-related changes, focusing on the bivalent gene expression and interactome. The work builds upon the idea of reciprocal cross-species comparison. The cross-species approach is informative because evolutionary distance enhances the contrast allowing the polyploidy-specific signature to appear [125].

The signal-to-noise filtration, where signal corresponds to polyploidy and noise to species- and tissue-specific signatures, is especially important for investigation of polyploidy because polyploidy preserves gene-dosage balance and thus may exert only weak and idiosyncratic effects on gene expression [126]. We performed the reciprocal pair-wise cross-species comparison using the transcriptomic data for polyploid vs. diploid organs. Specifically, we compared human heart (polyploid) vs. mouse heart (diploid) and mouse liver (polyploid) vs. human liver (diploid). The data were taken from the database obtained using RNA-seq [127].

The processed data were taken from the Supplement at the journal site [127]. We matched human-mouse orthologous genes and normalized the data in pairwise comparisons (human-mouse heart, human-mouse liver) using “quantile” normalization implemented in the “limma” package [128], as was done previously [124,129]. Finally, there were 13,913 orthologous gene pairs for which we found

stratigraphic data in Trigós et al. [38]. The transcriptomic data were uniformly obtained for all tissues and species [127]. This database was developed specially for interspecies comparisons (in particular, the samples were taken from the same parts of organs).

We detected the genes whose expression was changed in the same direction with regard to ploidy both in the heart and liver. In these comparisons the genes should have higher (or lower) expression in both polyploid tissues (human heart and mouse liver) compared with corresponding diploid tissues (mouse heart and human liver). Since we compared two different tissues in opposite directions in different species (human vs. mouse in the case of heart, and mouse vs. human in the case of liver), the tissue-specific and species-specific effects were presumably removed.

The one-to-one human-mouse orthologous genes were obtained from the NCBI database [130]. The expression levels of orthologous genes were analysed using the “limma” package specially developed for revealing differentially expressed genes in whole-transcriptome analyses [128]. A comparison of different software packages showed that limma is the method of choice for goals similar to those pursued in our work [131]. The data were normalized with “quantile” normalization implemented in “limma”. The differential gene expression (with statistical significance) was determined using the “voom” limma procedure. Then, we selected the genes with different expression contrasts between polyploid and diploid tissues as indicated in Results.

4.2. Principal Component Analysis

To determine whether the results of cross-species comparison can be confirmed by another approach, we applied principal component analysis (PCA) to the raw data matrix having samples as variables and genes as statistical units. The idea is to confirm the gene-by-gene a priori approach with a data-driven strategy, letting a ploidy-specific principal component to emerge from the data. The principal components are orthogonal to each other by construction; the data-driven emergence of a “ploidy” component distinct from tissue and “species” components is equivalent to an unsupervised normalization for tissue and species effects [132]. The genes endowed with extreme scores on such a “ploidy” component are the “image in light” of tissue and species independent ploidy effect on transcription pattern.

For this propose we used the same transcriptomic data for human and mouse heart and liver. This approach enabled us to evaluate the impact of shared variation (driven by housekeeping genes), species-specific, tissue-specific and ploidy-specific variables as separated mutually independent components [133].

As a result, we obtained two lists of genes demonstrating statistically significant ploidy-associated variation (above two standard deviations) for human and mouse heart and liver. Then these gene lists were subject to gene module enrichment analysis and the modules that are regulated by ploidy were identified. PCA is a purely geometrical non probabilistic procedure [132]. This means that each gene is simply projected into a rotated space (in this case having the same dimension of the original one, thus, with no loss of information) spanned by mutually orthogonal axes (components) extracted in decreasing order of explained variance. This unsupervised purely geometrical approach gave rise to a loading pattern mirroring the batch, tissue, species, ploidy a priori classification so demonstrating the tenability of the existence of “ploidy specific” genes. At this point the identification of genes having a score $> |2|$ as markers of the ploidy component corresponds to the usual 95% confidence intervals (component scores are equivalent to z scores). The actual *p*-values for phylostratigraphic analysis were based on relative enrichment of genes pertaining to different stratigraphic level based on the entire gene ontology. The samples having same tissue and species origin are practically coincident [see 132] for the presence of a common gene expression ideal profile for same tissue independent samples). RNA-seq analysis was based on the shared gene products across different samples; these shared genes were the pivots for coupling the relative vectors.

The species-specific and tissue-specific effects were automatically removed by PCA [124]. As a matter of fact the principal component analysis applied in an unsupervised way to the gene expression

profiles, generated a four-component solution correspondent to batch effect (PC1, 45.6% of variance explained), tissue-effect (PC2, 30.5% of variance); species-specific effect (PC3, 15% of variance) and ploidy effect (PC4, 9% of variance). We concentrated on genes having relevant score (higher than $|2|$ corresponding to two standard deviations from mean) on PC4. Principal components are each other independent by construction, therefore batch, tissue and species confounding are eliminated by the spectral decomposition of the dataset.

4.3. Analysis of Gene Modules

To determine which biological modules were over-represented among the ploidy-associated genes, we applied a double control. We tested the genes from all three datasets with higher and lower expression in polyploid vs. diploid tissues for enrichment of Gene Ontology (GO) categories and molecular pathways with regard to all human-mouse orthologous genes. The enriched GO categories and molecular pathways were found using the hypergeometric distribution of probability (implemented in R package) as previously [134,135]. GO categories were taken from GO database [136]. For each GO category, we collected all its subcategories using Gene Ontology acyclic directed graphs, and a gene was regarded as belonging to a given category if it was mapped to any of its subcategories. As a source of molecular pathways, the NCBI BioSystems was used, which is a most complete compendium of molecular pathways from different databases [130]. Redundancy of this compendium was removed by uniting entries with identical gene sets. The adjustment for multiple comparisons was done according to the method by [137]. This procedure gives a q -value, which can be considered a p -value corrected for multiple tests.

4.4. Protein-Protein Interaction Network

The protein-protein interaction networks (PPI) were constructed and visualized using the STRING server [138]. The analysis of network connectivity and the identification of causal regulators in modular and network organization were done with the same server.

4.5. Phylostratigraphic Analysis of Ploidy Associated Genes

The attribution of genes to phylostrata was taken from [38]. The phylostrata are as follows: 1—cellular organisms, 2—Eukaryota, 3—Opisthokonta, 4—Metazoa, 5—Eumetazoa, 6—Bilateria, 7—Chordata, 8—Euteleostomi, 9—Amniota, 10—Mammalia, 11—Theria, 12—Eutheria, 13—Euarchontoglires, 14—Catarrhini, 15—Homininae, 16—*Homo sapiens*.

4.6. Identification of Ploidy Associated Bivalent Gene

To find out how polyploidy affects bivalent gene expression landscape, we evaluated the expression of ploidy-associated genes that are known to be marked by bivalent chromatin in stem cells. The list of these genes was taken from [54].

5. Conclusions

The obtained results indicate that polyploidy activates the unicellular pathways of resistance to extinction fusing with ancient programs of ontogenesis related to carcinogenesis which originated in the early metazoa while suppressing the expression of genes from the late metazoa. This evolutionary retour is favoured by the activation of bivalent genes and deregulation of circadian rhythms. The data highlight the paramount role of polyploidy in the atavistic origin of cancer, the reason for the incurability of metastatic cancer, and indicate to targeting polyploidy for overcoming resistance to therapies.

Supplementary Materials: Supplementary materials can be found at <http://www.mdpi.com/1422-0067/21/22/8759/s1>.

Author Contributions: Conceptualization: J.E., O.V.A., A.E.V.; methodology: O.V.A., A.E.V., A.G.; investigation: O.V.A., A.E.V., A.G., N.M.V.; validation: O.V.A., A.E.V., A.G.; formal analysis: O.V.A., A.E.V., A.G.; data curation: O.V.A., A.E.V., A.G.; visualization: O.V.A., N.M.V.; literature analysis: J.E., O.V.A., A.E.V., A.G., N.M.V.;

writing—original draft preparation: J.E., O.V.A., A.E.V., A.G.; writing—review and editing: J.E., O.V.A., A.E.V., A.G., N.M.V. All authors have read and agreed to the published version of the manuscript.

Funding: This work was partly supported by a grant from the European Regional Development Fund (ERDF) project No. 1.1.1/18/A/099 for J.E and the Natural Sciences PhD Student Scholarship from the University of Latvia Foundation to N.M.V. Additionally, the work was partially supported by the Institute of Cytology Director’s Fund for OVA and AEV.

Acknowledgments: The authors are very grateful to Alexey N Tomilin for helpful comments.

Conflicts of Interest: The authors declare no conflict of interest.

References

- Comai, L. The advantages and disadvantages of being polyploid. *Nat. Rev. Genet.* **2005**, *6*, 836–846. [[CrossRef](#)] [[PubMed](#)]
- Fox, D.T.; Soltis, D.E.; Soltis, P.S.; Ashman, T.-L.; Van de Peer, Y. Polyploidy: A Biological Force from Cells to Ecosystems. *Trends Cell Biol.* **2020**, *30*, 688–694. [[CrossRef](#)] [[PubMed](#)]
- Avdeyev, P.; Alexeev, N.; Rong, Y.; Alekseyev, M.A. A unified ILP framework for core ancestral genome reconstruction problems. *Bioinformatics* **2020**, *36*, 2993–3003. [[CrossRef](#)] [[PubMed](#)]
- Anatskaya, O.V.; Vinogradov, A.E. Myocyte ploidy in heart chambers of birds with different locomotor activity. *J. Exp. Zool.* **2002**, *293*, 427–441. [[CrossRef](#)] [[PubMed](#)]
- Anatskaya, O.V.; Vinogradov, A.E. Heart and liver as developmental bottlenecks of mammal design: Evidence from cell polyploidization. *Biol. J. Linn. Soc.* **2004**, *83*, 175–186. [[CrossRef](#)]
- Sher, N.; Von Stetina, J.R.; Bell, G.W.; Matsuura, S.; Ravid, K.; Orr-Weaver, T.L. Fundamental differences in endoreplication in mammals and *Drosophila* revealed by analysis of endocycling and endomitotic cells. *Proc. Natl. Acad. Sci. USA* **2013**, *110*, 9368–9373. [[CrossRef](#)]
- Orr-Weaver, T.L. When bigger is better: The role of polyploidy in organogenesis. *Trends Genet.* **2015**, *31*, 307–315. [[CrossRef](#)]
- Lazzeri, E.; Angelotti, M.L.; Conte, C.; Anders, H.-J.; Romagnani, P. Surviving Acute Organ Failure: Cell Polyploidization and Progenitor Proliferation. *Trends Mol. Med.* **2019**, *25*, 366–381. [[CrossRef](#)]
- Derks, W.; Bergmann, O. Polyploidy in Cardiomyocytes: Roadblock to Heart Regeneration? *Circ. Res.* **2020**, *126*, 552–565. [[CrossRef](#)]
- Gan, P.; Patterson, M.; Sucov, H.M. Cardiomyocyte Polyploidy and Implications for Heart Regeneration. *Annu. Rev. Physiol.* **2020**, *82*, 45–61. [[CrossRef](#)]
- Anatskaya, O.V.; Vinogradov, A.E.; Kudryavtsev, B.N. Cardiomyocyte ploidy levels in birds with different growth rates. *J. Exp. Zool.* **2001**, *289*, 48–58. [[CrossRef](#)]
- Anatskaya, O.V.; Vinogradov, A.E. Genome multiplication as adaptation to tissue survival: Evidence from gene expression in mammalian heart and liver. *Genomics* **2007**, *89*, 70–80. [[CrossRef](#)] [[PubMed](#)]
- Silva, I.S.; Ghiraldini, F.G.; Veronezi, G.M.B.; Mello, M.L.S. Polyploidy and nuclear phenotype characteristics of cardiomyocytes from diabetic adult and normoglycemic aged mice. *Acta Histochem.* **2018**, *120*, 84–94. [[CrossRef](#)] [[PubMed](#)]
- Bensley, J.G.; Stacy, V.K.; De Matteo, R.; Harding, R.; Black, M.J. Cardiac remodelling as a result of pre-term birth: Implications for future cardiovascular disease. *Eur. Heart J.* **2010**, *31*, 2058–2066. [[CrossRef](#)]
- Gjelsvik, K.J.; Besen-McNally, R.; Losick, V.P. Solving the Polyploid Mystery in Health and Disease. *Trends Genet.* **2019**, *35*, 6–14. [[CrossRef](#)]
- Donne, R.; Saroul-Aïnama, M.; Cordier, P.; Celton-Morizur, S.; Desdouets, C. Polyploidy in liver development, homeostasis and disease. *Nat. Rev. Gastroenterol. Hepatol.* **2020**, *17*, 391–405. [[CrossRef](#)]
- Storchova, Z.; Pellman, D. From polyploidy to aneuploidy, genome instability and cancer. *Nat. Rev. Mol. Cell Biol.* **2004**, *5*, 45–54. [[CrossRef](#)]
- Coward, J.; Harding, A. Size Does Matter: Why Polyploid Tumor Cells are Critical Drug Targets in the War on Cancer. *Front. Oncol.* **2014**, *4*, 123. [[CrossRef](#)]
- Ben-Porath, I.; Thomson, M.W.; Carey, V.J.; Ge, R.; Bell, G.W.; Regev, A.; Weinberg, R.A. An embryonic stem cell-like gene expression signature in poorly differentiated aggressive human tumors. *Nat. Genet.* **2008**, *40*, 499–507. [[CrossRef](#)]

20. Salmina, K.; Jankevics, E.; Huna, A.; Perminov, D.; Radovica, I.; Klymenko, T.; Ivanov, A.; Jascenko, E.; Scherthan, H.; Cragg, M.; et al. Up-regulation of the embryonic self-renewal network through reversible polyploidy in irradiated p53-mutant tumour cells. *Exp. Cell Res.* **2010**, *316*, 2099–2112. [[CrossRef](#)]
21. Nguyen, H.G.; Ravid, K. Polyploidy: Mechanisms and Cancer Promotion in Hematopoietic and Other Cells. In *Polyploidization and Cancer*; Poon, R.Y.C., Ed.; Advances in Experimental Medicine and Biology; Springer: New York, NY, USA, 2010; Volume 676, pp. 105–122. ISBN 978-1-4419-6198-3.
22. Lagadec, C.; Vlashi, E.; Della Donna, L.; Dekmezian, C.; Pajonk, F. Radiation-Induced Reprogramming of Breast Cancer Cells: Radiation-Induced Cancer Stem Cells. *Stem Cells* **2012**, *30*, 833–844. [[CrossRef](#)] [[PubMed](#)]
23. Erenpreisa, J.; Cragg, M.S. Cancer: A matter of life cycle? *Cell Biol. Int.* **2007**, *31*, 1507–1510. [[CrossRef](#)] [[PubMed](#)]
24. Erenpreisa, J.; Cragg, M.S. Life-Cycle Features of Tumour Cells. In *Evolutionary Biology from Concept to Application*; Pontarotti, P., Ed.; Springer: Berlin/Heidelberg, Germany, 2008; pp. 61–71. ISBN 978-3-540-78992-5.
25. Mirzayans, R.; Andrais, B.; Scott, A.; Wang, Y.; Kumar, P.; Murray, D. Multinucleated Giant Cancer Cells Produced in Response to Ionizing Radiation Retain Viability and Replicate Their Genome. *Int. J. Mol. Sci.* **2017**, *18*, 360. [[CrossRef](#)] [[PubMed](#)]
26. Liu, J. The dualistic origin of human tumors. *Semin. Cancer Biol.* **2018**, *53*, 1–16. [[CrossRef](#)] [[PubMed](#)]
27. Salmina, K.; Bojko, A.; Inashkina, I.; Staniak, K.; Dudkowska, M.; Podlesniy, P.; Rumnieks, F.; Vainshelbaum, N.M.; Pjanova, D.; Sikora, E.; et al. “Mitotic Slippage” and Extranuclear DNA in Cancer Chemoresistance: A Focus on Telomeres. *Int. J. Mol. Sci.* **2020**, *21*, 2779. [[CrossRef](#)] [[PubMed](#)]
28. Mirzayans, R.; Andrais, B.; Murray, D. Roles of Polyploid/Multinucleated Giant Cancer Cells in Metastasis and Disease Relapse Following Anticancer Treatment. *Cancers* **2018**, *10*, 118. [[CrossRef](#)] [[PubMed](#)]
29. Vincent, M.D. Cancer: Beyond Speciation. In *Advances in Cancer Research*; Elsevier: Amsterdam, The Netherlands, 2011; Volume 112, pp. 283–350. ISBN 978-0-12-387688-1.
30. Davies, P.C.W.; Lineweaver, C.H. Cancer tumors as Metazoa 1.0: Tapping genes of ancient ancestors. *Phys. Biol.* **2011**, *8*, 015001. [[CrossRef](#)] [[PubMed](#)]
31. Davies, P. Exposing cancer’s deep evolutionary roots. *Phys. Cancer Phys. World* **2013**, *26*, 37–40. [[CrossRef](#)]
32. Aktipis, C.A.; Boddy, A.M.; Jansen, G.; Hibner, U.; Hochberg, M.E.; Maley, C.C.; Wilkinson, G.S. Cancer across the tree of life: Cooperation and cheating in multicellularity. *Philos. Trans. R. Soc. Lond. B Biol. Sci.* **2015**, *370*. [[CrossRef](#)]
33. Niculescu, V.F. Developmental and Non Developmental Polyploidy in Xenic and Axenic Cultured Stem Cell Lines of *Entamoeba invadens* and *E. histolytica*. *Insights Stem Cells* **2016**, *2*, 1–9.
34. Vinogradov, A.E. Human transcriptome nexuses: Basic-eukaryotic and metazoan. *Genomics* **2010**, *95*, 345–354. [[CrossRef](#)] [[PubMed](#)]
35. Vinogradov, A.E.; Anatskaya, O.V. Evolutionary framework of the human interactome: Unicellular and multicellular giant clusters. *Biosystems* **2019**, *181*, 82–87. [[CrossRef](#)] [[PubMed](#)]
36. Domazet-Lošo, T.; Tautz, D. Phylostratigraphic tracking of cancer genes suggests a link to the emergence of multicellularity in metazoa. *BMC Biol.* **2010**, *8*, 66. [[CrossRef](#)] [[PubMed](#)]
37. Gu, X.; Zou, Z.; Yang, J. Tracing Evolutionary Ages of Cancer-Driving Sites by Cancer Somatic Mutations. *bioRxiv* **2020**. [[CrossRef](#)]
38. Trigoso, A.S.; Pearson, R.B.; Papenfuss, A.T.; Goode, D.L. Altered interactions between unicellular and multicellular genes drive hallmarks of transformation in a diverse range of solid tumors. *Proc. Natl. Acad. Sci. USA* **2017**, *114*, 6406–6411. [[CrossRef](#)] [[PubMed](#)]
39. Bussey, K.J.; Cisneros, L.H.; Lineweaver, C.H.; Davies, P.C.W. Ancestral gene regulatory networks drive cancer. *Proc. Natl. Acad. Sci. USA* **2017**, *114*, 6160–6162. [[CrossRef](#)] [[PubMed](#)]
40. Trigoso, A.S.; Pearson, R.B.; Papenfuss, A.T.; Goode, D.L. How the evolution of multicellularity set the stage for cancer. *Br. J. Cancer* **2018**, *118*, 145–152. [[CrossRef](#)] [[PubMed](#)]
41. Vinogradov, A.E.; Anatskaya, O.V. Cell-cycle dependence of transcriptome gene modules: Comparison of regression lines. *FEBS J.* **2020**, *287*, 4427–4439. [[CrossRef](#)]
42. Bizzarri, M.; Giuliani, A.; Cucina, A.; D’Anselmi, F.; Soto, A.M.; Sonnenschein, C. Fractal analysis in a systems biology approach to cancer. *Semin. Cancer Biol.* **2011**, *21*, 175–182. [[CrossRef](#)]
43. Bizzarri, M.; Giuliani, A.; Minini, M.; Monti, N.; Cucina, A. Constraints Shape Cell Function and Morphology by Canalizing the Developmental Path along the Waddington’s Landscape. *Bioessays* **2020**, *42*, e1900108. [[CrossRef](#)]

44. Erenpreisa, J.; Cragg, M.S. Three steps to the immortality of cancer cells: Senescence, polyploidy and self-renewal. *Cancer Cell Int.* **2013**, *13*, 92. [[CrossRef](#)] [[PubMed](#)]
45. Van de Peer, Y.; Mizrachi, E.; Marchal, K. The evolutionary significance of polyploidy. *Nat. Rev. Genet.* **2017**, *18*, 411–424. [[CrossRef](#)] [[PubMed](#)]
46. Moein, S.; Adibi, R.; da Silva Meirelles, L.; Nardi, N.B.; Gheisari, Y. Cancer regeneration: Polyploid cells are the key drivers of tumor progression. *Biochim. Biophys. Acta (BBA) Rev. Cancer* **2020**, 188408. [[CrossRef](#)] [[PubMed](#)]
47. Mirzayans, R.; Murray, D. Intratumor Heterogeneity and Therapy Resistance: Contributions of Dormancy, Apoptosis Reversal (Anastasis) and Cell Fusion to Disease Recurrence. *Int. J. Mol. Sci.* **2020**, *21*, 1308. [[CrossRef](#)] [[PubMed](#)]
48. Bernstein, B.E.; Mikkelsen, T.S.; Xie, X.; Kamal, M.; Huebert, D.J.; Cuff, J.; Fry, B.; Meissner, A.; Wernig, M.; Plath, K.; et al. A bivalent chromatin structure marks key developmental genes in embryonic stem cells. *Cell* **2006**, *125*, 315–326. [[CrossRef](#)] [[PubMed](#)]
49. Mikkelsen, T.S.; Ku, M.; Jaffe, D.B.; Issac, B.; Lieberman, E.; Giannoukos, G.; Alvarez, P.; Brockman, W.; Kim, T.-K.; Koche, R.P.; et al. Genome-wide maps of chromatin state in pluripotent and lineage-committed cells. *Nature* **2007**, *448*, 553–560. [[CrossRef](#)]
50. Widschwendter, M.; Fiegl, H.; Egle, D.; Mueller-Holzner, E.; Spizzo, G.; Marth, C.; Weisenberger, D.J.; Campan, M.; Young, J.; Jacobs, I.; et al. Epigenetic stem cell signature in cancer. *Nat. Genet.* **2007**, *39*, 157–158. [[CrossRef](#)]
51. Balch, C.; Nephew, K.P.; Huang, T.H.-M.; Bapat, S.A. Epigenetic “bivalently marked” process of cancer stem cell-driven tumorigenesis. *Bioessays* **2007**, *29*, 842–845. [[CrossRef](#)]
52. Blanco, E.; González-Ramírez, M.; Alcaine-Colet, A.; Aranda, S.; Di Croce, L. The Bivalent Genome: Characterization, Structure, and Regulation. *Trends Genet.* **2020**, *36*, 118–131. [[CrossRef](#)]
53. Bernhart, S.H.; Kretzmer, H.; Holdt, L.M.; Jühling, F.; Ammerpohl, O.; Bergmann, A.K.; Northoff, B.H.; Doose, G.; Siebert, R.; Stadler, P.F.; et al. Changes of bivalent chromatin coincide with increased expression of developmental genes in cancer. *Sci. Rep.* **2016**, *6*, 37393. [[CrossRef](#)]
54. Court, F.; Arnaud, P. An annotated list of bivalent chromatin regions in human ES cells: A new tool for cancer epigenetic research. *Oncotarget* **2017**, *8*, 4110–4124. [[CrossRef](#)] [[PubMed](#)]
55. Kuroda, M.I.; Kang, H.; De, S.; Kassis, J.A. Dynamic Competition of Polycomb and Trithorax in Transcriptional Programming. *Annu. Rev. Biochem.* **2020**, *89*, 235–253. [[CrossRef](#)] [[PubMed](#)]
56. Sonnenschein, C.; Soto, A.M. Cancer Metastases: So Close and So Far. *JNCI J. Natl. Cancer Inst.* **2015**, *107*. [[CrossRef](#)] [[PubMed](#)]
57. Li, Q.; Dang, C.V. Myc Overexpression Uncouples DNA Replication from Mitosis. *Mol. Cell. Biol.* **1999**, *19*, 5339–5351. [[CrossRef](#)] [[PubMed](#)]
58. Grendler, J.; Lowgren, S.; Mills, M.; Losick, V.P. Wound-induced polyploidization is driven by Myc and supports tissue repair in the presence of DNA damage. *Development* **2019**, *146*, dev173005. [[CrossRef](#)]
59. Soucek, L.; Whitfield, J.; Martins, C.P.; Finch, A.J.; Murphy, D.J.; Sodik, N.M.; Karnezis, A.N.; Swigart, L.B.; Nasi, S.; Evan, G.I. Modelling Myc inhibition as a cancer therapy. *Nature* **2008**, *455*, 679–683. [[CrossRef](#)]
60. Evan, G. Taking a Back Door to Target Myc. *Science* **2012**, *335*, 293–294. [[CrossRef](#)]
61. Kortlever, R.M.; Sodik, N.M.; Wilson, C.H.; Burkhart, D.L.; Pellegrinet, L.; Brown Swigart, L.; Littlewood, T.D.; Evan, G.I. Myc Cooperates with Ras by Programming Inflammation and Immune Suppression. *Cell* **2017**, *171*, 1301–1315. [[CrossRef](#)]
62. Sui, Y.; Gu, R.; Janknecht, R. Crucial Functions of the JMJD1/KDM3 Epigenetic Regulators in Cancer. *Mol. Cancer Res.* **2020**. [[CrossRef](#)]
63. Neri, F.; Zippo, A.; Krepelova, A.; Cherubini, A.; Rocchigiani, M.; Oliviero, S. Myc Regulates the Transcription of the PRC2 Gene to Control the Expression of Developmental Genes in Embryonic Stem Cells. *Mol. Cell. Biol.* **2012**, *32*, 840–851. [[CrossRef](#)]
64. Ullius, A.; Luscher-Firzlaff, J.; Costa, I.G.; Walsemann, G.; Forst, A.H.; Gusmao, E.G.; Kapelle, K.; Kleine, H.; Kremmer, E.; Vervoorts, J.; et al. The interaction of MYC with the trithorax protein ASH2L promotes gene transcription by regulating H3K27 modification. *Nucleic Acids Res.* **2014**, *42*, 6901–6920. [[CrossRef](#)] [[PubMed](#)]
65. Vinogradov, A.E.; Shilina, M.A.; Anatskaya, O.V.; Alekseenko, L.L.; Fridlyanskaya, I.I.; Krasnenko, A.; Kim, A.; Korostin, D.; Ilynsky, V.; Elmuratov, A.; et al. Molecular Genetic Analysis of Human Endometrial Mesenchymal Stem Cells That Survived Sublethal Heat Shock. *Stem Cells Int* **2017**, *17*, 2362630. [[CrossRef](#)]

66. Kallioniemi, A. Bone morphogenetic protein 4—A fascinating regulator of cancer cell behavior. *Cancer Genet.* **2012**, *205*, 267–277. [[CrossRef](#)] [[PubMed](#)]
67. Bach, D.-H.; Park, H.J.; Lee, S.K. The Dual Role of Bone Morphogenetic Proteins in Cancer. *Mol. Ther. Oncolytics* **2018**, *8*, 1–13. [[CrossRef](#)] [[PubMed](#)]
68. Chen, H.; Liu, H.; Qing, G. Targeting oncogenic Myc as a strategy for cancer treatment. *Signal Transduct. Target. Ther.* **2018**, *3*, 5. [[CrossRef](#)] [[PubMed](#)]
69. Tovar, E.A.; Graveel, C.R. MET in human cancer: Germline and somatic mutations. *Ann. Transl. Med.* **2017**, *5*, 205. [[CrossRef](#)]
70. Mitra, P. Transcription regulation of MYB: A potential and novel therapeutic target in cancer. *Ann. Transl. Med.* **2018**, *6*, 443. [[CrossRef](#)]
71. Erenpreiss, J.O. *Current Concepts of Malignant Growth*; Zinâtne Publ.: Riga, Latvia, 1993.
72. Moore, A.R.; Rosenberg, S.C.; McCormick, F.; Malek, S. RAS-targeted therapies: Is the undruggable drugged? *Nat. Rev. Drug Discov.* **2020**, *19*, 533–552. [[CrossRef](#)]
73. Sigismund, S.; Avanzato, D.; Lanzetti, L. Emerging functions of the EGFR in cancer. *Mol. Oncol.* **2018**, *12*, 3–20. [[CrossRef](#)]
74. Hosaka, K.; Yang, Y.; Seki, T.; Du, Q.; Jing, X.; He, X.; Wu, J.; Zhang, Y.; Morikawa, H.; Nakamura, M.; et al. Therapeutic paradigm of dual targeting VEGF and PDGF for effectively treating FGF-2 off-target tumors. *Nat. Commun.* **2020**, *11*, 3704. [[CrossRef](#)]
75. Khurana, N.; Sikka, S.C. Interplay between SOX9, Wnt/ β -Catenin and Androgen Receptor Signaling in Castration-Resistant Prostate Cancer. *Int. J. Mol. Sci.* **2019**, *20*, 2066. [[CrossRef](#)] [[PubMed](#)]
76. Qin, Q.; Xu, Y.; He, T.; Qin, C.; Xu, J. Normal and disease-related biological functions of Twist1 and underlying molecular mechanisms. *Cell Res.* **2012**, *22*, 90–106. [[CrossRef](#)] [[PubMed](#)]
77. Petrizzo, A.; Caruso, F.P.; Tagliamonte, M.; Tornesello, M.L.; Ceccarelli, M.; Costa, V.; Aprile, M.; Esposito, R.; Ciliberto, G.; Buonaguro, F.M.; et al. Identification and Validation of HCC-specific Gene Transcriptional Signature for Tumor Antigen Discovery. *Sci. Rep.* **2016**, *6*, 29258. [[CrossRef](#)] [[PubMed](#)]
78. Davoli, T.; Xu, A.W.; Mengwasser, K.E.; Sack, L.M.; Yoon, J.C.; Park, P.J.; Elledge, S.J. Cumulative Haploinsufficiency and Triplosensitivity Drive Aneuploidy Patterns and Shape the Cancer Genome. *Cell* **2013**, *155*, 948–962. [[CrossRef](#)]
79. Justice, J.; Malhotra, S.; Ruano, M.; Li, Y.; Zavala, G.; Lee, N.; Morgan, R.; Beemon, K. The MET Gene Is a Common Integration Target in Avian Leukosis Virus Subgroup J-Induced Chicken Hemangiomas. *J. Virol.* **2015**, *89*, 4712–4719. [[CrossRef](#)] [[PubMed](#)]
80. Pienta, K.J.; Hammarlund, E.U.; Axelrod, R.; Amend, S.R.; Brown, J.S. Convergent Evolution, Evolving Evolvability, and the Origins of Lethal Cancer. *Mol. Cancer Res.* **2020**, *18*, 801–810. [[CrossRef](#)]
81. Walther, V.; Hiley, C.T.; Shibata, D.; Swanton, C.; Turner, P.E.; Maley, C.C. Can oncology recapitulate paleontology? Lessons from species extinctions. *Nat. Rev. Clin. Oncol.* **2015**, *12*, 273–285. [[CrossRef](#)]
82. Versteeg, R. Tumours outside the mutation box. *Nature* **2014**, *506*, 438–439. [[CrossRef](#)]
83. Gatenby, R.A. Is the Genetic Paradigm of Cancer Complete? *Radiology* **2017**, *284*, 1–3. [[CrossRef](#)]
84. Ganem, N.J.; Storchova, Z.; Pellman, D. Tetraploidy, aneuploidy and cancer. *Curr. Opin. Genet. Dev.* **2007**, *17*, 157–162. [[CrossRef](#)]
85. López, S.; Lim, E.L.; Horswell, S.; Haase, K.; Huebner, A.; Dietzen, M.; Mourikis, T.P.; Watkins, T.B.K.; Rowan, A.; Dewhurst, S.M.; et al. Interplay between whole-genome doubling and the accumulation of deleterious alterations in cancer evolution. *Nat. Genet.* **2020**, *52*, 283–293. [[CrossRef](#)] [[PubMed](#)]
86. Beach, R.R.; Ricci-Tam, C.; Brennan, C.M.; Moomau, C.A.; Hsu, P.-H.; Hua, B.; Silberman, R.E.; Springer, M.; Amon, A. Aneuploidy Causes Non-genetic Individuality. *Cell* **2017**, *169*, 229–242.e21. [[CrossRef](#)] [[PubMed](#)]
87. Salmina, K.; Huna, A.; Kalejs, M.; Pjanova, D.; Scherthan, H.; Cragg, M.S.; Erenpreisa, J. The Cancer Aneuploidy Paradox: In the Light of Evolution. *Genes* **2019**, *10*, 83. [[CrossRef](#)] [[PubMed](#)]
88. Mojtahedi, M.; Skupin, A.; Zhou, J.; Castaño, I.G.; Leong-Quong, R.Y.Y.; Chang, H.; Trachana, K.; Giuliani, A.; Huang, S. Cell Fate Decision as High-Dimensional Critical State Transition. *PLoS Biol.* **2016**, *14*, e2000640. [[CrossRef](#)]
89. Cavalli, G. Chromosome kissing. *Curr. Opin. Genet. Dev.* **2007**, *17*, 443–450. [[CrossRef](#)]
90. Lieberman-Aiden, E.; van Berkum, N.L.; Williams, L.; Imakaev, M.; Ragoczy, T.; Telling, A.; Amit, I.; Lajoie, B.R.; Sabo, P.J.; Dorschner, M.O.; et al. Comprehensive Mapping of Long-Range Interactions Reveals Folding Principles of the Human Genome. *Science* **2009**, *326*, 289–293. [[CrossRef](#)]

91. Solovei, I.; Thanisch, K.; Feodorova, Y. How to rule the nucleus: Divide et impera. *Curr. Opin. Cell Biol.* **2016**, *40*, 47–59. [[CrossRef](#)]
92. Bakhmet, E.I.; Nazarov, I.B.; Gazizova, A.R.; Vorobyeva, N.E.; Kuzmin, A.A.; Gordeev, M.N.; Sinenko, S.A.; Aksenov, N.D.; Artamonova, T.O.; Khodorkovskii, M.A.; et al. hnRNP-K Targets Open Chromatin in Mouse Embryonic Stem Cells in Concert with Multiple Regulators: hnRNP-K Targets Open Chromatin in Mouse ESCs. *Stem Cells* **2019**, *37*, 1018–1029. [[CrossRef](#)]
93. Nazarov, I.B.; Bakhmet, E.I.; Tomilin, A.N. KH-Domain Poly(C)-Binding Proteins as Versatile Regulators of Multiple Biological Processes. *Biochem. Mosc.* **2019**, *84*, 205–219. [[CrossRef](#)]
94. Kauffman, S.A. *The Origins of Order: Self-Organization and Selection in Evolution*; Series on Directions in Condensed Matter Physics; World Scientific: Singapore, 1992; Volume 6, pp. 61–100. ISBN 978-9971-5-0537-0.
95. Conant, G.C. Rapid reorganization of the transcriptional regulatory network after genome duplication in yeast. *Proc. Biol. Sci.* **2010**, *277*, 869–876. [[CrossRef](#)]
96. Conant, G.C. The lasting after-effects of an ancient polyploidy on the genomes of teleosts. *PLoS ONE* **2020**, *15*, e0231356. [[CrossRef](#)] [[PubMed](#)]
97. Cherstvy, A.G.; Teif, V.B. Structure-driven homology pairing of chromatin fibers: The role of electrostatics and protein-induced bridging. *J. Biol. Phys.* **2013**, *39*, 363–385. [[CrossRef](#)] [[PubMed](#)]
98. Jerković, I.; Szabo, Q.; Bantignies, F.; Cavalli, G. Higher-Order Chromosomal Structures Mediate Genome Function. *J. Mol. Biol.* **2020**, *432*, 676–681. [[CrossRef](#)]
99. Vinogradov, A.E. Buffering: A Possible Passive-homeostasis Role for Redundant DNA. *J. Theor. Biol.* **1998**, *193*, 197–199. [[CrossRef](#)] [[PubMed](#)]
100. Vinogradov, A.E. Genome size and chromatin condensation in vertebrates. *Chromosoma* **2005**, *113*, 362–369. [[CrossRef](#)] [[PubMed](#)]
101. Kanehisa, M.; Sato, Y.; Furumichi, M.; Morishima, K.; Tanabe, M. New approach for understanding genome variations in KEGG. *Nucleic Acids Res.* **2019**, *47*, D590–D595. [[CrossRef](#)]
102. Land, H.; Parada, L.F.; Weinberg, R.A. Tumorigenic conversion of primary embryo fibroblasts requires at least two cooperating oncogenes. *Nature* **1983**, *304*, 596–602. [[CrossRef](#)]
103. Knudson, A.G. Two genetic hits (more or less) to cancer. *Nat. Rev. Cancer* **2001**, *1*, 157–162. [[CrossRef](#)]
104. Wang, C.; Lisanti, M.P.; Liao, D.J. Reviewing once more the c-myc and Ras collaboration: Converging at the cyclin D1-CDK4 complex and challenging basic concepts of cancer biology. *Cell Cycle* **2011**, *10*, 57–67. [[CrossRef](#)]
105. Huang, S.; Ernberg, I.; Kauffman, S. Cancer attractors: A systems view of tumors from a gene network dynamics and developmental perspective. *Semin. Cell Dev. Biol.* **2009**, *20*, 869–876. [[CrossRef](#)]
106. Huang, S.; Kauffman, S. How to escape the cancer attractor: Rationale and limitations of multi-target drugs. *Semin. Cancer Biol.* **2013**, *23*, 270–278. [[CrossRef](#)] [[PubMed](#)]
107. Erenpreisa, J.; Roach, H.I. Epigenetic selection as a possible component of transdifferentiation. Further study of the commitment of hypertrophic chondrocytes to become osteocytes. *Mech. Ageing Dev.* **1996**, *87*, 165–182. [[CrossRef](#)]
108. Erenpreisa, J.; Salmiņa, K.; Belyayev, A.; Inashkina, I.; Cragg, M.S. Survival at the Brink. In *Autophagy: Cancer, Other Pathologies, Inflammation, Immunity, Infection, and Aging*; Elsevier: Amsterdam, The Netherlands, 2017; pp. 275–294. ISBN 978-0-12-812146-7.
109. Domazet-Lošo, T.; Klimovich, A.; Anokhin, B.; Anton-Erxleben, F.; Hamm, M.J.; Lange, C.; Bosch, T.C.G. Naturally occurring tumours in the basal metazoan Hydra. *Nat. Commun.* **2014**, *5*, 4222. [[CrossRef](#)] [[PubMed](#)]
110. Arthur, W. *Evolution: A Developmental Approach*; Wiley-Blackwell: Chichester, UK, 2011; ISBN 978-1-4051-8658-2.
111. Erenpreisa, J.; Salmina, K.; Huna, A.; Jackson, T.R.; Vazquez-Martin, A.; Cragg, M.S. The “virgin birth”, polyploidy, and the origin of cancer. *Oncoscience* **2014**, *2*, 3–14. [[CrossRef](#)]
112. Niu, N.; Mercado-Uribe, I.; Liu, J. Dedifferentiation into blastomere-like cancer stem cells via formation of polyploid giant cancer cells. *Oncogene* **2017**, *36*, 4887–4900. [[CrossRef](#)] [[PubMed](#)]
113. Fais, S.; Overholtzer, M. Cell-in-cell phenomena, cannibalism, and autophagy: Is there a relationship? *Cell Death Dis.* **2018**, *9*, 95. [[CrossRef](#)] [[PubMed](#)]

114. Goodkov, A.V.; Berdieva, M.A.; Podlipaeva, Y.I.; Demin, S.Y. The Chromatin Extrusion Phenomenon in *Amoeba proteus* Cell Cycle. *J. Eukaryot. Microbiol.* **2020**, *67*, 203–208. [[CrossRef](#)]
115. Arguello, F. Atavistic Metamorphosis: A New and Logical Explanation for the Origin and Biological Nature of Cancer: With a Discussion on a Novel Approach to Treat Cancer. CreateSpace: Scotts Valley, CA, USA, 2011; ISBN 978-1-4609-6899-4.
116. Lineweaver, C.H.; Davies, P.C.W.; Vincent, M.D. Targeting cancer's weaknesses (not its strengths): Therapeutic strategies suggested by the atavistic model: Insights & Perspectives. *BioEssays* **2014**, *36*, 827–835. [[CrossRef](#)] [[PubMed](#)]
117. Raikov, I.B. Nuclear apparatus of Mesokaryotic Protozoa. In *The Protozoan Nucleus, Morphology and Evolution*; Cell Biology Monographs; Springer: New York, NY, USA, 1982; pp. 1–174.
118. Demin, S.Y.; Berdieva, M.A.; Podlipaeva, Y.I.; Goodkov, A.V. Karyotypic instability of endoprophase and mitotic cells of *Amoeba* sp. strain Cont from the "proteus-type" group (Amoebozoa, Euamoebida, Amoebidae). *Eur. J. Protistol.* **2020**, *74*, 125691. [[CrossRef](#)]
119. Niculescu, V.F. The reproductive life cycle of cancer: Hypotheses of cell of origin, TP53 drivers and stem cell conversions in the light of the atavistic cancer cell theory. *Med Hypotheses* **2019**, *123*, 19–23. [[CrossRef](#)]
120. Nanjundiah, V. Cellular slime mold development as a paradigm for the transition from unicellular to multicellular life. In *Multicellularity: Origins and Evolution*; MIT Press: Cambridge, MA, USA, 2016.
121. Andreani, T.S.; Itoh, T.Q.; Yildirim, E.; Hwangbo, D.-S.; Allada, R. Genetics of Circadian Rhythms. *Sleep Med. Clin.* **2015**, *10*, 413–421. [[CrossRef](#)] [[PubMed](#)]
122. Camponeschi, I.; Damasco, A.; Uversky, V.N.; Giuliani, A.; Bianchi, M.M. Phenotypic suppression caused by resonance with light-dark cycles indicates the presence of a 24-hours oscillator in yeast and suggests a new role of intrinsically disordered protein regions as internal mediators. *J. Biomol. Struct. Dyn.* **2020**. [[CrossRef](#)] [[PubMed](#)]
123. Øvrebø, J.I.; Edgar, B.A. Polyploidy in tissue homeostasis and regeneration. *Development* **2018**, *145*. [[CrossRef](#)] [[PubMed](#)]
124. Vazquez-Martin, A.; Anatskaya, O.V.; Giuliani, A.; Erenpreisa, J.; Huang, S.; Salmina, K.; Inashkina, I.; Huna, A.; Nikolsky, N.N.; Vinogradov, A.E. Somatic polyploidy is associated with the upregulation of c-MYC interacting genes and EMT-like signature. *Oncotarget* **2016**, *7*, 75235–75260. [[CrossRef](#)] [[PubMed](#)]
125. Whitehead, A.; Crawford, D.L. Variation within and among species in gene expression: Raw material for evolution: Review of gene expression variation. *Mol. Ecol.* **2006**, *15*, 1197–1211. [[CrossRef](#)]
126. Otto, S.P. The Evolutionary Consequences of Polyploidy. *Cell* **2007**, *131*, 452–462. [[CrossRef](#)]
127. Brawand, D.; Soumillon, M.; Necsulea, A.; Julien, P.; Csárdi, G.; Harrigan, P.; Weier, M.; Liechti, A.; Aximu-Petri, A.; Kircher, M.; et al. The evolution of gene expression levels in mammalian organs. *Nature* **2011**, *478*, 343–348. [[CrossRef](#)]
128. Ritchie, M.E.; Phipson, B.; Wu, D.; Hu, Y.; Law, C.W.; Shi, W.; Smyth, G.K. limma powers differential expression analyses for RNA-sequencing and microarray studies. *Nucleic Acids Res.* **2015**, *43*, e47. [[CrossRef](#)]
129. Vinogradov, A.E.; Anatskaya, O.V. Systemic evolutionary changes in mammalian gene expression. *Biosystems* **2020**, *198*, 104256. [[CrossRef](#)]
130. Sayers, E.W.; Beck, J.; Brister, J.R.; Bolton, E.E.; Canese, K.; Comeau, D.C.; Funk, K.; Ketter, A.; Kim, S.; Kimchi, A.; et al. Database resources of the National Center for Biotechnology Information. *Nucleic Acids Res.* **2020**, *48*, D9–D16. [[CrossRef](#)]
131. Seyednasrollah, F.; Laiho, A.; Elo, L.L. Comparison of software packages for detecting differential expression in RNA-seq studies. *Brief. Bioinform.* **2015**, *16*, 59–70. [[CrossRef](#)] [[PubMed](#)]
132. Giuliani, A. The application of principal component analysis to drug discovery and biomedical data. *Drug Discov. Today* **2017**, *22*, 1069–1076. [[CrossRef](#)] [[PubMed](#)]
133. Roden, J.C.; King, B.W.; Trout, D.; Mortazavi, A.; Wold, B.J.; Hart, C.E. Mining gene expression data by interpreting principal components. *BMC Bioinform.* **2006**, *7*, 194. [[CrossRef](#)] [[PubMed](#)]
134. Vinogradov, A.E. 'Genome design' model and multicellular complexity: Golden middle. *Nucleic Acids Res.* **2006**, *34*, 5906–5914. [[CrossRef](#)]
135. Vinogradov, A.E.; Anatskaya, O.V. DNA helix: The importance of being AT-rich. *Mamm. Genome* **2017**, *28*, 455–464. [[CrossRef](#)]
136. The Gene Ontology Consortium. The Gene Ontology Resource: 20 years and still GOing strong. *Nucleic Acids Res.* **2019**, *47*, D330–D338. [[CrossRef](#)]

137. Storey, J.D.; Tibshirani, R. Statistical significance for genomewide studies. *Proc. Natl. Acad. Sci. USA* **2003**, *100*, 9440–9445. [[CrossRef](#)]
138. Szklarczyk, D.; Gable, A.L.; Lyon, D.; Junge, A.; Wyder, S.; Huerta-Cepas, J.; Simonovic, M.; Doncheva, N.T.; Morris, J.H.; Bork, P.; et al. STRING v11: Protein–protein association networks with increased coverage, supporting functional discovery in genome-wide experimental datasets. *Nucleic Acids Res.* **2019**, *47*, D607–D613. [[CrossRef](#)]

Publisher’s Note: MDPI stays neutral with regard to jurisdictional claims in published maps and institutional affiliations.



© 2020 by the authors. Licensee MDPI, Basel, Switzerland. This article is an open access article distributed under the terms and conditions of the Creative Commons Attribution (CC BY) license (<http://creativecommons.org/licenses/by/4.0/>).

3.3. Polyploidy is linked to circadian deregulation in malignant tumors from the TCGA database

This part of the study builds on the previously acquired result suggesting that polyploidy leads to circadian clock (CC) function suppression in normal tissues. To assess the impact of ploidy on CC function in cancer, a broad transcriptomics dataset of 11 tumor types from The Cancer Genome Atlas (TCGA) database was analyzed using the DeltaCCD method (Shilts et al., 2018), which measures circadian clock function in terms of core clock gene coexpression. The relationship between the DeltaCCD coefficient of circadian deregulation and approximate ploidy values (whole genome duplication/WGD status) inferred via the ABSOLUTE algorithm from copy number data of the same tumor samples was assessed statistically using Spearman correlation analysis and revealed to be significantly positive ($\rho=0.83$, $p<0.01$).

This work also reviews the particularities of circadian clock function in cell differentiation, reproduction and disease, and the results are subsequently interpreted from an embryonal theory of cancer standpoint.

Role of the Circadian Clock “Death-Loop” in the DNA Damage Response Underpinning Cancer Treatment Resistance

Ninel Miriam Vainshelbaum ^{1,2}, Kristine Salmina ¹, Bogdan I. Gerashchenko ³, Marija Lazovska ¹, Pawel Zayakin ¹, Mark Steven Cragg ⁴, Dace Pjanova ¹ and Jekaterina Erenpreisa ^{1,*}

¹ Cancer Research Division, Latvian Biomedicine Research and Study Centre, LV-1067 Riga, Latvia; ninela.vainshelbauma@biomed.lu.lv (N.M.V.); Latvia; salmina.kristine@gmail.com (K.S.); marija.lazovska@biomed.lu.lv (M.L.); pawel@biomed.lu.lv (P.Z.); dace@biomed.lu.lv (D.P.)

² Faculty of Biology, University of Latvia, LV-1050 Riga, Latvia

³ R.E. Kavetsky Institute of Experimental Pathology, Oncology and Radiobiology, National Academy of Sciences of Ukraine, 03022 Kyiv, Ukraine; bigerash63@gmail.com

⁴ Centre for Cancer Immunology, School of Cancer Sciences, Faculty of Medicine, University of Southampton, Southampton SO16 6YD, UK; m.s.cragg@soton.ac.uk

* Correspondence: katrina@biomed.lu.lv

Abstract: Here, we review the role of the circadian clock (CC) in the resistance of cancer cells to genotoxic treatments in relation to whole-genome duplication (WGD) and telomere-length regulation. The CC drives the normal cell cycle, tissue differentiation, and reciprocally regulates telomere elongation. However, it is deregulated in embryonic stem cells (ESCs), the early embryo, and cancer. Here, we review the DNA damage response of cancer cells and a similar impact on the cell cycle to that found in ESCs—overcoming G1/S, adapting DNA damage checkpoints, tolerating DNA damage, coupling telomere erosion to accelerated cell senescence, and favouring transition by mitotic slippage into the ploidy cycle (reversible polyploidy). Polyploidy decelerates the CC. We report an intriguing positive correlation between cancer WGD and the deregulation of the CC assessed by bioinformatics on 11 primary cancer datasets ($\rho = 0.83$; $p < 0.01$). As previously shown, the cancer cells undergoing mitotic slippage cast off telomere fragments with TERT, restore the telomeres by ALT-recombination, and return their depolyploidised offspring to telomerase-dependent regulation. By reversing this polyploidy and the CC “death loop”, the mitotic cycle and Hayflick limit count are thus again renewed. Our review and proposed mechanism support a life-cycle concept of cancer and highlight the perspective of cancer treatment by differentiation.

Keywords: cancer resistance; genotoxic treatments; circadian clock (CC); cell cycle; DNA damage response (DDR); reversible polyploidy; reprogramming; senescence; telomeres; Hayflick limit

Citation: Vainshelbaum, N.M.; Salmina, K.; Gerashchenko, B.I.; Lazovska, M.; Zayakin, P.; Cragg, M.S.; Pjanova, D.; Erenpreisa, J. Role of the Circadian Clock “Death-Loop” in the DNA Damage Response Underpinning Cancer Treatment Resistance. *Cells* **2022**, *11*, 880. <https://doi.org/10.3390/cells11050880>

Academic Editors: Michal Goldberg and Alessandro A. Sartori

Received: 12 December 2021

Accepted: 1 March 2022

Published: 3 March 2022

Publisher’s Note: MDPI stays neutral with regard to jurisdictional claims in published maps and institutional affiliations.



Copyright: © 2022 by the authors. Licensee MDPI, Basel, Switzerland. This article is an open access article distributed under the terms and conditions of the Creative Commons Attribution (CC BY) license (<https://creativecommons.org/licenses/by/4.0/>).

1. Introduction

Resistance to anticancer treatments remains a significant problem in medicine and society due to the high morbidity of cancer patients. In 1968, the first clinical report on the association of polyploidy with the progression of malignancy appeared [1]. The chronological landmarks in the field of cancer polyploidy from Virchow and Boveri in the 19th century until now have recently been excellently reviewed [2]. From this perspective article, we build on this framework to evaluate the current knowledge of the role of the circadian clock (CC) in genome deregulation under a lens of its relationship to cancer polyploidy and resistance to anticancer treatments.

It is established that malignant tumours are characterised by various degrees of aneu-polyploidy emerging from whole-genome duplications (WGD) that appear early in cancer evolution, progress with disease aggression, and correlate with resistance to anticancer treatments [3–7]. The first-line anticancer therapies (ionising radiation and gen-

otoxic drugs) kill most tumour cells in the first days after administration. However, these cells can also evoke transient polyploidy that can give rise to clonogenic depolyploidised survivors several weeks or months after treatment cessation, recovering mitotically cycling cells, which disseminate, cause metastases, and can repeatedly polyploidise with disease relapse [8–12]. Observations showed that advanced tumours paradoxically acquire this additive mechanism of clonogenic survival within a certain interval of increasing genotoxic challenge, proportional to induced polyploidy ([12–15] and unpublished observations). We previously suggested that for both intrinsic and therapy-induced cancer polyploidy, the two reciprocally joined reproduction cycles, the rapid mitotic cycle, and the slow polyploidy cycle can drive cancer cell immortality akin to the transmission of generations in unicellular organisms and termed it the “cancer cell life-cycle” [16–18]. A similar process was termed by Jinsong Liu the “giant cell cycle”, highlighting its operation in more malignant tumours [19], while Rajaraman termed this process “neosis” accenting the cycling, budding of young offspring from senescing polyploid cancer cells [10,20]. As proof of concept, in a seminal paper, Zhang Weihua et al. [21] showed that a single polyploid giant tumour cell with senescence landmarks can develop metastatic cancer when transplanted in a mouse. Examples of experimental evidence of this mechanism published in the 21st century from 26 laboratories over the world are gathered in Table 1 and a series of relevant reviews [3–8,12,20,22–24] and most recently in a Special Issue of Seminars in Cancer Biology [25].

The induction or enhancement of polyploidy by cancer progression or anticancer treatments does not only assign the evolutionary advantage of genome multiplication masking lethal mutations [26,27] and provides an option for effective DNA repair [4,14,28,29]. The accompanying aneuploidy is also trading off its advantages and disadvantages (chromosome mis-segregation) by driving clonal selection in cancer genetic contexts [30,31]. However, it may also contribute via whole-genome triploid bridges [26] between diploid and tetraploid generations. A similar bridge by the doubled maternal genome was identified in a proportion of male para-triploid cancer karyotypes and in vitro on HeLa [32,33]. It is important to stress that polyploidy induced in cancer by genotoxic treatment cannot be reduced to only the genome multiplication and re-arrangements, but it is also accompanied by a crucial change in cell biology—the reprogramming of tumour cells to a state of embryonal stemness [11,13,22,34–38] with germline markers [16,18,36,39–42]. At this point, the polyploidy facet of cancer biology fuses with that of cancer stem cells, currently considered the main mechanism of cancer cell immortality and treatment resistance [43,44].

Then, there arises an interesting question: how much polyploidy and stemness constitute cancer identity and treatment resistance potential in organisms (independently of somatic mutations)?

The first part of this question is addressed in Section 2 of this review through the evaluation of bioinformatic transcriptome studies of polyploidy in normal mammalian tissues [45,46]. These data revealed in the gene ontologies and gene phylostratigraphy of polyploid mammalian tissues already known mechanisms of carcinogenesis and drug resistance, including stemness, but also unexpectedly the suppression of the circadian clock. The latter finding gave impetus to the current perspective.

The other side of the same question, concerning stemness, was addressed in experiments on irradiation-resistant malignant lymphoma and non-cancerous hepatic stem cell cultures reviewed in Section 3. The mutual features of the DNA damage response (DDR) conferring resistance were found in the adaptation of the DNA damage checkpoints leading to polyploidy. Therefore, in Section 4, we discuss the regulation of the embryonic stem cell (ESC) cell cycle checkpoints and DDR—revealing parallels with cancer polyploidy—in particular, the tolerance to DNA damage. In turn, this highlighted the intrinsic link between the paradoxical coupling of accelerated cellular senescence (ACS) creating and tolerating the DNA double-strand breaks (DSBs) with reprogramming.

ACS was first described as irreversible growth arrest in response to oncogenic, genotoxic, and oxidative stress [47]. Senescent cells possess compromised telomeres signaling persistent DNA damage [48]. In cancer, both opposing phenomena, i.e., senescence and stemness, are interacting through the secretome via paracrine and intracellular mechanisms [49,50]—akin to the process of wound healing [2]. However, the relationship of this paradoxical pairing between ACS and reprogramming with reversible polyploidy as the third component of cancer resistance revealed in a number of studies [51–58], also seen in Table 1, remains poorly understood and often overlooked [25]. Therefore, Section 5 reviews the important actors of ACS and mitotic slippage—including the cGAS-STING pathway, which senses soluble cytoplasmic DNA, in turn, reciprocally activating the Hippo pathway. The latter is involved in the regulation of the correct mitotic segregation of chromosomes, stemness, cell fate change, and reciprocally... again ACS. The missing component of this puzzle, the fate of telomeres eroded by ACS, is analysed in Section 6. There we review and illustrate our own data on the transient alternative telomere lengthening in polyploid cancer giant cells (PGCCs), which ensures recombinative restoration of telomeres and the return of telomerase activity in the budding mitotic progeny of clonogenic survivors. Finally, with the knowledge extracted from previous sections under the lens of cancer polyploidy, we approach the main biological oscillator, the circadian clock (CC), in Section 7. We review the data on CC participation in regulating the normal and ESC cell cycle, DDR, telomere elongation, and the eventual Hayflick limit count by the CC through cell cycles. The following Section 8 is devoted to the deregulation of the CC in mammalian polyploidy and cancer and discusses our current study of the correlative link between the deregulation of CC and polyploidy in primary cancers from the TCGA database. As a result of this analysis, we propose in Section 9 a working hypothesis on the deterioration of circadian rhythm through mitotic slippage in the polyploid phase of the “cancer cell life-cycle”, subsequent telomere restoration by ALT, and reset in resistant de-polyploidised offspring of the telomerase-dependent circadian pacing and Hayflick count of the restored mitotic cycle. We finally outline some other relevant perspectives in the field.

Table 1. A summary of experimental evidence for anticancer treatment resistance acquired via reversible polyploidisation of mammalian cancer cells (where the species is not indicated, human material was investigated). PGCC—polyploid giant cancer cells.

Cancer Type	Anticancer Treatments	Experiment Type and The Results	Source
Burkitt’s lymphoma Namalwa and Ramos	Ionising radiation (single dose of 10 Gy)	In vitro. DNA flow cytometry of induced reversible polyploidy; separation of >4C DNA by FACS, clonogenicity of the labelled polyploid fraction; detailed microscopy.	[9,59]
Transformed cell lines, cervical carcinoma, renal adenocarcinoma, neuro-blastoma	Ionising radiation, etoposide	In vitro. Computerised video-time-lapse microscopy recording of polyploidisation followed by bursting or budding of small cells restarting mitosis	[10]
Colon carcinoma DHD-K12-TRb (PROb) (rat)	Cisplatin	In vitro. Prolonged observation revealed delayed emergence of a limited number of extensive colonies which originate from polyploid cells, as demonstrated by cell sorting analysis. These colonies are made of small diploid cells which differ from parental cells by increased resistance to cytotoxic drugs.	[55]

Colorectal carcinoma HT 116	Nocodazole	In vitro. Fluorescence-activated cell FACS-purified cells with an 8n DNA content formed colonies that gave rise to a ~2n generation, which was followed by video-microscopy; the plating efficiency was higher for the TP53 ^{-/-} subline.	[60]
Lymphoblastoma (WI-L2-NS, TK6), Burkitt's lymphoma (Namalwa)	Ionising radiation (single dose of 10 Gy)	In vitro. Induction of reversible polyploidy up-regulates OCT4, NANOG, and SOX2), which facilitate survival suppressed by retinoic acid. Dependence on mutant TP53 status.	[34]
Fibrosarcoma (mouse)	Doxorubicin	In vitro. Induced and isolated single giant cell allografts cause metastatic cancer.	[21]
NK/Ly lymphoma mouse	Vinblastine	In vivo. An increased number of giant cells were induced by vinblastine treatment and observed microscopically in tumour-bearing mice.	[61]
Colorectal carcinoma HCT116 modified lines	H ₂ O ₂	Tetraploid cell line established from parental diploid HCT116 via cell fusion revealed the superiority of tetraploidy over p53 for cell survival when compared by cell viability, cell cycle, and apoptotic response to H ₂ O ₂ with parental HCT116 and p53- inactivated sublines.	[62]
Breast carcinoma	Ionising radiation (single dose of 4 and 8 Gy)	Ex vivo. patient samples, ionising radiation re-programmed differentiated breast cancer cells into induced stem cells. They showed increased mammosphere formation and increased tumorigenicity in xenografts. Reprogramming occurred in a polyploid subpopulation of cells, coinciding with re-expression of the transcription factors Oct4, SOX2, Nanog, and Klf4, and could be partially prevented by Notch inhibition.	[13]
Non-small cell lung cancer in patients, NCI-H1299 cell line	Camptothecin, doxorubicin, cisplatin	Ex vivo: Clinicopathological study in patients with locally advanced non-small-cell lung cancer demonstrate that therapy-induced senescent cells following neoadjuvant therapy are prognostic of an adverse clinical outcome. In vitro: polyploid senescent cells represent transition states through which escape preferentially occurs.	[63]
Breast carcinoma T-47D and ZR-75-1	Genotoxic drugs and mTOR inhibitors	In vitro. Inhibition of mTOR signalling prevents the polyploidy/senescence induced by genotoxic drugs and increases cell chemosensitivity.	[64]
Colorectal carcinoma HCT-116 and Ca-co-2 cell lines	5-fluorouracil and oxaliplatin	In vitro. CoCl ₂ induction of hypoxia in colon cancer cells causes the formation of PGCCs, the expansion of a cell subpopulation with CSC characteristics and chemoresistance.	[65]
Virally transformed rat fibroblasts with sup-	Ionising radiation	In vitro. Permanent activation of DDR signalling due to impaired DNA repair results in the induction of cellular senescence in E1A + E1B cells.	[66]

pressed apoptosis in E1A + E1B cell lines		However, irradiated cells bypass senescence and restore the population by dividing cells, which have a near-normal size and ploidy and do not express senescence markers.	
Ovarian adenocarcinoma, breast carcinoma (HEY, SKOV3, and MDA-MB-231)	Cisplatin	In vitro and in vivo. Separation of induced PGCCs by CoCl ₂ ; characterisation of stemness, observation of budding offspring, A single PGCC formed cancer spheroids in vitro and generated tumorigenic xenografts.	[11]
Multiple human tumour types	Etoposide, doxorubicin, ionising radiation	In vitro and in vivo. Cell lines, time-lapse video microscopy observing budding of survivors from giant tumour cells; tumour xenografts.	[22,38]
Ovarian carcinoma (SKOV3, IGROV-1 cell lines)	carboplatin	In vitro. Generation and depolyploidisation of PGCCs by multipolar divisions and budding (time-lapse life cell imaging). Induction of EMT and senescence markers.	[67]
N-RA(61K)-mutant pigment cell culture cell	Doxycycline-inducible activation of oncogenic N-RAS	In vitro. Multinuclear senescent cells are induced, giving rise to mononuclear tumour progeny observed by time-lapse microscopy. The progeny is tumorigenic in xenografts.	[68]
Colorectal carcinoma (HC116)	Doxorubicin	In vitro. The cells which, along with therapy-induced senescence, undergo polyploidisation are prone to regaining the ability to proliferate.	[53]
Ovarian carcinoma (Hey, SKOV3, OVCAR433)	Paclitaxel	In vitro. Generation of genomically altered tumour-initiating cells through a giant cell cycle that contributes to tumour relapse was observed using live-cell fluorescence time-lapse microscopy. PGCCs were shown to self-renew via endoreplication and divide by nuclear budding or fragmentation.	[69]
Breast carcinoma	Doxorubicin + paclitaxel	Ex vivo. Sampling before and after neoadjuvant therapy. Induction of depolyploidising PGCCs positive for OCT4, SOX2, NANOG, and CD44 was mainly observed in near-triploid resistant cases.	[70]
Ovarian carcinoma (Hey, SKOV3, and MDA-HGSC-1 cell lines)	Paclitaxel	In vitro and in vivo. The obtained single PGCCs formed spheroids with the properties of blastomeres, including differentiation into three germ layers and formation of carcinoma, germ cell tumours, as well as benign tissue, in xenografts.	[37]
Prostate carcinoma PC3 line	Docetaxel	In vitro. A micro-fabricated “evolution accelerator” environment for controllable in vitro with a spatially varying drug concentration. The authors observed the rapid emergence of a large number of PGCCs with EMT marks at a very high drug concentration.	[15]

Glioblastoma T98G, A172, R2, T1 cell lines	Ionising radiation; Fotemustine	In vitro. The resistant cell lines displayed the PGCCs and high activity of tumour and micro-environment promoting genes.	[71]
Breast carcinoma and mouse melanoma	5-fluorouracil	In vitro and in vivo. The authors found IL 33 to be a key driver of cancer resistance through polyploidy.	[72]
Breast carcinoma (MDA MB 231 cell line)	Doxorubicin	In vitro. Resistant reversible polyploidisation registered by DNA cytometry; 7-week follow-up; IF, microscopy. Transient ALT in mitotic slippage; Budding of mitotic progeny from PGCCs.	[73]
Ovarian carcinoma (SCOV-3 and A2780 cell lines)	Cisplatin	In vitro. Bioinformatic analysis of induced PGCCs—upregulation of genes mainly related to gene regulatory mechanisms and nuclear processes, including negative chromatid segregation, microtubule polymerization and membrane budding.	[74]

2. Transcriptome Analysis of Polyploidy versus Diploidy in Normal Mammalian Tissues Reveals a *c-Myc*-Targeted Shift to Stemness and Other Known Mechanisms of Cancer Origin and Resistance

When the polyploid transcriptomes of normal mammalian tissues (heart, liver) are compared with diploid cells, the upregulation of *c-Myc*—an essential component of Yamanaka reprogramming [75]—is evident [45]. To evaluate its impact, a bioinformatic comparative study focused on multiple primary targets of *c-Myc*, alongside gene phylostratigraphic analysis of transcriptomes, was performed [46]. Surprisingly, they revealed in the gene ontologies of differentially the expressed genes (comparing polyploid and diploid) the already known mechanisms of cancer and drug resistance, such as the Warburg effect, the epithelial-mesenchymal transition (EMT), alongside atavistic features of unicellularity originating the ABC drug efflux, suppression of apoptosis, differentiation and cellular communication, immune evasion, enrichment of bivalent-chromatin genes, and suppression of the CC.

3. Resistance to Ionising Irradiation in Malignant Tumours and Tissue Stem Cells Is Associated with Induced ESC Stemness Concurrent with Senescence, Weak DNA Damage Checkpoints, and Polyploidy

The normal mitotic cell cycle consists of the G₁, S, G₂ and M phases. Progress through these is driven by corresponding cyclin-kinases. If DNA damage has occurred, cells can activate the G₁, intra-S, and G₂/M checkpoints and arrest the cell cycle to repair the damage. There are the two major DNA damage signalling pathways—regulated by ATM/CHK2 and ATR/CHK1. The ATM/CHK2 pathway is primarily activated by double-strand breaks (DSBs), while the ATR/CHK1 pathway is triggered in response to replication fork collapse. Following DNA double-strand breaks (DSB), the ATM protein is activated by autophosphorylation, which then activates CHK2. The p53 tumour suppressor, a major effector of the DDR pathway, is expressed at low levels and in an inactive form during normal conditions. Both ATM and CHK2 phosphorylate p53, causing its stabilisation and activation. Activated p53 arrests the cell cycle by inducing cell cycle inhibitors such as p21/CIP1. The DDR acting at the checkpoints normally allows the cell to repair its damaged DNA or alternatively undergo apoptosis [76].

Whereas normal healthy somatic cells have the fate indicated above, the response of malignant cancer cells can differ, leading to treatment resistance. Current data suggest

that resistance can be induced in malignant tumour cells by reprogramming to an ESC-like state accompanied by WGD [13,34,77]. As illustrated in Figure 1A,B, the master regulator of embryonic stemness OCT4 can be induced in the mtTP53 Burkitt's lymphoma cell line, Namalwa, alongside polyploidisation after 10-Gy irradiation [34]. In our study, the upregulated OCT4 alongside Nanog and SOX2 were shown to create a coordinated nuclear network, while all-trans-retinoic acid (an OCT4 antagonist and differentiation inducer) disrupted the nuclear localisation of Nanog, and subsequently cell survival. Similarly, the embryonal-type stemness could be partially suppressed by Notch inhibition [13,77].

Strikingly similar post-irradiation effects were found in the rat liver cell line WB-F344, which is a hepatic tissue-specific stem cell line capable of differentiating into hepatocytes and cholangiocytes [29]. This wtTP53 cell line, benign and incapable of inducing tumours *in vivo*, was shown to be radioresistant [78]. In common with genotoxically resistant cancers, the prominent feature of WB-F344 cells is a radiation dose-dependent enhancement of polyploidisation and micronucleation [29,78]. In this study, along with polyploidisation, there was also upregulation of the stemness transcription factors Oct4 and Nanog following 10-Gy irradiation [29], particularly enhanced in the polyploid fraction (Figure 1C). Thus, while one cell type is malignant (Namalwa) and the other benign (WB-F344), both radioresistant cell lines are similarly capable of the DNA damage-induced reprogramming—evoking the induction of ESC-type stemness alongside polyploidy. Finally, there was a radiation dose-dependent delay at the G2/M checkpoint (Figure 1D) that preceded and was proportional to the extent of polyploidisation within a considerable interval of increasing resistance. The same was found for malignant TP53-mutant lymphomas [14,59], as well in prostate cancer and colorectal cancer treated with genotoxic drugs [15,65], and in unpublished research. This response, characteristic for both benign and malignant resistant cell lines, reacting to irradiation with polyploidy-associated reprogramming to an ESC-state, is indicative of: (1) the weakness of the G1 checkpoint resulting in cell accumulation in G2M and, concurrently, (2) the insufficiency of the G2M damage checkpoint, the main DSB sensor and actor, showing the tolerance to DNA DSBs and allowing transition to polyploidy.

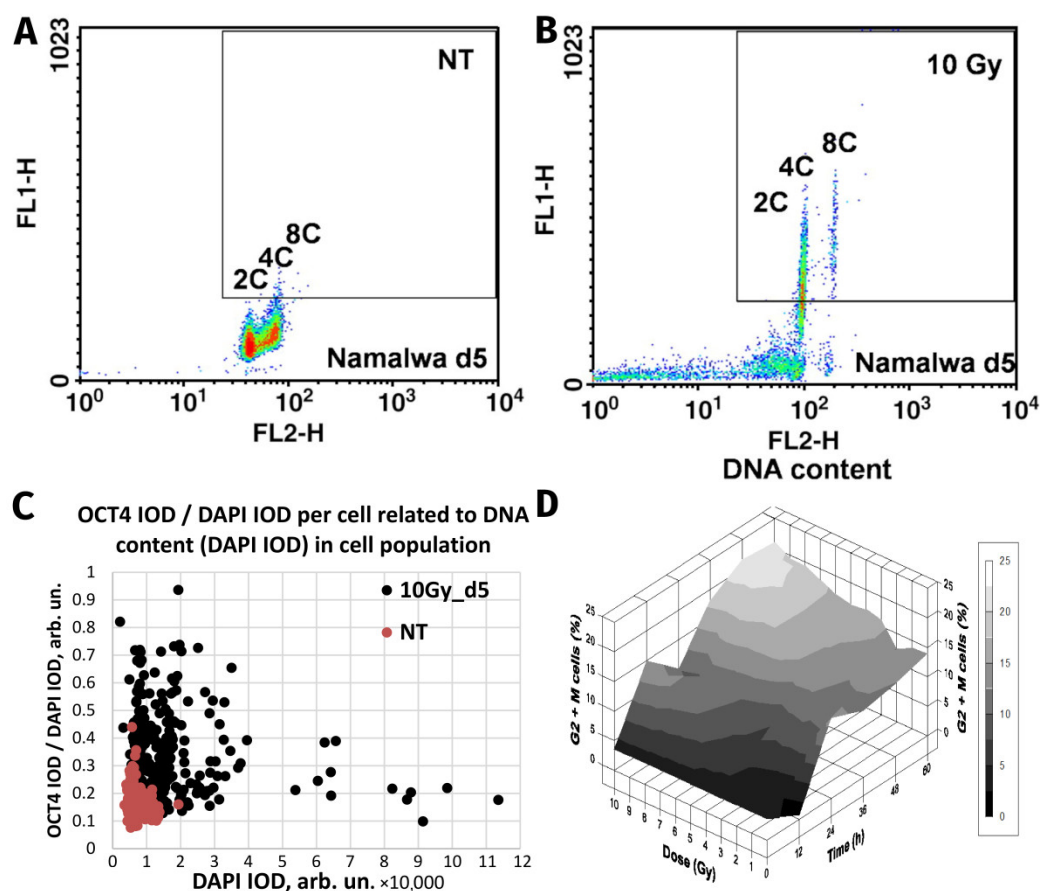


Figure 1. The similarity of responses to acute Irradiation (10 Gy) of the malignant human Burkitt's lymphoma cell line Namalwa and benign rat liver progenitor stem line WB-F344. Radiation-induced Oct4 upregulation in Namalwa cells as revealed by flow cytometry: panel (A) unirradiated cells (control); panel (B) irradiated cells on day 5 post-irradiation. According to the extent of the FL1-signal (immunofluorescence from Oct4), Oct4 is predominantly expressed in polyploid 4C and 8C cells whose DNA content was determined by propidium iodide staining for DNA (FL2-signal) (reprinted with permission from [34]. Copyright ID 1188250-1, 2022, Elsevier Science & Technology Journals). Panel (C) radiation-induced Oct4 upregulation in WB-F344 cells as revealed by two-parametric image analysis of integral optical densities (IOD): represented as Oct4 (IOD)/DAPI (IOD) versus DAPI (IOD). Panel (D) radiation-induced G2/M delay in WB-F344 cells which is dose- and time-dependent (image from [78]).

In addition, in both models, there is a dynamic toggle between two stemness and senescence regulators, NANOG and p16INK4a [29,34].

Concluding this section, the *in vitro* studies on irradiation-resistant malignant tumours and tissue stem cells revealed the following consistent features: induction of embryonic-type stemness (reprogramming) concurrent with senescence, attenuation of the DDR and transient polyploidisation. To better dissect this common mechanism, the regulation of the cell cycle checkpoints in ESCs will be reviewed in the next section.

4. Embryonic Stem Cells (ESCs) Have Defective Cell Cycle Checkpoints That Favour DNA Damage Tolerance and a Shift to Polyplody

There is a body of evidence indicating that ESCs have a short G1-phase and weak or absent G1/S checkpoint or a long S-phase and weak intra-S and G2/M checkpoints [79–81]. In response to stress, ESCs have a tendency to undergo mitotic slippage from the spindle checkpoint, shifting to G1-tetraploidy at a specific stage with non-degradable cyclin B1, which protects ESCs from mitotic catastrophe [82]. In irradiated tumour cells,

this stage may be preceded by delayed endo-prometaphase [83]. Under stress, ESCs epigenetically switch off the genome-guardian function of p53 [79,80]. The same is known for even TP53 wild-type tumours [84]. Presumably, the inherent risk of genome instability that this brings is offset by and required for their strategy for survival reliant upon explorative adaptation, which demands the freedom of choice [16,85]. The induction of stemness in the damaged tumour cells in many ways is akin to the induced reprogramming by Yamanaka factors in normal cells [75], which also simultaneously causes DNA damage-tolerating senescence [48] that paradoxically is indispensable for its induction [50].

Transcription factors of the basic embryonal stemness network also possess the properties of cyclin-kinases or can otherwise overcome the senescence-driving and cell cycle-arresting cyclin-kinase inhibitors of the corresponding checkpoints. In particular, OCT4 induces the adaptation of the G1/S checkpoint by activating Cdk2 in the Cyclin E/Cdk2 complex [86,87] and enhancing the transcription of cyclin-kinases CDK4 and CDC25A [79,88]. OCT4 also toggles p21CIP1 [89] in a p53-dependent (DDR-induced) manner [56,57,90]. Nanog activates Cdk6 by directly binding by its C-domain [79], thus competing in the G1/S checkpoint with p16INK4a, which inhibits cyclin D. In the DDR, p16 is also activated by exaggerated expression of p21 and can cause terminal senescence [91]. Concurrently, together with IL-6 secreted by senescent cells, p16 is paradoxically indispensable for reprogramming [49]. In turn, SOX2 directly interacts with p27(KIP1) in reprogramming to stimulate adaptation of the Cyclin E/Cdk2-dependent G1/S checkpoint [92] and also restricts the G2M checkpoint [93]. The most important activation of CDKs and opposing interactions between the embryonal stemness factors (OCT4, Nanog, and SOX2) with corresponding senescence regulators (p21, p16, p27) are shown in Figure 2.

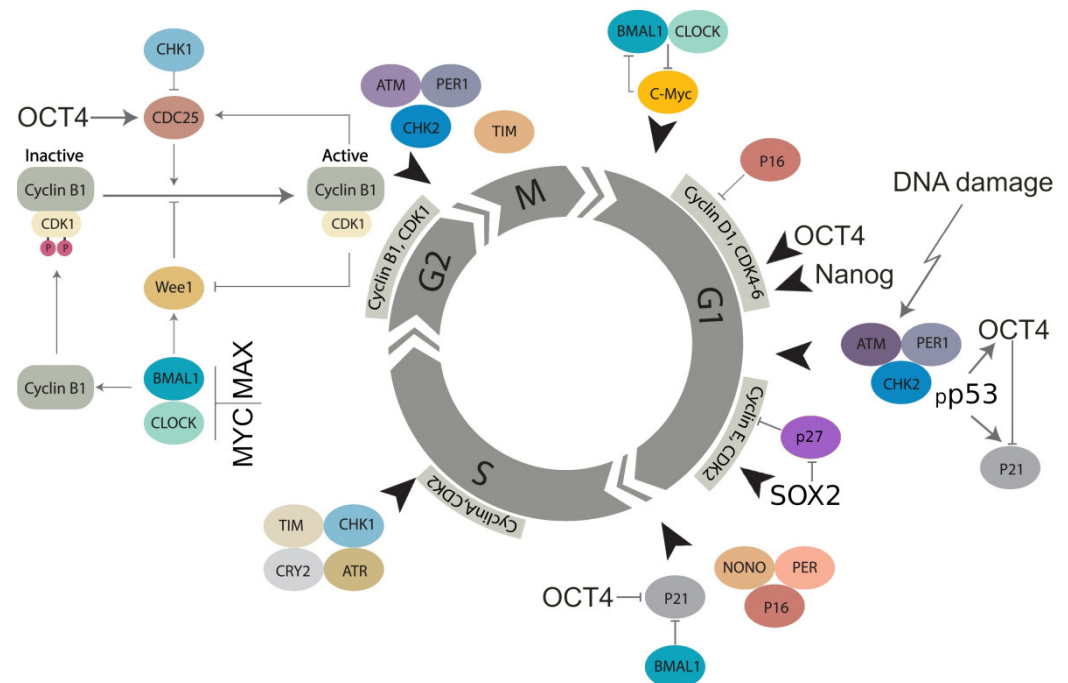


Figure 2. Molecular linkage between the regulators of the cell cycle in embryonic (cancer) stem cells with the checkpoints adapted by basic stemness transcription factors in their relationship with CDK inhibitors (not all of them are shown) and the circadian clock (adapted from [94] under Creative Commons Licence). The details of the action of the circadian clock regulators in DNA damage checkpoints and WGD are reviewed in Sections 7 and 8.

This scheme will be used again in Sections 7 and 8 to describe the role of the CC in the cell cycle, WGD, and cancer. The current analysis indicates that ESCs tend to adapt to the checkpoints of the normal cell cycle, especially as part of their DDR.

“He who dares wins” (*qui audet vincit*). Mitotic slippage (MS) represents a transition compartment between the mitotic cell cycle and polyploidy in tumours undergoing DDR-mediated reprogramming. Three additional issues about MS need to be understood: (1) How the centrosomal cycle is affected? (2) What happens to the telomeres? (3) What is occurring with the biological time upturning from cell senescence for the birth of a new mitotic offspring?

5. The Hyperactivated Hippo-YAP Pathway Relieves Control of Karyo-Cytokinesis, Reciprocally Favours MS, ACS, cGAS-STING Signalling and Polyploidy, and Enables Cell Fate Change

The Hippo pathway is an important regulator of genome stability, stem cell biology, and cell fate change [95]. It was also shown to be involved when deregulated in the origin of cancer polyploidy through cytokinesis failure [96–100]. Currently, it appears that the participation of Hippo deregulation in the events around MS is multifaceted, and here, we attempt to consolidate them. Normally, the main effector of the Hippo pathway, YAP1, is retained in its phosphorylated form in the cytoplasm. The nuclear import of the de-phosphorylated YAP1 initiated by LATS1/2 enables its binding in a (YAP1 + TEAD) complex to DNA, which facilitates hyper-transcription and replication stress due to multiple targets of hyperactivated YAP1 [101]. Interleukin-6, a pivotal senescence inducer indispensable for reprogramming [49], is one of these targets [102]. The feedback loop of cellular senescence in Hippo-YAP signalling has also been reported [103]. The ACSs were shown to release heterochromatin particles into the cytoplasm inducing autophagic lysosome activity [104] and production of cytoplasmic DNA. This activates the cytosolic DNA-sensing cGAS-STING pathway, producing diverse interferons and inflammatory cytokines [105,106]. The ACS-associated degradation of nuclear lamin B favours mitotic slippage and micronucleation of such cells, resetting interphase in a tetraploid state [107]. GAS-STING signalling, in turn, causes reciprocal deregulation of the Hippo-YAP1 pathway by inducing its upstream LATS1/2 kinase [108].

On the other side, the Hippo-related Aurora-A-Lats1/2-Aurora-B axis is pivotal for the centrosome cycle and accurate coordination between chromosome segregation, karyokinesis, and cytokinesis in anaphase and midbody abscission in telophase. Deregulation of this axis subsequently leads to aberrant metaphases, anaphase bridges, bi-nuclearity, multinuclearity, and fusion of daughter nuclei [96–100]. In addition, the stress-activated LATS1/2 causes the dysfunction of the pivotal guardian of genome stability and diploidy p53 [109] and thus can compromise its ploidy control [110].

The coordinated functions of the Hippo pathway ensure genome stability, whereas stress-induced dysfunction likely creates a vicious cycle through reciprocal activities and feedback loops starting with replication stress and around MS, which favour the transition of cancer cells to polyploidy with all its attributes—stemness, ACS and aneuploidy. Moreover, the stress-response is preceded by fast (0.5–2 h) oscillations of YAP1 nucleo-cytoplasmic localisation [111]. Interestingly, in response to DNA breaks induced by irradiation of MCF7 cells, p53 also oscillates in the p53-MDM2 loop with a similar periodicity [112] and drives the OCT4-p21CIP1 stemness-senescence toggle in embryonal carcinoma [56,57]. Cells that experience p53 oscillations recover from DNA damage, whereas cells exposed to sustained p53 signalling have poor survival [113]. It is tempting to suggest that both pulsing activities of two main tumour suppressors and genome guardians, when induced by lethal genotoxic challenge, coordinate their oscillations. In thermodynamic terms, such oscillations between the opposite genome and cell state favour explorative adaptation to the immediate alternative microenvironments to increase the chance of survival [16,114]. However, it is not immediately clear how this vicious circle solves the telomere problem of ACS in cancer resistance.

6. Under-Replication, Erosion, and Recovery of ACS-Compromised Telomeres in Mitotic Slippage and Transient Polyploidy through Transient Alternative Telomere Lengthening

Cancer cell lines undergoing mitotic slippage accompanied by the cytoplasmic release of chromatin after genotoxic challenge also exhibit the under-replication of DNA in the late S-phase [57,73]. Under-replication of heterochromatin has been widely described in plants and insects, and Walter Nagl [115] indicated that it was always and only associated with the endocycle. Recent studies on *Drosophila* polyploid cells associate telomere under-replication with inhibition of replication fork progression and control of DNA copy number [116,117].

ACS was defined by Campisi [118] as cell stress that is characterised by compromised shortened telomeres, which may be induced by oncogenic stress or DNA damage. As such, it appears that telomere erosion stemming from heterochromatin under-replication may, in fact, result from the replication stress observed in cancer development and treatment [119], occurring in the S-phase preceding polyploidisation by MS in the same or rather (as observed) next cell cycle (involving the relaxation of the “Hippo-genome-stability barrier” by YAP1-hyperactivation as already discussed). Tam et al. [120] likely were the first to define ACS as a reversible process that is determined by the balance of biological molecules which directly or indirectly control telomere length and telomerase activity by altering gene expression and/or modulating the epigenetic state of the chromatin. Our studies on the MDA-MB-231 breast cancer cell line treated with the Topoisomerase II inhibitor doxorubicin [73] revealed telomere ends enriched in DSBs were discarded during MS together with the telomere capping protein TRF2 and the telomerase catalytic subunit TERT (Figure 3A–C). In the inter- and post-MS polyploid cells, restoration of the telomeres by alternative telomere lengthening (ALT) marked by specific TRF2-positive PML bodies was found (Figure 3D). It was followed by the recovery of TERT activity in the budding offspring returning to the mitotic cell cycle (Figure 3E,F). Importantly, in this interim process of telomere restoration through ALT-driven homologous recombination, the telomere ends of the chromosomes were found closed [73]. Telomere shortening in diploid somatic cells is associated with the linear chromosome end replication problem, cutting telomeres in each cell cycle by ~50 bp [121]. This process is the molecular basis underpinning the Hayflick limit [122], permitting somatic cells to replicate only a limited number of times, proportional to the species’ lifespan. Thus, with the “trick” of under-replication signalling ACS and transient ALT, the chromosome end problem and the Hayflick (somatic mortality) limit may be circumvented by polyploid tumour cells.

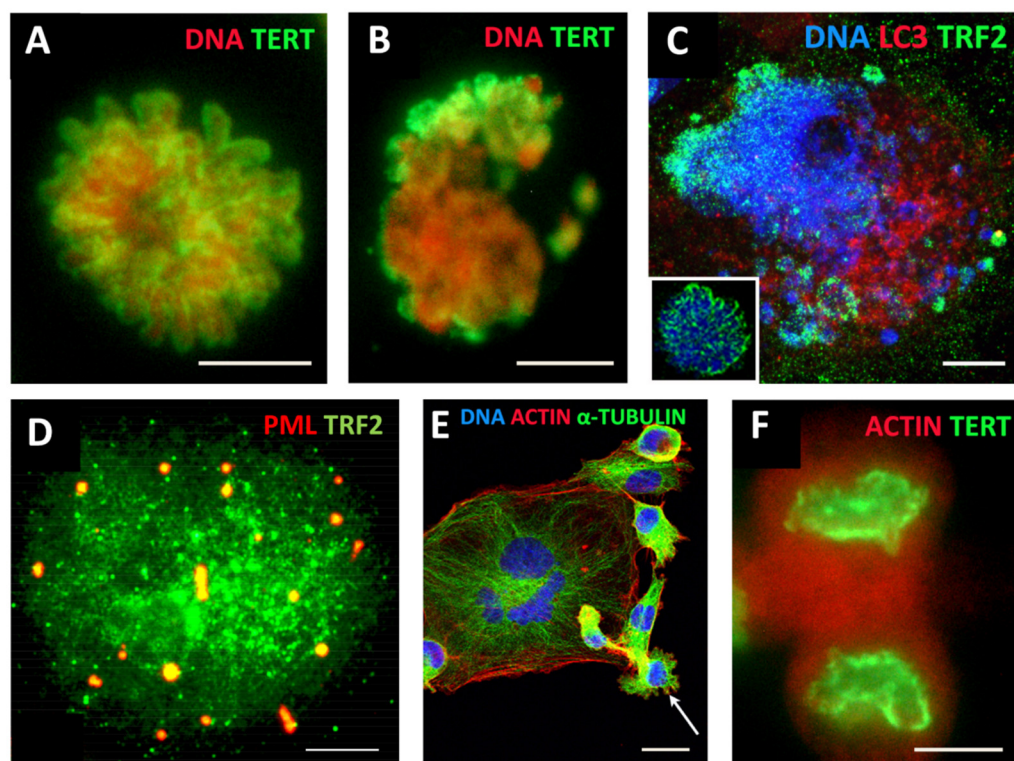


Figure 3. Mitotic slippage of the MDA-MB-231 breast cancer cell line. (A) TERT-positive metaphase in control cells (DNA counterstained by propidium iodide); (B) mitotic slippage with low TERT nuclear and enriched cytoplasmic DNA staining on Day 5 after DOX treatment; (C) preferential release of the telomere shelterin-TRF2-associated chromatin into the cytoplasm on Day 7 after DOX treatment (insert: normal metaphase); (D) polyploid cell marked by specific TRF2-positive PML bodies, suggesting the restoration of the telomeres by alternative telomere lengthening (ALT); (E) A giant multinuclear cell is budding subcells (arrow); (F) TERT-positive escape telophase cell on Day 22 after DOX treatment; Bars: (A–D,F) = 10 μ m; (E) = 25 μ m. Subfigures A–C,E,F are republished from [73] under Creative Commons Licence.

A positive regulator of telomere length, Sirtuin 1—a NAD-dependent histone deacetylase (HDAC)—binds directly to telomere repeats and attenuates telomere shortening associated with mouse ageing; this effect is dependent on telomerase activity [123]. At the same time, SIRT1 is very tightly associated with the regulation of the main cellular pacemaker—the CC. To analyse this aspect, we must first briefly describe the inner workings of this remarkable clock in the normal and ESC cell cycle (the latter is induced in tumours by DDR as described above in Section 4).

7. The Circadian Clock (CC) Paces the Mitotic Cell Cycle, DDR Checkpoints, and Reciprocally, the TERT-Dependent Hayflick Limit Count. It Is Absent in ESC, Early Embryo, and Germ Cells and Likely Becomes Dis-Engaged and Then Restored (By Reversible Polyploidy) in Cancer Cells

The bi-phasic CC is an autoregulatory transcriptional feedback loop-based oscillator involved in pacing the processes of living organisms with 24 h periodicity [124]. The CC also regulates the cell cycle and couples various metabolic oscillations with shorter ultradian periodicity [125].

The core structure of the CC's molecular oscillator contains a transcriptional activator, made up of *BMAL1* and *CLOCK*, and a transcription repressor consisting of *PER* (Period) and *CRY* (Cryptochrome) genes. The heterodimeric complex of *BMAL1* and *CLOCK*, which are basic helix-loop-helix transcription factors, binds the promoters and activates the expression of *PER1*, *PER2*, *PER3*, *CRY1*, and *CRY2*, which, in turn, hetero-

dimerize into PER/CRY complexes, translocate into the nucleus, and repress BMAL1/CLOCK [126]. The concentration of PER and CRY proteins is regulated by E3 ubiquitin ligases, resulting in their eventual depletion and BMAL1/CLOCK1 reactivation [127]. A second, adjacent feedback loop involves nuclear receptors that bind DNA in a periodic manner—the activating RORs and repressive REV-ERBs [128]. These nuclear receptors regulate the expression of BMAL1 and NFIL3 and are themselves rhythmically regulated by the action of NFIL3, CLOCK, BMAL1, and DBP. In this way, the expression patterns of the clock components induce oscillatory behaviours in their downstream interactants [94,124]. It was also shown that alternative splicing, as well as piRNA-mediated regulation of the transposons, could represent another level of clock control [129]. The CC, in general, is susceptible to stress—the circadian cortisol-mediated entrainment of ultradian transcription pulses that provide the normal feedback regulation of cellular function is then lost [130].

Several genes of the CC deliver the strictly synchronised oscillation frequencies of the cell cycle [94,131] and participate in the regulation of the DNA damage checkpoints [125,132], as presented in Figure 2 [94]. The CC becomes dysfunctional in reprogramming induced by Yamanaka transcription factors [133]. Interestingly, circadian oscillation is also not detectable in ESCs until differentiation starts [134]. This may be related to the overexpressed stemness transcription factors speeding the cell cycle and forcing adaptation of its checkpoints, as discussed in Section 4 and illustrated in Figure 2. In addition, the direct competition of the main reprogramming transcription factor, MYC/MAX, with the CLOCK/BMAL1 dimer [125] in the G1/S and G2M checkpoints [135], which can be overcome through upregulated MYC [136] (as designated on Figure 2), should be highlighted.

The loss of circadian rhythms impairs Hippo signalling, destabilises p53 [137], and potentiates tumour initiation [138]. On the contrary, in vitro differentiation of ESCs induces cell-autonomous robust circadian oscillation [139]. It is important to note that besides ESC, the CC is also not functional in normal primordial germ cells (PGCs) and both male and female gonocytes [140–142]; the germline-specific protein PIWIL2 suppresses circadian rhythms [143] by inactivating the *BMAL1* and *CLOCK* genes.

Noteworthy, in mammalian sperm, the telomere ends are joined, forming looped chromosomes [144], such as those observed in mitotic slippage of cancer cells [73] and also in bi-parental bi-chromatid genome segregation found by us alongside conventional mitoses in ovarian embryonal carcinoma [145]. Interestingly, early mammalian embryos also display segregation of biparental genomes in the first short cleavage cycles [146] and also lack circadian regulation, which initiates in late embryos, tightly coupled to cellular differentiation (in particular, somitogenesis) [147].

The above-mentioned telomere-specific nicotinamide adenine dinucleotide (NAD⁺)-dependent HDAC SIRT 1, maintaining telomeres through telomerase activity, was found to interact with CLOCK and to be recruited to circadian promoters in a cyclic manner [148]. In particular, Wang et al. [149] showed that *Sirt1*-deficient mice exhibited profound premature ageing and enhanced acetylation of histone H4 in the promoter of *Per2*—the latter leads to its overexpression. In turn, *Per2* suppresses *Sirt1* transcription through binding to the *Sirt1* promoter at the Clock/Bmal1 site. This negative reciprocal relationship between SIRT1 elongating telomeres and CC pace observed also in human hepatocytes [150] may perform the Hayflick limit count by CC.

We can subsequently rationalise that telomere shortening in ACS slows the circadian time-count, and further interruption of telomerase maintenance by TERT in MS substituted by recombination-based ALT with closed telomere ends should interrupt CC (arresting the biological time pace) while returning to the TERT mechanism in depolyploidised offspring restoring the mitotic cycle [73] should resume the CC oscillator and hence the Hayflick limit count. This manipulation of biological time in MS is reminiscent of a “death loop” in aviation.

8. The Circadian Clock Is Deregulated in Mammalian Polyploidy and Cancer

8.1. The Reciprocal Regulation of Polyploidy and CC Activity in Non-Malignant Tissues

The competitive antagonism of the overexpressed stemness/reprogramming master factor dimer MYC/MAX with CLOCK/BMAL1, which is the core component of the CC's activation arm and a regulator of the G2M DNA damage checkpoint, is likely to play a key role in impairing the CC in stem cells (including stressed cancer cells that have undergone reprogramming), where stemness features were shown to be tightly coupled to deregulation of the cell that leads to polyploidy. The Timeless (TIM) gene was shown to be involved in the S-phase checkpoint [76]. The circadian clock proteins PER1, PER2, and PER3 are involved in the ploidy regulation of non-cancerous liver cells, and their inactivation results in rampant polyploidisation (both in terms of polyploidisation frequency and increased ploidy counts in the polyploid hepatocytes) [151]. It is also important to mention that of the 16 core genes of the circadian clock (*CLOCK*, *ARNTL* (*BMAL1*), *ARNTL2*, *NPAS2*, *NR1D1*, *NR1D2*, *CRY1*, *CRY2*, *DBP*, *TEF*, *RORA*, *RORB*, *RORC*, *PER1*, *PER2*, and *PER3*) [152,153] 50% are bivalent genes [154] allowing rapid cell fate change. Interestingly, polyploidy (the endocycle) in plants was shown to decelerate the circadian rhythm [155]. In contrast, evidence from mouse and human transcriptome analyses suggests that the deregulation of the CC promotes polyploidisation and vice versa [46,151]. In turn, polyploidy in normal tissues, such as the mammalian heart and liver, is associated with upregulated *c-Myc* and the stemness and cancer-linked EMT targets [45]. The role of the CC in cell cycle integrity and DDR signalling is further showcased by its involvement in DNA repair after ionising irradiation damage (by inducing DDR-signalling genes) (Figure 2) [94,156,157].

The CC was reported as notably dysregulated in cancer [152,153,158], and perturbation of the CC is in itself carcinogenic [159,160]. Meta-analysis of 7476 cancer cases from 36 sources [161] revealed that low expression of PER1 and PER2 correlates with poor differentiation, worse TNM stage, metastases, and reduced patient survival.

Overall, the currently available information on the connection between the CC, stemness, and the cell cycle, as well CC deregulation in cancer, leads us to suggest that circadian dysregulation in human cancer may be largely associated with its polyploidy component as it is in normal mammalian heart and liver. In the next section, we describe an attempt to investigate this hypothesis through bioinformatic analysis of primary cancers.

8.2. Circadian Deregulation Correlates with Polyploidisation (Whole-Genome Doubling) in Malignant Tumour Patient Samples

In order to investigate the possible connection between polyploidy and CC deregulation in cancer, it was first necessary to calculate the measure of circadian deregulation. To that end, we used the Cancer Genome Atlas (TCGA), a large-scale collection of omics and clinical data on over 30 types of malignancies from over 11,000 patients [162]. TPM-normalised Rsubread-processed TCGA gene expression data were obtained from the GSE62944 GEO dataset [163]. In order to ensure statistical power, only TCGA transcriptomics datasets counterpart by at least 35 available normal samples were selected, resulting in a final cohort of 11 cancer types and 6667 samples (613 normal and 6054 tumours).

Circadian deregulation in TCGA cancer samples was determined using the CCD method and *deltaccd* R package developed by Shilts et al. [153], which compares core CC gene co-expression (Spearman rank-based correlation) between samples used in the study and a pan-tissue reference matrix calculated from eight normal mouse datasets with available time data. The Euclidean distance between CC gene correlation vectors of the samples and the mouse reference is referred to as the Clock Correlation Distance (CCD). The difference between normal vs. reference CCD, and the tumour vs. reference CCD, known as the Δ CCD, serves as a coefficient of circadian dysregulation, with the

“difference of differences” approach effectively negating the nuance of mouse–human comparison and accepting the common regulation of CC in mammals [164].

Tumour ploidy calculated from somatic DNA alteration data using the ABSOLUTE algorithm [165] was obtained from [166], and the relationship between the values of scaled Δ CCD for each of the 11 tumour types and the respective proportion of samples with at least one WGD was investigated using Spearman correlation analysis.

The results revealed a statistically significant positive correlation (Spearman’s $\rho = 0.83$; $p < 0.01$) between WGD and CC deregulation (Figure 4). While correlation does not necessarily equal causation, such a result seems logically sound when taking into account the known associations between polyploidy and the CC in normal tissues, deregulation of CC in cancers, as well as the impact of polyploidy on cancer evolution.

Correlation of circadian deregulation and polyploidy in 11 TCGA cancer types

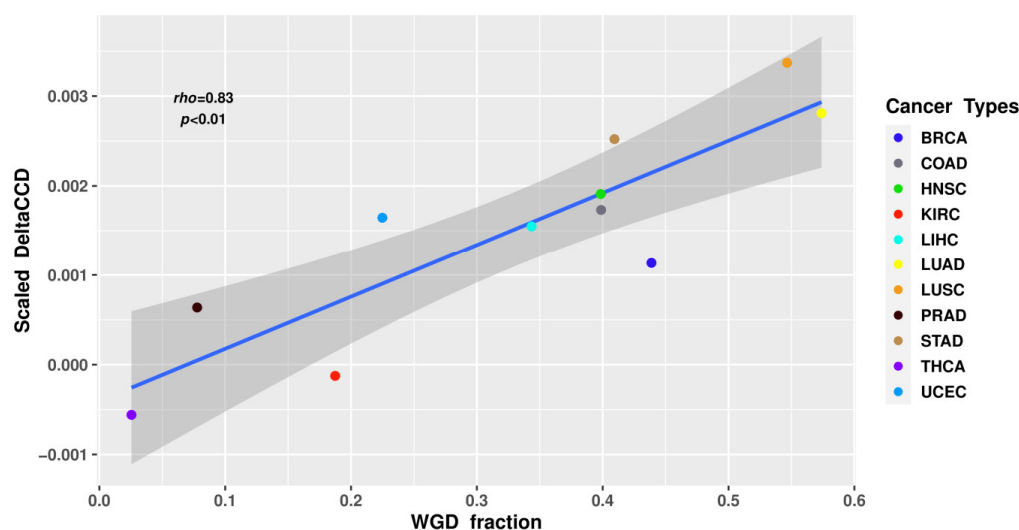


Figure 4. The Δ CCD coefficient of circadian deregulation positively correlates with the proportion of WGD in the samples of 11 tumour types from The Cancer Genome Atlas (TCGA) database. BRCA—breast carcinoma; COAD—colon adenocarcinoma; HNSC—head and neck squamous cell carcinoma; KIRC—kidney renal cell carcinoma; LIHC—liver hepatocellular carcinoma; LUAD—lung adenocarcinoma; LUSC—lung squamous cell carcinoma; PRAD—prostate adenocarcinoma; STAD—gastric adenocarcinoma; THCA—thyroid carcinoma; UCEC—uterine corpus endometrial carcinoma.

9. Conclusions, Hypothesis, Perspectives

Currently, data regarding the role and importance of circadian rhythms deregulation in cancer are accumulating. In this perspective article, we have attempted to untangle the involvement of this basic biological oscillator in the processes associated with one of the hallmarks of cancer aggression and resistance—aneu-polyploidy and its association with ACS and reprogramming. On the basis of our analysis, we propose a working hypothesis presented in Figure 5.

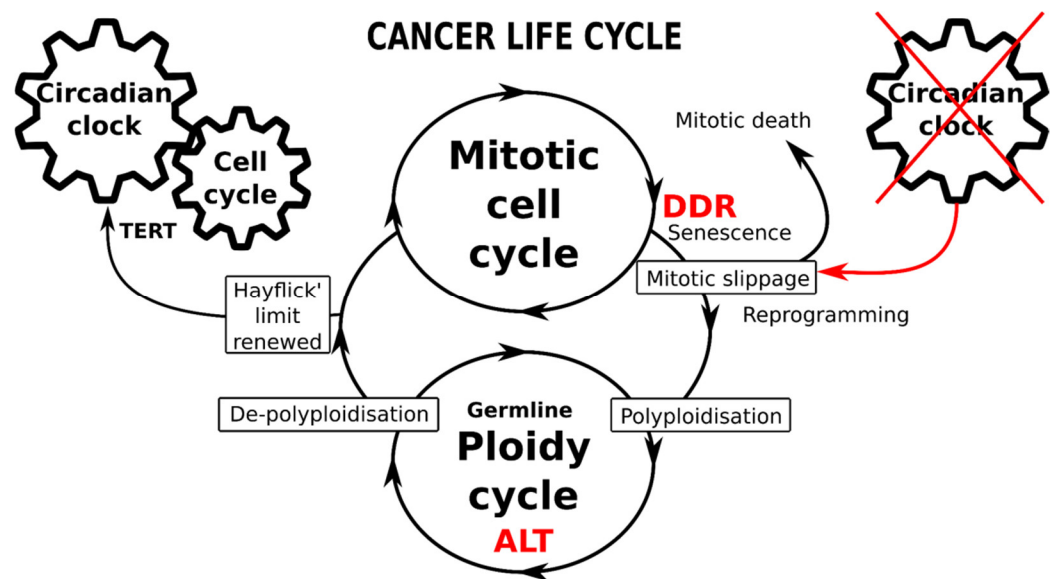


Figure 5. Schematic of the immortal cancer life-cycle composed of two reciprocally joined mitotic and ploidy cycles. The mitotic cell cycle is driven by the circadian clock (CC), particularly operating the telomerase-dependent telomere maintenance pathway (TERT). The transition from mitotic to ploidy cycle occurs after DNA checkpoints are adapted during the DNA damage response (DDR), through mitotic slippage coupling accelerated cellular senescence (with compromised telomeres) and reprogramming to whole-genome duplications. Transition into the ploidy cycle, concurrent with a germline expression signature, is associated with interruption of the circadian clock and restoration of eroded telomeres by alternative telomere lengthening (ALT). Return of depolyploidised offspring to the mitotic cycle restores the TERT-pathway and the CC-driven count of the Hayflick limit.

The adaptive response to genotoxic, oncogenic or oxidative stress induces ACS with telomere attrition coupled and toggled with stemness (reprogramming). While the former produces persistent DDR signalling, the latter concurrently attenuates the DDR checkpoints and supports DNA damage tolerance; such coupling is thus potentially redirecting stressed cancer cells from the mitotic cycle through mitotic slippage into polyploidy. The cell cycle drivers and DDR checkpoints are robustly regulated by CC genes; however, they become compromised by mitotic slippage into polyploidy (or even earlier, in the preceding replication stress). The data show that to get into transient polyploidy after receiving genotoxic stress, a cancer cell should perform a “death loop”—first, by falling out of the conventional mitotic cell cycle, driven by the CC, into a polyploidy cycle with a decelerated or dysfunctional CC and then undertaking a return to the mitotic cycle, re-engaging the CC to count the replication life-span again. This critical transition from the mitotic cycle into transient polyploidy appears focused on mitotic slippage interrupting the circadian regulation. The return to the normal biological time pace, which is associated with counting the Hayflick limit, needs the eroded telomeres to be restored and linked again to a telomerase-dependent mechanism (TERT). This telomere restitution mechanism may be performed by ALT coupled to a kind of meiotic homology search and recombination [73]. In some way, the “fall” into transient polyploidy resets the cell to a “timeless state”, the likes of which are normally displayed only by germ cells and early embryos which lack CC oscillation. It is noteworthy that cancers [40,167] and PGCCs, in particular, abundantly express the germline genes and proteins [39,41,42,83,168]. Furthermore, the connection between the mitotic slippage-induced cGAS-STING pathway and one of its targets—the transmembrane protein family Fragilis, is involved in the commitment of primordial germ cells and oogonia [169,170] may be also involved in this soma-to-germ transition. In summary, these current data on the CC suggest possible participation in cancer treatment resistance and provide an additional argument in support of the oldest embryonic concept of cancer with its parthenogenetic and parasexual

variants [17,32,33,36,37,171–173]. Within this logic, the various requirements of the above-discussed mechanisms of resistance to anticancer treatments may be provisionally met.

How can this knowledge be further used? Which drawbacks and perspectives for cancer research and treatment are illuminated?

In Section 5, we evaluated the pathways at play during mitotic slippage, particularly those surrounding the mitotic-to-polyploidy transition with its still poorly understood cross-talk between ACS and the cGAS-STING and Hippo pathways. We highlighted the induced oscillation of two pivotal genome stability guardians—the Hippo and p53 pathways, both components of the genotoxic stress-response and occur with a similar periodicity. In fact, these represent oscillations between senescence inducing DSBs and stemness, relaxing the DDR response and interfering with the CC regulation of the cell cycle. It may be speculated that these combined oscillations of the two pathways create fluctuation in a coherent mode to push cells from the conventional mitotic path into the new cell state of the polyploidy cycle uncoupled from the CC. Here, the laws of unstable thermodynamics of open systems [174] are acting. From the methodical point of view, such regulation by oscillation between opposing states needs a further appreciation of the circular causality implicit in any feedback process within certain parameters [114,175] and demands the design of dynamic studies on individual cells. Such a stress response incorporating an explorative oscillatory adaptation with a critical transition into the PGCC acquiring the germline or embryo-like potential, and a similar “timeless” CC state dangerously increases the chance of cancer relapse after aggressive genotoxic modalities [12,16,114,176].

However, the good news is that the initiation of cell differentiation in ESCs induces an autonomous circadian rhythm [139] that, in turn, drives a normal cell cycle from one checkpoint to another like a good operator drives a train from one station to the next. It currently appears, therefore, that instead of killing cancer cells with genotoxic treatments, the strategy of cancer normalisation by differentiation is more prospective. The embryonic features of PGCCs provide a fundamental basis for the epigenetic reversion of malignancy [36,37,177]. In such modalities, epigenetics can overcome genetics [178–180]. The various tumour-differentiation strategies, including environmental 3D structurisation, have been suggested and undergo testing [179,181,182]. The chronotherapy concept [183,184] may be considered in combination with differentiation-inducing modalities. In addition, as shown by our bioinformatic analysis, the measure of CC deregulation correlated with polyploidy obtained from transcriptome or other methods could have potential in new cancer diagnostic and prognostic settings.

Author Contributions: Conceptualization, J.E. and N.M.V.; methodology, N.M.V., B.I.G., K.S.; validation, P.Z.; investigation, N.M.V.; resources, N.M.V., D.P., K.S., J.E.; data curation, N.M.V. and P.Z.; writing—original draft preparation, J.E., N.M.V., M.L.; writing—review and editing, J.E. and M.S.C.; visualization, K.S., P.Z., J.E., N.M.V.; supervision, J.E.; project administration, D.P.; funding acquisition, N.M.V., K.S., D.P., J.E. All authors have read and agreed to the published version of the manuscript.

Funding: This research was funded by the University of Latvia Foundation’s PhD Student Scholarship in the Natural and Life Sciences (awarded to N.M.V.), a grant from the European Regional Development Fund (ERDF) projects No. 1.1.1.2/VIAA/3/19/463 for K.S. and ERDF 099 project No. 1.1.1.1/18/A/099) for D.P. and J.E.

Institutional Review Board Statement: Not applicable.

Informed Consent Statement: Not applicable.

Data Availability Statement: The reprocessed TCGA cancer and the normal transcriptomic dataset are available in the GEO repository under the GSE62944 accession number. TCGA tumour ploidy data calculated by ABSOLUTE from [166] are available in the Supplementary Materials of said study at <https://gdc.cancer.gov/about-data/publications/pancan-aneuploidy>, accessed on 5 November 2021.

Acknowledgments: Jekabs Krigerts is acknowledged for the cytometry of WB344 cells.

Conflicts of Interest: The authors declare no conflict of interest.

References

- Bauke, J.; Schöffling, K. Polyploidy in Human Malignancy. Hypopentaploid Chromosome Pattern in Malignant Reticulosis with Secondary Sideroachrestic Anemia. *Cancer* **1968**, *22*, 686–694.
- Moein, S.; Adibi, R.; da Silva Meirelles, L.; Nardi, N.B.; Gheisari, Y. Cancer Regeneration: Polyploid Cells Are the Key Drivers of Tumor Progression. *Biochim. Biophys. Acta Rev. Cancer* **2020**, *1874*, 188408.
- Bielski, C.M.; Zehir, A.; Penson, A.V.; Donoghue, M.T.A.; Chatila, W.; Armenia, J.; Chang, M.T.; Schram, A.M.; Jonsson, P.; Bandlamudi, C.; et al. Genome Doubling Shapes the Evolution and Prognosis of Advanced Cancers. *Nat. Genet.* **2018**, *50*, 1189–1195.
- Lee, H.O.; Davidson, J.M.; Duronio, R.J. Endoreplication: Polyploidy with Purpose. *Genes Dev.* **2009**, *23*, 2461–2477.
- Van de Peer, Y.; Mizrachi, E.; Marchal, K. The Evolutionary Significance of Polyploidy. *Nat. Rev. Genet.* **2017**, *18*, 411–424.
- Pienta, K.J.; Hammarlund, E.U.; Axelrod, R.; Brown, J.S.; Amend, S.R. Poly-Aneuploid Cancer Cells Promote Evolvability, Generating Lethal Cancer. *Evol. Appl.* **2020**, *13*, 1626–1634.
- Christodoulidou, A.; Raftopoulou, C.; Chiourea, M.; Papaioannou, G.K.; Hoshiyama, H.; Wright, W.E.; Shay, J.W.; Gagos, S. The Roles of Telomerase in the Generation of Polyploidy during Neoplastic Cell Growth. *Neoplasia* **2013**, *15*, 156–168.
- Coward, J.; Harding, A. Size Does Matter: Why Polyploid Tumor Cells Are Critical Drug Targets in the War on Cancer. *Front. Oncol.* **2014**, *4*, 123.
- Illidge, T.M.; Cragg, M.S.; Fringes, B.; Olive, P.; Erenpreisa, J.A. Polyploid Giant Cells Provide a Survival Mechanism for p53 Mutant Cells after DNA Damage. *Cell Biol. Int.* **2000**, *24*, 621–633.
- Sundaram, M.; Guernsey, D.L.; Rajaraman, M.M.; Rajaraman, R. Neosis: A Novel Type of Cell Division in Cancer. *Cancer Biol. Ther.* **2004**, *3*, 207–218.
- Zhang, S.; Mercado-Urbe, I.; Xing, Z.; Sun, B.; Kuang, J.; Liu, J. Generation of Cancer Stem-like Cells through the Formation of Polyploid Giant Cancer Cells. *Oncogene* **2014**, *33*, 116–128.
- Mirzayans, R.; Andrais, B.; Murray, D. Roles of Polyploid/Multinucleated Giant Cancer Cells in Metastasis and Disease Relapse Following Anticancer Treatment. *Cancers* **2018**, *10*, 118. <https://doi.org/10.3390/cancers10040118>.
- Lagadec, C.; Vlashi, E.; Della Donna, L.; Dekmezian, C.; Pajonk, F. Radiation-Induced Reprogramming of Breast Cancer Cells. *Stem Cells* **2012**, *30*, 833–844.
- Ivanov, A.; Cragg, M.S.; Erenpreisa, J.; Emzish, D.; Lukman, H.; Illidge, T.M. Endopolyploid Cells Produced after Severe Genotoxic Damage Have the Potential to Repair DNA Double Strand Breaks. *J. Cell Sci.* **2003**, *116*, 4095–4106.
- Lin, K.-C.; Torga, G.; Sun, Y.; Axelrod, R.; Pienta, K.J.; Sturm, J.C.; Austin, R.H. The Role of Heterogeneous Environment and Docetaxel Gradient in the Emergence of Polyploid, Mesenchymal and Resistant Prostate Cancer Cells. *Clin. Exp. Metastasis* **2019**, *36*, 97–108.
- Erenpreisa, J.; Salmina, K.; Anatskaya, O.; Cragg, M.S. Paradoxes of Cancer: Survival at the Brink. *Semin. Cancer Biol.* **2020**, *S1044*. <https://doi.org/10.1016/j.semcancer.2020.12.009>.
- Erenpreisa, J.; Cragg, M.S. Cancer: A Matter of Life Cycle? *Cell Biol. Int.* **2007**, *31*, 1507–1510.
- Erenpreisa, J.; Cragg, M.S. MOS, Aneuploidy and the Ploidy Cycle of Cancer Cells. *Oncogene* **2010**, *29*, 5447–5451.
- Liu, J. The Dualistic Origin of Human Tumors. *Semin. Cancer Biol.* **2018**, *53*, 1–16.
- Rajaraman, R.; Guernsey, D.L.; Rajaraman, M.M.; Rajaraman, S.R. Stem Cells, Senescence, Neosis and Self-Renewal in Cancer. *Cancer Cell Int.* **2006**, *6*, 25.
- Weihua, Z.; Lin, Q.; Ramoth, A.J.; Fan, D.; Fidler, I.J. Formation of Solid Tumors by a Single Multinucleated Cancer Cell. *Cancer* **2011**, *117*, 4092–4099.
- Díaz-Carballo, D.; Saka, S.; Klein, J.; Rennkamp, T.; Acikelli, A.H.; Malak, S.; Jastrow, H.; Wennemuth, G.; Tempfer, C.; Schmitz, I.; et al. A Distinct Oncogenerative Multinucleated Cancer Cell Serves as a Source of Stemness and Tumor Heterogeneity. *Cancer Res.* **2018**, *78*, 2318–2331.
- Chen, J.; Niu, N.; Zhang, J.; Qi, L.; Shen, W.; Donkena, K.V.; Feng, Z.; Liu, J. Polyploid Giant Cancer Cells (PGCCs): The Evil Roots of Cancer. *Curr. Cancer Drug Targets* **2019**, *19*, 360–367.
- Amend, S.R.; Torga, G.; Lin, K.-C.; Kosticka, L.G.; de Marzo, A.; Austin, R.H.; Pienta, K.J. Polyploid Giant Cancer Cells: Unrecognized Actuators of Tumorigenesis, Metastasis, and Resistance. *Prostate* **2019**, *79*, 1489–1497.
- Liu, J.; Erenpreisa, J.; Sikora, E. Polyploid Giant Cancer Cells: An Emerging New Field of Cancer Biology. *Semin. Cancer Biol.* **2021**. <https://doi.org/10.1016/j.semcancer.2021.10.006>.
- Comai, L. The Advantages and Disadvantages of Being Polyploid. *Nat. Rev. Genet.* **2005**, *6*, 836–846.
- Otto, S.P. The Evolutionary Consequences of Polyploidy. *Cell* **2007**, *131*, 452–462.
- Edgar, B.A.; Orr-Weaver, T.L. Endoreplication Cell Cycles. *Cell* **2001**, *105*, 297–306.
- Gerashchenko, B.I.; Salmina, K.; Krigerts, J.; Erenpreisa, J.; Babsky, A.M. Induced Polyploidy and Sorting of Damaged Dna by Micronucleation in Radioresistant Rat Liver Epithelial Stem-Like Cells Exposed to X-rays. *Probl. Radiat. Med. Radiobiol.* **2019**, *24*, 220–234.
- Holland, A.J.; Cleveland, D.W. Boveri Revisited: Chromosomal Instability, Aneuploidy and Tumorigenesis. *Nat. Rev. Mol. Cell*

- Biol.* **2009**, *10*, 478–487.
31. Ben-David, U.; Amon, A. Context Is Everything: Aneuploidy in Cancer. *Nat. Rev. Genet.* **2020**, *21*, 44–62.
 32. Vainshelbaum, N.M.; Zayakin, P.; Kleina, R.; Giuliani, A.; Erenpreisa, J. Meta-Analysis of Cancer Triploidy: Rearrangements of Genome Complements in Male Human Tumors Are Characterized by XXY Karyotypes. *Genes* **2019**, *10*, 613. <https://doi.org/10.3390/genes10080613>.
 33. Salmina; Gerashchenko; Hausmann; Vainshelbaum; Zayakin; Erenpreiss; Freivalds; Cragg; Erenpreisa When Three Isn't a Crowd: A Digyny Concept for Treatment-Resistant, Near-Triploid Human Cancers. *Genes* **2019**, *10*, 551.
 34. Salmina, K.; Jankevics, E.; Huna, A.; Perminov, D.; Radovica, I.; Klymenko, T.; Ivanov, A.; Jascenko, E.; Scherthan, H.; Cragg, M.; et al. Up-Regulation of the Embryonic Self-Renewal Network through Reversible Polyploidy in Irradiated p53-Mutant Tumour Cells. *Exp. Cell Res.* **2010**, *316*, 2099–2112.
 35. Liu, J. The “life Code”: A Theory That Unifies the Human Life Cycle and the Origin of Human Tumors. *Semin. Cancer Biol.* **2020**, *60*, 380–397.
 36. Erenpreisa, J.; Salmina, K.; Huna, A.; Jackson, T.R.; Vazquez-Martin, A.; Cragg, M.S. The “Virgin Birth”, Polyploidy, and the Origin of Cancer. *Oncoscience* **2015**, *2*, 3–14.
 37. Niu, N.; Mercado-Uribe, I.; Liu, J. Dedifferentiation into Blastomere-like Cancer Stem Cells via Formation of Polyploid Giant Cancer Cells. *Oncogene* **2017**, *36*, 4887–4900.
 38. Díaz-Carballo, D.; Gustmann, S.; Jastrow, H.; Acikelli, A.H.; Dammann, P.; Klein, J.; Dembinski, U.; Bardenheuer, W.; Malak, S.; Araúzo-Bravo, M.J.; et al. Atypical Cell Populations Associated with Acquired Resistance to Cytostatics and Cancer Stem Cell Features: The Role of Mitochondria in Nuclear Encapsulation. *DNA Cell Biol.* **2014**, *33*, 749–774.
 39. Pjanova, D.; Vainshelbaum, N.M.; Salmina, K.; Erenpreisa, J. The Role of the Meiotic Component in Reproduction of B-RAF-Mutated Melanoma: A Review and “Brainstorming” Session. In *Melanoma*; Lasfar, A., Cohen-Solal, K., Eds.; IntechOpen: London, UK, 2020; doi:10.5772/intechopen.93641.
 40. McFarlane, R.J.; Wakeman, J.A. Meiosis-like Functions in Oncogenesis: A New View of Cancer. *Cancer Res.* **2017**, *77*, 5712–5716.
 41. Ianzini, F.; Kosmacek, E.A.; Nelson, E.S.; Napoli, E.; Erenpreisa, J.; Kalejs, M.; Mackey, M.A. Activation of Meiosis-Specific Genes Is Associated with Depolyploidisation of Human Tumor Cells Following Radiation-Induced Mitotic Catastrophe. *Cancer Res.* **2009**, *69*, 2296–2304.
 42. Erenpreisa, J.; Cragg, M.S.; Salmina, K.; Hausmann, M.; Scherthan, H. The Role of Meiotic Cohesin REC8 in Chromosome Segregation in Gamma Irradiation-Induced Endopolyploid Tumour Cells. *Exp. Cell Res.* **2009**, *315*, 2593–2603.
 43. Bomken, S.; Fiser, K.; Heidenreich, O.; Vormoor, J. Understanding the Cancer Stem Cell. *Br. J. Cancer* **2010**, *103*, 439–445.
 44. Ayob, A.Z.; Ramasamy, T.S. Cancer Stem Cells as Key Drivers of Tumour Progression. *J. Biomed. Sci.* **2018**, *25*, 20.
 45. Vazquez-Martin, A.; Anatskaya, O.V.; Giuliani, A.; Erenpreisa, J.; Huang, S.; Salmina, K.; Inashkina, I.; Huna, A.; Nikolsky, N.N.; Vinogradov, A.E. Somatic Polyploidy Is Associated with the Upregulation of c-MYC Interacting Genes and EMT-like Signature. *Oncotarget* **2016**, *7*, 75235–75260.
 46. Anatskaya, O.V.; Vinogradov, A.E.; Vainshelbaum, N.M.; Giuliani, A.; Erenpreisa, J. Phylostratic Shift of Whole-Genome Duplications in Normal Mammalian Tissues towards Unicellularity Is Driven by Developmental Bivalent Genes and Reveals a Link to Cancer. *Int. J. Mol. Sci.* **2020**, *21*, 8759. <https://doi.org/10.3390/ijms21228759>.
 47. Roninson, I.B.; Broude, E.V.; Chang, B.-D. If Not Apoptosis, Then What? Treatment-Induced Senescence and Mitotic Catastrophe in Tumor Cells. *Drug Resist. Updates* **2001**, *4*, 303–313.
 48. Campisi, J.; d'Adda di Fagagna, F. Cellular Senescence: When Bad Things Happen to Good Cells. *Nat. Rev. Mol. Cell Biol.* **2007**, *8*, 729–740.
 49. Mosteiro, L.; Pantoja, C.; de Martino, A.; Serrano, M. Senescence Promotes in vivo Reprogramming through p16 and IL-6. *Aging Cell* **2018**, *17*, e12711. <https://doi.org/10.1111/accel.12711>.
 50. Lee, S.; Schmitt, C.A. The Dynamic Nature of Senescence in Cancer. *Nat. Cell Biol.* **2019**, *21*, 94–101.
 51. Davoli, T.; de Lange, T. Telomere-Driven Tetraploidization Occurs in Human Cells Undergoing Crisis and Promotes Transformation of Mouse Cells. *Cancer Cell* **2012**, *21*, 765–776.
 52. Erenpreisa, J.; Cragg, M.S. Three Steps to the Immortality of Cancer Cells: Senescence, Polyploidy and Self-Renewal. *Cancer Cell Int.* **2013**, *13*, 92.
 53. Mosieniak, G.; Sliwinska, M.A.; Alster, O.; Strzeszewska, A.; Sunderland, P.; Piechota, M.; Was, H.; Sikora, E. Polyploidy Formation in Doxorubicin-Treated Cancer Cells Can Favor Escape from Senescence. *Neoplasia* **2015**, *17*, 882–893.
 54. Mosieniak, G.; Sikora, E. Polyploidy: The Link between Senescence and Cancer. *Curr. Pharm. Des.* **2010**, *16*, 734–740.
 55. Puig, P.-E.; Guilly, M.-N.; Bouchot, A.; Droin, N.; Cathelin, D.; Bouyer, F.; Favier, L.; Ghiringhelli, F.; Kroemer, G.; Solary, E.; et al. Tumor Cells Can Escape DNA-Damaging Cisplatin through DNA Endoreduplication and Reversible Polyploidy. *Cell Biol. Int.* **2008**, *32*, 1031–1043.
 56. Jackson, T.R.; Salmina, K.; Huna, A.; Inashkina, I.; Jankevics, E.; Riekstina, U.; Kalnina, Z.; Ivanov, A.; Townsend, P.A.; Cragg, M.S.; et al. DNA Damage Causes TP53-Dependent Coupling of Self-Renewal and Senescence Pathways in Embryonal Carcinoma Cells. *Cell Cycle* **2013**, *12*, 430–441.
 57. Huna, A.; Salmina, K.; Erenpreisa, J.; Vazquez-Martin, A.; Krigerts, J.; Inashkina, I.; Gerashchenko, B.I.; Townsend, P.A.; Cragg, M.S.; Jackson, T.R. Role of Stress-Activated OCT4A in the Cell Fate Decisions of Embryonal Carcinoma Cells Treated with Etoposide. *Cell Cycle* **2015**, *14*, 2969–2984.

58. Suzuki, M.; Boothman, D.A. Stress-Induced Premature Senescence (SIPS)-Influence of SIPS on Radiotherapy. *J. Radiat. Res.* **2008**, *49*, 105–112.
59. Erenpreisa, J.A.; Cragg, M.S.; Fringes, B.; Sharakhov, I.; Illidge, T.M. Release of Mitotic Descendants by Giant Cells from Irradiated Burkitt's Lymphoma Cell Line. *Cell Biol. Int.* **2000**, *24*, 635–648.
60. Vitale, I.; Senovilla, L.; Jemaà, M.; Michaud, M.; Galluzzi, L.; Kepp, O.; Nanty, L.; Criollo, A.; Rello-Varona, S.; Manic, G.; et al. Multipolar Mitosis of Tetraploid Cells: Inhibition by p53 and Dependency on Mos. *EMBO J.* **2010**, *29*, 1272–1284.
61. Horbay, R.; Stoika, R. Giant Cell Formation: The Way to Cell Death or Cell Survival? *Open Life Sci.* **2011**, *6*, 675–684.
62. Park, S.U.; Choi, E.S.; Jang, Y.S.; Hong, S.-H.; Kim, I.-H.; Chang, D.K. Effects of chromosomal polyploidy on survival of colon cancer cells. *Korean J. Gastroenterol.* **2011**, *57*, 150.
63. Wang, Q.; Wu, P.C.; Dong, D.Z.; Ivanova, I.; Chu, E.; Zeliadt, S.; Vesselle, H.; Wu, D.Y. Polyploidy Road to Therapy-Induced Cellular Senescence and Escape. *Int. J. Cancer* **2013**, *132*, 1505–1515.
64. Sharma, S.; Yao, H.-P.; Zhou, Y.-Q.; Zhou, J.; Zhang, R.; Wang, M.-H. Prevention of BMS-777607-Induced Polyploidy/senescence by mTOR Inhibitor AZD8055 Sensitizes Breast Cancer Cells to Cytotoxic Chemotherapeutics. *Mol. Oncol.* **2014**, *8*, 469–482.
65. Lopez-Sánchez, L.M.; Jimenez, C.; Valverde, A.; Hernandez, V.; Peñarando, J.; Martinez, A.; Lopez-Pedraza, C.; Muñoz-Castañeda, J.R.; De la Haba-Rodríguez, J.R.; Aranda, E.; et al. CoCl₂, a Mimic of Hypoxia, Induces Formation of Polyploid Giant Cells with Stem Characteristics in Colon Cancer. *PLoS ONE* **2014**, *9*, e99143.
66. Chitikova, Z.V.; Gordeev, S.A.; Bykova, T.V.; Zubova, S.G.; Pospelov, V.A.; Pospelova, T.V. Sustained Activation of DNA Damage Response in Irradiated Apoptosis-Resistant Cells Induces Reversible Senescence Associated with mTOR Downregulation and Expression of Stem Cell Markers. *Cell Cycle* **2014**, *13*, 1424–1439.
67. Rohnalter, V.; Roth, K.; Finkernagel, F.; Adhikary, T.; Obert, J.; Dorzweiler, K.; Bensberg, M.; Müller-Brüsselbach, S.; Müller, R. A Multi-Stage Process Including Transient Polyploidisation and EMT Precedes the Emergence of Chemoresistant Ovarian Carcinoma Cells with a Dedifferentiated and pro-Inflammatory Secretory Phenotype. *Oncotarget* **2015**, *6*, 40005–40025.
68. Leikam, C.; Hufnagel, A.L.; Otto, C.; Murphy, D.J.; Mühling, B.; Kneitz, S.; Nanda, I.; Schmid, M.; Wagner, T.U.; Haferkamp, S.; et al. In Vitro Evidence for Senescent Multinucleated Melanocytes as a Source for Tumor-Initiating Cells. *Cell Death Dis.* **2015**, *6*, e1711.
69. Niu, N.; Zhang, J.; Zhang, N.; Mercado-Uribe, I.; Tao, F.; Han, Z.; Pathak, S.; Multani, A.S.; Kuang, J.; Yao, J.; et al. Linking Genomic Reorganization to Tumor Initiation via the Giant Cell Cycle. *Oncogenesis* **2016**, *5*, e281.
70. Gerashchenko, B.I.; Salmina, K.; Eglitis, J.; Huna, A.; Grjunberga, V.; Erenpreisa, J. Disentangling the Aneuploidy and Senescence Paradoxes: A Study of Triploid Breast Cancers Non-Responsive to Neoadjuvant Therapy. *Histochem. Cell Biol.* **2016**, *145*, 497–508.
71. Kiseleva, L.N.; Kartashev, A.V.; Vartanyan, N.L.; Pinevich, A.A.; Samoilovich, M.P. Multinucleated Cells Resistant to Genotoxic Factors within Human Glioblastoma Cell Lines. *Cell Tissue Biol.* **2019**, *13*, 1–7.
72. Kudo-Saito, C.; Miyamoto, T.; Imazeki, H.; Shoji, H.; Aoki, K.; Boku, N. IL33 Is a Key Driver of Treatment Resistance of Cancer. *Cancer Res.* **2020**, *80*, 1981–1990.
73. Salmina, K.; Bojko, A.; Inashkina, I.; Staniak, K.; Dudkowska, M.; Podlesniy, P.; Rumnieks, F.; Vainshelbaum, N.M.; Pjanova, D.; Sikora, E.; et al. "Mitotic Slippage" and Extranuclear DNA in Cancer Chemoresistance: A Focus on Telomeres. *Int. J. Mol. Sci.* **2020**, *21*, 2779. <https://doi.org/10.3390/ijms21082779>.
74. Adibi, R.; Moein, S.; Gheisari, Y. Cisplatin Resistant Ovarian Cancer Cells Reveal a Polyploid Phenotype with Remarkable Activation of Nuclear Processes. *Res. Square* **2021**. doi:10.21203/rs.3.rs-440506/v1
75. Takahashi, K.; Yamanaka, S. Induction of Pluripotent Stem Cells from Mouse Embryonic and Adult Fibroblast Cultures by Defined Factors. *Cell* **2006**, *126*, 663–676.
76. Yang, X.; Wood, P.A.; Hrushesky, W.J.M. Mammalian TIMELESS Is Required for ATM-Dependent CHK2 Activation and G2/M Checkpoint Control. *J. Biol. Chem.* **2010**, *285*, 3030–3034.
77. Vlashi, E.; Pajonk, F. Cancer Stem Cells, Cancer Cell Plasticity and Radiation Therapy. *Semin. Cancer Biol.* **2015**, *31*, 28–35.
78. Gerashchenko, B.I.; Azzam, E.I.; Howell, R.W. Characterization of Cell-Cycle Progression and Growth of WB-F344 Normal Rat Liver Epithelial Cells Following Gamma-Ray Exposure. *Cytometry A* **2004**, *61*, 134–141.
79. Neganova, I.; Lako, M. G1 to S Phase Cell Cycle Transition in Somatic and Embryonic Stem Cells. *J. Anat.* **2008**, *213*, 30–44.
80. Suvorova, I.I.; Grigorash, B.B.; Chuykin, I.A.; Pospelova, T.V.; Pospelov, V.A. G1 Checkpoint Is Compromised in Mouse ESCs due to Functional Uncoupling of p53-p21Waf1 Signaling. *Cell Cycle* **2016**, *15*, 52–63.
81. Liu, L.; Michowski, W.; Kolodziejczyk, A.; Sicinski, P. The Cell Cycle in Stem Cell Proliferation, Pluripotency and Differentiation. *Nat. Cell Biol.* **2019**, *21*, 1060–1067.
82. Mantel, C.; Guo, Y.; Lee, M.R.; Han, M.K.; Rhorabough, S.; Kim, K.S.; Broxmeyer, H.E. Cells Enter a Unique Intermediate 4N Stage, Not 4N-G1, after Aborted Mitosis. *Cell Cycle* **2008**, *7*, 484–492.
83. Erenpreisa, J.; Kalejs, M.; Cragg, M.S. Mitotic Catastrophe and Endomitosis in Tumour Cells: An Evolutionary Key to a Molecular Solution. *Cell Biol. Int.* **2005**, *29*, 1012–1018.
84. Kastan, M.B. Wild-Type p53: Tumors Can't Stand It. *Cell* **2007**, *128*, 837–840.
85. Huang, S. Reprogramming Cell Fates: Reconciling Rarity with Robustness. *Bioessays* **2009**, *31*, 546–560.
86. Zhang, X.; Neganova, I.; Przyborski, S.; Yang, C.; Cooke, M.; Atkinson, S.P.; Anyfantis, G.; Fenyk, S.; Keith, W.N.; Hoare, S.F.; et al. A Role for NANOG in G1 to S Transition in Human Embryonic Stem Cells through Direct Binding of CDK6 and

- CDC25A. *J. Cell Biol.* **2009**, *184*, 67–82.
87. Neganova, I.; Vilella, F.; Atkinson, S.P.; Lloret, M.; Passos, J.F.; von Zglinicki, T.; O'Connor, J.-E.; Burks, D.; Jones, R.; Armstrong, L.; et al. An Important Role for CDK2 in G1 to S Checkpoint Activation and DNA Damage Response in Human Embryonic Stem Cells. *Stem Cells* **2011**, *29*, 651–659.
88. Greco, S.J.; Liu, K.; Rameshwar, P. Functional Similarities among Genes Regulated by OCT4 in Human Mesenchymal and Embryonic Stem Cells. *Stem Cells* **2007**, *25*, 3143–3154.
89. Keyes, W.M.; Wu, Y.; Vogel, H.; Guo, X.; Lowe, S.W.; Mills, A.A. p63 Deficiency Activates a Program of Cellular Senescence and Leads to Accelerated Aging. *Genes Dev.* **2005**, *19*, 1986–1999.
90. Baryshev, M.; Inashkina, I.; Salmina, K.; Huna, A.; Jackson, T.R.; Erenpreisa, J. DNA Methylation of the Oct4A Enhancers in Embryonal Carcinoma Cells after Etoposide Treatment Is Associated with Alternative Splicing and Altered Pluripotency in Reversibly Senescent Cells. *Cell Cycle* **2018**, *17*, 362–366.
91. Kulaberoglu, Y.; Gundogdu, R.; Hergovich, A. The Role of p53/p21/p16 in DNA-Damage Signaling and DNA Repair. In *Genome Stability*; Elsevier: Amsterdam, Netherlands, 2016; pp. 243–256. ISBN 9780128033098.
92. Li, H.; Collado, M.; Villasante, A.; Matheu, A.; Lynch, C.J.; Cañamero, M.; Rizzoti, K.; Carneiro, C.; Martínez, G.; Vidal, A.; et al. p27(Kip1) Directly Represses Sox2 during Embryonic Stem Cell Differentiation. *Cell Stem Cell* **2012**, *11*, 845–852.
93. She, S.; Wei, Q.; Kang, B.; Wang, Y.-J. Cell Cycle and Pluripotency: Convergence on Octamer-binding Transcription Factor 4 (Review). *Mol. Med. Rep.* **2017**, *16*, 6459–6466.
94. Farshadi, E.; van der Horst, G.T.J.; Chaves, I. Molecular Links between the Circadian Clock and the Cell Cycle. *J. Mol. Biol.* **2020**, *432*, 3515–3524.
95. Yu, F.-X.; Guan, K.-L. The Hippo Pathway: Regulators and Regulations. *Genes Dev.* **2013**, *27*, 355–371.
96. Steigemann, P.; Wurzenberger, C.; Schmitz, M.H.A.; Held, M.; Guizzetti, J.; Maar, S.; Gerlich, D.W. Aurora B-Mediated Abscission Checkpoint Protects against Tetraploidization. *Cell* **2009**, *136*, 473–484.
97. Bui, D.A.; Lee, W.; White, A.E.; Harper, J.W.; Schackmann, R.C.J.; Overholtzer, M.; Selfors, L.M.; Brugge, J.S. Cytokinesis Involves a Nontranscriptional Function of the Hippo Pathway Effector YAP. *Sci. Signal.* **2016**, *9*, ra23.
98. Yabuta, N.; Mukai, S.; Okada, N.; Aylon, Y.; Nojima, H. The Tumor Suppressor Lats2 Is Pivotal in Aurora A and Aurora B Signaling during Mitosis. *Cell Cycle* **2011**, *10*, 2724–2736.
99. Vitale, I.; Galluzzi, L.; Castedo, M.; Kroemer, G. Mitotic Catastrophe: A Mechanism for Avoiding Genomic Instability. *Nat. Rev. Mol. Cell Biol.* **2011**, *12*, 385–392.
100. Ganem, N.J.; Cornils, H.; Chiu, S.-Y.; O'Rourke, K.P.; Arnaud, J.; Yimlamai, D.; Théry, M.; Camargo, F.D.; Pellman, D. Cytokinesis Failure Triggers Hippo Tumor Suppressor Pathway Activation. *Cell* **2014**, *158*, 833–848.
101. Lavado, A.; Park, J.Y.; Paré, J.; Finkelstein, D.; Pan, H.; Xu, B.; Fan, Y.; Kumar, R.P.; Neale, G.; Kwak, Y.D.; et al. The Hippo Pathway Prevents YAP/TAZ-Driven Hypertranscription and Controls Neural Progenitor Number. *Dev. Cell* **2018**, *47*, 576–591.e8.
102. Kim, T.; Yang, S.-J.; Hwang, D.; Song, J.; Kim, M.; Kyum Kim, S.; Kang, K.; Ahn, J.; Lee, D.; Kim, M.-Y.; et al. A Basal-like Breast Cancer-Specific Role for SRF-IL6 in YAP-Induced Cancer Stemness. *Nat. Commun.* **2015**, *6*, 10186.
103. He, C.; Lv, X.; Huang, C.; Hua, G.; Ma, B.; Chen, X.; Angeletti, P.C.; Dong, J.; Zhou, J.; Wang, Z.; et al. YAP1-LATS2 Feedback Loop Dictates Senescent or Malignant Cell Fate to Maintain Tissue Homeostasis. *EMBO Rep.* **2019**, *20*, e44948. <https://doi.org/10.15252/embr.201744948>.
104. Ivanov, A.; Pawlikowski, J.; Manoharan, I.; van Tuyn, J.; Nelson, D.M.; Rai, T.S.; Shah, P.P.; Hewitt, G.; Korolchuk, V.I.; Passos, J.F.; et al. Lysosome-Mediated Processing of Chromatin in Senescence. *J. Cell Biol.* **2013**, *202*, 129–143.
105. Dou, Z.; Ghosh, K.; Vizioli, M.G.; Zhu, J.; Sen, P.; Wangenstein, K.J.; Simithy, J.; Lan, Y.; Lin, Y.; Zhou, Z.; et al. Cytoplasmic Chromatin Triggers Inflammation in Senescence and Cancer. *Nature* **2017**, *550*, 402–406.
106. Kwon, J.; Bakhom, S.F. The Cytosolic DNA-Sensing cGAS-STING Pathway in Cancer. *Cancer Discov.* **2020**, *10*, 26–39.
107. Lezaja, A.; Altmeyer, M. Dealing with DNA Lesions: When One Cell Cycle Is Not Enough. *Curr. Opin. Cell Biol.* **2021**, *70*, 27–36.
108. Wang, S.; Zhou, L.; Ling, L.; Meng, X.; Chu, F.; Zhang, S.; Zhou, F. The Crosstalk Between Hippo-YAP Pathway and Innate Immunity. *Front. Immunol.* **2020**, *11*, 323.
109. Furth, N.; Bossel Ben-Moshe, N.; Pozniak, Y.; Porat, Z.; Geiger, T.; Domany, E.; Aylon, Y.; Oren, M. Down-Regulation of LATS Kinases Alters p53 to Promote Cell Migration. *Genes Dev.* **2015**, *29*, 2325–2330.
110. Raj, N.; Bam, R. Reciprocal Crosstalk Between YAP1/Hippo Pathway and the p53 Family Proteins: Mechanisms and Outcomes in Cancer. *Front. Cell Dev. Biol.* **2019**, *7*, 159.
111. Franklin, J.M.; Ghosh, R.P.; Shi, Q.; Reddick, M.P.; Liphardt, J.T. Concerted Localization-Resets Precede YAP-Dependent Transcription. *Nat. Commun.* **2020**, *11*, 4581.
112. Lahav, G. Oscillations by the p53-Mdm2 Feedback Loop. *Adv. Exp. Med. Biol.* **2008**, *641*, 28–38.
113. Purvis, J.E.; Karhohs, K.W.; Mock, C.; Batchelor, E.; Loewer, A.; Lahav, G. p53 Dynamics Control Cell Fate. *Science* **2012**, *336*, 1440–1444.
114. Erenpreisa, J.; Giuliani, A. Resolution of Complex Issues in Genome Regulation and Cancer Requires Non-Linear and Network-Based Thermodynamics. *Int. J. Mol. Sci.* **2019**, *21*, 240. <https://doi.org/10.3390/ijms21010240>.
115. Nagl, W. *Endopolyploidy and Polyteny in Differentiation and Evolution: Towards an Understanding of Quantitative and Qualitative Variation of Nuclear DNA in Ontogeny and Phylogeny*; North-Holland Publish: Amsterdam, the Netherlands; New York, NY,

- USA; Oxford, UK, 1978; 283p.
116. Munden, A.; Rong, Z.; Sun, A.; Gangula, R.; Mallal, S.; Nordman, J.T. Rif1 Inhibits Replication Fork Progression and Controls DNA Copy Number in *Drosophila*. *Elife* **2018**, *7*, e39140. <https://doi.org/10.7554/eLife.39140>.
 117. Das, S.; Caballero, M.; Kolesnikova, T.; Zhimulev, I.; Koren, A.; Nordman, J. Replication Timing Analysis in Polyploid Cells Reveals Rif1 Uses Multiple Mechanisms to Promote Underreplication in *Drosophila*. *Genetics* **2021**, *219*, iyab147. <https://doi.org/10.1093/genetics/iyab147>.
 118. Campisi, J. Aging, Cellular Senescence, and Cancer. *Annu. Rev. Physiol.* **2013**, *75*, 685–705.
 119. Bartek, J.; Mistrik, M.; Bartkova, J. Thresholds of Replication Stress Signaling in Cancer Development and Treatment. *Nat. Struct. Mol. Biol.* **2012**, *19*, 5–7.
 120. Tam, W.-L.; Ang, Y.-S.; Lim, B. The Molecular Basis of Ageing in Stem Cells. *Mech. Ageing Dev.* **2007**, *128*, 137–148.
 121. Olovnikov, A.M. Telomeres, Telomerase, and Aging: Origin of the Theory. *Exp. Gerontol.* **1996**, *31*, 443–448.
 122. Hayflick, L. The Limited in Vitro Lifetime of Human Diploid Cell Strains. *Exp. Cell Res.* **1965**, *37*, 614–636.
 123. Palacios, J.A.; Herranz, D.; De Bonis, M.L.; Velasco, S.; Serrano, M.; Blasco, M.A. SIRT1 Contributes to Telomere Maintenance and Augments Global Homologous Recombination. *J. Cell Biol.* **2010**, *191*, 1299–1313.
 124. Rijo-Ferreira, F.; Takahashi, J.S. Genomics of Circadian Rhythms in Health and Disease. *Genome Med.* **2019**, *11*, 82.
 125. Feillet, C.; van der Horst, G.T.J.; Levi, F.; Rand, D.A.; Delaunay, F. Coupling between the Circadian Clock and Cell Cycle Oscillators: Implication for Healthy Cells and Malignant Growth. *Front. Neurol.* **2015**, *6*, 96.
 126. Langmesser, S.; Tallone, T.; Bordon, A.; Rusconi, S.; Albrecht, U. Interaction of Circadian Clock Proteins PER2 and CRY with BMAL1 and CLOCK. *BMC Mol. Biol.* **2008**, *9*, 41.
 127. Takahashi, J.S. Transcriptional Architecture of the Mammalian Circadian Clock. *Nat. Rev. Genet.* **2017**, *18*, 164–179.
 128. Yang, X. A Wheel of Time: The Circadian Clock, Nuclear Receptors, and Physiology. *Genes Dev.* **2010**, *24*, 741–747.
 129. Cusumano, P.; Damulewicz, M.; Carbognin, E.; Caccin, L.; Puricella, A.; Specchia, V.; Bozzetti, M.P.; Costa, R.; Mazzotta, G.M. The RNA Helicase BELLE Is Involved in Circadian Rhythmicity and in Transposons Regulation in *Drosophila melanogaster*. *Front. Physiol.* **2019**, *10*, 133. doi:10.3389/fphys.2019.00133
 130. Stavreva, D.A.; Garcia, D.A.; Fettweis, G.; Gudla, P.R.; Zaki, G.F.; Soni, V.; McGowan, A.; Williams, G.; Huynh, A.; Palangat, M.; et al. Transcriptional Bursting and Co-Bursting Regulation by Steroid Hormone Release Pattern and Transcription Factor Mobility. *Mol. Cell* **2019**, *75*, 1161–1177.e11.
 131. Yan, J.; Goldbeter, A. Robust Synchronization of the Cell Cycle and the Circadian Clock through Bidirectional Coupling. *J. R. Soc. Interface* **2019**, *16*, 20190376.
 132. Kowalska, E.; Ripperger, J.A.; Hoegger, D.C.; Bruegger, P.; Buch, T.; Birchler, T.; Mueller, A.; Albrecht, U.; Contaldo, C.; Brown, S.A. NONO Couples the Circadian Clock to the Cell Cycle. *Proc. Natl. Acad. Sci. USA* **2013**, *110*, 1592–1599.
 133. Umemura, Y.; Yagita, K. Development of the Circadian Core Machinery in Mammals. *J. Mol. Biol.* **2020**, *432*, 3611–3617.
 134. Vallone, D.; Lahiri, K.; Dickmeis, T.; Foulkes, N.S. Start the Clock! Circadian Rhythms and Development. *Dev. Dyn.* **2007**, *236*, 142–155.
 135. Raleigh, J.M.; O’Connell, M.J. The G(2) DNA Damage Checkpoint Targets Both Wee1 and Cdc25. *J. Cell Sci.* **2000**, *113*, 1727–1736.
 136. Burchett, J.B.; Knudsen-Clark, A.M.; Altman, B.J. MYC Ran Up the Clock: The Complex Interplay between MYC and the Molecular Circadian Clock in Cancer. *Int. J. Mol. Sci.* **2021**, *22*, 7761. <https://doi.org/10.3390/ijms22147761>.
 137. Gotoh, T.; Vila-Caballer, M.; Santos, C.S.; Liu, J.; Yang, J.; Finkielstein, C.V. The Circadian Factor Period 2 Modulates p53 Stability and Transcriptional Activity in Unstressed Cells. *Mol. Biol. Cell* **2014**, *25*, 3081–3093.
 138. Stokes, K.; Nunes, M.; Trombley, C.; Flôres, D.E.F.L.; Wu, G.; Taleb, Z.; Alkhateeb, A.; Banskota, S.; Harris, C.; Love, O.P.; et al. The Circadian Clock Gene, *Bmal1*, Regulates Intestinal Stem Cell Signaling and Represses Tumor Initiation. *Cell. Mol. Gastroenterol. Hepatol.* **2021**, *12*, 1847–1872.e0.
 139. Jiang, L.; Zhang, F.; Fan, W.; Zheng, M.; Kang, J.; Huang, F.; He, H. Expression of Circadian Clock Genes during Differentiation of Rat Dental Papilla Cells in Vitro. *Biol. Rhythm Res.* **2020**, doi:10.1080/09291016.2020.1777049
 140. Morse, D.; Cermakian, N.; Brancorsini, S.; Parvinen, M.; Sassone-Corsi, P. No Circadian Rhythms in Testis: Period 1 Expression Is Clock Independent and Developmentally Regulated in the Mouse. *Mol. Endocrinol.* **2003**, *17*, 141–151.
 141. Beaver, L.M.; Rush, B.L.; Gvakharia, B.O.; Giebultowicz, J.M. Noncircadian Regulation and Function of Clock Genes Period and Timeless in Oogenesis of *Drosophila melanogaster*. *J. Biol. Rhythm.* **2003**, *18*, 463–472.
 142. Bittman, E.L. Timing in the Testis. *J. Biol. Rhythms* **2016**, *31*, 12–36.
 143. Lu, Y.; Zheng, X.; Hu, W.; Bian, S.; Zhang, Z.; Tao, D.; Liu, Y.; Ma, Y. Cancer/testis Antigen PIWIL2 Suppresses Circadian Rhythms by Regulating the Stability and Activity of BMAL1 and CLOCK. *Oncotarget* **2017**, *8*, 54913–54924.
 144. Solov’eva, L.; Svetlova, M.; Bodinski, D.; Zalensky, A.O. Nature of Telomere Dimers and Chromosome Looping in Human Spermatozoa. *Chromosome Res.* **2004**, *12*, 817–823.
 145. Salmina, K.; Huna, A.; Kalejs, M.; Pjanova, D.; Scherthan, H.; Cragg, M.S.; Erenpreisa, J. The Cancer Aneuploidy Paradox: In the Light of Evolution. *Genes* **2019**, *10*, 83. <https://doi.org/10.3390/genes10020083>.
 146. Mayer, W.; Smith, A.; Fundele, R.; Haaf, T. Spatial Separation of Parental Genomes in Preimplantation Mouse Embryos. *J. Cell Biol.* **2000**, *148*, 629–634.
 147. Curran, K.L.; Allen, L.; Porter, B.B.; Dodge, J.; Lope, C.; Willadsen, G.; Fisher, R.; Johnson, N.; Campbell, E.; VonBergen, B.; et al. Circadian Genes, *xBmal1* and *xNocturnin*, Modulate the Timing and Differentiation of Somites in *Xenopus Laevis*. *PLoS*

- ONE **2014**, *9*, e108266.
148. Bellet, M.M.; Orozco-Solis, R.; Sahar, S.; Eckel-Mahan, K.; Sassone-Corsi, P. The Time of Metabolism: NAD⁺, SIRT1, and the Circadian Clock. *Cold Spring Harb. Symp. Quant. Biol.* **2011**, *76*, 31–38.
 149. Wang, R.-H.; Zhao, T.; Cui, K.; Hu, G.; Chen, Q.; Chen, W.; Wang, X.-W.; Soto-Gutierrez, A.; Zhao, K.; Deng, C.-X. Negative Reciprocal Regulation between Sirt1 and Per2 Modulates the Circadian Clock and Aging. *Sci. Rep.* **2016**, *6*, 28633.
 150. Asher, G.; Gatfield, D.; Stratmann, M.; Reinke, H.; Dibner, C.; Kreppel, F.; Mostoslavsky, R.; Alt, F.W.; Schibler, U. SIRT1 Regulates Circadian Clock Gene Expression through PER2 Deacetylation. *Cell* **2008**, *134*, 317–328.
 151. Chao, H.-W.; Doi, M.; Fustin, J.-M.; Chen, H.; Murase, K.; Maeda, Y.; Hayashi, H.; Tanaka, R.; Sugawa, M.; Mizukuchi, N.; et al. Circadian Clock Regulates Hepatic Polyploidy by Modulating Mkp1-Erk1/2 Signaling Pathway. *Nat. Commun.* **2017**, *8*, 2238.
 152. Wu, Y.; Tao, B.; Zhang, T.; Fan, Y.; Mao, R. Pan-Cancer Analysis Reveals Disrupted Circadian Clock Associates with T Cell Exhaustion. *Front. Immunol.* **2019**, *10*, 2451.
 153. Shilts, J.; Chen, G.; Hughey, J.J. Evidence for Widespread Dysregulation of Circadian Clock Progression in Human Cancer. *PeerJ* **2018**, *6*, e4327.
 154. Bernstein, B.E.; Mikkelsen, T.S.; Xie, X.; Kamal, M.; Huebert, D.J.; Cuff, J.; Fry, B.; Meissner, A.; Wernig, M.; Plath, K.; et al. A Bivalent Chromatin Structure Marks Key Developmental Genes in Embryonic Stem Cells. *Cell* **2006**, *125*, 315–326.
 155. Fung-Uceda, J.; Lee, K.; Seo, P.J.; Polyn, S.; De Veylder, L.; Mas, P. The Circadian Clock Sets the Time of DNA Replication Licensing to Regulate Growth in Arabidopsis. *Dev. Cell* **2018**, *45*, 101–113.e4.
 156. Dakup, P.P.; Porter, K.I.; Gajula, R.P.; Goel, P.N.; Cheng, Z.; Gaddameedhi, S. The Circadian Clock Protects against Ionizing Radiation-Induced Cardiotoxicity. *FASEB J.* **2020**, *34*, 3347–3358.
 157. Dakup, P.P.; Porter, K.I.; Gaddameedhi, S. The Circadian Clock Protects against Acute Radiation-Induced Dermatitis. *Toxicol. Appl. Pharmacol.* **2020**, *399*, 115040.
 158. Relógio, A.; Thomas, P.; Medina-Pérez, P.; Reischl, S.; Bervoets, S.; Gloc, E.; Riemer, P.; Mang-Fatehi, S.; Maier, B.; Schäfer, R.; et al. Ras-Mediated Deregulation of the Circadian Clock in Cancer. *PLoS Genet.* **2014**, *10*, e1004338.
 159. Van Dycke, K.C.G.; Rodenburg, W.; van Oostrom, C.T.M.; van Kerkhof, L.W.M.; Pennings, J.L.A.; Roenneberg, T.; van Steeg, H.; van der Horst, G.T.J. Chronically Alternating Light Cycles Increase Breast Cancer Risk in Mice. *Curr. Biol.* **2015**, *25*, 1932–1937.
 160. Papagiannakopoulos, T.; Bauer, M.R.; Davidson, S.M.; Heimann, M.; Subbaraj, L.; Bhutkar, A.; Bartlebaugh, J.; Vander Heiden, M.G.; Jacks, T. Circadian Rhythm Disruption Promotes Lung Tumorigenesis. *Cell Metab.* **2016**, *24*, 324–331.
 161. Zhang, J.; Lv, H.; Ji, M.; Wang, Z.; Wu, W. Low Circadian Clock Genes Expression in Cancers: A Meta-Analysis of Its Association with Clinicopathological Features and Prognosis. *PLoS ONE* **2020**, *15*, e0233508.
 162. Tomczak, K.; Czerwińska, P.; Wiznerowicz, M. The Cancer Genome Atlas (TCGA): An Immeasurable Source of Knowledge. *Contemp. Oncol.* **2015**, *19*, A68–A77.
 163. Rahman, M.; Jackson, L.K.; Johnson, W.E.; Li, D.Y.; Bild, A.H.; Piccolo, S.R. Alternative Preprocessing of RNA-Sequencing Data in The Cancer Genome Atlas Leads to Improved Analysis Results. *Bioinformatics* **2015**, *31*, 3666–3672.
 164. Lu, C.; Yang, Y.; Zhao, R.; Hua, B.; Xu, C.; Yan, Z.; Sun, N.; Qian, R. Role of Circadian Gene Clock during Differentiation of Mouse Pluripotent Stem Cells. *Protein Cell* **2016**, *7*, 820–832.
 165. Carter, S.L.; Cibulskis, K.; Helman, E.; McKenna, A.; Shen, H.; Zack, T.; Laird, P.W.; Onofrio, R.C.; Winckler, W.; Weir, B.A.; et al. Absolute Quantification of Somatic DNA Alterations in Human Cancer. *Nat. Biotechnol.* **2012**, *30*, 413–421.
 166. Taylor, A.M.; Shih, J.; Ha, G.; Gao, G.F.; Zhang, X.; Berger, A.C.; Schumacher, S.E.; Wang, C.; Hu, H.; Liu, J.; et al. Genomic and Functional Approaches to Understanding Cancer Aneuploidy. *Cancer Cell* **2018**, *33*, 676–689.e3.
 167. Bruggeman, J.W.; Irie, N.; Lodder, P.; van Pelt, A.M.M.; Koster, J.; Hamer, G. Tumors Widely Express Hundreds of Embryonic Germline Genes. *Cancers* **2020**, *12*, 3812. <https://doi.org/10.3390/cancers12123812>.
 168. Kalejs, M.; Ivanov, A.; Plakhins, G.; Cragg, M.S.; Emzins, D.; Illidge, T.M.; Erenpreisa, J. Upregulation of Meiosis-Specific Genes in Lymphoma Cell Lines Following Genotoxic Insult and Induction of Mitotic Catastrophe. *BMC Cancer* **2006**, *6*, 6.
 169. Lange, U.C.; Saitou, M.; Western, P.S.; Barton, S.C.; Surani, M.A. The Fragilis Interferon-Inducible Gene Family of Transmembrane Proteins Is Associated with Germ Cell Specification in Mice. *BMC Dev. Biol.* **2003**, *3*, 1.
 170. Sheng, X.; Tian, C.; Liu, L.; Wang, L.; Ye, X.; Li, J.; Zeng, M.; Liu, L. Characterization of Oogonia Stem Cells in Mice by Fragilis. *Protein Cell* **2019**, *10*, 825–831.
 171. Grundmann, E. The concept of Julius Cohnheim on tumor formation and metastasis from the viewpoint of new research results. *Zentralbl. Allg. Pathol.* **1985**, *130*, 323–331.
 172. Vinnitsky, V. The Development of a Malignant Tumor Is due to a Desperate Asexual Self-Cloning Process in Which Cancer Stem Cells Develop the Ability to Mimic the Genetic Program of Germline Cells. *Intrinsically Disord. Proteins* **2014**, *2*, e29997.
 173. Rajaraman, R.; Guernsey, D.L.; Rajaraman, M.M.; Rajaraman, S.R. Neosis-A Parasexual Somatic Reduction Division in Cancer. *Int. J. Hum. Genet.* **2007**, *7*, 29–48.
 174. Prigogine, I. Time, Structure and Fluctuations: Nobel Lecture, 8 December 1977. Available online: <https://www.nobelprize.org/uploads/2018/06/prigogine-lecture.pdf> (accessed on 5 November 2021).
 175. Noble, R.; Tasaki, K.; Noble, P.J.; Noble, D. Biological Relativity Requires Circular Causality but Not Symmetry of Causation: So, Where, What and When Are the Boundaries? *Front. Physiol.* **2019**, *10*, 827.
 176. Huang, S. On the Intrinsic Inevitability of Cancer: From Foetal to Fatal Attraction. *Semin. Cancer Biol.* **2011**, *21*, 183–199.

177. Niculescu, V.F. Is Cancer Cell Reversion to Normalcy Possible? Un Update. In *Novel Approaches in Cancer Study*; Crimson Publishers: New York, NY, USA, 2020; Volume 5.
178. Lotem, J.; Sachs, L. Epigenetics Wins over Genetics: Induction of Differentiation in Tumor Cells. *Semin. Cancer Biol.* **2002**, *12*, 339–346.
179. Telerman, A.; Amson, R. The Molecular Programme of Tumour Reversion: The Steps beyond Malignant Transformation. *Nat. Rev. Cancer* **2009**, *9*, 206–216.
180. Krigerts, J.; Salmina, K.; Freivalds, T.; Zayakin, P.; Rumnieks, F.; Inashkina, I.; Giuliani, A.; Hausmann, M.; Erenpreisa, J. Differentiating Cancer Cells Reveal Early Large-Scale Genome Regulation by Pericentric Domains. *Biophys. J.* **2021**, *120*, 711–724.
181. Bizzarri, M.; Giuliani, A.; Cucina, A.; Minini, M. Redifferentiation Therapeutic Strategies in Cancer. *Drug Discov. Today* **2020**, *25*, 731–738.
182. Nelson, C.M.; Bissell, M.J. Of Extracellular Matrix, Scaffolds, and Signaling: Tissue Architecture Regulates Development, Homeostasis, and Cancer. *Annu. Rev. Cell Dev. Biol.* **2006**, *22*, 287–309.
183. Lévi, F. Circadian Chronotherapy for Human Cancers. *Lancet Oncol.* **2001**, *2*, 307–315.
184. Battaglin, F.; Chan, P.; Pan, Y.; Soni, S.; Qu, M.; Spiller, E.R.; Castanon, S.; Roussos Torres, E.T.; Mumenthaler, S.M.; Kay, S.A.; et al. Clocking Cancer: The Circadian Clock as a Target in Cancer Therapy. *Oncogene* **2021**, *40*, 3187–3200.

3.4. Polyploidy upregulates gametogenetic genes and enriches meiotic modules in TCGA malignant tumors

This section of the work focuses on the impact of polyploidy on the expression of reproductive genes in cancer, using gene expression and ABSOLUTE purity/ploidy data of 29 tumor types from the TCGA database and an integrated gene set of 1474 gametogenetic (GG) genes. The differentially expressed genes from the experimentally validated work of (Quinton et al., 2021) are assessed for GG gene enrichment, cooperation in networks (STRING and coexpression), and enrichment of reproduction-related GO and KEGG functional modules in the giant components of their interaction networks. The results show that in a majority of tumor types polyploidy significantly upregulates at least several GG genes (in 17 of 29 - more than 10 GG genes), with 10 tumor types demonstrating significant enrichment ($p < 0.05$) of the GG gene set. Phylostratigraphic analysis shows that the evolutionary emergence of polyploidy-upregulated gametogenic genes used by tumors spans the whole timeline of life evolution. Furthermore, 9 tumor types demonstrate STRING networks enriched with GO and KEGG modules pertaining to meiosis and gametogenesis (oogenesis-related modules being of particular interest). Of the 6 tumor types eligible for network validation with the coexpression method (Article VI Table 2), all demonstrate robust coexpression networks enriched with reproductive modules, suggesting a ploidy-induced cooperative process with reproductive characteristics, the nature of which is further discussed in the manuscript. While this process was only observed in a subset of TCGA tumors and cannot be confidently referred to as “pan-cancer” based on the results of this study alone, these results nonetheless seem promising in the context of previous findings.

3.5. Gametogenetic genes are expressed and networked in malignant melanoma and breast carcinoma proteomes

This section of the study focuses on the expression and cooperation of gametogenetic genes in cancer on the protein level. Two high-throughput proteomics datasets (MM500 melanoma and PXD008841 breast carcinoma) were filtered for GG genes, and coexpression network analysis was used to assess their cooperation. The analysis revealed that in both cancer types, gametogenetic genes are significantly expressed by the hundreds, and over 50% them make up the giant component of a hard-threshold coexpression network. MCL clustering analysis extracted the most interconnected components of said networks, which were enriched for meiotic modules (Article VI Fig. S2) hint that the cancer reproductive process is an attractor state.



Article

The Transcriptome and Proteome Networks of Malignant Tumours Reveal Atavistic Attractors of Polyploidy-Related Asexual Reproduction

Ninel M. Vainshelbaum ^{1,2,*}, Alessandro Giuliani ³ , Kristine Salmina ¹, Dace Pjanova ¹
and Jekaterina Erenpreisa ^{1,*}

¹ Cancer Research Division, Latvian Biomedicine Research and Study Centre, LV-1067 Riga, Latvia

² Faculty of Biology, The University of Latvia, LV-1586 Riga, Latvia

³ Environment and Health Department, Istituto Superiore di Sanità, 00161 Rome, Italy

* Correspondence: ninela.vainshelbaum@biomed.lu.lv (N.M.V.); katrina@biomed.lu.lv (J.E.)

Abstract: The expression of gametogenesis-related (GG) genes and proteins, as well as whole genome duplications (WGD), are the hallmarks of cancer related to poor prognosis. Currently, it is not clear if these hallmarks are random processes associated only with genome instability or are programmatically linked. Our goal was to elucidate this via a thorough bioinformatics analysis of 1474 GG genes in the context of WGD. We examined their association in protein–protein interaction and coexpression networks, and their phylostratigraphic profiles from publicly available patient tumour data. The results show that GG genes are upregulated in most WGD-enriched somatic cancers at the transcriptome level and reveal robust GG gene expression at the protein level, as well as the ability to associate into correlation networks and enrich the reproductive modules. GG gene phylostratigraphy displayed in WGD+ cancers an attractor of early eukaryotic origin for DNA recombination and meiosis, and one relative to oocyte maturation and embryogenesis from early multicellular organisms. The upregulation of cancer–testis genes emerging with mammalian placentation was also associated with WGD. In general, the results suggest the role of polyploidy for soma–germ transition accessing latent cancer attractors in the human genome network, which appear as pre-formed along the whole Evolution of Life.

Keywords: cancer; whole genome duplications; biological interaction networks; gene phylostratigraphy; atavism; basic meiosis attractor; female meiosis; early embryo; pseudo-placentation; soma–germ transition



Citation: Vainshelbaum, N.M.; Giuliani, A.; Salmina, K.; Pjanova, D.; Erenpreisa, J. The Transcriptome and Proteome Networks of Malignant Tumours Reveal Atavistic Attractors of Polyploidy-Related Asexual Reproduction. *Int. J. Mol. Sci.* **2022**, *23*, 14930. <https://doi.org/10.3390/ijms232314930>

Academic Editor: Konrad Huppi

Received: 10 October 2022

Accepted: 26 November 2022

Published: 29 November 2022

Publisher's Note: MDPI stays neutral with regard to jurisdictional claims in published maps and institutional affiliations.



Copyright: © 2022 by the authors. Licensee MDPI, Basel, Switzerland. This article is an open access article distributed under the terms and conditions of the Creative Commons Attribution (CC BY) license (<https://creativecommons.org/licenses/by/4.0/>).

1. Introduction

Metastatic cancer is one of the leading causes of death in the world [1,2]. A major determinant of its lethality is the ability of late-stage solid tumours to become increasingly resistant to anti-cancer treatments. Cancer research still lags in understanding the biological reasons for this resistance. Somatic cancers are known to ectopically express the genes related to reproductive processes, such as cancer–testis antigens [3–7] and meiosis-specific genes [7–13], as well as a wide range of genes specific both to primordial and adult germ cells [14]. Based on the existing overlap between the three aforementioned lists of genes (meiotic, cancer–testis and germ cell-specific), we shall refer to them as a united group of “gametogenesis-related genes” (GG). GG expression is generally associated with a worse patient prognosis [14–19]. Reproductive genes paradoxically play a role in promoting the severity and lethality of cancers, which by their origin are somatic. Another notable hallmark of cancer lies in the tendency of tumour cells to acquire whole genome duplications (WGD) and unstable aneuploidy karyotypes, which are also associated with poor outcomes [20]. While at first glance it seems that aneuploidy would interfere with mitotic division and proliferation of tumours, it paradoxically favours resistance to treatment, cancer relapse and metastatic growth [21–24]. This puzzle of cancer could be

overcome by the assumption that reproduction-related genes in cancer cells are involved in an atavistic life-cycle-like process ensuring the perpetuation of generations [25], which is realized through reversible polyploidy (ploidy cycles) that gave evolutionary origin to meiosis and sex [26]. This cancer unicellular life-cycle hypothesis was inspired by the observations of tumour giant cells in their prolonged response to ionising irradiation, finding the phenotypes comparable with those of some protists undergoing cycling polyploidy in their life-cycle [25,27–29].

From that standpoint, “dormant” polyploid giant cancer cells (PGCCs), which are heavily implicated in resistance, are presumed to represent a kind of “cancer germline” that is reciprocally linked to a mitotically dividing cell line, cyclically renewing its immortality [30].

The reproductive role of cancer polyploidy has been intensively studied and reviewed over the last two decades in our and about 20 other laboratories, and also earlier, becoming more and more recognised worldwide. It was shown that a single PGCC is able to induce a metastatic tumour at xenotransplantation [31] and appears similar to an early embryo [32–42]. A summary table of these studies is available in [43], the historical arrow diagram of cancer polyploidy research milestones—in Moein et al. [42], the latest advances united in a special issue [44]. This, along with the exchangeability of tumour and embryo nuclei and cells, already shown in the 20th century, has thus awakened and led to the emergence of a new, polyploidy-related twist on the embryonal theory of cancer, which initially originated in the 19th century [32–42].

Meiosis requires a tetranemic bivalent from two replicated parental homologous chromosomes for the main event of meiosis I—meiotic recombination and crossover, which effectively repair DNA, prevent accumulation of deleterious mutations with loss of heterozygosity (LOH), and provide genetic diversity [45,46]. The next important role of meiosis is the ordered halving of DNA content (suppressing one DNA replication cycle between two cell divisions), which might be involved, as suggested in [11,47], in the depolyploidisation of PGCCs whose progeny can start a new life-cycle.

In multicellular organisms, the germ cells are either specified during embryonic development or generated from somatic cells in a soma-to-germ transition (e.g., in plants, this is a very common phenomenon) [48]. Bruggeman et al. [14], who had observed the widespread expression of germ cell-specific (from embryonic to adult) genes in a wide database set from cancer cell lines and primary malignant tumours, proposed the involvement of such a soma-to-germ transition process in cancer evolution; the same was proposed by [5,8,34], while we have reported the induction of the embryonic stem cell-like markers (POU5F1, SOX2, NANOG) starting after DNA damage together with the polyploidy cycles [49]. In turn, cancer–testis (CT) genes are also considered cancer stem cell biomarkers [50,51]. The expression of cancer–testis genes may contribute to the ploidy cycle in both its poly- and depolyploidisation stages. Some of them are involved in meiosis and germ cell development, and some, particularly members of the Melanoma Antigen Gene (MAGE) family and PRAME, are implicated in the downregulation of the *p53* tumour suppressor [52–54], epigenetic reprogramming to stemness, and germline initiation [55,56], along with suppression of differentiation [57] and poor clinical prognosis [56,58].

However, it still remains to be seen whether this association between GG expression and cancer is pre-programmed (correlated, networked, and module-hubbed), or, as suggested by some authors [59], coincidental and random. On the other side, between those who do not doubt the programmatic atavistic development of cancer, there is a controversy over the time of its evolutionary origin, unicellular or early multicellular [60–62]. More fundamentally, there is also no clarity on the functional role of the meiotic toolkit in polyploidy-including life-cycles of the obligatory agamic protists [63,64]. In this study, we approach these questions by means of complex network analysis on publicly available cancer patient datasets (transcriptomes, inferred ploidy/WGD values, phylostratigraphy, and proteomes). To explain our goals, it is important to highlight the prerequisites in more detail.

Firstly, Stuart Kauffman, and then together with Sui Huang and Ernberg, proposed an idea that human cancer is driven by an attractor of the genome network that was evolutionary pre-formed (but not used) near the top of the onto-phylogenetic tree [65,66]. Indeed, phylostratigraphic studies revealed the evolutionary origin of cancer-driving genes [67] and a cancer transcriptome evolutionary gene profile shift to the emergence of multicellularity from unicellularity [60,68–70], likely disrupting the normal gene balance between uni- and multicellularity gene expression in the mammalian genome [61]. Interestingly, the earliest naturally occurring tumour was observed as far back as in the basal Eumetazoan *Hydra* [71]. However, the role of polyploidy in this phylostratigraphic shift of primary tumours, to our knowledge, has not been investigated.

Polyploidy as such (in normal mammalian tissues) induces a similar epigenetic shift favouring upregulation of unicellular and early multicellular genes (phylogenetic strata 1–5, from Prokaryotes to Eumetazoa), accompanied by downregulation of the genes of complex multicellularity, responsible for apoptosis, differentiation, immunity, and cell communication [72]. This shift towards unicellularity is aided by the ploidy-upregulated key proto-oncogene *c-myc* (originated in Opisthokonta) opening the chromatin for reprogramming [73], leading to epithelial-mesenchymal transition (EMT) [72,74–76] and hubbing the network nest of upregulated bivalent genes (in the same phylogenetic strata 1–5). The latter enable a critically rapid switch of the gene promoter activity from a suppressed to an active state. Moreover, cancer gene ontology (GO) modules embracing the c-MYC-HRAS axis and EGFR nest become activated by polyploidy [72,74–76].

Here it is worth adding that the current experimental evidence of cancer's resistant response to conventional therapy can be summed up in three stages: induction of cellular senescence (with telomere attrition and persistent DNA damage signalling), polyploidisation, and reciprocal reprogramming/self-renewal [77]. The link between stress-induced accelerated cell senescence and reprogramming has been shown in many studies [30,78–81].

The meiotic pachytene recombination checkpoint has initially evolved from the mitotic G2/DNA damage checkpoint and uses some proteins from it [82,83]. As such, the persistent DNA damage induced in accelerated cellular senescence by oncogenes, drugs, or oxidative stress may enable cancer cells to slip from the mitotic DNA damage checkpoint into the meiotic prophase, as suggested in [77], assuming a polyploidisation variant in the form of Mos-driven endomitosis [27]. The other (or the same) route are the cycles of so-called mitotic slippage (reversal of metaphase arrest after DNA re-replication, not accomplishing mitosis) expressing the meiotic proteins (DMC1, SPO11, MOS, REC8, STAG3, SCYP1, SCYP3, POU5F1) observed in vitro on the irradiated *p53*-mutant lymphoma cell lines [12,27], and doxorubicin-treated basal breast cancer cell line [81] and some meiotic genes in luminal MCF7 cancer after TOPO I inhibitor [84].

The problem is that, although GG genes were found abundantly expressed in tumours and associated with poor survival of patients, thus assigning fitness advantage to cancer cells, the conventional meiosis has never been microscopically observed, but instead, the polyploidy associated with meiotic markers was found [30,85]. On the other hand, there exist valid gene phylostratigraphic results demonstrating the converging of both WGD and the origin of cancer-driving genes to the same paleontological period of early eukaryotic evolution (as indicated above). Moreover, Quinton et al. [86] detected differences between transcriptomes of diploid (WGD-) and polyploid (WGD+) in the Cancer Genome Atlas (TCGA) tumours highlighting suppression of immunity, but the relationship between polyploidy and meiosis was not addressed there. The evidence of GG expression in cancer might have a programmatic evolutionary significance, if not only their presence but also networking and cooperation were to be proven in the context of polyploidy. The theoretical basis of these insights from the literature and the bioinformatics work in similar studies converging to the aim and design of the current work is schematised in Figure 1. The goal was to evaluate, through bioinformatics analysis of GG genes and proteins, their programmatically atavistic link with cancer polyploidy and to define the relevant attractor(s) in the human genome.

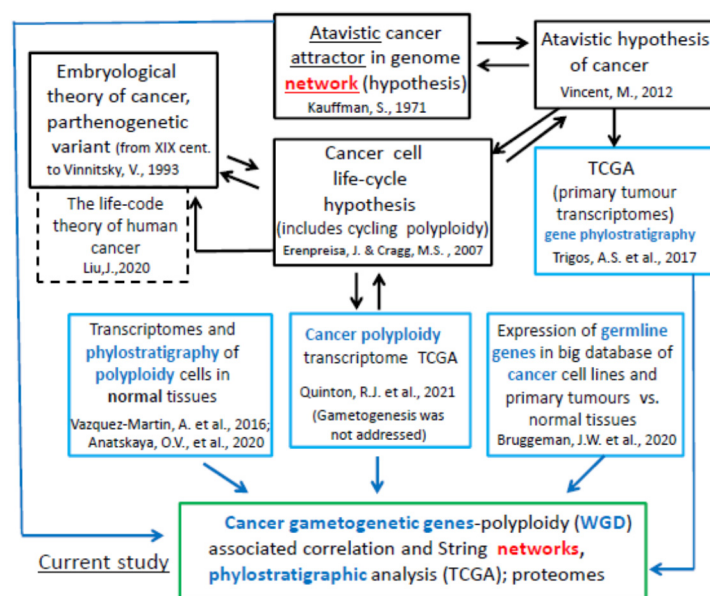


Figure 1. The context, aims, and design of the current bioinformatics study: in black boxes, the theoretical prerequisites; in blue boxes, what has been performed in previous similar studies (see the citations in the reference list [14,25,38,41,60,65,69,72,74,86]); in a green box, the aims and design addressed in the current study.

In synthesis, our results rule out the purely coincidental/random hypothesis of GG expression in favour of the re-activation of highly structured latent coexpression modules. Even if in this work, we do not make any direct PGCC observation, the emerging picture of robust GG upregulation by polyploidy (WGD) in multiple tumour types, as well as the highly organized coexpression networks that include them, give a relevant (albeit implicit) support to this hypothesis. Moreover, the obtained results suggest the role of polyploidy in soma–germ transition by visiting and interconnecting cancer attractors, pre-formed in the human genome network, during the origin and development of reproductive life-cycles, along the whole Evolution of Life.

2. Results

2.1. Whole-Genome Duplication Enriches GG Genes in TCGA Cancer Transcriptomes

Upon filtering the WGD-related differentially expressed (DE) genes (from [86]) for GG genes (Table S1), we observed non-zero GG gene upregulation in 23 of the overall 29 tumour types. A total of 10 tumour types (BLCA, BRCA, GBM, LIHC, LUAD, LUSC, OV, PRAD, SARC, STAD) possess a statistically significant enrichment of GG genes among upregulated genes, compared to the whole transcriptome (right-tailed binomial test $p < 0.05$) (Table 1).

Of 29 cancer types, 7 (BLCA, BRCA, GBM, LIHC, LUAD, PRAD, SARC) used in the tumour WGD study by Quinton et al. [86] have >100 ploidy-upregulated genes, of which more than 10% belong to the GG group (the maximum being BRCA at 25.27%). Furthermore, the GG genes are clearly depleted among ploidy-down-regulated genes (left-tailed binomial test $p < 0.05$ in all cancer types with any down-regulated GG), with the maximum proportion of GG genes among down-regulated genes being just 3.54% (Table 1). A statistically significant (binomial test $p < 0.05$) trend towards GG upregulation rather than downregulation can be observed in 13 cancer types (BLCA, BRCA, GBM, HNSC, KICH, LIHC, LUAD, OV, PRAD, SARC, STAD, TCGT, UCEC). Furthermore, 17 of 29 tumour types have at least one gene from the GG group fall into the top-25 genes when ranked by the highest logFC. A total of 10 of these tumour cohorts have MAGE group members in their top-25 upregulated genes; 3 (BRCA, HNSC, LUAD) have both MAGEs and PRAME in their top-25 upregulated genes.

Table 1. The prevalence of GG genes found among ploidy-upregulated and downregulated differentially expressed genes (DEGs) *.

TCGA Cancer Type	% of WGD+ Samples	Number of Ploidy-Upregulated Genes	Upregulated Genes Enriched with GG ($p < 0.05$)	Number of Ploidy-Downregulated Genes	Downregulated Genes Enriched with GG ($p < 0.05$)
ACC	53.7%	84	FALSE	443	FALSE
BLCA	60.2%	424	TRUE	1000	FALSE
BRCA	44.0%	277	TRUE	1395	FALSE
CESC	33.7%	16	FALSE	157	FALSE
CHOL	22.2%	1	FALSE	0	FALSE
COAD	40.0%	431	FALSE	641	FALSE
ESCA	55.4%	0	FALSE	1	FALSE
GBM	17.6%	164	TRUE	850	FALSE
HNSC	39.4%	309	FALSE	867	FALSE
KICH	15.4%	164	FALSE	204	FALSE
KIRC	22.2%	305	FALSE	658	FALSE
KIRP	7.3%	36	FALSE	5	FALSE
LIHC	35.0%	435	TRUE	894	FALSE
LUAD	57.1%	431	TRUE	1445	FALSE
LUSC	54.5%	97	TRUE	1106	FALSE
MESO	22.6%	0	FALSE	4	FALSE
OV	57.6%	400	TRUE	1374	FALSE
PAAD	29.1%	11	FALSE	1083	FALSE
PCPG	21.4%	3	FALSE	6	FALSE
PRAD	11.6%	427	TRUE	610	FALSE
READ	52.3%	0	FALSE	4	FALSE
SARC	47.4%	573	TRUE	1040	FALSE
STAD	41.3%	1047	TRUE	928	FALSE
TGCT	95.3%	549	FALSE	523	FALSE
THCA	9.0%	686	FALSE	1138	FALSE
THYM	20.0%	1562	FALSE	1046	FALSE
UCEC	22.3%	1671	FALSE	1691	FALSE
UCS	82.8%	1	FALSE	1	FALSE
UVM	6.3%	13	FALSE	69	FALSE

Abbreviations: TCGA—The Cancer Genome Atlas, ACC—Adrenocortical Carcinoma, BLCA—Bladder Urothelial Carcinoma, BRCA—Breast Invasive Carcinoma, CESC—Cervical Squamous Cell Carcinoma and Endocervical Adenocarcinoma, CHOL—Cholangiocarcinoma, COAD—Colon Adenocarcinoma, ESCA—Esophageal Carcinoma, GBM—Glioblastoma Multiforme, HNSC—Head and Neck Squamous Cell Carcinoma, KICH—Kidney Chromophobe, KIRC—Kidney Renal Clear Cell Carcinoma, KIRP—Kidney Renal Papillary Cell Carcinoma, LIHC—Liver Hepatocellular Carcinoma, LUAD—Lung Adenocarcinoma, LUSC—Lung Squamous Cell Carcinoma, MESO—Mesothelioma, OV—Ovarian Serous Cystadenocarcinoma, PAAD—Pancreatic Adenocarcinoma, PCPG—Pheochromocytoma and Paraganglioma, PRAD—Prostate Adenocarcinoma, READ—Rectum Adenocarcinoma, SARC—Sarcoma, STAD—Stomach Adenocarcinoma, TCGT—Testicular Germ Cell Tumours, THCA—Thyroid carcinoma, THYM—Thymoma, UCEC—Uterine Corpus Endometrial Carcinoma, UCS—Uterine Carcinosarcoma, UVM—Uveal Melanoma. *—genes with $> |0.5| \log_{2}FC$ from the [86] dataset of 29 TCGA tumour type transcriptomes.

In an attempt to uncover the evolutionary meaning of GG gene upregulation in polyploid cancer, we next decided to investigate the evolutionary history of GG gene origin using gene-phylostratigraphic information.

2.2. The Phylostratigraphic Distribution of GG Genes

After plotting the phylostratigraphic distribution of GG genes based on the gene phylostrata classification used by Trigos et al. [60], we observed significant peaks in phylostrata 2 (Eukaryota) and 8 (Euteleostomi) (Figure 2). Overall, this distribution was approximately concurrent with the reference of all available genes for which phylostratigraphy information was available. However, compared to the reference, GG genes show higher enrichment in the 12th and 14th phylostrata of placental animals and ancestral primates. The list of GG genes per phylostratum is presented in Table S1.

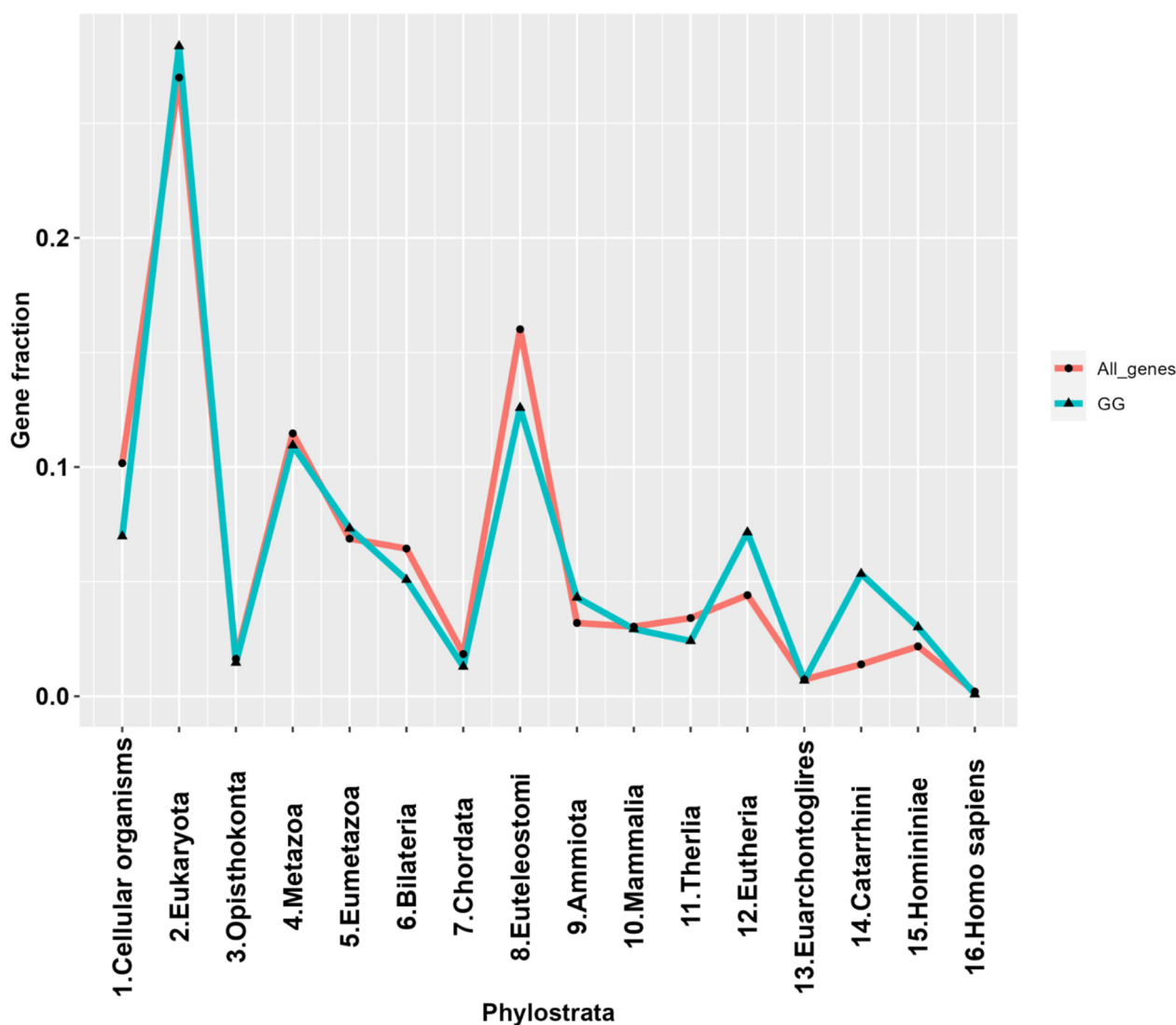


Figure 2. The phylostratigraphic distribution line plot of genes in the GG list ($n = 1474$), with all available genes serving as a reference.

Briefly, from this GG list, it can be seen that the powerful meiosis-specific recombinase *DMC1* (the homolog of bacterial *RecA* which appeared in the Archaea in two forms [87,88]), along with the recombinase *RAD51*, fall into the Prokaryotic stratum 1, while most of the meiotic recombination toolkit with *HORMAD* (which can organise the axial element for chromosome pairing [89]), and the meiotic Aurora kinase variant C (cooperating with mitotic *AURKB*), are already present in the 2nd Eukaryota stratum. DNA damage response elements (*ATR* and *CHEK1*, integrating *ATR* and *ATM* signalling) also appear in strata 2 and 3, respectively, and the *MOS*-kinase, responsible for the main steps of female meiosis—the recombination-dependent monopolar spindle and oocyte maturation [34,90,91]—in stratum 4 (Metazoa). Stratum 5 adds *PRDM14*, *PRDM9* and *DAZL* for the commitment of primordial germ cells. The important element of the conventional meiosis—the protein of the synaptonemal complex central element (*SYCP1*), together with the *SGO* stabilisers of the meiotic centromeric cohesin *REC8*, developed by stratum 8, coinciding with the Cambrian explosion. Late strata 12 and 14, starting from the Eutherians (placental mammals), added the majorly X-chromosome-linked CT genes (*PRAME*, most *MAGEA* genes in stratum 12, the *GAGE* and *PAGE* groups in stratum 14 (Catarrhini—Old World monkeys)—normally found in both gonads and the placenta [92]. The *Homo sapiens* stratum 16 added only the *STAG2* component of the meiotic cohesin complex. The STRING network representation of

the GG genes falling into the respectively oldest and dominant 1st and 2nd strata can be seen in Figure 3.

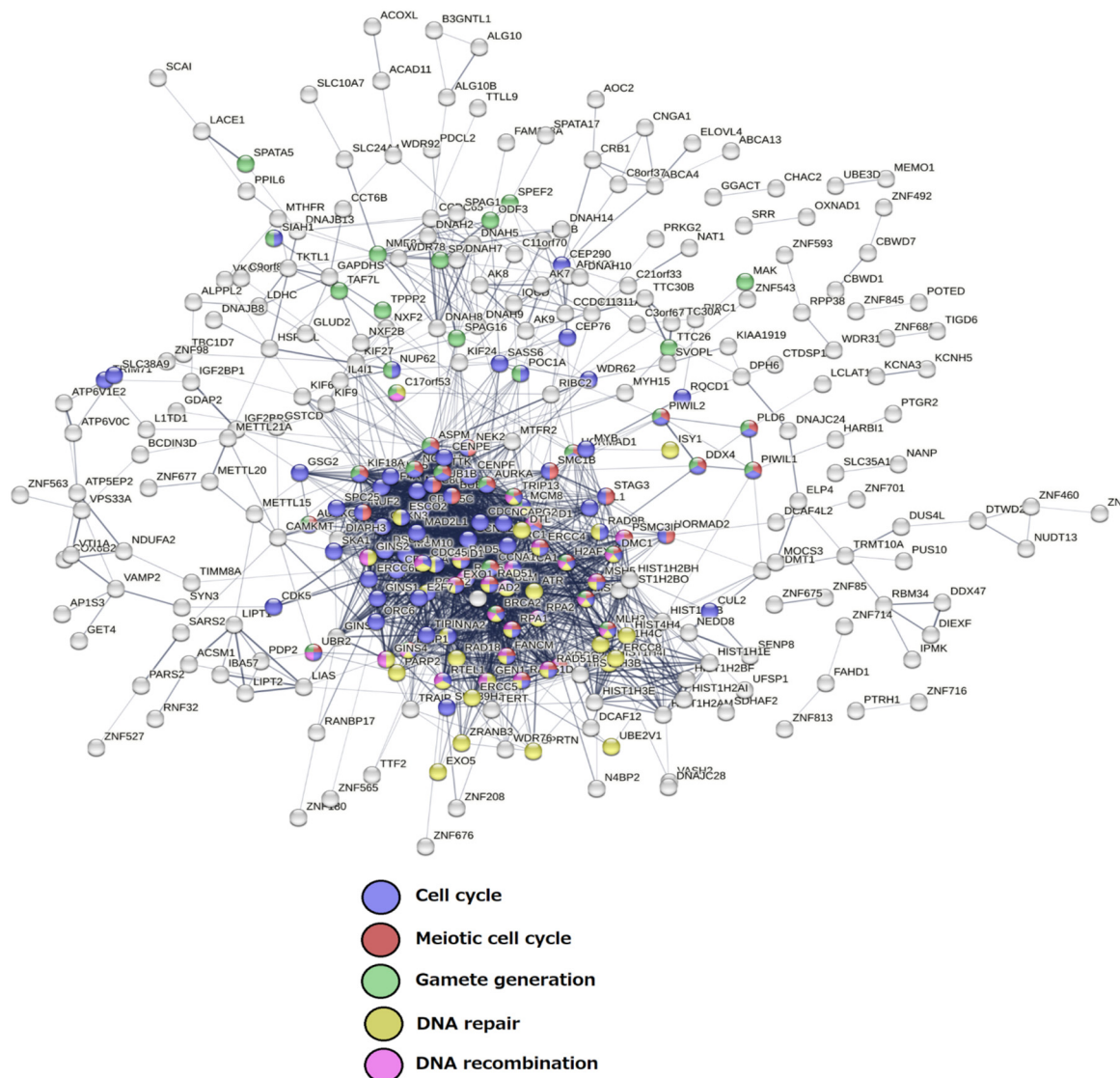


Figure 3. The STRING network of GG genes in the 1st and 2nd evolutionary phylostrata with enriched GO biological process modules highlighted in colours.

It is seen that the meiotic cell cycle appeared in Eukaryota, coupled with the recombination DNA repair, along with sex (gamete generation). Applying the same method to ploidy-upregulated GG genes in the TCGA dataset (Figure 4) revealed a dominant peak at phylostratum 2 in 15 of the 17 tumour types eligible for analysis (having >10 upregulated GG genes), along with high variability of the other part of the histogram occupying the whole evolutionary timeline, still highlighting a notable peak at stratum 8 (save for the TGCT cancer, which is also depleted of the later ploidy-upregulated GG genes). In all other tumours including PRAD, CT genes of the strata 12–14 (placental and hominid animals, respectively) are more or less overexpressed; in LUSC, this peak is dominating. The CT genes found, besides tumours and testis, in normal ovaries and placenta, inspired Lloyd Old’s witty conclusion: “Cancer is a somatic cell pregnancy” [93]—a paradox which will be later discussed.

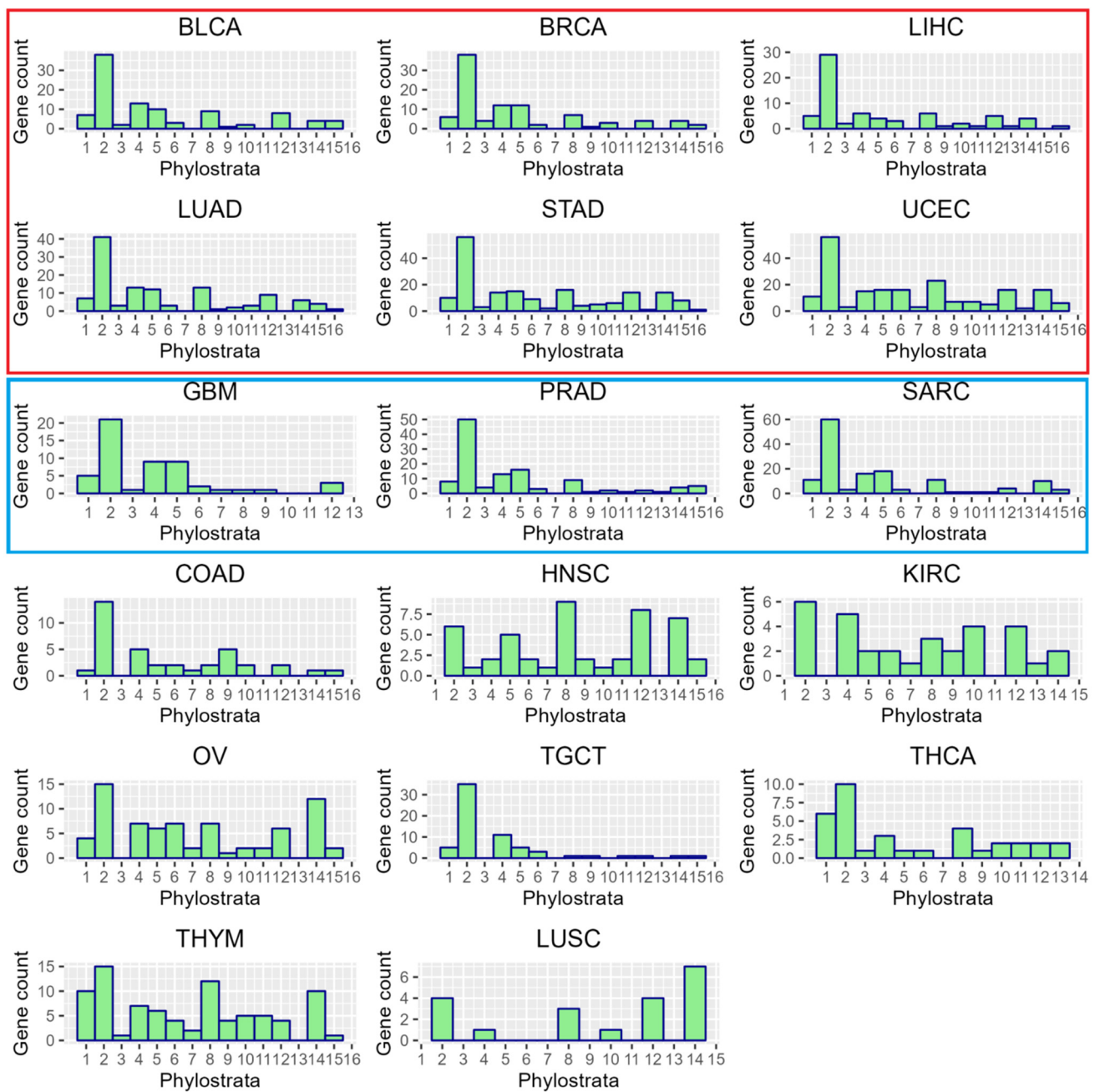


Figure 4. The phylostratigraphic distribution of ploidy-upregulated GG genes in 17 primary TCGA tumour types (that meet the criteria of having >10 ploidy-upregulated GG genes). The histograms of the 6 tumour types whose STRING and coexpression networks of upregulated genes are enriched for meiosis and gametogenesis-related GO and KEGG modules are highlighted in red, the 3 tumour types for which the former is true only in the case of STRING networks—in blue. Notably, they have a similar pattern of phylostratigraphic distribution of GG genes along the evolutionary tree, which is also similar in COAD and represents the most frequent types of somatic human cancers. Abbreviations are the same as in Table 1.

Examining the STRING protein–protein interaction (PPI) networks of the 29 TCGA tumours at both medium and high confidence revealed that nine of them (bladder carcinoma, breast carcinoma, glioblastoma, liver hepatocellular carcinoma, lung adenocarcinoma, stomach adenocarcinoma, prostate adenocarcinoma, sarcoma, uterine corpus carcinoma) possess the ploidy-upregulated meiotic GO and KEGG modules. An example of such a network in BRCA samples is shown in Figure 5. It demonstrates a tightly associated sub-network of the

meiotic cell cycle with strictly meiosis-specific (i.e., *HORMAD1*, *MND1*, *SMC1B*) genes and includes CT genes such as *TTK* and *PBK* (known also for metastatic prostate carcinoma [94]). Furthermore, the giant sub-network is connected through *PRAME* to a cluster of *MAGE*-family of CT-proteins, which are considered to be metastasis-favouring oncogenes playing an important role in the soma-to-germ transition—by epigenetic reprogramming, germ commitment, and differentiation suppression (reviewed in Introduction).

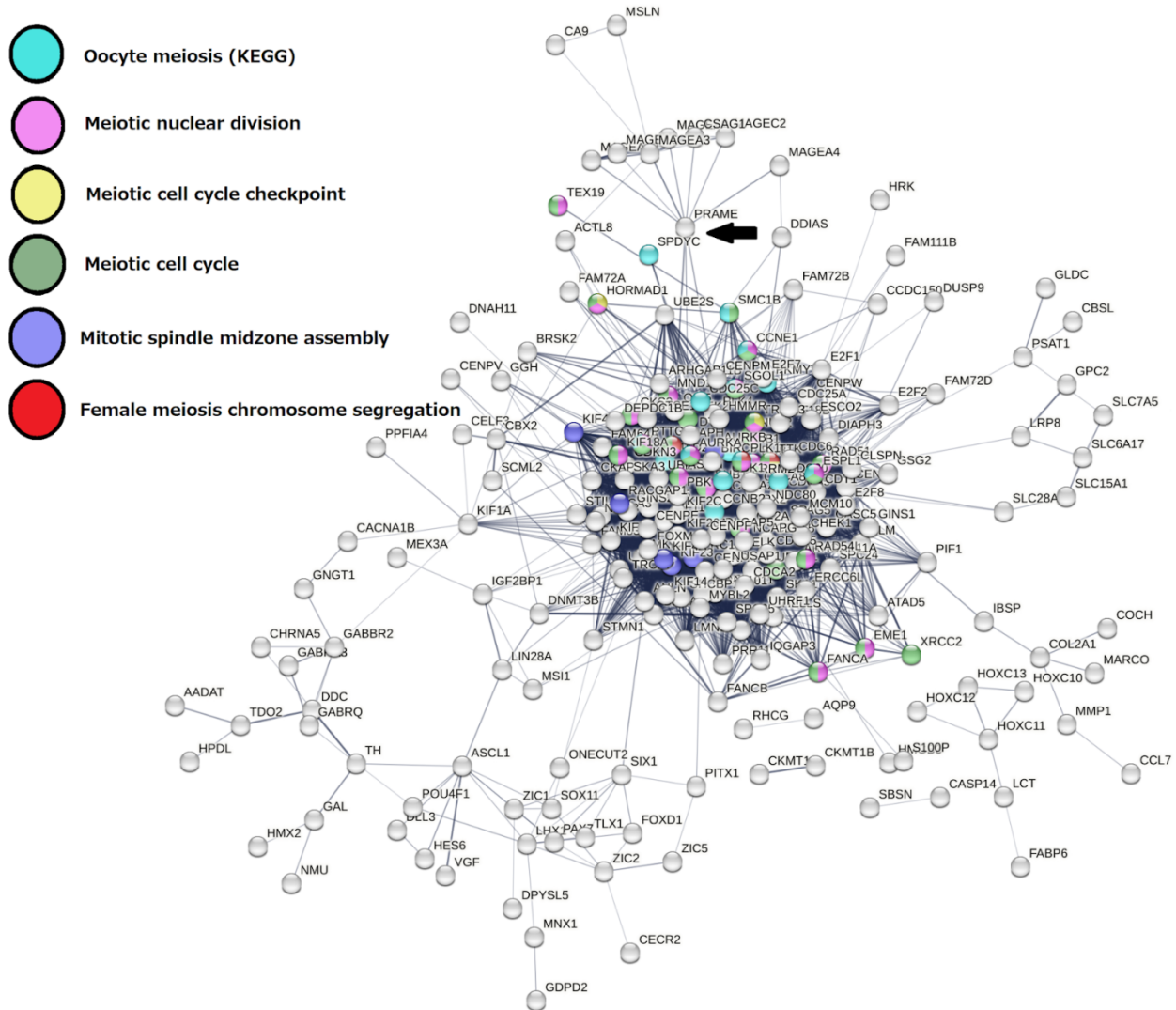


Figure 5. A STRING network of the ploidy-upregulated genes in TCGA-BRCA with colour-highlighted genes of meiosis-related enriched GO and KEGG modules (at medium confidence) connected by *PRAME* to a CT gene cluster (*MAGE*s) (arrow).

In Figure 5, besides the elements of the meiotic cell cycle composed of functional nodes: meiotic cell cycle checkpoint (responsible for meiotic DNA recombination) and female meiosis including oocyte maturation, the polyploidy-related network contains an element of mitotic karyokinesis—spindle midzone assembly, which will be later discussed. The enrichment of GO and KEGG modules related to oocyte meiosis is seen in the six STRING networks of nine meiotic module-enriched tumour cohorts (Files S1).

Moreover, performing coexpression network analysis on six of the total nine meiosis module-enriched tumour types (the other three were rejected from coexpression network analysis due to not meeting both criteria of at least 100 upregulated genes and at least 50 polyploid samples with a purity > 0.5), in line with the STRING results, also revealed that the giant component of the ploidy-upregulated gene coexpression network is enriched

for meiosis-related GO and KEGG modules in general, and modules relating to oogenesis/female meiosis in particular. The tumour types selected for coexpression network analysis are listed in Table 2.

Table 2. Parameters of the ploidy-upregulated genes, the coexpression network thereof, and gametogenesis-related modules in (WGD+) samples of six TCGA tumour types *.

Tumour Type	Number of Samples (WGD+, >0.5 Purity)	Number of Upregulated Genes (pAdj < 0.05; logFC > 0.5) Expressed in High-Purity Samples	Percent of Upregulated Genes in the Giant Component of Network	Average Clustering Coefficient of Network	Meiotic GO/KEGG Modules Enriched in Coexpression Network (Y/N)	Female-Specific Meiotic GO/KEGG Modules Enriched in Coexpression Network (Y/N)
BRCA	277	220	56.8%	0.68	Y	Y
LUAD	103	340	52.9%	0.74	Y	Y
LIHC	91	290	94.5%	0.61	Y	Y
STAD	82	756	58.6%	0.47	Y	Y
BLCA	142	348	54.9%	0.5	Y	Y
UCEC	97	1217	48.5%	0.56	Y	Y

* These tumour samples were selected for analysis due to meeting the criteria of meiotic module enrichment in ploidy-upregulated gene STRING networks, at least 100 upregulated genes (as seen in Table 1), and at least 50 polyploid samples with a purity > 0.5. Y—Yes; N—No.

The analysis revealed a high proportion of the ploidy-upregulated genes associating into a network enriched with the meiotic and female-specific meiotic GO/KEGG modules with high average clustering coefficients. An example of one such coexpression network (TCGA-BRCA), with 125 nodes, 1700 edges, and an average clustering coefficient of 0.68 can be observed in Figure 6A, and the functional enrichment results thereof in Figure 6B. The rest of the networks have been deposited and are publicly available in the Network Data Exchange (NDEX) database (see Data Availability Statement below).

The Senescence Module of the Ploidy-Upregulated Gene Network

Among the six tumour types with highly WGD-upregulated GG genes and enriched meiotic (among them, female-specific) modules in both STRING and coexpression networks, three (BRCA, LUAD and LIHC) demonstrated the enrichment of the cellular senescence KEGG module (seen in File S2). There, we found that the well-known G1/S transition inhibitor CDKN2A (encoding p14 and p16) and the upregulation of CHEK1 Checkpoint kinase 1 integrating signals from ATM and ATR, the two cell cycle proteins involved in DNA damage responses G2M transition regulation, also associate with chromatin in meiotic prophase. Additionally, FOXM1 participating in DNA damage response should be highlighted. The upregulated member of the MYB family of transcription factor genes family MYBL2 has been shown to activate cyclin D1 (involved in polyploidisation) and interact with multiple insulin-like growth factor-binding proteins [95]. This auto-regulating loop is associated with the frequent deregulation of the insulin growth factor signalling pathway in cancer [96]. Interestingly, 14 of the 29 TCGA cancer types, including the three with the enriched senescence module, show ploidy-upregulation of IGF2BPs and IGF2BPs, IGF2BP1 and IGF2BP3 being the most frequently encountered. IGF2BP1 and IGF2BP3 are oncofoetal proteins that are involved in stem cell renewal, organogenesis, and gametogenesis [97–99], and are also listed as MYBL2 interactants in the Harmonizome database [95].

This may be related to the fact that senescence induces DNA double-stranded breaks (DSBs), which, viewed in the context of GG gene expression and meiosis, may be interpreted as conferring the capability for a soma–germ transition from the mitotic DNA damage checkpoint in G2 (equivalent to WGD, in case of interrupted mitotic cell division, as

discussed in Introduction). The insulin-like growth factor (IGF1)-related pathways may play the same or a converging role in a soma–germ transition. Insulin can substitute progesterone for inducing female oogenesis through direct activation of MOS by Ras upregulation in senescent somatic cells [34]. IGF1-related pathways are activated by hypoxia/an acidic environment [100].

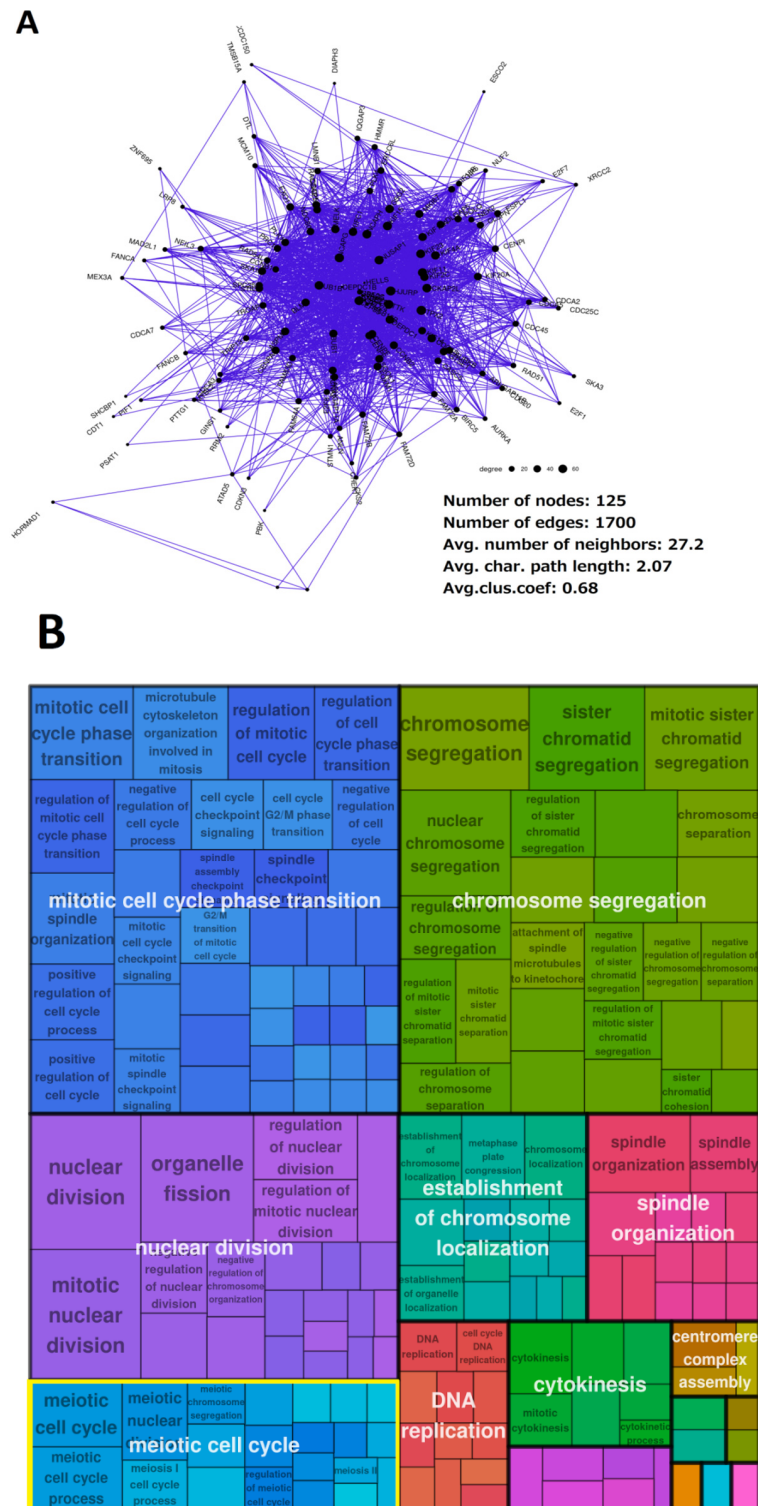


Figure 6. The cooperation of the ploidy-upregulated genes in TCGA-BRCA: (A) The giant component of the coexpression network of ploidy-upregulated genes. (B) A tree map plot of GO biological process modules enriched in this network. Modules related to meiosis are highlighted (yellow).

As for the ploidy-down-regulated genes, the results of GO and KEGG enrichment analysis on both STRING and coexpression networks largely skew towards immunity-related processes in all nine analysed GG-enriched tumour types. The same was shown by [74] as related to polyploidy in normal tissues, and by [86] as related to polyploidy in tumours. Modules related to apoptosis and tissue homeostasis are also stably present in the ploidy-down-regulated gene networks (File S3).

2.3. Malignant Melanoma (MM) and BRCA Proteome Analysis Reveal Robust Expression and Coexpression of GG Proteins

In order to investigate GG gene expression and coexpression in cancer on the protein level, we selected and analysed two recently published high-throughput proteomics datasets of MM and BRCA.

2.3.1. The Malignant Melanoma Proteome

Hierarchical clustering had stratified the MM500 database [101] patient cohort into six clusters (Figure S1). Taking into account the limited available clinical data, as well as the presence of non-random missing patterns provoking the impossibility to discriminate the existence of distinct biological subtypes from a batch effect, we decided to focus on the largest distinctive patient subset ($n = 142$), or Cluster 3 on Figure S1 for further analysis.

Overall, in the whole MM500 database melanoma proteome matrix, 411 proteoforms of reproduction-related genes (382 unique gene IDs) were found to be expressed in at least 20% of the samples (101 of 505). Patient Cluster 3, which was selected separately for further analysis, demonstrated the expression of 513 such proteoforms (501 unique gene IDs) in at least 20% of its constituent samples (>28 of 142).

After calculating correlations, thresholding the protein pairwise correlation matrix at $|0.6|$, and transforming it into a binary adjacency matrix, it was revealed that the vast majority ($n = 452$) of the expressed GG genes are also significantly coexpressed, forming the giant component of a network with a total of 3035 edges. Upon analysing the network with base Cytoscape [102] functionalities, it was determined to have an average clustering coefficient of 0.34 and an average shortest path length of 3.43.

Ranking the nodes in the network by degree (Figure 7A) reveals a highly interconnected “core” sub-network in its middle. Markov Cluster Algorithm (MCL) clustering at a granularity parameter of 2.5 extracted that interconnected component of 134 nodes and 1432 edges, with an average clustering coefficient of 0.58 and average shortest path length of 2.26 (Figure 7B).

In addition, GO biological process (BP) and KEGG enrichment analysis (right-sided hypergeometric test using all proteins identified in the MM500 proteome as the background, with the Bonferroni Step-Down (Holm) p -value adjustment method) identified meiotic GO and KEGG modules enriched in both the whole giant component of the network and, in particular, its most interconnected MCL cluster, including meiosis I, reciprocal meiotic recombination, female meiotic nuclear division, meiotic nuclear division, meiotic chromosome segregation, meiotic cell cycle checkpoint signalling, and blastocyst growth (Figure S2A).

2.3.2. The Breast Carcinoma Proteome

Overall, in the PXD008841 [103] proteome matrix of 45 BRCA (pre-filtered for insufficiently expressed proteins), 316 proteoforms of reproduction-related genes (316 unique gene IDs) were found to be expressed. A total of 196 (62%) of them were found to make up the giant component of a highly interconnected coexpression network (Figure 8A), with 3068 edges and an average clustering coefficient of 0.6. MCL clustering at a granularity parameter of 2.5 extracted the most interconnected component of 127 nodes and 2812 edges, with an average clustering coefficient of 0.77 and an average shortest path length of 1.86 (Figure 8B).

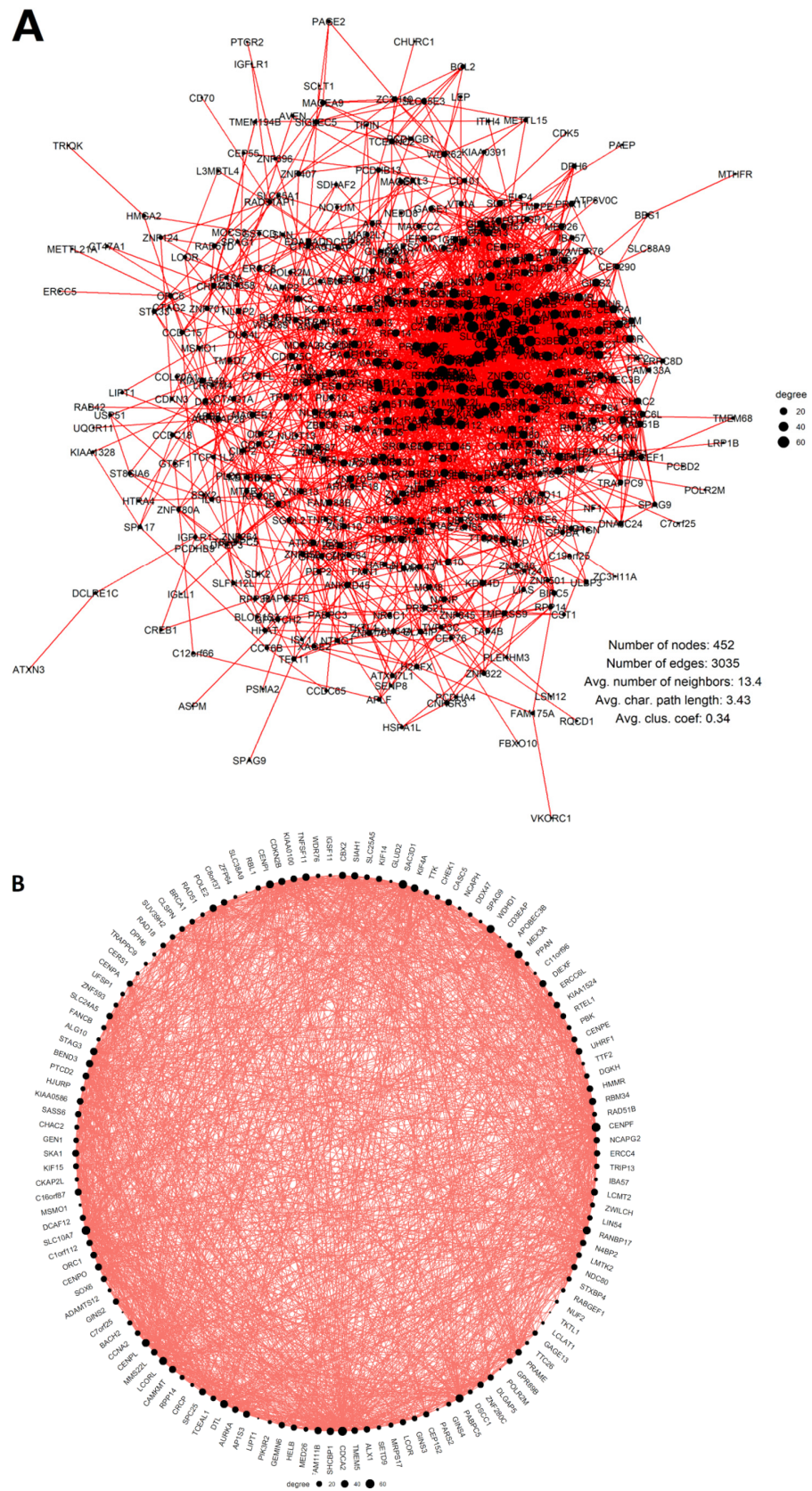


Figure 7. The coexpression networks of GG proteins in the MM500 database [101] melanoma proteomes (node size scaled to a degree): (A) The full network of GG proteins in 142 late-stage MM samples; (B) The most interconnected component (MCL Cluster 1) of the GG protein coexpression network, displayed in a circular layout.

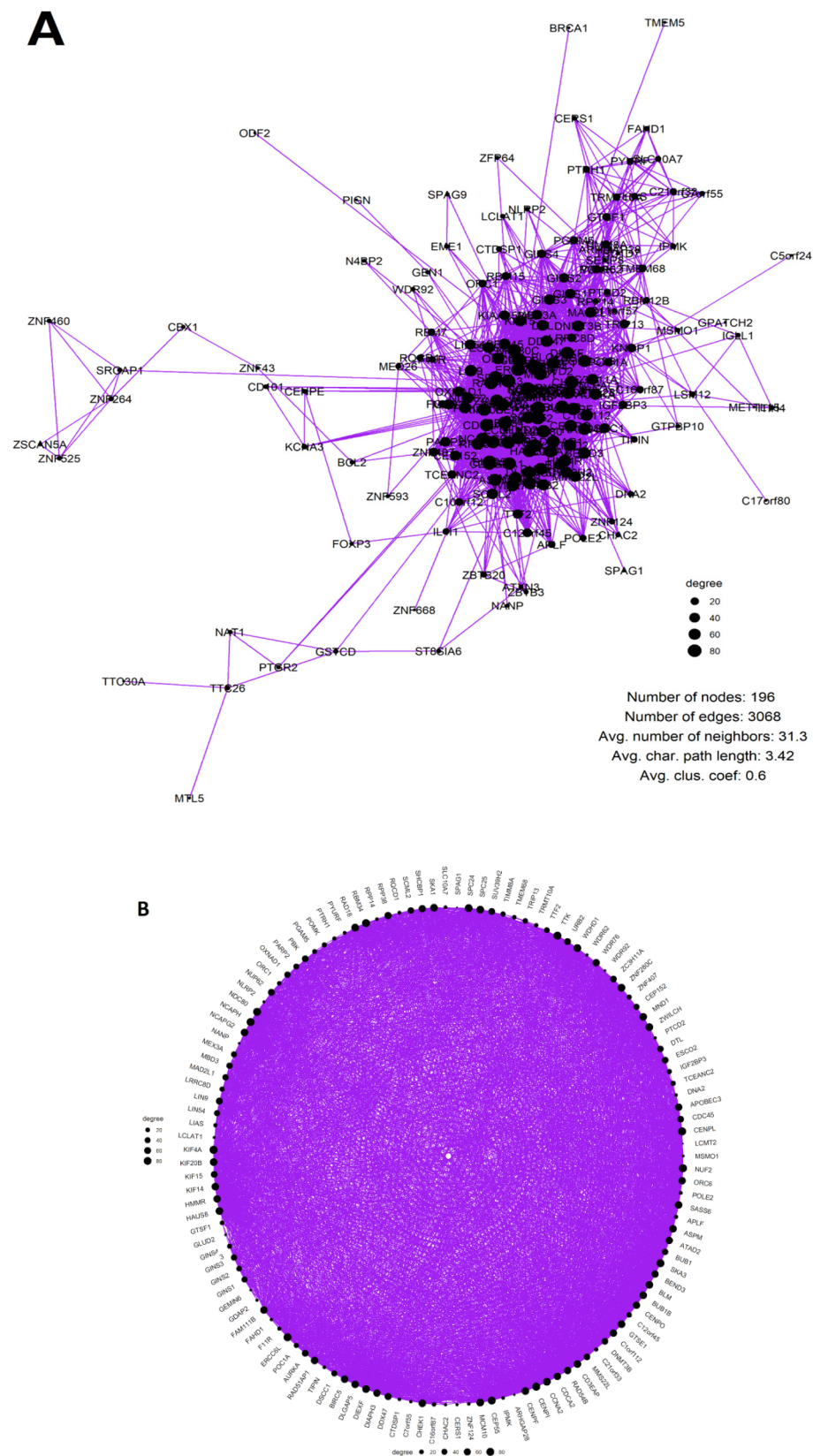


Figure 8. The coexpression networks of GG proteins in the PXD008841 [103] dataset of BRCA proteomes (node size scaled to a degree): (A) The full network of GG proteins in 45 BRCA tumour samples (B) The most interconnected component (MCL Cluster 1) of the GG protein coexpression network, displayed in a circular layout.

GO BP and KEGG enrichment analysis) identified meiotic GO and KEGG modules enriched in both the whole giant component of the network and, in particular, its most-interconnected MCL cluster (Figure S2B) including meiosis I, meiotic nuclear division, meiotic chromosome segregation and inner cell mass proliferation (Figure S2B). In this analysis, the right-sided hypergeometric test, using all proteins identified in the BRCA proteome as the background with the Bonferroni Step-Down (Holm) *p*-value adjustment method, was applied.

3. Discussion

In this study, we have addressed a working hypothesis that the genes involved in gametogenesis also cooperate in cancer development as part of a polyploidy-associated, coordinated, and pre-programmed process. To test the hypothesis and attempt to “capture” evidence of this cooperation and ploidy association, we have performed a bioinformatics study, including network analysis, on twenty-nine transcriptomic and two proteomic datasets of malignant tumour patient samples.

In this context, it is important to mention the limitations of the methods employed to acquire the results. This study focuses on bulk-sequenced samples, which complicates the capability to fully assess the complexity of the heterogeneous tumour. As such, the limitations of bulk transcriptome sequencing restrict the analysis of the biology of PGCCs, which are hypothesized to be the reproductive component of cancer, but may represent a very small part of the population, increasing in numbers when the tumour undergoes oncogenic and oxidative stress displayed as reversible cellular senescence [77]. The analysis to identify differentially expressed genes in bulk RNA-seq samples also only assesses the difference between WGD+ and WGD– samples, while taking into consideration sample purity (the proportion of cancerous cells), but not the cancer cell population heterogeneity. We partially bypassed the above-mentioned limitations with the phylostratigraphic analysis of GG genes in WGD+ tumours.

With these restrictions and rigorous statistical selection criteria for each part of our bioinformatics analysis, we obtained “an upturned pyramid”: from 17 of 29 tumour types with >10 ploidy-upregulated GG genes, 9 have ploidy-upregulated gene STRING networks enriched with meiotic GO and KEGG modules, and 6 of these 9 tumour types that met the criteria for coexpression network analysis also showed coexpression networks enriched for meiotic modules in general and female meiotic modules in particular, while 3 of the latter (BRCA, LUAD, LIHC) also displayed the KEGG module of cellular senescence (which likely increased the proportion of PGCCs in them).

Altogether, despite the aforementioned limitations, the results obtained in this study show that, in a considerable number of tumour types, gametogenesis-related genes are not only robustly expressed (by the hundreds), but also coexpressed on both the transcriptome and proteome levels and associated with whole genome duplications. As previously mentioned, PGCCs (induced in various tumour cell lines after severe anti-cancer treatments and also found in smaller quantities in the control samples), were shown to be positive for meiotic proteins (MOS, REC8, DMC1, SPO11, POU5F1, DDX4, IFITM3), as revealed in individual cells by immunofluorescence [13,27,81,104,105] and time-series qPCR analysis after genotoxic treatments, along with senescence markers [7–13]; [13,27,81,104,105]. It is therefore logical to consider that these findings complement the evidence of a link between polyploidy and GG genes from the above-mentioned polyploid cancer single-cell immunofluorescence studies and reinforce the hypothesis. Interestingly, we have also observed that the networks of ploidy-upregulated genes in the datasets are also enriched for functional modules related to female meiosis (apparently regardless of patient sex), which thus favour cancer cell survival.

So, the evidence we currently possess—that of a robust GG gene (germ–meiosis–CT) network expressed in malignant tumours on both the transcriptome and proteome levels and showing links to polyploidy, oocyte development, and preimplantation embryogenesis—is indicative of a non-random pre-programmed process related to the reproduction.

But what kind of reproductive process could it be? Quite clearly, the process is (1) asexual and (2) hardly employs canonical gametic meiosis, which in its full form has never been observed in cancers [30,59,85]. It appears from current data that this cancer-, meiosis- and embryonicity-related story is linked to polyploidy through its atavistic, evolutionary roots. In particular, the marked dominance of the phylostratum 2 for upregulated GG genes in WGD+ tumours points towards the association of cancer polyploidy with the origins of the eukaryotic life-cycle. As we have seen from the examined phylostratigraphic distribution of 1474 gametogenic genes, the origin of meiosis associated with DNA damage and recombination repair (the hypothesis of meiosis origin proposed by [106] appearing together with the origin of sex (gamete generation) in the very early eukaryote cells was confirmed here. In concord, another study on ancestral character state reconstruction for representatives of 106 eukaryotic taxa indicates that LECA (the last eukaryote common ancestor which likely gave rise to the first eukaryote cell (phylostratum 2) from a symbiosis of archaea and bacteria), in addition to possessing mitochondria, was sexual, meiotic, and multinucleate [107], and thus, polyploid. However, in the case of cancer, the reproduction process is an asexual one; it is thus worth mentioning some features of this kind of atavistic reproduction.

From the point of view of evolutionary genetics, the prevention of the so-called Muller's ratchet [108]—the deleterious loss of heterozygosity (LOH) in asexual reproduction—can replace sexual reproduction (outweighing the “cost of sex”) only if it is associated with at least triploidy or tetraploidy [109], or if polyploidy is associated with inverted meiosis and/or cell fusion [110]. Archetti came to the conclusion that “polyploidy has a selective advantage against LOH shown for the evolution of different types of asexual reproduction in nature. This provides an adaptive explanation for cyclical ploidy, mitotic slippage, and cell fusion in cancer cells” [111]. As indicated by the author, DNA recombination in polyploids, occurring also between sister chromatids, can counteract LOH or act along with gene conversion. The latter mechanism was found in polyploid Archaea [112]. It follows that the mechanisms of genome protection by polyploidy were already in action in very early Eukaryota and, according to Kondrashov [26], gave origin to meiosis, which was immediately followed by sex. This mechanism possibly determines the earliest GG-related cancer attractor in the 2nd phylostratum, seen by us in all meiotic module-enriched TCGA WGD+ tumour types.

Indeed, asexual Amoebozoa display cyclical polyploidy along with expression of the basic meiotic toolkit of 12–15 genes [63,113]. These genes have been observed in human tumours as well [14,81,114,115], while amoeboid multi-nucleated cell patterns and even macrocysts were encountered in cancers treated with genotoxic agents [29,62,81,116]. The dominant basic 2nd phylostratum peak of meiotic recombination and DNA repair was in fact WGD-upregulated in 15 of the 17 eligible tumour types. It is indispensable for any sexual or asexual reproductive process, as it processes the function of meiosis I, which may also be non-conventional, e.g., inverted [81,110] or preceded by biparental genome segregation [23,117]. The budding or bursting of offspring from PGCCs followed in some models after one or several multi-nuclear-bridged reconstruction cycles, preceding the cellularisation of subnuclei by postponed radial cytotomy. This kind of nuclear reconstruction (including pedogamic exchange of the division products in tripolar a-cytotomic karyotomy) of the giant cell shows further the extended central spindles associated with Aurora B kinase converging to a monopolar composed centrosome [118,119]. This process was particularly typical for irradiated HeLa and lymphoblastoma, but also described in senescent mouse fibroblast cultures [119]. It can explain the presence of the mitotic spindle midzone assembly GO BP found enriched in the STRING network of WGD+ BRCA (Figure 5). Further, these cells underwent cellularisation of subnuclei and disintegration by bursting or budding. Such cell division with postponed cellularisation within multinuclear cells created by a-cytokinetic karyotomy is known in evolutionary biology terms as coenocytosis, which is often associated with reproduction [120]. It is very likely that similar reproductive adaptations could originate at the early transitions from uni- to multicellularity [121].

Besides the basic cancer attractor in the 2nd phylostratum, we observed in the TCGA tumour dataset of ploidy-upregulated GG genes the engagement of the phylostrata of early multicellular organisms (strata 4 and 5), where the oocyte meiosis and preimplantation embryo were already evolutionarily stabilized.

The origin of cancer driver genes is also focused on the first five phylostrata, embracing the origin of unicellular and embryonic reproduction life-cycles and supporting the atavistic ancestry of cancer [60,67,69,70,122].

Our GG phylostratigraphic study also revealed a large group of CT-genes in strata 12–14, for placental animals and Old World monkeys; some were evolutionary amplified in the hominid genome. These CT-GGs were also ploidy-upregulated in TCGA tumours. In particular, they include the MAGEA, B group, multiple SPANX members, and PRAME, which binds CT-GG cluster to the giant meiotic cluster of the human WGD+ cancer network. In fact, this is also a cancer attractor conferring stemness, germline induction, loss of differentiation, immunity modulation, metastases, and poor clinical prognosis [56,58]. It may further reinforce the embryonic attractor by insulin-like-growth factor-related, progesterone-independent pathway [30,34]. One of the CT protein families, SPANX, warrants special attention in association with the budding of survival descendents from PGCCs, claimed by many authors to be amitotic [123,124]. In this context, it is necessary to refer our electron microscopic study applied after 10Gy irradiation or mitotic spindle inhibitor SK&F in Burkitt's lymphoma cell lines. Within induced multiple PGCCs, the intra-cytoplasmic sequestration of nuclear buds and micronuclei was revealed to be started by annulate lamellae (AL), the derivatives of the nuclear envelope, branching from the nuclear membrane of the main nucleus, along with the emergence of the folds of the nuclear envelope limited chromatin sheets (ELCS). The process was occurring at the brink of mitotic death with survival of <1% PGCCs resistant cells producing offspring [125]. A somewhat similar transformation of the nuclear membrane with blistering of ELCS and AL is occurring in spermiogenesis, reducing the nuclear volume by blebbing the redundant nuclear envelope into the mammalian sperm cytoplasmic droplet [126]. This process is regulated by SPANX, which is a component of lamin A [127]. The Xq27-located CT-protein SPAN-X family is overexpressed in melanoma, testicular, breast, prostate, lung, and other cancers [126]. Transfection of SPANXA into mammalian cells causes nuclear budding and micronucleation, which are also characteristic of senescing giant cancer cells [127]. Interestingly, the SPANX family originated in rodents from SPANX-N, which is located in the acrosome for sperm motility, and split (via locus amplification) into the SPANX-A/D group specific for hominids (phylostratum 14) with a new function—that of nuclear membrane reduction in spermatids [128]. Some other X-chromosome-linked CT genes (mostly MAGEA group) also appeared late in evolution together with placentation and were amplified in hominids. This may be associated with the human trophoblast developing polyploid giant cells with high invasiveness, which could be evolutionarily necessitated by the large size of the primate foetus and the prolonged pregnancy period [129]. It is also interesting to note that the evolution of placental invasion and cancer metastasis appears to be causally linked [129,130], sharing as reported IGF/MAPK, BCL2, Wnt-signalling [131,132] and, most importantly, immune evasion.

4. Materials and Methods

4.1. TCGA Polyploid versus Diploid Tumour Transcriptome Comparison

We followed a strategy of analysis tailored upon Quinton et al. [86], who bioinformatically detected and experimentally validated differences between transcriptomes of diploid (WGD−) and polyploid (WGD+) TCGA tumours. The approximate ploidy of analysed samples determined by the ABSOLUTE algorithm (which uses whole-genome copy number information to reconstruct the trajectory of tumour genome evolution and estimate the presence of WGD) [133] was obtained from the supplementary data of Taylor et al. [134]. DE genes obtained from the supplementary materials of [86] were filtered by the adoption of the inferential/effect-size threshold: ($p_{Adj} < 0.05$, $|\log_{2}FC| > 0.5$).

In order to assess the possible presence of germ–soma transition and/or pseudo-meiotic features related to polyploidy in the TCGA datasets, a combined gametogenesis-related (GG) gene set comprised of cancer–testis genes from the CTDatabase [135], cancer–germ cell (primordial and adult male) genes from [14] and the MeiosisOnline [136] human meiosis-involved gene database that was updated with a manually-curated set of additional genes (SYCP1, SYCP2, SYCP3, SYCE1, SYCE2, HORMAD2, MAEL, MEIKIN, MEIOB, MEIOC, SYC E1L, TEX11, MAJIN, FAM9C, FAM9B, FAM9A, REC114, TEX19, BRME1, TEX14, MSH4, TEX15), numbering a total of 1474 genes, was used to filter the ploidy-upregulated and downregulated differentially expressed (DE) gene lists. To test for enrichment or depletion of GG genes among DE genes, binomial tests were performed with the R stats package. Information on gene phylostratigraphy was obtained from [60] and phylostratigraphic distributions of GG genes were visualised with ggplot2.

The potential relationship between ploidy and reproductive features was further investigated by constructing networks (a STRING [137] PPI network and a coexpression network). The STRING web interface was used for constructing the STRING networks from the filtered lists of DE genes. The coexpression network analysis was used on cancer types that were shown to have meiotic modules enriched in their STRING networks at least at medium confidence, in order to assess whether these genes are indeed cooperating in this particular dataset.

For the construction of coexpression networks, Rsubread-processed TPM-normalised TCGA data for 9264 tumour samples and 741 normal samples across 24 cancer types [138] were obtained from the Gene Expression Omnibus repository (GSE62944). Using the ABSOLUTE-calculated values, the data for each cancer type were split by the presence or absence of whole-genome duplications (into WGD+ and WGD-, or diploid and polyploid sample cohorts). To minimise the impact of tumour heterogeneity, a purity cutoff of 0.5 was implemented. Of the nine cancer types shown to have meiosis-related modules enriched in STRING, six of them met the conditions for at least 100 ploidy-upregulated genes, and at least 50 WGD+ samples post-purity cutoff (BRCA, LUAD, STAD, UCEC, LIHC, BLCA) were selected for coexpression network construction. The gene expression matrices were filtered for lowly expressed genes with a cutoff of at least 2 TPM in at least 20% of the samples.

The coexpression network (unsigned, with both positive and negative correlation coefficients counting as an edge) was obtained by computing pairwise Pearson correlations between DE genes.

A hard threshold of pairwise correlation coefficients was determined by comparing the number of links (pairwise correlations equal to or exceeding the threshold in absolute value) between 50 randomly picked sets of 300 genes and surrogate data—shuffling of these datasets across columns (50 shuffling for each set). This approach serves to determine a “mean correlation field” linking the genes (or, in the case of the proteomic data described in the next sections, the proteins), and the amount of noise/randomness present in the data [139]. In this case, a list of four possible thresholds, ranging from 0.6 to 0.9, were tested in this manner, and a threshold of 0.6 was found to be sufficient to define an edge in the network, with the number of interactions in “real” data vastly and highly significantly (Wilcoxon test $p < 0.001$) exceeding that of surrogate data (as seen in Table S2), indicating that the normalisation procedure in the initial data was successful at reducing the noise.

The selected threshold was used to transform the correlation matrix into a binary adjacency matrix, which was imported into Cytoscape via the RCy3 R package [140] and the aMatReader app [141]. The giant components of the upregulated and downregulated gene networks were then extracted for further enrichment analysis to determine.

Gene-set enrichment (Gene Ontology (GO) and Kyoto Encyclopaedia of Genes and Genomes (KEGG)) was adopted (using clusterProfileR in R and ClueGO in Cytoscape for visualisation of enrichment maps) as a proxy of genes’ biological functions, and the gene sets were checked for their statistical relevance by tests based upon hypergeometric distribution enrichment analysis with Bonferroni Step-Down (Holm) correction, which is more stringent in terms of false positives than the Benjamini–Hochberg correction implemented

in the STRING web tool, for the p -value. For ease of interpretation, the large number of enriched processes was reduced, clustered, and visualised as treemap plots using the *rvvgo* R package [142] and/or ClueGO enrichment maps. Igraph [143] and graph [144] R packages were used to supplement Cytoscape's network visualisation functionalities for interpretability and aesthetic reasons.

The NDEX database [145] was used for depositing the networks.

4.2. Analysis of GG Protein Expression in the MM and BRCA Proteomes

This analysis was performed to assess the relationships between GG gene expressions on the protein (whole-proteome) level. For that purpose, two high-throughput proteomics datasets of two cancer types (MM and BRCA) from public databases were used.

A matrix of normalised relative protein abundances determined by high-throughput LC-MS/MS from 505 late-stage melanoma patient tumour samples and over 12,000 protein-coding genes was obtained from the supplementary materials of the MM500 Melanoma Proteome Atlas study [101]. Hierarchical clustering (*hclust* in the R stats package) was performed to stratify the samples by abundance and value missingness. Cutting the tree at a height of 1400 (an ultrametrics based on Euclidean Distance) stratified the patient samples into six clusters (Figure 4). Patient Cluster 3 ($n = 142$) was selected for further analysis due to technical considerations.

The lowly expressed proteoforms were filtered out of the resulting 142-sample matrix, with a cut-off of at least five units of normalised relative expression in at least 20% of the samples. For the rest, the missing values were replaced using minimum imputation (the \log_2 -scale value of the minimum possible measurement) with the assumption of low protein expression as the reason for their missingness.

A matrix of normalised relative protein abundances for 45 BRCA samples (mainly grades 2–3) was obtained from the ProteomeXChange PXD008841 repository [103]. Unlike the MM dataset, the BRCA dataset had already been filtered to only include proteins expressed in every sample, for a total of 9995 proteins. As such, no further low-expression filtering was necessary.

In order to assess the possible presence of soma–germ transition and/or pseudo-meiotic features related to embryonalization in late-stage melanoma and grade 2–3 breast carcinoma, the GG gene set ($n = 1474$) was used to filter out the proteins related to the aforementioned processes.

To investigate the relationship between the expressed proteins, the resulting GG protein abundance matrix was used to calculate pairwise correlations and construct a coexpression network with the same procedure as described in Section 4.1. In the proteome data, the threshold of 0.6 in absolute value was found to be sufficient, as can be seen in Tables S3 and S4. To determine the most interconnected network components or modules, the coexpression network was subjected to MCL clustering with a granularity parameter of 2.5, implemented in Cytoscape's clusterMaker app [146]. GO Biological Process enrichment analysis was performed as described in Section 4.1, but unlike the case of the TCGA transcriptomes, in which all genes in the database were used, for proteomics data, the whole proteome of the cancer dataset in question (respectively, MM and BRCA) was used as the background gene set ("universe"). The enrichment analysis was done separately on the whole giant component of the protein–protein coexpression network, and its most highly interconnected part (MCL cluster 1).

The NDEX database [145] was used for depositing the networks.

5. Conclusions and Perspectives

We can conclude that human tumours can likely employ three or more cancer-polyploidy associated reproduction attractors of soma–germ transition, pre-formed and developed during life evolution on Earth. While the first, early eukaryotic and basic, is directly associated with DNA damage repair by recombination with the functions of the meiotic prophase, which seems indispensable for starting any reproductive life-cycle (and may be displayed

in cancers by the amoeboid reproduction mode with an asexual macrocyst), the second, associated with oocyte maturation and early embryogenesis, is linked to the transition from unicellular to multicellular forms of life [60] (and can induce in cancers the parthenogenesis-like reproduction process). The current results provide a hint to the existence of a link between the WGD-related oocyte maturation and cellular senescence, as was suggested earlier [77]. The latest, placental attractor links the embryonic sub-network to germline determination in placental mammals through ectopic activation of PRAME/CT-genes (which presumably may favour “pseudo-placentation”—invasion and metastases). In addition, the coupling of the polyploidising mitotic slippage (that results in the acquisition of meiotic features) with the interruption of the circadian clock in WGD-positive TCGA cancers, shown by us recently [43], likely enables this scanning of the genome evolutionary memory through all aeons, revealing the permissive paths to cancer attractors of asexual reproduction and connecting the most adaptive among them into the very dense network disclosed in this study. Our data and their analysis confirm the view of the extreme adaptability of human cancers to the general pattern states of the genome network, neighbouring and distant tissues, and the microenvironment [147], by means of polyploidy-aided atavistic variable mechanisms of asexual reproduction. Tightly clustered and correlated gametogenesis- and WGD-related cancer networks found here in the common aggressive cancers present an argument in favour of epigenetic cancer evolution “as a model of cell learning”, providing its causal potential for anti-cancer therapies [148]. At the same time, carcinogenesis and tumour evolution remain very complex, and the present study is only a step to their better understanding.

Supplementary Materials: The supporting information can be downloaded at: <https://www.mdpi.com/article/10.3390/ijms232314930/s1>.

Author Contributions: Conceptualization, N.M.V., A.G. and J.E.; methodology, A.G. and N.M.V.; software, N.M.V. and A.G.; validation, A.G., J.E. and D.P.; formal analysis, N.M.V.; investigation, N.M.V., J.E., A.G., D.P. and K.S.; resources, N.M.V.; data curation, N.M.V. and A.G.; writing—original draft preparation, N.M.V., J.E. and A.G.; editing N.M.V., A.G., J.E., D.P. and K.S.; visualisation, N.M.V., J.E. and K.S.; supervision, J.E. and A.G.; project administration, D.P.; funding acquisition, N.M.V., D.P. All authors have read and agreed to the published version of the manuscript.

Funding: This research was supported by the University of Latvia Doctoral Student Scholarship in the Life, Exact, and Medical Sciences and the 8.2.2.0/20/I/006 “University of Latvia Doctoral Study Program Capacity Enhancement Through a New PhD Model” project for N.M.V., by a grant from the European Regional Development Fund (ERDF) project No. 1.1.1.2/VIAA/3/19/463 for KS.

Institutional Review Board Statement: Not applicable.

Informed Consent Statement: Not applicable.

Data Availability Statement: The coexpression networks resulting from this study have been deposited in the NDEX database, with the transcriptome and proteome network sets available, respectively, under the following URLs: <https://www.ndexbio.org/#/networkset/c4934da2-3cf7-11ed-b7d0-0ac135e8bacf?accesskey=5d269780b0440e6cf61633b03121b398598d19307be4c23760642ae33acbf749> (accessed on 5 October 2022). <https://www.ndexbio.org/#/networkset/5e0ba954-3cf5-11ed-b7d0-0ac135e8bacf?accesskey=e29f7a1571fba879aa0b38158550baae147b7ea39a384f08f7c52a11a6165428> (accessed on 5 October 2022).

Acknowledgments: Regina Kleina is acknowledged for providing consultations in cancer pathology; Pawel Zayakin is acknowledged for bioinformatics advice.

Conflicts of Interest: The authors declare no conflict of interest.

References

1. Murray, C.J.; Lopez, A.D. Mortality by cause for eight regions of the world: Global Burden of Disease Study. *Lancet* **1997**, *349*, 1269–1276. [[CrossRef](#)] [[PubMed](#)]
2. Mahase, E. Cancer overtakes CVD to become leading cause of death in high income countries. *BMJ* **2019**, *366*, 15368. [[CrossRef](#)] [[PubMed](#)]

3. Scanlan, M.J.; Gure, A.O.; Jungbluth, A.A.; Old, L.J.; Chen, Y.-T. Cancer/testis antigens: An expanding family of targets for cancer immunotherapy. *Immunol. Rev.* **2002**, *188*, 22–32. [[CrossRef](#)] [[PubMed](#)]
4. Caballero, O.L.; Chen, Y.-T. Cancer/testis (CT) antigens: Potential targets for immunotherapy. *Cancer Sci.* **2009**, *100*, 2014–2021. [[CrossRef](#)] [[PubMed](#)]
5. Old, L.J. Cancer/testis (CT) antigens—A new link between gametogenesis and cancer. *Cancer Immun.* **2001**, *1*, 1.
6. Kalejs, M.; Erenpreisa, J. Cancer/testis antigens and gametogenesis: A review and “brain-storming” session. *Cancer Cell Int.* **2005**, *5*, 4. [[CrossRef](#)]
7. Gantchev, J.; Martínez Villarreal, A.; Gunn, S.; Zetka, M.; Ødum, N.; Litvinov, I.V. The Ectopic Expression of meiCT Genes Promotes Meiomitosis and May Facilitate Carcinogenesis. *Cell Cycle* **2020**, *19*, 837–854. [[CrossRef](#)]
8. McFarlane, R.J.; Wakeman, J.A. Meiosis-like Functions in Oncogenesis: A New View of Cancer. *Cancer Res* **2017**, *77*, 5712–5716. [[CrossRef](#)]
9. Feichtinger, J.; McFarlane, R.J. Meiotic gene activation in somatic and germ cell tumours. *Andrology* **2019**, *7*, 415–427. [[CrossRef](#)]
10. Fujiwara, Y.; Horisawa-Takada, Y.; Inoue, E.; Tani, N.; Shibuya, H.; Fujimura, S.; Kariyazono, R.; Sakata, T.; Ohta, K.; Araki, K.; et al. Meiotic cohesins mediate initial loading of HORMAD1 to the chromosomes and coordinate SC formation during meiotic prophase. *PLoS Genet.* **2020**, *16*, e1009048. [[CrossRef](#)]
11. Ianzini, F.; Kosmacek, E.A.; Nelson, E.S.; Napoli, E.; Erenpreisa, J.; Kalejs, M.; Mackey, M.A. Activation of Meiosis-Specific Genes Is Associated with Depolyloidization of Human Tumor Cells following Radiation-Induced Mitotic Catastrophe. *Cancer Res.* **2009**, *69*, 2296–2304. [[CrossRef](#)] [[PubMed](#)]
12. Kalejs, M.; Ivanov, A.; Plakhins, G.; Cragg, M.S.; Emzins, D.; Illidge, T.M.; Erenpreisa, J. Upregulation of meiosis-specific genes in lymphoma cell lines following genotoxic insult and induction of mitotic catastrophe. *BMC Cancer* **2006**, *6*, 6. [[CrossRef](#)]
13. Erenpreisa, J.; Cragg, M.S.; Salmina, K.; Hausmann, M.; Scherthan, H. The Role of Meiotic Cohesin REC8 in Chromosome Segregation in Gamma Irradiation-Induced Endopolyploid Tumour Cells. *Exp. Cell Res.* **2009**, *315*, 2593–2603. [[CrossRef](#)] [[PubMed](#)]
14. Bruggeman, J.W.; Irie, N.; Lodder, P.; Van Pelt, A.M.M.; Koster, J.; Hamer, G. Tumors Widely Express Hundreds of Embryonic Germline Genes. *Cancers* **2020**, *12*, 3812. [[CrossRef](#)] [[PubMed](#)]
15. da Silva, V.L.; Fonseca, A.F.; Fonseca, M.; da Silva, T.E.; Coelho, A.C.; Kroll, J.E.; de Souza, J.E.S.; Stransky, B.; de Souza, G.A.; de Souza, S.J. Genome-wide identification of cancer/testis genes and their association with prognosis in a pan-cancer analysis. *Oncotarget* **2017**, *8*, 92966–92977. [[CrossRef](#)] [[PubMed](#)]
16. Planells-Palop, V.; Hazazi, A.; Feichtinger, J.; Jezkova, J.; Thallinger, G.G.; Alsiwiehri, N.O.; Almutairi, M.; Parry, L.; Wakeman, J.; McFarlane, R.J. Human germ/stem cell-specific gene TEX19 influences cancer cell proliferation and cancer prognosis. *Mol. Cancer* **2017**, *16*, 84. [[CrossRef](#)]
17. Nichols, B.A.; Oswald, N.W.; McMillan, E.A.; McGlynn, K.; Yan, J.; Kim, M.S.; Saha, J.; Mallipeddi, P.L.; LaDuke, S.A.; Villa-lobos, P.A.; et al. HORMAD1 Is a Negative Prognostic Indicator in Lung Adenocarcinoma and Specifies Resistance to Oxidative and Genotoxic Stress. *Cancer Res.* **2018**, *78*, 6196–6208. [[CrossRef](#)]
18. Chung, J.-Y.; Kitano, H.; Takikita, M.; Cho, H.; Noh, K.H.; Kim, T.W.; Ylaja, K.; Hanaoka, J.; Fukuoka, J.; Hewitt, S.M. Synaptonemal Complex Protein 3 as a Novel Prognostic Marker in Early Stage Non-Small Cell Lung Cancer. *Hum. Pathol.* **2013**, *44*, 472–479. [[CrossRef](#)]
19. Gu, E.A.Y.; Wang, C.; Zhu, R.; Yang, J.; Yuan, W.; Zhu, Y.; Zhou, Y.; Qin, N.; Shen, H.; Ma, H.; et al. The cancer-testis gene, MEIOB, sensitizes triple-negative breast cancer to PARP1 inhibitors by inducing homologous recombination deficiency. *Cancer Biol. Med.* **2021**, *18*, 74–87. [[CrossRef](#)]
20. Bielski, C.M.; Zehir, A.; Penson, A.V.; Donoghue, M.T.A.; Chatila, W.; Armenia, J.; Chang, M.T.; Schram, A.M.; Jonsson, P.; Bandlamudi, C.; et al. Genome doubling shapes the evolution and prognosis of advanced cancers. *Nat. Genet.* **2018**, *50*, 1189–1195. [[CrossRef](#)]
21. Sheltzer, J.M.; Amon, A. The aneuploidy paradox: Costs and benefits of an incorrect karyotype. *Trends Genet.* **2011**, *27*, 446–453. [[CrossRef](#)] [[PubMed](#)]
22. Gerashchenko, B.I.; Salmina, K.; Eglitis, J.; Huna, A.; Grjunberga, V.; Erenpreisa, J. Disentangling the Aneuploidy and Senescence Paradoxes: A Study of Triploid Breast Cancers Non-Responsive to Neoadjuvant Therapy. *Histochem. Cell Biol.* **2016**, *145*, 497–508. [[CrossRef](#)] [[PubMed](#)]
23. Salmina, K.; Huna, A.; Kalejs, M.; Pjanova, D.; Scherthan, H.; Cragg, M.S.; Erenpreisa, J. The Cancer Aneuploidy Paradox: In the Light of Evolution. *Genes* **2019**, *10*, 83. [[CrossRef](#)] [[PubMed](#)]
24. Pienta, K.J.; Hammarlund, E.U.; Brown, J.S.; Amend, S.R.; Axelrod, R.M. Cancer recurrence and lethality are enabled by enhanced survival and reversible cell cycle arrest of polyaneploid cells. *Proc. Natl. Acad. Sci. USA* **2021**, *118*, e2020838118. [[CrossRef](#)] [[PubMed](#)]
25. Erenpreisa, J.; Cragg, M.S. Cancer: A Matter of Life Cycle? *Cell Biol. Int.* **2007**, *31*, 1507–1510. [[CrossRef](#)] [[PubMed](#)]
26. Kondrashov, A.S. The asexual ploidy cycle and the origin of sex. *Nature* **1994**, *370*, 213–216. [[CrossRef](#)]
27. Erenpreisa, J.; Kalejs, M.; Cragg, M.S. Mitotic Catastrophe and Endomitosis in Tumour Cells: An Evolutionary Key to a Molecular Solution. *Cell Biol. Int.* **2005**, *29*, 1012–1018. [[CrossRef](#)]
28. Erenpreisa, J.; Cragg, M.S. Life-Cycle Features of Tumour Cells. In *Evolutionary Biology from Concept to Application*; Pontarotti, P., Ed.; Springer: Berlin/Heidelberg, Germany, 2008; pp. 61–71; ISBN 9783540789932.

29. Niculescu, V.F. Developmental and Non Developmental Polyploidy in Xenic and Axenic Cultured Stem Cell Lines of Entamoeba histolytica and E. Histolytica. *Insights Stem Cells* **2016**, *2*, 14.
30. Erenpreisa, J.; Salmina, K.; Anatskaya, O.; Cragg, M.S. Paradoxes of cancer: Survival at the brink. *Review. Semin Cancer Biol.* **2022**, *81*, 119–131. [[CrossRef](#)]
31. Weihua, Z.; Lin, Q.; Ramoth, A.J.; Fan, D.; Fidler, I.J. Formation of solid tumors by a single multinucleated cancer cell. *Cancer* **2011**, *117*, 4092–4099. [[CrossRef](#)]
32. Cohnheim, J. *Vorlesungen über Allgemeine Pathologie: Ein Handbuch für Aertze und Studirende*; A. Hirschwald: Berlin, Germany, 1882.
33. Pierce, G.B.; Pantazis, C.G.; Caldwell, E.J.; Wells, R.S. Specificity of the control of tumor formation by the blastocyst. *Cancer Res.* **1982**, *42*, 1082–1087. [[PubMed](#)]
34. Erenpreiss, J. *Current Concepts of Malignant Growth. Part A: From a Normal Cell to Cancer*; Zvaigzne: Riga, Latvia, 1993.
35. Niu, N.; Mercado-Urbe, I.; Liu, J. Dedifferentiation into blastomere-like cancer stem cells via formation of polyploid giant cancer cells. *Oncogene* **2017**, *36*, 4887–4900. [[CrossRef](#)] [[PubMed](#)]
36. Bignold, L.P.; Coghlan, B.L.D.; Jersmann, H.P.A. *David Paul von Hansemann: Contributions to Oncology: Context, Comments and Translations*; Birkhauser Verlag: Basel, Switzerland, 2007.
37. Erenpreisa, J.; Salmina, K.; Huna, A.; Jackson, T.R.; Vazquez-Martin, A.; Cragg, M.S. The “Virgin Birth”, Polyploidy, and the Origin of Cancer. *Oncoscience* **2015**, *2*, 3–14. [[CrossRef](#)] [[PubMed](#)]
38. Vinnitsky, V. Oncogerminative hypothesis of tumor formation. *Med. Hypotheses* **1993**, *40*, 19–27. [[CrossRef](#)]
39. Vinnitsky, V. The development of a malignant tumor is due to a desperate asexual self-cloning process in which cancer stem cells develop the ability to mimic the genetic program of germline cells. *Intrinsically Disord. Proteins* **2014**, *2*, e29997. [[CrossRef](#)]
40. Pierce, G.B. Carcinoma is to Embryology as Mutation is to Genetics. *Am. Zool.* **1985**, *25*, 707–712. [[CrossRef](#)]
41. Liu, J. The “Life Code”: A Theory That Unifies the Human Life Cycle and the Origin of Human Tumors. *Semin. Cancer Biol.* **2020**, *60*, 380–397. [[CrossRef](#)] [[PubMed](#)]
42. Moein, S.; Adibi, R.; Meirelles, L.D.S.; Nardi, N.B.; Gheisari, Y. Cancer regeneration: Polyploid cells are the key drivers of tumor progression. *Biochim. Biophys. Acta* **2020**, *1874*, 188408. [[CrossRef](#)] [[PubMed](#)]
43. Vainshelbaum, N.M.; Salmina, K.; Gerashchenko, B.I.; Lazovska, M.; Zayakin, P.; Cragg, M.S.; Pjanova, D.; Erenpreisa, J. Role of the Circadian Clock “Death-Loop” in the DNA Damage Response Underpinning Cancer Treatment Resistance. *Cells* **2022**, *11*, 880. [[CrossRef](#)]
44. Liu, J.; Erenpreisa, J.; Sikora, E. Polyploid giant cancer cells: An emerging new field of cancer biology. *Semin. Cancer Biol.* **2022**, *81*, 1–4. [[CrossRef](#)] [[PubMed](#)]
45. Lenormand, T.; Engelstädter, J.; Johnston, S.E.; Wijnker, E.; Haag, C.R. Evolutionary mysteries in meiosis. *Philos. Trans. R. Soc. B Biol. Sci.* **2016**, *371*, 20160001. [[CrossRef](#)]
46. Mirzaghaderi, G.; Hörandl, E. The evolution of meiotic sex and its alternatives. *Proc. R. Soc. B Boil. Sci.* **2016**, *283*, 20161221. [[CrossRef](#)] [[PubMed](#)]
47. Erenpreisa, J.A.; Cragg, M.S.; Fringes, B.; Sharakhov, I.; Illidge, T.M. Release of mitotic descendants by giant cells from irradiated burkitt’s lymphoma cell lines. *Cell Biol. Int.* **2000**, *24*, 635–648. [[CrossRef](#)] [[PubMed](#)]
48. Bai, S.-N. Two Types of Germ Cells, the Sexual Reproduction Cycle, and the Double-Ring Mode of Plant Developmental Program. *Plant Signal. Behav.* **2017**, *12*, e1320632. [[CrossRef](#)] [[PubMed](#)]
49. Salmina, K.; Jankevics, E.; Huna, A.; Perminov, D.; Radovica, I.; Klymenko, T.; Ivanov, A.; Jascenko, E.; Scherthan, H.; Cragg, M.; et al. Up-regulation of the embryonic self-renewal network through reversible polyploidy in irradiated p53-mutant tumour cells. *Exp. Cell Res.* **2010**, *316*, 2099–2112. [[CrossRef](#)]
50. Gordeeva, O. Cancer-testis antigens: Unique cancer stem cell biomarkers and targets for cancer therapy. *Semin. Cancer Biol.* **2018**, *53*, 75–89. [[CrossRef](#)]
51. Miranda, A.; Hamilton, P.T.; Zhang, A.W.; Pattnaik, S.; Becht, E.; Mezheyski, A.; Bruun, J.; Micke, P.; de Reynies, A.; Nelson, B.H. Cancer stemness, intratumoral heterogeneity, and immune response across cancers. *Proc. Natl. Acad. Sci. USA* **2019**, *116*, 9020–9029. [[CrossRef](#)]
52. Marcar, L.; Maclaine, N.J.; Hupp, T.R.; Meek, D.W. Mage-A Cancer/testis Antigens Inhibit p53 Function by Blocking Its Inter-action with Chromatin. *Cancer Res.* **2010**, *70*, 10362–10370. [[CrossRef](#)]
53. Yang, B.; O’Herrin, S.M.; Wu, J.; Reagan-Shaw, S.; Ma, Y.; Bhat, K.M.; Gravekamp, C.; Setaluri, V.; Peters, N.; Hoffmann, F.M.; et al. MAGE-A, mMage-b, and MAGE-C Proteins Form Complexes with KAP1 and Suppress p53-Dependent Apoptosis in MAGE-Positive Cell Lines. *Cancer Res* **2007**, *67*, 9954–9962. [[CrossRef](#)]
54. Ladelfa, M.F.; Peche, L.Y.; Toledo, M.F.; Laiseca, J.E.; Schneider, C.; Monte, M. Tumor-specific MAGE proteins as regulators of p53 function. *Cancer Lett.* **2012**, *325*, 11–17. [[CrossRef](#)]
55. Wei, Y.; Wang, Y.; Gong, J.; Rao, L.; Wu, Z.; Nie, T.; Shi, D.; Zhang, L. High expression of MAGE-A9 contributes to stemness and malignancy of human hepatocellular carcinoma. *Int. J. Oncol.* **2017**, *52*, 219–230. [[CrossRef](#)]
56. Nettersheim, D.; Arndt, I.; Sharma, R.; Riesenberger, S.; Jostes, S.; Schneider, S.; Hölzel, M.; Kristiansen, G.; Schorle, H. The Cancer/testis-Antigen PRAME Supports the Pluripotency Network and Represses Somatic and Germ Cell Differentiation Programs in Seminomas. *Br. J. Cancer* **2016**, *115*, 454–464. [[CrossRef](#)] [[PubMed](#)]
57. Al-Khadairi, G.; Decock, J. Cancer Testis Antigens and Immunotherapy: Where Do We Stand in the Targeting of PRAME? *Cancers* **2019**, *11*, 984. [[CrossRef](#)] [[PubMed](#)]

58. Zhao, Q.; Zhang, Z.; Wu, Y. PRAME Is a Potential Carcinogenic Biomarker That Correlates with Patient Prognosis and Tumor Immunity Based on Pan-Cancer Analysis. *Ann. Clin. Lab. Sci.* **2022**, *52*, 185–195. [[PubMed](#)]
59. Lindsey, S.F.; Byrnes, D.M.; Eller, M.S.; Rosa, A.M.; Dabas, N.; Escandon, J.; Grichnik, J.M. Potential Role of Meiosis Proteins in Melanoma Chromosomal Instability. *J. Ski. Cancer* **2013**, *2013*, 190109. [[CrossRef](#)] [[PubMed](#)]
60. Trigos, A.S.; Pearson, R.B.; Papenfuss, A.T.; Goode, D.L. Altered interactions between unicellular and multicellular genes drive hallmarks of transformation in a diverse range of solid tumors. *Proc. Natl. Acad. Sci. USA* **2017**, *114*, 6406–6411. [[CrossRef](#)] [[PubMed](#)]
61. Trigos, A.S.; Pearson, R.B.; Papenfuss, A.T.; Goode, D.L. Somatic mutations in early metazoan genes disrupt regulatory links between unicellular and multicellular genes in cancer. *eLife* **2019**, *8*, 947. [[CrossRef](#)]
62. Niculescu, V.F. Cancer genes and cancer stem cells in tumorigenesis: Evolutionary deep homology and controversies. *Genes Dis.* **2022**, *9*, 1234–1247. [[CrossRef](#)]
63. Maciver, S.K.; Koutsogiannis, Z.; Valle, A.D.O.F.D. ‘Meiotic genes’ are constitutively expressed in an asexual amoeba and are not necessarily involved in sexual reproduction. *Biol. Lett.* **2019**, *15*, 20180871. [[CrossRef](#)]
64. Lorenz, A.; Mpaulo, S.J. Gene conversion: A non-Mendelian process integral to meiotic recombination. *Heredity* **2022**, *129*, 56–63. [[CrossRef](#)]
65. Kauffman, S. Differentiation of malignant to benign cells. *J. Theor. Biol.* **1971**, *31*, 429–451. [[CrossRef](#)] [[PubMed](#)]
66. Huang, S.; Ernberg, I.; Kauffman, S. Cancer Attractors: A Systems View of Tumors from a Gene Network Dynamics and Developmental Perspective. *Semin. Cell Dev. Biol.* **2009**, *20*, 869–876. [[CrossRef](#)] [[PubMed](#)]
67. Domazet-Lošo, T.; Tautz, D. Phylostratigraphic tracking of cancer genes suggests a link to the emergence of multicellularity in metazoa. *BMC Biol.* **2010**, *8*, 66. [[CrossRef](#)] [[PubMed](#)]
68. Vinogradov, A.E. Human transcriptome nexuses: Basic-eukaryotic and metazoan. *Genomics* **2010**, *95*, 345–354. [[CrossRef](#)] [[PubMed](#)]
69. Vincent, M. Cancer: A de-Repression of a Default Survival Program Common to All Cells?: A Life-History Perspective on the Nature of Cancer. *Bioessays* **2012**, *34*, 72–82. [[CrossRef](#)] [[PubMed](#)]
70. Lineweaver, C.H.; Bussey, K.J.; Blackburn, A.C.; Davies, P.C.W. Cancer progression as a sequence of atavistic reversions. *BioEssays* **2021**, *43*, e2000305. [[CrossRef](#)]
71. Domazet-Lošo, T.; Klimovich, A.; Anokhin, B.; Anton-Erxleben, F.; Hamm, M.J.; Lange, C.; Bosch, T.C. Naturally occurring tumours in the basal metazoan Hydra. *Nat. Commun.* **2014**, *5*, 4222. [[CrossRef](#)]
72. Anatskaya, O.V.; Vinogradov, A.E.; Vainshelbaum, N.M.; Giuliani, A.; Erenpreisa, J. Phylostratic Shift of Whole-Genome Duplications in Normal Mammalian Tissues towards Unicellularity Is Driven by Developmental Bivalent Genes and Reveals a Link to Cancer. *Int. J. Mol. Sci.* **2020**, *21*, 8759. [[CrossRef](#)]
73. Vinogradov, A.E.; Anatskaya, O.V. Growth of Biological Complexity from Prokaryotes to Hominids Reflected in the Human Genome. *Int. J. Mol. Sci.* **2021**, *22*, 11640. [[CrossRef](#)]
74. Vazquez-Martin, A.; Anatskaya, O.V.; Giuliani, A.; Erenpreisa, J.; Huang, S.; Salmina, K.; Inashkina, I.; Huna, A.; Nikolsky, N.N.; Vinogradov, A.E. Somatic polyploidy is associated with the upregulation of c-MYC interacting genes and EMT-like signature. *Oncotarget* **2016**, *7*, 75235–75260. [[CrossRef](#)]
75. Anatskaya, O.V.; Vinogradov, A.E. Polyploidy as a Fundamental Phenomenon in Evolution, Development, Adaptation and Diseases. *Int. J. Mol. Sci.* **2022**, *23*, 3542. [[CrossRef](#)] [[PubMed](#)]
76. Anatskaya, O.V.; Vinogradov, A.E. Polyploidy and Myc Proto-Oncogenes Promote Stress Adaptation via Epigenetic Plasticity and Gene Regulatory Network Rewiring. *Int. J. Mol. Sci.* **2022**, *23*, 9691. [[CrossRef](#)] [[PubMed](#)]
77. Erenpreisa, J.; Cragg, M.S. Three steps to the immortality of cancer cells: Senescence, polyploidy and self-renewal. *Cancer Cell Int.* **2013**, *13*, 92. [[CrossRef](#)] [[PubMed](#)]
78. Ayob, A.Z.; Ramasamy, T.S. Cancer Stem Cells as Key Drivers of Tumour Progression. *J. Biomed. Sci.* **2018**, *25*, 20. [[CrossRef](#)]
79. Yu, Z.; Pestell, T.G.; Lisanti, M.P.; Pestell, R.G. Cancer Stem Cells. *Int. J. Biochem. Cell Biol.* **2012**, *44*, 2144–2151. [[CrossRef](#)] [[PubMed](#)]
80. Battle, E.; Clevers, H. Cancer stem cells revisited. *Nat. Med.* **2017**, *23*, 1124–1134. [[CrossRef](#)] [[PubMed](#)]
81. Salmina, K.; Bojko, A.; Inashkina, I.; Staniak, K.; Dudkowska, M.; Podlesniy, P.; Rumnieks, F.; Vainshelbaum, N.M.; Pjanova, D.; Sikora, E.; et al. “Mitotic Slippage” and Extranuclear DNA in Cancer Chemoresistance: A Focus on Telomeres. *Int. J. Mol. Sci.* **2020**, *21*, 2779. [[CrossRef](#)]
82. Roeder, G.S.; Bailis, J.M. The Pachytene Checkpoint. *Trends Genet.* **2000**, *16*, 395–403. [[CrossRef](#)] [[PubMed](#)]
83. Subramanian, V.V.; Hochwagen, A. The Meiotic Checkpoint Network: Step-by-Step through Meiotic Prophase. *Cold Spring Harb. Perspect. Biol.* **2014**, *6*, a016675. [[CrossRef](#)]
84. Czarnecka-Herok, J.; Sliwinska, M.A.; Herok, M.; Targonska, A.; Strzeszewska-Potyrala, A.; Bojko, A.; Wolny, A.; Mosieniak, G.; Sikora, E. Therapy-Induced Senescent/Polyploid Cancer Cells Undergo Atypical Divisions Associated with Altered Expression of Meiosis, Spermatogenesis and EMT Genes. *Int. J. Mol. Sci.* **2022**, *23*, 8288. [[CrossRef](#)]
85. Berdieva, M.; Demin, S.; Goodkov, A. Amoeba proteus and ploidy cycles: From simple model to complex issues. *Protistology* **2019**, *13*, 166–173. [[CrossRef](#)]

86. Quinton, R.J.; DiDomizio, A.; Vittoria, M.A.; Kotýnková, K.; Ticas, C.J.; Patel, S.; Koga, Y.; Vakhshoorzadeh, J.; Hermance, N.; Kuroda, T.S.; et al. Whole-genome doubling confers unique genetic vulnerabilities on tumour cells. *Nature* **2021**, *590*, 492–497. [[CrossRef](#)] [[PubMed](#)]
87. Yang, S.; Yu, X.; Seitz, E.M.; Kowalczykowski, S.C.; Egelman, E.H. Archaeal RadA Protein Binds DNA as Both Helical Filaments and Octameric Rings. *J. Mol. Biol.* **2001**, *314*, 1077–1085. [[CrossRef](#)] [[PubMed](#)]
88. Sauvageau, S.; Masson, J.-Y. Exploring the multiple facets of the meiotic recombinase Dmcl1. *BioEssays* **2004**, *26*, 1151–1155. [[CrossRef](#)] [[PubMed](#)]
89. Shin, Y.-H.; Choi, Y.; Erdin, S.U.; Yatsenko, S.A.; Kloc, M.; Yang, F.; Wang, P.J.; Meistrich, M.L.; Rajkovic, A. Hormad1 Mutation Disrupts Synaptonemal Complex Formation, Recombination, and Chromosome Segregation in Mammalian Meiosis. *PLoS Genet.* **2010**, *6*, e1001190. [[CrossRef](#)]
90. Erenpreisa, J.; Cragg, M.S. MOS, aneuploidy and the ploidy cycle of cancer cells. *Oncogene* **2010**, *29*, 5447–5451. [[CrossRef](#)]
91. Yamamoto, A.; Hiraoka, Y. Monopolar spindle attachment of sister chromatids is ensured by two distinct mechanisms at the first meiotic division in fission yeast. *EMBO J.* **2003**, *22*, 2284–2296. [[CrossRef](#)]
92. Jungbluth, A.A.; Silva, A.W.; Iversen, K.; Frosina, D.; Zaidi, B.; Coplan, K.; Eastlake-Wade, S.K.; Castelli, S.B.; Spagnoli, G.C.; Old, L.J.; et al. Expression of cancer-testis (CT) antigens in placenta. *Cancer Immun.* **2007**, *7*, 15.
93. Old, L.J. Cancer is a somatic cell pregnancy. *Cancer Immun.* **2007**, *7*, 19.
94. Kulkarni, P.; Shiraiishi, T.; Rajagopalan, K.; Kim, R.; Mooney, S.M.; Getzenberg, R.H. Cancer/testis antigens and urological malignancies. *Nat. Rev. Urol.* **2012**, *9*, 386–396. [[CrossRef](#)]
95. Rouillard, A.D.; Gunderson, G.W.; Fernandez, N.F.; Wang, Z.; Monteiro, C.D.; McDermott, M.G.; Ma’Ayan, A. The harmonizome: A collection of processed datasets gathered to serve and mine knowledge about genes and proteins. *Database* **2016**, *2016*, baw100. [[CrossRef](#)] [[PubMed](#)]
96. Arcaro, A. Targeting the insulin-like growth factor-1 receptor in human cancer. *Front. Pharmacol.* **2013**, *4*, 30. [[CrossRef](#)] [[PubMed](#)]
97. Git, A.; Allison, R.; Perdiguero, E.; Nebreda, A.R.; Houliston, E.; Standart, N. Vg1RBP phosphorylation by Erk2 MAP kinase correlates with the cortical release of Vg1 mRNA during meiotic maturation of *Xenopus* oocytes. *RNA* **2009**, *15*, 1121–1133. [[CrossRef](#)] [[PubMed](#)]
98. Andrabi, S.M.; Ganai, N.A. *Long Non-Coding RNA: From Disease Biomarkers to Targeted Therapeutics*; Cambridge Scholars Publishing: Cambridge, UK, 2020; ISBN 9781527559103.
99. Hammer, N.A.; Hansen, T.O.; Byskov, A.G.; Rajpert-De Meyts, E.; Grøndahl, M.L.; Bredkjaer, H.E.; Wewer, U.M.; Christiansen, J.; Nielsen, F.C. Expression of IGF-II mRNA-Binding Proteins (IMPs) in Gonads and Testicular Cancer. *Reproduction* **2005**, *130*, 203–212. [[CrossRef](#)] [[PubMed](#)]
100. Liu, Q.; Xu, Z.; Mao, S.; Chen, W.; Zeng, R.; Zhou, S.; Liu, J. Effect of hypoxia on hypoxia inducible factor-1 α , insulin-like growth factor I and vascular endothelial growth factor expression in hepatocellular carcinoma HepG2 cells. *Oncol. Lett.* **2015**, *9*, 1142–1148. [[CrossRef](#)]
101. Betancourt, L.H.; Gil, J.; Kim, Y.; Doma, V.; Çakır, U.; Sanchez, A.; Murillo, J.R.; Kuras, M.; Parada, I.P.; Sugihara, Y.; et al. The human melanoma proteome atlas—Defining the molecular pathology. *Clin. Transl. Med.* **2021**, *11*, e473. [[CrossRef](#)] [[PubMed](#)]
102. Shannon, P.; Markiel, A.; Ozier, O.; Baliga, N.S.; Wang, J.T.; Ramage, D.; Amin, N.; Schwikowski, B.; Ideker, T. Cyto-scape: A Software Environment for Integrated Models of Biomolecular Interaction Networks. *Genome Res.* **2003**, *13*, 2498–2504. [[CrossRef](#)]
103. Johansson, H.J.; Consortia Oslo Breast Cancer Research Consortium (OSBREAC); Socciarelli, F.; Vacanti, N.M.; Haugen, M.H.; Zhu, Y.; Siavelis, I.; Fernandez, A.; Aure, M.R.; Sennblad, B.; et al. Breast cancer quantitative proteome and proteogenomic landscape. *Nat. Commun.* **2019**, *10*, 1600. [[CrossRef](#)]
104. Pjanova, D.; Vainshelbaum, M.N.; Salmina, K.; Erenpreisa, J. The Role of the Meiotic Component in Reproduction of B-RAF-Mutated Melanoma: A Review and “brainstorming” Session. In *Melanoma*; IntechOpen: London, UK, 2021; ISBN 9781838808785.
105. Erenpreisa, J.; Cragg, M.S.; Anisimov, A.P.; Illidge, T.M. Tumor Cell Embryonality and the Ploidy Number 32n: Is It a Developmental Checkpoint? *Cell Cycle* **2011**, *10*, 1873–1874. [[CrossRef](#)]
106. Bernstein, H.; Bernstein, C.; Michod, R.E. Meiosis as an Evolutionary Adaptation for DNA Repair. *DNA Repair* **2011**, *11*, 357. [[CrossRef](#)]
107. Skejo, J.; Garg, S.G.; Gould, S.B.; Hendriksen, M.; Tria, F.D.K.; Bremer, N.; Franjević, D.; Blackstone, N.W.; Martin, W.F. Evidence for a Syncytial Origin of Eukaryotes from Ancestral State Reconstruction. *Genome Biol. Evol.* **2021**, *13*, evab096. [[CrossRef](#)] [[PubMed](#)]
108. Muller, H. The relation of recombination to mutational advance. *Mutat. Res. Mol. Mech. Mutagen.* **1964**, *1*, 2–9. [[CrossRef](#)] [[PubMed](#)]
109. Archetti, M. Recombination and loss of complementation: A more than two-fold cost for parthenogenesis. *J. Evol. Biol.* **2004**, *17*, 1084–1097. [[CrossRef](#)] [[PubMed](#)]
110. Archetti, M. Inverted meiosis and the evolution of sex by loss of complementation. *J. Evol. Biol.* **2019**, *33*, 460–467. [[CrossRef](#)]
111. Archetti, M. Polyploidy as an Adaptation against Loss of Heterozygosity in Cancer. *Int. J. Mol. Sci.* **2022**, *23*, 8528. [[CrossRef](#)]
112. Soppa, J. Ploidy and gene conversion in Archaea. *Biochem. Soc. Trans.* **2011**, *39*, 150–154. [[CrossRef](#)]
113. Hofstatter, P.G.; Brown, M.; Lahr, D.J.G. Comparative Genomics Supports Sex and Meiosis in Diverse Amoebozoa. *Genome Biol. Evol.* **2018**, *10*, 3118–3128. [[CrossRef](#)]

114. Nielsen, A.Y.; Gjerstorff, M.F. Ectopic Expression of Testis Germ Cell Proteins in Cancer and Its Potential Role in Genomic Instability. *Int. J. Mol. Sci.* **2016**, *17*, 890. [[CrossRef](#)]
115. Rivera, M.; Wu, Q.; Hamerlik, P.; Hjelmeland, A.B.; Bao, S.; Rich, J.N. Acquisition of meiotic DNA repair regulators maintain genome stability in glioblastoma. *Cell Death Dis.* **2015**, *6*, e1732. [[CrossRef](#)]
116. Erenpreisa, J.; Giuliani, A.; Vinogradov, A.E.; Anatskaya, O.V.; Vazquez-Martin, A.; Salmina, K.; Cragg, M.S. Stress-Induced Polyploidy Shifts Somatic Cells towards a pro-Tumourigenic Unicellular Gene Transcription Network. *Cancer Hypotheses* **2018**, *1*, 1–20.
117. Walen, K.H. Epigenetic Enabled Normal Human Cells, Lead to First Cell's Unique Division System, Driving Tumorigenesis Evolution. *J. Cancer Ther.* **2022**, *13*, 48–69. [[CrossRef](#)]
118. Erenpreisa, J.; Ivanov, A.; Wheatley, S.P.; Kosmacek, E.A.; Ianzini, F.; Anisimov, A.P.; Mackey, M.; Davis, P.J.; Plakhins, G.; Illidge, T.M. Endopolyploidy in irradiated p53-deficient tumour cell lines: Persistence of cell division activity in giant cells expressing Aurora-B kinase. *Cell Biol. Int.* **2008**, *32*, 1044–1056. [[CrossRef](#)]
119. Salmina, K.; Gerashchenko, B.I.; Hausmann, M.; Vainshelbaum, N.M.; Zayakin, P.; Erenpreiss, J.; Freivalds, T.; Cragg, M.S.; Erenpreisa, J. When Three Isn't a Crowd: A Digyny Concept for Treatment-Resistant, Near-Triploid Human Cancers. *Genes* **2019**, *10*, 551. [[CrossRef](#)] [[PubMed](#)]
120. Adl, S.M.; Simpson, A.G.B.; Lane, C.E.; Lukes, J.; Bass, D.; Bowser, S.S.; Brown, M.; Burki, F.; Dunthorn, M.; Hampl, V.; et al. The Revised Classification of Eukaryotes. *J. Eukaryot. Microbiol.* **2012**, *59*, 429–514. [[CrossRef](#)] [[PubMed](#)]
121. Raïkov, I.B. *The Protozoan Nucleus, Morphology and Evolution*; Springer: Berlin/Heidelberg, Germany, 1982; ISBN 9780387816784.
122. Davies, P. Exposing cancer's deep evolutionary roots. *Phys. World* **2013**, *26*, 37–40. [[CrossRef](#)]
123. Sundaram, M.; Guernsey, D.L.; Rajaraman, M.M.; Rajaraman, R. Neosis: A Novel Type of Cell Division in Cancer. *Cancer Biol. Ther.* **2004**, *3*, 207–218. [[CrossRef](#)] [[PubMed](#)]
124. Zhang, S.; Mercado-Urbe, I.; Xing, Z.; Sun, B.; Kuang, J.; Liu, J. Generation of Cancer Stem-like Cells through the For-mation of Polyploid Giant Cancer Cells. *Oncogene* **2014**, *33*, 116–128. [[CrossRef](#)]
125. Erenpreisa, J.; Ivanov, A.; Cragg, M.; Selivanova, G.; Illidge, T. Nuclear envelope-limited chromatin sheets are part of mitotic death. *Histochem. Cell Biol.* **2002**, *117*, 243–255. [[CrossRef](#)]
126. Westbrook, V.A.; Schoppee, P.D.; Diekman, A.B.; Klotz, K.L.; Allietta, M.; Hogan, K.T.; Slingluff, C.L.; Patterson, J.W.; Frierson, H.F.; Irvin, W.P.; et al. Genomic Organization, Incidence, and Localization of the SPAN-X Family of Cancer-Testis Antigens in Melanoma Tumors and Cell Lines. *Clin. Cancer Res.* **2004**, *10*, 101–112. [[CrossRef](#)]
127. Lazar, I.; Fabre, B.; Feng, Y.; Khateb, A.; Turko, P.; Gomez, J.M.M.; Frederick, D.T.; Levesque, M.P.; Feld, L.; Zhang, G.; et al. SPANX Control of Lamin A/C Modulates Nuclear Architecture and Promotes Melanoma Growth. *Mol. Cancer Res.* **2020**, *18*, 1560–1573. [[CrossRef](#)]
128. Kouprina, N.; Noskov, V.N.; Pavlicek, A.; Collins, N.K.; Bortz, P.D.S.; Ottolenghi, C.; Loukinov, D.; Goldsmith, P.; Risinger, J.I.; Kim, J.-H.; et al. Evolutionary Diversification of SPANX-N Sperm Protein Gene Structure and Expression. *PLoS ONE* **2007**, *2*, e359. [[CrossRef](#)] [[PubMed](#)]
129. Zybina, T. Genome Modifications Involved in Developmental Programs of the Placental Trophoblast. In *Cytogenetics-Classical and Molecular Strategies for Analysing Heredity Material*; IntechOpen: London, UK, 2021; ISBN 9781839689413.
130. Kshitiz; Afzal, J.; Maziarz, J.D.; Hamidzadeh, A.; Liang, C.; Erkenbrack, E.M.; Kim, H.N.; Haeger, J.-D.; Pfarrer, C.; Ho-ang, T.; et al. Evolution of Placental Invasion and Cancer Metastasis Are Causally Linked. *Nat. Ecol. Evol.* **2019**, *3*, 1743–1753.
131. Costanzo, V.; Bardelli, A.; Siena, S.; Abrignani, S. Exploring the links between cancer and placenta development. *Open Biol.* **2018**, *8*, 180081. [[CrossRef](#)] [[PubMed](#)]
132. Lala, P.K.; Nandi, P.; Hadi, A.; Halari, C. A Crossroad between Placental and Tumor Biology: What Have We Learnt? *Placenta* **2021**, *116*, 12–30. [[CrossRef](#)]
133. Carter, S.L.; Cibulskis, K.; Helman, E.; McKenna, A.; Shen, H.; Zack, T.; Laird, P.W.; Onofrio, R.C.; Winckler, W.; Weir, A.B.; et al. Absolute quantification of somatic DNA alterations in human cancer. *Nat. Biotechnol.* **2012**, *30*, 413–421. [[CrossRef](#)] [[PubMed](#)]
134. Taylor, A.M.; Shih, J.; Ha, G.; Gao, G.F.; Zhang, X.; Berger, A.C.; Schumacher, S.E.; Wang, C.; Hu, H.; Liu, J.; et al. Genomic and Functional Approaches to Understanding Cancer Aneuploidy. *Cancer Cell* **2018**, *33*, 676–689.e3. [[CrossRef](#)]
135. Almeida, L.G.; Sakabe, N.J.; Deoliveira, A.R.; Silva, M.C.C.; Mundstein, A.S.; Cohen, T.; Chen, Y.-T.; Chua, R.; Gurung, S.; Gnjatic, S.; et al. CTdatabase: A knowledge-base of high-throughput and curated data on cancer-testis antigens. *Nucleic Acids Res.* **2008**, *37*, D816–D819. [[CrossRef](#)]
136. Jiang, X.; Zhao, D.; Ali, A.; Xu, B.; Liu, W.; Wen, J.; Zhang, H.; Shi, Q.; Zhang, Y. MeiosisOnline: A Manually Curated Database for Tracking and Predicting Genes Associated With Meiosis. *Front. Cell Dev. Biol.* **2021**, *9*, 673073. [[CrossRef](#)]
137. Szklarczyk, D.; Gable, A.L.; Nastou, K.C.; Lyon, D.; Kirsch, R.; Pyysalo, S.; Doncheva, N.T.; Legeay, M.; Fang, T.; Bork, P.; et al. The STRING Database in 2021: Customizable Protein–protein Networks, and Functional Characterization of User-Uploaded Gene/measurement Sets. *Nucleic Acids Res.* **2021**, *49*, D605–D612. [[CrossRef](#)]
138. Rahman, M.; Jackson, L.K.; Johnson, W.; Li, D.Y.; Bild, A.H.; Piccolo, S.R. Alternative preprocessing of RNA-Sequencing data in The Cancer Genome Atlas leads to improved analysis results. *Bioinformatics* **2015**, *31*, 3666–3672. [[CrossRef](#)]
139. Censi, F.; Giuliani, A.; Bartolini, P.; Calcagnini, G. A Multiscale Graph Theoretical Approach to Gene Regulation Net-works: A Case Study in Atrial Fibrillation. *IEEE Trans. Biomed. Eng.* **2011**, *58*, 2943–2946. [[CrossRef](#)] [[PubMed](#)]

140. Gustavsen, J.A.; Pai, S.; Isserlin, R.; Demchak, B.; Pico, A.R. RCy3: Network Biology Using Cytoscape from within R. *F1000Research* **2019**, *8*, 1774. [[CrossRef](#)] [[PubMed](#)]
141. Settle, B.; Otasek, D.; Morris, J.H.; Demchak, B. aMatReader: Importing adjacency matrices via Cytoscape Automation. *F1000Research* **2018**, *7*, 823. [[CrossRef](#)]
142. Sayols, S. Rrvgo: A Bioconductor Package to Reduce and Visualize Gene Ontology Terms. Available online: <https://ssayols.github.io/rrvgo/> (accessed on 1 September 2022).
143. Csardi, N. The Igraph Software Package for Complex Network Research. *Interf. Complex Syst.* **2006**, *1695*, 1–9.
144. Pedersen, T.L. *Ggraph: An Implementation of Grammar of Graphics for Graphs and Networks, R Package Version 1.0. 2*; R Foundation: Vienna, Austria, 2018.
145. Pratt, D.; Chen, J.; Welker, D.; Rivas, R.; Pillich, R.; Rynkov, V.; Ono, K.; Miello, C.; Hicks, L.; Szalma, S.; et al. NDEx, the Network Data Exchange. *Cell Syst.* **2015**, *1*, 302–305. [[CrossRef](#)]
146. Morris, J.H.; Apeltsin, L.; Newman, A.M.; Baumbach, J.; Wittkop, T.; Su, G.; Bader, G.D.; Ferrin, T.E. clusterMaker: A multi-algorithm clustering plugin for Cytoscape. *BMC Bioinform.* **2011**, *12*, 436. [[CrossRef](#)]
147. Dujon, A.M.; Aktipis, A.; Alix-Panabières, C.; Amend, S.R.; Boddy, A.M.; Brown, J.S.; Capp, J.; DeGregori, J.; Ewald, P.; Gatenby, R.; et al. Identifying key questions in the ecology and evolution of cancer. *Evol. Appl.* **2020**, *14*, 877–892. [[CrossRef](#)]
148. Gyurko, D.M.; Veres, D.; Modos, D.; Lenti, K.; Korcsmáros, T.; Csermely, P. Adaptation and learning of molecular networks as a description of cancer development at the systems-level: Potential use in anti-cancer therapies. *Semin. Cancer Biol.* **2013**, *23*, 262–269. [[CrossRef](#)]

3.6. Reproductive functional modules related to embryogenesis are activated in MDA-MB-231 breast cancer cells after doxorubicin treatment and subsequent polyploidization via mitotic slippage

In the following two articles, we explored the biology of chemoresistance development, using MDA-MB-231 TP53-mutant triple-negative breast cancer cell line cells treated with the DNA-damaging agent doxorubicin (DOX). Evolutionary adaptation of MDA-MB-231 cells after treatment with DOX (100 nM, 24 h) involves mitotic slippage (MS) - an incomplete mitosis that follows the DNA under-replication and metaphase arrest caused by DOX and results in polyploidization and a rebound to interphase, repeating in several cycles.

3.6.1. Mitotic slippage in MDA-MB-231 cells is associated with meiotic gene expression, alternative telomere lengthening, and the emergence of two distinct PGCC subtypes

In this part of the studies, where my contribution was mostly limited to data analysis and visualization, PGCCs that resulted from MDA-MB-231 cells undergoing MS were observed undergoing reversible senescence, extruding damaged telomeric DNA to the cytoplasm, repairing their telomeres by RAD51-dependent homologous recombination (alternative telomere lengthening) in PML bodies (as evidenced by the co-localization of RAD51, γ H2AX and PML foci in immunofluorescence experiments), and expressing a number of meiotic/germline genes. Interestingly, these cells also displayed amoeboid-like phenotypes, as well as a lack of sister chromatid cohesion and holokinetic kinetochore arrangements morphologically reminiscent of inverted meiosis. Furthermore, on the second and third weeks, two distinct subpopulations of PGCCs diverged - the reproductive subpopulation drove mitotic regrowth by ploidy reduction, while the other continued to increase in ploidy and seemed to perform a supportive function for the depolyploidized offspring.



Article

“Mitotic Slippage” and Extranuclear DNA in Cancer Chemoresistance: A Focus on Telomeres

Kristine Salmina ¹, Agnieszka Bojko ² , Inna Inashkina ¹, Karolina Staniak ²,
Magdalena Dudkowska ², Petar Podlesniy ³ , Felikss Rumnieks ^{1,4}, Ninel M Vainshelbaum ^{1,4},
Dace Pjanova ¹, Ewa Sikora ² and Jekaterina Erenpreisa ^{1,*}

¹ Cancer Research Division, Latvian Biomedicine Research and Study Centre, LV-1067 Riga, Latvia; salmina.kristine@gmail.com (K.S.); inna@biomed.lu.lv (I.I.); felikss.rumnieks@gmail.com (F.R.); ninela.vainshelbauma@biomed.lu.lv (N.M.V.); dace@biomed.lu.lv (D.P.)

² Nencki Institute of Experimental Biology, Polish Academy of Sciences, 3 Pasteura St., 02-093 Warsaw, Poland; a.bojko@nencki.gov.pl (A.B.); k.staniak@nencki.edu.pl (K.S.); m.dudkowska@nencki.edu.pl (M.D.); e.sikora@nencki.edu.pl (E.S.)

³ CiberNed (Centro Investigacion Biomedica en Red Enfermedades Neurodegenerativas), IIBB, Rosello 161, 08036 Barcelona, Spain; ppodlesniy@gmail.com

⁴ Faculty of Biology, University of Latvia, LV-1586 Riga, Latvia

* Correspondence: katrina@biomed.lu.lv

Received: 25 February 2020; Accepted: 14 April 2020; Published: 16 April 2020



Abstract: Mitotic slippage (MS), the incomplete mitosis that results in a doubled genome in interphase, is a typical response of *TP53*-mutant tumors resistant to genotoxic therapy. These polyploidized cells display premature senescence and sort the damaged DNA into the cytoplasm. In this study, we explored MS in the MDA-MB-231 cell line treated with doxorubicin (DOX). We found selective release into the cytoplasm of telomere fragments enriched in telomerase reverse transcriptase (hTERT), telomere capping protein TRF2, and DNA double-strand breaks marked by γ H2AX, in association with ubiquitin-binding protein SQSTM1/p62. This occurs along with the alternative lengthening of telomeres (ALT) and DNA repair by homologous recombination (HR) in the nuclear promyelocytic leukemia (PML) bodies. The cells in repeated MS cycles activate meiotic genes and display holocentric chromosomes characteristic for inverted meiosis (IM). These giant cells acquire an amoeboid phenotype and finally bud the depolyploidized progeny, restarting the mitotic cycling. We suggest the reversible conversion of the telomerase-driven telomere maintenance into ALT coupled with IM at the sub-telomere breakage sites introduced by meiotic nuclease SPO11. All three MS mechanisms converging at telomeres recapitulate the amoeba-like agamic life-cycle, decreasing the mutagenic load and enabling the recovery of recombined, reduced progeny for return into the mitotic cycle.

Keywords: *mtTP53* cancer; genotoxic treatment; cellular senescence; polyploidization; extranuclear DNA; amoeboid conversion; ALT; inverted meiosis; budding of mitotic progeny; *SQSTM1/p62*

1. Introduction

Once exposed to DNA damaging therapy, tumor cells (particularly *TP53* mutants) undergo a spindle checkpoint arrest, which can be released by mitotic slippage (MS), i.e. mitosis failure and reversal to interphase with a doubled genome [1]. Several laboratories independently found that, after passing several such polyploidizing cycles, a proportion of the surviving giant tumor cells undertake the reverse path, depolyploidization, returning “escapers” into the mitotic cycle [2–8]. Using different cancer treatment models, this recovery process was found to have several characteristic features: (a) duration of about one to three weeks; (b) tumor cell reprogramming [5,9]; (c) the death of most

polyploid participants of the process leading to a remarkably small minority that inevitably survives severe DNA damage [2,9–12]; and (d) serves as a source of cancer metastatic relapse [13–15]. Although the amount of MS is roughly proportional to the drug dosage, it improves cancer cell survival [16].

The mechanisms of this MS-aided cancer resistance, which paradoxically integrates the features of cellular senescence with reprogramming, are poorly understood [8,17–29]. The paracrine tumor- and resistance-stimulating effects of the secretome of senescing cells are of interest [30] but the role of polyploidy as the third component of the paradoxical senescence–self-renewal duality of the chemoresistance is not sufficiently understood [8,26,31–34]. The release of extranuclear DNA in senescent cells via polyploidizing MS requires more study [10]. Extranuclear DNA was reported to be released in senescent cells through the defects or blebs in the nuclear lamina, and digested by lysosomal DNase II, either directly or via macro-autophagy [35–41], causing Sting-mediated inflammation and suppression of innate immunity.

The capability of cancer cells to release cytosolic DNA enriched in DNA strand breaks in response to chemotherapy is proportional to the chromosome instability of cancer cell lines; surprisingly, this favors the epithelial–mesenchymal transition (EMT) and metastases in animal models [42]. MS and associated micronucleation may play a role in escaping cell death via sorting of the intrinsically damaged DNA [27]. However, the origin of this intrinsic damage, how sorting is regulated, and the cause of its survival advantage remain unanswered questions. A secondary origin of the DNA damage induced by chemotherapy and caused by upregulation of the meiotic program was proposed but only partly explored [12,43–45], leaving open the question of the mechanism and biological significance of the meiomitosis in cancer [46,47]. Here, we attempted to address these puzzles in the MDA-MB-231 cell line found previously to display a very high proportion of MS with cytosolic DNA [42]—by studying the response of this cancer cells line to the conventional chemotherapy drug doxorubicin (DOX), the inhibitor of topoisomerase II [48].

2. Results

2.1. Breast Cancer MDA-MB-231 Cell Line, before and after Doxorubicin (DOX) Treatment: The Phenotypes, Cell Growth, and Outlines of the Findings

This metastatic triple-negative breast cancer cell line was obtained from ECACC and cytogenetic analysis of its untreated culture was performed, confirming the reported characteristics [42]: a near-triploid karyotype with multiple chromosomal aberrations and karyotypic heterogeneity. MDA-MB-231 cell line is known to bear three oncogene driver mutations: *TP53R280K*, *KRASG13D*, and *BRAFV600E* [49]. In non-treated (NT) cell culture, it has a mostly fibroblastoid phenotype and contains a small proportion of polyploid cells (Figure 1A,B). After DOX treatment, the cells polyploidize, gradually acquire giant size, amoeboid phenotype, and by the end of the second week or later bud the mitotic progeny (Figure 1C–E) returning it to mitotic cycle (Figure 1F–H) and reconstituting the initial phenotype in escape clones (Figure 1H). During this process, the cell growth was seen steeply retarded in the second week and then very slowly elevated from the beginning of the third week (Figure 2A), when the first recovery clones appeared. The colony formation capacity was $0.009\% \pm 0.002\%$ ($n = 3$). These are very small numbers. Despite this, in 16 experimental series performed on this model (each time seeing a very prolonged and significant drop in cell growth), the recovery consistently occurred. Trying to disclose the mechanisms of this incredible resistance, we studied several aspects of the recovery process—reversible polyploidy, reversible senescence, mitotic slippage, repair and sorting of the DNA damage, mechanisms of telomere maintenance, amoeboidization with the change of reproductive modus, and the involved genes—which all converged on telomeres and the atavistic variant of meiosis as a possible novel mechanism of survival escape.

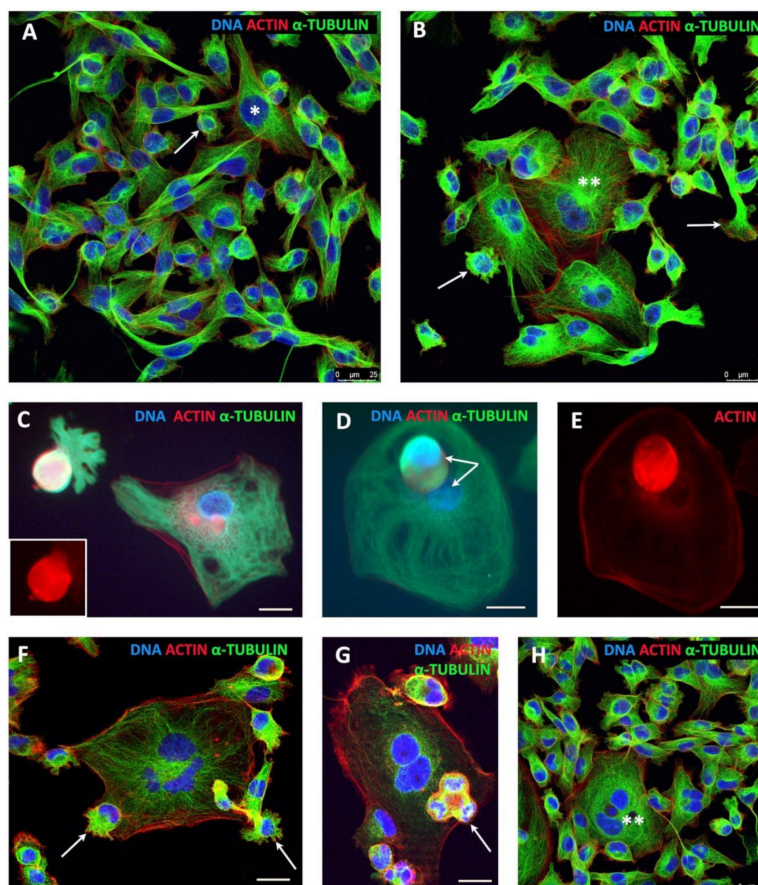


Figure 1. MDA-MB-231 cell culture (grown for 24 h in chamber slides), untreated and in the course of recovery after doxorubicin (DOX) treatment: (A,B) untreated control (arrows, mobile cells in epithelial–mesenchymal transition (EMT); * 8C; ** a multinuclear cell); (C–E) giant amoeboid cells on Day 13 post-DOX treatment budding spore-like subcells, which are extremely enriched in actin and tubulin; and (F–H) seven-week cell culture explanted from the escaped clone on Day 19 after DOX treatment. (F) A giant multinuclear cell is budding two subcells (arrows); the bi-polar ana-telophase on the right is spinning one daughter by the actin structure twisting around a spindle. (G) From the same culture, the progeny in a tripolar division (arrow) is situated on the giant cell. (H) View of the escaped clone with a general phenotype similar to the non-treated control. Bars = 25 μ m.

2.2. Cell Cycle Dynamics and Mitotic Slippage (MS) after DOX-Treatment

Cell cycle measurements by DNA cytometry revealed the induction of reversible polyploidy, in a reciprocal relationship with the mitotic cell cycle (Figure 2B, $n = 3$). A detailed description of the cell cycle changes, along with counts of aberrant mitosis, MS, and cell viability in one of the representative experiments (green line in Figure 2A) is shown in Figure 2C,D and the DNA histograms are presented in Figure 3.

On Day 0, the non-treated (NT) cells had the usual DNA cytometry histograms for the cell cycle in interphase and for cell divisions (measured separately), with negligible admix of 8C cells (Figure 3, first row). The mitotic index was 2.2% (Figure 2C), divisions proceeded in a bi-polar manner as shown in Figure 4A (insert) and, in rare cases, also through tripolar mitosis. Besides major 4C, the 8C metaphases were also encountered (Figure 3, first row, right).

On Day 4 (one day of 100 nM DOX treatment plus three days after the change of the medium), as shown in Figure 3 (second row), the majority of cells accumulated in late S–G2-phase with strongly under-replicated DNA ($\ll 4C$), 3% of cells were arrested in metaphase (Figure 2C), whereas a subpopulation of the under-replicated cells had already overcome the barrier of tetraploidy, doubling its DNA content, reaching a peak $<8C$, and also accumulating in the next $<8C$ metaphase arrest.

The arrested metaphases displayed aberrant features, without exception (Figure 2C), and contained DNA double-strand breaks (DSB), as detected by γ H2AX (not shown). Microscopy performed on Days 4–5 revealed the disordered metaphase figures, often with loopy chromosomes lacking sister cohesion, and the peripheral linear or circular chromosome fragments. Their typical appearance (also characteristic for further days after DOX-treatment) is shown in Figure 4A–C. Anaphases and telophases on Days 4–5 were absent. A proportion of the arrested metaphases undergo MS—a reversal to interphase with the doubled genome (for the counts, see Figure 2C). The microscopic patterns of MS are shown in Figure 4D–K. MS is usually exhibited by one large interphase nucleus with irregular contours and LAMIN B1 defects, surrounded by chromatin clusters and lamin-enveloped micronuclei (Figure 4D). Clusters of the chromatin released into the cytoplasm are enriched with DNA double-strand breaks (DSBs), which were densely stained for γ H2AX (Figure 4E).

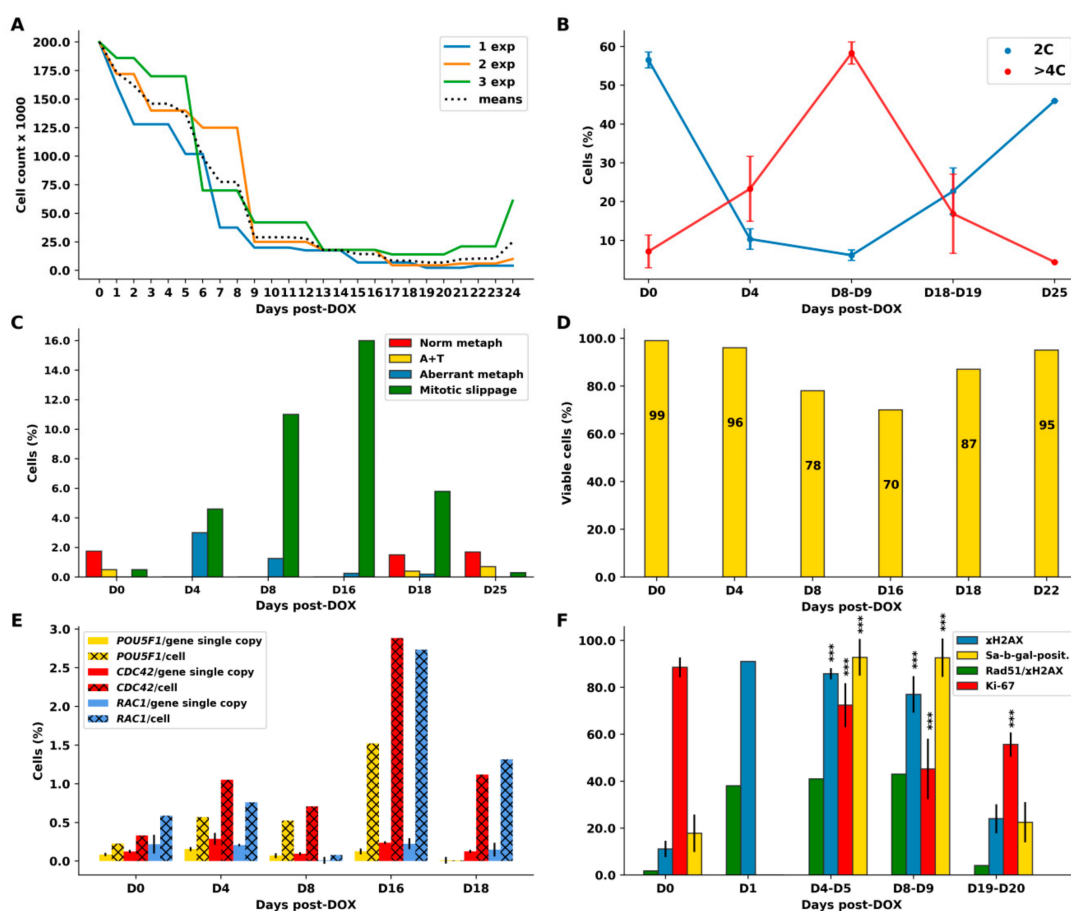


Figure 2. The quantified parameters of MDA-MB-231 cells following DOX treatment: (A) the cell growth curves of three independent experiments with a mean (a dashed line); (B) the reciprocal relationship between mitotic (2C) and polyploid (>4C) cell numbers overtime for three independent experiments (with SD); (C) representative differential mitotic counts (from Experiment 3, shown in (A) by the green line); (D) viability test with trypan blue from Experiment 3 (green curve in (A) and in (C)); (E) results of gene transcription evaluation obtained by Selfie digital PCR for three gene transcripts quantified per gene copy and per cell (as transcripts per gene copy multiplied by the average ploidy in the same experiment)—the average of three technical replicates with SEM; and (F) the dynamics of the senescence marker Sa- β -gal and proliferation marker Ki-67 along with DNA double-strand breaks (γ H2AX) in three independent experiments and their repair by homologous recombination—cells with colocalized Rad51/ γ H2AX foci. (ANOVA with post hoc analysis (Tukey's HSD test), *** $p < 0.001$).

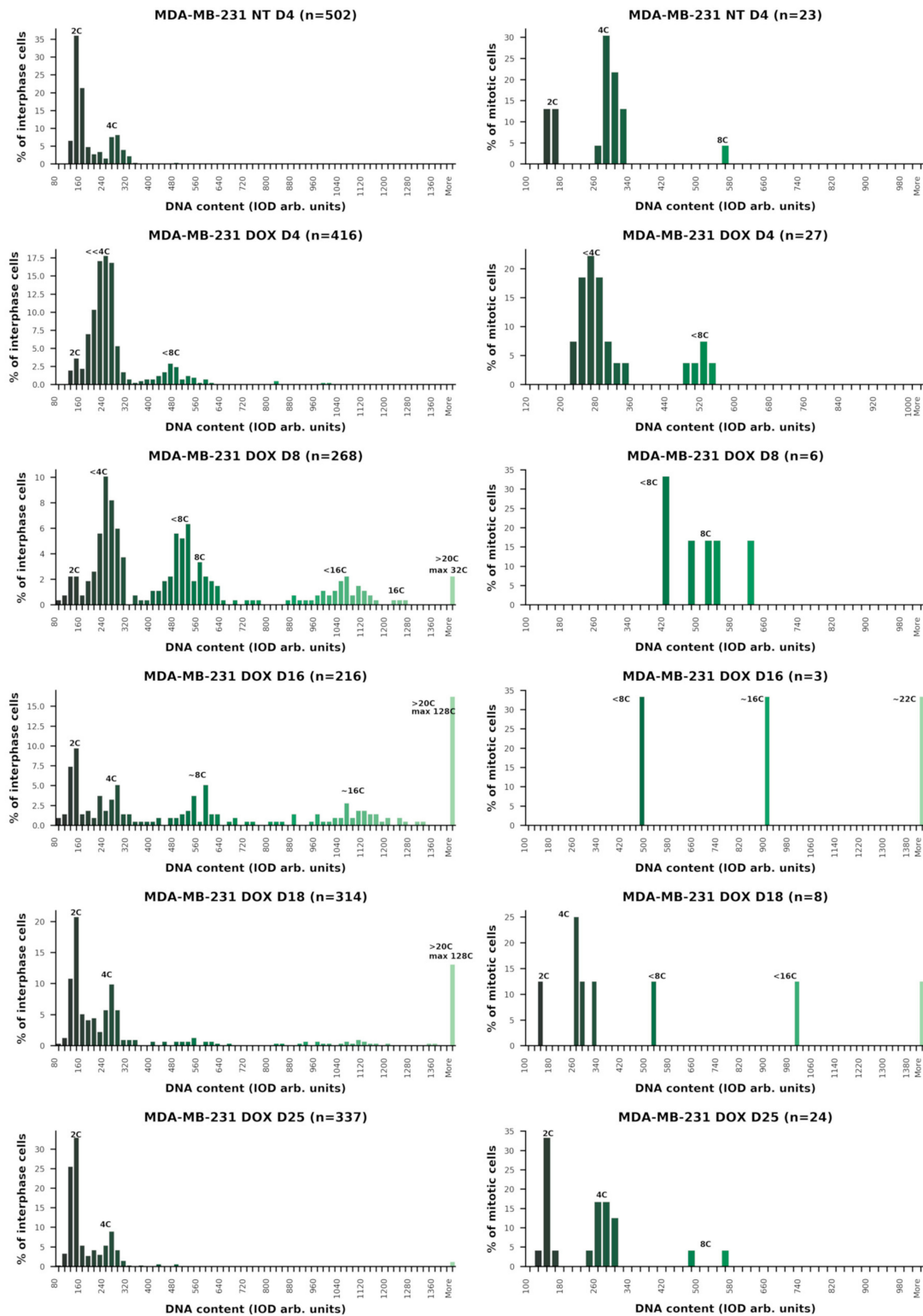


Figure 3. Representative cell cycle changes monitored with in situ DNA cytometry in the dynamics of the DOX treatment experiment: (Left) DNA histograms of interphase cell nuclei; and (Right) the DNA content in mitosis. Interruption of normal mitoses (Days 4–16) coincides with polyploidizing cycles. Bifurcation for depolyploidizing and continuing polyploidization sublines on Day 16 precedes resumption of the normal mitotic cycle on Day 18.

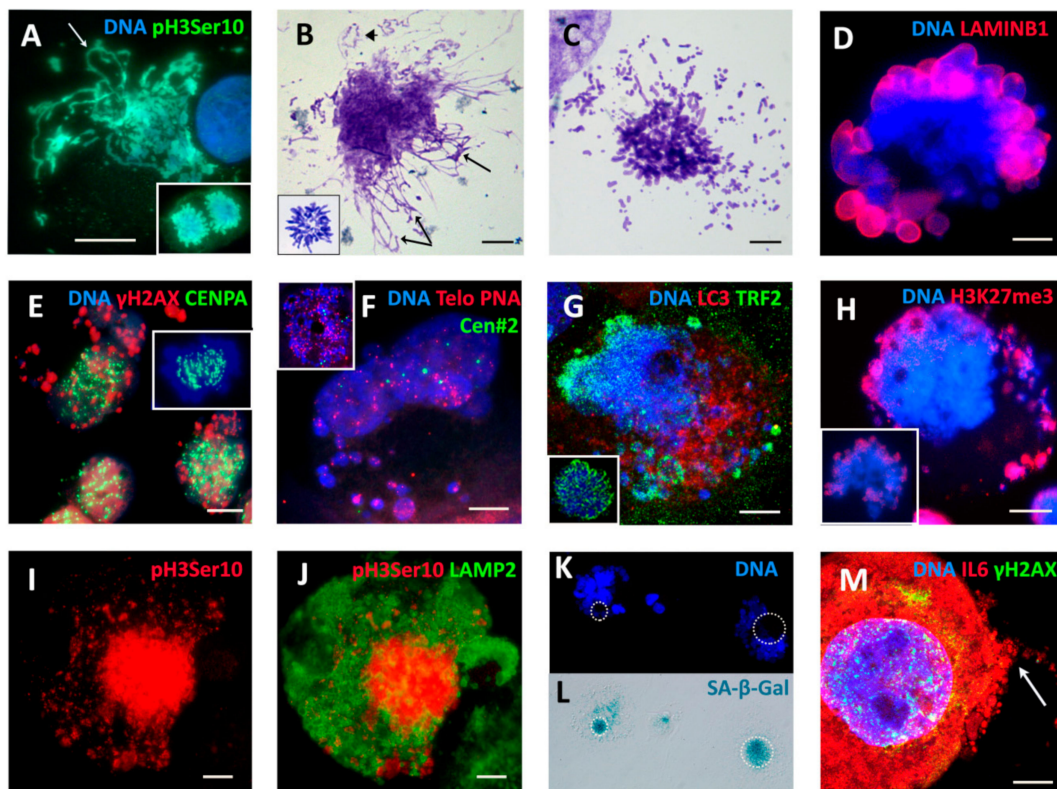


Figure 4. Characterization of aberrant mitosis and mitotic slippage (MS) by several in situ methods applied post-DOX treatment. Representative pictures from three or more experiments for each issue. (A–C) Aberrant metaphases with loopy chromosomes ((A,B) arrows) and their fragments, some circular ((B) arrowhead). (A) DOX-D4. (insert: normal anaphase of the non-treated (NT) control). (B,C) DNA staining with Toluidine blue (DOX-D16 and D18) (insert: normal 4C metaphase of NT). (D–K) Mitotic slippage: (D) defects of the lamina in the main nucleus and most cytoplasmic DNA clumps (DOX-D11); (E) holokinetic arrangement of kinetochores in the main nucleus and release of the damaged DNA into the cytoplasm (DOX-D5) (insert: metaphase of NT); (F) Fluorescence In Situ Hybridization (FISH) with the telomere and cen#2 probes showing retention of centromeres in the cell nucleus and release of a proportion of telomeres into the cytoplasm (DOX-D4) (insert: normal metaphase of NT); (G) preferential release of the telomere shelterin-TRF2-associated chromatin into the cytoplasm (DOX-D7) (insert: normal metaphase of NT); (H) the lamina-associated heterochromatin mark H3K27me3 (DOX-D5) showing partial release into the cytoplasm (insert: normal mitosis of NT with preferential localization of H3K27me3 mark on telomere ends); (I,J) early MS (yet pH3ser10-positive) with finely fragmented cytoplasmic DNA is surrounded by the LAMP2-positive lysosomal material (DOX-D7); (K,L) two cells in MS stained with 4',6-diamidino-2-phenylindole (DAPI) for DNA and positively for Sa- β -gal (DOX-D4); and (M) a giant cell with senescence marks: DNA DSBs in cell nuclei and enrichment of cytoplasm with secreted (arrow) Interleukin-6 (IL6) (DOX-D8). Bars = 10 μ m.

On Day 8 (Figure 3, the third row), the cells further underwent the genome duplication cycles, forming ~4C, ~8C, and ~16C peaks of under-replicated DNA, and, in small proportions, the euploid 8C and 16C peaks. A small amount of ~32C cells also appeared. The degree of the DNA under-replication, compared by DNA cytometry on Day 4, diminished (Figure 3) and the proportion of aberrant metaphases also dropped; they were near-octoploid, but normal cytokinetic cell division still had not resumed (Figure 2C). Reciprocal to the decrease in the proportion of aberrant metaphases, the proportion of MS increased along with the degree of polyploidy (Figures 2C and 3), thus these cells more easily reset interphase after spindle checkpoint adaptation. All cells undergoing mitotic slippage continued to sort the increasing amounts of damaged DNA into the cytoplasm. Simultaneously, many cells detached from the flask bottom and died. As a result, by Days 7–9, the cell number steeply decreased

(Figure 2A), however, about 80% of the cells attached to support excluded Trypan blue, i.e. were viable (Figure 2D).

On Day 16, a dramatic change occurred: the proportion of cells in the polyploidization cycles revealed on the DNA cytometry histograms as ~4C, ~8C, and ~16C peaks diminished, while the proportion of diploid cells increased (Figure 3, the fourth row, left). The back-route of this part of the DNA histogram points to the start of the depolyploidization phase for recovery. However, cytokinetic mitoses were not found (they could be extremely rare); only very aberrant polyploid metaphases with continued chromosome looping and fragmentation of the peripheral chromatin were observed (Figure 3, the fourth row, right); one is depicted in Figure 4B. The proportion of hyperploidy cells (>32C) and mitotic slippage continued to increase (to 16% in both counts; Figure 2C). This bifurcation in the DNA histogram points toward the separation of the two giant cell sublines: one undergoing depolyploidization starting with ~32C–16C cells and the other continuing to re-replicate DNA and undergo MS. Thus, the proportion of mitotic slippage on Days 8 and 16 continued to increase, while 4C mitoses and 2C anaphases were still not evident.

The time point of bifurcation of the two cell lines coincided with the minimum of the cell growth curve (Figure 2A) and the lowest viability (70%) of the cells attached to support (Figure 2D), both signaling the population crisis. At this critical point, we recorded the highest average DNA content per cell (12.15 C; Table 1, first column). Some cells reached 128 C-ploidy. It means that giant and supergiant cells were dominating, filling up the cell population by their mass. In some other experiments with somewhat slower recovery, the maximum encountered DNA amount in the (endo)metaphase was 52C and the largest interphase cell reached 396 C DNA content (not shown).

Table 1. The dynamics of the cell cycle and MS after DOX treatment.

Sample	Average Ploidy *	Normal Cycle	Aberrant Metaphase	Mitotic Slippage	Polyploidy Cycles	Hyperploidy > 20C	Normal Mitosis
Day 0	2.68C	+	–	–	–	–	+
Day 4	3.65C	– ¹	++	+	+	–	–
Day 8	7.47C	–	+	++	+++	+	–
Day 16	12.15C	+/-	+/-	+++	++	+++	–
Day 18	8.87C	+	–	+	+	++	+
Day 25	3.26C	+	–	–	–	-/+	++

* For the experiment presented on Figure 3; ¹ severe DNA under-replication.

On Day 18, the normal cell cycle was restored (Figure 3, the fifth row, left) and normal cytokinetic mitoses (with 2C anaphase/telophase) reappeared (Figure 3, the fifth row, right). The proportion of hyperploids and MS reciprocally decreased (Figures 2C and 3); however, a small amount of the polyploidizing cycles and MS (continuing to sort the damage-signaling DNA) was still encountered for several weeks. The cell number started to increase (Figure 2A, green line). In the other two experiments presented in Figure 2A (blue and orange lines), this regrowth started a few days later.

On Days 24–25 (Figure 3, the sixth row), the cell cycling was similar to the NT control with a larger proportion of ana-telophase/metaphase (Figure 2C), pointing to hasty cell divisions. Mitotic slippage became negligible (<0.2%), as in the NT control (Figure 2C). However, rare giant cells were still present in the samples.

A summary of the typical relationship between observed cell cycle phenomena presented in Figures 2A–C and 3 in their dynamics after DOX treatment is provided in Table 1.

In Table 1, the chain of events can be deduced as follows: DOX causes DNA under-replication, M-arrest, and MS, initiating polyploidization cycles, which increase ploidy through further rounds of re-replication coupled with repeated MS. However, between the second and third weeks (in the particularly described experiment, it was recorded on Day 16), the two diverging polyploid sublines emerged, one starting depolyploidization and the other continuing the increase in ploidy through

repeated cycles of re-replication and MS for a few more days until the stabilization of the normal cell cycle. When this was achieved, hyperploid cells gradually died (as observed by necrosis).

This inevitable survival outcome recovering a very small proportion of resistant cells poses a question of how it is possible. This is the main question of cancer resistance to therapy. Several phenomena with unusual features accompany the process of cancer cell recovery after DOX treatment through the reversible polyploidy. The most striking is the budding of mitotic progeny from late giant cells; the phenomenon has been previously described [3,5,6,50–53] and termed “neosis” [3]. We found that it is part of the amoeboid conversion of giant cells. Below, we provide a short description of our model.

2.3. The Amoeboid Transition of Polyploidized Breast Cancer Cells and Budding of the Mitotic Progeny

By the end of the second week after DOX treatment onward, most cells reached a diameter of 50–300 μm , acquired a powerful microtubular cytoskeleton, enriched with actin, also nuclear (Figure 1C–G), and sometimes encysted (Figure S1A). On chamber slides, we observed the giant cells assuming variable shapes (Figures 1C and S1D, and not shown), some with front–rear polarity, pseudopodia, lamellipodia, and filopodia, which indicate that the EMT-amoeboid invasion phenotype was acquired [54]. Some polynuclear giant cells began to bud spore-like cellularized progeny, highly enriched with microtubules and actin (Figures 1C–E and S1B,D). The budded progeny usually immediately performed bi-polar (more rarely tripolar or tetrapolar) cell division, sometimes even before or during the process of budding (Figure 1F,G) or after homing at the surface of their “mothers” or the nearest giant neighbor (Figure S1C and not shown). The remaining nucleus of a giant cell was often seen in the process of autophagy induction (Figure S1B) and deterioration (Figure S1C). At this very early stage of recovery, the new-born small and giant cells seemed to be cooperating as a system, with the giants providing not only nutritive but also mechanical support for the young generation (Figure S1C,D). Rare budding from polynuclear giant cells was still found even 7–10 weeks post-DOX treatment (Figure 1F); however, on the whole, the culture phenotype returned to that of the untreated cells (Figure 1H). We decided to check the cells for the transcription of the Rho GTPases that are responsible for cell motility involved in the amoeboid transition, cell membrane protrusion for spore budding, and for invasion, *CDC42* and *RAC1* [55,56], as well as for the main stemness transcription factor *POU5F1/OCT4A* in the prolonged time course post-DOX. The results of Selfie digital PCR expressed per gene copy and per cell (multiplied by the average ploidy number, shown in Table 1, determined in the same culture) for each sampling term are presented in Figure 2E, per gene copy and gene dosage. These genes were upregulated on Day 4 (starting with the ploidy cycles); by Day 16, the three markers were particularly high due to high gene dosage in giant cells. Later, together with the recovery of the normal mitotic cycle and reciprocal decrease of polyploidy, the amoeboid regulators went down. Thus, amoeboid phenotype was linked to the DOX-induced polyploidy, and through the spore-like intermediates triggered the recovery of escape mitotic clones. As mentioned above, during the entire prolonged transition period, up to recovery of the mitotic cell cycle, cell polyploidization was accompanied by mitotic slippage, releasing cytoplasmic DNA, and this phenomenon was further studied.

2.4. Extranuclear DNA Released by MS in DOX-Treated Cells Contains Telomere Heterochromatin Enriched with the TRF2-Shelterin but Not Centromeres

The aberrant arrested metaphases contain DNA double-strand breaks (Figure 4B,C); however, during MS, a considerable amount of the fragmented chromatin is sorted into the cytoplasm, thus the remaining nucleus becomes free of the DNA damage (Figure 4E). This creation of the extranuclear damaged DNA and its sorting do not decrease; they increase with repeated cycles of polyploidization and the accompanied MS. To elucidate if there is any cytogenetic selectivity of the sorted DNA, we stained cell nuclei for centromeric kinetochore protein CENPA, telomere capping shelterin TRF2 [57,58], and performed Fluorescent in Situ Hybridization (FISH) with the

telomere-sequence-specific probe combined with the probe for chromosome 2 centromere, for internal control. The typical results of both experiments on Days 4–9 post-DOX-treatment are presented in Figures 4E–G and 5F. We found that in MS the centromeres/kinetochores remain within the restituted cell nuclei. The telomeres in the MS nucleus as compared with NT control (on insert) have variable size and the tendency to cluster; part of the telomere sequenced label was observed in cytoplasmic clusters of the damage-signaling chromatin. The extranuclear DNA was enriched with telomere-capping protein TRF2 (Figure 4G). We also paid attention to the fact that, in arrested metaphases undergoing MS and extending loopy chromosomes into the cytoplasm, their ends are often closed and circular structures detach (Figure 4A,B). The multiple kinetochores were arranged along the chromosomes of the MS nucleus in tandem arrays (Figure 4E), while the centromeres of chr#2 were normally represented by three doublets in control metaphase (Figure 4F, insert) and six separate dots in a (4C) slippage nucleus (Figure 4F). DNA methylation determined by the antibody to 5'-methyl-cytosine after DOX revealed the decreased methylation in the lamin-associated marginal chromatin as well as poor DNA methylation in some clusters of extranuclear chromatin in MS. The H3K27me3-marked heterochromatin, which in control metaphases is located at telomere ends (Figure 4H, insert), becomes partially released from cell nuclei into cytoplasmic clumps in MS (Figure 4H), apparently along with LAMIN B1 defects (compare Figure 4D,H). The intensity of the lysosome marker LAMP2 was enhanced by DOX before the mitosis-slipping cells became deprived of the mitotic marker pH3ser10 staining (Figure 4I,J). In other words, the damage-signaling DNA that is released from the cell nucleus during MS is enriched with the fragmented and circularized telomere heterochromatin but is selectively void of centromeres and kinetochores which are likely indispensable for repeated cycles of MS. The chromosomes in aberrant metaphases and MS, however, exhibited holokinetic distribution of kinetochores, weak or absent sister chromatid cohesion, and often closed ends. Simultaneously, these same cells display cellular senescence.

2.5. The Features of Cellular Senescence in the MDA-MB-231-DOX-Treated Cells with Persistent DNA Damage, Ki-67 Positivity, and HR DNA Repair are Related to MS

In our MDA-MB-231-DOX model, we registered the typical hallmarks of cellular senescence: a high percentage of Sa- β -gal-positivity (Figure 2F), including MS cells (Figure 4K,L), persistent DNA damage (Figure 2F) associated with the Il6-rich secretome (Figure 4M) [49], LAMIN B1 insufficiency (Figure 4D), and release of extranuclear circular DNA (Figure 4B and see below). These canonic senescence hallmarks were combined with the opposite features— positive cell cycle hallmark Ki-67 and DNA repair by homologous recombination (HR)—in a large proportion of these cells (Figure 2F). The p21 senescence marker was also upregulated by DOX [49] but the terminal senescence CDNK4A/p16 protein was usually observed sequestered in cytoplasmic vacuoles. Both groups of opposite phenomena were upregulated by DOX and expressed in the same polyploid cells (at least, half of them) over the period of two weeks (Figure 2F) but became downregulated with restitution of the mitotic cycle, also in accordance. Our data suggest that restitution of the mitotic progeny from these polyploid amoeboid cells seen as budding (Figure 1C–F) was prepared during this prolonged senescence period including the repeated MS. Erosion of telomeres accompanies cellular senescence and favors a transition to tetraploidy [59,60]. The cytogenetic study and staining for TRF2 showed that telomere marks were observed both in restituted giant nuclei and in the released chromatin. The question then became: How are telomeres involved in the DNA repair and sorting of cytoplasmic DNA during MS?

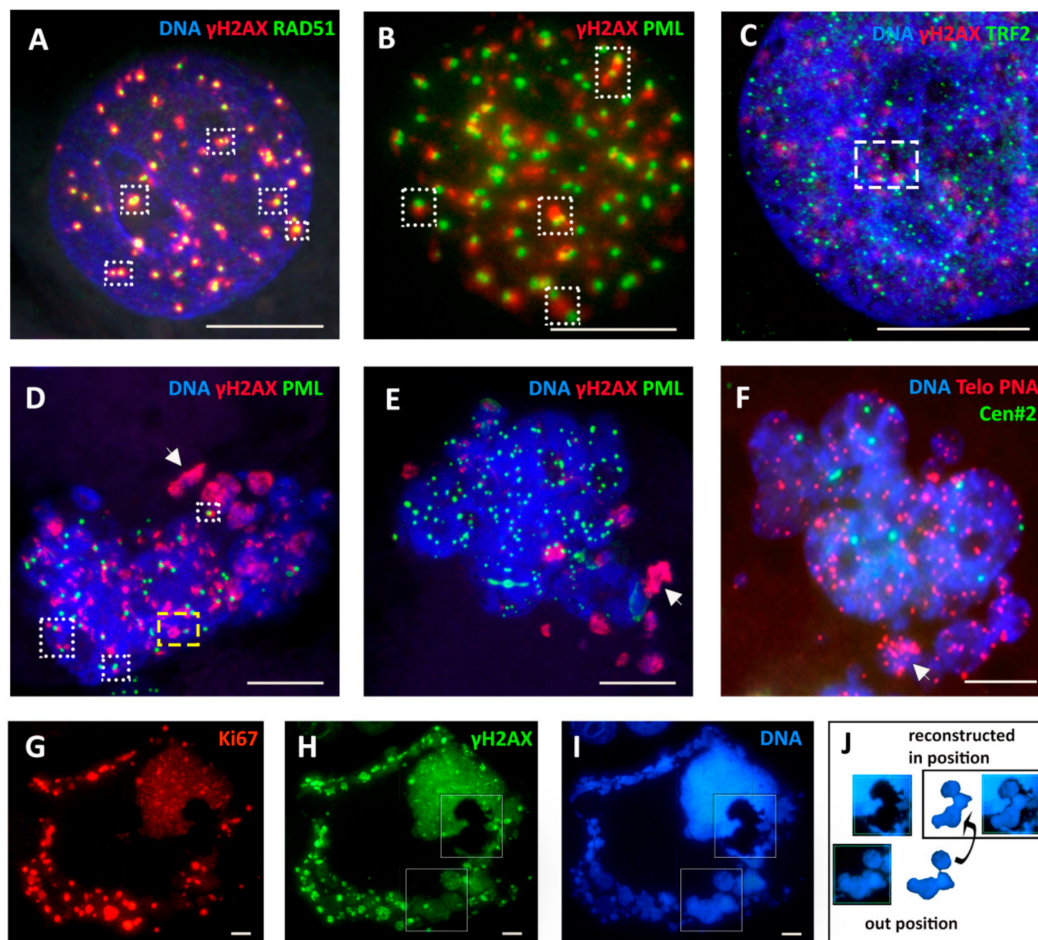


Figure 5. Representative pictures of DNA repair of telomere DNA double-strand breaks by RAD51-dependent homologous recombination (HR) involving promyelocytic leukemia (PML) bodies, a sign of alternative lengthening of telomeres (ALT) in giant post-DOX cell nuclei undergoing MS cycles with sorting the damage signaling DNA out into the cytoplasm and reconstituting subnuclei free of it: (A–D) Days 5–8 post-DOX ($n = 3$). The typical HR configurations are boxed, the extranuclear damaged DNA on (D) arrowed. (E,F) Reconstitution of subnuclei in two similar cells (DOX-D8-9): (E) the extranuclear damaged DNA (arrowed) does not contain PML bodies; and (F) FISH with the telomere and cen#2 probes ($n = 3$) showing the telomere label cluster in the extranuclear DNA (arrowed). (G–I) The release of four repaired subnuclei (boxed) from a defect in the giant mother nucleus (reconstructed in J); high Ki-67 positivity of the sorted DNA signaling damage by γ H2AX-label on DOX-D19 ($n = 3$). Bars = 10 μ m.

2.6. Homologous Recombination (HR) Repair in Giant Interphase and MS Cells is Associated with Promyelocytic Leukemia (PML) Bodies and is Featured by Alternative Lengthening of Telomeres (ALT)

The aberrant metaphases that emerged in the first cell cycles after DOX were all positive for DNA double-strand breaks. From the γ H2AX-positive cell counts, presented in Figure 2F, about 85% of interphase cells possessed the DSBs in the first week, and nearly as many in the second week after DOX. Similar counts showed the proportion of SA- β -gal-positive cells and about half of them were involved in HR (Figure 2F). This persistent DNA damage signaling and persistent HR continued through the transient period of polyploidization and amoeboid conversion. Applying a detailed microscopic study of HR during Days 5–10 post-DOX (three independent experiments), besides colocalization of RAD51 and γ H2AX foci in giant cells (Figure 5A), we unexpectedly found another participant of the DSB repair process—the PML nuclear bodies (Figure 5B,D)—a marker of alternative telomere lengthening (ALT). ALT-associated PML bodies (APBs) are known to provide the nuclear compartment for the ALT

mechanism, clustering and aligning the telomere ends together, for the homologous recombination repair of the eroded telomere on the non-defective double strand [61].

The APB bodies join telomeres for HR with the invading RAD51 (with or without RAD52) filament, so PML bodies become colocalized with RAD51 foci [61]. In post-DOX polyploid interphase cells and in the body of some restituted nuclei of MS cells, we found these typical compositions of the relationship between the foci of the doublets of the γ H2AX-positive chromosome fragments and RAD51 single and double foci, and the same for PML (boxes in Figure 5A,B,D). The foci of telomere shelterin TRF2 were also found in a similar relationship with γ H2AX fragments in some giant cell nuclear parts (boxed in Figure 5C). This mechanism was likely involved in the sorting of the damaged DNA, as we found PML within the repairing giant cell nuclei and MS associated with foci of γ H2AX and Rad51. However, PML bodies were absent in the γ H2AX-labeled DNA cytoplasmic clumps (Figure 5D,E). Here, we present three MS cells in the deduced dynamics of the repair process. HR DNA repair and sorting are occurring in the cell MS nucleus in Figure 5D (DOX-Day 5) where the typical configurations are boxed. We see the formation of a circular non-repaired DNA, still linked to PML, at the nuclear border (yellow box), which might then be released into the cytoplasm. Clusters of the damaged DNA are separated in the cytoplasm (arrowhead). Figure 5E shows MS in the development of the process (DOX-Day 10), with the restituted giant nucleus free of the DNA damage, reconstructing into subnuclei, each with its own nucleolus, while clusters of the damaged DNA are separated in the cytoplasm (arrowhead). Figure 5F shows a very similar composition in the FISH sample (DOX-Day 9), where two reconstituting subnuclei contain 2 + 4 cen#2 labels and multiple telomere labels, while the discarded chromatin is enriched with the clustered telomere label (arrowhead). The next row (Figure 5G–J) shows a giant cell (DOX-Day 19) performing the nuclear release of four repaired sub-nuclei (boxed in Figure 5H,I and reconstructed in Figure 5J) with simultaneous sorting of large amounts of the damaged DNA (γ H2AX-positive). The whole-cell DNA content measured by DAPI was about 32C. The main nucleus and its four extruded sub-nuclei were free from DNA damage signaling and weakly stained for Ki-67. The huge amount of the damaged discarded chromatin was colocalized with bright Ki-67 staining (positive in MS also at earlier terms), which may suggest the amplification of this material with the rolling circle mechanism. Indeed, this cytoplasmic DNA material shows the unscheduled DNA synthesis in BrdU pulse experiments (Figure S2A,B).

2.7. Telomere Ends are Released into the Cytoplasm by MS

To study the process further, we applied the antibody for the catalytic unit of telomerase, reverse transcriptase (hTERT), and combined the available markers of the ALT process (PML, RAD51, and γ H2AX) with TRF2 immunofluorescent staining. We conducted a detailed microscopic study, focusing on the nuclear and cytoplasmic distribution of the components in MS. The results are presented in Figure 6A–F.

MDA-MB-231 cells are known for maintaining their telomeres by telomerase and this cell line is strongly positive for hTERT in the non-treated control outlining the metaphase chromosomes (Figure 6A). During the post-DOX transition of the aberrant mitosis into repeated MS, multiple circular hTERT-positive DNA structures were observed being released into the cytoplasm (Figure 6B), resulting in the relative enrichment of discarded cytoplasmic DNA fragments with hTERT (Figure 6C); this process was also observed in some late giant cells on Day 19 (Figure S2C). However, in the recovery clones, the hTERT staining is again in its place (Figure 6D). The monoclonal antibody for TRF2, similarly, stains normal telophases of the untreated control (Figure 6E, insert) but enriches the released cytoplasmic DNA after DOX treatment (Figures 4G and 6E). This material contains the γ H2AX-positive fragments as presented in Figure 6F (boxed). Thus, these data show that, during MS, the DNA structures of the telomere-end origin, which are often circularized, are transferred into the cytoplasm, signaling DNA damage. From these observations, we suggest that, in giant MS cell nuclei, ALT is substituting the telomerase-driven repair of telomeres, while the telomerase overhang and rolling circles are cut off into the cytoplasm retaining hTERT. In turn, having been repaired by ALT-HR,

the trimmed telomeres in cell nuclei interrupt the DNA damage signaling and further bud the mitotic progeny shifted back to the telomerase maintenance of telomeres.

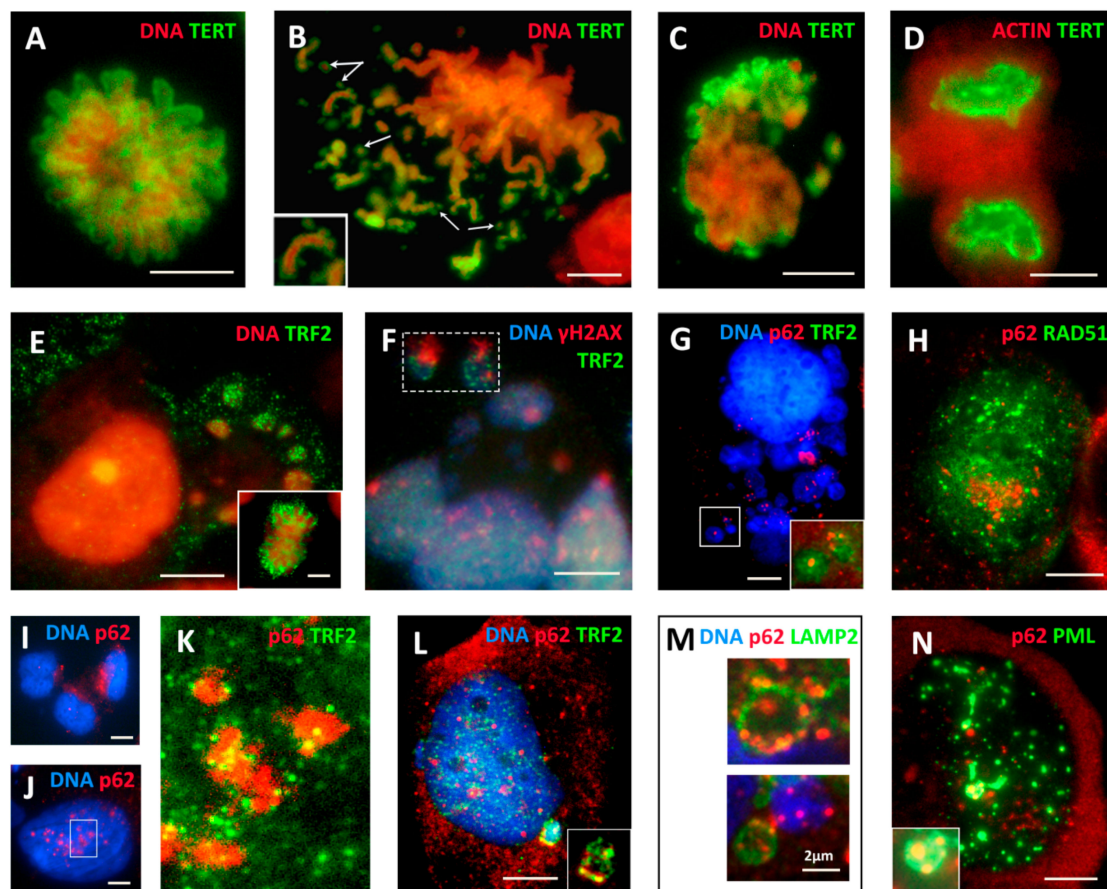


Figure 6. (A–F) The release of the TERT-TRF2- γ H2AX-marked chromatin into the cytoplasm of DOX-treated cells (DOX-Days 5–8, if not specified otherwise; $n \geq 3$) accompanied by the autophagy adaptor SQSTM1/p62: (A) TERT-positive metaphase in NT control (DNA counterstained by propidium iodide); (B) separation of the TERT-enriched circular fragments (arrows) in the restituting polyploid metaphase (insert: a chromosome doublet ending by two circular structures); (C) mitotic slippage with TERT-enriched cytoplasmic DNA, poor in the nucleus (DOX-Day 5); (D) the conventional TERT-positivity in the escape telophase cell (DOX-Day 22); (E) a giant cell after MS surrounded by clumps of extranuclear DNA enriched with TRF2 (insert: the TRF2-positive telophase of the NT); (F) a fragment of the giant MS cell with two boxed chromatin TRF2-enriched fragments marked by DNA damage (γ H2AX) in the cytoplasm; (G) the giant MS cell with abundant extranuclear chromatin enriched with TRF2 and attached SQSTM1/62 protein using RGB filter (the green channel was removed) (insert: from the boxed fragment, the blue channel is removed); (H) the bi-nuclear giant cell with RAD51 repair foci that are apart from the cluster of p62 foci; (I) p62 is scarce in the nuclei of NT cells; (J) nuclear clustering of p62 foci in a giant DOX-treated cell; (K) enlarged nuclear fragment boxed in (J) with removed blue DAPI channel reveals the attachment of TRF2 foci to the p62 clusters; (L) an octoploid cell with several p62 nuclear foci surrounded by TRF2 and a cytoplasmic chromatin fragment, shown enlarged in the insert without the blue channel with clear colocalization of TRF2 and p62; (M) cytoplasmic fragments of the MS cell co-stained for p62, LAMP2, and DNA showing accumulation of p62 in the membrane of lysosomal vesicles, perhaps attracting cytoplasmic DNA to them; and (N) the giant cell in the terminal senescence with typical nuclear polymorphic enlarged PML bodies accumulating p62 (enlarged on the insert). Bars = 10 μ m.

These observations explain the two-week-long coupling between DNA DSBs and HR repair documented in Figure 2F. However, the source of the secondary DNA DSBs for this intrusive coupling

with HR discarding the chromosome ends in giant cells is unclear. The most immediate source of DSBs is the under-replication of heterochromatin caused by DOX-induced topoisomerase II inhibition, leading to accumulation of DNA DSBs [62] associated with fragile sub-telomeric sites of the late-replicating heterochromatin [63]. However, over time, the under-replication induced by DOX decreases (Figure 3) but MS, with the release of extranuclear DNA, increases along with continued nuclear HR up to recovery of the mitotic cycle by Days 18–20, when both decrease (Figure 2C,F).

The recombination repair of telomeres by ALT needs the whole-genome homology search of the complementary telomere matrices for the eroded ones. Arnoult and Karlseder [64] revealed the rapid whole-nuclei spanning of telomeres involved in ALT and suggested that ALT participates in whole-genome homology search by a mechanism evolutionarily related to meiosis. Amoeboid sporogenesis-like mechanism of reproduction also puts the question about possible meiosis. Therefore, further, we focused on the expression of meiotic features and meiotic genes in our model.

2.8. The Meiotic Features of “Mitotic Slippage”

In the untreated control, this cell line expressed very low meiotic *MOS-kinase* but the transcription was several-fold enhanced after DOX-treatment (Figure 7A). Western blot analysis also revealed the upregulation of MOS after DOX treatment (Figure 7B,C).

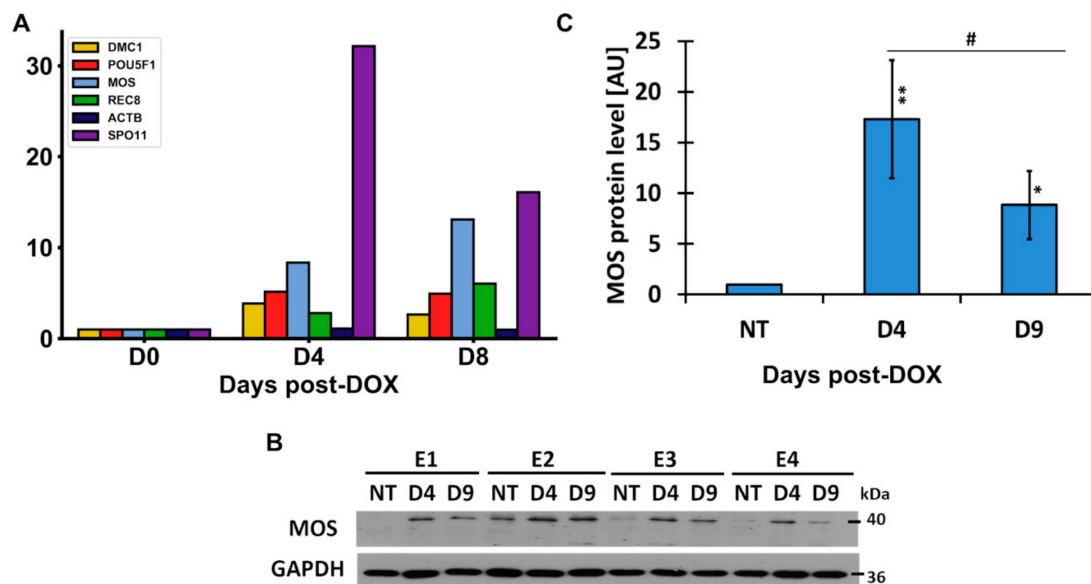


Figure 7. Expression of the meiotic genes and proteins after DOX treatment. (A) RT-PCR results of gene transcription are shown in folds. Representative charts of two independent experiments, with three technical replicates; (B) MOS protein induction on Days 4 and 9 after DOX treatment, analyzed by Western Blot in four independent experiments. (C) The protein level of MOS; densitometry analysis of Western blot bands ($n = 4$) (the p -value is stated as: * $0.01 < p < 0.05$; ** $0.001 < p < 0.01$); # statistical significance between subsequent days of DOX treatment.

In the control, MOS-staining was found by immunofluorescence (IF) being colocalized or juxtaposed with cyclin B1 in rare G2 cell nuclei and in some metaphases, but this expression was enhanced in DOX-treated cells from the second day post-DOX treatment (Figure 8A). MOS-protein was also seen interacting with a centrosome in interphase cells, spindle poles in arrested metaphases (Figure 8B,C), and forming a monopolar spindle (needed for the homology search) in the prophase-like cells (Figure 8C, detailed in [12]). A remnant monopolar spindle was occasionally found in some MS cells (Figure 8D, asterisk), which usually contained two centrosomes (not shown). In the development of MS, MOS, and CYCLIN B1 proteins degraded along with the restitution of the interphase nucleus (Figure 8E).

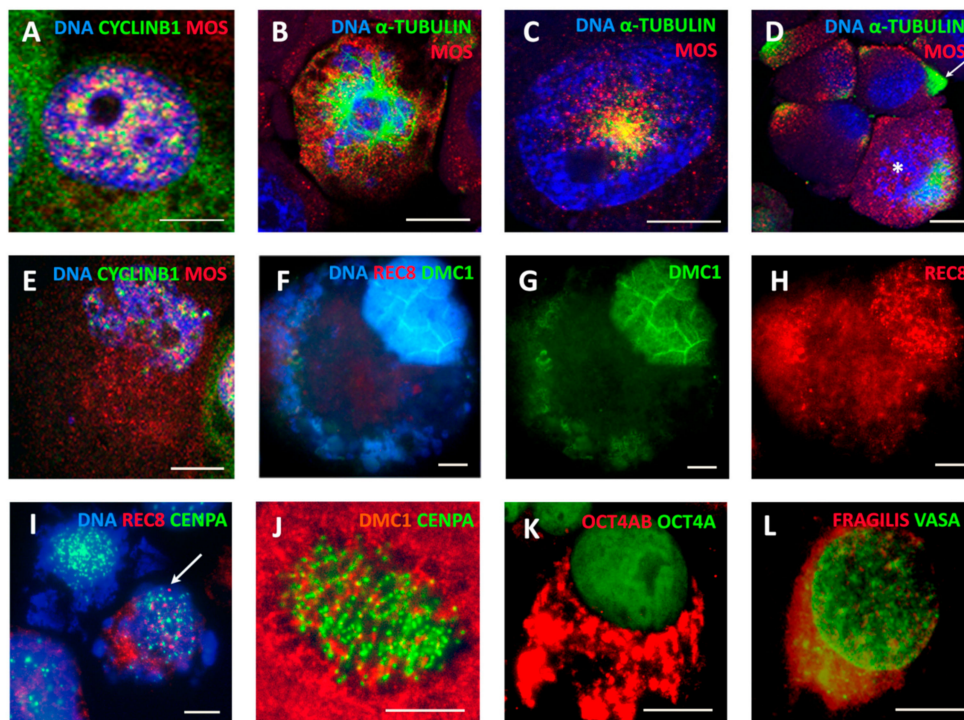


Figure 8. Expression of meiotic and germline proteins in MS and giant cells found by Immunofluorescence—representative images for at least three experiments: (A) a tetraploid cell nucleus enriched with MOS-kinase (sc-86) colocalized and juxtaposed with CYCLIN B1 (DOX-D2); (B) an attachment of MOS to the centrosomes and microtubules of the tripolar mitosis (DOX-D4); (C) MOS and α -TUBULIN form a monopolar spindle in the early prophase (DOX-D4); (D) MOS is attached to interphase centrosomes (arrow) and shows a remnant of a monopolar spindle in MS (asterisk) [12]; (E) the restituting nucleus in MS becomes poor with MOS and CYCLIN B1 (DOX-D4); (F–H) a giant cell in MS releasing cytoplasmic DNA shows the enrichment of the cell nucleus with DMC1 (meiotic recombinase) and REC8 (meiotic cohesin) (DOX-D19); (I) REC8 grains are scarcely inserted in the kinetochore chains in the MS cell (arrow) (DOX-D4); (J) DMC1 grains are scarcely inserted in the MS cell (DOX-D7; [12]); (K) a giant cell enriched with OCT4A in the cell nucleus (a monoclonal Ab) and OCT4B in the cytoplasm (DOX-D5); and (L) a giant cell enriched with the germ markers, DDX4/VASA in the cell nucleus and FRAGILIS in the cytoplasm (DOX-D7). Bars = 10 μ m.

In general, the IF observations can be interpreted as imposing by MOS-kinase of the meiotic prophase upon mitosis, likely starting between the G2 and M arrest. The notable changes in MOS production coincide with the period of the emergence of aberrant “metaphases”, MS, and release of extranuclear chromatin (Figures 2C and 4A). However, even stronger upregulation from practically zero levels in the control was found in the transcription of *SPO11* meiotic nuclease induced by DOX (Figure 7A, DNA contamination excluded). Alongside, we found mild transcription increase of the meiotic cohesin *REC8* and meiotic recombinase *DMC1* after DOX treatment (Figure 7A). These proteins were, however, scarcely inserted in the tandem chains of kinetochores in some arrested and slipping metaphases (Figure 8I,J) but accumulated in the MS nuclei of later giant cells (Figure 8F–H; DOX-Day 19, comparable with Figure 5G–I). These data allowed us to link MS and the release of extranuclear DNA enriched with telomere sequences with a meiotic component (more detailed mechanistic studies on this aspect are planned). The DOX-treated giant cells (heterogeneously) acquired higher positivity for OCT4A/POU5F1 (also confirmed by RT-PCR (Figures 2E and 7A), whereas its alternatively spliced variant OCT4B also can be very strong in the cytoplasm (Figure 8K) and the truncated *OCT4B1* variant, which was expressed in the control, considerably increased. The giant cells were also positive for other germline markers (DDX4/VASA protein, found also in non-treated cells), but the marker of the oocyte maturation, FRAGILIS, was found particularly enhanced by DOX in giant cells (Figure 8L). As already

indicated, the holocentric chromosomes in DOX-treated MS cells typical for inverted meiosis (IM) were also identified (Figures 4E and 8J) (more details and control are described in [12]). Thus, it was revealed that the repeated cycles of MS possessed in many aspects the meiotic features.

2.9. Extranuclear Sorting of the Cut-Off Telomere Ends in MS Being Regulated with the Participation of the Polyubiquitination Adaptor Protein SQSTM1/p62

The question remains if cell degrading systems are involved in the extranuclear sorting of cut-off telomere ends. SQSTM1/p62, a multifunctional polyubiquitination adaptor protein that plays an important role in cell signaling and autophagic degradation of protein aggregates, may be involved. We noted that the damaged chromatin released into the cytoplasm was also enriched with p62 foci (Figure 6G), but, in the repairing nuclei, the p62 clusters (if present) avoided colocalization with RAD51 foci (Figure 6H) but were surrounded by attached and embedded TRF2 foci (see Figure 6I,K,L for NT control), and colocalized with TRF2 in the extranuclear chromatin fragments (Figure 6L, boxed and shown without DAPI in insert). The microscopy using staining for DNA, lysosome activating protein LAMP2, and p62 did not rule out the mediator role of p62 for the link of the damaged telomere DNA to lysosomes (Figures 4I and 6M). However, in terminally senescing cells, where PML bodies enlarge and become polymorphic, p62 was poorly exported from cell nuclei but became incorporated into these enlarged nuclear PML bodies (Figure 6N). These observations correspond well with the data reported by Hewitt et al. [65] on the role of the HR-negative regulating function of p62 in ALT by degradation recombination proteins, in particular RAD51. From this study, we also conclude that the release of the circular damaged DNA into the cytoplasm is part of the ALT telomere repair process processed by HR in the cell nucleus and influenced by p62. In agreement with the opinion of Hewitt et al. [65], this mechanism for genome integrity surveillance very likely depends on the autophagic flux, whose capacity in terminally senescing cells can become exhausted, leading to excessive accumulation of p62 [20]. A more detailed investigation of the degradation pathways of the soluble DNA was outside the scope of the current study.

3. Discussion

After treatment of breast cancer MDA-MB-231 cells with DOX, we observed several phenomena: (1) cellular senescence; (2) polyploidization by mitotic slippage; (3) activation of meiotic genes; (4) extranuclear sorting of the cut-off circularized telomere ends along with the signs of the telomere maintenance mechanism by ALT in these polyploidized cell nuclei; and (5) amoeboid conversion of these cells with final sporogenesis-like budding of their depolyploidized progeny restarting mitotic cycling. In terms of cell mobility, the process of epithelial-to-mesenchymal-amoeboid transition is associated with metastatic cancer spread [54]. All these complex phenomena need to be placed into a mutual context explaining, in particular, why MS improves cell survival [16].

The dynamics of these processes that we evaluated over the period from the mitotic cycle of the untreated population up to its return in survivors, two to three weeks after DOX treatment, may provide a clue. Firstly, the relationships between mitotic and polyploidy cycles are clearly reciprocal. Secondly, the shift from telomerase-driven to ALT-like TMM was also reversible. Thirdly, the amoeboid conversion associated with polyploidy cycles through MS and the change of the reproduction modus, from mitotic to sporogony-like, was also reversible. All these concerted changes induced by 24 h 100 nM DOX treatment continued for 10–14 days in the background of the drug-induced cell senescence, which hence was also not terminal. We speculate that the transient shift in TMM was associated with the change of the tumor cell reproduction modus serving a prerequisite for its realization. The amoeboid cell conversion, including reproduction by spores, is akin to the asexual lifecycle of unicellular organisms [52,53,66,67]. Therefore, these coordinated events could not be random but bore the features of the atavistic program executed in quite a prolonged time.

One of the central observations in this model was the change of the TMM in the MDA MB 231 cell line, known as telomerase-driven, for ALT. The well-known markers of ALT include a high level of

telomere–sister chromatid exchanges (may be seen as closed chromosome ends); extrachromosomal circular telomere repeats; and a specialized telomeric nuclear structure, ALT-associated PML [68]—all these hallmarks were found in our MDA MB 231-DOX model. Analysis of the literature showed that this change of TMM in the telomerase-driven tumors is possible, and is favored by cellular senescence and telomeric DNA damage [68–70] and we observed both. Although the telomerase mechanism is characteristic for epithelial cancers, while primary ALT for the mesenchymal ones [70], the epithelial tumor cells with depleted hTERT undergo epithelial–mesenchymal transition (EMT) and ALT [71]. Again, we observed this transition to ALT after physical depletion of hTERT with its substrate (in the cytoplasm) of amoeboid cells. In turn, stable expression of PML in telomerase-primed MCF7 breast cancer cells also results in ALT [72], whereas ectopic expression of hTERT in primary ALT cells maintains their telomeres with both TMMs [68,69]. The control of telomere length by trimming of telomere ends, generating the amplifying circles, was reported as likely involving the ALT mechanism [73], which is considered by us here, too.

However, a source of these telomere trimming breaks and the biological advantage of the TMM shift for survival escape remained elusive. Here, we found that the process occurs along with upregulation of meiotic genes along with self-renewal and germ master gene *OCT4A* and some other germ genes—*VASA* and *FRAGILIS*. The expression of meiotic genes in cancers with poor prognosis and their involvement in resistance to irradiation and drugs are known and have been studied [12,43–45,74–80]. However, the mechanisms of so-called “meiomitosis”, whose evolutionary origin was earlier proposed [81], are poorly understood, and whether they stabilize or destabilize the genome is currently disputed [46,47,76,82].

The observed MOS-kinase associated phenotypes suggested the imposing of the meiotic prophase onto the cells in G2M arrest caused by DOX. Among the cohort of upregulated meiotic genes in our model, we found the meiotic recombination nuclease *SPO11*. The *SPO11* nuclease is a conservative regulator known from archaea [83] that can introduce the DNA double-strand breaks in the telomere fragile sites [84]. We suggest here for the first time that ALT may be coupled by HR in polyploid tumor cells with inverted meiosis (IM) in PML-APB bodies for recombination (and possibly counting) of homologous chromosomes. If so, *SPO11* may drive the whole process of TMM shift during MS by cutting off the telomere ends, as schematized in Figure 9, and possibly sorting the non-homologous chromosome pairs.

The IM, which has only recently received wider attention from researchers, is an evolutionary ancient variant of meiosis in which the homologous chromosomes specifically synapse and undergo recombination by their sub-telomeric ends, terminalize chiasma [85], and segregate sisters in the first and homologs in the second meiotic division [86–90]. For that, holocentric (holokinetic) chromosomes with diffuse kinetochores distributed along the chromosome length, capable of karyokinesis but disabling the centromeric cohesion of sister chromatids, are needed. We found holocentric chromosomes in DOX-treated MDA MB 231 cells undergoing polyploidization and MS and recently described some more elements of IM in this and other human tumors, such as irradiated Burkitt’s lymphoma [12]. IM has been reported not only in protists, plants, and insects but also in each third normal human oocyte, sorting the non-recombined chromosomes in aneuploid polar bodies [91,92]. Thus, whereas ALT in human tumors is compatible with the telomerase mechanism of TMM [68,93], the IM is compatible with monocentric chromosomes, in both human tumors and embryos. In addition, TERT was shown stabilizing telomere caps even without telomere lengthening and reversibly leaving cell nuclei under stress conditions [94].

IM coupling to telomere maintenance by ALT (or even substituting it) could resolve the long-standing puzzle of the Muller’s Ratchet [95] in the obligately agamic amoeba existing on Earth for eons. They undergo cyclic polyploidy accompanied by chromatin diminution and express the orthologs of genes employed in meiosis of sexual eukaryotes *Spo11*, *Mre11*, *Rad50*, *Rad51*, *Rad52*, *Mnd1*, *Dmc1*, *Msh*, and *Mlh* [83,87,96–99]. Archetti [100] recently presented calculations showing that asexual reproduction can replace sexual reproduction with inverted meiosis due to recombinative gene

conversion, providing protection from the deleterious loss of heterozygosity and outweighing the cost of sex. The same consequence and biological advantage can enable the use of polyploidy and IM as an archaic adaptive mechanism that limits hypermutation, for tumor cell immortality and resistance to extinction.

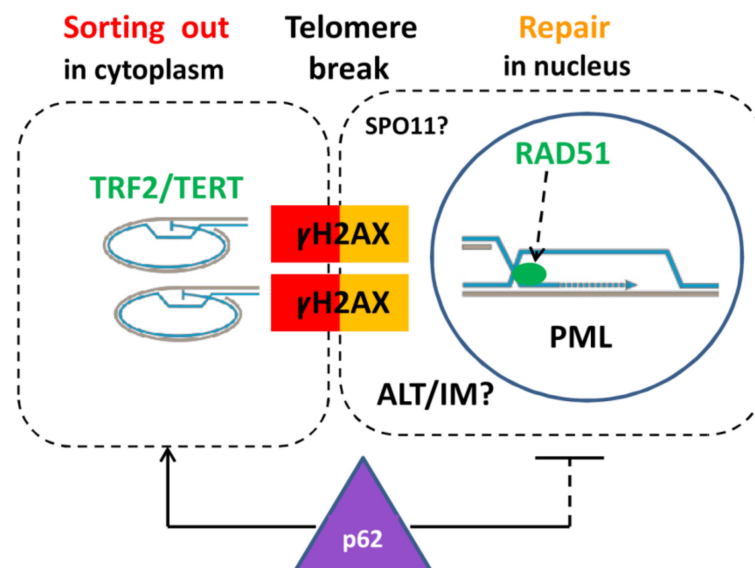


Figure 9. A schematic showing the cytoplasmic sorting of hTERT/TRF2-marked DNA damage signaling telomere ends cut off by a telomere break during mitotic slippage. This process is associated with the ALT-RAD51-driven repair by homologous recombination of the two co-aligned trimmed telomeres occurring in specific nuclear PML (APB) bodies. ALT may be coupled with inverted meiosis (IM) by recombining homologous chromosomes conjugated by telomeres at the same breakage site. In this case, the breakage sites can be introduced by meiotic nuclease SPO11. The ubiquitination protein SQSTM1/62 participates in the sorting of the extranuclear DNA.

The nutritive significance of soluble cytoplasmic DNA and the mechanical support of the budded cancer “spores”, which we observed in this study homed and likely fed with the nucleotide soup by the giant amoeboid “mothers and aunts” before they were able to stabilize clones and the microenvironment on their own (Figure S1B,C), should not be underestimated. The divergence of the reproductive depolyploidizing fraction and the apparently vegetative “nurses”, continuing to re-replicate and produce soluble DNA through MS until stabilization of the normal mitotic cycle, all acting as a tissue system, is an example of the histiotrophic co-operation, which was also noted by Zybina and Zybina [101,102] in the development of the mammalian trophoblast.

Finally, we briefly discuss the relationship of the phenomenology in DOX-treated breast cancer cells to cell senescence. We observed six hallmarks of premature cell senescence: Sa-β-gal-positivity, persistent DNA double-strand breaks [103], reduction of lamin B1, the release of heterochromatin [35,36], erosion of telomeres associated with tetraploidy [60], and secretion of cytokines (in particular, IL6) during a prolonged period post-DOX damage [49]. However, we simultaneously found that the persistent chromatin damage and its repeated sorting from cell nuclei occurring during polyploidization cycles are necessarily coupled with proliferation, self-renewal, and meiotic markers, and bear a programmed characteristic discussed above. The dependence of reprogramming capacity on accelerated senescence is clearly established [8,24,25,32,104]. Thus, although displaying basic hallmarks of senescence, for quite a long period of time, the DOX-treated polyploidizing MDA-MB-231 cells are not really senescent but rather reproductive (paradoxically, both).

In conclusion, the present results investigating the link between cellular senescence, MS, and the processes of ALT and IM in chemoresistant cancer cells, all converging on telomeres, open a new avenue for further research and possible targeting.

4. Materials and Methods

4.1. Cell Line and Treatment

The breast adenocarcinoma MDA-MB-231 cell line was obtained from the ECACC (European Collection of Authentic Cell Cultures, Wiltshire, UK). Cells were cultured in flasks in Dulbecco's modified Eagle's media (DMEM) supplemented with 10% fetal bovine serum (FBS; Sigma-Aldrich, St. Louis, MO, USA) at 37 °C in a 5% CO₂ humidified incubator without antibiotics. For experimental studies, cells were maintained in the log phase of growth and treated with 100 nM DOX (doxorubicin) for 24 h. After drug removal, cells were maintained by replenishing culture medium every 2–3 days and sampled over a 3-week period post-treatment until the appearance of escape clones. In some, we further followed the re-seeded recovery fractions for 5–8 weeks. Some issues were repeatedly addressed in the shorter time periods, provided that the recovery of escape clones was further achieved. In some experiments, cells were grown on chamber slides.

For testing the unscheduled DNA replication, the cells were incubated with 5 μM BrdU for 90 min before sampling.

4.2. Cell Growth, Viability, and Colony Formation

To determine growth kinetics, cells were seeded and treated at a density of 200,000 cells per well in a 6-well plate and counts were performed using a Neubauer camera (Heinz Herenz Medizinalbedarf GmbH Hamburg, Germany) and Trypan blue dye (0.4%) exclusion. After treatment, cell number changes were monitored at several time points until the recovery. Cell viability was calculated as the proportion of the cells attached to the support with Trypan blue exclusion.

To determine colony formation capability, 1.5–2 million cells in a T25 flask were treated with 100 nM DOX. On Day 22 after treatment, the cells were rinsed with phosphate-buffered saline (PBS), then fixed and stained with Trypan blue, and the number of colonies exceeding 50 cells was counted. Colony formation capability was calculated as a percentage of the initial cell number before treatment with DOX.

4.3. Immunofluorescence

Cells were pelleted, suspended in warm FBS, and pelleted by cytocentrifuge again onto polylysine-coated glass slides or grown and fixed on chamber slides. Cytospins were fixed in methanol for 7 min at –20 °C, dipped 10 times in ice-cold acetone, and allowed to briefly dry. Slides were then washed three times in Tris-buffered saline (TBS) 0.01% Tween20 (TBST) for 5 min. Slides were subsequently blocked for 15 min in TBS, 0.05% Tween 20%, and 1% bovine serum albumin (BSA) at room temperature. Samples were covered with TBS, 0.025% Tween 20%, and 1% BSA containing the primary antibody, and incubated overnight at 4 °C in a humidified chamber. Samples were then washed three times in TBST and covered with TBST containing the appropriate secondary antibodies (goat anti-mouse IgG Alexa Fluor 488, goat anti-rabbit IgG Alexa Fluor 594, or sheep anti-human IgG Alexa Fluor 488 (Invitrogen, Carlsbad, CA, USA)) and incubated for 40 min at room temperature in the dark. Slides were washed three times for 5 min with TBST and once for 2 min in PBS. Samples were then counterstained with DAPI (0.25 μg/mL) for 2 min or with propidium iodide (5 μg/mL) and finally embedded in Prolong Gold (Invitrogen, Carlsbad, CA, USA). When staining for α-tubulin, actin, or IL-6, the post-fixation drying step was omitted and fixation in 4% paraformaldehyde was performed. For 5-methylcytosine and BrdU staining, DNA denaturation was performed by 2 N HCl at 37 °C for 20 min before the blocking step. Primary antibodies and their sources are listed in Table 2.

Table 2. The antibodies used, their specificity, and source.

Antibody Against	Description	Specificity/Immunogen	Used Concentration	Product No. and Manufacturer
AURORA B	Rabbit polyclonal	A peptide derived from within residues 1–100 of human Aurora B	1:300	ab2254, Abcam, Cambridge, UK
BrdU	Mouse monoclonal	Recognizes the thymidine analog 5-bromo-2'-deoxyuridine (BrdU)	1:100	A21300, Invitrogen, Carlsbad, CA, USA
α -Tubulin	Mouse monoclonal	Recognizes an epitope located at the C-terminal end of the α -tubulin isoform in a variety of organisms	1:1000	T5168, Sigma-Aldrich, St. Louis, MO, USA
Centromere protein	Human	Derived from human CREST patient serum	1:50	15–234, Antibodies Inc., Davis, CA, USA
CYCLIN B1	Mouse monoclonal	Raised against a recombinant protein corresponding to human cyclin B1	1:100	sc-245, Santa Cruz, Dallas, TX, USA
DMC1	Mouse monoclonal	Specific for DMC1, does not cross-react with the related protein Rad51	1:100	ab11054, Abcam, Cambridge, UK
F-ACTIN		Phalloidin-iFlour 594 Conjugate	1:500	ab176757, Abcam, Cambridge, UK
FRAGILIS	Rabbit polyclonal	The details of the immunogen for this antibody are not available	1:50	ab65183-100, Abcam, Cambridge, UK
GAPDH	Mouse monoclonal	Raised against recombinant GAPDH of human origin	1:50000	sc-47724, Santa Cruz, Dallas, TX, USA
IL6	Rabbit polyclonal	Synthetic peptide	1:50	orb87798, Biorbyt, Cambridge, UK
γ -H2AX	Rabbit polyclonal	Recognizes mammalian, yeast <i>Drosophila melanogaster</i> and <i>Xenopus laevis</i> γ -H2AX	1:200	4411-PC-100, Trevigen, Gaithersburg, MD, USA
γ -H2AX	Mouse monoclonal	Synthetic peptide sequence surrounding phosphorylated Ser140	1:200	Ma1-2022, Pierce, Waltham, MA, USA
H3K27me3	Rabbit polyclonal	Synthetic peptide within human Histone H3 aa 1–100	1:200	ab6147, Abcam, Cambridge, UK
Ki67	Rabbit polyclonal	Synthetic peptide from C-terminus of human Ki-67	1:50	PA5-16785, Pierce, Waltham, MA, USA
LAMIN B1	Rabbit polyclonal	Peptide mapping at the C-terminus of Lamin B1 of human origin	1:200	ab1604, Abcam, Cambridge, UK
LAMP2	Mouse monoclonal	The details of the immunogen for this antibody are not available	1:500	555803, BD Pharmingen™, Franklin Lakes, NJ, USA
MOS (C237)	Rabbit polyclonal	Epitope mapping at the C-terminus	1:50	sc-86, Santa Cruz, Dallas, TX, USA
MOS	Rabbit polyclonal	Synthetic peptide corresponding to a region within internal sequence amino acids 107–156	1:500	Ab99017, Abcam, Cambridge, UK
OCT 3/4	Mouse monoclonal	Peptide raised against amino acids 1–134 of Oct-3/4 of human origin non-cross-reactive with Oct-3/4 isoforms B and B1	1:50	sc-5279, Santa Cruz, Dallas, TX, USA
OCT4	Rabbit polyclonal	A peptide derived from within residues 300 to the C-terminus of human Oct4	1:200	ab19857, Abcam, Cambridge, UK
p-AMPK α 1/2 (Thr183/172)	Rabbit polyclonal	Epitope corresponding to phosphorylated Thr172 of AMPK α 1 of human origin	1:50	sc-101630, Santa Cruz, Dallas, TX, USA
pH3Ser10	Mouse monoclonal	Recognizes Phospho- S10 on Histone H3	1:200	ab14955, Abcam, Cambridge, UK
PML	Mouse monoclonal	Epitope corresponding to amino acids 37–51 mapping near the N-terminal of PML of human origin	1:200	sc-966, Santa Cruz, Dallas, TX, USA
P62/SQSTM1	Rabbit polyclonal	A synthetic peptide corresponding to Human SQSTM1/ p62 (C-terminal)	1:200	ab91526, Abcam, Cambridge, UK
RAD51	Mouse monoclonal	Recombinant full-length protein corresponding to human Rad51 aa 1–338	1:50	ab213, Abcam, Cambridge, UK
REC8	Rabbit polyclonal	Peptide mapping near the N-terminus of Rec8 of human origin	1:50	10793-1-AP, Proteintech Group, Manchester, UK
TERT	Mouse monoclonal	Recombinant full-length protein (human) from insect cells	1:50	ab5181, Abcam, Cambridge, UK
TRF2	Mouse monoclonal	His-tagged, fusion protein, corresponding to full-length TRF2 (Telomeric Repeat binding Factor 2)	1:100	05-521, Millipore, Temecula, CA, USA
VASA/DDX4	Mouse monoclonal	A synthetic peptide corresponding to residues near the N-terminus of human DDX4	1:50	MA5-15565, Pierce, Waltham, MA, USA
5-Methylcytosine	Mouse monoclonal	Detects methylated DNA or RNA	1:200	NA81, Calbiochem, Merck, Burlington, MA, USA

For microscopic observations, a fluorescence light microscope (Leitz Ergolux L03-10, Leica, Wetzlar, Germany) equipped with a color video camera (Sony DXC 390P, Sony, Tokyo, Japan) and laser scanning confocal microscope (LEICA TCS SP8, Wetzlar, Germany) were used. To capture fluorescent images, in addition to separate optical filters, a three-band BRG (blue, red, green) optical filter (Leica, Wetzlar, Germany) was used.

4.4. Toluidine Blue DNA Staining and Image Cytometry

Cytospins were prepared and fixed in ethanol/acetone (1:1) for >30 min at 4 °C and air-dried. Slides were then hydrolyzed with 5 N HCl for 20 min at room temperature. In some experiments, shortened hydrolysis (30–60 s) was performed, preserving cytoplasmic RNA staining. Slides were then washed in distilled water (5 × 1 min) and stained for 10 min with 0.05% toluidine blue in 50% citrate-phosphate McIlvain buffer at pH 4. Slides were rinsed with distilled water, blotted dry, and dehydrated by incubating twice in butanol for 3 min each at 37 °C. Samples were then incubated twice in xylene for 3 min each at room temperature before being embedded in DPX. Digital images were collected using a Sony DXC 390P color video camera (Sony, Tokyo, Japan) calibrated in the green channel. DNA content was measured as the integral optical density (IOD), using Image-Pro Plus 4.1 software (Media Cybernetics, Rockville, MD, USA). The stoichiometry of DNA staining was verified using the values obtained for metaphases compared with anaphases and telophases (ratio 2.0); arbitrary diploid (2C) DNA values were averaged from measuring anaphases in untreated tumor cells. The method error was estimated to be less than 10%. For cell cycle measurements, 200–500 interphase cells were collected at each point. For DNA measurements, 500–2000 cells were collected for each point. The counts of the normal and aberrant mitoses and mitotic slippage were recorded microscopically per 500 or more cells.

4.5. Fluorescence in Situ Hybridization (FISH)

Cells were harvested, washed with warm PBS, treated with 75 mM KCl at room temperature, incubated for 40 min at 37 °C, and centrifuged. Serum and KCl solution (1:1) were added to cells and suspension was pelleted by cytocentrifuge on slides and air-dried. Then, slides were fixed for 1 h with two changes of fresh methanol/glacial acetic acid (3:1) at –20 °C. Telomere FISH for Telo PNA Cy3/Cen#2 FITC was done with a peptide nucleic acid (PNA) telomere probe (Dako Inc., Glostrup, Denmark) in conjunction with a differentially colored centromere 2 PNA probe (a gift from Dako, Inc., Glostrup, Denmark) as an internal reference point as previously described [105,106]. FISH was carried out using 1 M NaSC pretreatment (56 °C for 20 min), denaturation step for 3 min at 83 °C and hybridization at 37 °C overnight. Denaturation and hybridization steps were performed on a ThermoBrite (Leica, Wetzlar, Germany) programmable temperature controlled slide processing system. Slides were mounted in antifade solution (Vector Laboratories, Burlingame, CA, USA) or in Prolong Gold with DAPI (Invitrogen, Carlsbad, CA, USA).

4.6. Detection of Senescence-Associated- β -Galactosidase

Detection of senescence-associated- β -galactosidase (SA- β -gal) was performed according to [107]. Briefly, cells were fixed in 2% formaldehyde and 0.2% glutaraldehyde in PBS, washed, and incubated overnight at 37 °C with a solution containing 1 mg/mL 5-bromo-4-chloro-3-indolyl- β -d-galactopyranoside, 2.5 mM potassium ferrocyanide, 2.5 mM potassium ferricyanide, 150 mM NaCl, 2 mM MgCl₂, and 0.1 M phosphate buffer, pH 6. Cell nuclei were stained with DAPI (1 μ M in PBS) or Hoechst 33342 (1 μ g/mL in PBS). Cells were observed under a Nikon Eclipse Ti (Nikon, Tokyo, Japan), a fluorescent microscope with a 40 \times /0.6 Nikon lens, and analyzed using the NIS Elements Basic Research software. The percentage of SA- β -gal positive cells was calculated.

4.7. RT-PCR

Total RNA was extracted from MDA-MB-231 (10^6 cells) using TRIZOL (Invitrogen, Carlsbad, CA, USA). First-strand cDNA was synthesized using 2 μ g of RNA, random hexamers, and RevertAidTM M-MuLV Reverse Transcriptase (Fermentas, Vilnius, Lithuania) according to the manufacturer's instructions, and subsequently diluted with nuclease-free water 10 times. The absence of contamination with chromosomal DNA was verified by PCR using β -actin primers (Table 3). Amplification was carried out in a total volume of 20 μ L with 2 μ L of diluted cDNA, 4 μ L of 5 \times HOT FIREPol[®] Blend Master Mix (Solis BioDyne, Tartu, Estonia) and the following primers: *OCT4A* F/R, *OCT4B* F/R, *OCT4B1* F/R, *MOS* F/R, *REC8* F/R, *DMC1* F/R, and *SPO11* F/R under the manufacturer's recommended conditions. Amplified PCR products were analyzed by direct sequencing after ExoI/FastAP treatment (Thermo Scientific, Waltham, MA, USA) using the fluorescent Bigdye Terminator v3.1 Cycle Sequencing protocol on a 3130xl Genetic Analyzer (Applied Biosystems, Waltham, MA, USA) and verified using the BLAST NCBI (National Center for Biotechnology Information) platform (Bethesda, MD, USA). Amplified PCR products were visualized on 1.2% agarose gels and quantified using ImageJ software [108].

Table 3. The primers applied in RT-PCR for *POU5F1* and meiotic proteins.

Gene	Forward Primer Sequence	Reverse Primer Sequence	Amplicon Length	Tann (°C)	Reference	Sequence ID
<i>POU5F1-A (Oct4A)</i>	TCGCAAGCCCTCATTTCACC	GCCAGGTCGAGGATCAAC	157	56	[109]	NM_002701.5
<i>POU5F1-B (Oct4B)</i>	AGACTATTCTTGGGGCCACAC	GGCTGAATACCTTCCCAAATAGA	244	58	[109]	NM_203289.5
<i>POU5F1-B1 (Oct4B1)</i>	TGACCGCATCTCCCTCTAA	AGCTTACCACCTCTTCCCAG	134	58	[109]	NM_001285986.1
<i>MOS</i>	CGGTGTTCTGTGGCCATAA	GCAGGCCGTTACAAACATC	250	58	[75]	NM_005372.1
<i>REC8</i>	TGAGGGTGAATGTGGTAAA	CTGGGATTGCAGCCTCTAAG	400	56	[75]	NM_005132.2
<i>DMC1</i>	AGCAGCAAAGTCCATGAAG	TGAGTCTCTCTTCCCTTT	300	54	[75]	NM_007068.3
<i>SPO11</i>	TGAGGTTCTTGCATATAGAAA	AAATTTTTGAGCTGATTTGGTG	240	58	in house	NM_012444.2
<i>ACTB</i>	AGTGTGACGTGGACATCCG	AATCTCATCTGTTTCTGCGC	349	56	[110]	NA

4.8. Selfie-Digital RT-PCR

To preserve the content of the nucleic acids in the sample, selfie-digital PCR analysis was performed using lysate as previously described [111]. Briefly, cell culture media were aspirated from the culture flasks and the cell layer was lysed in 100ST DNA/RNA/Protein Solubilization Reagent (#DCQ100ST, DireCtQuant, Lleida, Spain) at 250,000 cells/mL. The lysate was incubated at 90 °C for 3 min, centrifuged at 10,000 rpm for 10 min and the supernatant used directly. Strand-specific, absolute expression level analysis of gene transcription was performed using Selfie-digital PCR as previously described [111]. The reverse transcription step was performed using the reverse primer listed in Table 4. Digital PCR was performed using EvaGreen SuperMix (186-4005, Bio-Rad, Hercules, CA, USA) on the QX200 ddPCR platform. PCR amplification was performed in a thermal cycler (C1000 Touch Thermal Cycler, Bio-Rad, Hercules, CA, USA) using the following thermal profile: 95 °C 5 min; 40 cycles of 95 °C for 30 s and 60 °C for 1 min; 4 °C for 5 min; and 90 °C for 10 min. Non-template controls containing all the reagents and the corresponding amount of solubilization buffer without sample lysate were included in all steps of the procedure. The number of RNA transcripts was calculated by subtracting the number of amplicons measured in the reaction without reverse transcriptase (RT-) from the reaction with reverse transcriptase (RT+) and dividing by (RT-). The results are expressed as the number of transcripts per gene. The specificity of the primers was checked using BLAST analysis and the correct size and homogeneity of the amplicons after gel analysis of the PCR products.

Table 4. The primers used for selfie-digital PCR.

Gene Symbol	Amplicon Size	Forward Primer Sequence 5'-3'	Reverse Primer Sequence 5'-3'
<i>RAC-1</i>	75 bp.	AAACCGGTGAATCTGGGCTT	CGGATAGGATAGGGGGCGTA
<i>POU5F1</i>	97 bp.	GAGTAGTCCCTTCGCAAGCC	GAGAAGGCGAAATCCGAAGC
<i>CDC-42</i>	95 bp.	TGTTGAACCAATGCTTCTCATGT	CTCAGGCTGGCTTGTGAAGG

4.9. Western Blot Analysis

Living adherent cells were harvested into Laemmli SDS sample lysis buffer, sonicated, and centrifuged at $10,000\times g$ for 10 min. The concentration of proteins was estimated by the BCA method; 100 mM DTT and 0.01% bromophenol were added to lysates before separation by SDS-PAGE (12% gels were used). Total protein concentrations were determined using bicinchoninic acid (BCA) protein assay kit, according to the manufacturer's instructions. The same protein amount (20 μ g) was loaded into each well. Membranes were blocked in 5% nonfat milk dissolved in TBS containing 0.1% Tween-20 for 1 h at room temperature (RT). Then, the membranes were probed overnight at 4 °C with primary antibodies. The respective proteins were detected after incubation with the horseradish peroxidase-conjugated secondary antibodies (1:2000) (Dako, Glostrup, Denmark), using an ECL system (Thermo Scientific, Rockford, IL, USA; according to the manufacturer's instructions).

4.10. Statistical Analysis

Statistical analysis was performed with the use of the STATISTICA 11 program, TIBCO Software Inc, Palo Alto CA, USA. ANOVA (analysis of variance) was used for the analysis of differences among three or more groups, followed by post hoc analysis (Tukey's honestly significant difference; HSD test). Normal distribution of the data was tested with the Shapiro–Wilk test. The *p*-value was stated as: * $0.01 < p < 0.05$; ** $0.001 < p < 0.01$ *** $p < 0.001$.

Supplementary Materials: The following figures are available online at <http://www.mdpi.com/1422-0067/21/8/2779/s1>, Figure S1: Amoeboid giant cells formed by DOX-treated MDA MB 231 cells grown on chamber slides on days 19–21 post-DOX-treatment; Figure S2: The increased extranuclear release of the TERT-enriched DNA in late giant cells post-DOX treatment maybe associated with unscheduled DNA synthesis.

Author Contributions: Conceptualization, J.E. and K.S. (Kristine Salmina); methodology, K.S. (Kristine Salmina), J.E., I.I., and P.P.; validation, K.S. (Kristine Salmina), A.B., I.I., K.S. (Karolina Staniak), and M.D.; formal analysis, K.S. (Kristine Salmina) and A.B.; investigation, J.E., K.S. (Kristine Salmina), A.B., I.I., P.P., K.S. (Karolina Staniak), F.R., D.P., and M.D.; resources, E.S. and D.P.; data curation, N.M.V.; writing—original draft preparation, K.S. (Kristine Salmina) and J.E.; writing—review and editing, J.E., N.M.V., and E.S.; visualization, K.S. (Kristine Salmina), F.R., N.M.V., and J.E.; supervision, J.E.; project administration, D.P.; and funding acquisition, K.S. (Kristine Salmina), D.P., E.S., P.P., and N.M.V. All authors have read and agreed to the published version of the manuscript.

Funding: This work was supported by a grant from the European Regional Development Fund (ERDF) projects No. 1.1.1.2/VIAA/3/19/463 for K.S., partly from No. 1.1.1.1/18/A/099 for J.E. and D.P., partly supported by the Polish National Science Center grant UMO-2015/17/B/NZ3/03531 for E.S., grant from the Ministerio de Ciencia, Innovación y Universidades of Spain (Grant: SAF2017-89791-R) for P.P., and the Natural Sciences PhD Student Scholarship from the University of Latvia Foundation to N.M.V.

Acknowledgments: The authors thank A. Goodkow and S. Demin (St. Petersburg) for discussion of the observations, Harry Scherthan (Munich) for the kind donation of the materials for FISH, Nuria Serra for help with selfie-digital PCR, Ramon Trullas (Barcelona) for providing access to the ddPCR platform, and Pawel Zayakin for reading the manuscript.

Conflicts of Interest: The authors declare no conflict of interest. The funders had no role in the design of the study; in the collection, analyses, or interpretation of data; in the writing of the manuscript, or in the decision to publish the results.

Abbreviations

DOX	Doxorubicin
MS	Mitotic slippage
IM	Inverted meiosis
HR	Homologous recombination
PML	Promyelocytic leukemia (protein)
DSB	Double-strand break
ALT	Alternative telomere lengthening
TMM	Telomere maintenance mechanism
EMT	Epithelial–mesenchymal transition
NT	Non-treated
FBS	Fetal bovine serum

References

- Riffell, J.L.; Zimmerman, C.; Khong, A.; McHardy, L.M.; Roberge, M. Effects of chemical manipulation of mitotic arrest and slippage on cancer cell survival and proliferation. *Cell Cycle* **2009**, *8*, 3025–3038. [[CrossRef](#)] [[PubMed](#)]
- Illidge, T.M.; Cragg, M.S.; Fringes, B.; Olive, P.; Erenpreisa, J.A. Polyploid giant cells provide a survival mechanism for p53 mutant cells after DNA damage. *Cell Biol. Int.* **2000**, *24*, 621–633. [[CrossRef](#)] [[PubMed](#)]
- Sundaram, M.; Guernsey, D.L.; Rajaraman, M.M.; Rajaraman, R. Neosis: A novel type of cell division in cancer. *Cancer Biol. Ther.* **2004**, *3*, 207–218. [[CrossRef](#)] [[PubMed](#)]
- Erenpreisa, J.; Cragg, M.S. Cancer: A matter of life cycle? *Cell Biol. Int.* **2007**, *31*, 1507–1510. [[CrossRef](#)] [[PubMed](#)]
- Zhang, S.; Mercado-Urbe, I.; Xing, Z.; Sun, B.; Kuang, J.; Liu, J. Generation of cancer stem-like cells through the formation of polyploid giant cancer cells. *Oncogene* **2014**, *33*, 116–128. [[CrossRef](#)] [[PubMed](#)]
- Díaz-Carballo, D.; Gustmann, S.; Jastrow, H.; Acikelli, A.H.; Dammann, P.; Klein, J.; Dembinski, U.; Bardenheuer, W.; Malak, S.; Araúzo-Bravo, M.J.; et al. Atypical cell populations associated with acquired resistance to cytostatics and cancer stem cell features: The role of mitochondria in nuclear encapsulation. *DNA Cell Biol.* **2014**, *33*, 749–774. [[CrossRef](#)] [[PubMed](#)]
- Díaz-Carballo, D.; Saka, S.; Klein, J.; Rennkamp, T.; Acikelli, A.H.; Malak, S.; Jastrow, H.; Wennemuth, G.; Tempfer, C.; Schmitz, I.; et al. A Distinct Oncogenetic Multinucleated Cancer Cell Serves as a Source of Stemness and Tumor Heterogeneity. *Cancer Res.* **2018**, *78*, 2318–2331. [[CrossRef](#)]
- Mosieniak, G.; Sliwiska, M.A.; Alster, O.; Strzeszewska, A.; Sunderland, P.; Piechota, M.; Was, H.; Sikora, E. Polyploidy Formation in Doxorubicin-Treated Cancer Cells Can Favor Escape from Senescence. *Neoplasia* **2015**, *17*, 882–893. [[CrossRef](#)]
- Salmina, K.; Jankevics, E.; Huna, A.; Perminov, D.; Radovica, I.; Klymenko, T.; Ivanov, A.; Jascenko, E.; Scherthan, H.; Cragg, M.; et al. Up-regulation of the embryonic self-renewal network through reversible polyploidy in irradiated p53-mutant tumour cells. *Exp. Cell Res.* **2010**, *316*, 2099–2112. [[CrossRef](#)]
- Erenpreisa, J.; Salmina, K.; Belyayev, A.; Inashkina, I.; Cragg, M.S. Survival at the Brink. In *Autophagy: Cancer, Other Pathologies, Inflammation, Immunity, Infection, and Aging*; Elsevier: Amsterdam, The Netherlands, 2017; pp. 275–294, ISBN 9780128121467.
- Shaffer, S.M.; Dunagin, M.C.; Torborg, S.R.; Torre, E.A.; Emert, B.; Krepler, C.; Beqiri, M.; Sproesser, K.; Brafford, P.A.; Xiao, M.; et al. Rare cell variability and drug-induced reprogramming as a mode of cancer drug resistance. *Nature* **2017**, *546*, 431–435. [[CrossRef](#)]
- Salmina, K.; Huna, A.; Kalejs, M.; Pjanova, D.; Scherthan, H.; Cragg, M.S.; Erenpreisa, J. The Cancer Aneuploidy Paradox: In the Light of Evolution. *Genes* **2019**, *10*, 83. [[CrossRef](#)] [[PubMed](#)]
- Mirzayans, R.; Andrais, B.; Scott, A.; Wang, Y.W.; Kumar, P.; Murray, D. Multinucleated Giant Cancer Cells Produced in Response to Ionizing Radiation Retain Viability and Replicate Their Genome. *Int. J. Mol. Sci.* **2017**, *18*, 360. [[CrossRef](#)] [[PubMed](#)]
- Mirzayans, R.; Andrais, B.; Murray, D. Roles of Polyploid/Multinucleated Giant Cancer Cells in Metastasis and Disease Relapse Following Anticancer Treatment. *Cancers* **2018**, *10*, 118. [[CrossRef](#)] [[PubMed](#)]

15. Chen, J.; Niu, N.; Zhang, J.; Qi, L.; Shen, W.; Donkena, K.V.; Feng, Z.; Liu, J. Polyploid Giant Cancer Cells (PGCCs): The Evil Roots of Cancer. *Curr. Cancer Drug Targets* **2019**, *19*, 360–367. [[CrossRef](#)] [[PubMed](#)]
16. Raab, M.; Krämer, A.; Hehlhans, S.; Sanhaji, M.; Kurunci-Csacsko, E.; Dötsch, C.; Bug, G.; Ottmann, O.; Becker, S.; Pahl, F.; et al. Mitotic arrest and slippage induced by pharmacological inhibition of Polo-like kinase 1. *Mol. Oncol.* **2015**, *9*, 140–154. [[CrossRef](#)]
17. Rajaraman, R.; Guernsey, D.L.; Rajaraman, M.M.; Rajaraman, S.R. Stem cells, senescence, neosis and self-renewal in cancer. *Cancer Cell Int.* **2006**, *6*, 25. [[CrossRef](#)]
18. Puig, P.-E.; Guilly, M.-N.; Bouchot, A.; Droin, N.; Cathelin, D.; Bouyer, F.; Favier, L.; Ghiringhelli, F.; Kroemer, G.; Solary, E.; et al. Tumor cells can escape DNA-damaging cisplatin through DNA endoreduplication and reversible polyploidy. *Cell Biol. Int.* **2008**, *32*, 1031–1043. [[CrossRef](#)]
19. Sliwinska, M.A.; Mosieniak, G.; Wolanin, K.; Babik, A.; Piwocka, K.; Magalska, A.; Szczepanowska, J.; Fronk, J.; Sikora, E. Induction of senescence with doxorubicin leads to increased genomic instability of HCT116 cells. *Mech. Ageing Dev.* **2009**, *130*, 24–32. [[CrossRef](#)]
20. Huna, A.; Salmina, K.; Erenpreisa, J.; Vazquez-Martin, A.; Krigerts, J.; Inashkina, I.; Gerashchenko, B.I.; Townsend, P.A.; Cragg, M.S.; Jackson, T.R. Role of stress-activated OCT4A in the cell fate decisions of embryonal carcinoma cells treated with etoposide. *Cell Cycle* **2015**, *14*, 2969–2984. [[CrossRef](#)]
21. Sikora, E.; Mosieniak, G.; Sliwinska, M.A. Morphological and Functional Characteristic of Senescent Cancer Cells. *Curr. Drug Targets* **2016**, *17*, 377–387. [[CrossRef](#)]
22. Leikam, C.; Hufnagel, A.; Walz, S.; Kneitz, S.; Fekete, A.; Müller, M.J.; Eilers, M.; Schartl, M.; Meierjohann, S. Cystathionase mediates senescence evasion in melanocytes and melanoma cells. *Oncogene* **2014**, *33*, 771–782. [[CrossRef](#)] [[PubMed](#)]
23. Was, H.; Barszcz, K.; Czarnecka, J.; Kowalczyk, A.; Bernas, T.; Uzarowska, E.; Koza, P.; Klejman, A.; Piwocka, K.; Kaminska, B.; et al. Bafilomycin A1 triggers proliferative potential of senescent cancer cells in vitro and in NOD/SCID mice. *Oncotarget* **2017**, *8*, 9303–9322. [[CrossRef](#)] [[PubMed](#)]
24. Mosteiro, L.; Pantoja, C.; de Martino, A.; Serrano, M. Senescence promotes in vivo reprogramming through p16 and IL-6. *Ageing Cell* **2018**, *17*, e12711. [[CrossRef](#)]
25. Milanovic, M.; Fan, D.N.Y.; Belenki, D.; Däbritz, J.H.M.; Zhao, Z.; Yu, Y.; Dörr, J.R.; Dimitrova, L.; Lenze, D.; Monteiro Barbosa, I.A.; et al. Senescence-associated reprogramming promotes cancer stemness. *Nature* **2018**, *553*, 96–100. [[CrossRef](#)] [[PubMed](#)]
26. Gerashchenko, B.I.; Salmina, K.; Eglitis, J.; Huna, A.; Grjunberga, V.; Erenpreisa, J. Disentangling the aneuploidy and senescence paradoxes: A study of triploid breast cancers non-responsive to neoadjuvant therapy. *Histochem. Cell Biol.* **2016**, *145*, 497–508. [[CrossRef](#)] [[PubMed](#)]
27. Gerashchenko, B.I.; Salmina, K.; Krigerts, J.; Erenpreisa, J.; Babsky, A.M. Induced polyploidy and sorting of damaged DNA by micronucleation in radioresistant rat liver epithelial stem-like cells exposed to X-rays. *Probl. Radiac. Med. Radiobiol.* **2019**, *24*, 220–234. [[CrossRef](#)]
28. Mirzayans, R.; Murray, D. Intratumor Heterogeneity and Therapy Resistance: Contributions of Dormancy, Apoptosis Reversal (Anastasis) and Cell Fusion to Disease Recurrence. *Int. J. Mol. Sci.* **2020**, *21*, 1308. [[CrossRef](#)]
29. Pluquet, O.; Abbadie, C.; Coqueret, O. Connecting cancer relapse with senescence. *Cancer Lett.* **2019**, *463*, 50–58. [[CrossRef](#)]
30. Krtolica, A.; Campisi, J. Cancer and aging: A model for the cancer promoting effects of the aging stroma. *Int. J. Biochem. Cell Biol.* **2002**, *34*, 1401–1414. [[CrossRef](#)]
31. Erenpreisa, J.; Cragg, M.S. Three steps to the immortality of cancer cells: Senescence, polyploidy and self-renewal. *Cancer Cell Int.* **2013**, *13*, 92. [[CrossRef](#)]
32. Erenpreisa, J.; Salmina, K.; Cragg, M.S. Accelerated Senescence of Cancer Stem Cells: A Failure to Thrive or a Route to Survival? In *Senescence Physiology or Pathology*; Dorszewska, J., Kozubski, W., Eds.; InTechOpen: London, UK, 2017; ISBN 9789535134619.
33. Bharadwaj, D.; Mandal, M. Senescence in polyploid giant cancer cells: A road that leads to chemoresistance. *Cytokine Growth Factor Rev.* **2020**, *52*, 68–75. [[CrossRef](#)] [[PubMed](#)]
34. Amend, S.R.; Torga, G.; Lin, K.-C.; Kostecka, L.G.; de Marzo, A.; Austin, R.H.; Pienta, K.J. Polyploid giant cancer cells: Unrecognized actuators of tumorigenesis, metastasis, and resistance. *Prostate* **2019**, *79*, 1489–1497. [[CrossRef](#)]

35. Ivanov, A.; Pawlikowski, J.; Manoharan, I.; van Tuyn, J.; Nelson, D.M.; Rai, T.S.; Shah, P.P.; Hewitt, G.; Korolchuk, V.I.; Passos, J.F.; et al. Lysosome-mediated processing of chromatin in senescence. *J. Cell Biol.* **2013**, *202*, 129–143. [[CrossRef](#)] [[PubMed](#)]
36. Dou, Z.; Xu, C.; Donahue, G.; Shimi, T.; Pan, J.-A.; Zhu, J.; Ivanov, A.; Capell, B.C.; Drake, A.M.; Shah, P.P.; et al. Autophagy mediates degradation of nuclear lamina. *Nature* **2015**, *527*, 105–109. [[CrossRef](#)] [[PubMed](#)]
37. Dou, Z.; Ghosh, K.; Vizioli, M.G.; Zhu, J.; Sen, P.; Wangensteen, K.J.; Simithy, J.; Lan, Y.; Lin, Y.; Zhou, Z.; et al. Cytoplasmic chromatin triggers inflammation in senescence and cancer. *Nature* **2017**, *550*, 402–406. [[CrossRef](#)] [[PubMed](#)]
38. Lan, Y.Y.; Londoño, D.; Bouley, R.; Rooney, M.S.; Hacoheh, N. Dnase2a deficiency uncovers lysosomal clearance of damaged nuclear DNA via autophagy. *Cell Rep.* **2014**, *9*, 180–192. [[CrossRef](#)]
39. Lan, Y.Y.; Heather, J.M.; Eisenhaure, T.; Garris, C.S.; Lieb, D.; Raychowdhury, R.; Hacoheh, N. Extranuclear DNA accumulates in aged cells and contributes to senescence and inflammation. *Aging Cell* **2019**, *18*, e12901. [[CrossRef](#)]
40. Glück, S.; Guey, B.; Gulen, M.F.; Wolter, K.; Kang, T.-W.; Schmacke, N.A.; Bridgeman, A.; Rehwinkel, J.; Zender, L.; Ablasser, A. Innate immune sensing of cytosolic chromatin fragments through cGAS promotes senescence. *Nat. Cell Biol.* **2017**, *19*, 1061–1070. [[CrossRef](#)]
41. Jakhar, R.; Luijten, M.N.H.; Wong, A.X.F.; Cheng, B.; Guo, K.; Neo, S.P.; Au, B.; Kulkarni, M.; Lim, K.J.; Maimaiti, J.; et al. Autophagy Governs Protumorigenic Effects of Mitotic Slippage-induced Senescence. *Mol. Cancer Res.* **2018**, *16*, 1625–1640. [[CrossRef](#)]
42. Bakhoun, S.F.; Ngo, B.; Laughney, A.M.; Cavallo, J.-A.; Murphy, C.J.; Ly, P.; Shah, P.; Sriram, R.K.; Watkins, T.B.K.; Taunk, N.K.; et al. Chromosomal instability drives metastasis through a cytosolic DNA response. *Nature* **2018**, *553*, 467–472. [[CrossRef](#)]
43. Erenpreisa, J.; Cragg, M.S.; Salmina, K.; Hausmann, M.; Scherthan, H. The role of meiotic cohesin REC8 in chromosome segregation in gamma irradiation-induced endopolyploid tumour cells. *Exp. Cell Res.* **2009**, *315*, 2593–2603. [[CrossRef](#)] [[PubMed](#)]
44. Ianzini, F.; Kosmacek, E.A.; Nelson, E.S.; Napoli, E.; Erenpreisa, J.; Kalejs, M.; Mackey, M.A. Activation of meiosis-specific genes is associated with depolyploidization of human tumor cells following radiation-induced mitotic catastrophe. *Cancer Res.* **2009**, *69*, 2296–2304. [[CrossRef](#)] [[PubMed](#)]
45. Cho, H.; Noh, K.H.; Chung, J.-Y.; Takikita, M.; Chung, E.J.; Kim, B.W.; Hewitt, S.M.; Kim, T.W.; Kim, J.-H. Synaptonemal complex protein 3 is a prognostic marker in cervical cancer. *PLoS ONE* **2014**, *9*, e98712. [[CrossRef](#)] [[PubMed](#)]
46. Lindsey, S.F.; Byrnes, D.M.; Eller, M.S.; Rosa, A.M.; Dabas, N.; Escandon, J.; Grichnik, J.M. Potential role of meiosis proteins in melanoma chromosomal instability. *J. Skin Cancer* **2013**, *2013*, 190109. [[CrossRef](#)]
47. Yant, L.; Bomblies, K. Genome management and mismanagement—cell-level opportunities and challenges of whole-genome duplication. *Genes Dev.* **2015**, *29*, 2405–2419. [[CrossRef](#)]
48. Tacar, O.; Sriamornsak, P.; Dass, C.R. Doxorubicin: An update on anticancer molecular action, toxicity and novel drug delivery systems. *J. Pharm. Pharmacol.* **2013**, *65*, 157–170. [[CrossRef](#)]
49. Bojko, A.; Czarnecka-Herok, J.; Charzynska, A.; Dabrowski, M.; Sikora, E. Diversity of the Senescence Phenotype of Cancer Cells Treated with Chemotherapeutic Agents. *Cells* **2019**, *8*, 1501. [[CrossRef](#)]
50. Walen, K.H. Spontaneous cell transformation: Karyoplasts derived from multinucleated cells produce new cell growth in senescent human epithelial cell cultures. *In Vitro Cell. Dev. Biol. Anim.* **2004**, *40*, 150–158. [[CrossRef](#)]
51. Erenpreisa, J.; Cragg, M.S. Life-Cycle Features of Tumour Cells. In *Evolutionary Biology from Concept to Application*; Pontarotti, P., Ed.; Springer: Berlin/Heidelberg, Germany, 2008; Volume 75, pp. 61–71, ISBN 9783540789925.
52. Fais, S.; Fauvarque, M.-O. TM9 and cannibalism: How to learn more about cancer by studying amoebae and invertebrates. *Trends Mol. Med.* **2012**, *18*, 4–5. [[CrossRef](#)]
53. Erenpreisa, J.; Giuliani, A.; Vinogradov, A.E.; Anatskaya, O.V. Stress-induced polyploidy shifts somatic cells towards a pro-tumorigenic unicellular gene transcription network. *Cancer Hypotheses* **2018**, *1*, 1–20, CH-ErenpreisaFinal2-DWFE.pdf.
54. Hecht, I.; Bar-El, Y.; Balmer, F.; Natan, S.; Tsarfaty, I.; Schweitzer, F.; Ben-Jacob, E. Tumor invasion optimization by mesenchymal-amoeboid heterogeneity. *Sci. Rep.* **2015**, *5*, 10622. [[CrossRef](#)]

55. Leblanc, J.; Zhang, X.; McKee, D.; Wang, Z.-B.; Li, R.; Ma, C.; Sun, Q.-Y.; Liu, X.J. The small GTPase Cdc42 promotes membrane protrusion during polar body emission via ARP2-nucleated actin polymerization. *Mol. Hum. Reprod.* **2011**, *17*, 305–316. [[CrossRef](#)] [[PubMed](#)]
56. Yamao, M.; Naoki, H.; Kunida, K.; Aoki, K.; Matsuda, M.; Ishii, S. Distinct predictive performance of Rac1 and Cdc42 in cell migration. *Sci. Rep.* **2015**, *5*, 17527. [[CrossRef](#)] [[PubMed](#)]
57. Palm, W.; de Lange, T. How shelterin protects mammalian telomeres. *Annu. Rev. Genet.* **2008**, *42*, 301–334. [[CrossRef](#)] [[PubMed](#)]
58. De Lange, T. Shelterin-Mediated Telomere Protection. *Annu. Rev. Genet.* **2018**, *52*, 223–247. [[CrossRef](#)]
59. Davoli, T.; Denchi, E.L.; de Lange, T. Persistent telomere damage induces bypass of mitosis and tetraploidy. *Cell* **2010**, *141*, 81–93. [[CrossRef](#)]
60. Davoli, T.; de Lange, T. Telomere-driven tetraploidization occurs in human cells undergoing crisis and promotes transformation of mouse cells. *Cancer Cell* **2012**, *21*, 765–776. [[CrossRef](#)]
61. Chung, I.; Osterwald, S.; Deeg, K.I.; Rippe, K. PML body meets telomere: The beginning of an ALternate ending? *Nucleus* **2012**, *3*, 263–275. [[CrossRef](#)]
62. Andreyeva, E.N.; Kolesnikova, T.D.; Belyaeva, E.S.; Glaser, R.L.; Zhimulev, I.F. Local DNA underreplication correlates with accumulation of phosphorylated H2Av in the *Drosophila melanogaster* polytene chromosomes. *Chromosome Res.* **2008**, *16*, 851–862. [[CrossRef](#)]
63. Glover, L.; Alford, S.; Horn, D. DNA break site at fragile subtelomeres determines probability and mechanism of antigenic variation in African trypanosomes. *PLoS Pathog.* **2013**, *9*, e1003260. [[CrossRef](#)]
64. Arnoult, N.; Karlseder, J. ALT telomeres borrow from meiosis to get moving. *Cell* **2014**, *159*, 11–12. [[CrossRef](#)] [[PubMed](#)]
65. Hewitt, G.; Carroll, B.; Sarallah, R.; Correia-Melo, C.; Ogrodnik, M.; Nelson, G.; Otten, E.G.; Manni, D.; Antrobus, R.; Morgan, B.A.; et al. SQSTM1/p62 mediates crosstalk between autophagy and the UPS in DNA repair. *Autophagy* **2016**, *12*, 1917–1930. [[CrossRef](#)] [[PubMed](#)]
66. Niculescu, V.F. The reproductive life cycle of cancer: Hypotheses of cell of origin, TP53 drivers and stem cell conversions in the light of the atavistic cancer cell theory. *Med. Hypotheses* **2019**, *123*, 19–23. [[CrossRef](#)] [[PubMed](#)]
67. Niculescu, V.F. Carcinogenesis: Recent Insights in Protist Stem Cell Biology Lead To a Better Understanding of Atavistic Mechanisms Implied in Cancer Development. *MOJ Tumor Res.* **2018**, *1*, 00004. [[CrossRef](#)]
68. De Vitis, M.; Berardinelli, F.; Sgura, A. Telomere Length Maintenance in Cancer: At the Crossroad between Telomerase and Alternative Lengthening of Telomeres (ALT). *Int. J. Mol. Sci.* **2018**, *19*, 606. [[CrossRef](#)]
69. Hu, Y.; Shi, G.; Zhang, L.; Li, F.; Jiang, Y.; Jiang, S.; Ma, W.; Zhao, Y.; Songyang, Z.; Huang, J. Switch telomerase to ALT mechanism by inducing telomeric DNA damages and dysfunction of ATRX and DAXX. *Sci. Rep.* **2016**, *6*, 32280. [[CrossRef](#)]
70. Dilley, R.L.; Greenberg, R.A. ALternative Telomere Maintenance and Cancer. *Trends Cancer Res.* **2015**, *1*, 145–156. [[CrossRef](#)]
71. Xue, Y.; Li, L.; Zhang, D.; Wu, K.; Chen, Y.; Zeng, J.; Wang, X.; He, D. Twisted epithelial-to-mesenchymal transition promotes progression of surviving bladder cancer T24 cells with hTERT-dysfunction. *PLoS ONE* **2011**, *6*, e27748. [[CrossRef](#)]
72. Yong, J.W.Y.; Yeo, X.; Khan, M.M.; Lee, M.B.; Hande, M.P. Stable expression of promyelocytic leukaemia (PML) protein in telomerase positive MCF7 cells results in alternative lengthening of telomeres phenotype. *Genome Integr.* **2012**, *3*, 5. [[CrossRef](#)]
73. Pickett, H.A.; Cesare, A.J.; Johnston, R.L.; Neumann, A.A.; Reddel, R.R. Control of telomere length by a trimming mechanism that involves generation of t-circles. *EMBO J.* **2009**, *28*, 799–809. [[CrossRef](#)]
74. Kalejs, M.; Erenpreisa, J. Cancer/testis antigens and gametogenesis: A review and “brain-storming” session. *Cancer Cell Int.* **2005**, *5*, 4. [[CrossRef](#)] [[PubMed](#)]
75. Kalejs, M.; Ivanov, A.; Plakhins, G.; Cragg, M.S.; Emzinsh, D.; Illidge, T.M.; Erenpreisa, J. Upregulation of meiosis-specific genes in lymphoma cell lines following genotoxic insult and induction of mitotic catastrophe. *BMC Cancer* **2006**, *6*, 6. [[CrossRef](#)] [[PubMed](#)]
76. Erenpreisa, J.; Cragg, M.S. MOS, aneuploidy and the ploidy cycle of cancer cells. *Oncogene* **2010**, *29*, 5447–5451. [[CrossRef](#)] [[PubMed](#)]
77. Erenpreisa, J.; Salmina, K.; Huna, A.; Jackson, T.R.; Vazquez-Martin, A.; Cragg, M.S. The “virgin birth”, polyploidy, and the origin of cancer. *Oncoscience* **2015**, *2*, 3–14. [[CrossRef](#)]

78. Niu, N.; Mercado-Urbe, I.; Liu, J. Dedifferentiation into blastomere-like cancer stem cells via formation of polyploid giant cancer cells. *Oncogene* **2017**, *36*, 4887–4900. [[CrossRef](#)]
79. Liu, J. The dualistic origin of human tumors. *Semin. Cancer Biol.* **2018**, *53*, 1–16. [[CrossRef](#)]
80. Old, L.J. Cancer/testis (CT) antigens—A new link between gametogenesis and cancer. *Cancer Immun.* **2001**, *1*, 1.
81. Erenpreisa, J.; Kalejs, M.; Cragg, M.S. Mitotic catastrophe and endomitosis in tumour cells: An evolutionary key to a molecular solution. *Cell Biol. Int.* **2005**, *29*, 1012–1018. [[CrossRef](#)]
82. McFarlane, R.J.; Wakeman, J.A. Meiosis-like Functions in Oncogenesis: A New View of Cancer. *Cancer Res.* **2017**, *77*, 5712–5716. [[CrossRef](#)]
83. Hofstatter, P.G.; Lahr, D.J.G. All Eukaryotes Are Sexual, unless Proven Otherwise: Many So-Called Asexuals Present Meiotic Machinery and Might Be Able to Have Sex. *Bioessays* **2019**, *41*, 1800246. [[CrossRef](#)]
84. Forche, A.; Alby, K.; Schaefer, D.; Johnson, A.D.; Berman, J.; Bennett, R.J. The parasexual cycle in *Candida albicans* provides an alternative pathway to meiosis for the formation of recombinant strains. *PLoS Biol.* **2008**, *6*, e110. [[CrossRef](#)] [[PubMed](#)]
85. Viera, A.; Page, J.; Rufas, J.S. Inverted meiosis: The true bugs as a model to study. *Genome Dyn.* **2009**, *5*, 137–156. [[PubMed](#)]
86. Kuznetsova, V.G. The Chromosomes of the Holokinetic Type and Their Distribution among Insects and Other Invertebrate Animals. In *Kariosistematika Bespozvonochnykh Zhivotnykh (Karyosystematics of Invertebrates)*; Nauka: Leningrad, Russia, 1979; pp. 5–19.
87. Solari, A.J. Primitive forms of meiosis: The possible evolution of meiosis. *Biocell* **2002**, *26*, 1–13.
88. Heckmann, S.; Jankowska, M.; Schubert, V.; Kumke, K.; Ma, W.; Houben, A. Alternative meiotic chromatid segregation in the holocentric plant *Luzula elegans*. *Nat. Commun.* **2014**, *5*, 4979. [[CrossRef](#)] [[PubMed](#)]
89. Bogdanov, Y.F. Inverted meiosis and its place in the evolution of sexual reproduction pathways. *Russ. J. Genet.* **2016**, *52*, 473–490. [[CrossRef](#)]
90. Loidl, J. Conservation and Variability of Meiosis Across the Eukaryotes. *Annu. Rev. Genet.* **2016**, *50*, 293–316. [[CrossRef](#)]
91. Ottolini, C.S.; Newnham, L.; Capalbo, A.; Natesan, S.A.; Joshi, H.A.; Cimadomo, D.; Griffin, D.K.; Sage, K.; Summers, M.C.; Thornhill, A.R.; et al. Genome-wide maps of recombination and chromosome segregation in human oocytes and embryos show selection for maternal recombination rates. *Nat. Genet.* **2015**, *47*, 727–735. [[CrossRef](#)]
92. Ottolini, C.S. Chromosome Segregation and Recombination in Human Meiosis: Clinical Applications and Insight Into Disjunction Errors. Ph.D. Thesis, University of Kent, Canterbury, UK, 2015. Doctor of Philosophy.
93. Perrem, K.; Colgin, L.M.; Neumann, A.A.; Yeager, T.R.; Reddel, R.R. Coexistence of alternative lengthening of telomeres and telomerase in hTERT-transfected GM847 cells. *Mol. Cell. Biol.* **2001**, *21*, 3862–3875. [[CrossRef](#)]
94. Chiodi, I.; Mondello, C. Telomere-independent functions of telomerase in nuclei, cytoplasm, and mitochondria. *Front. Oncol.* **2012**, *2*, 133. [[CrossRef](#)]
95. Maciver, S.K. Asexual Amoebae Escape Muller’s Ratchet through Polyploidy. *Trends Parasitol.* **2016**, *32*, 855–862. [[CrossRef](#)]
96. Khan, N.A.; Siddiqui, R. Is there evidence of sexual reproduction (meiosis) in *Acanthamoeba*? *Pathog. Glob. Health* **2015**, *109*, 193–195. [[CrossRef](#)] [[PubMed](#)]
97. Demin, S.Y.; Berdieva, M.A.; Goodkov, A.V. Cyclic Polyploidy in Obligate Agamic Amoebae. *Cell Tissue Biol.* **2019**, *13*, 242–246. [[CrossRef](#)]
98. Goodkov, A.V.; Berdieva, M.A.; Podlipaeva, Y.I.; Demin, S.Y. The Chromatin Extrusion Phenomenon in *Amoeba proteus* Cell Cycle. *J. Eukaryot. Microbiol.* **2019**, *67*, 203–208. [[CrossRef](#)] [[PubMed](#)]
99. Berdieva, M.; Demin, S.; Goodkov, A. *Amoeba proteus* and ploidy cycles: From simple model to complex issues. *Protistology* **2019**, *13*, 166–173. [[CrossRef](#)]
100. Archetti, M. Inverted meiosis and the evolution of sex by loss of complementation. *J. Evol. Biol.* **2019**. [[CrossRef](#)]
101. Zybina, T.G. Genome variation in the trophoblast cell lifespan: Diploidy, polyteny, depolytenization, genome segregation. *WJMG* **2014**, *4*, 77. [[CrossRef](#)]
102. Zybina, T.G.; Stein, G.I.; Pozhariski, K.M.; Zybina, E.V. Invasion and genome reproduction of the trophoblast cells of placenta junctional zone in the field vole, *Microtus rossiaemeridionalis*. *Cell Biol. Int.* **2014**, *38*, 136–143. [[CrossRef](#)]

103. Campisi, J.; d'Adda di Fagagna, F. Cellular senescence: When bad things happen to good cells. *Nat. Rev. Mol. Cell Biol.* **2007**, *8*, 729–740. [[CrossRef](#)]
104. Jackson, T.R.; Salmina, K.; Huna, A.; Inashkina, I.; Jankevics, E.; Riekstina, U.; Kalnina, Z.; Ivanov, A.; Townsend, P.A.; Cragg, M.S.; et al. DNA damage causes TP53-dependent coupling of self-renewal and senescence pathways in embryonal carcinoma cells. *Cell Cycle* **2013**, *12*, 430–441. [[CrossRef](#)]
105. Narath, R.; Lörch, T.; Greulich-Bode, K.M.; Boukamp, P.; Ambros, P.F. Automatic telomere length measurements in interphase nuclei by IQ-FISH. *Cytometry A* **2005**, *68*, 113–120. [[CrossRef](#)]
106. Scherthan, H.; Sotnik, N.; Peper, M.; Schrock, G.; Azizova, T.; Abend, M. Telomere Length in Aged Mayak PA Nuclear Workers Chronically Exposed to Internal Alpha and External Gamma Radiation. *Radiat. Res.* **2016**, *185*, 658–667. [[CrossRef](#)] [[PubMed](#)]
107. Dimri, G.P.; Lee, X.; Basile, G.; Acosta, M.; Scott, G.; Roskelley, C.; Medrano, E.E.; Linskens, M.; Rubelj, I.; Pereira-Smith, O. A biomarker that identifies senescent human cells in culture and in aging skin in vivo. *Proc. Natl. Acad. Sci. USA* **1995**, *92*, 9363–9367. [[CrossRef](#)] [[PubMed](#)]
108. Schneider, C.A.; Rasband, W.S.; Eliceiri, K.W. NIH Image to ImageJ: 25 years of image analysis. *Nat. Methods* **2012**, *9*, 671–675. [[CrossRef](#)] [[PubMed](#)]
109. Asadi, M.H.; Khalifeh, K.; Mowla, S.J. OCT4 spliced variants are highly expressed in brain cancer tissues and inhibition of OCT4B1 causes G2/M arrest in brain cancer cells. *J. Neurooncol.* **2016**, *130*, 455–463. [[CrossRef](#)]
110. Vandesompele, J.; De Preter, K.; Pattyn, F.; Poppe, B.; Van Roy, N.; De Paepe, A.; Speleman, F. Accurate normalization of real-time quantitative RT-PCR data by geometric averaging of multiple internal control genes. *Genome Biol.* **2002**, *3*, RESEARCH0034. [[CrossRef](#)]
111. Podlesniy, P.; Trullas, R. Absolute measurement of gene transcripts with Selfie-digital PCR. *Sci. Rep.* **2017**, *7*, 8328. [[CrossRef](#)]



© 2020 by the authors. Licensee MDPI, Basel, Switzerland. This article is an open access article distributed under the terms and conditions of the Creative Commons Attribution (CC BY) license (<http://creativecommons.org/licenses/by/4.0/>).

3.6.2. The trophoblast-like capacity of supergiant PGCCs, and its cooperation with the reproductive PGCC function in the MDA-MB-231 model

Building on the results of the previous study, the features of reproductive and supergiant PGCCs of DOX-treated MDA-MB-231 cells were studied. Four time-points after DOX treatment were selected to be compared against non-treated cells - days 5, 8, 16 and 22. Immunofluorescence showed hallmarks of soma-germ transition during mitotic slippage (nuclear translocation of the embryonal stemness factor OCT4A and the expression of the MOS and EMI2 oocyte meiosis genes in the nucleus). Furthermore, the Hippo pathway was observed to be inactivated by YAP1/TEAD1, linking cell fate change with the sensing of cytosolic DNA in MS.

Bioinformatic comparison of non-treated and DOX-treated MDA-MB-231 transcriptomes, carried out by me, revealed bivalent gene upregulation and a widespread enrichment of GO modules related to cytosolic DNA sensing and the pro-inflammatory immune response characteristic of senescence (Turzanski et al., 2004; Wojtuszkiewicz et al., 2016). Furthermore, GO modules of reproduction (including multi-organism development, female pregnancy and placenta development) with placental genes were also activated. Clonogenicity assays performed by Dr. K. Salmina also showed the trophoblast lineage specifier (Y. Liu et al., 2020) CDC42 (identified in giant PGCCs and their nearby-located offspring by immunofluorescence) to be crucial for DOX-treated cell regrowth.

Overall, the results indicate that the process linking reversible polyploidization and the subsequent support of the offspring via the secretome of senescent supergiant PGCCs may be an atavistic cancer cell “pregnancy” system, with a “parthenogenetic” and “trophoblastic” component. Both components could potentially develop in the same PGCC.



Article

The Role of Mitotic Slippage in Creating a “Female Pregnancy-like System” in a Single Polyploid Giant Cancer Cell

Kristine Salmina ^{1,*}, Ninel Miriam Vainshelbaum ^{1,2}, Madara Kreishmane ¹, Inna Inashkina ¹,
Mark Steven Cragg ³, Dace Pjanova ¹ and Jekaterina Erenpreisa ^{1,*}

¹ Cancer Research Division, Latvian Biomedical Research and Study Centre, LV-1067 Riga, Latvia

² Faculty of Biology, The University of Latvia, LV-1586 Riga, Latvia

³ Centre for Cancer Immunology, Faculty of Medicine, University of Southampton, Southampton SO16 6YD, UK

* Correspondence: salmina.kristine@gmail.com (K.S.); katrina@biomed.lu.lv (J.E.)

Abstract: In our recent work, we observed that triple-negative breast cancer MDA-MB-231 cells respond to doxorubicin (DOX) via “mitotic slippage” (MS), discarding cytosolic damaged DNA during the process that provides their resistance to this genotoxic treatment. We also noted two populations of polyploid giant cells: those budding surviving offspring, versus those reaching huge ploidy by repeated MS and persisting for several weeks. Their separate roles in the recovery from treatment remained unclear. The current study was devoted to characterising the origin and relationship of these two sub-populations in the context of MS. MS was hallmarked by the emergence of nuclear YAP1/OCT4A/MOS/EMI2-positivity featuring a soma-germ transition to the meiotic-metaphase-arrested “maternal germ cell”. In silico, the link between modules identified in the inflammatory innate immune response to cytosolic DNA and the reproductive module of female pregnancy (upregulating placenta developmental genes) was observed in polyploid giant cells. Asymmetry of the two subnuclei types, one repairing DNA and releasing buds enriched by CDC42/ACTIN/TUBULIN and the other persisting and degrading DNA in a polyploid giant cell, was revealed. We propose that when arrested in MS, a “maternal cancer germ cell” may be parthenogenetically stimulated by the placental proto-oncogene parathyroid-hormone-like-hormone, increasing calcium, thus creating a “female pregnancy-like” system within a single polyploid giant cancer cell.

Keywords: cancer; polyploid giant cell; resistance to treatment; mitotic slippage; soma-germ transition; maternal germ cell; innate immune response; placental developmental genes; parthenogenesis; budding; female pregnancy system



Citation: Salmina, K.; Vainshelbaum, N.M.; Kreishmane, M.; Inashkina, I.; Cragg, M.S.; Pjanova, D.; Erenpreisa, J. The Role of Mitotic Slippage in Creating a “Female Pregnancy-like System” in a Single Polyploid Giant Cancer Cell. *Int. J. Mol. Sci.* **2023**, *24*, 3237. <https://doi.org/10.3390/ijms24043237>

Academic Editor: Daniela Grimm

Received: 2 January 2023

Revised: 30 January 2023

Accepted: 31 January 2023

Published: 6 February 2023



Copyright: © 2023 by the authors. Licensee MDPI, Basel, Switzerland. This article is an open access article distributed under the terms and conditions of the Creative Commons Attribution (CC BY) license (<https://creativecommons.org/licenses/by/4.0/>).

1. Introduction

After Cancer-Testis-Antigens (CTA) were discovered in ovaries and placenta and the link between cancer and gametogenesis became apparent [1,2] Lloyd J. Old published an Editorial entitled “Cancer Is a Somatic Cell Pregnancy” [3]. Recently, we reported mitotic slippage (MS) as a means of discarding cytosolic damaged DNA and a key process for cancer cells undergoing recovery from genotoxic treatment by reversible senescence, polyploidy, and alternative telomere repair [4]. The experiments were carried out in vitro on the triple-negative breast cancer cell-line MDA-MB-231 in response to doxorubicin (DOX). Among other observations, we noted super-giant cells, which reach huge ploidy and display an amoeboid phenotype. They diverge in DNA content from the smaller, de-polyploidising recovery fraction and persist for a few weeks. Their role in the recovery process remained unclear. Therefore, here we devoted a deeper analysis to the origin and function of these two populations in reference to MS over the recovery time-course post-DOX treatment, combining immunofluorescence with bioinformatic methods. The link between the transcriptional modules sensing inflammatory innate immune responses to

cytosolic DNA, including the response to viral and bacterial infection and host defence, with the emergence of reproductive modules of maternal soma-to-germ transition, including the maternal placenta development pathways in super-giant cancer cells, was observed bioinformatically and confirmed by immunofluorescence analysis. Thus, we revealed a system of somatic cell pregnancy for cancer as postulated by L.J. Old [3] within a single multinucleated polyploidy giant cell during the response to genotoxic drugs. The data are discussed in view of recent discoveries regarding the role of endogenous retrovirus (HERV) domestication in human evolutionary placental development [5], HERV activation in stressed cancer cells [6], participation in cancer metastases [7,8], and the well-known poor prognosis implications of placental markers in many human cancers. Finally, the implication of these findings for cancer treatment is briefly discussed.

2. Results

2.1. DNA Cytometry to Identify Appropriate Time Points for Studying the Origin and Features of Small Versus Super-Giant Polyploid Cells by Bulk Transcriptomic Analysis

Based upon DNA cytometry and mitotic counts, we selected time points where we could collect predominantly small and predominantly giant and super-giant polyploid cells. With this approach, in the response of MDA-MB-231 cells to DOX (100 μ M, 24 h) treatment, we selected four time points (Figure 1A): (1) non-treated (NT) cells showing a normal cell cycle; (2) the period of replicative stress, S-G2-delay, and DNA under-replication (days 4–5) where MS begins (red-dash circled on Figure 1A; resulting in the first double peak, <8C and 8C; the cycles of MS, increasing ploidy, were further repeating as seen on day 8, resulting in an additional double peak: <16C and 16C); (3) the point of dichotomy between cells starting depolyploidisation (from ~8C to 16C, illustrated by corresponding reductive divisions, shown and discussed below) of the reproductive fraction to the re-establishment of the normal cell cycle (days 16–18), contrasted with the simultaneous accumulation of giant and even super-giant cells (>20C–396C, the highest found ploidy) which continued undergoing MS and increased in number. This second fraction of super-giants is identified with a blue-dashed narrow circle in Figure 1A, while in Figure 1B a similar circle outlines the highest proportion of MS (~16% of cells) counted at this time point. Both fractions gave a high average polyploidy on day 16 (12.15C). Finally (4) the time period of full (or close to full) return to the initial point, with the gradual disappearance of both giant cells and MS (usually seen between days 22 and 29) and represented on Figure 1A by day 25 coinciding with the restart of normal mitoses (Figure 1B) and clonal cell re-growth [4]. The average ploidy content per cell at this time is returning to the control. Up until this recovery, most treated cells expressed the hallmarks of cellular senescence, Sa- β -gal, and IL-6 staining [4].

2.2. Differential Gene Expression

The full list of differentially expressed (DE) genes after DOX is presented in File S1. In line with the chosen transcriptome sampling time points in three independent experiments, the DE genes formed clusters when presented on the multidimensional scaling plot: for day 5 this was sharply different from the cluster of non-treated (NT) samples and from day 16; for day 16 all three samples were closely converged, different from the NT samples and from day 5; for day 8 the cluster was between those of day 5 and day 16; and for day 22 the samples showed the tendency to return (likely with somewhat different dynamics in each separate case) to the initial NT pattern (Figure 2A). The amount of differentially expressed genes (compared with the NT control) as presented in Figure 2B–D was the highest for days 5 and 16 (similar for day 8), and very much reduced on day 22. The high convergence of the DE pattern for three samples on day 16 was apparently due to the dominant presence of the hyperploid cells, which thus unified the data. It is clear that on days 4–5, along with MS, the cells underwent a very strong change of cell fate. Therefore we first directed our transcriptome analysis to the

study of bivalent genes, whose activation is usually characteristic for the developmental changes particularly associated with polyploidy [9].

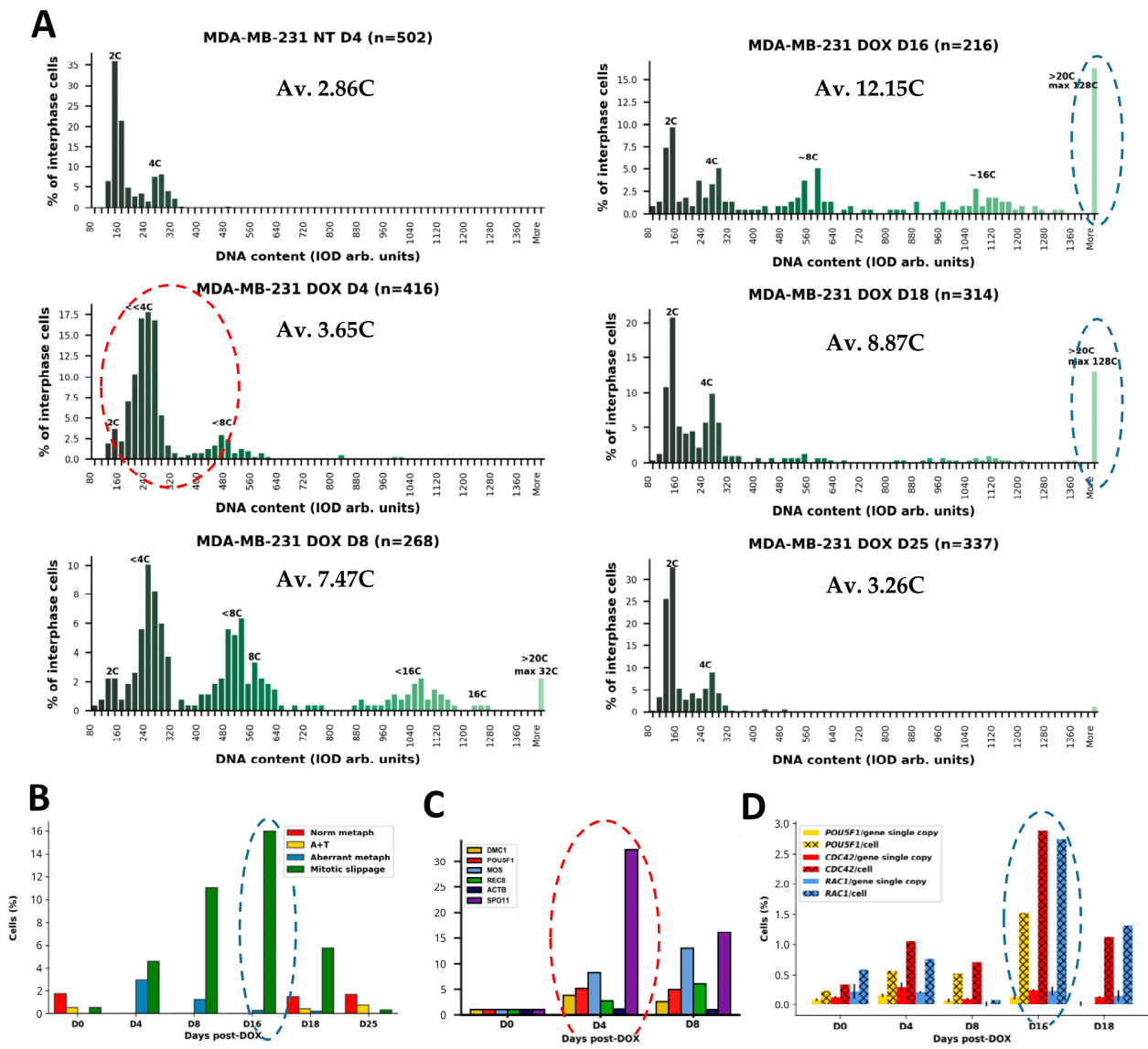


Figure 1. Quantified parameters of MDA-MB-231 cells following DOX treatment: (A) Cell cycle changes monitored with in situ DNA cytometry after DOX treatment in a representative experiment; the average ploidy content per cell (AV) is shown for each day. (B) Representative differential mitotic counts showing the absence of cell division at the period of increasing MS (D4-D16). (C) RT-qPCR results of meiotic gene transcription after DOX treatment, shown as fold change. Representative charts of two independent experiments, with three technical replicates. (D) Results of gene transcription evaluation obtained by Selfie digital PCR for three gene transcripts quantified per gene copy and per cell (as transcripts per gene copy multiplied by the average ploidy in the same experiment)—the average of three technical replicates with SEM. Red-dashed circle (in A) highlights the period of S-G2-M-delay with DNA under-replication in the late S-phase starting the MS, polyploidisation, and the expression of meiotic genes (in C); blue-dashed circles outline the diverged subpopulation of super-giant cells (in A) with the highest proportion of MS (in B) and the highest proportion of the *POU5F1*, *CDC42*, *RAC1* gene expression per cell (in D) (republished from [4] with an open access CC BY 4.0 license).

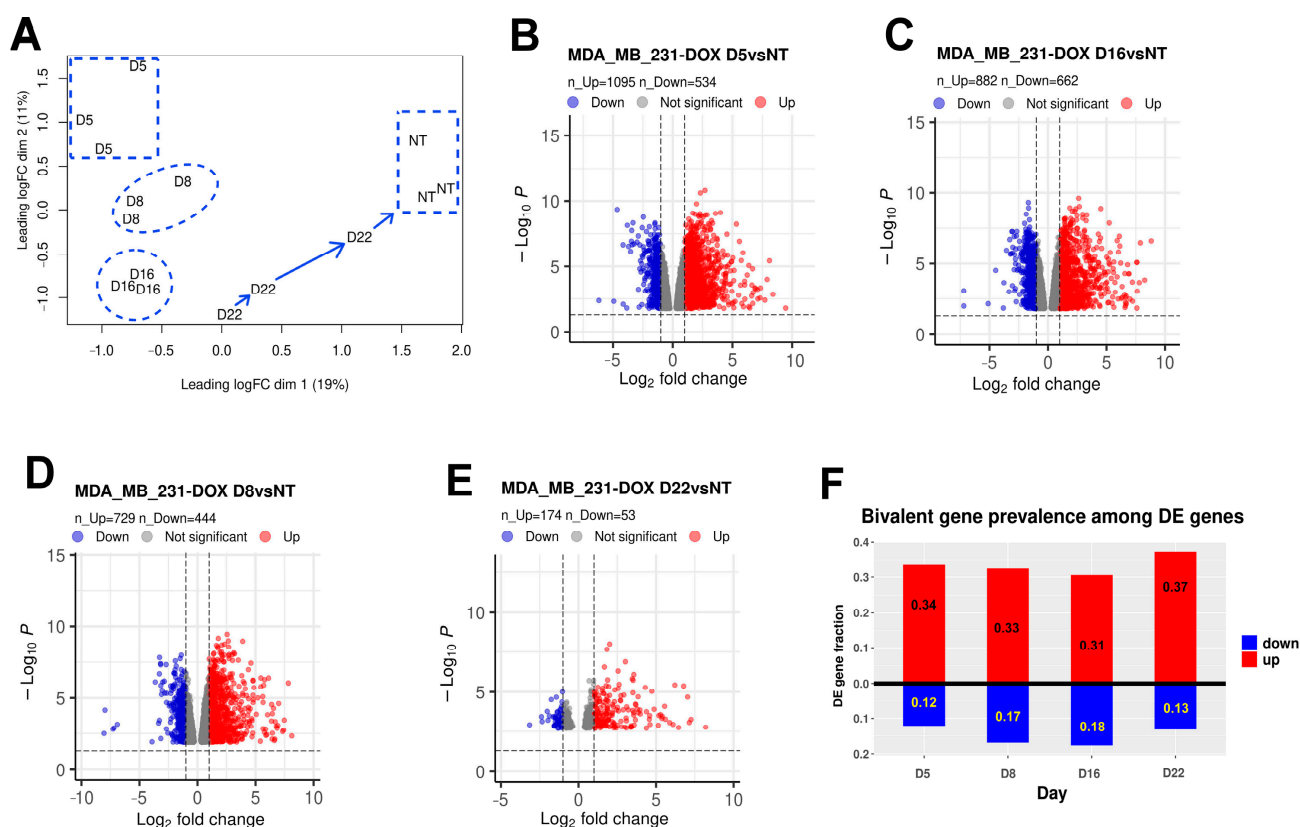


Figure 2. Transcriptome characteristics of DOX-treated MDA-MB-231 compared to non-treated samples from three independent experiments. (A) The multidimensional scaling (MDS) plot of MDA-MB-231 RNA-seq samples at days 0 (non-treated, NT), 5, 8, 16, and 22 post-DOX treatment showing (by dashed outline) the separation of the sampled cohorts, with the cohorts on day 22 returning to the NT pattern. (B–E) Volcano plots of differentially expressed (DE) genes ($FDR < 0.05$, $|\text{Log}_2\text{FC}| > 1$) on: (B) day 5 versus NT; (C) day 8 versus NT; (D) day 16 versus NT; (E) day 22 versus NT. (F) The proportions of bivalent genes amongst DE genes, up- and downregulated, respectively, on days 5, 8, 16, and 22 post-DOX.

2.2.1. Quantitation of Up- and Downregulated Bivalent Genes

The activation of bivalent genes (harbouring both transcription-suppressing H3K27me3 and activating H3K4me3 histone H3 modalities at their promoters) is capable of immediately changing their transcription and thus, can impact cell fate. Our results here revealed the enrichment of DOX-treated samples with upregulated bivalent genes. Among the DE genes (presented as volcano plots in Figure 2), the proportion of bivalent genes, as seen in Figure 2F, is $>30\%$ among upregulated genes for all time points, and up to 18% among downregulated genes. The revealed up- and downregulated bivalent gene lists are presented in File S2. The proportion of downregulated bivalent genes decreases along with an eight-fold decrease of DE genes on day 22, during recovery. The annotation of upregulated bivalent genes revealed two main module groups—innate immune response to soluble DNA and reproduction—on days 5 and 16 after DOX treatment.

2.2.2. Gene Ontology (GO) Enrichment Analysis of DE Bivalent Genes Reveals Modules of Cytokine Signaling and Response to Cytosolic DNA

A GO enrichment analysis of the upregulated bivalent genes of day 5, presented in Figure 3 as a treemap plot, revealed the activation of a stress response and oscillating processes—both typical for reversible senescence [10,11].

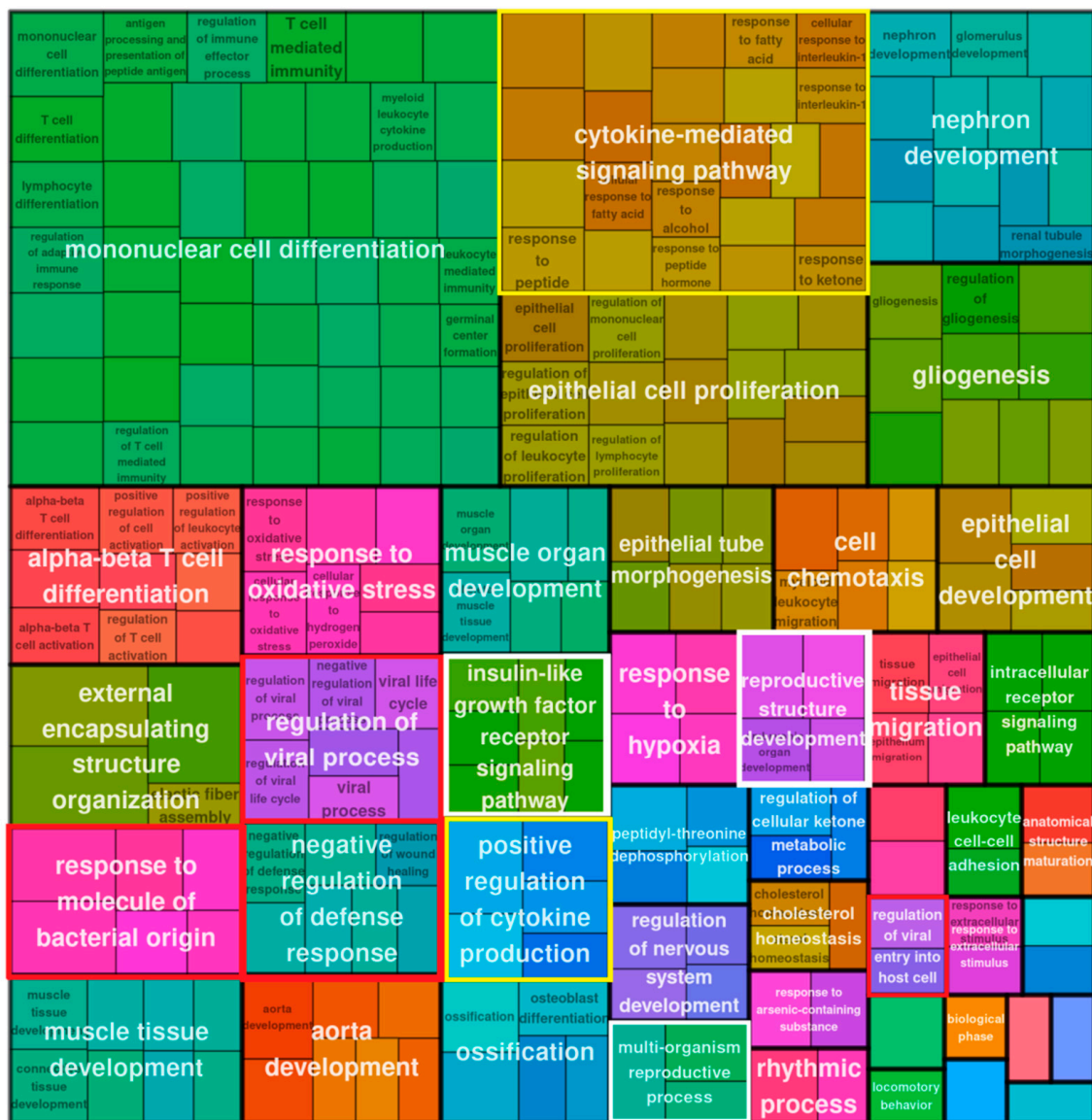


Figure 3. Treemap plot representation of the Gene Ontology Biological Process (GO BP) enrichment analysis (GO modules with hypergeometric test $p_{Adj} < 0.05$ classed as enriched) for bivalent genes upregulated in MDA-MB-231 cells on day 5 post-DOX.

Both settings on day 5 and day 16 revealed several modules describing morphogenesis and a response to the decreased oxygen level. The prominent GO terms of cytokine signaling, regulation of viral process, and response to molecules of bacterial origin (framed by yellow and red boxes) included sensing of soluble DNA by cGAS-Sting or other pathways of adaptive and inflammatory immune response [12]. It was also similar on day 5 and day 16 (Figure 4).

However, a negative regulation of the defense response and a negative regulation of the biotic stimuli were also found. To better dissect the reaction to cytosolic DNA accompanying MS, we analysed the other sensing pathway triggered by intracellular DNA, the AIM2 inflammasome which may reduce the activation of the STING pathway [12]. The cytosolic DNA-sensing pathway M39837 was obtained from MSigDB [13] and the list of DE genes for each time point was filtered against it. The M39837 pathway genes present among DE genes are listed in Table 1.



Figure 4. Treemap plot representation of the GO BP enrichment analysis results (GO modules with hypergeometric test $p_{Adj} < 0.05$ classed as enriched) for bivalent genes upregulated in MDA-MB-231 cells on day 16 post-DOX.

Table 1. The expression of differentially expressed (LogFC, compared to NT) genes sensing cytosolic DNA triggered by the AIM2 inflammasome.

Genes	Up/Down	D5	D8	D16	D22
<i>IL1B</i>	Up	5.58	4.78	3.87	NA
<i>IL6</i>	Up	3.77	3.23	2.73	NA
<i>CCL4L2</i>	Up	2.89	3.46	6.21	4.87
<i>CCL5</i>	Up	2.05	1.76	2.95	1.7
<i>NFKB1A</i>	Up	1.88	1.85	1.64	NA
<i>NFKBκB</i>	Up	NA	NA	1.26	NA
<i>CXCL10</i>	Up	1.86	1.44	NA	NA
<i>CASP1</i>	Up	1.38	NA	NA	NA
<i>RNF125</i>	Up	1.29	NA	1.06	NA
<i>AIM2</i>	Up	1.14	NA	NA	NA
<i>RELA</i>	Up	1.04	NA	NA	NA
<i>DDX58</i>	Up	NA	1.5	1.59	NA
<i>POLR3G</i>	Down	-1.25	-2.07	-1.47	NA
<i>POLR3K</i>	Down	-1.14	NA	-1.02	NA
<i>POLR2F</i>	Down	-1.16	-1.11	-1.09	NA
<i>POLR2L</i>	Down	-1.09	-1.11	-1.11	NA

It appears that the AIM2-receptor pathway recognizing cytosolic DNA was activated on day 5 but no further. In contrast, other cytosolic DNA sensors, the receptors of POL II and POL III, were downregulated on days 5–16. I.e., in spite of intense pro-inflammatory signalling (*IL-1B*, *IL-6*, *CCL4L2*, *CCL10*, *CCL4L2*) by senescent polyploidising cells, the sensing of cytosolic DNA produced by MS was at least partially protected from the innate and inflammatory immune response, particularly at the beginning of the MS process.

2.2.3. GO Enrichment Analysis of DE Bivalent Genes Reveals Reproductive Modules

Along with the powerful cytokine signaling and sensing of cytosolic DNA, we found the biological processes “multiorganism reproduction process” and “reproductive structure development” (Figure 3, framed in white) on day 5 among the GO modules of upregulated bivalent genes. The former (GO:0044703) lists, among other processes, meiotic cell cycle and female pregnancy, and includes among other processes “ovarian nurse cell to oocyte transport” [14]. The definition of the “reproductive structure development” process reads: “The reproductive developmental process whose specific outcome is the progression of somatic structures that will be used in the process of creating new individuals . . . ” (GO:0048608). The latter reproductive module and also “molting processes” (which in our context may correspond with excystation and budding from giant cells) were found on day 16; however, subsequently this process of “creating new individuals” progressed to “maternal placenta development” (Figure 4, all reproductive modules framed in white). The cells also show upregulation of locomotory behavior and migration compatible with their amoeboid phenotype, highlighted by the development of a powerful, microtubule-actin-rich cytoskeleton and budding offspring from late polyploidy giant cells, as described by us previously [4] and detailed further below.

The GO modules among the downregulated bivalent genes were not significantly enriched on days 5 and 16. Notably, on day 8, the downregulated bivalent genes show enrichment for the circadian rhythm GO BP (File S2), suggesting circadian deregulation removing cells from the normal cell cycle, which was associated in our previous work with senescence, MS, polyploidy, and a cancer soma-to-germ transition [9,15].

2.2.4. The GO Enrichment of All DE Genes on Day 16

At this stage, the GO enrichment of all upregulated genes (Figure 5) revealed a considerable role of the cellular microenvironment and intercellular communication including the senescence secretome, hallmarked by the regulation of interleukin-6 and the cellular response to interleukin-1 (a master regulator of inflammation controlling a variety of innate immune processes), as well as the negative regulation of viral genome replication, the regulation of T-cell activation and mononuclear cell differentiation, the response to glucose starvation and the regulation of protein import, and the intrinsic apoptotic signalling pathway. In addition, the modules of “reproductive structure development” were also present (framed in white). As for the downregulated genes, the GO modules enriched among them mostly pertained to the mitotic cell cycle, and the regulation thereof (File S1).

Because of renewed interest in the atavistic theory of cancer [16], and an understanding of how cancer attractors during evolution are associated with polyploidy related to asexual reproduction, as recently identified in the TCGA database, including for breast carcinoma [17], we were interested in if and how these differences in gene expression changed the phylostratigraphic gene profiles.

2.2.5. Phylostratigraphic Distribution of the Differentially Expressed Genes over Time after DOX-Treatment

The results are presented in Figure 6A, with the general phylostratigraphy histogram of human genes used as a background. We see that the most crucial change occurred on day 5, with the relative downregulation of genes originating in Phylostratum 2, corresponding to unicellular Eukaryota (responsible for the evolving cell cycle, DNA damage signalling, and recombination repair mechanisms [15,18]) and the upregulation of the eighth multicellular

phylostratum Euteleostomi. Phylostratum 6 (Bilateria) associated, in particular, with polyploidy-cancer-linked angiogenesis [9] is also slightly upregulated. On days 8 and 16 the gene balance situation remained the same. On day 22, the suppressed phylostratum 2 partially reverted to the control (along with a return to the normal cell cycle).



Figure 5. Treemap plot representation of the GO BP enrichment analysis results (GO modules with hypergeometric test $p_{Adj} < 0.05$ classed as enriched) for all genes upregulated in MDA-MB-231 cells on day 16 post-DOX.

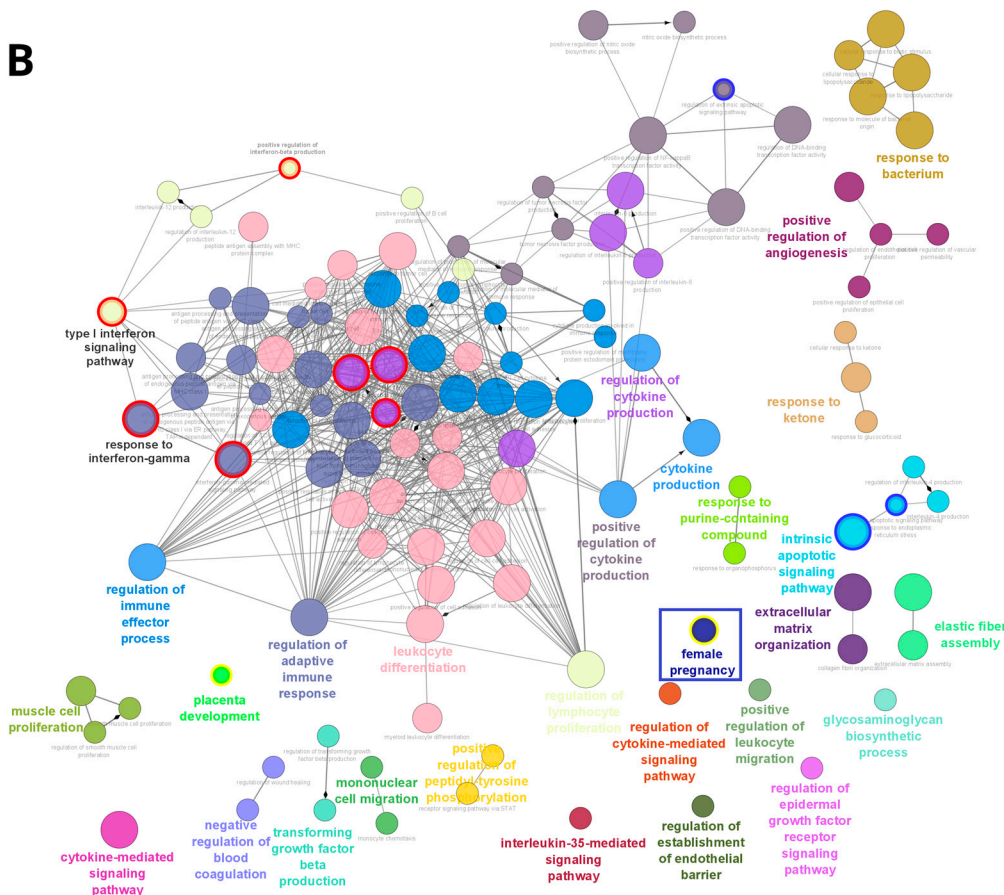
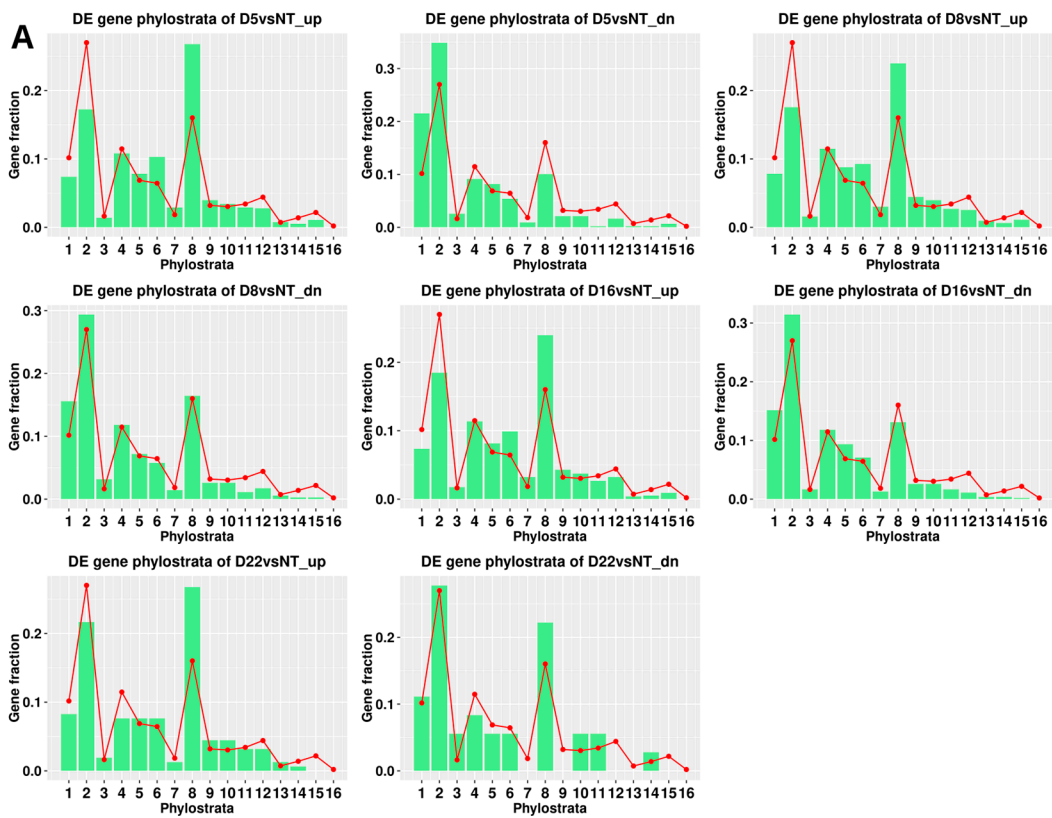


Figure 6. Cont.

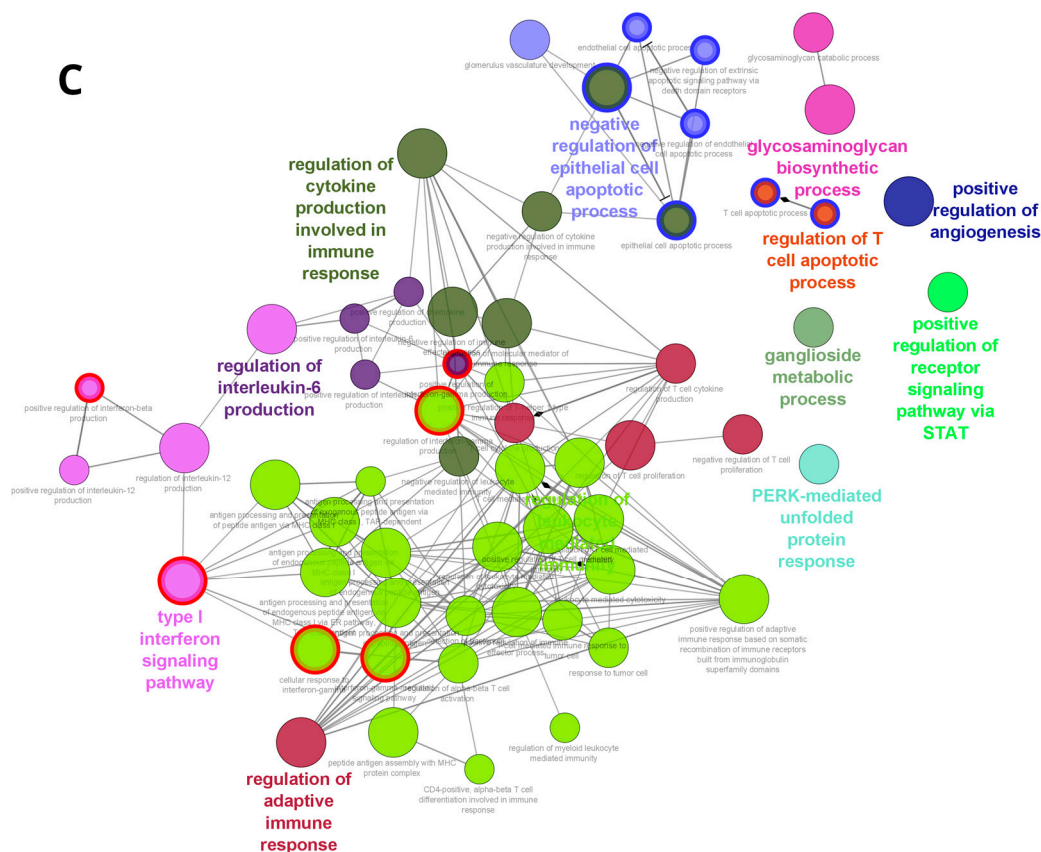


Figure 6. Phylostratigraphic analysis of MDA-MB-231 cells over the time course after DOX treatment. (A) The phylostratigraphic distributions of differentially expressed (up- and downregulated, abbreviated as “up” and “dn”) genes on days 5, 8, 16, and 22 post-DOX, with the whole-genome phylostratigraphic distribution (red line) serving as the background reference. (B) The ClueGO enrichment map representation of GO biological processes enriched (hypergeometric test $pAdj < 0.05$) in the STRING network of day 5 versus NT upregulated genes corresponding to the eighth phylostratum. The presence of both adaptive and innate immunity modules (including interferon-related pathways), angiogenesis, apoptosis, and female pregnancy (blue-framed) is noteworthy. (C) ClueGO enrichment map representation of GO biological processes enriched (hypergeometric test $pAdj < 0.05$) in the STRING network of day 16 versus NT upregulated genes corresponding to the eighth phylostratum. The modules of interferon-related pathways are circled in red; those pertaining to apoptosis are circled in blue. Figure 6B,C can also be viewed interactively in NDEX data base <https://www.ndexbio.org/#/networkset/326907d3-a2f3-11ed-9a1f-005056ae23aa?accesskey=d13703d9d6c991087b20776c62648d36c27d4d92e7c4fea1b7e177a03221963b>.

In the upregulated eighth phylostratum of our DOX-treated material, the ClueGO enrichment map representation of GO biological processes enriched in the STRING network of day 5 versus NT upregulated genes revealed (Figure 6B) a dominant network of inflammatory cytokine production, which is consistent with a cellular senescence secretome and also immune response including a STING / Type 1 interferon component. Both senescence and immunity emerged around this period during evolution [18]. The module “response to bacterium” which reacts to soluble self-, mitochondrial, and viral/bacterial DNA as well, may be associated with cytosolic DNA accompanying mitotic slippage. In addition, a GO module designated as “female pregnancy” was revealed (Figure 6B, framed). The “female pregnancy” module (GO:0007565) is part of “multicellular organism development” and includes, mainly, the embryo implantation and maternal process involved in female pregnancy, in addition to multiple sub-sub networks, including secretion by tissues and viral processes. The latter paradoxically relates to placental biology [5], expanded further

in the Discussion section. The upregulated genes of the module “female pregnancy” in our DOX-treated material include: FOS (logFC = 1.48) and JUNB (logFC = 2.40), indispensable regulators of embryonic and cancer stem cells with a positive loop to OCT4 [19]; IL-1 β , a potent inflammatory cytokine involved in host defence through innate immunity (logFC = 5.58); VEGFA (vascular endothelial growth factor), acting in placenta and dysregulated in senescent and cancer cells (logFC = 1.82); THBD (thrombomodulin; logFC = 1.52); AREG, a ligand of the EGF receptor/EGFR, which regulates invasive phenotypes in cancers (logFC = 2.23); AGT (angiotensin; logFC = 3.38); PGF (placenta growth factor; logFC = 1.19); PTHLH, an intra/autocrine/paracrine parathyroid hormone-like-hormone found in the placenta DNA library [20] causing humoral hypercalcemia, and a poor prognosis marker in many cancers [21] (logFC = 2.06); and STC2 (stanniocalcin-hypocalcemic action) a universal tumor marker [22] (logFC = 2.21). In addition, the modules of the foetal-maternal interface such as the regulation and establishment of an endothelial barrier and the negative regulation of blood coagulation are also included.

Thus, GO modules for reproductive processes appeared in all in silico analyses. In Figure 6C, showing the network of phylostratum 8 on day 16, in addition to interleukin 6 and type 1 interferon signaling, the STAT pathway was revealed. The JAK/STAT pathway can be related to the trophoblast-like biology of the reproductive process [23] through the stress-activated MAPK cascade, which was also bivalently activated on day 16 (Figure 4).

In summary, in all of our in silico transcriptome studies, the emergence of reproductive modules (soma-to-germ transition), co-opting with sensing and the response to cytosolic DNA linked through pervasive “female pregnancy” to the placental module, was found, along with the accumulation of super-giant cells by repeated MS.

2.3. Immunofluorescence (IF) and Clonogenicity Studies

2.3.1. Change of Cell Fate through MS on Days 4–5 Is Hallmarked by Soma-to-Maternal Germ Transition

As indicated above, the reproductive process was highlighted by transcriptome studies from day 5 to day 16 after DOX treatment. Although previously we associated MS with meiotic traits based on IF and qPCR investigations [4], the mechanism of this transition remained unclear. Here, we noted the entry of OCT4A into the cell nucleus coinciding with MS (Figure 7A,B). To explore this further, fixed preparations were stained with an antibody for both A- and B-forms of OCT4. While in the NT sample, OCT4 was expressed in the cytoplasm (Figure 7A) corresponding to the spliced B-form lacking the first exon required for transactivation; after DOX treatment and the induction of MS, we found the clear transition of OCT4 into the reconstituting cell nuclei from the centrosome pole, on days 4–5 (Figure 7B). The shift between full A- and spliced B-form of the *POU5F1* gene can occur by the reversible methylation of its enhancers [24]. In our previous work using qPCR and digital PCR, we observed a two-fold increase in *OCT4A* transcription when referred per gene on day 4 (republished in Figure 1C,D). The importance of this observation is underscored by the role of *OCT4A* (*POU5F1*) as a maternally expressed germline-specifying factor [25,26]. The link of mitotic slippage to maternal soma-to-germ transition is also in line with the previously reported activation of the meiotic kinase MOS (Figure 7C) and the expression of several meiosis-specific genes found by qPCR and IF on days 4–8 (Figure 1C). Here, we also found the upregulation of EMI2, the co-activator of MOS, in the oocyte meiotic arrest of the anaphase-promoting complex during MS (Figure 7D,E).

In addition to these hallmarks of soma-to-germ transition associated with mitotic arrest and slippage, we also decided to study the YAP1/TEAD1 distribution as a possible link between the sensing of cytosolic DNA in MS and the inactivation of the Hippo pathway as reported in the literature [27]. Here, we confirmed on day 5–8 post DOX treatment this important hallmark of cell-fate change—i.e., the inactivation of the Hippo pathway, with the transition of YAP1 along with MS from the cytoplasm into the cell nucleus and interacting there with its partner transcription factor TEAD1 (Figure 7F). The reproductive modules of “female pregnancy” and “maternal placenta development”, as well as the upregulated

genes, indicate the presence of placenta components seen during evolution. Therefore, we suspected that polyploid giant cells may recapitulate a function of the atavistic intercellular communication placed in placenta development, precursors that further evolved in mammals as embryo invasion and the “fetus-mother” trophoblast relationship. In this context, we decided to investigate the cellular location and functionality of CDC42-kinase, a small Rho GTP-ase which is engaged in trophoblast lineage specification in mammals [28].

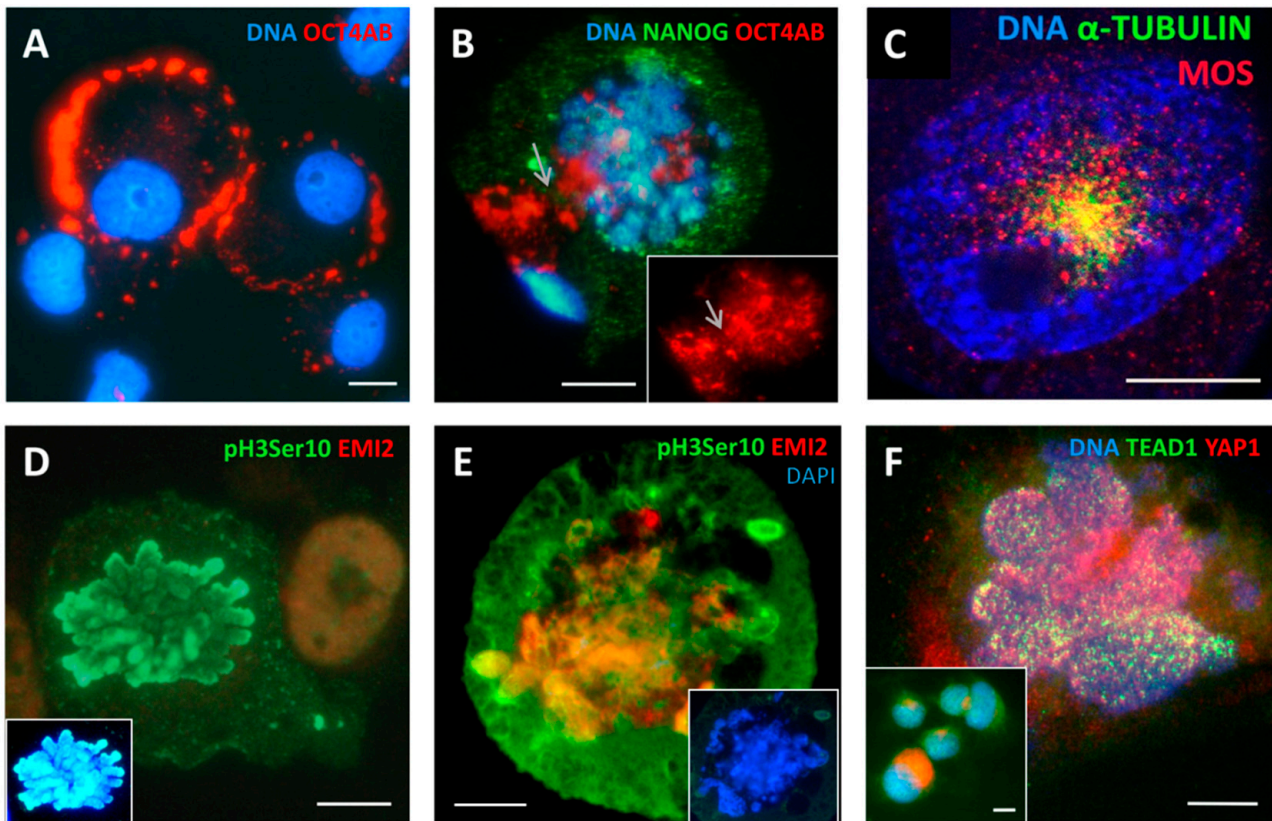


Figure 7. Cell fate change during MS where maternal germline specification and the inactivation of the Hippo pathway are observed on days 4–5 post DOX treatment: (A) OCT4-antibody-positive cells in NT control showing the cytoplasmic location of OCT4B; (B) the entrance of OCT4A into the cell nucleus (likely from the centrosome pole, arrowed) during MS; (C) the meiotic kinase MOS and α -TUBULIN form a monopolar spindle (arrowed) in the early prophase; (D) mitotic marker pH3ser10-positive and EMI2-negative metaphase in NT control; insert: metaphase-pH3ser10 with DAPI; (E) the chromosomes swelling and fusing in MS while losing the pH3Ser10 label become positive for EMI2 (insert: only DAPI staining); (F) the inactivation of the Hippo pathway, with the transition of YAP1 in its active form along with MS from the cytoplasm into the cell nucleus and interacting there with its partner transcription factor TEAD1 (insert: NT control cells). Imaged in RGB optical filters. Bars = 10 μ m. Figure 7C is republished from [4] with an open access CC BY 4.0 license.

2.3.2. Inhibition of the Trophoblast Lineage Specifier CDC42 Suppresses the Clonogenic Survival of DOX-Treated MDA-MB-231 Cells

CDC42, together with the substrate-phosphorylating RAC1 component, is indispensable in the biology of various solitary and social amoebae, parasitic protists, budding yeast, and mammalian animals, including female pregnancy. It was also shown to promote tumor progression and metastases, particularly in triple-negative breast cancer [29]. The activated CDC42 acts by modulating the structure of actin and tubulin dynamics, creating and modifying the cytoskeleton, cell–cell interaction, and multiple invasion processes [30]. In amoeba, CDC42 participates in the excysting of spores from macrocysts, the same function as for budding yeast. In humans, CDC42 is also involved in the creation of the immuno-

logical synapse [31]. In relation to female pregnancy, activated CDC42 has two membrane invasive functions, polar body emission and placentation, with the migration and invasion of the human extravillous trophoblast, where CDC42 is directly located in microvilli [32,33]. In our previous work, we highlighted the initial increase in CDC42 transcription on days 4–5 after DOX treatment and the many-fold accumulation of transcripts in polyploidy giant cells, due to high gene dosage (presented here in Figure 1D).

The presence of CDC42 in NT and DOX-treated cells was confirmed by Western blotting (WB) (Figure 8A). Using the inhibitor of CDC42, ML141, we found a three-fold suppression of the clonogenicity of the DOX-treated MDA-MB-231 cells, in five independent experiments scored on day 23, although the colony formation capability on NT control cells was not significantly changed (Figure 8B,C). The stained colonies are shown in Supplementary Figure S1.

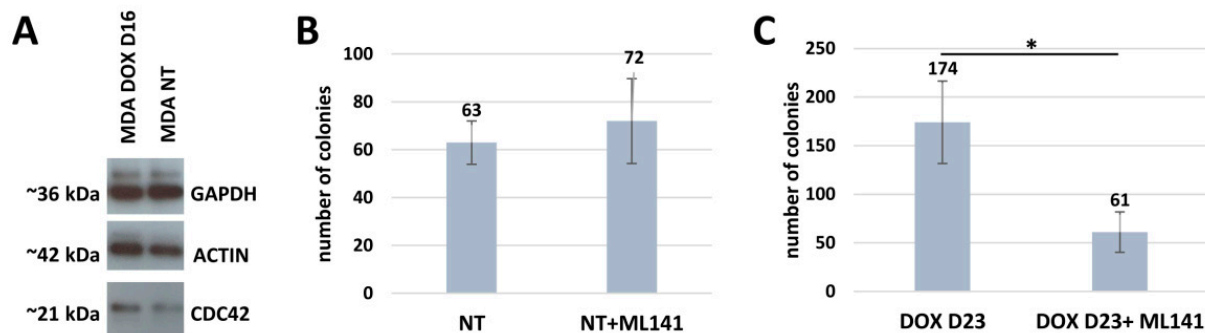


Figure 8. The evaluation of CDC42 by WB and clonogenicity assay: (A) Western blot analysis of CDC42 expression in MDA-MB-231 cells before and after DOX treatment. The GAPDH antibody is used as a loading control. (B,C) The evaluation of clonogenicity after DOX treatment and CDC42 suppression. (B) Clonogenicity of MDA-MB-231 NT cells on day 23 after CDC42 inhibitor, ML141, treatment (100 cells seeded per well). (C) Three-fold decrease in the clonogenicity of MDA-MB-231 cells after DOX and CDC42 inhibitor, ML141, treatment (counted from $\sim 1.5 \times 10^6$ cells initially seeded per flask) on day 23 after treatment evaluated in five independent experiments. * $p < 0.05$.

2.3.3. CDC42 Is Located at the Periphery, Buds, and Their Microvilli of Late DOX-Treated Polyploid Giant Cells

The immunofluorescent detection of CDC42 in the chamber slide cultures, showed CDC42 to be highly enriched in the polyploid giant cell buds (appearing at the end of the second week post-DOX and beyond), which are also very rich in actin and tubulin and occasionally can be found asymmetrically originating beside a sub-nucleus lacking these components (Figure 9A–D, E for NT control). When outside the polyploid giant cells, these buds often display the peripheral microvilli enriched with all three components: actin, tubulin, and CDC42, indicating their mobility and invasive capacity (Figure 9C,D).

In some cases, such small cells were seen branched from the polyploidy giant cells on a thin actin “foot” (Figure 9H). In addition, CDC42 staining was more intense at the periphery of these cells where their smaller CDC42-enriched offspring/neighbors may be homing (Figure 9G). The participation of CDC42 in ejecting the structures filled with diffuse low-density DNA was also seen (Figure 9I). The staining for the preimplantation trophectoderm lineage specifier, CDX2, in late giant cells showed weak co-staining with Ki67 in polyploid giant cells and their intracellular buds, with accumulation in the autophagosomes but absence in the recovered cell nuclei (Figure 9J).

It is somewhat difficult to ascertain when the mobile CDC42/ACTIN/TUBULIN-enriched buds are ejected from giant cells and when they are homing to them. In the current study, we tried to clarify how the budding cancer “babies” develop from the “maternal germ cell” and the remnant super-giant with the features of the “maternal placenta”, as extrapolated from our in silico analysis, to attain different fates.

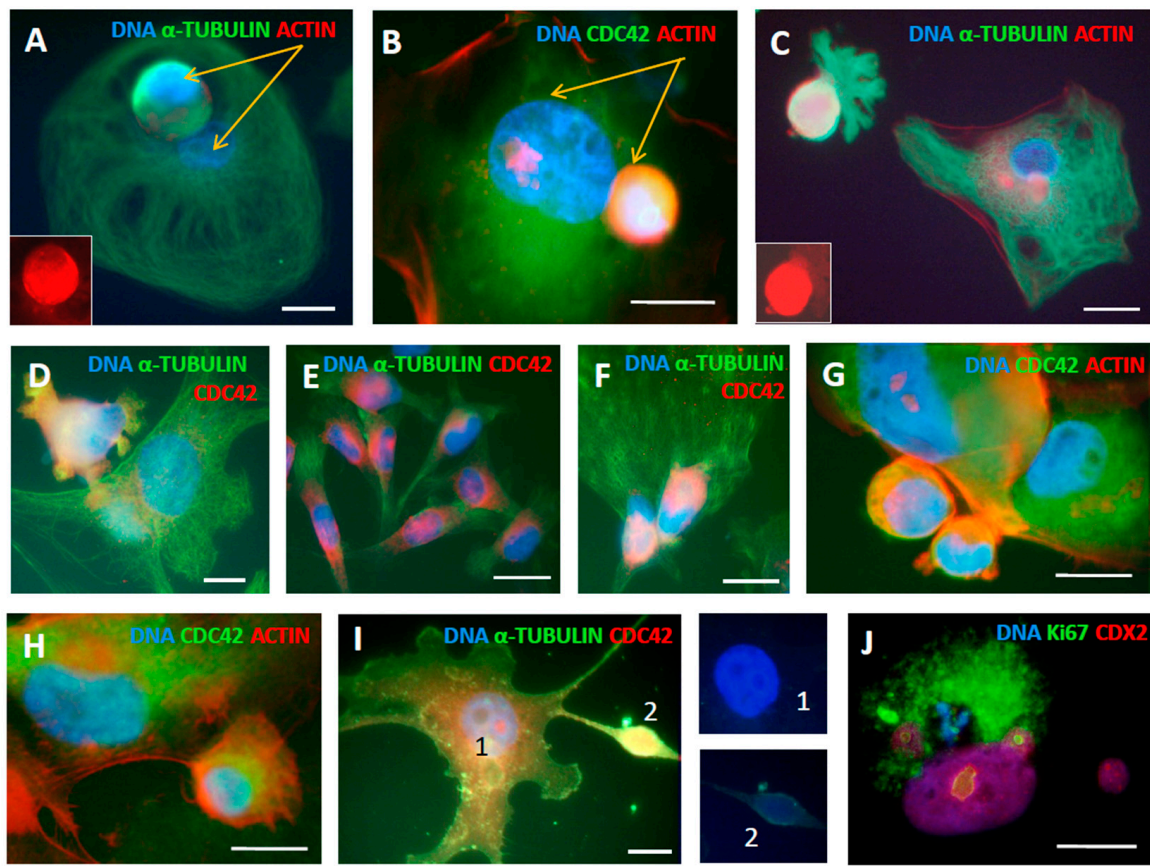


Figure 9. CDC42 kinase acting together with actin and tubulin in late (second–third week) DOX-treated polyploid giant MDA-MB-231 cells participates in collective activities for survival: budding, homing, invasion, and DNA transfer: (A–D) giant amoeboid cells on days 13–18 post-DOX treatment budding budding mobile spore-like sub-cells, which are highly enriched in actin and tubulin and contain CDC42, particularly in the microvilli (in D); (A,B) arrows indicate two type of subnuclei, one in the mobile bud and another immobile remaining at place; (E) CDC42 is found in the cytoplasm of NT control cells; (F) CDC42-rich small sub-cells located on the surface of the polyploid giant cell; (G) CDC42 is found intensely at the periphery of the polyploid giant cell possibly providing homing for their smaller neighbors; (H) a giant cell budding a sub-cell; (I) the participation of CDC42 in branching the structures filled with diffuse DNA; (J) the trophoblast lineage marker CDX2 weakly positive in a polyploid giant cell nucleus and its two buds, on day 19 after DOX treatment. Bars = 20 μm . Figure 9A,C are reproduced from [4] with an open access CC BY 4.0 license.

2.3.4. DNA Repair, Autophagy, and DNA Damage Sorting in Small and Super-Giant Cells

The asymmetric a-mitotic segregation of polyploid giant cancer cell subnuclei in relation to DNA repair was already reported by us in this [4] and other models of genotoxic treatment. The whirling of the whole polyploid giant cell genome and the rotation at the nuclear periphery, together with the looping nuclear lamin, presumably in search of homology for the recombination repair and sorting of the damage by autophagy, has been proposed and partially examined [34–37] (occurring at the brink between survival and death by mitotic catastrophe, indirectly supported in studies of anastasis (return from apoptosis)) [38,39]. Therefore here, in this model, we present just a few examples (Figure 10A,B,D) of DNA damage sorting with the participation of autophagy (pAMPK-positivity in Figure 10D) and two examples of reduction division (Figure 10C,E), as well a unique picture of a polyploid super-giant cell homing three offspring just at the state of mitosis, while its own nucleus is deteriorating (Figure 10F). We also know from dozens of experimental repeats that the super-giants die alongside the establishment of the mitotic clonogenic growth, as exemplified in Figure 1A [4].

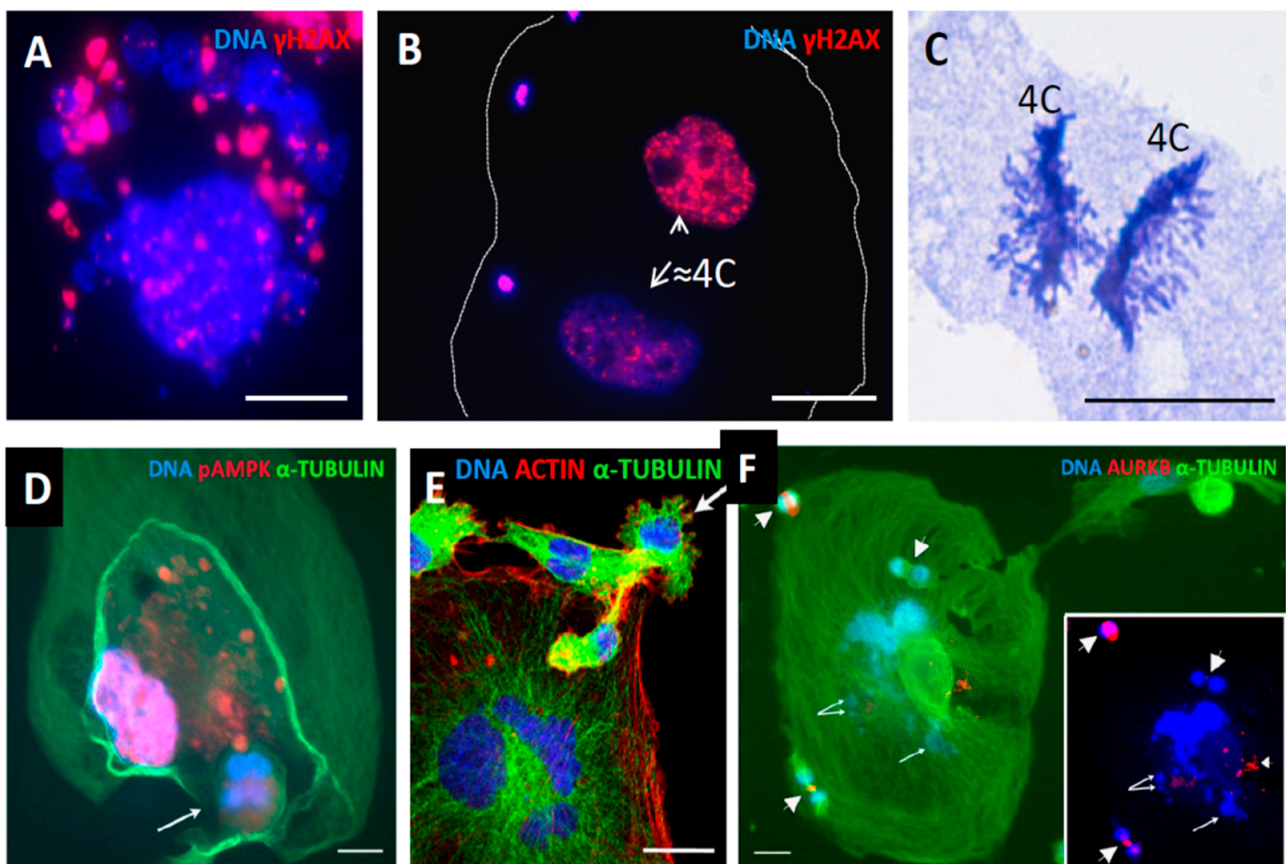


Figure 10. The production of fragmented cytosolic DNA in repeated cycles of MS in polyploid giant cells; its separation from the repairing sub-nucleus by autophagy and support from a polyploid giant for the budding and homing of mitotic survivors. (A) MS positive for DNA DSBs (second week post DOX). (B) A giant cell with two $\sim 4C$ sub-nuclei, one is $\gamma H2AX$ positive, while the other is free of DNA DSBs, and three small clusters of the sorted DSB-enriched DNA at the cytoplasm periphery. (C) Bi-polar anaphase of the equal $4C$ binemic chromosome groups from an $8C$ MDA-MB-231 cell—a clear indication of reduction division—on day 19 post-DOX-treatment. (D) The possible excystation of a tetra-nuclear subcell (arrow) leaving a giant cell, while another subnucleus ($\sim 8C$) is positive for pAMPK, indicating its autophagic degradation (republished from [4]). (E) A giant multinuclear cell is budding a sub-cell (arrow) from a fragment of a polyploid giant cell 7 weeks post-DOX treatment, expelling a daughter cell, with the actin twisting around the anaphase spindle. (F) A super-giant amoeboid cell with a deteriorating nucleus (arrowed, better seen on the DAPI-stained image in insert) homing three small cells performing mitosis (arrowheads): metaphase, anaphase, and telophase. Bars = $25 \mu m$. (E,F) republished from [4] with an open access CC BY 4.0 license; (C,D) from [11], the article can be found <https://www.researchgate.net/publication/322581015>.

Accordingly, it appears that polyploid giant cells sort the DNA damage between subnuclei and deliver small viable survivors, but themselves only produce even more cytosolic DNA, degraded by autophagy for recycling, and also energy to feed the offspring and to stimulate their mitoses, also by a secreted microenvironment, until they are self-sufficient and capable of forming clones. Additional data are presented in Figure 11.

It is seen that the polyploid giant cells (large nuclei) remain after DOX treatment predominantly with DNA DSBs, while the small cells (presumably delivered from them) become repaired. WB analysis of the DNA autophagy mediator p62 (Figure 11B), shows its upregulation in terms of DNA-damage response, in line with literature [40].

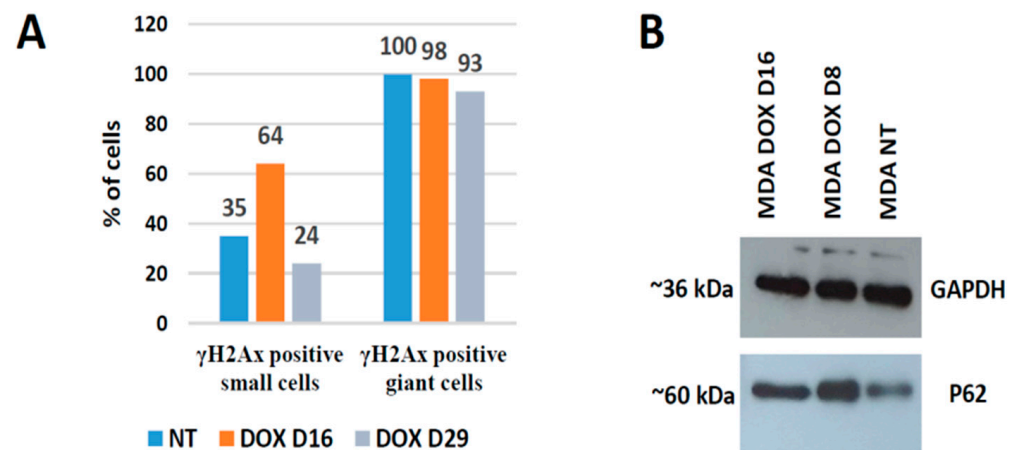


Figure 11. DNA damage, repair, and autophagy in MDA-MB-231 cells after DOX treatment. (A) Microscopic counts of gamma-H2AX-positive cells showing recovery after DOX of small cells without DNA DSBs, while late polyploidy giant cells remain with DNA breaks. (B) Western blot analysis of autophagy marker p62 expression in NT control cells and after DOX treatment. The GAPDH antibody is used as a loading control at the same time points.

3. Discussion

We began our observations of the basal breast cancer cell-line MDA-MB-231's response to DOX by finding the replication stress and under-replication of DNA in the late S-phase. This response has several consequences. First, as shown by us previously, it produces DNA damage, telomere attrition, and cytosolic DNA, and induces accelerated senescence [4]. The DNA under-replication changes cell fate by DNA-damage signaling and by preceding replicative stress [41].

To be precise, the replicative stress and under-replication induce a soma-meiotic germ transition, leading to metaphase arrest and slippage (most likely in the second altered cycle preceded by aberrant mitosis). MS is mediated by cooperation between the meiotic kinase MOS, which suppresses the degradation of cyclin B, and EMI2 (both preventing the induction of the anaphase-promoting complex). MS apparently belongs not to a mitotic but rather a female meiotic cell cycle, leading to a state similar to oocyte maturation, in expectation of fertilisation or parthenogenetic stimulus. Both stimuli should start embryonic development by cleavage divisions of blastomeres [42–44], which are considered by Niu and colleagues as equivalent to polyploid giant cancer cells [45].

In line with our earlier observations, this soma-germ transition state appears in a transcriptome analysis as the earliest feature of reproduction on the same 4–5 days with the GO module “multiorganism reproductive process”. Secondly, in parallel with MS, the pro-inflammatory immune response is activated, sensing the cytosolic DNA through the cGAS-STING pathway [46]. This soluble, unrepaired, and cleaved-by-autophagy DNA accumulates along with duplications of the DNA in the polyploid cells with each subsequent MS cycle. It is important to note that the soma-germ transition induced by MS also coincided with inactivation of the Hippo tumor-suppressor pathway and the transition of YAP1 in the cell nucleus, colocalising and activating TEAD1, along with the nuclear activation of OCT4A. Accordingly, the meiotic soma-germ transition of maternal origin resulting in MS was accompanied by YAP1/Hippo nuclear-cytoplasmic redistribution, known as sensing cytosolic DNA, resulting from the same MS as referred to in [27], and likely circularly linking both events. In turn, and thirdly, the accumulating soluble DNA induces the innate and adaptive immune response (transcriptionally, although requiring evidence in vivo) increasingly revealed by the activation of relevant genes in the PPI STRING network in the super-giant cancer cells. In its turn, and fourthly, this soluble DNA was not only used for re-utilisation but was also related to the induction of the maternal placenta module from day 5 onwards, as seen in the GO biological process of

“female pregnancy”. The latter was best revealed by bivalent genes and particularly in the DOX-upregulated eighth gene phylostratum (integrating the appearance of cellular senescence and immunity in multicellular organisms through evolution [18]).

Therefore it is interesting that recently we revealed oocyte maturation and meiotic cell division in the STRING PPI network of the TCGA database BRCA (and some other cancers) patient sample cohort in association with whole genome duplications [17]. So, the current in silico and immunofluorescence data in our MDA-MB-231-DOX model confirm the reality of such cell-fate change of somatic cancer cells. Notably, this pathway takes place not only in female but likely also triploid male cancers, through the doubling of the maternal genome [47].

However, the question remains, how does the mature maternal cancer “germ” originating from somatic cells establish a link to “maternal placenta development”? Here, we should recall the viral component. In our transcriptome analysis, the response to viral cell cycle and bacterial molecules, both positive and negative, evolutionarily emerged in multicellular eukaryotic cells for defense from viral and bacterial infection as the cGAS-STING-interferon-related immunity pathway was found. During MS, this pathway is activated presumably through the fragmentation of the self-DNA. Concurrently, the under-replication of heterochromatin would also cause its de-methylation and the activation of retroviral DNAs concealed there, which ultimately can end in cell death by transposition [48]. The situation is potentially even more complex, because Edward Chuong [5] showed the domestication of endogenous retroviruses (HERV) in the human genome, enabling, in his opinion, the evolution of proto-mammals.

These endoviruses, which constitute 8% of the human genome, can produce syncytin, causing cell–cell fusion that enables the creation of the syncytiotrophoblast for the separation of the fetal and maternal bloodstreams, preventing mutual destruction by competing immune systems. In this way HERVs are at work in the human placenta. Moreover, the activated HERVs were found by Diaz-Carballo and colleagues [49] to be mobilised in drug-treated polyploid giant cancer cells, participating in horizontal gene transfer together with mitochondrial DNA through ejections, similar to that described here in Figure 9I (and also observed by us in patient material; unpublished observations). Moreover, the same group described the mitochondrial encapsulation around cell nuclei of giant cancer cells resulting from genotoxic treatments [49], while Aarreberg et al. [50] reported that interleukin-1 β induces a mitochondrial DNA release to activate innate immune signaling via cGAS-STING. Moreover, interleukin-1 β from the phylostratum 8, upregulated by DOX, as revealed here 48-fold, is a component of the GO “female pregnancy”. Collectively, this data potentially provides a unifying resolution for the various aspects of the response: MS, resulting from cell senescence and energised by active mitochondria (counteracting cell death by anastasis [39]), both releases fragmented self-DNA and activates HERVs. Through the inflammatory interleukin-1 β immune response and cGAS-STING signaling, these programs become linked with the induced trophectoderm and placental proto-genes.

Returning to the female pregnancy module, it presumes not only the ectopic expression of placental genes, but also the presence of an “embryo proper” to invade. The MS preceded by replication stress supports the conversion of cancer somatic cells into a mimic of the arrested “mature oocyte” awaiting fertilisation or parthenogenetic stimulus to start early embryo development. Building on this observation, we propose a hypothesis that one of the known carcinogenic placental hormones, PTPLH, when activated, can intra-autocrinally and paracrinally elevate the humoral calcium level. PTPLH was isolated from a placental DNA library by Yasuda et al. [20], it regulates fetal-placental calcium transport [51], and is a poor prognosis marker in several somatic cancers [21]. PTPLH activity may also counteract calcium precipitation in the acidic microenvironment typical of cancers [52]. Calcium elevation mimics fertilisation and is widely used to cause parthenogenesis in experiments and domestic animals [53]. In this way, chemotherapeutic drugs can induce MS and therein, in a stressed senescent cancer cell, two key components—the imitation

of a mature egg arrested before fertilisation and a placental imitation, which can cause the parthenogenesis of this arrested “egg” (formation of the embryo proper) in the same super-giant multinucleated polyploid cell. The latter, in addition, also serves to feed and home the delivered offspring. In other words, a system of “female pregnancy” is obtained, regulated by positive feedback, including the secreted microenvironment, which creates a self-reproducing metastatic cancer.

Innate immunity has a very important role in normal pregnancy [54], with the strictly controlled processes allowing the baby to be nourished whilst the mutual immune destruction of both baby and mother is prevented. In view of the obtained results, the evasion mechanisms of tumor immunity may be related to the evolutionary fetal-maternal relationship.

Cdc42, an invasive placental component, shown here as intrinsically involved in the activities of the super-giant polyploid cancer cells, developed post-MS and favored the resistant clonogenic survival of DOX-treated MDA MB 231 cells. As a result, the targeting of CDC42 may be an attractive therapeutic strategy for preventing drug resistance. Strategies to target CDC42 are already available [29,55]. Similarly, other therapeutic strategies are also worthy of consideration. For example, the use of anti-viral medicines for treating cancers more generally, as well those aimed directly against HERV, have been undertaken [56]. Bisphosphonates, decreasing lipid droplets to target senescent chemo-resistant polyploid giant cancer cells, were also recently described [57]. Potentially, this treatment with zoledronic acid can decrease humoral calcium and interrupt the parthenogenetic link of the “female pregnancy system” revealed here in polyploid giant cancer cells. These approaches likely deserve attention and development in the future.

4. Materials and Methods

4.1. Cell Line and Treatment

The breast adenocarcinoma MDA-MB-231 cell line (triple-negative, modal chromosome number 64) was obtained from the European Collection of Authentic Cell Cultures (ECACC, Wiltshire, UK). The cells were grown in flasks or on chamber slides in Dulbecco’s Modified Eagle’s Medium (DMEM) supplemented with 10% fetal bovine serum (FBS; Sigma-Aldrich, St. Louis, MO, USA) at 37 °C in a 5% CO₂ humidified incubator without antibiotics. For the experimental studies, the cells were maintained in the log phase of growth and treated with 100 nM DOX (doxorubicin) for 24 h. After drug removal, the cells were maintained by replenishing the culture medium every 2–3 days and sampled over a 3-week period post-treatment until the appearance of escape clones. To suppress CDC42 activity cells after DOX removal, the cells were treated with 20 µM of the CDC42 inhibitor, ML141 (Sigma-Aldrich, St. Louis, MO, USA) until the appearance of escape clones. The concentration of ML141 as CDC42-inhibitory in the MDA MB 231 cells was based on [55].

4.2. Cell Colony Formation

Preliminary experiments showed that colony formation after DOX treatment was very low; therefore, to determine the colony formation ability after DOX treatment, it was performed in T25 flasks (along with immunofluorescence experiments carried out from the parallel T25 flasks). In a T25 flask $\sim 1.5 \times 10^6$ cells were seeded and treated with 100 nM DOX, alone, or in combination with 20 µM ML141. For NT control, cells were also seeded in 6 well plates (100 cells per well). On day 23 after treatment, the cells were rinsed with phosphate buffered saline (PBS), then fixed in methanol for 10 min and stained with 0.5% crystal violet solution (in 25% methanol) for 10 min, rinsed with ddH₂O, air dried, and the number of the eye-visible colonies counted. The colony formation capability was calculated from the initially seeded 1.5×10^6 cells per T25 flask on day 23 after treatment with DOX and ML141. For the NT control, the clonogenicity was calculated on day 23 after ML141 treatment from initially 100 cells seeded per well. The Student’s *t*-test for

unpaired samples was used to calculate the statistical significance of the difference of means (GraphPad Software Inc.). Statistical significance was accepted with $p < 0.05$.

4.3. Immunofluorescence (IF)

Standard IF staining was performed according to the procedures detailed previously [4]. Briefly, the cell cytopins or chamber slides were fixed in methanol for 7 min at $-20\text{ }^{\circ}\text{C}$, dipped 10 times in ice-cold acetone, and allowed to briefly dry. When staining for α -tubulin and actin, the post-fixation drying step was omitted and fixation in 4% paraformaldehyde with a triple wash in PBS was performed. Blocking for 15 min in Tris buffered saline (TBS), 0.05% Tween 20%, and 1% bovine serum albumin (BSA) at room temperature followed. Incubations with primary antibodies overnight at $4\text{ }^{\circ}\text{C}$ and appropriate secondary antibodies (goat anti-mouse IgG Alexa Fluor 488, goat anti-rabbit IgG Alexa Fluor 594 (Invitrogen, Carlsbad, CA, USA)) for 40 min at room temperature were carried out. The samples were counterstained with DAPI ($0.25\text{ }\mu\text{g}/\text{mL}$) and embedded in Prolong Gold (Invitrogen, Carlsbad, CA, USA). The primary antibodies and their sources are listed in Table 2.

Table 2. Antibodies used, their specificity, and source.

Antibody Against	Description	Specificity/Immunogen	Concentration Used	Product No. and Manufacturer
AURORA B	Rabbit polyclonal	A peptide derived from within residues 1–100 of human Aurora B.	1:300	ab2254, Abcam, Cambridge, UK
α -Tubulin	Mouse monoclonal	Recognizes an epitope located at the C-terminal end of the α -tubulin isoform in a variety of organisms.	1:1000	T5168, Sigma-Aldrich, St. Louis, MO, USA
β -Actin	Mouse monoclonal	Synthetic peptide corresponding to human β -actin aa 1–100.	1:500 1:2000 WB	ab8226, Abcam, Cambridge, UK
CDC42	Rabbit polyclonal	The details of the immunogen for this antibody are not available.	1:100 1:500 WB	ab187643, Abcam, Cambridge, UK
CDC42	Mouse monoclonal	Specific for an epitope mapping between amino acids 166–182 at the C-terminus of CDC42 of human origin.	1:50	sc-8401, Santa Cruz, Dallas, TX, USA
CDX2	Rabbit monoclonal	A synthetic peptide corresponding to residues near the N-terminus of human CDX2.	1:50	MA5-14494, Thermo Fisher Scientific, Rockford, IL, USA
EMI2	Rabbit polyclonal	Recombinant protein corresponding to human EMI2.	1:100	PA5-55042, Invitrogen, Carlsbad, CA, USA
F-ACTIN		Phalloidin-iFluor 594 conjugate.	1:500	ab176757, Abcam, Cambridge, UK
GAPDH	Mouse monoclonal	Raised against recombinant GAPDH of human origin.	1:5000 WB	sc-47724, Santa Cruz, Dallas, TX, USA
γ -H2AX	Rabbit polyclonal	Recognizes human and mouse γ -H2AX.	1:200	4411-PC-100, Trevigen, Gaithersburg, MD, USA
MOS (C237)	Rabbit polyclonal	Epitope mapping at the C-terminus.	1:50	sc-86, Santa Cruz, Dallas, TX, USA
NANOG	Mouse monoclonal	Recombinant human Nanog.	1:50	N3038, Sigma-Aldrich, St. Louis, MO, USA
OCT4	Rabbit polyclonal	A peptide derived from within residues 300 to the C-terminus of human Oct4.	1:200	ab19857, Abcam, Cambridge, UK
p-AMPK α 1/2 (Thr183/172)	Rabbit polyclonal	Epitope corresponding to phosphorylated Thr172 of AMPK α 1 of human origin.	1:50	sc-101630, Santa Cruz, Dallas, TX, USA
pH3Ser10	Mouse monoclonal	Recognizes phospho-S10 on histone H3.	1:200	ab14955, Abcam, Cambridge, UK
P62/SQSTM1	Rabbit polyclonal	A synthetic peptide corresponding to human SQSTM1/ p62 (C-terminal).	1:500 WB	ab91526, Abcam, Cambridge, UK
TEAD1	Mouse monoclonal	Carrier-protein-conjugated synthetic peptide encompassing a sequence within the centre region of human TEAD1.	1:100	GT13112, Invitrogen, Carlsbad, CA, USA
YAP1	Rabbit polyclonal	Recombinant YAP1 protein expressed in bacteria.	1:400	PA-46189, Invitrogen, Carlsbad, CA, USA

For microscopic observations, a fluorescence light microscope (Leitz Ergolux L03-10, Leica, Wetzlar, Germany) equipped with a color video camera (Sony DXC 390P, Sony, Tokyo, Japan) and laser scanning confocal microscope (LEICA TCS SP8, Wetzlar, Germany) were used.

4.4. Toluidine Blue DNA Staining and Image Cytometry

Toluidine blue DNA staining and image cytometry were performed as detailed previously [4]. The cytopins were fixed in ethanol: acetone (1:1) for ≥ 30 min at 4 °C, air-dried and hydrolyzed with 5 N HCl for 20 min at room temperature. The slides were then washed in distilled water (5 × 1 min), stained for 10 min with 0.05% toluidine blue in 50% citrate-phosphate McIlvain buffer at pH 4, and rinsed with distilled water. The samples were then blotted dry and incubated twice in butanol for 3 min each at 37 °C and twice in xylene for 3 min each at room temperature before being embedded in DPX. The DNA content was measured as the integral optical density (IOD), using Image-Pro Plus 4.1 software (Media Cybernetics, Rockville, MD, USA). The stoichiometry of DNA staining was verified using the values obtained for metaphases compared with anaphases and telophases (ratio 2.0); the (2C) DNA values in arbitrary units were averaged from measuring the anaphases in untreated tumor cells. For the cell cycle measurements, 200–500 interphase cells were collected at each point.

4.5. RT-PCR and Selfie-Digital RT-PCR

The total RNA was extracted from MDA-MB-231 (10^6) cells using TRIZOL (Invitrogen, Carlsbad, CA, USA) and for the Selfie-digital RT-PCR the cells were lysed in the 100ST DNA/RNA/protein solubilization reagent (#DCQ100ST, DireCtQuant, Lleida, Spain) at 250,000 cells/mL. RT-PCR and Selfie-digital RT-PCR was performed and the primers were used as described in [4].

4.6. Western Blot Analysis

Living adherent cells were washed with PBS, harvested into an ice-cold RIPA lysis buffer using a cold plastic cell scraper, and centrifuged at $10,000 \times g$ for 20 min at 4 °C. The concentration of proteins was estimated with the Qubit protein Assay kit (Invitrogen, Carlsbad, CA, USA). Equal protein loading in each lane was checked by Ponceau S staining. SDS PAGE was used to separate 20 μ g of each protein sample on 15% gels and then blotted onto nitrocellulose membranes (Amersham, Buckinghamshire, UK). The membranes were blocked in 3% BSA dissolved in TBS containing 0.1% Tween-20 for 1 h at room temperature (RT). Subsequently, the membranes were probed overnight at 4 °C with the primary antibodies listed in Table 2. The respective proteins were detected after incubation with horseradish peroxidase-conjugated secondary antibodies (1:2000, rabbit anti-mouse IgG-HRP, 61-6520, Invitrogen; goat anti-rabbit IgG-HRP 32460, Thermo Fisher Scientific, Rockford, IL, USA), using an ECL system (Thermo Scientific, Rockford, IL, USA) according to the manufacturer's instructions.

4.7. Transcriptome Library Preparation

RNA isolation was performed using the AllPrep DNA/RNA/miRNA Universal Kit (Qiagen, Hilden, Germany). RNA quality was determined using the RNA 6000 Pico Kit and Agilent 2100 bioanalyzer (Agilent Technologies, Santa Clara, CA, USA). The cells for RNA isolation were collected on days 0, 5, 8, 16, and 22. The experiments were performed in triplicate. A transcriptome library preparation was performed using the MGIEasy RNA Directional Library Prep Kit (MGI, Shenzhen, China). The Veriti 96 Well Thermal Cycler (Applied Biosystems, Bedford, MA, USA) was used to carry out all reactions and incubations as intended in the library preparation protocol. The RNA enrichment was performed by depleting rRNA with the MGIEasy rRNA Depletion Kit (MGI, China). Work continued accordingly with the instructions for the 250bp insert size. The DNBSEQ-G400 sequencing platform (MGI, China) was used for sequencing the libraries. The RNA concentrations after extraction, dsDNA concentrations after amplification, and ssDNA concentrations after multiplexing were determined using the appropriate Qubit assays: QubitTM RNA HS Assay Kit, QubitTM dsDNA HS Assay, QubitTM ssDNA HS Assay Kit, and Qubit[®] 2.0 Fluorometer (Thermo Fisher Scientific, Rockford, IL, USA). The fragment size after amplification was determined using a high sensitivity DNA kit and Agilent 2100 bioanalyzer (Agilent

Technologies, USA). The transcriptome FASTQ files were quality checked with a FastQC, trimmed of 3' adapters and low-quality reads with Cutadapt (with parameters of -m 70 and -q 10), pseudo-aligned to the GRCh38.p13 human transcriptome (downloaded from the GENCODE site) with Salmon [58], and then the tximport package [59] in R was used to acquire gene-level count matrices for each sample.

4.8. Differentially Expressed Gene (DEG) Identification and GO Enrichment Analysis

A differential expression analysis comparing treated samples with the NT control at the D5, D8, D16, and D22 time points was performed using edgeR [60], obtaining the differentially expressed genes (DEGs) with the glmQLFTest approach. The threshold for differential expression was selected to be FDR < 0.05 and LogFC > 1 (in absolute value). The EdgeR's plotMDS visualization function was used to construct a MDS (multidimensional scaling) plot of the samples, while volcano plots of the DEGs were generated with EnhancedVolcano [61]. The resulting lists of upregulated and downregulated genes for each time point were subsequently subjected to a Gene Ontology (GO) [14] enrichment analysis with the hypergeometric test method and Benjamini-Hochberg *p*-value correction (*p*Adj < 0.05 threshold for enrichment) implemented in the clusterProfiler [62] package. The enrichment results were visualized in treemap plot form using the rrvgo [63] R package.

4.9. Bivalent Gene Enrichment Analysis, Phylostratigraphic Analysis, and Eighth Phylostratum STRING Protein–Protein Interaction Network Analysis

The list of 3590 bivalent genes was obtained from Court and Arnaud, 2017 [64]. The DEG lists (upregulated and downregulated genes, separately) for each time point were assessed for statistically significant enrichment with bivalent genes using the binomial test method. The differentially expressed bivalent genes were assessed separately with a GO enrichment analysis and the results visualized as described in the previous section.

The whole-genome phylostratigraphy data separating the genes into evolutionary groups referred to as phylostrata was obtained from Trigos et al., 2017 [18]. The phylostratigraphic distributions of the differentially expressed genes at each of the time points were plotted with ggplot2 [65], with the whole-genome phylostratigraphic distribution serving as a reference.

Due to the prevalence of eighth phylostratum genes among the upregulated genes, it was further decided to subject these eighth phylostratum DEGs to a STRING PPI (protein–protein interaction) network analysis in order to determine the functional relationship between them. Protein–protein interaction data for these genes of interest was downloaded from the STRING database and visualized in network form using Cytoscape [66]. After extracting the giant component of each network, the resulting networks were subjected to a GO-enrichment analysis with the ClueGO [67] Cytoscape app. The resulting enriched GO modules were subsequently visualized in an enrichment map format.

Supplementary Materials: The following supporting information can be downloaded at: <https://www.mdpi.com/article/10.3390/ijms24043237/s1>.

Author Contributions: Conceptualization, K.S., N.M.V. and J.E.; methodology, K.S., N.M.V., M.K., I.I. and J.E.; validation, K.S., N.M.V., M.K., I.I. and D.P.; investigation, K.S., N.M.V., M.K., I.I. and D.P.; resources, K.S. and N.M.V.; data curation, N.M.V.; writing—original draft preparation, K.S., J.E., and N.M.V.; writing—review and editing, J.E., M.S.C., N.M.V. and K.S.; visualization, K.S. and N.M.V.; supervision, J.E.; project administration, D.P.; funding acquisition, K.S. and N.M.V. All authors have read and agreed to the published version of the manuscript.

Funding: This research was supported by a grant from the European Regional Development Fund (ERDF) project No. 1.1.1.2/VIAA/3/19/463 for K.S. and the 8.2.2.0/20/1/006 "University of Latvia Doctoral Study Program Capacity Enhancement Through a New PhD Model" project for N.M.V.

Acknowledgments: Petar Podlesniy for the digital PCR, Agnieszka Bojko for help with the Sa- β -gal staining (republished from [4] under CC BY 4.0 licence), and Pawel Zayakin for the bioinformatic advice are acknowledged.

Conflicts of Interest: The authors declare no conflict of interest.

References

- Old, L.J. Cancer/testis (CT) Antigens—A New Link between Gametogenesis and Cancer. *Cancer Immun.* **2001**, *1*, 1. [[PubMed](#)]
- Kalejs, M.; Erenpreisa, J. Cancer/testis Antigens and Gametogenesis: A Review and “Brain-Storming” Session. *Cancer Cell Int.* **2005**, *5*, 4. [[CrossRef](#)]
- Old, L.J. Cancer Is a Somatic Cell Pregnancy. *Cancer Immun.* **2007**, *7*, 19. [[PubMed](#)]
- Salmina, K.; Bojko, A.; Inashkina, I.; Staniak, K.; Dudkowska, M.; Podlesniy, P.; Rumnieks, F.; Vainshelbaum, N.M.; Pjanova, D.; Sikora, E.; et al. “Mitotic Slippage” and Extranuclear DNA in Cancer Chemoresistance: A Focus on Telomeres. *Int. J. Mol. Sci.* **2020**, *21*, 2779. [[CrossRef](#)] [[PubMed](#)]
- Chuong, E.B. The Placenta Goes Viral: Retroviruses Control Gene Expression in Pregnancy. *PLoS Biol.* **2018**, *16*, e3000028. [[CrossRef](#)] [[PubMed](#)]
- Diaz-Carballo, D.; Klein, J.; Acikelli, A.H.; Wilk, C.; Saka, S.; Jastrow, H.; Wennemuth, G.; Dammann, P.; Giger-Pabst, U.; Khosrawipour, V.; et al. Cytotoxic Stress Induces Transfer of Mitochondria-Associated Human Endogenous Retroviral RNA and Proteins between Cancer Cells. *Oncotarget* **2017**, *8*, 95945–95964. [[CrossRef](#)]
- Kshitiz; Afzal, J.; Maziarz, J.D.; Hamidzadeh, A.; Liang, C.; Erkenbrack, E.M.; Kim, H.N.; Haeger, J.-D.; Pfarrer, C.; Hoang, T.; et al. Evolution of Placental Invasion and Cancer Metastasis Are Causally Linked. *Nat. Ecol. Evol.* **2019**, *3*, 1743–1753. [[CrossRef](#)]
- Lala, P.K.; Nandi, P.; Hadi, A.; Halari, C. A Crossroad between Placental and Tumor Biology: What Have We Learnt? *Placenta* **2021**, *116*, 12–30. [[CrossRef](#)]
- Anatskaya, O.V.; Vinogradov, A.E.; Vainshelbaum, N.M.; Giuliani, A.; Erenpreisa, J. Phylostratic Shift of Whole-Genome Duplications in Normal Mammalian Tissues towards Unicellularity Is Driven by Developmental Bivalent Genes and Reveals a Link to Cancer. *Int. J. Mol. Sci.* **2020**, *21*, 8759. [[CrossRef](#)]
- Martínez-Zamudio, R.I.; Roux, P.-F.; de Freitas, J.A.N.L.F.; Robinson, L.; Doré, G.; Sun, B.; Belenki, D.; Milanovic, M.; Herbig, U.; Schmitt, C.A.; et al. AP-1 Imprints a Reversible Transcriptional Programme of Senescent Cells. *Nat. Cell Biol.* **2020**, *22*, 842–855. [[CrossRef](#)]
- Erenpreisa, J.; Salmina, K.; Anatskaya, O.; Cragg, M.S. Paradoxes of Cancer: Survival at the Brink. *Semin. Cancer Biol.* **2022**, *81*, 119–131. [[CrossRef](#)] [[PubMed](#)]
- Corrales, L.; Woo, S.-R.; Williams, J.B.; McWhirter, S.M.; Dubensky, T.W., Jr.; Gajewski, T.F. Antagonism of the STING Pathway via Activation of the AIM2 Inflammasome by Intracellular DNA. *J. Immunol.* **2016**, *196*, 3191–3198. [[CrossRef](#)] [[PubMed](#)]
- Liberzon, A.; Subramanian, A.; Pinchback, R.; Thorvaldsdóttir, H.; Tamayo, P.; Mesirov, J.P. Molecular Signatures Database (MSigDB) 3.0. *Bioinformatics* **2011**, *27*, 1739–1740. [[CrossRef](#)] [[PubMed](#)]
- Harris, M.A.; Clark, J.; Ireland, A.; Lomax, J.; Ashburner, M.; Foulger, R.; Eilbeck, K.; Lewis, S.; Marshall, B.; Mungall, C.; et al. The Gene Ontology (GO) Database and Informatics Resource. *Nucleic Acids Res.* **2004**, *32*, D258–D261.
- Vainshelbaum, N.M.; Salmina, K.; Gerashchenko, B.I.; Lazovska, M.; Zayakin, P.; Cragg, M.S.; Pjanova, D.; Erenpreisa, J. Role of the Circadian Clock “Death-Loop” in the DNA Damage Response Underpinning Cancer Treatment Resistance. *Cells* **2022**, *11*, 880. [[CrossRef](#)] [[PubMed](#)]
- Lineweaver, C.H.; Bussey, K.J.; Blackburn, A.C.; Davies, P.C.W. Cancer Progression as a Sequence of Atavistic Reversions. *Bioessays* **2021**, *43*, e2000305. [[CrossRef](#)]
- Vainshelbaum, N.M.; Giuliani, A.; Salmina, K.; Pjanova, D.; Erenpreisa, J. The Transcriptome and Proteome Networks of Malignant Tumours Reveal Atavistic Attractors of Polyploidy-Related Asexual Reproduction. *Int. J. Mol. Sci.* **2022**, *23*, 14930. [[CrossRef](#)]
- Trigos, A.S.; Pearson, R.B.; Papenfuss, A.T.; Goode, D.L. Altered Interactions between Unicellular and Multicellular Genes Drive Hallmarks of Transformation in a Diverse Range of Solid Tumors. *Proc. Natl. Acad. Sci. USA* **2017**, *114*, 6406–6411. [[CrossRef](#)]
- Hadjimichael, C.; Chanoumidou, K.; Papadopoulou, N.; Arampatzi, P.; Papamatheakis, J.; Kretsovali, A. Common Stemness Regulators of Embryonic and Cancer Stem Cells. *World J. Stem Cells* **2015**, *7*, 1150–1184.
- Yasuda, T.; Banville, D.; Hendy, G.N.; Goltzman, D. Characterization of the Human Parathyroid Hormone-like Peptide Gene. Functional and Evolutionary Aspects. *J. Biol. Chem.* **1989**, *264*, 7720–7725. [[CrossRef](#)] [[PubMed](#)]
- Chang, W.-M.; Lin, Y.-F.; Su, C.-Y.; Peng, H.-Y.; Chang, Y.-C.; Hsiao, J.-R.; Chen, C.-L.; Chang, J.-Y.; Shieh, Y.-S.; Hsiao, M.; et al. Parathyroid Hormone-Like Hormone Is a Poor Prognosis Marker of Head and Neck Cancer and Promotes Cell Growth via RUNX2 Regulation. *Sci. Rep.* **2017**, *7*, 41131. [[CrossRef](#)]
- Qie, S.; Sang, N. Stanniocalcin 2 (STC2): A Universal Tumour Biomarker and a Potential Therapeutical Target. *J. Exp. Clin. Cancer Res.* **2022**, *41*, 161. [[CrossRef](#)]
- Suman, P.; Malhotra, S.S.; Gupta, S.K. LIF-STAT Signaling and Trophoblast Biology. *JAKSTAT* **2013**, *2*, e25155. [[CrossRef](#)]
- Baryshev, M.; Inashkina, I.; Salmina, K.; Huna, A.; Jackson, T.R.; Erenpreisa, J. DNA Methylation of the *Oct4A* Enhancers in Embryonal Carcinoma Cells after Etoposide Treatment Is Associated with Alternative Splicing and Altered Pluripotency in Reversibly Senescent Cells. *Cell Cycle* **2018**, *17*, 362–366. [[CrossRef](#)]
- Schöler, H.R.; Dressler, G.R.; Balling, R.; Rohdewohld, H.; Gruss, P. Oct-4: A Germline-Specific Transcription Factor Mapping to the Mouse T-Complex. *EMBO J.* **1990**, *9*, 2185–2195. [[CrossRef](#)]
- Pesce, M.; Anastassiadis, K.; Schöler, H.R. Oct-4: Lessons of Totipotency from Embryonic Stem Cells. *Cells Tissues Organs* **1999**, *165*, 144–152. [[CrossRef](#)] [[PubMed](#)]

27. Motwani, M.; Pesiridis, S.; Fitzgerald, K.A. DNA Sensing by the cGAS-STING Pathway in Health and Disease. *Nat. Rev. Genet.* **2019**, *20*, 657–674. [[CrossRef](#)]
28. Deb, K.; Sivaguru, M.; Yong, H.Y.; Roberts, R.M. Cdx2 Gene Expression and Trophectoderm Lineage Specification in Mouse Embryos. *Science* **2006**, *311*, 992–996. [[CrossRef](#)] [[PubMed](#)]
29. Zhang, Y.; Li, J.; Lai, X.-N.; Jiao, X.-Q.; Xiong, J.-P.; Xiong, L.-X. Focus on Cdc42 in Breast Cancer: New Insights, Target Therapy Development and Non-Coding RNAs. *Cells* **2019**, *8*, 146. [[CrossRef](#)]
30. Fu, J.; Liu, B.; Zhang, H.; Fu, F.; Yang, X.; Fan, L.; Zheng, M.; Zhang, S. The Role of Cell Division Control Protein 42 in Tumor and Non-Tumor Diseases: A Systematic Review. *J. Cancer* **2022**, *13*, 800–814. [[CrossRef](#)] [[PubMed](#)]
31. Kalailingam, P.; Tan, H.B.; Pan, J.Y.; Tan, S.H.; Thanabalu, T. Overexpression of CDC42SE1 in A431 Cells Reduced Cell Proliferation by Inhibiting the Akt Pathway. *Cells* **2019**, *8*, 117. [[CrossRef](#)]
32. Leblanc, J.; Zhang, X.; McKee, D.; Wang, Z.-B.; Li, R.; Ma, C.; Sun, Q.-Y.; Liu, X.J. The Small GTPase Cdc42 Promotes Membrane Protrusion during Polar Body Emission via ARP2-Nucleated Actin Polymerization. *Mol. Hum. Reprod.* **2011**, *17*, 305–316. [[CrossRef](#)]
33. Liu, Y.; Shan, N.; Yuan, Y.; Tan, B.; He, C.; Tong, C.; Qi, H. Knockdown of Activated Cdc42-Associated Kinase Inhibits Human Extravillous Trophoblast Migration and Invasion and Decreases Protein Expression of Pho-Akt and Matrix Metalloproteinase. *J. Matern. Fetal. Neonatal Med.* **2020**, *33*, 1125–1133. [[CrossRef](#)]
34. Erenpreisa, J.; Ivanov, A.; Cragg, M.; Selivanova, G.; Illidge, T. Nuclear Envelope-Limited Chromatin Sheets Are Part of Mitotic Death. *Histochem. Cell Biol.* **2002**, *117*, 243–255. [[CrossRef](#)] [[PubMed](#)]
35. Erenpreisa, J.; Salmina, K.; Huna, A.; Kosmacek, E.A.; Cragg, M.S.; Ianzini, F.; Anisimov, A.P. Polyploid Tumour Cells Elicit Paradiploid Progeny through Depolyploidizing Divisions and Regulated Autophagic Degradation. *Cell Biol. Int.* **2011**, *35*, 687–695. [[CrossRef](#)]
36. Erenpreisa, J.; Huna, A.; Salmina, K.; Jackson, T.R.; Cragg, M.S. Macroautophagy-Aided Elimination of Chromatin: Sorting of Waste, Sorting of Fate? *Autophagy* **2012**, *8*, 1877–1881. [[CrossRef](#)] [[PubMed](#)]
37. Erenpreisa, J.; Salmina, K.; Belyayev, A.; Inashkina, I.; Cragg, M.S. Chapter 12—Survival at the Brink: Chromatin Autophagy of Tumor Cells in Response to Genotoxic Challenge. In *Autophagy: Cancer, Other Pathologies, Inflammation, Immunity, Infection, and Aging*; Hayat, M.A., Ed.; Academic Press: Cambridge, MA, USA, 2017; pp. 275–294. ISBN 9780128121467.
38. Mirzayans, R.; Murray, D. Intratumor Heterogeneity and Therapy Resistance: Contributions of Dormancy, Apoptosis Reversal (Anastasis) and Cell Fusion to Disease Recurrence. *Int. J. Mol. Sci.* **2020**, *21*, 1308. [[CrossRef](#)]
39. Zaitceva, V.; Kopeina, G.S.; Zhivotovsky, B. Anastasis: Return Journey from Cell Death. *Cancers* **2021**, *13*, 3671. [[CrossRef](#)] [[PubMed](#)]
40. Hewitt, G.; Carroll, B.; Sarallah, R.; Correia-Melo, C.; Ogrodnik, M.; Nelson, G.; Otten, E.G.; Manni, D.; Antrobus, R.; Morgan, B.A.; et al. SQSTM1/p62 Mediates Crosstalk between Autophagy and the UPS in DNA Repair. *Autophagy* **2016**, *12*, 1917–1930. [[CrossRef](#)]
41. Walen, K.H. Mitotic Slippage Process Concealed Cancer-Sought Chromosome Instability Mechanism (S-CIN). *J. Cancer Ther.* **2017**, *8*, 608–623. [[CrossRef](#)]
42. Madgwick, S.; Hansen, D.V.; Levasseur, M.; Jackson, P.K.; Jones, K.T. Mouse Emi2 Is Required to Enter Meiosis II by Reestablishing Cyclin B1 during Interkinesis. *J. Cell Biol.* **2006**, *174*, 791–801. [[CrossRef](#)]
43. Erenpreisa, J.; Cragg, M.S. MOS, Aneuploidy and the Ploidy Cycle of Cancer Cells. *Oncogene* **2010**, *29*, 5447–5451. [[CrossRef](#)]
44. Fukasawa, K.; Murakami, M.S.; Blair, D.G.; Kuriyama, R.; Hunt, T.; Fischinger, P.; Vande Woude, G.F. Similarities between Somatic Cells Overexpressing the Mos Oncogene and Oocytes during Meiotic Interphase. *Cell Growth Differ.* **1994**, *5*, 1093–1103.
45. Niu, N.; Mercado-Urbe, I.; Liu, J. Dedifferentiation into blastomere-like cancer stem cells via formation of polyploid giant cancer cells. *Oncogene* **2017**, *36*, 4887–4900. [[CrossRef](#)]
46. Kwon, J.; Bakhom, S.F. The Cytosolic DNA-Sensing cGAS-STING Pathway in Cancer. *Cancer Discov.* **2020**, *10*, 26–39. [[CrossRef](#)] [[PubMed](#)]
47. Vainshelbaum, N.M.; Zayakin, P.; Kleina, R.; Giuliani, A.; Erenpreisa, J. Meta-Analysis of Cancer Triploidy: Rearrangements of Genome Complements in Male Human Tumors Are Characterized by XXY Karyotypes. *Genes* **2019**, *10*, 613. [[CrossRef](#)]
48. Sedivy, J.M.; Kreiling, J.A.; Neretti, N.; De Cecco, M.; Criscione, S.W.; Hofmann, J.W.; Zhao, X.; Ito, T.; Peterson, A.L. Death by Transposition—The Enemy Within? *Bioessays* **2013**, *35*, 1035–1043. [[CrossRef](#)]
49. Díaz-Carballo, D.; Gustmann, S.; Jastrow, H.; Acikelli, A.H.; Dammann, P.; Klein, J.; Dembinski, U.; Bardenheuer, W.; Malak, S.; Araúzo-Bravo, M.J.; et al. Atypical Cell Populations Associated with Acquired Resistance to Cytostatics and Cancer Stem Cell Features: The Role of Mitochondria in Nuclear Encapsulation. *DNA Cell Biol.* **2014**, *33*, 749–774. [[CrossRef](#)] [[PubMed](#)]
50. Aarreberg, L.D.; Esser-Nobis, K.; Driscoll, C.; Shuvarikov, A.; Roby, J.A.; Gale, M., Jr. Interleukin-1 β Induces mtDNA Release to Activate Innate Immune Signaling via cGAS-STING. *Mol. Cell* **2019**, *74*, 801–815.e6. [[CrossRef](#)]
51. Kovacs, C.S.; Lanske, B.; Hunzelman, J.L.; Guo, J.; Karaplis, A.C.; Kronenberg, H.M. Parathyroid Hormone-Related Peptide (PTHrP) Regulates Fetal-placental Calcium Transport through a Receptor Distinct from the PTH/PTHrP Receptor. *Proc. Natl. Acad. Sci. USA* **1996**, *93*, 15233–15238. [[CrossRef](#)] [[PubMed](#)]
52. Fais, S.; Marunaka, Y. The Acidic Microenvironment: Is It a Phenotype of All Cancers? A Focus on Multiple Myeloma and Some Analogies with Diabetes Mellitus. *Cancers* **2020**, *12*, 3226. [[CrossRef](#)] [[PubMed](#)]

53. Wang, W.H.; Macháty, Z.; Abeydeera, L.R.; Prather, R.S.; Day, B.N. Parthenogenetic Activation of Pig Oocytes with Calcium Ionophore and the Block to Sperm Penetration after Activation. *Biol. Reprod.* **1998**, *58*, 1357–1366. [[CrossRef](#)]
54. Burwick, R.M.; Lokki, A.I.; Fleming, S.D.; Regal, J.F. Editorial: Innate Immunity in Normal and Adverse Pregnancy. *Front. Immunol.* **2021**, *12*, 646596. [[CrossRef](#)] [[PubMed](#)]
55. Chen, H.-Y.; Yang, Y.M.; Stevens, B.M.; Noble, M. Inhibition of redox/Fyn/c-Cbl pathway function by Cdc42 controls tumour initiation capacity and tamoxifen sensitivity in basal-like breast cancer cells. *EMBO Mol. Med.* **2013**, *5*, 723–736. [[CrossRef](#)]
56. Díaz-Carballo, D.; Saka, S.; Acikelli, A.H.; Homp, E.; Erwes, J.; Demmig, R.; Klein, J.; Schröer, K.; Malak, S.; D'Souza, F.; et al. Enhanced antitumoral activity of TLR7 agonists via activation of human endogenous retroviruses by HDAC inhibitors. *Commun Biol.* **2021**, *4*, 276. [[CrossRef](#)]
57. Adibi, R.; Moein, S.; Gheisari, Y. Bisphosphonates Fight against Cancer Roots: Zoledronic Acid Targets Chemo-Resistant Polyploid Giant Cancer Cells. *Res. Square* **2022**, *13*, 419.
58. Patro, R.; Duggal, G.; Love, M.I.; Irizarry, R.A.; Kingsford, C. Salmon Provides Fast and Bias-Aware Quantification of Transcript Expression. *Nat. Methods* **2017**, *14*, 417–419. [[CrossRef](#)]
59. Soneson, C.; Love, M.I.; Robinson, M.D. Differential Analyses for RNA-Seq: Transcript-Level Estimates Improve Gene-Level Inferences. *F1000Research* **2015**, *4*, 1521. [[CrossRef](#)] [[PubMed](#)]
60. Robinson, M.D.; McCarthy, D.J.; Smyth, G.K. edgeR: A Bioconductor Package for Differential Expression Analysis of Digital Gene Expression Data. *Bioinformatics* **2010**, *26*, 139–140. [[CrossRef](#)] [[PubMed](#)]
61. Blighe, K.; Rana, S.; Lewis, M. *EnhancedVolcano: Publication-Ready Volcano Plots with Enhanced Colouring and Labeling*; R Package Version 1.2.0; GitHub, Inc.: San Francisco, CA, USA, 2019.
62. Wu, T.; Hu, E.; Xu, S.; Chen, M.; Guo, P.; Dai, Z.; Feng, T.; Zhou, L.; Tang, W.; Zhan, L.; et al. clusterProfiler 4.0: A Universal Enrichment Tool for Interpreting Omics Data. *Innovation* **2021**, *2*, 100141. [[CrossRef](#)] [[PubMed](#)]
63. Sayols, S. Rrvgo: A Bioconductor Package to Reduce and Visualize Gene Ontology Terms. 2020. Available online: <https://ssayols.github.io/rrvgo> (accessed on 30 January 2023).
64. Court, F.; Arnaud, P. An Annotated List of Bivalent Chromatin Regions in Human ES Cells: A New Tool for Cancer Epigenetic Research. *Oncotarget* **2017**, *8*, 4110–4124. [[CrossRef](#)] [[PubMed](#)]
65. Villanueva, R.A.M.; Chen, Z.J. ggplot2: Elegant Graphics for Data Analysis (2nd Ed.). *Measurement* **2019**, *17*, 160–167. [[CrossRef](#)]
66. Shannon, P.; Markiel, A.; Ozier, O.; Baliga, N.S.; Wang, J.T.; Ramage, D.; Amin, N.; Schwikowski, B.; Ideker, T. Cytoscape: A Software Environment for Integrated Models of Biomolecular Interaction Networks. *Genome Res.* **2003**, *13*, 2498–2504. [[CrossRef](#)] [[PubMed](#)]
67. Bindea, G.; Mlecnik, B.; Hackl, H.; Charoentong, P.; Tosolini, M.; Kirilovsky, A.; Fridman, W.-H.; Pagès, F.; Trajanoski, Z.; Galon, J. ClueGO: A Cytoscape Plug-in to Decipher Functionally Grouped Gene Ontology and Pathway Annotation Networks. *Bioinformatics* **2009**, *25*, 1091–1093. [[CrossRef](#)] [[PubMed](#)]

Disclaimer/Publisher's Note: The statements, opinions and data contained in all publications are solely those of the individual author(s) and contributor(s) and not of MDPI and/or the editor(s). MDPI and/or the editor(s) disclaim responsibility for any injury to people or property resulting from any ideas, methods, instructions or products referred to in the content.

4. Discussion

The literature data indicates that the attractor state of highly aggressive treatment-resistant cancer is characterized by embryonal stemness, atavistic co-option of traits from more ancient organisms (including amoeboid transition), expression of gametogenetic (meiotic, cancer-testis and germ cell) genes, as well as modes of cell division much unlike conventional mitosis (e.g. PGCC budding by coenocytosis). In this work, we have attempted to find out whether these features of cancer resistance are mutually related and could be united in the context of the life cycle-like reversible polyploidy as components or prerequisites of a “cancer reproductive process”. This study places a particular emphasis on patient tumor material.

We have opted for a bioinformatic and systems-biological approach focusing on high-throughput data. For analysis, we have used data from several open-access databases (*ex vivo* samples) and cell line experimental material from the Latvian Biomedical Research and Study Centre’s Cancer Cell Biology and Melanoma Research Laboratory (Table 1). This data covers multiple -omics layers (genomic in the form of ABSOLUTE ploidy values and Mitelman database karyotypes, transcriptomic, and proteomic). The results of these studies were presented in 7 articles.

Overall, five linked “layers” of results were acquired:

- (1) The isolated impact of polyploidy on the transcriptome in normal tissues, highlighting unicellularity and early multicellularity, a potential cancer-promoting component, upregulation of bivalent developmental genes, and downregulation of the circadian clock.
- (2) The impact of polyploidy on the cancer transcriptome.
- (3) The positive relationship between polyploidy and activation of reproductive functional modules in cancer transcriptomes (highlighting the evolutionarily early oocyte-meiotic component in TCGA patient data and the later component of pseudo-pregnancy and trophoblast-like functions in the MDA-MB-231-doxorubicin model)
- (4) The expression and networking of gametogenetic genes in cancer on the protein level
- (5) A particular example of a likely reproductive process in cancer (a presumable cancer digyny in the form of X-disomic near-triploid karyotypes).

The comparison of polyploid and diploid normal organs revealed that polyploidy can increase the activity of bivalent genes - genes that contain both activating and repressive histone modifications in their promoters and/or enhancers, enabling them to switch their activity rapidly

(D. Kumar et al., 2021). Thus, polyploidy inherently increases epigenetic plasticity and the ability for critical cooperative transitions regardless of whether it's present in a normal or a cancer cell. Coupled with the fact that most bivalent genes are involved in development and embryogenesis (Court & Arnaud, 2017), this evidence further reinforces the idea that PGCCs bear a similarity to ESCs and/or early embryos.

The results of this study also suggest that polyploidy changes the balance of gene expression in the whole transcriptome (driving an atavistic shift to more ancient, unicellular or early multicellular phenotypes), however, that it uses latent or creates novel reproductive attractors (likely by using gene paralogs) that span the whole phylostratigraphic axis. This is in line with both the study of Trigos et al. (Trigos et al., 2019) that shows a link between cancer and heightened unicellular gene expression, and the morphological observations on polyploid cancer cells induced in genotoxically treated cultures (J. Erenpreisa et al., 2018; Ianzini et al., 2009), which demonstrate amoeboid phenotypes such as budding (release of cellularized subnuclei) and encystment. Furthermore, normal tissue polyploidy also upregulates oncogenes, downregulates tumor suppressor genes, suppresses the circadian clock and stimulates the activity of the key proto-oncogene c-Myc's interactome. Strikingly, as prerequisites for such a process have been observed in normal endopolyploid cells, a cancer-favoring environment can thus be generated via genome copy multiplication alone, without the profound mutational load inherent in cancer. At the same time, the interphase chromosomes of PGCCs show expansion and overlap of their territories (Schwarz-Finsterle et al., 2013), c-Myc-induced acetylation of nucleosomal histone H3 and H4 tails, which likely increases accessibility of the chromatin common fragile sites as a source of juxtaposed gene mutations, translocations and amplification of the mutant genes (Shubernetskaya et al., 2017); as well as activation of retrotransposons that increases genome instability, production of carcinogenic microRNAs (Lavia et al., 2022) and similar processes which can probabilistically and reciprocally favour cancer origin and development.

Furthering the investigation from normal tissues to TCGA cancer patient samples, it was revealed that, like in the normal tissues, polyploidy (WGD) is associated with circadian deregulation (namely, a higher coefficient thereof - the Δ CCD value). Embryonic stem and germ cells also demonstrate a lack of circadian function, which returns during differentiation and is coordinated with the cell cycle (Bittman, 2016; Farshadi et al., 2020; Vallone et al., 2007). Thus, the obtained results regarding circadian deregulation reinforce the association between ESCs, germ cells and polyploid cancer displaying tolerance to DNA damage as an essential feature of cancer's adaptive system.

In the following part of the study, we have observed that polyploidy upregulates gametogenesis-related (GG) genes in TCGA cancer patient transcriptomes, with 10 of the 29 studied cancer types demonstrating significant GG gene enrichment among their ploidy-upregulated genes. The upregulated GG genes were also revealed to be largely evolutionarily ancient (with the exception of MAGE group CT genes). Furthermore, ploidy-upregulated genes associate into highly-interconnected STRING (in 9 tumor types) and coexpression (in 6 tumor types) networks enriched for multiple modules related to meiosis (including oogenesis-related ones). The relation of polyploidy to female meiosis and pseudo-placentation, shown in TCGA tumors and in experiments on breast cancer cell line samples, as well as XXY karyotypes in triploid male tumors, represent a strong argument for the involvement of a non-accidental but pre-programmed reproductive process in the resistant escape from various cancer treatments. The fact that GG genes were observed to be both expressed and co-expressed on the proteome level in high-throughput proteomics data of melanoma and breast cancer also contributes to the evidence for a reproductive process. Moreover, many GG proteins (MOS, SYCP3, PRAME, the MAGE group and others) are linked to poor prognosis in cancer patients independently of experimental studies (Bruggeman et al., 2020; Z. Chen et al., 2018; da Silva et al., 2017; Lingg et al., 2022).

The cancer reproductive process is by its nature asexual in somatic tumors. Multiple mechanisms of this process can be proposed, starting from the ploidy cycles of protozoans that help them avoid Muller's ratchet and ending with the implementation of actual modified meiosis variants observed in plants and animals, such as inverted meiosis and/or digyny (triploid parthenogenesis), both found in IVF clinics (Chamayou et al., 2013; Ottolini et al., 2015). It likely involves at least some part or modification of oocyte meiosis and displays some parthenogenetic characteristics. Evidence for a digyny-like process, in particular, was observed upon analyzing karyotype data of 15 malignant tumor patient cohorts from the Mitelman database, wherein a robust and non-random association between a near-triploid chromosome count and X chromosome disomy has been demonstrated.

Furthermore, both the results of Mitelman database karyotype analysis and doxorubicin-treated MDA-MB-231 cell culture comparison with untreated samples demonstrate the importance of interactions and transitions between different polyploidy levels in cancer evolution and adaptation to treatment. In renal carcinoma samples from the Mitelman database, diploid and tetraploid subpopulations are shown to exist alongside X-disomic (likely reproductive) triploid ones, while the MDA-MB-231 experiments showcase the existence of reproductive PGCCs (that depolyploidize) and supergiant PGCCs that further senesce and seem

to serve a supportive function for their reproductive dependants via extruded and autophagically recycled cytosolic DNA, homing, and pro-inflammatory SASP. A single PGCC can possibly serve both a reproductive function and a feeding, homing, invasive “pseudo-trophoblastic” function that complements its descendants after depolyploidization until they become capable of independent division and tumor repopulation. Thus, different types of PGCC cell populations coexist in the tumor, and a cooperation between them can drive evolution, metastasis and resistance to treatment.

The ability of ectopically expressed meiotic genes to increase genomic instability for subsequent clonal selection certainly warrants attention as well. Still, due to the properties of cancer as a complex adaptive system, channeling pre-programmed processes, such a role for meiotic genes isn't in contradiction with the existence of a reproductive process (and our work is in line with that).

The attractor state of advanced, therapy-resistant cancer (embodied by the reproductive PGCC) is reached in a crucial yet low-probability event through adaptive exploration (“learning”) of the gene regulatory network that occurs on the “edge of chaos” in response to stimuli (stress). Both bivalent gene activation and circadian clock failure can be viewed as signs of such critical cooperative transition. This process of self-organization would inevitably result in the emergence of errors and many other cell fates (i.e polyloid cancer cells that don't become reproductive PGCC) alongside the rare resistant attractor. The fact that reproduction-related gene activation in polyloid cancer skews towards oogenesis rather than spermatogenesis is another piece of evidence in favor of a pre-programmed role other than the indiscriminate genome instability-promoting one.

Altogether, the relationship between the results yielded by the separate components of the work appears to be one of mutual reinforcement. The observed phenomena seem to coalesce, indicating the existence of a uniting mechanism for cancer ploidy cycling, reproduction, evolution, reprogramming, and therapy resistance development. Neither of those observations contradict any previously established cancer theory (e.g. embryonal and parthenogenetic cancer theory, somatic mutation theory, cancer stem cell theory, cancer life-cycle, atavistic theory), but rather complement them.

The success of this comparative study may be dependent on the chosen methodical approach - network analysis, study of bivalent genes changing cell fate, and phylostratigraphic inquiry. A major drawback is the lack of actual single-cell PGCC data in favor of bulk sequencing

(whole-genome copy number data, aka ABSOLUTE ploidy values, transcriptome, proteome) and karyotyping. This was mostly substituted by *in situ* immunofluorescence analysis of single cells in chamber slides carried out in parallel by collaborators, with supporting results. Still, difficulties remain concerning bioinformatic analysis of large-scale open-access patient datasets due to the growing importance of being able to distinguish between the heterogeneous components of the malignant tumor, which is known to consist of a wide variety of cell types, including tumor-associated immune cells, pericytes, fibroblasts, mesenchymal stromal cells, parenchymal cancer cells and cancer stem cells (including PGCCs and their depolyploidized progeny) (Albini et al., 2015; Cho, 2017; White-Gilbertson & Voelkel-Johnson, 2020). The existence and ongoing rapid expansion of open-access cancer scRNA-seq material databases opens an intriguing direction for potential continuation of this work. Given access to high-quality scRNA-seq datasets of multiple cancer types and stages, it could be possible to explore the biology of PGCCs and their interactions with the cancerous and non-cancerous cells of the surrounding tumor microenvironment in more detail. However, such an approach is currently bottlenecked by difficulties in single-cell ploidy inference from scRNA-seq data (hitherto attempted in only one study using the InferCNV algorithm (M. Kumar et al., 2020)).

While it is evident that further research is necessary to improve the precision of the described findings, they could potentially have applications for future endeavors in cancer diagnostics, prognostics and/or therapeutics (for example, efforts to counteract cancer stemness via epigenetic normalization, which are currently yielding slow yet promising progress (Ishay-Ronen & Christofori, 2019; Zheng & Gao, 2019)).

5. Conclusions

1. Polyploidy induces an atavistic whole-transcriptome phylostratigraphic shift and rewiring of the gene regulatory network that involves epigenetic plasticity enhancement via bivalent gene activation and promotes cancer cell reprogramming to an embryonal stem- or germ-like state.
2. Polyploidy is associated with circadian clock deregulation, which may be exploited by cancer cells to bypass DNA damage checkpoints. Measuring the degree of circadian deregulation may have practical applications.

3. Polyploidy also promotes the acquisition of an asexual reproductive function that employs some components of oocyte meiosis and should serve, through recombination events, to prevent deleterious mutation accumulation and reduce ploidy.
4. The likely cancer reproductive process, while mostly ancient, employs phylostratigraphically diverse genes and may borrow its functions from a variety of potential sources such as inverted meiosis, parthenogenesis (e.g. triploid digyny), and coenocytosis.
5. In addition to their “reproductive” function, some PGCCs instead (or afterwards) perform a trophoblast-like function (associated with cytosolic DNA, the senescence secretome and immunity) for the depolyploidized mitotic progeny. These novel data showcase the importance of cooperation between different cancer cell subpopulations and highlight the necessity for further exploration of this topic via investigation methods focusing on single-cell sequencing.
6. Taking into account the ability of cancer stem cell GRNs to switch between rigidity and plasticity (Csermely, 2021), the study of the GG genes’ first neighbors could present an interesting direction for continuation of this work.

6. Theses for defense

- I. Polyploidy is a major driver of atavistic and cancer-promoting rewiring of the gene regulatory network.
- II. Cancer polyploidy is associated with circadian deregulation, both leading to DNA damage tolerance.
- III. Cancers are prone to undergoing asexual reproductive processes driven by gametogenetic genes, which employ components of the oocyte meiosis pathway and proto-placental mechanisms of cell communication between PGCCs and their reproductive offspring.
- IV. X-disomic cancer triploidy in male patient karyotypes may be indicative of a digyny-like parthenogenesis that confers adaptive benefits.

7. Acknowledgements

Funding:

- European Regional Development Fund project “Understanding the biology of the minimal residual disease after targeted therapy of BRAF mutant melanoma” (ERDF 1.1.1.1/18/A/099)
- University of Latvia Foundation Doctoral Scholarship in the Exact, Medical and Life Sciences
- “Strengthening of the Capacity of Doctoral Studies at the University of Latvia within the Framework of the New Doctoral Model”, project identification No. 8.2.2.0/20/I/006.
- FLPP projekts “The role of PML in the ALT-coupled senescence-meiosis-stemness pathway involved in tumour cell resistance to targeted and genotoxic treatment” (lzp-2022/1-0114)

I would like to extend my sincere gratitude to my thesis supervisor J. Erenpreisa and thesis consultant A. Giuliani, my co-authors, my funding providers, the cherished friends who kept me in good spirits, and the good coffee that fueled my creativity.

References

- Adibi, R., Moein, S., & Gheisari, Y. (2021). Cisplatin resistant ovarian cancer cells reveal a polyploid phenotype with remarkable activation of nuclear processes. In *Research Square*. Research Square. <https://doi.org/10.21203/rs.3.rs-440506/v1>
- Adl, S. M., Simpson, A. G. B., Lane, C. E., Lukeš, J., Bass, D., Bowser, S. S., Brown, M. W., Burki, F., Dunthorn, M., Hampl, V., Heiss, A., Hoppenrath, M., Lara, E., Le Gall, L., Lynn, D. H., McManus, H., Mitchell, E. A. D., Mozley-Stanridge, S. E., Parfrey, L. W., ... Spiegel, F. W. (2012). The revised classification of eukaryotes. *The Journal of Eukaryotic Microbiology*, 59(5), 429–493.
- Albini, A., Bruno, A., Gallo, C., Pajardi, G., Noonan, D. M., & Dallaglio, K. (2015). Cancer stem cells and the tumor microenvironment: interplay in tumor heterogeneity. *Connective Tissue Research*, 56(5), 414–425.
- Allada, R., & Chung, B. Y. (2010). Circadian organization of behavior and physiology in *Drosophila*. *Annual Review of Physiology*, 72, 605–624.
- Almeida, L. G., Sakabe, N. J., deOliveira, A. R., Silva, M. C. C., Mundstein, A. S., Cohen, T., Chen, Y.-T., Chua, R., Gurung, S., Gnjatic, S., Jungbluth, A. A., Caballero, O. L., Bairoch, A., Kiesler, E., White, S. L., Simpson, A. J. G., Old, L. J., Camargo, A. A., & Vasconcelos, A. T. R. (2009). CTdatabase: a knowledge-base of high-throughput and curated data on cancer-testis antigens. *Nucleic Acids Research*, 37(Database issue), D816–D819.
- Anatskaya, O. V., & Vinogradov, A. E. (2004). Paradoxical relationship between protein content and nucleolar activity in mammalian cardiomyocytes. *Genome / National Research Council Canada = Genome / Conseil National de Recherches Canada*, 47(3), 565–578.
- Anatskaya, O. V., & Vinogradov, A. E. (2022). Polyploidy as a Fundamental Phenomenon in Evolution, Development, Adaptation and Diseases. *International Journal of Molecular Sciences*, 23(7). <https://doi.org/10.3390/ijms23073542>

- Archetti, M. (2004). Recombination and loss of complementation: a more than two-fold cost for parthenogenesis. *Journal of Evolutionary Biology*, *17*(5), 1084–1097.
- Archetti, M. (2022). Polyploidy as an Adaptation against Loss of Heterozygosity in Cancer. *International Journal of Molecular Sciences*, *23*(15). <https://doi.org/10.3390/ijms23158528>
- Austin, C. R. (1960). Anomalies of fertilization leading to triploidy. *Journal of Cellular and Comparative Physiology*, *56*(Suppl 1), 1–15.
- Ayob, A. Z., & Ramasamy, T. S. (2018). Cancer stem cells as key drivers of tumour progression. *Journal of Biomedical Science*, *25*(1), 20.
- Barnum, K. J., & O’Connell, M. J. (2014). Cell Cycle Regulation by Checkpoints. *Methods in Molecular Biology*, *1170*, 29–40.
- Bernhart, S. H., Kretzmer, H., Holdt, L. M., Jühling, F., Ammerpohl, O., Bergmann, A. K., Northoff, B. H., Doose, G., Siebert, R., Stadler, P. F., & Hoffmann, S. (2016). Changes of bivalent chromatin coincide with increased expression of developmental genes in cancer. In *Scientific Reports* (Vol. 6, Issue 1). <https://doi.org/10.1038/srep37393>
- Bernstein, H., & Bernstein, C. (2013). Evolutionary origin and adaptive function of meiosis. *Meiosis*, *1*, 56557.
- Bernstein, H., Bernstein, C., & E., R. (2011). Meiosis as an evolutionary adaptation for DNA repair. In *DNA Repair*. InTech.
- Betancourt, L. H., Gil, J., Kim, Y., Doma, V., Çakır, U., Sanchez, A., Murillo, J. R., Kuras, M., Parada, I. P., Sugihara, Y., Appelqvist, R., Wieslander, E., Welinder, C., Velasquez, E., de Almeida, N. P., Woldmar, N., Marko-Varga, M., Pawłowski, K., Eriksson, J., ... Marko-Varga, G. (2021). The human melanoma proteome atlas-Defining the molecular pathology. *Clinical and Translational Medicine*, *11*(7), e473.
- Bindea, G., Mlecnik, B., Hackl, H., Charoentong, P., Tosolini, M., Kirilovsky, A., Fridman, W.-H., Pagès, F., Trajanoski, Z., & Galon, J. (2009). ClueGO: a Cytoscape plug-in to

- decipher functionally grouped gene ontology and pathway annotation networks. *Bioinformatics*, 25(8), 1091–1093.
- Bittman, E. L. (2016). Timing in the Testis. *Journal of Biological Rhythms*, 31(1), 12–36.
- Bizzarri, M., & Giuliani, A. (2022). Soft Statistical Mechanics for Biology. *Methods in Molecular Biology*, 2449, 263–280.
- Bizzarri, M., Giuliani, A., Cucina, A., D'Anselmi, F., Soto, A. M., & Sonnenschein, C. (2011). Fractal analysis in a systems biology approach to cancer. *Seminars in Cancer Biology*, 21(3), 175–182.
- Blighe, K., Rana, S., & Lewis, M. (2019). *EnhancedVolcano: Publication-ready volcano plots with enhanced colouring and labeling*. R package version 1.2.0. GitHub.
- Boisselier, B., Dugay, F., Belaud-Rotureau, M.-A., Coutolleau, A., Garcion, E., Menei, P., Guardiola, P., & Rousseau, A. (2018). Whole genome duplication is an early event leading to aneuploidy in IDH-wild type glioblastoma. *Oncotarget*, 9(89), 36017–36028.
- Brawand, D., Soumillon, M., Necsulea, A., Julien, P., Csárdi, G., Harrigan, P., Weier, M., Liechti, A., Aximu-Petri, A., Kircher, M., Albert, F. W., Zeller, U., Khaitovich, P., Grützner, F., Bergmann, S., Nielsen, R., Pääbo, S., & Kaessmann, H. (2011). The evolution of gene expression levels in mammalian organs. *Nature*, 478(7369), 343–348.
- Bruggeman, J. W., Irie, N., Lodder, P., van Pelt, A. M. M., Koster, J., & Hamer, G. (2020). Tumors Widely Express Hundreds of Embryonic Germline Genes. *Cancers*, 12(12). <https://doi.org/10.3390/cancers12123812>
- Buhr, E. D., & Takahashi, J. S. (2013). Molecular Components of the Mammalian Circadian Clock. In *Circadian Clocks* (pp. 3–27). https://doi.org/10.1007/978-3-642-25950-0_1
- Cancer Genome Atlas Research Network, Weinstein, J. N., Collisson, E. A., Mills, G. B., Shaw, K. R. M., Ozenberger, B. A., Ellrott, K., Shmulevich, I., Sander, C., & Stuart, J. M. (2013). The Cancer Genome Atlas Pan-Cancer analysis project. *Nature Genetics*, 45(10),

1113–1120.

- Carter, S. L., Cibulskis, K., Helman, E., McKenna, A., Shen, H., Zack, T., Laird, P. W., Onofrio, R. C., Winckler, W., Weir, B. A., Beroukhi, R., Pellman, D., Levine, D. A., Lander, E. S., Meyerson, M., & Getz, G. (2012). Absolute quantification of somatic DNA alterations in human cancer. *Nature Biotechnology*, *30*(5), 413–421.
- Censi, F., Giuliani, A., Bartolini, P., & Calcagnini, G. (2011). A multiscale graph theoretical approach to gene regulation networks: a case study in atrial fibrillation. *IEEE Transactions on Bio-Medical Engineering*, *58*(10), 2943–2946.
- Chamayou, S., Patrizio, P., Storaci, G., Tomaselli, V., Alecci, C., Ragolia, C., Crescenzo, C., & Guglielmino, A. (2013). The use of morphokinetic parameters to select all embryos with full capacity to implant. *Journal of Assisted Reproduction and Genetics*, *30*(5), 703–710.
- Chao, H.-W., Doi, M., Fustin, J.-M., Chen, H., Murase, K., Maeda, Y., Hayashi, H., Tanaka, R., Sugawa, M., Mizukuchi, N., Yamaguchi, Y., Yasunaga, J.-I., Matsuoka, M., Sakai, M., Matsumoto, M., Hamada, S., & Okamura, H. (2017). Circadian clock regulates hepatic polyploidy by modulating Mkp1-Erk1/2 signaling pathway. *Nature Communications*, *8*(1), 2238.
- Chen, J., Niu, N., Zhang, J., Qi, L., Shen, W., Donkena, K. V., Feng, Z., & Liu, J. (2019). Polyploid Giant Cancer Cells (PGCCs): The Evil Roots of Cancer. *Current Cancer Drug Targets*, *19*(5), 360–367.
- Chen, Z. J. (2010). Molecular mechanisms of polyploidy and hybrid vigor. *Trends in Plant Science*, *15*(2), 57–71.
- Chen, Z., Qiao, J., Wang, Q., & Xiao, Q. (2018). Data on tumor progression of c-mos deficiency in murine models of KrasG12D lung and ApcMin colorectal cancer. *Data in Brief*, *20*, 1124–1132.
- Chitikova, Z. V., Gordeev, S. A., Bykova, T. V., Zubova, S. G., Pospelov, V. A., & Pospelova, T.

- V. (2014). Sustained activation of DNA damage response in irradiated apoptosis-resistant cells induces reversible senescence associated with mTOR downregulation and expression of stem cell markers. *Cell Cycle*, 13(9), 1424–1439.
- Cho, C.-H. (2017). *Therapeutic Targets For Inflammation And Cancer: Novel Therapies For Digestive Diseases*. World Scientific.
- Comai, L. (2005). The advantages and disadvantages of being polyploid. *Nature Reviews. Genetics*, 6(11), 836–846.
- Coppé, J.-P., Desprez, P.-Y., Krtolica, A., & Campisi, J. (2010). The senescence-associated secretory phenotype: the dark side of tumor suppression. *Annual Review of Pathology*, 5, 99–118.
- Costanzo, V., Bardelli, A., Siena, S., & Abrignani, S. (2018). Exploring the links between cancer and placenta development. *Open Biology*, 8(6). <https://doi.org/10.1098/rsob.180081>
- Court, F., & Arnaud, P. (2017). An annotated list of bivalent chromatin regions in human ES cells: a new tool for cancer epigenetic research. *Oncotarget*, 8(3), 4110–4124.
- Creighton, H., & Waddington, C. H. (1958). The strategy of the genes. *AIBS Bulletin*, 8(2), 49.
- Csermely, P. (2021). Adaptation of molecular interaction networks in cancer cells. In *Rethinking Cancer*. The MIT Press.
- da Silva, V. L., Fonseca, A. F., Fonseca, M., da Silva, T. E., Coelho, A. C., Kroll, J. E., de Souza, J. E. S., Stransky, B., de Souza, G. A., & de Souza, S. J. (2017). Genome-wide identification of cancer/testis genes and their association with prognosis in a pan-cancer analysis. *Oncotarget*, 8(54), 92966–92977.
- Davis, S., & Meltzer, P. S. (2007). GEOquery: a bridge between the Gene Expression Omnibus (GEO) and BioConductor. *Bioinformatics*, 23(14), 1846–1847.
- Díaz-Carballo, D., Gustmann, S., Jastrow, H., Acikelli, A. H., Dammann, P., Klein, J., Dembinski, U., Bardenheuer, W., Malak, S., Araúzo-Bravo, M. J., Schultheis, B., Aldinger,

- C., & Strumberg, D. (2014). Atypical cell populations associated with acquired resistance to cytostatics and cancer stem cell features: the role of mitochondria in nuclear encapsulation. *DNA and Cell Biology*, *33*(11), 749–774.
- Díaz-Carballo, D., Saka, S., Klein, J., Rennkamp, T., Acikelli, A. H., Malak, S., Jastrow, H., Wennemuth, G., Tempfer, C., Schmitz, I., Tannapfel, A., & Strumberg, D. (2018). A Distinct Oncogenerative Multinucleated Cancer Cell Serves as a Source of Stemness and Tumor Heterogeneity. *Cancer Research*, *78*(9), 2318–2331.
- Dou, Z., & Berger, S. L. (2018). Senescence Elicits Stemness: A Surprising Mechanism for Cancer Relapse [Review of *Senescence Elicits Stemness: A Surprising Mechanism for Cancer Relapse*]. *Cell Metabolism*, *27*(4), 710–711.
- Duffy, M. J., O’Grady, S., Tang, M., & Crown, J. (2021). MYC as a target for cancer treatment. *Cancer Treatment Reviews*, *94*, 102154.
- Dvorak, H. F. (1986). Wounds that do not heal. Similarities between tumor stroma generation and wound healing. *New Eng J Med*, *25*, 1650–1659.
- Epping, M. T., Hart, A. A. M., Glas, A. M., Krijgsman, O., & Bernards, R. (2008). PRAME expression and clinical outcome of breast cancer. *British Journal of Cancer*, *99*(3), 398–403.
- Erenpreisa, J. (2000). Tamed" chaos in embryonal development and carcinogenesis: a holistic view. *Proceedings of the Latvian Academy of Sciences. Section B: Natural, Exact and Applied Sciences*, *54*, 1–8.
- Erenpreisa, J. A., Cragg, M. S., Fringes, B., Sharakhov, I., & Illidge, T. M. (2000). Release of mitotic descendants by giant cells from irradiated Burkitt’s lymphoma cell line. *Cell Biology International*, *24*(9), 635–648.
- Erenpreisa, J., & Cragg, M. S. (2007). Cancer: a matter of life cycle? *Cell Biology International*, *31*(12), 1507–1510.

- Erenpreisa, J., & Cragg, M. S. (2010). MOS, aneuploidy and the ploidy cycle of cancer cells. *Oncogene*, *29*(40), 5447–5451.
- Erenpreisa, J., Cragg, M. S., Salmina, K., Hausmann, M., & Scherthan, H. (2009). The role of meiotic cohesin REC8 in chromosome segregation in gamma irradiation-induced endopolyploid tumour cells. *Experimental Cell Research*, *315*(15), 2593–2603.
- Erenpreisa, J., & Giuliani, A. (2019). Resolution of Complex Issues in Genome Regulation and Cancer Requires Non-Linear and Network-Based Thermodynamics. *International Journal of Molecular Sciences*, *21*(1). <https://doi.org/10.3390/ijms21010240>
- Erenpreisa, J., Giuliani, A., & Vinogradov, A. E. (2018). Stress-induced polyploidy shifts somatic cells towards a pro-tumorigenic unicellular gene transcription network. *Cancer Hypotheses*, *1*(1), 1–20.
- Erenpreisa, J., Salmina, K., Anatskaya, O., & Cragg, M. S. (2022). Paradoxes of cancer: Survival at the brink. *Seminars in Cancer Biology*, *81*, 119–131.
- Erenpreisa, J., Salmina, K., Huna, A., Kosmacek, E. A., Cragg, M. S., Ianzini, F., & Anisimov, A. P. (2011). Polyploid tumour cells elicit paradiploid progeny through depolyploidizing divisions and regulated autophagic degradation. *Cell Biology International*, *35*(7), 687–695.
- Erenpreiss. (1993). *Current concepts of malignant growth. Part A: From a normal cell to cancer*. Zvaigzne.
- Faggioli, F., Velarde, M., & Wiley, C. D. (2022). Cellular senescence, a novel area of investigation for metastatic diseases. In *Preprints*. <https://doi.org/10.20944/preprints202211.0564.v1>
- Farshadi, E., van der Horst, G. T. J., & Chaves, I. (2020). Molecular Links between the Circadian Clock and the Cell Cycle. *Journal of Molecular Biology*, *432*(12), 3515–3524.
- Feichtinger, J., & McFarlane, R. J. (2019). Meiotic gene activation in somatic and germ cell tumours. *Andrology*, *7*(4), 415–427.

- Fu, L., Pelicano, H., Liu, J., Huang, P., & Lee, C. (2002). The circadian gene *Period2* plays an important role in tumor suppression and DNA damage response in vivo. *Cell*, *111*(1), 41–50.
- Gantchev, J., Martínez Villarreal, A., Gunn, S., Zetka, M., Ødum, N., & Litvinov, I. V. (2020). The ectopic expression of *meiCT* genes promotes meiomitosis and may facilitate carcinogenesis. *Cell Cycle*, *19*(8), 837–854.
- Gerashchenko, B. I., Salmina, K., Eglitis, J., Huna, A., Grjunberga, V., & Erenpreisa, J. (2016). Disentangling the aneuploidy and senescence paradoxes: a study of triploid breast cancers non-responsive to neoadjuvant therapy. *Histochemistry and Cell Biology*, *145*(4), 497–508.
- Gerber, N., & Kokko, H. (2018). Abandoning the ship using sex, dispersal or dormancy: multiple escape routes from challenging conditions. *Philosophical Transactions of the Royal Society of London. Series B, Biological Sciences*, *373*(1757). <https://doi.org/10.1098/rstb.2017.0424>
- Goh, K.-I., Cusick, M. E., Valle, D., Childs, B., Vidal, M., & Barabási, A.-L. (2007). The human disease network. *Proceedings of the National Academy of Sciences of the United States of America*, *104*(21), 8685–8690.
- Goodkov, A. V., Berdieva, M. A., Podlipaeva, Y. I., & Demin, S. Y. (2019). The Chromatin Extrusion Phenomenon in *Amoeba proteus* Cell Cycle. *The Journal of Eukaryotic Microbiology*. <https://doi.org/10.1111/jeu.12771>
- Gordeeva, O. (2018). Cancer-testis antigens: Unique cancer stem cell biomarkers and targets for cancer therapy. *Seminars in Cancer Biology*, *53*, 75–89.
- Graziani, V., Rodriguez-Hernandez, I., Maiques, O., & Sanz-Moreno, V. (2022). The amoeboid state as part of the epithelial-to-mesenchymal transition programme. *Trends in Cell Biology*, *32*(3), 228–242.
- Griffiths, J. G., & Bonser, S. P. (2013). Is sex advantageous in adverse environments? A test of

- the abandon-ship hypothesis. *The American Naturalist*, 182(6), 718–725.
- Gustavsen, J. A., Pai, S., Isserlin, R., Demchak, B., & Pico, A. R. (2019). RCy3: Network biology using Cytoscape from within R. *F1000Research*, 8, 1774.
- Gyurkó, D. M., Veres, D. V., Módos, D., Lenti, K., Korcsmáros, T., & Csermely, P. (2013). Adaptation and learning of molecular networks as a description of cancer development at the systems-level: Potential use in anti-cancer therapies. In *Seminars in Cancer Biology* (Vol. 23, Issue 4, pp. 262–269). <https://doi.org/10.1016/j.semcancer.2013.06.005>
- Harris, M. A., Clark, J., Ireland, A., Lomax, J., Ashburner, M., Foulger, R., Eilbeck, K., Lewis, S., Marshall, B., Mungall, C., Richter, J., Rubin, G. M., Blake, J. A., Bult, C., Dolan, M., Drabkin, H., Eppig, J. T., Hill, D. P., Ni, L., ... Gene Ontology Consortium. (2004). The Gene Ontology (GO) database and informatics resource. *Nucleic Acids Research*, 32(Database issue), D258–D261.
- Hofstatter, P. G., Brown, M. W., & Lahr, D. J. G. (2018). Comparative Genomics Supports Sex and Meiosis in Diverse Amoebozoa. *Genome Biology and Evolution*, 10(11), 3118–3128.
- Hojsgaard, D. (2018). Transient Activation of Apomixis in Sexual Neotriploids May Retain Genomically Altered States and Enhance Polyploid Establishment. *Frontiers in Plant Science*, 9, 230.
- Horbay, R., & Stoika, R. (2011). Giant cell formation: the way to cell death or cell survival? *Open Life Sciences*, 6(5), 675–684.
- Huang, S. (2021). The logic of cancer treatment: Treatment-induced progression, hyper-progression, and the Nietzsche effect. In *Rethinking Cancer*. The MIT Press.
- Huang, S., Eichler, G., Bar-Yam, Y., & Ingber, D. E. (2005). Cell fates as high-dimensional attractor states of a complex gene regulatory network. *Physical Review Letters*, 94(12), 128701.
- Huang, S., Ernberg, I., & Kauffman, S. (2009). Cancer attractors: a systems view of tumors from

- a gene network dynamics and developmental perspective. *Seminars in Cell & Developmental Biology*, 20(7), 869–876.
- Huna, A., Salmina, K., Erenpreisa, J., Vazquez-Martin, A., Krigerts, J., Inashkina, I., Gerashchenko, B. I., Townsend, P. A., Cragg, M. S., & Jackson, T. R. (2015). Role of stress-activated OCT4A in the cell fate decisions of embryonal carcinoma cells treated with etoposide. *Cell Cycle*, 14(18), 2969–2984.
- Hunter. (2007). *Matplotlib: A 2D Graphics Environment*. 9, 90–95.
- Huskins, C. L. (1948). Chromosome multiplication and reduction in somatic tissues; their possible relation to differentiation, reversion and sex. *Nature*, 161(4081), 80–83.
- Ianzini, F., Kosmacek, E. A., Nelson, E. S., Napoli, E., Erenpreisa, J., Kalejs, M., & Mackey, M. A. (2009). Activation of meiosis-specific genes is associated with depolyploidization of human tumor cells following radiation-induced mitotic catastrophe. *Cancer Research*, 69(6), 2296–2304.
- Ibrahim, S. S., Eldeeb, M. A. R., Rady, M. A. H., Hady, K. M. A., Lotfy, M. S., Farag, N. S., Verleysdonk, S., & Bagowski, C. P. (2011). The role of protein interaction domains in the human cancer network. *Network Biology*, 1(1), 59.
- Illidge, T. M., Cragg, M. S., Fringes, B., Olive, P., & Erenpreisa, J. A. (2000). Polyploid giant cells provide a survival mechanism for p53 mutant cells after DNA damage. *Cell Biology International*, 24(9), 621–633.
- Ishay-Ronen, D., & Christofori, G. (2019). Targeting Cancer Cell Metastasis by Converting Cancer Cells into Fat. *Converting Cancer Cells into Fat Cells*. *Cancer Research*. <https://aacrjournals.org/cancerres/article-abstract/79/21/5471/657672>
- Jiang, X., Zhao, D., Ali, A., Xu, B., Liu, W., Wen, J., Zhang, H., Shi, Q., & Zhang, Y. (2021). MeiosisOnline: A Manually Curated Database for Tracking and Predicting Genes Associated With Meiosis. *Frontiers in Cell and Developmental Biology*, 9, 673073.

- Johansson, H. J., Socciarelli, F., Vacanti, N. M., Haugen, M. H., Zhu, Y., Siavelis, I., Fernandez-Woodbridge, A., Aure, M. R., Sennblad, B., Vesterlund, M., Branca, R. M., Orre, L. M., Huss, M., Fredlund, E., Beraki, E., Garred, Ø., Boekel, J., Sauer, T., Zhao, W., ... Lehtiö, J. (2019). Breast cancer quantitative proteome and proteogenomic landscape. *Nature Communications*, *10*(1), 1600.
- Jungbluth, A. A., Silva, W. A., Jr, Iversen, K., Frosina, D., Zaidi, B., Coplan, K., Eastlake-Wade, S. K., Castelli, S. B., Spagnoli, G. C., Old, L. J., & Vogel, M. (2007). Expression of cancer-testis (CT) antigens in placenta. *Cancer Immunity*, *7*, 15.
- Kalejs, M., & Erenpreisa, J. (2005). Cancer/testis antigens and gametogenesis: a review and “brain-storming” session. *Cancer Cell International*, *5*(1), 4.
- Kanehisa, M., Sato, Y., Kawashima, M., Furumichi, M., & Tanabe, M. (2016). KEGG as a reference resource for gene and protein annotation. In *Nucleic Acids Research* (Vol. 44, Issue D1, pp. D457–D462). <https://doi.org/10.1093/nar/gkv1070>
- Kauffman, S. (1971). Differentiation of malignant to benign cells. *Journal of Theoretical Biology*, *31*(3), 429–451.
- Kauffman, S. A., & Johnsen, S. (1991). Coevolution to the edge of chaos: coupled fitness landscapes, poised states, and coevolutionary avalanches. *Journal of Theoretical Biology*, *149*(4), 467–505.
- Kiseleva, L. N., Kartashev, A. V., Vartanyan, N. L., Pinevich, A. A., & Samoilovich, M. P. (2019). Multinucleated cells resistant to genotoxic factors within human glioblastoma cell lines. *Cell and Tissue Biology*, *13*(1), 1–7.
- Ko, A., Han, S. Y., Choi, C. H., Cho, H., Lee, M.-S., Kim, S.-Y., Song, J. S., Hong, K.-M., Lee, H.-W., Hewitt, S. M., Chung, J.-Y., & Song, J. (2018). Oncogene-induced senescence mediated by c-Myc requires USP10 dependent deubiquitination and stabilization of p14ARF. *Cell Death and Differentiation*, *25*(6), 1050–1062.

- Korentzelos, D., Clark, A. M., & Wells, A. (2020). A Perspective on Therapeutic Pan-Resistance in Metastatic Cancer. *International Journal of Molecular Sciences*, 21(19). <https://doi.org/10.3390/ijms21197304>
- Kshitiz, Afzal, J., Maziarz, J. D., Hamidzadeh, A., Liang, C., Erkenbrack, E. M., Kim, H. N., Haeger, J.-D., Pfarrer, C., Hoang, T., Ott, T., Spencer, T., Pavličev, M., Antczak, D. F., Levchenko, A., & Wagner, G. P. (2019). Evolution of placental invasion and cancer metastasis are causally linked. *Nature Ecology & Evolution*, 3(12), 1743–1753.
- Kudo-Saito, C., Miyamoto, T., Imazeki, H., Shoji, H., Aoki, K., & Boku, N. (2020). IL33 Is a Key Driver of Treatment Resistance of Cancer. *Cancer Research*, 80(10), 1981–1990.
- Kumar, D., Cinghu, S., Oldfield, A. J., Yang, P., & Jothi, R. (2021). Decoding the function of bivalent chromatin in development and cancer. *Genome Research*, 31(12), 2170–2184.
- Kumar, M., Bowers, R. R., & Delaney, J. R. (2020). Single-cell analysis of copy-number alterations in serous ovarian cancer reveals substantial heterogeneity in both low- and high-grade tumors. *Cell Cycle*, 19(22), 3154–3166.
- Lagadec, C., Vlashi, E., Della Donna, L., Dekmezian, C., & Pajonk, F. (2012). Radiation-induced reprogramming of breast cancer cells. *Stem Cells*, 30(5), 833–844.
- Langmesser, S., Tallone, T., Bordon, A., Rusconi, S., & Albrecht, U. (2008). Interaction of circadian clock proteins PER2 and CRY with BMAL1 and CLOCK. *BMC Molecular Biology*, 9, 41.
- Lavia, P., Sciamanna, I., & Spadafora, C. (2022). An Epigenetic LINE-1-Based Mechanism in Cancer. *International Journal of Molecular Sciences*, 23(23). <https://doi.org/10.3390/ijms232314610>
- Lee, H. O., Davidson, J. M., & Duronio, R. J. (2009). Endoreplication: polyploidy with purpose. *Genes & Development*, 23(21), 2461–2477.
- Leikam, C., Hufnagel, A. L., Otto, C., Murphy, D. J., Mühling, B., Kneitz, S., Nanda, I., Schmid,

- M., Wagner, T. U., Haferkamp, S., Bröcker, E.-B., Scharl, M., & Meierjohann, S. (2015). In vitro evidence for senescent multinucleated melanocytes as a source for tumor-initiating cells. *Cell Death & Disease*, 6, e1711.
- Lenormand, T., Engelstädter, J., Johnston, S. E., Wijnker, E., & Haag, C. R. (2016). Evolutionary mysteries in meiosis. *Philosophical Transactions of the Royal Society of London. Series B, Biological Sciences*, 371(1706). <https://doi.org/10.1098/rstb.2016.0001>
- Lewin, R. (1999). *Complexity: Life at the Edge of Chaos*. University of Chicago Press.
- Lindsey, S. F., Byrnes, D. M., Eller, M. S., Rosa, A. M., Dabas, N., Escandon, J., & Grichnik, J. M. (2013). Potential Role of Meiosis Proteins in Melanoma Chromosomal Instability. In *Journal of Skin Cancer* (Vol. 2013, pp. 1–9). <https://doi.org/10.1155/2013/190109>
- Lingg, L., Rottenberg, S., & Francica, P. (2022). Meiotic Genes and DNA Double Strand Break Repair in Cancer. *Frontiers in Genetics*, 13, 831620.
- Lin, K.-C., Torga, G., Sun, Y., Axelrod, R., Pienta, K. J., Sturm, J. C., & Austin, R. H. (2019). The role of heterogeneous environment and docetaxel gradient in the emergence of polyploid, mesenchymal and resistant prostate cancer cells. *Clinical & Experimental Metastasis*, 36(2), 97–108.
- Liu, J. (2020). The “life code”: A theory that unifies the human life cycle and the origin of human tumors. *Seminars in Cancer Biology*, 60, 380–397.
- Liu, Y., Shan, N., Yuan, Y., Tan, B., He, C., Tong, C., & Qi, H. (2020). Knockdown of activated Cdc42-associated kinase inhibits human extravillous trophoblast migration and invasion and decreases protein expression of p-Akt and matrix metalloproteinase. *The Journal of Maternal-Fetal & Neonatal Medicine: The Official Journal of the European Association of Perinatal Medicine, the Federation of Asia and Oceania Perinatal Societies, the International Society of Perinatal Obstetricians*, 33(7), 1125–1133.
- Lopez-Sánchez, L. M., Jimenez, C., Valverde, A., Hernandez, V., Peñarando, J., Martinez, A.,

- Lopez-Pedrerera, C., Muñoz-Castañeda, J. R., De la Haba-Rodríguez, J. R., Aranda, E., & Rodríguez-Ariza, A. (2014). CoCl₂, a mimic of hypoxia, induces formation of polyploid giant cells with stem characteristics in colon cancer. *PloS One*, *9*(6), e99143.
- Maciver, S. K. (2016). Asexual Amoebae Escape Muller's Ratchet through Polyploidy. *Trends in Parasitology*, *32*(11), 855–862.
- Madlung, A. (2013). Polyploidy and its effect on evolutionary success: old questions revisited with new tools. *Heredity*, *110*(2), 99–104.
- McKinney, W. (2010). Data Structures for Statistical Computing in Python. *Proceedings of the 9th Python in Science Conference*. Python in Science Conference, Austin, Texas. <https://doi.org/10.25080/majora-92bf1922-00a>
- Mitelman, F., Johansson, B., & Mertens, F. (2000). *Mitelman Database of Chromosome Aberrations and Gene Fusions in Cancer*. <http://cgap.nci.nih.gov/Chromosomes/Mitelman>
- Mittal, K., Donthamsetty, S., Kaur, R., Yang, C., Gupta, M. V., Reid, M. D., Choi, D. H., Rida, P. C. G., & Aneja, R. (2017). Multinucleated polyploidy drives resistance to Docetaxel chemotherapy in prostate cancer. *British Journal of Cancer*, *116*(9), 1186–1194.
- Moein, S., Adibi, R., da Silva Meirelles, L., Nardi, N. B., & Gheisari, Y. (2020). Cancer regeneration: Polyploid cells are the key drivers of tumor progression. *Biochimica et Biophysica Acta, Reviews on Cancer*, *1874*(2), 188408.
- Morris, J. H., Apeltsin, L., Newman, A. M., Baumbach, J., Wittkop, T., Su, G., Bader, G. D., & Ferrin, T. E. (2011). clusterMaker: a multi-algorithm clustering plugin for Cytoscape. *BMC Bioinformatics*, *12*, 436.
- Mosieniak, G., & Sikora, E. (2010). Polyploidy: the link between senescence and cancer. *Current Pharmaceutical Design*, *16*(6), 734–740.
- Mosieniak, G., Sliwinska, M. A., Alster, O., Strzeszewska, A., Sunderland, P., Piechota, M., Was, H., & Sikora, E. (2015). Polyploidy Formation in Doxorubicin-Treated Cancer Cells

- Can Favor Escape from Senescence. *Neoplasia* , 17(12), 882–893.
- Muller, H. J. (1964). THE RELATION OF RECOMBINATION TO MUTATIONAL ADVANCE. *Mutation Research*, 106, 2–9.
- Neganova, I., & Lako, M. (2008). G1 to S phase cell cycle transition in somatic and embryonic stem cells. *Journal of Anatomy*, 213(1), 30–44.
- Newcomb, R., Dean, E., McKinney, B. J., & Alvarez, J. V. (2021). Context-dependent effects of whole-genome duplication during mammary tumor recurrence. *Scientific Reports*, 11(1), 14932.
- Niu, N., Mercado-Uribe, I., & Liu, J. (2017). Dedifferentiation into blastomere-like cancer stem cells via formation of polyploid giant cancer cells. *Oncogene*, 36(34), 4887–4900.
- Niu, N., Zhang, J., Zhang, N., Mercado-Uribe, I., Tao, F., Han, Z., Pathak, S., Multani, A. S., Kuang, J., Yao, J., Bast, R. C., Sood, A. K., Hung, M.-C., & Liu, J. (2016). Linking genomic reorganization to tumor initiation via the giant cell cycle. In *Oncogenesis* (Vol. 5, Issue 12, pp. e281–e281). <https://doi.org/10.1038/oncsis.2016.75>
- Oliphant, T. E. (2006). *A guide to NumPy* (Vol. 1). Trelgol Publishing USA.
- Ottolini, C. S., Newnham, L., Capalbo, A., Natesan, S. A., Joshi, H. A., Cimadomo, D., Griffin, D. K., Sage, K., Summers, M. C., Thornhill, A. R., Housworth, E., Herbert, A. D., Rienzi, L., Ubaldi, F. M., Handyside, A. H., & Hoffmann, E. R. (2015). Genome-wide maps of recombination and chromosome segregation in human oocytes and embryos show selection for maternal recombination rates. *Nature Genetics*, 47(7), 727–735.
- Pandit, S. K., Westendorp, B., & de Bruin, A. (2013). Physiological significance of polyploidization in mammalian cells. *Trends in Cell Biology*, 23(11), 556–566.
- Park, S. U., Choi, E. S., Jang, Y. S., Hong, S.-H., Kim, I.-H., & Chang, D. K. (2011). Effects of chromosomal polyploidy on survival of colon cancer cells. *The Korean journal of gastroenterology = Taehan Sohwagi Hakhoe chi*, 57(3), 150.

- Patro, R., Duggal, G., Love, M. I., Irizarry, R. A., & Kingsford, C. (2017). Salmon provides fast and bias-aware quantification of transcript expression. *Nature Methods*, *14*(4), 417–419.
- Pienta, K. J., Hammarlund, E. U., Axelrod, R., Amend, S. R., & Brown, J. S. (2020). Convergent Evolution, Evolving Evolvability, and the Origins of Lethal Cancer. *Molecular Cancer Research: MCR*, *18*(6), 801–810.
- Pierce, G. B. (1985). Carcinoma is to embryology as mutation is to genetics. *American Zoologist*, *25*(3), 707–712.
- Pierce, G. B., Pantazis, C. G., Caldwell, J. E., & Wells, R. S. (1982). Specificity of the control of tumor formation by the blastocyst. *Cancer Research*, *42*(3), 1082–1087.
- Pratt, D., Chen, J., Welker, D., Rivas, R., Pillich, R., Rynkov, V., Ono, K., Miello, C., Hicks, L., Szalma, S., Stojmirovic, A., Dobrin, R., Braxenthaler, M., Kuentzer, J., Demchak, B., & Ideker, T. (2015). NDEx, the Network Data Exchange. *Cell Systems*, *1*(4), 302–305.
- Prigogine, I., & Stengers, I. (1984). *Order Out of Chaos: Man's New Dialogue with Nature*. Bantam Books.
- Puig, P.-E., Guilly, M.-N., Bouchot, A., Droin, N., Cathelin, D., Bouyer, F., Favier, L., Ghiringhelli, F., Kroemer, G., Solary, E., Martin, F., & Chauffert, B. (2008). Tumor cells can escape DNA-damaging cisplatin through DNA endoreduplication and reversible polyploidy. *Cell Biology International*, *32*(9), 1031–1043.
- Quinton, R. J., DiDomizio, A., Vittoria, M. A., Kotýnková, K., Ticas, C. J., Patel, S., Koga, Y., Vakhshoorzadeh, J., Hermance, N., Kuroda, T. S., Parulekar, N., Taylor, A. M., Manning, A. L., Campbell, J. D., & Ganem, N. J. (2021). Whole-genome doubling confers unique genetic vulnerabilities on tumour cells. *Nature*, *590*(7846), 492–497.
- Rahman, M., Jackson, L. K., Johnson, W. E., Li, D. Y., Bild, A. H., & Piccolo, S. R. (2015). Alternative preprocessing of RNA-Sequencing data in The Cancer Genome Atlas leads to improved analysis results. *Bioinformatics*, *31*(22), 3666–3672.

- Rajaraman, R., Guernsey, D. L., Rajaraman, M. M., & Rajaraman, S. R. (2007). Neosis - A Parasexual Somatic Reduction Division in Cancer. *International Journal of Human Genetics*, 7(1), 29–48.
- Ram, Y., & Hadany, L. (2016). Condition-dependent sex: who does it, when and why? *Philosophical Transactions of the Royal Society of London. Series B, Biological Sciences*, 371(1706). <https://doi.org/10.1098/rstb.2015.0539>
- Rijo-Ferreira, F., & Takahashi, J. S. (2019). Genomics of circadian rhythms in health and disease. *Genome Medicine*, 11(1), 82.
- Rivera, M., Wu, Q., Hamerlik, P., Hjelmeland, A. B., Bao, S., & Rich, J. N. (2015). Acquisition of meiotic DNA repair regulators maintain genome stability in glioblastoma. *Cell Death & Disease*, 6, e1732.
- Robinson, M. D., McCarthy, D. J., & Smyth, G. K. (2010). edgeR: a Bioconductor package for differential expression analysis of digital gene expression data. *Bioinformatics*, 26(1), 139–140.
- Roeder, G. S. (1997). Meiotic chromosomes: it takes two to tango. *Genes & Development*, 11(20), 2600–2621.
- Rohnalter, V., Roth, K., Finkernagel, F., Adhikary, T., Obert, J., Dorzweiler, K., Bensberg, M., Müller-Brüsselbach, S., & Müller, R. (2015). A multi-stage process including transient polyploidization and EMT precedes the emergence of chemoresistent ovarian carcinoma cells with a dedifferentiated and pro-inflammatory secretory phenotype. In *Oncotarget* (Vol. 6, Issue 37, pp. 40005–40025). <https://doi.org/10.18632/oncotarget.5552>
- Salmina, K., Bojko, A., Inashkina, I., Staniak, K., Dudkowska, M., Podlesniy, P., Rumnieks, F., Vainshelbaum, N. M., Pjanova, D., Sikora, E., & Erenpreisa, J. (2020). “Mitotic Slippage” and Extranuclear DNA in Cancer Chemoresistance: A Focus on Telomeres. *International Journal of Molecular Sciences*, 21(8), 2779.

- Salmina, K., Huna, A., Inashkina, I., Belyayev, A., Krigerts, J., Pastova, L., Vazquez-Martin, A., & Erenpreisa, J. (2017). Nucleolar aggresomes mediate release of pericentric heterochromatin and nuclear destruction of genotoxically treated cancer cells. *Nucleus*, 8(2), 205–221.
- Salmina, K., Huna, A., Kalejs, M., Pjanova, D., Scherthan, H., Cragg, M. S., & Erenpreisa, J. (2019). The Cancer Aneuploidy Paradox: In the Light of Evolution. *Genes*, 10(2). <https://doi.org/10.3390/genes10020083>
- Salmina, K., Jankevics, E., Huna, A., Perminov, D., Radovica, I., Klymenko, T., Ivanov, A., Jascenko, E., Scherthan, H., Cragg, M., & Erenpreisa, J. (2010). Up-regulation of the embryonic self-renewal network through reversible polyploidy in irradiated p53-mutant tumour cells. *Experimental Cell Research*, 316(13), 2099–2112.
- Sasieni, P. D., Shelton, J., Ormiston-Smith, N., Thomson, C. S., & Silcocks, P. B. (2011). What is the lifetime risk of developing cancer?: the effect of adjusting for multiple primaries. *British Journal of Cancer*, 105(3), 460–465.
- Savvidis, C., & Koutsilieris, M. (2012). Circadian Rhythm Disruption in Cancer Biology. In *Molecular Medicine* (Vol. 18, Issue 9, pp. 1249–1260). <https://doi.org/10.2119/molmed.2012.00077>
- Sayols. (2020). rrvgo: a Bioconductor package to reduce and visualize Gene Ontology terms. *Australian Dental Journal*.
- Schinkel, C. C. F., Kirchheimer, B., Dullinger, S., Geelen, D., De Storme, N., & Hörandl, E. (2017). Pathways to polyploidy: indications of a female triploid bridge in the alpine species (Ranunculaceae). *Plant Systematics and Evolution = Entwicklungsgeschichte Und Systematik Der Pflanzen*, 303(8), 1093–1108.
- Schwarz-Finsterle, J., Scherthan, H., Huna, A., González, P., Mueller, P., Schmitt, E., Erenpreisa, J., & Hausmann, M. (2013). Volume increase and spatial shifts of chromosome territories in

- nuclei of radiation-induced polyploidizing tumour cells. *Mutation Research*, 756(1-2), 56–65.
- Settle, B., Otasek, D., Morris, J. H., & Demchak, B. (2018). aMatReader: Importing adjacency matrices via Cytoscape Automation. *F1000Research*, 7. <https://doi.org/10.12688/f1000research.15146.2>
- Shannon, P., Markiel, A., Ozier, O., Baliga, N. S., Wang, J. T., Ramage, D., Amin, N., Schwikowski, B., & Ideker, T. (2003). Cytoscape: a software environment for integrated models of biomolecular interaction networks. *Genome Research*, 13(11), 2498–2504.
- Sharma, S., Yao, H.-P., Zhou, Y.-Q., Zhou, J., Zhang, R., & Wang, M.-H. (2014). Prevention of BMS-777607-induced polyploidy/senescence by mTOR inhibitor AZD8055 sensitizes breast cancer cells to cytotoxic chemotherapeutics. *Molecular Oncology*, 8(3), 469–482.
- Sheltzer, J. M., & Amon, A. (2011). The aneuploidy paradox: costs and benefits of an incorrect karyotype. *Trends in Genetics: TIG*, 27(11), 446–453.
- Shilts, J., Chen, G., & Hughey, J. J. (2018). Evidence for widespread dysregulation of circadian clock progression in human cancer. In *PeerJ* (Vol. 6, p. e4327). <https://doi.org/10.7717/peerj.4327>
- Shubernetskaya, O., Skvortsov, D., Evfratov, S., Rubtsova, M., Belova, E., Strelkova, O., Cherepaninets, V., Zhironkina, O., Olovnikov, A., Zvereva, M., Dontsova, O., & Kireev, I. (2017). Interstitial telomeric repeats-associated DNA breaks. *Nucleus*, 8(6), 641–653.
- Skejo, J., Garg, S. G., Gould, S. B., Hendriksen, M., Tria, F. D. K., Bremer, N., Franjević, D., Blackstone, N. W., & Martin, W. F. (2021). Evidence for a Syncytial Origin of Eukaryotes from Ancestral State Reconstruction. *Genome Biology and Evolution*, 13(7). <https://doi.org/10.1093/gbe/evab096>
- Soneson, C., Love, M. I., & Robinson, M. D. (2015). Differential analyses for RNA-seq: transcript-level estimates improve gene-level inferences. *F1000Research*, 4(1521), 1521.

- Storch, K.-F., Lipan, O., Leykin, I., Viswanathan, N., Davis, F. C., Wong, W. H., & Weitz, C. J. (2002). Extensive and divergent circadian gene expression in liver and heart. *Nature*, *417*(6884), 78–83.
- Sulli, G., Lam, M. T. Y., & Panda, S. (2019). Interplay between Circadian Clock and Cancer: New Frontiers for Cancer Treatment. *Trends in Cancer Research*, *5*(8), 475–494.
- Sundaram, M., Guernsey, D. L., Rajaraman, M. M., & Rajaraman, R. (2004). Neosis: a novel type of cell division in cancer. *Cancer Biology & Therapy*, *3*(2), 207–218.
- Szklarczyk, D., Gable, A. L., Nastou, K. C., Lyon, D., Kirsch, R., Pyysalo, S., Doncheva, N. T., Legeay, M., Fang, T., Bork, P., Jensen, L. J., & von Mering, C. (2020). The STRING database in 2021: customizable protein–protein networks, and functional characterization of user-uploaded gene/measurement sets. *Nucleic Acids Research*, *49*(D1), D605–D612.
- Takahashi, J. S. (2017). Transcriptional architecture of the mammalian circadian clock. *Nature Reviews. Genetics*, *18*(3), 164–179.
- Takahashi, K., & Yamanaka, S. (2006). Induction of pluripotent stem cells from mouse embryonic and adult fibroblast cultures by defined factors. *Cell*, *126*(4), 663–676.
- Tan, C., Pan, Q., Cui, C., Xiang, Y., Ge, X., & Li, Z. (2016). Genome-Wide Gene/Genome Dosage Imbalance Regulates Gene Expressions in Synthetic Brassica napus and Derivatives (AC, AAC, CCA, CCAA). *Frontiers in Plant Science*, *7*, 1432.
- Taylor, A. M., Shih, J., Ha, G., Gao, G. F., Zhang, X., Berger, A. C., Schumacher, S. E., Wang, C., Hu, H., Liu, J., Lazar, A. J., Cancer Genome Atlas Research Network, Cherniack, A. D., Beroukhim, R., & Meyerson, M. (2018). Genomic and Functional Approaches to Understanding Cancer Aneuploidy. *Cancer Cell*, *33*(4), 676–689.e3.
- Treasure, T., Farewell, V., Macbeth, F., Batchelor, T., Milošević, M., King, J., Zheng, Y., Leonard, P., Williams, N. R., Brew-Graves, C., Fallowfield, L., & PulMiCCinvestigators. (2021). The Pulmonary Metastectomy in Colorectal Cancer cohort study: Analysis of

- case selection, risk factors and survival in a prospective observational study of 512 patients. *Colorectal Disease: The Official Journal of the Association of Coloproctology of Great Britain and Ireland*, 23(7), 1793–1803.
- Trigos, A. S., Pearson, R. B., Papenfuss, A. T., & Goode, D. L. (2017). Altered interactions between unicellular and multicellular genes drive hallmarks of transformation in a diverse range of solid tumors. *Proceedings of the National Academy of Sciences of the United States of America*, 114(24), 6406–6411.
- Trigos, A. S., Pearson, R. B., Papenfuss, A. T., & Goode, D. L. (2018). How the evolution of multicellularity set the stage for cancer. *British Journal of Cancer*, 118(2), 145–152.
- Trigos, A. S., Pearson, R. B., Papenfuss, A. T., & Goode, D. L. (2019). Somatic mutations in early metazoan genes disrupt regulatory links between unicellular and multicellular genes in cancer. *eLife*, 8. <https://doi.org/10.7554/eLife.40947>
- Tubbs, A., & Nussenzweig, A. (2017). Endogenous DNA Damage as a Source of Genomic Instability in Cancer. *Cell*, 168(4), 644–656.
- Turzanski, J., Grundy, M., Russell, N. H., & Pallis, M. (2004). Interleukin-1beta maintains an apoptosis-resistant phenotype in the blast cells of acute myeloid leukaemia via multiple pathways. *Leukemia*, 18(10), 1662–1670.
- Vainshelbaum, N. M., Salmina, K., Gerashchenko, B. I., Lazovska, M., Zayakin, P., Cragg, M. S., Pjanova, D., & Erenpreisa, J. (2022). Role of the Circadian Clock “Death-Loop” in the DNA Damage Response Underpinning Cancer Treatment Resistance. *Cells*, 11(5), 880.
- Vallone, D., Lahiri, K., Dickmeis, T., & Foulkes, N. S. (2007). Start the clock! Circadian rhythms and development. *Developmental Dynamics: An Official Publication of the American Association of Anatomists*, 236(1), 142–155.
- Villanueva, R. A. M., & Chen, Z. J. (2019). ggplot2: Elegant Graphics for Data Analysis (2nd ed.). *Measurement: Interdisciplinary Research and Perspectives*, 17(3), 160–167.

- Vincent, M. D. (2010). The animal within: carcinogenesis and the clonal evolution of cancer cells are speciation events sensu stricto. *Evolution; International Journal of Organic Evolution*, 64(4), 1173–1183.
- Vincent, M. D. (2011). Cancer: beyond speciation. *Advances in Cancer Research*, 112, 283–350.
- Vinogradov, A. E. (2010). Human transcriptome nexuses: basic-eukaryotic and metazoan. *Genomics*, 95(6), 345–354.
- Vitale, I., Senovilla, L., Jemaà, M., Michaud, M., Galluzzi, L., Kepp, O., Nanty, L., Criollo, A., Rello-Varona, S., Manic, G., Métivier, D., Vivet, S., Tajeddine, N., Joza, N., Valent, A., Castedo, M., & Kroemer, G. (2010). Multipolar mitosis of tetraploid cells: inhibition by p53 and dependency on Mos. *The EMBO Journal*, 29(7), 1272–1284.
- Walen, K. H. (2014). Neoplastic-like CELL changes of normal fibroblast cells associated with evolutionary conserved maternal and paternal genomic autonomous behavior (gonomery). *Journal of Cancer Therapy*, 05(09), 860–877.
- Wang, C., Gu, Y., Zhang, K., Xie, K., Zhu, M., Dai, N., Jiang, Y., Guo, X., Liu, M., Dai, J., Wu, L., Jin, G., Ma, H., Jiang, T., Yin, R., Xia, Y., Liu, L., Wang, S., Shen, B., ... Hu, Z. (2016). Systematic identification of genes with a cancer-testis expression pattern in 19 cancer types. *Nature Communications*, 7, 10499.
- Wang, Q., Wu, P. C., Dong, D. Z., Ivanova, I., Chu, E., Zeliadt, S., Vesselle, H., & Wu, D. Y. (2013). Polyploidy road to therapy-induced cellular senescence and escape. *International Journal of Cancer. Journal International Du Cancer*, 132(7), 1505–1515.
- Waskom, M. (2021). seaborn: statistical data visualization. *Journal of Open Source Software*, 6(60), 3021.
- Weihua, Z., Lin, Q., Ramoth, A. J., Fan, D., & Fidler, I. J. (2011). Formation of solid tumors by a single multinucleated cancer cell. *Cancer*, 117(17), 4092–4099.
- Weismann, A. (1890, February 1). *Prof. Weismann's Theory of Heredity*. Nature Publishing

Group UK. <https://doi.org/10.1038/041317g0>

- Wei, Y., Wang, Y., Gong, J., Rao, L., Wu, Z., Nie, T., Shi, D., & Zhang, L. (2018). High expression of MAGE-A9 contributes to stemness and malignancy of human hepatocellular carcinoma. *International Journal of Oncology*, *52*(1), 219–230.
- Wendel, J. F. (2000). Genome evolution in polyploids. *Plant Molecular Biology*, *42*(1), 225–249.
- White-Gilbertson, S., & Voelkel-Johnson, C. (2020). Giants and monsters: Unexpected characters in the story of cancer recurrence. *Advances in Cancer Research*, *148*, 201–232.
- Wojtuszkiewicz, A., Schuurhuis, G. J., Kessler, F. L., Piersma, S. R., Knol, J. C., Pham, T. V., Jansen, G., Musters, R. J. P., van Meerloo, J., Assaraf, Y. G., Kaspers, G. J. L., Zweegman, S., Cloos, J., & Jimenez, C. R. (2016). Exosomes Secreted by Apoptosis-Resistant Acute Myeloid Leukemia (AML) Blasts Harbor Regulatory Network Proteins Potentially Involved in Antagonism of Apoptosis. *Molecular & Cellular Proteomics: MCP*, *15*(4), 1281–1298.
- Wu, C.-H., Hsieh, C.-S., Chang, Y.-C., Huang, C.-C., Yeh, H.-T., Hou, M.-F., Chung, Y.-C., Tu, S.-H., Chang, K.-J., Chattopadhyay, A., Lai, L.-C., Lu, T.-P., Li, Y.-H., Tsai, M.-H., & Chuang, E. Y. (2021). Differential whole-genome doubling and homologous recombination deficiencies across breast cancer subtypes from the Taiwanese population. *Communications Biology*, *4*(1), 1052.
- Wu, T., Hu, E., Xu, S., Chen, M., Guo, P., Dai, Z., Feng, T., Zhou, L., Tang, W., Zhan, L., Fu, X., Liu, S., Bo, X., & Yu, G. (2021). clusterProfiler 4.0: A universal enrichment tool for interpreting omics data. *Innovation (Cambridge (Mass.))*, *2*(3), 100141.
- Wu, Y., Tao, B., Zhang, T., Fan, Y., & Mao, R. (2019). Pan-Cancer Analysis Reveals Disrupted Circadian Clock Associates With T Cell Exhaustion. *Frontiers in Immunology*, *10*, 2451.
- Yang, B., O'Herrin, S. M., Wu, J., Reagan-Shaw, S., Ma, Y., Bhat, K. M. R., Gravekamp, C., Setaluri, V., Peters, N., Hoffmann, F. M., Peng, H., Ivanov, A. V., Simpson, A. J. G., &

- Longley, B. J. (2007). MAGE-A, mMage-b, and MAGE-C proteins form complexes with KAP1 and suppress p53-dependent apoptosis in MAGE-positive cell lines. *Cancer Research*, 67(20), 9954–9962.
- Yang, X. (2010). A wheel of time: the circadian clock, nuclear receptors, and physiology [Review of *A wheel of time: the circadian clock, nuclear receptors, and physiology*]. *Genes & Development*, 24(8), 741–747.
- Yu, G., Wang, L.-G., Han, Y., & He, Q.-Y. (2012). clusterProfiler: an R package for comparing biological themes among gene clusters. *Omics: A Journal of Integrative Biology*, 16(5), 284–287.
- Zaidi, S. K., Frieze, S. E., Gordon, J. A., Heath, J. L., Messier, T., Hong, D., Boyd, J. R., Kang, M., Imbalzano, A. N., Lian, J. B., Stein, J. L., & Stein, G. S. (2017). Bivalent Epigenetic Control of Oncofetal Gene Expression in Cancer. *Molecular and Cellular Biology*, 37(23). <https://doi.org/10.1128/MCB.00352-17>
- Zhang, R., Lahens, N. F., Ballance, H. I., Hughes, M. E., & Hogenesch, J. B. (2014). A circadian gene expression atlas in mammals: implications for biology and medicine. *Proceedings of the National Academy of Sciences of the United States of America*, 111(45), 16219–16224.
- Zhang, S., Mercado-Uribe, I., Xing, Z., Sun, B., Kuang, J., & Liu, J. (2014). Generation of cancer stem-like cells through the formation of polyploid giant cancer cells. *Oncogene*, 33(1), 116–128.
- Zhang, X., & Sjöblom, T. (2021). Targeting Loss of Heterozygosity: A Novel Paradigm for Cancer Therapy. *Pharmaceuticals*, 14(1). <https://doi.org/10.3390/ph14010057>
- Zhao, Q., Zhang, Z., & Wu, Y. (2022). PRAME Is a Potential Carcinogenic Biomarker that Correlates with Patient Prognosis and Tumor Immunity Based on Pan-Cancer Analysis. *Annals of Clinical Laboratory Science*, 52(2), 185–195.
- Zheng, J., & Gao, P. (2019). Toward Normalization of the Tumor Microenvironment for Cancer

Therapy. *Integrative Cancer Therapies*, 18, 1534735419862352.

Zickler, D., & Kleckner, N. (2015). Recombination, Pairing, and Synapsis of Homologs during Meiosis. In *Cold Spring Harbor Perspectives in Biology* (Vol. 7, Issue 6, p. a016626). <https://doi.org/10.1101/cshperspect.a016626>